

Ligand Strategies based on Electronically Flexible Carbon Donors in Magnesium and Bismuth Chemistry

Akachukwu D. Obi

B.S. Chemistry, Bates College, 2015
M.Ed., University of Pennsylvania Graduate School of Education, 2017

A Dissertation presented to the
Graduate Faculty of the University of Virginia Department of Chemistry
in Candidacy for the degree of

Doctor of Philosophy

November 2022

Abstract

Main-group (*s*- and *p*-block) organometallic reagents based on environmentally benign and biocompatible metals are increasingly being adopted in chemical synthesis for bond activation events competitive with the more versatile transition metal complexes. Central to these advances is the correct choice of ancillary ligand for stabilizing well-defined species with unusual bonding scenarios (e.g., low coordinate, low valent or highly electrophilic complexes), in order to mimic the synergistic effect of *d*-orbitals for canonical organometallic reactivities (i.e., oxidative addition, reductive elimination, insertion and elimination reactions). In addition to their practical application for “greener” catalysis, inquests into unusual bonding in main group species typically enable enigmatic reactivities with fundamental and pedagogical significance. To this end, it is widely accepted that bulky, polydentate, anionic ligands based on electronegative elements (e.g., N, O) are critical for kinetic stabilization, especially for electropositive metals such as magnesium and bismuth, which tend to form metastable bonds with neutral donors. This dissertation investigates the stabilization of organo-magnesium and -bismuth complexes primarily through sterically unencumbered, electronically-flexible donor ligands such as carbenes and carbones.

Chapter One addresses ligand stabilization strategies in group 2 chemistry through the lens of periodic trends, which suggests that a one-size-fits-all is not appropriate. As an alternative, the electronic diversity achievable using carbenes and carbones is presented. In the *p*-block, these carbon-based donors are widely adopted, except for the heaviest element, bismuth. Therefore, new strategies for stabilizing organobismuth complexes using carbones were highlighted (and further elaborated in Chapter Seven). Chapter Two discusses the stabilization of redox-flexible magnesium complexes using redox non-innocent diimines, with unprecedented multiple bonding at magnesium due to electromeric carbene-diimine interactions. It was also discovered that multiple carbenes at the same magnesium center discouraged deleterious redox disproportionation.

The same strategy enabled the stabilization of highly electrophilic, organomagnesium cations benefitting from bis- or tris-carbene stabilization in Chapter Three. The electronic influence of carbenes for stabilizing small molecule building blocks at magnesium was further demonstrated in the isolation of thermally-stable magnesium phosphoethynolate ($\text{O}-\text{C}\equiv\text{P}$) complexes in Chapter Four.

Chapter Five introduces the first example of reversible migratory insertion chemistry at normal valent *s*-block species. This process is mediated by N-heterocyclic carbenes (NHCs), which shuttle unsaturated aminoboranes ($\text{Me}_2\text{N}=\text{BH}_2$) within the coordination sphere of magnesium amidoboranes. Notably, the utilization of sterically unencumbered NHCs was critical to the thermodynamic stability of these species. Analogous calcium amides are described in Chapter Six, and no dynamic migratory insertion processes were observed. Therefore, the NHC-assisted aminoborane migration at magnesium was attributed to comparative Lewis acidities of base-free magnesium amides and $\text{Me}_2\text{N}=\text{BH}_2$.

Finally, Chapter Seven details the isolation of remarkably air-stable carbene-bismuth halides, which benefit from geometrically-constrained, persistent carbene coordination. Their unprecedented *trans* carbene-Bi-halide ligation facilitated rapid dehydrosilylation redox catalysis, and the transient Bi-H intermediate was captured using $\text{B}(\text{C}_6\text{F}_5)_3$ as the first isolable bismuth hydridoborate.

Copyright Information

Chapters 1–7 contain modified versions of published manuscripts reproduced in accordance with the American Chemical Society Journal Publishing Agreement and John Wiley and Sons Publication Agreement. Proper citation for each chapter is given below and on the first page of each of the chapters within this thesis.

Chapter 1:

Obi, A. D.; Gilliard, R. J., Ligand Stabilization Strategies in Alkaline Earth Metal Chemistry. *In Preparation*

Chapter 2:

Obi, A. D.; Freeman, L. A.; Dickie, D. A.; Gilliard, R. J., N-Heterocyclic Carbene-Mediated Ring Opening of Reduced Diazamagnesacycles. *Organometallics* **2020**, *39*, 4575-4583

Chapter 3:

Obi, A. D.; Walley, J. E.; Frey, N. C.; Wong, Y. O.; Dickie, D. A.; Webster, C. E.; Gilliard, R. J., Tris(carbene) Stabilization of Monomeric Magnesium Cations: A Neutral, Nontethered Ligand Approach. *Organometallics* **2020**, *39*, 4329-4339

Chapter 4:

Obi, A. D.; Machost, H. R.; Dickie, D. A.; Gilliard, R. J., A Thermally Stable Magnesium Phosphaethynolate Grignard Complex. *Inorg. Chem.* **2021**, *60*, 12481-12488

Chapter 5:

Obi, A. D.; Frey, N. C.; Dickie, D. A.; Webster, C. E.; Gilliard, R. J., N-Heterocyclic Carbene-Assisted Reversible Migratory Coupling of Aminoborane at Magnesium. *Angew. Chem. Int. Ed.* **2022**, <https://doi.org/10.1002/anie.202211496>

Chapter 6:

Obi, A. D.; Freeman, L. A.; Coates, S.J.; Alexis, A.J.H.; Frey, N. C.; Dickie, D. A.; Webster, C. E.; Gilliard, R. J., Carbene-Calcium Silylamides and Amidoboranes. *Submitted*.

Chapter 7:

Obi, A. D.; Dickie, D. A.; Tiznado, W.; Frenking, G.; Pan S.; Gilliard, R. J., A Multi-Dimensional Carbodiphosphoranyl Approach to Bismuth Coordination Chemistry: Cationization, Redox-Flexibility, and Stabilization of a Crystalline Bismuth Hydridoborate. *Submitted*.

Acknowledgements

First, I thank my advisor and lab group. Easily the best decision I made in graduate school. Robert, advisors like you are very difficult to come by. Thank you for always being available to check-in, never running out of good ideas, fighting for resources, and never missing an opportunity to promote your students and their work. I'm very grateful that I joined the lab in its early days because I've learned a great deal by watching how your refined leadership, mentorship and outreach skills established a formidable research group within an impossibly short period.

Nod to the first students and postdocs that laid the foundations. Luke and Jacob, most of my dissertation was inspired by your work. Your understanding of the field, high level of science communication, and patient mentorship of undergraduate and graduate students around you set a high standard for everyone. Kelsie, your diligence in research and efforts at building community in the lab will never be forgotten. To the current crew – Levi, Kim, Eric, Nathan, Josh, Samir, Chunlin, Tyler – thanks for being great colleagues and friends. You make my life substantially better within and outside of lab. To the undergrads, especially my mentees Sam and Andrew, thanks for your hard work and for keeping it lively in lab.

I thank all the teachers, academic staff, and students that brought me to this point. I acknowledge that this adventure was spurred by my brilliant Chemistry students at Tabor Academy. Our stimulating conversations about fundamental chemistry concepts laid the groundwork for research interests in fundamental Inorganic Chemistry. Your joy for learning encouraged me greatly as a young teacher, and supported me through the most difficult parts of the Ph.D. I also thank my undergraduate advisors (Prof. Jen Koviach-Cote and Prof. Matt Cote) for strongly encouraging this pursuit, and my Ph.D. committee for keeping their doors open for regular, spontaneous conversations that enriched my research and career goals. To Diane, you're undoubtedly my most valuable collaborator. Thanks for delivering unbelievable miracles on some

truly terrible crystals. Jeff, thanks for your invaluable assistance with NMR. Earl, Ed, Jerry, Cindy, Susie, Cam, Madi, Sage – thank you!

This adventure would not be possible at all without the unwavering support of family and friends. Unwavering, also, in their unanimous support to quit this voluntary servitude and make real money. We made it out!! To my parents and siblings, thank you for the regular calls and texts, and for being incredibly patient even when it's difficult to explain exactly what I'm doing or why it's so hard to always stay in touch. Thanks for your occasional surprise gifts – they were very timely and always uplifting! I've been blessed many incredible friends within UVa and the greater Charlottesville community along the way, and while too numerous to mention, your contribution to this Ph.D. cannot possibly be exaggerated. Thanks for helping me maintain good mental and emotional health.

Finally, to my incredible, loving partner Tenzin, these last five years have been easy because of you. Thank you from the bottom of my heart!

To Faith. Don't give up on your dreams.

To Sonam. Can't wait to meet you.

I will search and stop at nothing / but you're just not that hard to find

Table of Contents

<i>Abstract</i>	2
<i>Copyright Information</i>	4
<i>Acknowledgements</i>	6
<i>List of Abbreviations</i>	13
<i>List of Figures</i>	14
<i>List of Schemes</i>	16
<i>List of Tables</i>	18
Chapter One: Introduction and Overview	19
<i>1.1 Ligand Stabilization Strategies in Alkaline Earth Metal Chemistry</i>	20
1.1.1 Periodic Trends and The Schlenk Equilibrium	21
1.1.2 Multidentate Ancillary Ligands	24
1.1.3 The “Big R”	26
1.1.4 Donor ligands	28
<i>1.2 Electronic Influence of Carbenes and Carbones</i>	29
Chapter Two: N-Heterocyclic Carbene-Mediated Ring Opening of Reduced Diazamagnesacycles	35
<i>2.1 Redox Non-innocent α-Diimines in Magnesium Chemistry</i>	36
<i>2.2 Synthesis of Bis(NHC)-stabilized Magnesium Diazabutadienyl Complexes</i>	38
<i>2.3 Ring Expansion and Contraction in NHC-stabilized Magnesium Diazabutadienyl Complexes</i>	42
<i>2.4 Conclusion and Outlook</i>	49
Chapter Three: Tris(carbene) Stabilization of Monomeric Magnesium Cations: A Neutral, Nontethered Ligand Approach	51
<i>3.1 Contrasting ligand stabilization strategies towards reactive alkaline earth cations</i>	52
<i>3.2 A Bis(N-heterocyclic carbene)-Stabilized Magnesium Dication</i>	54
<i>3.3 Ligand Rearrangements of Bis- to Tris-NHC Stabilized Cations</i>	56
<i>3.4 Direct Syntheses and Structural analyses of Tris(NHC)-stabilized Mg Cations</i>	58
<i>3.5 NHC-mediated Heterolysis of MgBr₂</i>	62
<i>3.6 Theoretical Analysis</i>	65
<i>3.7 Conclusion and Outlook</i>	67
Chapter Four: A Thermally Stable Magnesium Phosphaethynolate Grignard Complex	68
<i>4.1 Overview of s-Block Phosphaethynolate Chemistry</i>	69

4.2 Dioxane Activation via a Phosphaethynolate-containing Grignard Complex	70
4.3 Isolation of a Stable Magnesium Phosphaethynolate Grignard Complex	76
4.4 Isolation and Thermal Decarbonylation of a Carbene-Magnesium Diphosphaethynolate	79
4.5 Conclusion and Outlook	84
Chapter Five: N-Heterocyclic Carbene-Assisted Reversible Migratory Coupling of Aminoborane at Magnesium	85
5.1 Overview of <i>s</i> -block amidoboranes in hydrogen storage and catalysis	86
5.2 Aminoborane Coupling at Carbene-Magnesium Centers	89
5.3 Synthesis of Homoleptic Mg(NMe ₂ BH ₃) ₂ Complexes	92
5.4 Dynamic Aminoborane Coupling in Complexes Containing the ⁻ {NMe ₂ BH ₂ NMe ₂ BH ₃ } Anion	95
5.5 Computational Studies	103
5.6 Conclusion and Outlook	107
Chapter Six: Carbene-Calcium Silylamides and Amidoboranes	108
6.1 Overview of Calcium Bis(silylamide) Organometallic Chemistry	109
6.2 Assessment of Steric and Solvent Effects in Carbene-Stabilized Silylamides.	111
6.3 Isolation of a cyclic (alkyl)(amino) carbene Calcium Complex	114
6.4 Involvement of Carbenes in Calcium-mediated Amine Borane Dehydrocoupling	117
6.5 Conclusion and Outlook	123
Chapter Seven: A Multi-Dimensional Carbodiphosphoranyl Approach to Bismuth Coordination Chemistry: Cationization, Redox-Flexibility, and Stabilization of a Crystalline Bismuth Hydridoborate.	125
7.1 Ligand Stabilization Strategies Towards Redox Active Organobismuth Reagents	126
7.2 Carbene Trans Influence in the Isolation of Carbodiphosphoranyl Bismuth(III) Halides	129
7.3 Stabilization of Low-Coordinate Ionic Bismuth(III) Complexes	132
7.4 Redox Catalysis and Isolation of a Bismuth Hydridoborate Complex	139
7.5 Isolation of Bismuth(V) Complexes with Non-innocent Ligand Participation	145
7.6 Theoretical analysis	148
7.7 Conclusion and Outlook	152
Appendix I: Experimental	154
General Considerations.	154
Synthetic Procedures.	155
Chapter Two:	155

Chapter Three:	160
Chapter Four:	165
Chapter Five:	171
Chapter Six:	177
Chapter Seven:	181
Appendix II: Spectral Data	191
Chapter Two:	191
Chapter Three:	201
Chapter Four:	213
Chapter Five:	232
Chapter Six:	254
Chapter Seven:	267
Appendix III: Crystallographic Details and Crystal Structures	297
<i>General Considerations.</i>	297
Chapter Two:	297
Chapter Three:	304
Chapter Four:	311
Chapter Five:	319
Chapter Six:	329
Chapter Seven:	336
Appendix IV: Computational Details	351
Chapter Three:	351
Chapter Five:	357
Chapter Six:	361
Chapter Seven:	363
References	369

List of Abbreviations

Å	angstrom
°C	degree Celsius
CAAC	cyclic (alkyl)(amino) carbene
cm ⁻¹	inverse centimeters or wavenumbers (ν)
DFT	density functional theory
DCM	dichloromethane
deg	degree(s) (°)
EDA	energy decomposition analysis
FTIR	Fourier transform infrared
g	gram
mg	milligram
HOMO	highest occupied molecular orbital
IPr	1,3-bis(2,6-diisopropylphenyl)imidazoline-2-ylidene
kcal	kilocalorie
LUMO	lowest unoccupied molecular orbital
mol	mole
M	molarity
NBO	natural bond orbital
NHC	N-heterocyclic carbene
Me ^e NHC	1,3,4,5-tetramethylimidazol-2-ylidene
ⁱ PrNHC	1,3-diisopropyl-4,5-dimethylimidazol-2-ylidene
NMR	nuclear magnetic resonance

SC-XRD	single crystal X-ray diffraction
THF	tetrahydrofuran

List of Figures

Figure 2.1 Reported Examples of Carbene-Stabilized Alkaline Earth Complexes Bearing Dianionic Diimines

Figure 2.2. Molecular structures of **2.2** (a), **2.3** (b) and **2.4** (c)

Figure 2.3. Molecular structure of **2.6** (a), and its 10-membered ring core showing boat conformation and *trans* NCCN configurations (b)

Figure 2.4. Molecular structure of **2.8** showing (a) monomeric and (b) polymeric fragments

Figure 3.1. Bonding Comparison of Neutral and Anionic Ligand-Supported Cations

Figure 3.2. Molecular structure of **3.2**

Figure 3.3. X-ray structure of **3.5**[BPh₄] including 4% co-crystallized



Figure 3.4. X-ray structures of BPh₄ salts for **3.3** (a) and **3.4** (b)

Figure 3.5. X-ray structure of **3.7**

Figure 3.6. X-ray structure of **3.8a** and **3.8b**

Figure 3.7. Comparison of NAO-Wiberg Bond Index (WBI) values for each reported compound

Figure 4.1. Molecular structures of **4.3^{Me}** (a) and **4.4^{Me}** (b)

Figure 4.2. Molecular structure of **4.6**

Figure 4.3. Molecular structure of **4.2^{iPr}**

Figure 4.4. Molecular structure of **4.9** (a) and **4.10** (b)

Figure 4.5. Molecular structure of **4.11**

Figure 5.1. a) Simplified catalytic amine borane dehydrogenation by molecular species (R, R' = H, alkyl, aryl). b) Select examples of solution-stable group 2 bis(amidoboranes). c) Dynamic depolymerization of aminoboranes by N-heterocyclic carbenes (NHCs). d) This work: NHC-assisted reversible migratory insertion of aminoborane at magnesium (L = NHC, N' = silylamide or amidoborane).

Figure 5.2. Molecular structures of **5.2** (a) and **5.4** (b).

Figure 5.3. Molecular structures of **5.5** (a), **5.6** (b), **5.7** (c) and **5.8** (d).

Figure 5.4. Molecular structures of **5.9** (a) and **5.11** (b).

Figure 5.5. Stack plot of ^{11}B NMR spectra showing the presence of multiple species in **5.9** (a, bottom), and disappearance of $\text{Mg}(\text{NMe}_2\text{BH}_2\text{NMe}_2\text{BH}_3)$ units upon reaction with two equivalents of $i^{\text{Pr}}\text{NHC}$ (b, top).

Figure 5.6. Molecular structure of **5.12**.

Figure 5.7. Calculated relative free energies (ΔG , $\text{kcal}\cdot\text{mol}^{-1}$) for the dehydrocoupling of **5.1** to **5.2** at the $\omega\text{B97X-D/cc-PVDZ}$ level of theory.

Figure 5.8. Relative free energies (ΔG , $\text{kcal}\cdot\text{mol}^{-1}$) of aminoborane insertion/elimination between compounds **5.8**, **5.9**, **5.10**, and **5.12**.

Figure 6.1. Molecular structures of **6.2** (a) and **6.4** (b).

Figure 6.2. Molecular structure of **6.5**.

Figure 6.3. Molecular structures of **6.7** (a) and **6.8** (b).

Figure 6.4. Molecular structure of **6.9**.

Figure 7.1. Selected examples of redox-flexible bismuth platforms highlighting design strategies based on pincer ligands and/or redox-flexible electronegative elements (R = alkyl, silyl, aryl).

Figure 7.2. Electronic flexibility in carbene bismuth bonding highlighting (a) non-reductive carbene-Bi(III) multiple bonding via double dative interactions, and (b) redox flexibility within a tethered, anionic carbodiphosphorane bismuth framework with multidimensional bonding and reactivity (WCA = weakly coordinating anion).

Figure 7.3. Molecular structures of **7.1** and **7.2**.

Figure 7.4. Molecular structures of **7.3-7.5**.

Figure 7.5. Molecular structures of **7.6-7.8**.

Figure 7.6. Molecular structures of **7.9** (A) and **7.9'** (B), showing cation-cation stacking in **7.9'** (C).

Figure 7.7. Molecular structure of **7.10**.

Figure 7.8. Molecular structure of **7.11** and **7.12**.

Figure 7.9. The contour plots of Laplacian of electron density at the plane of $^{CDP}C-Bi-^{Ph}C$ of the studied complexes at the BP86-D3(BJ)/def2-TZVPP level including solvation effect where blue solid lines show $\nabla^2\rho(r) > 0$ and red dotted lines show $\nabla^2\rho(r) < 0$.

Figure 7.10. The highest occupied molecular orbital (HOMO) showing π lone-pair on CDP in the studied complexes. A low isovalue of 0.02 au is used to visualize the small MO coefficient on Bi center.

List of Schemes

Scheme 2.1. Synthesis of Bis(*N*-Heterocyclic Carbene)-Stabilized Magnesium Diazabutadienyl (DAB) Complexes

Scheme 2.2. Ring Expansion and Contraction in the Synthesis of **2.5**

Scheme 2.3. Proposed Ring Expansion/Contraction Mechanism

Scheme 2.4. KBr capture in a mono(*N*-heterocyclic carbene) Mg(DAB) species

Scheme 3.1. Synthesis of a Bis(carbene)-Stabilized Magnesium Dication

Scheme 3.2. Ligand rearrangements of bis- to tris-NHC species: differences in solvent and borate anion stabilization

Scheme 3.3. Syntheses of tris(NHC)-stabilized Mg cations **3.3-3.4**

Scheme 3.1. NHC-mediated heterolysis of MgBr₂: syntheses and calculated reaction energetics^a

Scheme 4.1. Dioxane activation in the attempted synthesis of a phosphaehtynolate-containing Grignard complex

Scheme 4.2. Dynamic carbene coordination and solvent effects in the direct synthesis of **4.4^{Me}**

Scheme 4.3. Synthesis of a stable magnesium phosphaehtynolate Grignard complex

Scheme 4.4. Role of carbene stereoelectronics in the stabilization of a magnesium bis(2-phosphaehtynolate) complex

Scheme 4.5. Thermal decomposition of a magnesium diphosphaehtynolate complex

Scheme 5.1. Dimethylamine borane dehydrocoupling in the synthesis of a heteroleptic magnesium amidoborane complex.

Scheme 5.2. Dimethylamine borane dehydrocoupling in the synthesis of a heteroleptic magnesium amidoborane complex.

Scheme 5.3. Carbene-mediated shuttling of Me₂N=BH₂ in an Mg(NMe₂BH₂NMe₂BH₃)₂ complex.

Scheme 5.4. Proposed mechanism for the disproportionation of carbene-stabilized RMg(NMe₂BH₂NMe₂BH₃) complexes.

Scheme 5.5. Isolation of (ⁱPrNHC)Mg(NMe₂BH₃)(NMe₂BH₂NMe₂BH₃) (**5.12**).

Scheme 6.1. Synthesis of (Et₂O)₂Ca(HMDS)₂ (**6.1**)

Scheme 6.2. Synthesis of N-heterocyclic carbene-stabilized calcium silylamides (6.2-6.4)

Scheme 6.3. Synthesis of CAAC-coordinated calcium amide (6.5)

Scheme 6.4. Isolation and decomposition of an N-heterocyclic carbene-stabilized calcium amidoborane

Scheme 6.5. Aminoborane capture at N-heterocyclic carbene-stabilized calcium amides

Scheme 7.1. Stabilization of bismuth halides at a dianionic carbodiphosphoranyl framework

Scheme 7.2. Cationization of 7.1 and 7.2 towards stronger ^{carbone}C–Bi bonding

Scheme 7.3. Formation and dehydrohalogenation of 7.6[BPh₄]

Scheme 7.4. Synthesis of a bismuth hydridoborate complex

Scheme 7.5. Isolation of carbodiphosphoranyl bismuth(V) complexes

List of Tables

Table 2.1. Selected Bond Distances^a and Angles^b for Compounds 2.2-2.4 and 2.6.

Table 3.1. Selected Bond Distances^a and Angles^b for Compounds 3.2-3.5 and 3.7-3.8

Table 4.1. Comparison of selected spectroscopic data and bond metrics^a for the isolated phosphaehtynolate complexes.

Table 7.1. Selected Spectroscopic and Structural Data for 7.1-7.6

Table 7.2. Reactions conditions and conversion data for catalysis experiments

Chapter One: Introduction and Overview

Contains work that was originally published in:

Obi, A. D.; Gilliard, R. J., Ligand Stabilization Strategies in Alkaline Earth Metal Chemistry. *In*
Preparation

1.1 Ligand Stabilization Strategies in Alkaline Earth Metal Chemistry

Typified by organolithium and Grignard reagents, *s*-block reagents are indispensable in chemical synthesis.¹ Yet, their organometallic chemistry is significantly less developed than their *p*- and *d*-block counterparts. *s*-Block elements form highly polarized M–R complexes (R = organic group) because of their high electropositivities and ionicity. While desirable for developing highly reactive nucleophiles, these attributes often result in weak metal-ligand bonding and poor solubility due to oligomerization, which can be detrimental to their kinetic stability. However, the last two decades ushered in new paradigms in *s*-block chemistry with the emergence of early main-group metal catalysis,¹⁻³ *s*-block element-mediated synergistic reactivity,⁴⁻⁶ and formally reduced molecular complexes.⁷⁻¹⁰ This renaissance is motivated in one part by rational kinetic stabilization strategies due to improved synthetic and computational technologies, and another by global efforts towards more sustainable resources. In particular, the alkaline earth (Ae) metals magnesium and calcium are among the most earth abundant, environmentally benign and biocompatible elements in the Earth's crust.¹¹ Therefore, their molecular reagents are attractive targets for stoichiometric or catalytic transformations currently dominated by noble metals, whose scarcity and toxicity can be disadvantageous.³ On this basis, there has been a reevaluation of organoalkaline earth chemistry towards the discovery of novel reactivity which are comparable to, or even unattainable with the noble metals.^{1-10, 12-18} Many remarkable advances have inspired an exploration into bonding scenarios previously considered inaccessible for molecular Ae complexes (e.g., low oxidation states, metal-metal bonding, multiple bonding), but desirable for designing effective molecular catalysts.

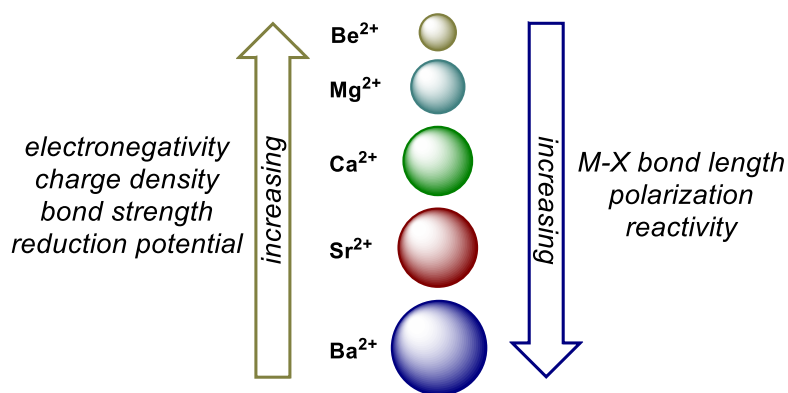
The versatility of transition metal complexes in catalysis is owed to their partially filled and energetically accessible *d*-orbitals, which allow for facile coordination of diverse substrates and reversible changes in metal oxidation states. It is now known that frontier orbital shapes and

energies for main group element (*s*- and *p*-block) complexes can be rationally modified by ligand stabilization strategies in order to mimic the synergistic effect of *d*-orbitals in challenging bond activation events such as small molecule activation (H₂, CO, N₂O, etc.) and reversible C–H and C=C activation.¹⁹⁻²³ In their own right, organoalkaline earth reagents have found extensive application in redox-invariant stoichiometric and catalytic bond activation events (i.e., σ -bond metathesis and polarized insertion reactions) controlled by metal Lewis acidity and ligand basicity similar to lanthanides and early *d*⁰ species.^{2, 3} Their capacity for multiple bonding or metal-based redox activity is impeded by their high electropositivities and extremely low reduction potentials,²⁴ resulting in a near immutable conformation of group 2 complexes as ionic salts in their +2 oxidation states. These conventions were challenged with the isolation of stable covalently bonded magnesium(I) dimers by Jones in 2007.²⁵ Following this landmark achievement, researchers have pursued ambitious undertakings leading to the discovery of other low valent complexes,^{9, 26-30} metal-metal bonds¹⁰ potent for the reduction of arenes and inert gases,³⁰⁻³⁵ energetically accessible *d*-orbitals,³⁶ well-defined molecular hydrides,^{37,38} and multiple bonding.³⁹⁻⁴¹ While these examples present strategies for achieving unique bonding modes in the *s*-block, fundamental differences in the periodic properties and trends for group 2 elements (*vide infra*) suggest that a one-size-fits-all approach cannot be adopted. Hence, it is pertinent to highlight breakthroughs in the organometallic chemistry of alkaline earth elements in the light of ligand stabilization strategies and periodic differences within the group.

1.1.1 Periodic Trends and The Schlenk Equilibrium

Differences in mass-to-charge ratio (*m/z*), electronegativity (EN) and polarizability down the group can result in profound variations in the bonding, structure and reactivity of the alkaline earth elements (Figure 1.1). The first three elements (Be, Mg, Ca) show markedly different coordination

chemistry and reactivity profiles, whereas the heavier elements (Ca, Sr, Ba) have relatively similar reactivity trends consistent with changes in their ionic size.



M^{2+}	r (Å, CN = 6)	E^0_{red} (V)	EN ⁴²	% ionicity (for M-CH ₃) ²
Be²⁺	0.45	-1.97	1.576	74
Mg²⁺	0.72	-2.36	1.293	77
Ca²⁺	1.00	-2.84	1.034	89
Sr²⁺	1.18	-2.89	0.963	91
Ba²⁺	1.35	-2.92	0.881	94

Figure 1.1. Periodic Properties and Trends for the Alkaline Earth Elements.

The least electropositive group 2 element, Be, can engage in covalent bonding interactions with organic elements (e.g., B, C, N, Si, P, Cl, Br with $\Delta\text{EN} \lesssim 1.5$), often resulting in stable ligand coordination. For instance, AeCl₂ salts (Ae = Mg, Ca, Sr, Ba) dissociate into their ionic components (Ae²⁺ and Cl⁻) in water, while BeCl₂ reacts vigorously to form Be(OH)₂ and HCl due to the polar covalent nature of the Be-Cl bond. Although magnesium is known to form covalent interactions in some cases, examples for the heavier Ae elements are essentially non-existent. Furthermore, the Ae²⁺ cations of Be, Mg and Ca have high charge densities (with Be²⁺ being the highest), hence are potent for Lewis acid reactivity. Although heavier Ae²⁺ cations are softer Lewis acids, the increasing ionic size and electropositive character down the group result in highly

polarized Ae–X bonds (X = reactive functional group) with concomitantly increasing reactivity based on σ -bond metathesis and polarized insertion. Thus, the heavier Ae elements are more attractive for homogenous catalysis. However, the same attributes present substantial difficulty in stabilizing well-defined functionalities for the heavy Ae elements due to weaker metal-ligand bonding. The propensity for ligand redistributions via the Schlenk equilibrium⁴³ worsen as the group is descended, and increasingly favors kinetic L_nAe and thermodynamic AeX_2 products (Figure 1.2).⁴⁴

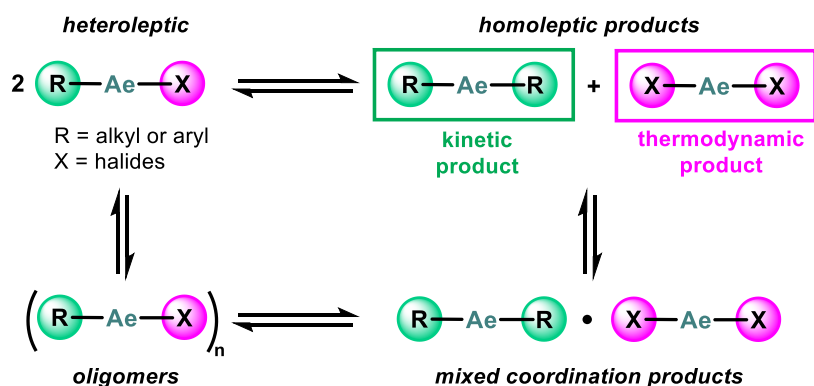


Figure 1.2. The Schlenk Equilibrium.

The poor solubility of ionic or salt-like AeX_2 products (e.g., halides, hydrides, hydroxides) in organic solvents often drives the equilibrium to the left. Moreover, the large ionic size of heavier group 2 metals makes coordinative saturation difficult, and may result in poorly defined insoluble oligomers, ether degradation and Wurtz-type R–R coupling products (R = alkyl/aryl).^{15, 16, 45, 46} The challenging syntheses of heavy $RAeX$ or AeR_2 complexes are well documented,^{2, 45-51} whereas magnesium Grignards and dialkyls have been established for more than a century as shelf-stable reagents. Indeed, pure dimethylcalcium was only reported in 2018, and further enabled the first crystallographically characterized “heavy” Grignard complexes (e.g., $[(\text{THF})_3\text{Ca}(\mu\text{-CH}_3)]_2$).⁵²

1.1.2 Multidentate Ancillary Ligands

To mitigate Schlenk-type rearrangements and isolate discrete, soluble Ae–R species, multidentate, sterically demanding ancillary ligands based on electronegative elements (e.g., N or O) are often necessary. Multidentate ligands discourage the formation of poorly defined oligomers, improve complex solubility in hydrocarbon solvents, and utilize their steric demand for kinetic stabilization of reactive functionalities. Rationally stabilized discrete species feature enhanced metal Lewis acidity and lower coordination numbers than their polymeric adducts, thus permitting facile substrate interaction, selective derivatization, and even energetically accessible *d*-orbitals.

The most versatile ancillary ligand class in group 2 chemistry is the bidentate β -diketiminate ($^{\text{Ar}}\text{Nacnac}$; $\text{Nacnac} = \text{CH}[\text{C}(\text{Me})\text{N-Ar}]_2$, Ar = aryl) with desirable characteristics such as i) monoanionic and *N*-chelating persistent bonding, ii) steric and electronic tunability via the backbone or pendant *N*-aryl substituents, and iii) ability to adapt coordination sphere to metal size (Figure 1.3).⁵³ This ligand class has enabled the isolation of well-defined, hydrocarbon soluble reagents encompassing all of the Ae elements, including low-coordinate Mg^0 and Mg^{I} reagents,^{9, 27} and catalytically active magnesium and calcium hydrides, alkyls and amides.^{37, 38, 54, 55} The most common proligand, $^{\text{Dipp}}\text{NacnacH}$ (Dipp = 2,6-diisopropylphenyl), is easily synthesized in one step from commercial reagents, and can be converted to useful Ae starting materials via one-pot protonolysis and/or (trans)metallation reactions.⁵⁶⁻⁵⁸ Coordinative saturation around the Ae metal center can be modified by substituting the backbone methyls for *tert*-butyl groups, which enable larger metal shielding by forcing the aryl groups to bend towards the metal, and further impedes any potentially deleterious deprotonation of the ligand backbone. The six-membered $\text{C}_3\text{N}_2\text{Ae}$ ring encapsulating the metal center adopts an envelope or chair transformation, except in the case of beryllium for which it is planar presumably due to Be–N π -bonding.⁵⁹ The same planarity is

observed in the isoelectronic tricoordinate $[(^{\text{Ar}}\text{Nacnac})\text{Al-R}]^+$ cation, whose empty p -orbital is symmetric with the ligand π -system.⁶⁰

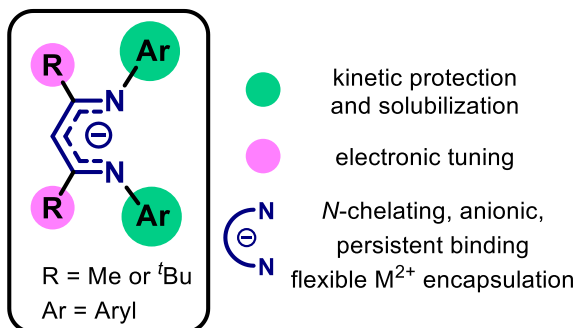


Figure 1.3. The $^{\text{Ar}}\text{Nacnac}$ ligand embodying favorable design principles for Ae complexes.

In addition to the steric encumbrance and bidentate nature of the ligand, the stability of heteroleptic $(^{\text{Ar}}\text{Nacnac})\text{AeR}$ complexes to Schlenk-type disproportionation may also be owed to a coordinatively saturated binuclear intermediate.⁶¹ Since coordinative saturation in heavier Ae elements is difficult, DippNacnac complexes of strontium and barium are prone to disproportionation to the unreactive homoleptic L_2Ae species,⁵⁶ often necessitating solvation⁶²⁻⁶⁴ and non-covalent interactions (e.g., electrostatic $\text{M}\cdots\text{C}_\pi$, $\text{M}\cdots\text{F}$, anagostic $\text{M}\cdots\text{H-C}$ or $\text{M}\cdots\text{H-Si}$)^{17, 18, 64-66} for auxiliary stabilization. A “super bulky” Nacnac ligand (DiPePNacnac ; DiPeP = 2,6-diisopentylphenyl) stabilized dimeric strontium hydrides and alkyls, for a remarkable nucleophilic alkylation of benzene,⁶⁷ which was similarly achieved at a calcium center.⁶⁸ Thermally stable Nacnac barium complexes are limited to iodides and silyl amides, and there remains a severe paucity of ligands for accessing discrete functionalities at Ba.^{18, 69} Suitably robust ligands should ideally stabilize smaller functionalities such as hydrides, which are active species in hydroelementation catalysis. Indeed, only a few examples of low nuclearity heavy Ae hydrides have been reported, and they are mostly stabilized by N -chelating anionic ligands including $^{\text{Ar}}\text{Nacnac}$,^{62, 67, 70} amidinate,⁷¹ hydrotris(pyrazolyl)borate,⁷² and Me_3TACD^- ($(\text{Me}_3\text{TACD})\text{H} =$

1,4,7-trimethyl-1,4,7,10-tetraazacyclododecane).⁷³ Recently, a bulky penta-arylcyclopentadienyl ligand (^{Ar}Cp; Ar = 3,5-C₆H₃) stabilized [Ae(μ -H)]₂ complexes across all the heavy Ae elements (Ae = Ca, Sr, Ba) for the first time, and these hydrides were indeed catalytically active for hydroolefination.⁷⁴ A bis(imino)carbazolate ligand enabled the isolation of a rare solvent-free barium amide for catalytic styrene hydrophosphination, and the long sought molecular barium fluoride (as (THF)₃(Carb^{Dipp}Ba(μ -F))₂; Carb^{Dipp} = 1,8-bis-(2,6-diisopropylphenyl)imino-3,6-di-*tert*-butylcarbazole).⁷⁵ The latter heralds the ligand's potential to similarly stabilize small functionalities (e.g., alkyls and hydrides) at barium, and expand the library of discrete functionalities at strontium.

1.1.3 The “Big R”

An alternative strategy avoids the Schlenk equilibrium altogether through the use of base-free homoleptic complexes. Low nuclearity AeR₂ complexes with polyhaptic (e.g., cyclopentadienyl) or sterically encumbered R groups (e.g., bis(trialkylsilyl) alkyls/amides, benzyl) are typically highly active reagents in their own right, especially for the heavier Ae elements. Prior to the introduction of bulky spectator ligands such as Nacnac, the syntheses and structural study of Ae metallocenes and their Lewis base adducts enabled an early fundamental understanding of bonding and coordination behavior within the alkaline earth metals.^{48, 49, 76-79} In the solid-state, magnesocene is structurally analogous to ferrocene (i.e., linear M(η^5 -Cp)₂, Cp = C₅H₅), whereas MCp₂ adducts of the heavier group 2 elements are oligomeric or polymeric adducts with mixed $\eta^1/\eta^3/\eta^5$ Cp coordination due to their larger size. For the lightest element, Cp₂Be has an η^1/η^5 “slip-sandwich” structure, albeit with fluxional solution-state dynamics.⁸⁰ The bulkier pentamethylcyclopentadienyl ligand (C₅Me₅ or Cp*) affords monomeric M(η^5 -Cp*)₂ adducts for all the group 2 elements, and those of the larger atoms (Ca, Sr and Ba) are non-VSEPR structures,

which are bent despite the absence of a lone pair.⁸¹ The higher polarizability of heavy Ae elements results in a permanent dipole moment in their MCp^*_2 structures, and their bent configuration largely results from charge-dipole interactions such as pregostic-type interactions between the Ae metal and methyl groups on the Cp^* rings.⁸¹

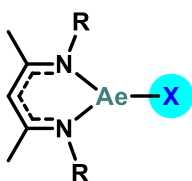
Simple dimeric $[\text{Ae}(\text{N}(\text{SiMe}_3)_2)_2]_2$ adducts of Mg, Ca, Sr and Ba have been established as potent catalysts in the hydrogenation of unactivated alkenes^{82, 83} and imines.⁸⁴ Their highly polarized Ae–N bonds enable facile metathesis or insertion reactions with hydride sources, and subsequent hydrogenation of unsaturated substrates via the Ae–H fragment. A slight increase in the steric demand of the amide can improve the stability of the intermediary heteroleptic hydride (i.e., H–Ae–NR₂) for increased activity.⁸⁵ Indeed, stable $[\text{H–Ae–NR}_2]_n$ clusters (Ae = Mg, Ca, Sr, Ba) have been isolated as solvated or base-stabilized crystalline complexes. An isolable Ba–H aggregate $[(\text{C}_6\text{H}_6)_2\text{Ba}_7\text{H}_7(\text{N}(\text{SiMe}_3)_2)_7]$ displayed greater reducing power than LiAlH_4 , and was active for the hydrogenation of ethylene under mild conditions (20 °C, 1 bar).⁸³


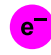

In contrast to its heavier counterparts, $\text{Be}(\text{N}(\text{SiMe}_3)_2)_2$ is monomeric and relatively inert.⁸⁶ The linear N–Be–N angle (178.73(16)°), short Be–N bonds (1.525(2) and 1.519(2) Å), and sp^2 hybridization around the N atoms suggest some Be–N π -bonding character, which may further contribute to its stability.⁸⁶ An activated base-stabilized adduct was targeted by sequential dechlorination of $(\text{CDC})\text{BeCl}_2$ (CDC = carbodicarbene), but the reaction of potassium hexamethyldisilazide ($\text{KN}(\text{SiMe}_3)_2$) with the heteroleptic $(\text{CDC})\text{BeCl}(\text{N}(\text{SiMe}_3)_2)$ resulted in a deprotonation of the ligand's pendant isopropyl $\text{C}(\text{sp}^3)\text{–H}$ bond acidified by a highly polarizing Be^{2+} cation.⁸⁷

1.1.4 Donor ligands

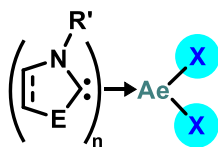
Donor ligands can modulate the electronics of alkaline earth complexes towards the stabilization of diverse homo- and hetero-leptic functionalities. Since monoanionic ancillary ligands consume one electron in bonding, leaving only one reactive functionality for Ae complexes, donor ligands are desirable for their versatility as they can support stepwise one- and two-electron reductions, as well as cationization towards mono- and di-cations for enhanced metal Lewis acidity (Figure 1.4).

A: Bulky anionic ligands (e.g., NacNac)



-  one reactive group
-  one electron reduction
-  restricted ligand tuning (R = aryl)

B: Neutral monodentate donors (e.g., carbenes)








-   two reactive groups
-   two electron reduction
-  flexible ligand tuning (R' = alkyl, aryl; E = NR or CR'₂)

Figure 1.4. Contrasting anionic vs neutral ancillary ligands in group 2 chemistry

Excluding donor solvents, the most common neutral ligands in Ae chemistry are macrocyclic *N*-donors such as tetramethyl-tetraazacyclododecane (Me₄TACD), tetramethylethylenediamine (TMEDA) and pentamethyldiethylenediamine (PMDTA), with widespread application for stabilizing small functionalities (e.g., hydrides) at Mg, Ca and Sr.^{37, 38, 73, 88-96} Their polydentate nature is critical to their persistent coordination, since they form donor-acceptor adducts with Ae²⁺ cations rather than charged interactions. Indeed, the tetradentate Me₄TACD (as well as its anionic counterpart Me₃TACD⁻) is the most versatile ligand within this category.

Conversely, monodentate donors (e.g., pyridines, phosphines, ethers) are disadvantaged by weak coordination and deleterious ligand dissociation. In recent years, exceptionally strong donor and electronically flexible carbon-based ligands such as carbenes and carbones have been increasingly adopted in organoalkaline earth chemistry as monodentate Lewis bases for stabilizing low coordinate Ae complexes.^{97,98} Cyclic carbenes (such as *N*-heterocyclic carbenes (NHCs) and cyclic (alkyl)(amino) carbenes (CAACs)) are two-electron σ -donor and π -acceptor ligands (Figure 1.4), and have facilitated remarkable advances in low valent Ae chemistry,^{99,100} small molecule activation,¹⁰¹ catalysis,^{102,103} hydrogen storage,^{104,105} and multiple bonding.^{26,28,40,106,107} Carbones (such as carbodicarbenes (CDC) and carbodiphosphanes (CDP)) are stronger σ -donors than carbenes, but are also exceptional π -donors. The latter property was instrumental in stabilizing a Be=C double bond, the first example of a formal double bond in the *s*-block.³⁹

Despite their strong donor ability and potential for multiple bonding (through π -interactions), hard-soft acid-base (HSAB) effects can result in dynamic coordination of these carbon-based ligands, often with destabilizing effects on reactive complexes. The coordination of multiple monodentate carbenes at divalent alkaline earth complexes is increasingly being adopted to ensure ligand stabilized intermediates upon base dissociation.^{79,102,103,107-111} Typically, this necessitates a reduction in sterics, leading to species with predominant electronic stabilization from the ligand. Indeed, it has been realized that unencumbered carbenes form robust coordination complexes with simple magnesium and calcium compounds (e.g., amides, alkyls, halides), whereas bulkier carbenes readily dissociate in solution, or fail to coordinate altogether.

1.2 Electronic Influence of Carbenes and Carbones

Due to their burgeoning influence in various aspects of main group chemistry,⁹⁸ it is worth elaborating on the electronic nature of these carbon donor ligands, towards their broader adoption in group 2 chemistry. Carbenes (CR₂, divalent C(II) ligands) were long known as laboratory

curiosities, only observed in the coordination sphere of transition metals. Classically recognized as Fisher- ($M=CR(OR)$) or Schrock-type ($M=CH_2$) ligands, carbenes are comprised of a high lying σ -symmetric HOMO and low-lying π -symmetric LUMO, usually stabilized by donor-acceptor multiple-bonding interactions with transition-metal d -orbitals. In 1991, Arduengo reported that installation of the carbene carbon within a heterocycle enabled the isolation of metal-free, “bottleable” N-heterocyclic carbenes (NHCs),¹¹² predominantly stabilized by electromeric effects (e.g., $N_{2p} \rightarrow C_{\pi^*}(LUMO)$ and $C_{\sigma(HOMO)} \rightarrow \sigma^*_{N-C}$).¹¹³ Consequently, simple coordination complexes of NHCs and other main group complexes were easily obtained without necessary π -back-bonding stabilization, and NHCs rapidly became one of the most useful ligands in organometallic chemistry.¹¹⁴ Furthermore, the realization that π -back-bonding is negligible in certain NHC-transition-metal complexes rekindled debate on the nature of bonding in the acyclic Fisher and Schrock carbenes.⁹⁷ Nevertheless, cyclic carbenes are desirable for their ease of synthesis and stereoelectronic tunability (Figure 1.5).

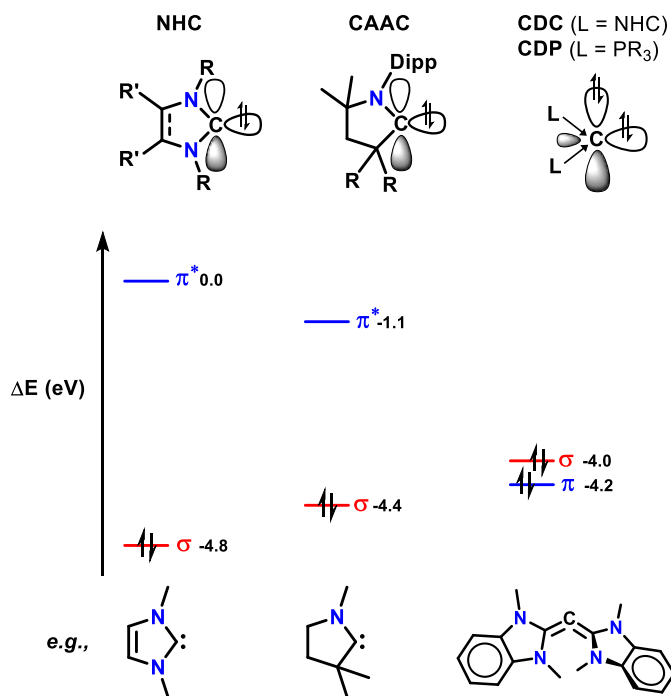


Figure 1.5. Frontier orbitals of electronically flexible, carbon-based donor ligands. NHC = *N*-heterocyclic carbene (R, R' = H, alkyl, aryl); CAAC = cyclic (alkyl)(amino) carbene (R = alkyl); CDC = carbodicarbene; CDP = carbodiphosphorane.

In 2007, Bertrand realized that substituting one of the nitrogen atoms in classical NHCs by carbon enabled a more reactive, but stronger σ -donor and π -acceptor carbene – the so-called cyclic (alkyl)(amino) carbene (CAAC).¹¹⁵ Since then, CAACs have made an immediate impact,^{116, 117} especially in low valent main group chemistry,¹¹⁸ whereby their enhanced π -acidity enables facile π -back-bonding with electron-rich metals. In group 2, CAACs enabled the isolation of several low valent beryllium complexes as di-coordinate, multiply-bonded (CAAC)₂Be^{0/1} species. The seminal (CAAC)₂Be⁰ complex was synthesized by the KC₈ reduction of (CAAC)BeCl₂ in the presence of free CAAC, and features a three-center two-electron π -bond between Be⁰ (1s², 2s⁰, 2p²) and the strongly σ -donating and π -accepting CAAC ligands (i.e., CAAC \rightleftharpoons Be \rightleftharpoons CAAC).²⁶ It is noteworthy that the attempted reduction of (NacNac)BeX complexes led to ligand activation and intractable mixtures, in lieu of a well-defined species.^{59, 119} Because comparative magnesium species have been isolated (e.g., [LMg]₂ and [LMgNa]₂, L = NacNac),^{25, 27} it is assumed that the smaller atomic radius of Be results in unfavorable steric interactions, and the enhanced metal Lewis acidity (vs Mg) may enable facile ligand activation. CAAC complexes of Mg, Ca, Sr and Ba have also been isolated, but their likewise reduction is thwarted by weak coordination and deleterious ligand activation.^{120, 121}

In contrast to the octet defying carbenes, carbones (CL₂, divalent C(0) compounds) satisfy the octet rule. The first stable carbene – hexaphenylcarbodiphosphorane (C(PPh₃)₂) – was prepared in 1961 by Ramirez *et al.*,¹²² who described it as “formally related to the carbodiimides and the allenes,” hence the representation Ph₃P=C=PPh₃. Structural analysis by X-ray diffraction indicates

a bent geometry about the central carbon ($\angle\text{P-C-P}$ 131.7°), thus raising much debate on the bonding scenario in $\text{C}(\text{PPh}_3)_2$ when compared to related allenes which are typically linear. It took more than four decades for this compound and related carbodiphosphoranes (CDPs, i.e., $\text{C}(\text{PR}_3)_2$) to be unambiguously recognized as divalent $\text{C}(0)$ donors, whereby two lone pairs are localized on the central carbon in the free molecule and occupy frontier orbitals (HOMO and HOMO-1), leading to the observed bent geometry.¹²³ Therefore, the donor-acceptor representation $\text{Ph}_3\text{P}\rightarrow\text{C}\leftarrow\text{PPh}_3$ is the predominant resonance contributor, and the carbene carbon has been established as a two- and four-electron donor atom.¹²³⁻¹²⁵ Following this realization, Frenking theorized that the same CL_2 scaffold is possible using NHCs.¹²⁶ The first $\text{C}(\text{NHC})_2$ (carbodicarbene or CDC) reported by Bertrand in 2008 features a comparable bend angle ($\angle\text{C-C-C}$ 134.8°) to that of CDPs, which already suggests that both compounds are electronically similar.¹²⁷ The frontier orbitals of CDCs resemble those of CDPs, although the π -symmetric lone pair (HOMO) is more delocalized than those of CDPs due to more substantial negative hyperconjugation effects (lone pair $\rightarrow \pi^*_{\text{C-C}}$) in the former. Owing to an improved understanding of their electronics, the coordination chemistry of carbenes has rapidly developed during the last decade,^{128, 129} and there is now an extensive library of synthetically accessible carbenes with high stereoelectronic variety.¹²⁹⁻¹³² Recently, Ong introduced a new class of asymmetric carbenes, carbophosphinocarbenes (CPCs, i.e., $\text{NHC}=\text{C}=\text{PR}_3$), that combines the electronics of CDCs and CDPs, and further expands the structural diversity of carbenes.¹³³

Despite their electronic appeal, there are very few carbene-alkaline earth complexes. The first carbene-alkaline earth complex was $(\text{CDP})\text{BeCl}_2$, synthesized to investigate the influence of the double Lewis base (CDP) on a double Lewis acid (BeCl_2).¹³⁴ However, the bonding situation in $(\text{CDP})\text{BeCl}_2$, as well as the comparative $(\text{CDC})\text{BeCl}_2$,⁸⁷ is predominantly $\text{C}\rightarrow\text{BeCl}_2$ σ -donation,

with negligible contribution of the π -symmetric lone pairs. The reaction of (CDC)BeCl₂ and K[N(SiMe₃)₂] lead to deprotonation of the ligand isopropyl pendant arm, likely polarized by the unoccupied Be²⁺ 2*p* orbital. Notably, the same reactivity was observed at a CDC-stabilized boron scaffold, wherein agostic CH₃---B interactions were evident in the solid-state.¹³⁵ By geometrically constraining the carbene-Be interaction, Buchner and coworkers recently isolated the elusive double dative (σ and π) C=Be interaction, which represents the first reported example of multiple bonding in the *s*-block.³⁹ The attempted coordination of C(PPh₃)₂ to magnesium resulted in C-H activation of one of the phenyl groups, and subsequent cyclometallation of the ligand.¹³⁶ Indeed, simple coordination complexes of carbenes and heavier group 2 salts are nearly absent in the literature, which is surprising since their carbene complexes are relatively ubiquitous. Access to heavier Ae carbene or methanediide complexes typically involves the utilization of alkaline earth bis(alkyl) or bis(amide) bases to activate (deprotonate) the ligand such that the metal center loses at least one reactive functionality, and the ligand becomes mono- or di-anionic.

In contrast to their underdeveloped and challenging chemistry in the *s*-block, carbon-based donors have remarkably transformed *p*-block organometallic chemistry.⁹⁸ Because *p*-block elements below the second row are predisposed to multiple stable oxidation states (e.g. P(III)/P(V), Sn(II)/Sn(IV), Bi(III)/Bi(V)), ligand effects may further lower the energy penalty for M(*n*)/M(*n*+2) redox cycles towards transition-metal-like catalysis, as well as stabilize unusual oxidation states.²³ Indeed, carbenes enabled the isolation of low valent molecular complexes for nearly every *p*-block metal or metalloid, typically (but not necessarily) stabilized by π -backdonation into the unoccupied and symmetry-correct carbene C_{2*p*} orbital. This includes unusual zero oxidation state molecular complexes such as carbene-stabilized di-boron,¹³⁷ di-silicon,¹³⁸ and even carbodicarbenes (CDCs).¹²⁷ Although the adoption of carbenes has been more sluggish, the introduction of CDCs

in 2008 revitalized carbene *p*-block chemistry with alternative electronic tuning strategies that contrast or even compliment those of carbenes.^{128, 139} For example, NHCs react with BH₃ to form air-stable donor-acceptor adducts (i.e., NHC-BH₃), whereas the much stronger σ -donor CDCs formally displace two hydride anions from BH₃ to form the much more reactive di-cationic hydrido boron complex [(CDC)₂BH]²⁺.¹⁴⁰ This observation further implicates the capacity of carbones to stabilize highly electrophilic main group species, wherein the stabilization from carbenes is typically insufficient.^{141, 142} Among the heavier elements, carbene-bismuth complexes are known to be highly reactive and susceptible to small changes in their coordination environments.^{143, 144} This is partly because the large atomic size of bismuth makes coordinative saturation difficult, leading to facile oligomerization, deleterious solvent effects and/or ligand activation. Conversely, carbene-bismuth complexes are typically low-coordinate, monomeric and thermally stable in solution.^{142, 145} In addition to their superior σ -donor capacity, CDCs can contribute their π electrons in double-dative bonding with Lewis acidic bismuth species to form robust C=Bi bonds through non-reductive multiple bonding.¹⁴²

Chapter Two: N-Heterocyclic Carbene-Mediated Ring Opening of Reduced Diazamagnesacycles

Contains work that was originally published in:

Obi, A. D.; Freeman, L. A.; Dickie, D. A.; Gilliard, R. J., N-Heterocyclic Carbene-Mediated Ring Opening of Reduced Diazamagnesacycles. *Organometallics* **2020**, *39*, 4575-4583

2.1 Redox Non-innocent α -Diimines in Magnesium Chemistry

Since the turn of the century, advances in ligand stabilization strategies have enabled the isolation of well-defined molecular alkaline earth reagents for bond activation,^{2, 3, 20} as well as the synthesis of rare subvalent beryllium,^{26, 28, 146} magnesium,^{25, 27, 147, 148} and calcium^{29, 30} complexes. Of these exotic complexes, Jones' Mg(I) dimers are the most investigated, and have demonstrated an impressive array of reactivity, primarily as hydrocarbon-soluble reducing agents.^{8, 9, 33, 34, 149} We have also demonstrated that low valent Be(0) species can be used as specialty reducing agents.^{28, 150} However, redox chemistry at group 2 centers remains challenging due to their extremely low reduction potentials, and a penchant for their highly stable +2 oxidation state.^{21, 151} As an alternative to a formally reduced metal center, non-innocent α -diimines can permit redox activity in organometallic systems due to their capacity to serve as electron and proton reservoirs.¹⁵² Fedushkin reported C–H activation of phenylacetylene and subsequent diphenylketone insertion within a THF-stabilized ^{Dipp}BIAN (BIAN = 1,2-bis[(aryl)imino]acenaphthene, aryl = Dipp = 2,6-diisopropylphenyl) magnesium complex.¹⁵³ This seminal report inspired concerted effort towards developing reactive alkaline earth complexes bearing redox active ligands with unusual bonding and reactivity,^{106, 119, 154-163} including Mg–Mg bonded complexes.¹⁶⁴⁻¹⁶⁷

More recently, the research groups of Hill,¹⁵⁴ Jones,¹¹⁹ and this laboratory¹⁰⁶ reported carbene-stabilized alkaline earth complexes bearing reduced α -diimines such as diazabutadienyl (DAB) or 2,2-bipyridyl (bpy) anions (Figure 2.1, I–VI). Due to their exceptional donor ability, and tunable steric and electronic properties,^{97, 112, 114-117, 168} cyclic carbenes (i.e. *N*-heterocyclic carbenes (NHCs) and cyclic(alkyl)(amino) carbene (CAACs)) have enabled the isolation of organometallic complexes with attractive redox activity.^{21, 98, 169} CAACs, being more π -acidic than NHCs, have been exploited to stabilize low valent, monomeric beryllium^{26, 28, 146} and magnesium¹⁷⁰⁻¹⁷² complexes with ^{carbene}C \rightleftharpoons M multiple bonding. Likewise, the π -acidity of both CAACs and NHCs

enabled carbene-diimine cooperative bonding in tricoordinate doubly reduced α -diimine complexes (e.g., **II–IV**).¹⁰⁶ This involves electromeric stabilization of unoccupied p -orbitals of carbene and metal by the π -symmetric diimine nitrogen lone pairs. Indeed, calculated MOs and WBI values for the CAAC-stabilized magnesium-diimine complex (**II**) support partial double-bond character for the $^{\text{CAAC}}\text{C–Mg}$ bond. The comparative stabilization of Mg(DAB) or Mg(bpy) using classical diamidocarbenes (i.e. NHCs) such as 1,3-bis(2,6-diisopropylphenyl)-4,5-dihydroimidazole-2-ylidene (SIPr) was not achieved, likely due to the relatively weak coordination of SIPr in the starting dihalide $[(\text{SIPr})\text{MgBr}_2]$.^{106, 108} Nevertheless, NHC-stabilized analogues of reduced magnesium complexes are attractive targets due to the potential for achieving unique bonding and reactivity in the reduced complexes.

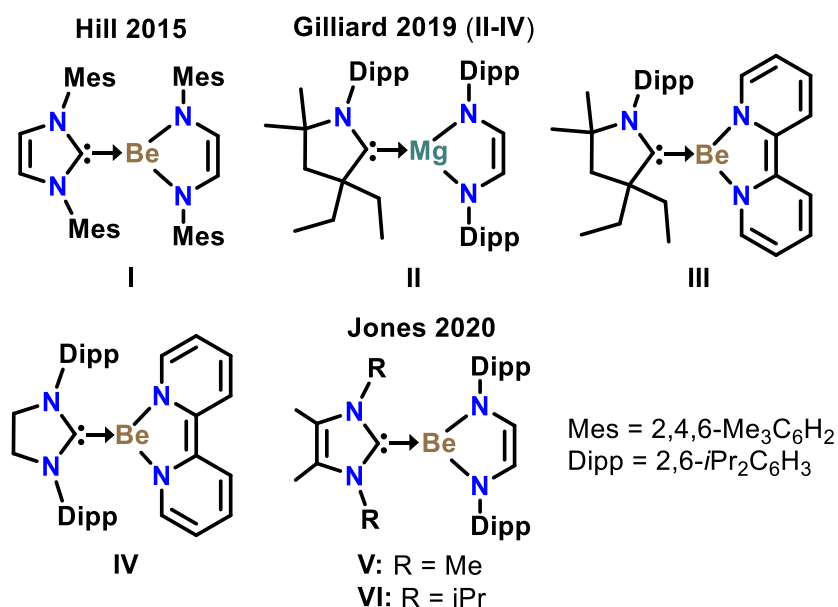


Figure 2.1 Reported Examples of Carbene-Stabilized Alkaline Earth Complexes Bearing Dianionic Diimines.

Since we have recently discovered that dual- or tris-stabilization of magnesium centers using sterically unencumbered NHCs (e.g. $(^{\text{iPr}}\text{NHC})_2\text{MgBr}_2$, (**1**); $^{\text{iPr}}\text{NHC}$ = 1,3-diisopropyl-4,5-

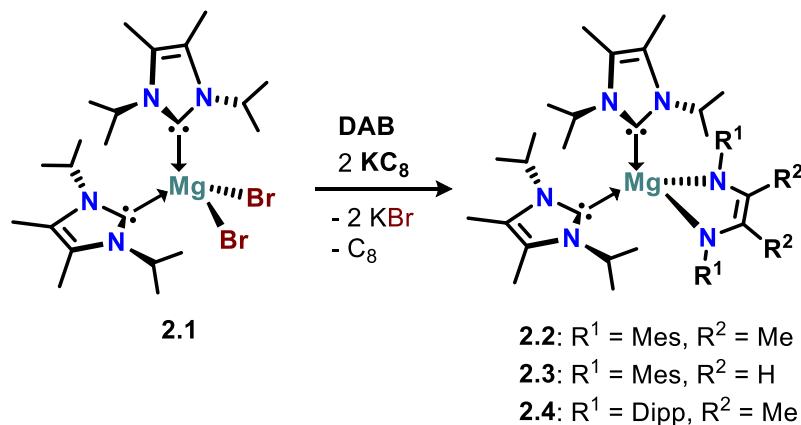
dimethylimidazol-2-ylidene) can result in persistent carbene coordination to Lewis acidic magnesium reagents,^{108, 109, 173, 174} we sought to stabilize the reduced complexes using a bis(NHC) approach. The coordination of two non-tethered NHCs may permit access to a “masked” Lewis acidic magnesium center due to dynamic association and dissociation of the carbene ligand. Herein, we report the syntheses and structural studies of tetracoordinate magnesium complexes of reduced diazabutadienes stabilized by dual NHC-coordination: (ⁱPrNHC)₂Mg(^{Mes}DAB^{Me}) (**2.2**), (ⁱPrNHC)₂Mg(^{Mes}DAB^H) (**2.3**), (ⁱPrNHC)₂Mg(^{Dipp}DAB^{Me}) (**2.4**) and (ⁱPrNHC)₂Mg(^{Dipp}DAB^H) (**2.5**) (^{Mes}DAB^{Me} = *N,N'*-bis(2,4,6-trimethylphenyl)-2,3-dimethyl-1,4-diaza-1,3-diene, ^{Mes}DAB^H = *N,N'*-bis(2,4,6-trimethylphenyl)-1,4-diazabutadiene, ^{Dipp}DAB^{Me} = *N,N'*-bis(2,6-diisopropylphenyl)-2,3-dimethyl-1,4-diaza-1,3-diene and ^{Dipp}DAB^H = *N,N'*-bis(2,6-diisopropylphenyl)-1,4-diazabutadiene). Compounds **2.2-2.4** are mononuclear complexes with tetracoordinate metal centers, and surprisingly, **2.5** crystallizes as the dinuclear 10-membered metallocycle [(ⁱPrNHC)Mg(μ -^{Dipp}DAB^H)]₂ (**2.6**) with tricoordinate magnesium atoms. To the best of our knowledge, compounds **2.2-2.6**, and the mono(NHC)-stabilized species (ⁱPrNHC)Mg(^{Dipp}DAB^{Me})·KBr (**2.8**) represent the first examples of NHC magnesium complexes bearing α -diimines. Promoted by dynamic carbene coordination and dissociation in solution, the ring expansion and contraction between **2.5** and **2.6** offer insight into the potential reactivity of these complexes as synthons in carbene-magnesium coordination chemistry.

2.2 Synthesis of Bis(NHC)-stabilized Magnesium Diazabutadienyl Complexes

The doubly reduced complexes **2.2-2.4** were prepared in 60 – 79% yields by the addition of KC₈ to a homogenous toluene solution of (ⁱPrNHC)₂MgBr₂ (**2.1**)¹⁰⁸ and the respective diimine ligand, or the addition of **2.1** to K₂(DAB) (prepared *in situ* from DAB and 2 equiv KC₈) in toluene (Scheme 2.1). Crystalline yellow-orange solids were obtained after workup, and characterized by NMR

spectroscopy and single-crystal X-ray diffraction. ^1H NMR analyses suggest symmetric coordination environments due to single resonances for the NHC methine protons (δ 4.77, 4.90 and 4.69 ppm for **2.2**, **2.3**, and **2.4** respectively), which are significantly upfield shifted from **2.1** (δ 5.69 ppm). A broad singlet (δ 4.69 ppm) attributed to the NHC methine protons on **2.4** indicate restricted rotation of the carbenes, resulting in asymmetry in the Dipp- ^iPr methyl protons which resonate as two doublets at 1.47 ppm and 1.21 ppm. Comparatively, the mesityl *ortho*- CH_3 substituents on **2.2** and **2.3** appear as single resonances (δ 2.50 and 2.56 ppm respectively), indicating free rotation of carbene and mesityl groups.

Scheme 2.1. Synthesis of Bis(*N*-Heterocyclic Carbene)-Stabilized Magnesium Diazabutadienyl (DAB) Complexes.



Yellow or orange plate-like single crystals of **2.2-2.4** suitable for X-ray diffraction studies were obtained from their respective saturated hydrocarbon solutions at room temperature or -37°C . Each structure revealed two NHCs coordinated to a single Mg atom which lies within a five-membered metallacycle containing the diimine core (Figure 2.2). Three chemically equivalent but crystallographically independent molecules are contained in the asymmetric unit of **2.4**, one of which is discussed herein for comparison of metrical parameters. The C–C and C–N bond distances within the DAB heterocycle in **2.2-2.4** maintain the expected N–C=C–N sequence, and

are within the range for dianionic diimines.^{106, 119, 154-163} The N–Mg–N' DAB bite angles in **2.2**–**2.4** (Table 1) are slightly smaller than that of **II** (90.79(7)°). The metallocycle in **2.3** is nearly flat, with the magnesium atom deviating only -0.0428(10) Å from the plane of the ring, whereas the rings in **2.2** and **2.4** are slightly more distorted (Mg 0.0887(9) and -0.1041(8) Å out of plane, respectively) due to steric effects of the DAB backbone methyl substituents. Additional electronic influence of the methyl substituents is observed in slightly elongated ^{NHC}C–Mg distances for **2.2** (2.275(2) and 2.277(3) Å) and **2.4** (2.269(2) and 2.308(2) Å) when compared to **2.3** (2.248(3) and 2.237(2) Å). Indeed, this electronic effect is reflected in the ¹H NMR, where the NHC methine protons in **2.2** (δ 4.77 ppm) are upfield of those of **2.3** (δ 4.90 ppm). These ^{NHC}C–Mg distances are expectedly longer than the ^{CAAC}C–Mg in **II** (2.194(2) Å)¹⁰⁶ due to absence of carbene-diimine π-interactions, and the presence of an additional stabilizing Lewis base. Nevertheless, they are comparable to **2.1** and in the range of reported values.^{104, 106, 108, 109, 173, 174} Notably, these compounds are stable as solids for more than five months under an inert atmosphere and ambient conditions, and in anhydrous hydrocarbon solvents for more than three months at room temperature.

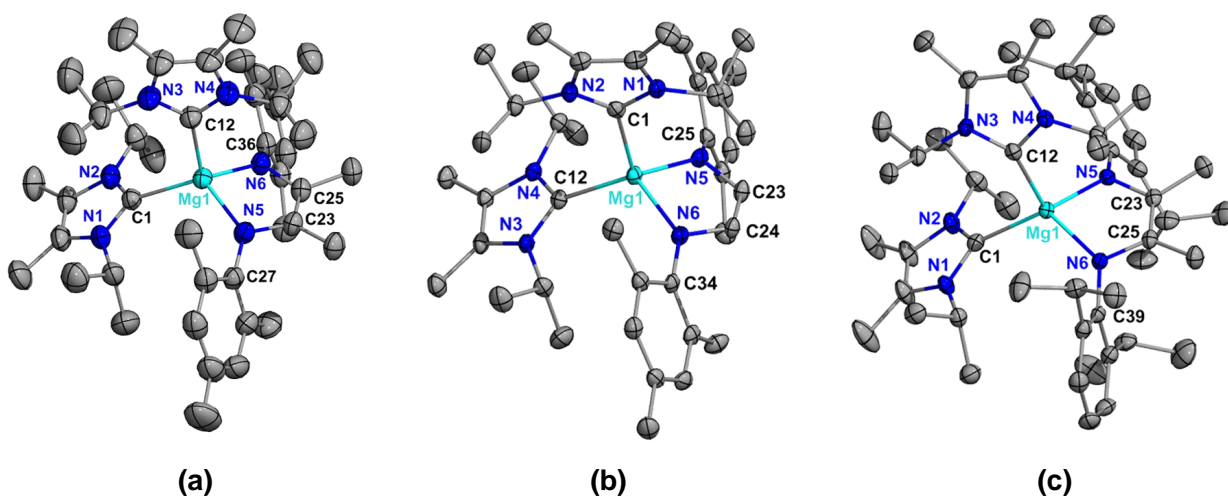


Figure 2.2. Molecular structures of **2.2** (a), **2.3** (b) and **2.4** (c). Thermal ellipsoids are shown at a probability level of 50%. All H atoms, and co-crystallized toluene molecules for **2.3** are omitted for clarity. One of three crystallographically independent molecules in the asymmetric unit of **2.4** is shown. Selected bond distances (Å) and angles (°) are described in table 2.1.

Table 2.2. Selected Bond Distances^a and Angles^b for Compounds **2.2-2.4** and **2.6**.

	2.2	2.3	2.4^c	2.6	2.8^c
Mg1–C1	2.275(2)	2.248(3)	2.269(2)	2.205(6)	2.196(10)
Mg1–C12	2.277(2)	2.236(3)	2.308(2)	2.204(6) ^e	
Mg1–N5	2.0356(19)	2.024(2)	2.0546(18)	1.986(5)	2.043(6) ^h
Mg1–N6	2.0259(18)	2.053(2)	2.0106(19)	1.975(5) ^e	2.043(6) ^f
Mg1–Br1	-	-	-	-	2.606(3)
K1–Br1	-	-	-	-	3.233(2)
C23–C25	1.353(3)	1.342(3) ^d	1.355(3)	1.332(7) ^d	1.387(15) ⁱ
N5–C23	1.423(3)	1.412(3)	1.426(3)	1.405(6)	1.408(9) ^{g, i}
N6–C25	1.423(3)	1.410(3) ^d	1.428(3)	1.423(6) ^d	1.408(9) ^{f, j}
C1–Mg1–C12	112.06(8)	111.39(9)	105.31(8)		94.3(3) ^k
N5–Mg1–N6	86.59(7)	88.30(8)	86.15(8)	133.11(19) ^f	83.9(3) ^{f, h}
C1–Mg1–N5	118.19(8)	112.71(9)	120.48(8)	113.0(2)	129.7(2) ^h
C1–Mg1–N6	116.33(8)	109.57(9)	118.07(8)	113.9(2) ^f	129.7(2) ^f
C12–Mg1–N5	110.39(8)	114.77(9)	110.75(8)	132.75(19) ^g	
C12–Mg1–N6	110.85(8)	118.24(9)	115.71(8)	112.9(2) ^e	
Mg1–N6–C25–C23	10.9(3)	-5.9(3) ^d	-11.9(3)		7.2(4) ^l
N6–Mg1–N5–C23	12.71(15)	-5.97(16)	-15.18(14)		-8.5(4) ^m

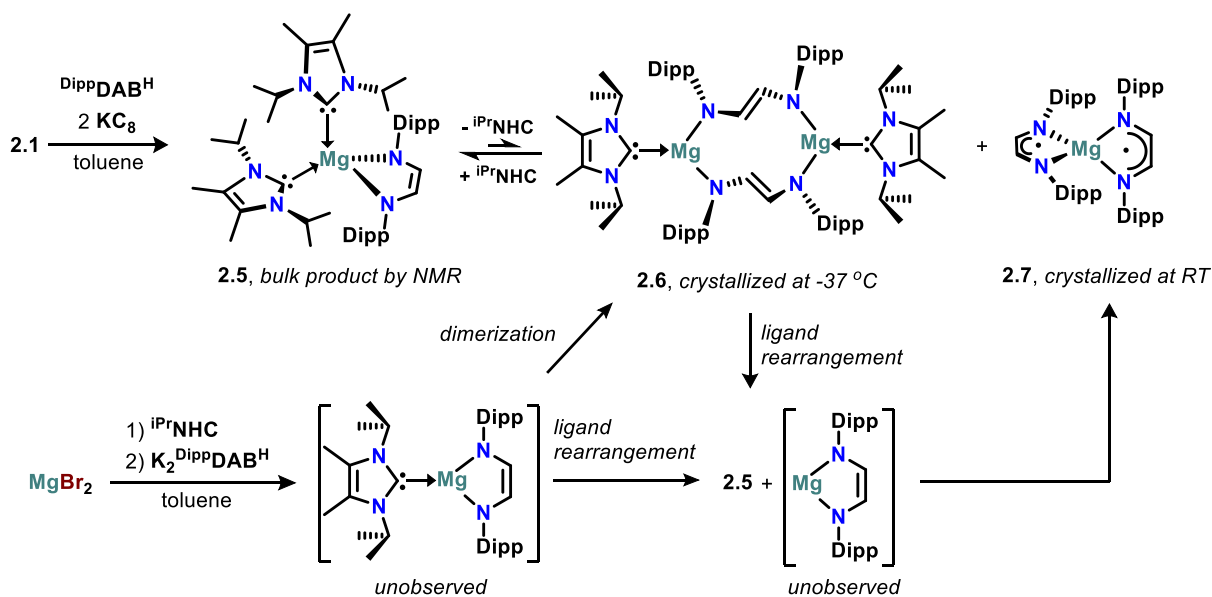
^aIn angstroms. ^bIn degrees. ^cValues reported for only one of two (**2.8**) or three (**2.4**) chemically equivalent but crystallographically unique molecules in the asymmetric unit. ^dC24 instead of C25.

^eMg2 instead of Mg1. ^fN8 (**2.6**) or N2 (**2.8**) instead of N6. ^gN7–Mg2–N6. ^hN2' instead of N5. ⁱC7 instead of C23. ^jC7' instead of C25. ^kBr1 instead of C12. ^lMg1–N2–C7–C7'. ^mN2–Mg1–N2'–C7'.

2.3 Ring Expansion and Contraction in NHC-stabilized Magnesium Diazabutadienyl Complexes

Similar to the syntheses of **2.2-2.4**, 2 equiv of KC_8 were added to a stirring toluene solution of **2.1** and neutral $\text{DippDAB}^{\text{H}}$ (Scheme 2.2). A yellow solid was obtained after workup, and the ^1H NMR (Figure A2.7) is consistent with the expected bis(NHC)-stabilized magnesacycle $(i\text{PrNHC})_2\text{Mg}(\text{DippDAB}^{\text{H}})$ (**2.5**), with a 1:1 integral ratio with respect to the NHC and Dipp methine protons. As is similarly observed between the mesityl analogues **2.2** and **2.3**, the absence of methyl substituents on the DAB backbone resulted in a downfield ^1H NMR resonance for the NHC methine protons (δ 4.85 ppm) relative to those of **2.4** (δ 4.69 ppm).

Scheme 2.2. Ring Expansion and Contraction in the Synthesis of **2.5**.



Although compounds **2.2-2.4** are isostructural, subtle changes in *N*-substitution (mesityl to diisopropylphenyl from **2.3**) or diimine backbone substitution (Me to H from **2.4**) resulted in an unexpected structural variation. Yellow block-like single crystals were obtained at -37°C from a saturated toluene solution of **2.5**, and analyzed by X-ray diffraction. The crystal structure revealed

a dinuclear $\text{Mg}_2(\mu\text{-DAB})_2$ ten-membered metallacycle where two magnesium atoms are bridged by DAB ligands in an η^1, η^1 -enediamide coordination ($[(\text{iPrNHC})\text{Mg}(\mu\text{-DippDAB}^{\text{H}})]_2$ (**2.6**), Figure 2.3a). Each magnesium atom is supported by a single NHC, and lies within a slightly distorted trigonal planar environment. The $^{\text{NHC}}\text{C-Mg}$ distances (2.204(6) and 2.205(6) Å) are significantly shortened from those in **2.2-2.4** (2.236 – 2.308 Å), and are comparable to the $^{\text{CAAC}}\text{C-Mg}$ bond in **II** (2.194(2) Å). Similarly, the Mg–N bonds (e.g., Mg1–N5: 1.986(5) Å, Mg2–N6: 1.975(5) Å) are shortened from **2.2-2.4** (average 2.034 Å). These data support stronger bonding in the $^{\text{NHC}}\text{C-Mg-DABN}$ core, and are suggestive of carbene-diimine cooperative bonding as observed in **II**, with stabilizing interactions across their π -symmetric orbitals.¹⁰⁶ The molecular structure of **2.6** also features a boat-shaped conformation for the heterocycle, where the diazabutadiene NCCN units adopt *trans* configurations (Figure 2.3b), which minimize steric repulsion between the *N*-Dipp groups. Notably, the $^{\text{DAB}}\text{C}=\text{C}\cdots\text{Mg}$ contacts in **2.2-2.4** and **2.6** (2.666 – 2.864 Å) are within the range of electrostatic Mg– C_π interactions.¹⁷⁵ However, the $^{\text{DAB}}\text{C}=\text{C}$ bonds in **2.6** are slightly shortened from **2.2-2.4**, and the corresponding C–N bonds lengthened (see Table 2.1), as the coordination mode of the diimine ligands in **2.6** does not position them for substantial Mg–(C=C) $_\pi$ interactions.¹⁷⁶

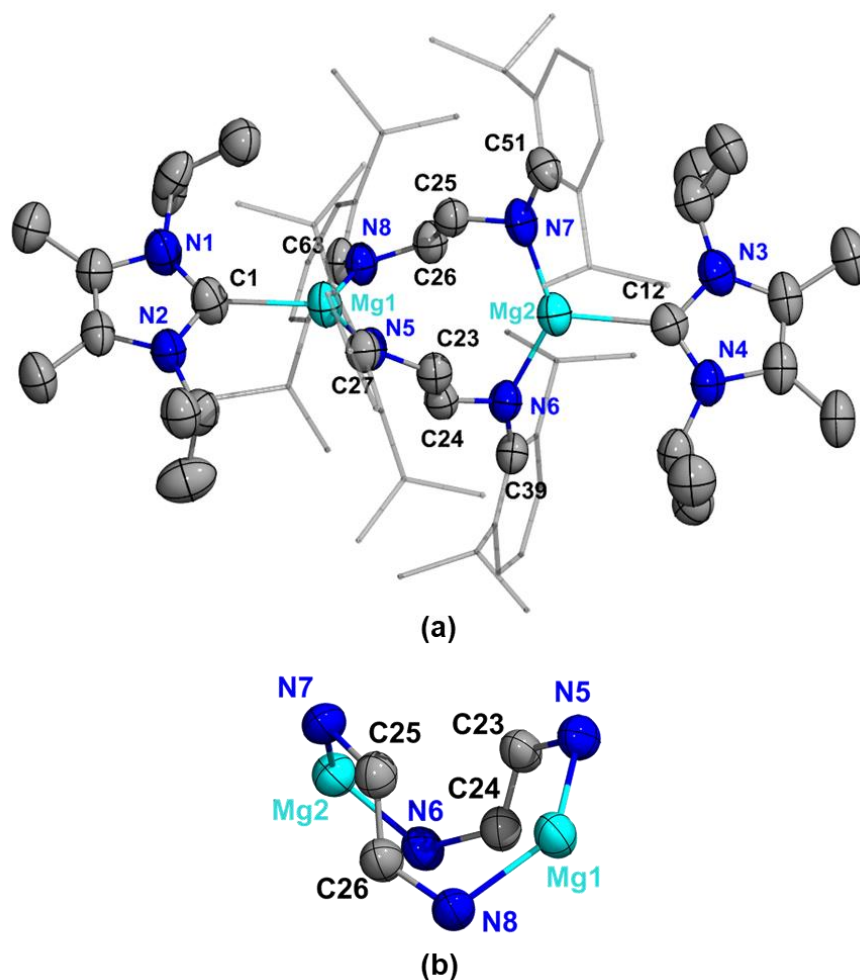


Figure 2.3. Molecular structure of **2.6** (a), and its 10-membered ring core showing boat conformation and *trans* NCCN configurations (b). Thermal ellipsoids are shown at the 50% probability level. For clarity, H atoms and co-crystallized toluene molecules have been omitted, and the Dipp groups are styled as wireframe. Only the major occupied positions are shown for the disordered isopropyl substituents on N2.

Because the coordination environment in **2.6** is different from the ^1H NMR spectrum of the bulk sample (**2.5**), diffusion ordered spectroscopy (DOSY) experiments were conducted to ascertain the solution phase structure. In the DOSY NMR, similar diffusion coefficients, and consequently comparable hydrodynamic volume were obtained for **2.2-2.5** (see Appendix II). These results

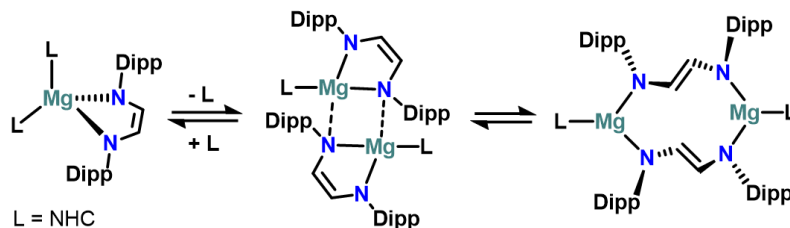
indicate that the structure of **2.5** in solution is isostructural to complexes **2.2-2.4**. Notably, ^1H NMR resonances corresponding to **2.6** were not observed in solution, despite variable temperature (VT) NMR experiments (toluene- d_8 , 298 – 213 K). Thus, the transience of **2.6** in solution, and the possibility for a fast equilibrium process between **2.5** and **2.6** were considered.

The reaction of equimolar amounts of $i\text{PrNHC}$, MgBr_2 and $\text{K}_2(\text{DippDAB}^{\text{H}})$ yielded similar results as the analogous reaction via the bis(NHC) stabilized dihalide, **2.1** (Scheme 2.2). This suggests that bis(NHC)-stabilized species is favored in solution, even without the introduction of an additional carbene. The expected byproduct of a rearrangement from **2.6** to **2.5** is a transient $\text{Mg}(\text{DAB}^{2-})$ species that is not stabilized by a Lewis base, which is known to initiate ligand exchange and intramolecular disproportionation to form stable $\text{Mg}(\text{DAB}^{\cdot-})_2$ diradical species.^{156, 157, 164} Indeed, a few crystals of the diradical $\text{Mg}(\text{DippDAB}^{\text{H}})_2$ (**2.7**, Figure A3.5) precipitated from a toluene solution of **2.5** after one week at room temperature. Due to the trace amount isolated, spectroscopic analyses on **2.7** could not be performed. However, similar diradical species have been reported.^{164, 177-179} It is noteworthy that single crystals of **2.6** were also only obtained in extremely poor yields, thus limiting spectroscopic studies on a crystalline sample. After the initial deposition of few single crystals, prolonged times led to the precipitation of a powdery solid, which was spectroscopically characterized as **2.5** and an unidentified product (Figure A2.11). Although the combined observation of **2.6** and **2.7** from solutions of **2.5** are suggestive of a reversible equilibrium as described in Scheme 2.2, the possibility that **2.7** is a product of an irreversible decomposition of **2.5** cannot be discounted.

Notably, the DAB coordination mode in **2.6** is uncommon for main-group-element–diimine complexes, and is, to the best of our knowledge, the first reported example for *s*-block complexes. However, a comparable binding arrangement has been observed for tetracoordinate aluminum

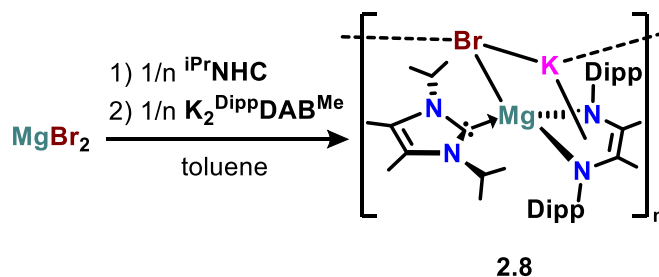
diamide complexes.¹⁸⁰ In the formation of **2.6**, we propose an initial ligand dissociation resulting in a more electrophilic metal center,¹⁸¹ which initiates dimerization and further polarizes the covalent Mg–N bonds (Scheme 2.3). In a concerted σ -bond metathesis fashion, new covalent Mg–N bonds are formed from the dimeric interactions, driven by the formation of stronger bonds via NHC–Mg–diimine π -interactions as observed in **II**. Notably, Fedushkin et al. observed base dissociation when $(\text{THF})_n\text{Mg}(\text{R}^n\text{BIAN})$ ($\text{R} = \text{alkyl or aryl, } n = 2 \text{ or } 3$) complexes are dissolved in non-coordinating solvents such as toluene, resulting in complete conversion to the diradical $\text{Mg}(\text{R}^n\text{BIAN})_2$.^{156, 157} Therefore, upon base dissociation, it is expected that the persistence of one electronically flexible Lewis base (i.e., a carbene) in this case stabilizes the isolation of the dinuclear species, **2.6**. In contrast to **2.6**, the lighter group 2 congener $(\text{iPrNHC})\text{Be}(\text{DippDAB}^{\text{H}})$ ¹¹⁹ and related carbene beryllium diimine complexes are mononuclear (see Figure 2.1). It should be noted that mononuclear tricoordinate complexes are common for beryllium, and relatively rare for magnesium, except in cases where bulky ligands are employed to protect the Mg complex from dimerization. Indeed, the significant increase in mass to charge ratio (m/z) and consequent polarizability down the group plays a role in the differences in bonding preferences for heavier group 2 elements. Therefore, upon carbene dissociation, the larger size of the Mg^{2+} cation (relative to Be^{2+}) promotes the suggested dimerization and consequent ring expansion towards the formation of **2.6**.

Scheme 2.3. Proposed Ring Expansion/Contraction Mechanism



Given that complexes **2.2** and **2.3** are isostructural, it is assumed that the Dipp groups play an important role in non-covalent interactions in **2.5/2.6**, resulting in the dynamic structural variation observed. Therefore, to further probe the suggested mechanism, we explored a comparative mono(NHC) stabilization of $\text{Mg}(\text{DippDAB}^{\text{Me}})$ bearing the saturated DAB backbone (Scheme 2.4). The addition of *in situ* prepared $\text{K}_2(\text{DippDAB}^{\text{Me}})$ to a toluene solution of equimolar MgBr_2 and $i\text{PrNHC}$ yielded a yellow powder after workup. The ^1H NMR is consistent with a mono(NHC) coordinated species, where the $i\text{PrNHC}$ methine protons resonate upfield of those for **2.2-2.5** at 4.50 ppm. The carbene carbon (δ 181.9 ppm) is similarly upfield shifted, as expected for a more Lewis acidic magnesium atom.¹⁸² Asymmetry in this molecule is indicated by slightly overlapping septets at 3.93 ppm and 3.89 ppm for the Dipp- $\text{CH}(\text{Me})_2$ protons, and their distinctively resolved methyl doublets at 1.20 ppm and 1.11 ppm.

Scheme 2.4. KBr capture in a mono(*N*-heterocyclic carbene) Mg(DAB) species



Structural disambiguation by single crystal X-ray diffraction affords a centrosymmetric polymer, whereby K–Br units are interacting with mononuclear $\text{Mg}(\text{DippDAB}^{\text{Me}})$ heterocycles each stabilized by one $i\text{PrNHC}$ ligand (Figure 2.4). An analysis of the bonding in this complex suggests a strong electrostatic or weakly covalent interaction of a KBr salt with the polarized $\text{Mg}(\text{DippDAB}^{\text{Me}})$ unit, and supports the dimerization speculated for the homologous $(i\text{PrNHC})\text{Mg}(\text{DippDAB}^{\text{H}})$ species. Analogous alkali halide salt interactions have been observed for solvated DAB^{2-} complexes of highly electropositive lanthanides and heavy alkaline earth

elements.^{161, 162, 183} It is thus assumed that unfavorable steric interactions due to the DAB backbone methyl substitution hinders dimerization in the isolation of **2.8**.

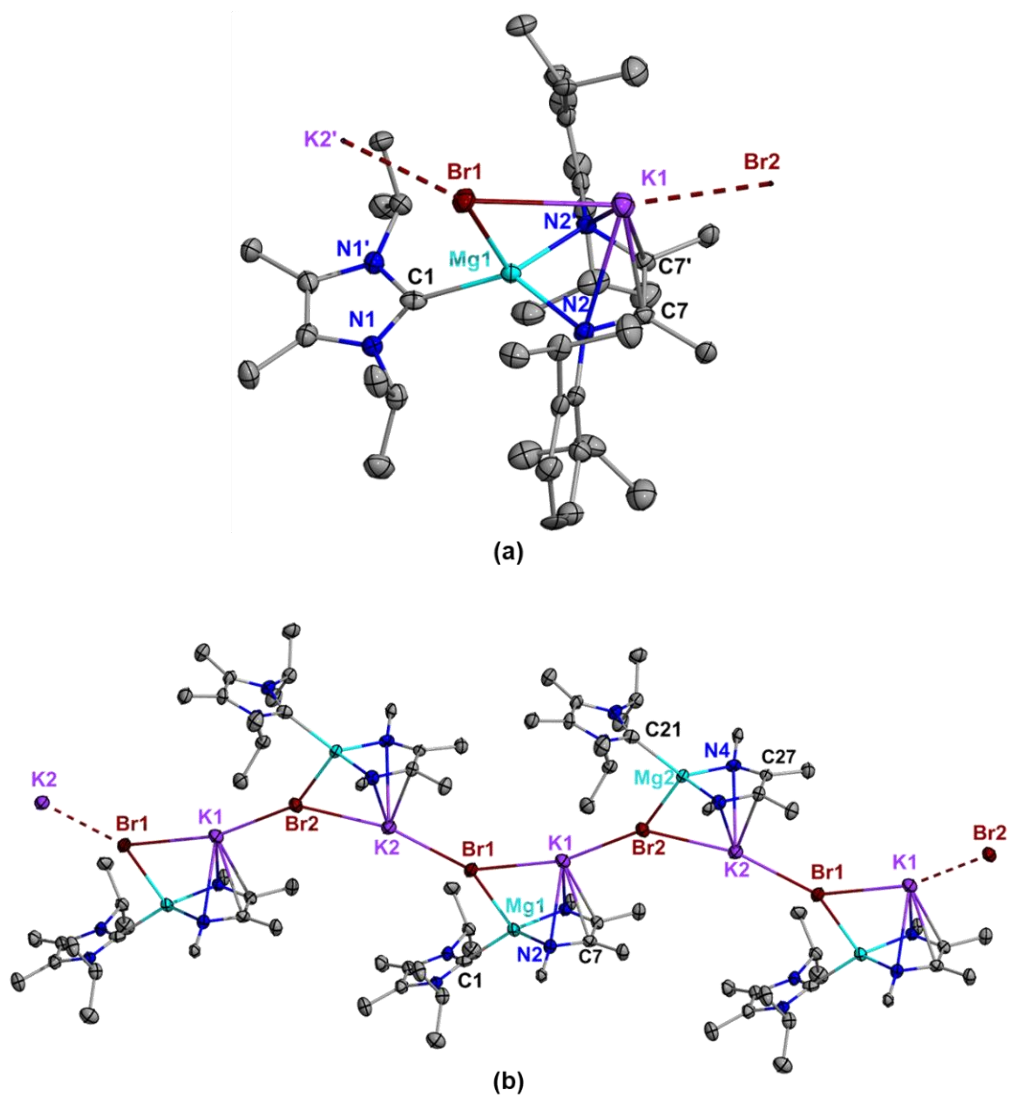


Figure 2.4. Molecular structure of **2.8** showing (a) monomeric and (b) polymeric fragments.

Thermal ellipsoids are shown at a probability level of 50%. For clarity, Dipp groups in (b) and all H atoms are hidden. Selected bond distances (Å) and angles (°): Mg1–C1: 2.196(10); Mg2–C21: 2.210(11); Mg1–Br1: 2.606(3); Mg2–Br2: 2.591(3); Mg1–N2: 2.043(6); Mg2–N4: 2.029(6); C7–C7': 1.387(15); C27–C27': 1.370(15); Br1–K1: 3.233(2); Br1–K2: 3.136(2); Br2–K1: 3.103(2);

Br2–K2: 3.246(2); K1–C7: 2.907(7); K1–N2: 2.936(6); K2–C27: 2.915(7); K2–N4: 2.927(6); N2–Mg1–N2': 83.9(3); N2–Mg1–C1: 129.7(2); C1–Mg1–Br1: 94.3(3); N2–Mg1–Br1: 109.45(19).

The adjoining K–Br distances in **2.8** (K1–Br2: 3.103(2) Å and K2'–Br1: 3.136(2) Å) are more closely correlated with their expected additive covalent radii (3.10 Å),¹⁸⁴ than the intramolecular KBr interactions (K1–Br1: 3.233(2) Å and K2–Br2: 3.246(2) Å). The Mg1–Br1 bond (2.606(3) Å) is significantly elongated from the Mg–Br distances in **2.1** (2.4822(2) Å and 2.4939(6) Å)¹⁰⁸ and similar terminal Mg–Br bonds.^{108, 109} The ^{centroid}(NCCN)–K1 distance is 2.642 Å, and the K1–C7 (2.907(7) Å) and K1–N2 (2.936(6) Å) bonds are in the range of reported K–DAB interactions.¹⁶¹ This electrostatic interaction is further supported by a slight elongation of the ^{DAB}C=C bond (C7–C7': 1.387(15) Å) compared to **2.2–2.4** and **2.6** (1.332 – 1.355 Å), and a concomitant shortening of the C–N bonds (both 1.408(9) Å). The C1–Mg1 bond in **2.8** (2.196(10) Å) is identical to the ^{carbene}C–Mg bond distances in **II** and **2.6** within their estimated standard deviations. Notably, the bond parameters in **2.8** differ significantly from those observed in the paramagnetic complex (CAAC)Mg(Br)(^{Dipp}DAB^H) bearing a singly-reduced DAB ligand.¹⁰⁶ Thus, this diamagnetic polymer may be considered an (^{iPr}NHC)Mg(^{Dipp}DAB^{Me})-KBr complex, or an ionic K[(^{iPr}NHC)Mg(Br)(^{Dipp}DAB^{Me})] salt.

2.4 Conclusion and Outlook

The first examples of NHC-stabilized magnesium complexes bearing doubly reduced α -diimines have been synthesized and structurally characterized. Dynamic carbene coordination permits reversible ring expansion and contraction in complexes **2.5** and **2.6**. The η^1, η^1 -enediamide coordination in **2.6** is facilitated by dimerization of an intermediary (^{iPr}NHC)Mg(^{Dipp}DAB^H) upon carbene dissociation from **2.5**, and stabilized by cooperative π -interactions between carbene and diimine ligands. The isolation of (^{iPr}NHC)Mg(^{Dipp}DAB^{Me})-KBr (**2.8**) suggests that a reduction in

carbene steric demand and electrophilicity (compared to **II**, Figure 2.1) permits facile substrate interaction with the polarized Mg(DAB) unit, and supports the mechanism postulated for the formation of **2.6**. The electronic flexibility in these carbene-stabilized magnesium bis-amido complexes heralds promise for their application as synthons in magnesium coordination chemistry. Furthermore, bimetallic species such as **2.8** may have desirable potential for *s*-block synergistic reactivity, where both metals through charge separation or charge transfer may stabilize transition states otherwise inaccessible by the neutral species.⁴

Chapter Three: Tris(carbene) Stabilization of Monomeric Magnesium

Cations: A Neutral, Nontethered Ligand Approach

Contains work that was originally published in:

Obi, A. D.; Walley, J. E.; Frey, N. C.; Wong, Y. O.; Dickie, D. A.; Webster, C. E.; Gilliard, R. J.,

Tris(carbene) Stabilization of Monomeric Magnesium Cations: A Neutral, Nontethered Ligand

Approach. *Organometallics* **2020**, *39*, 4329-4339

3.1 Contrasting ligand stabilization strategies towards reactive alkaline earth cations

The study of alkaline earth (Ae) metals in unusual coordination environments is currently experiencing a renaissance, attracting broad interest across the fields of chemical synthesis and catalysis.¹⁻³ Indeed, these elements were fairly recently discovered to facilitate stoichiometric and catalytic bond activations when the metal center resides in a low oxidation state or in a bonding situation that renders the metal electrophilic.^{8, 9, 185-187} Due to the vital importance of electrostatic interactions between alkaline earth metals and substrates,^{68, 188-191} a trend in utilizing charge separation to enhance the electrophilicity of the metal has emerged. Harder and Hill have reported an array of β -diketiminato (NacNac)-stabilized cationic alkaline earth complexes which formed stable, unsupported bonding interactions with a diverse array of arenes, terminal alkynes, silyl ethers and phosphines.^{32, 175, 192-196} Notably, these cations have been utilized as frustrated Lewis pair-type reagents mediating two-electron dearomatization of benzene,³¹ aromatization of cyclooctatetraene,³² and diverse reactivity at carbon–carbon multiple bonds.^{195, 197}

When alkaline earth metals bind to the anionic β -diketiminato framework, one electron is immediately consumed in bonding, leaving one terminal or bridging metal–organic unit. Thus, the formation of electrophilic cations via abstraction of an organic group affords an alkaline-earth center that is free of an exocyclic functional group (excluding weakly coordinating anions, Figure 3.1). In contrast, the use of L-type neutral ligands for the stabilization of cationic Ae complexes provides a well-defined functional group (e.g. CH_3^-) at the metal.^{89, 93, 111, 198} To this end, *N*-heterocyclic carbenes (NHCs) are particularly attractive as neutral ancillary ligands due to their high donor strength, tunable sterics, and electronic flexibility.^{97, 112, 115-117, 168} However, despite being popular ligands in *p*-block and transition metal chemistry, NHC-*s*-block chemistry remains underexplored.^{98, 114, 169, 199-202} Thus, carbene-stabilized alkaline earth cations are rare. This is mostly due to the fact that the solution-phase coordination chemistry of such species can be

complex, where Schlenk-type ligand redistributions and reversible solvent coordination are prominent, especially in their monodentate ligand supported adducts.⁴⁴ Nevertheless, recent remarkable advances in carbene-stabilized group 2 organometallics necessitate a reevaluation of the unique potential of NHCs for unusual transformations at these highly electropositive metal centers.^{26, 28, 33, 98, 101, 104, 119, 150, 154, 203, 204}

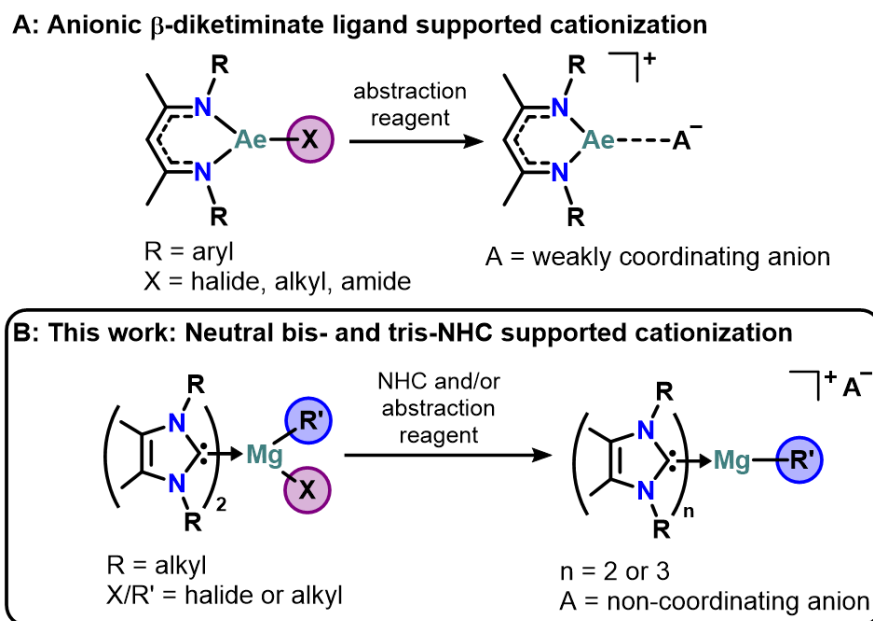


Figure 3.1. Bonding Comparison of Neutral and Anionic Ligand-Supported Cations

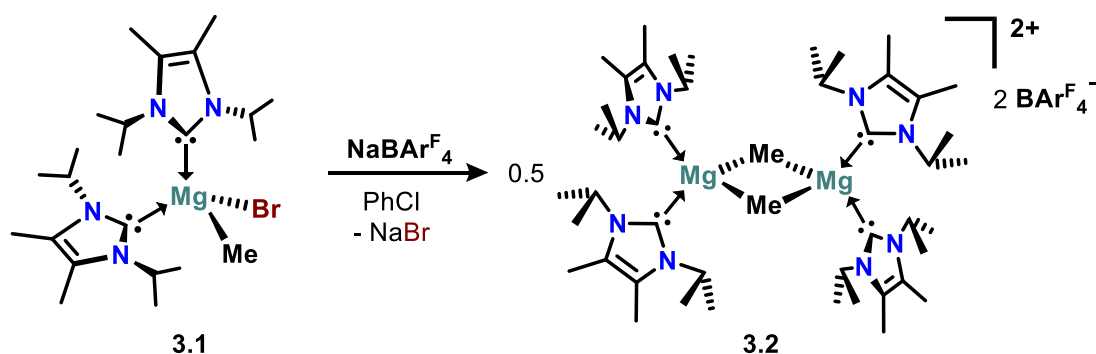
The utilization of NHCs in group 2 chemistry often requires sterically demanding aryl *N*-substitutions at the carbenes to induce kinetic stabilization around the metal center in a manner similar to NacNac-stabilized species. However, we recently initiated studies on the electronic influence of less sterically demanding NHCs on the structure and chemical properties of organoalkaline earth reagents.^{106, 108, 173, 174, 205} Employing a dual NHC coordination strategy with 1,3-diisopropyl-4,5-dimethylimidazol-2-ylidene (ⁱPrNHC), we isolated the first carbene-stabilized terminal Grignard (i.e. (ⁱPrNHC)₂MgMeBr, **3.1**) along with a series of unsolvated monomeric magnesium alkyls and halides.¹⁰⁸ This system resulted in persistent ligand coordination in contrast

to dynamic solvent interaction observed in the mono-NHC stabilized magnesium complexes.^{108, 198, 206} We now report the syntheses and structural characterization of solvent-free organomagnesium cations stabilized by a non-tethered multi-carbene system. Notably, complexes **3.2-3.5** and **3.8** represent the first examples of cationic organomagnesium complexes benefitting from bis- and tris-carbene stabilization.²⁰⁷ Solvent-dependent ligand rearrangements from bis- to tris(NHC)-stabilized cations are also observed. The electronic influence of multiple carbenes on magnesium halides is demonstrated in the carbene-mediated cationization of magnesium bromide in the absence of halide abstraction reagents, resulting in the remarkable isolation of geometrically unique Mg cations (**3.8a** and **3.8b**) of the type $[(^{\text{Me}}\text{NHC})_3\text{MgBr}][\text{Br}]$ ($^{\text{Me}}\text{NHC} = 1,3,4,5$ -tetramethylimidazol-2-ylidene).

3.2 A Bis(*N*-heterocyclic carbene)-Stabilized Magnesium Dication

The bis-NHC Grignard ($i^{\text{Pr}}\text{NHC}$)₂MgMeBr (**3.1**)¹⁰⁸ was treated with Na[BAr^F₄] (Ar^F = 3,5-bis(trifluoromethyl)phenyl) in chlorobenzene to afford compound **3.2** as a colorless solid in 63% yield (Scheme 3.1). The ¹H NMR spectrum of **3.2** in C₆D₅Br is consistent with two chemically equivalent $i^{\text{Pr}}\text{NHC}$ ligands stabilizing a cationic Mg–Me fragment, where the characteristic carbene and methyl protons all resonate upfield of **3.1** (e.g., δ Mg–CH₃: -1.02 ppm for **3.2** and -0.82 ppm for **3.1**).

Scheme 3.1. Synthesis of a Bis(carbene)-Stabilized Magnesium Dication



The molecular structure of **3.2** was unambiguously determined by single-crystal X-ray diffraction, which revealed a dinuclear complex where the Mg atoms are each stabilized by two *i*PrNHC ligands and dissymmetrically bridged by their methyl substituents (Figure 3.2). The resulting dication is balanced by two non-coordinating BARF₄ anions, indicating that formation of the [Mg(μ -Me)]₂²⁺ core (Mg...Mg: 2.737(4) Å) is preferred over anion or arene solvent interactions. The ^{NHC}C–Mg bond distances (2.209(10) – 2.233(12) Å) are slightly shortened from **3.1** (2.258(3) and 2.261(3) Å) and in the range of reported examples.^{106, 108, 173, 174, 206} Likely due to the dicationic nature of **3.2**, the Mg(μ -Me) interactions (avg. 2.242(11) Å) are shorter than the terminal Mg–Me bond in **3.1** (2.277(5) Å). In contrast to similar homometallic organomagnesium complexes which feature planar dimers,²⁰⁸⁻²¹² the [Mg(μ -Me)]₂²⁺ core in **3.2** exhibits a distorted metallacyclobutane “butterfly” configuration (Mg1–C46–Mg2: 74.3(3)°, C45–Mg1–C46: 102.7(4)°) where both Mg atoms lie slightly above the C46–Mg2–C45–Mg1 plane (torsion angle of 17.2(4)°) and the methyl groups slightly below. This rare distortion has been observed within an octamethyltrimagnesiato dianion.²¹³

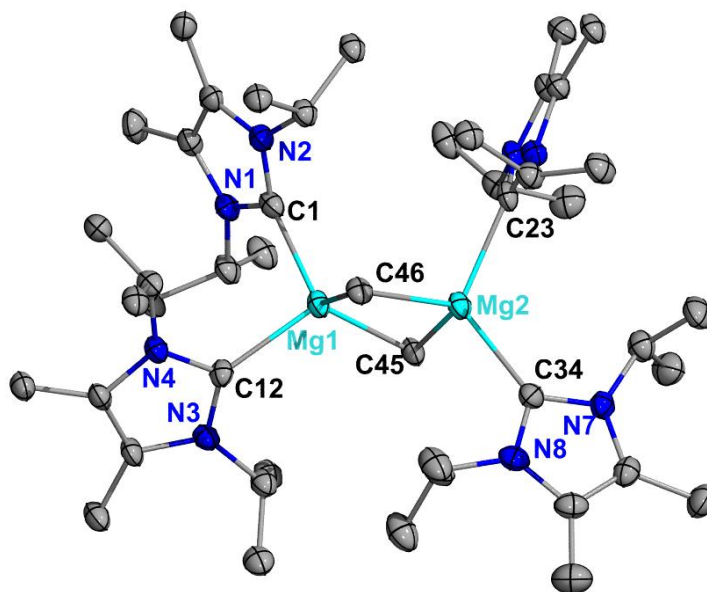
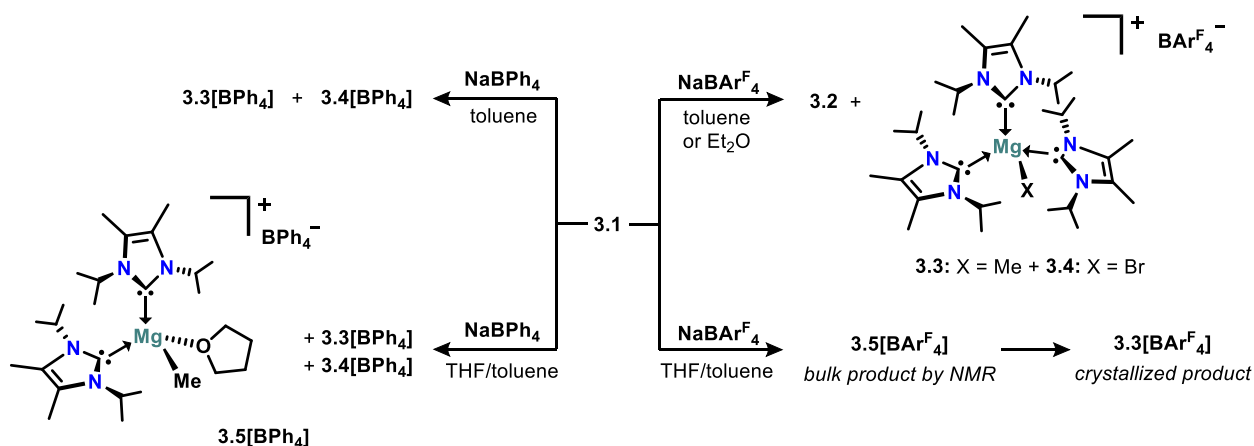


Figure 3.2. Molecular structure of **3.2** (thermal ellipsoids shown at 30% probability; H atoms, BAr^{F_4} anions and one co-crystallized chlorobenzene solvent molecule are omitted for clarity).

3.3 Ligand Rearrangements of Bis- to Tris-NHC Stabilized Cations

The reaction between **3.1** and $\text{Na}[\text{BAr}^{\text{F}_4}]$ in toluene or diethyl ether yielded a mixture of **3.2** and the tris-NHC coordinated species $[(^{\text{iPr}}\text{NHC})_3\text{Mg}(\text{Me})][\text{BAr}^{\text{F}_4}]$ (**3.3** $[\text{BAr}^{\text{F}_4}]$) and $[(^{\text{iPr}}\text{NHC})_3\text{Mg}(\text{Br})][\text{BAr}^{\text{F}_4}]$ (**3.4** $[\text{BAr}^{\text{F}_4}]$) via Schlenk-type ligand rearrangements (Scheme 3.2). In notable contrast, the reaction of **3.1** and $\text{Na}[\text{BPh}_4]$ in toluene afforded exclusively tris-carbene coordinated products **3.3** $[\text{BPh}_4]$ and **3.4** $[\text{BPh}_4]$. These observations suggest that the BAr^{F_4} anions stabilize the formation of **3.2**, possibly due to intermediary $[\text{Mg}]^+\cdots\text{F}(\text{BAr}^{\text{F}_4})$ contacts prior to dimerization to the dication. Similarly, the utilization of halogenated arene solvents may provide further halide-contact stabilization as was previously observed for cationic alkaline earth complexes.¹⁷⁵ Therefore, we expect that the combined stabilizing effects of the BAr^{F_4} anion and chlorobenzene influenced the isolation of **3.2** as a pure product.

Scheme 3.2. Ligand rearrangements of bis- to tris-NHC species: differences in solvent and borate anion stabilization.



We further investigated the influence of THF solvation on the isolation of these cations. The reaction between **3.1** and $\text{Na}[\text{BPh}_4]$ in THF or toluene/THF mixtures yielded a complex mixture

of products including $[(\text{THF})(^i\text{PrNHC})_2\text{Mg}(\text{Me})][\text{BPh}_4]$ (**3.5**[BPh₄]) and the tris-NHC species **3.3**[BPh₄] and **3.4**[BPh₄] as observed by NMR. Recrystallization of this mixture in bromobenzene/hexanes yielded colorless crystals identified by X-ray diffraction as the expected monomeric structure, which also included $[(^i\text{PrNHC})_2(\text{THF})\text{Mg}(\text{Br})][\text{BPh}_4]$ in 4% population (Figure 3.3). Notably, the bulk solid recovered from the reaction between **3.1** and Na[BAr^F₄] in THF was spectroscopically determined to be the single species **3.5**[BAr^F₄]. However, **3.5**[BAr^F₄] rearranges and crystallizes from a concentrated THF/toluene solution as the tris-NHC species **3.3**[BAr^F₄] over two days at room temperature.

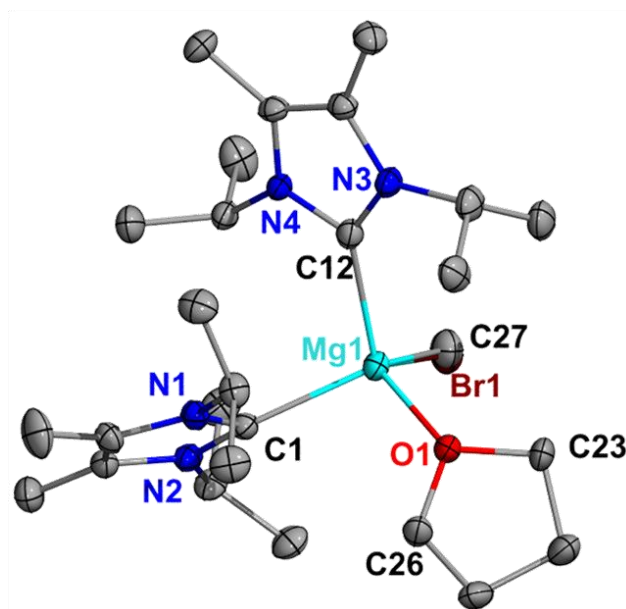


Figure 3.3. X-ray structure of **3.5**[BPh₄] including 4% co-crystallized $[(^i\text{PrNHC})_2(\text{THF})\text{Mg}(\text{Br})][\text{BPh}_4]$ (thermal ellipsoids shown at 50% probability; H atoms and BPh₄ anion are omitted for clarity). Selected bond distances and angles are shown in Table 3.1.

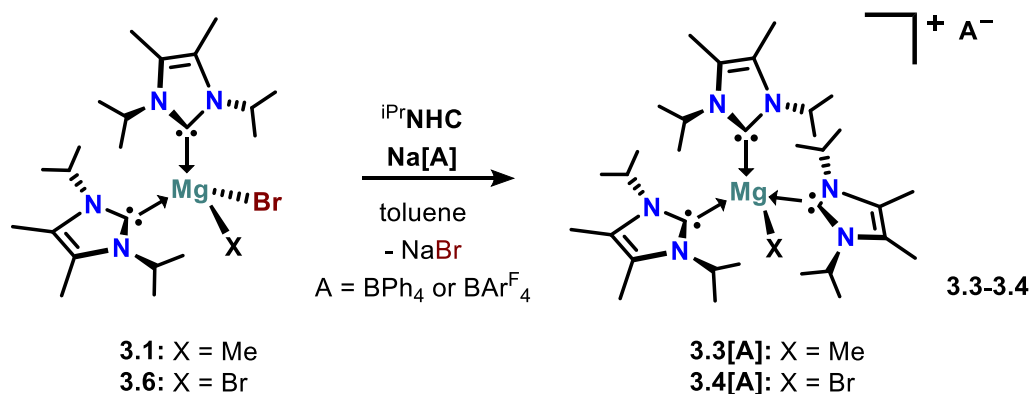
Gas-phase DFT ($\omega\text{B97X-D/BS1}$) suggest a thermodynamic preference for the formation of **3.3** (−55.1 kcal/mol relative to **3.1**) over the bis-NHC complexes **3.2** (−40.3 kcal/mol) and **3.5** (−41.4 kcal/mol, Figure A4.1). Notably, the inclusion of solvation models for toluene resulted in a

preference for **3.5** (−80.0 kcal/mol) over **3.3** (−33.1 kcal/mol), highlighting the observed stabilization of THF-coordinated bis-NHC cations in the solvent. In addition to the dynamic THF-coordination observed, the rearrangements in **3.5** are perhaps unsurprising as coordinating solvents play a significant role in Schlenk-type ligand redistributions.^{214, 215} Therefore we targeted the solvent-free tris(NHC)-stabilized cations as single products using common hydrocarbon solvents.

3.4 Direct Syntheses and Structural analyses of Tris(NHC)-stabilized Mg Cations

Colorless crystalline solids of complexes **3.3–3.4** were isolated in 49 – 80% yields by combining (ⁱPrNHC)₂Mg(X)(Br) (**3.1**: X = Me; **3.6**: X = Br),¹⁰⁸ ⁱPrNHC and Na[BAr^F₄] or Na[BPh₄] in toluene (Scheme 3.3). Evidence of donor-rich metal centers can be found in higher-field resonances of the carbene methine protons (δ 4.72 ppm for **3.3**[BAr^F₄] and δ 4.73 ppm for **3.3**[BPh₄] in C₆D₆) with respect to **3.1** (δ 5.62 ppm). The nearly identical methine resonances in **3.3** are similarly observed for **3.4** (δ 4.90 ppm for both **3.4**[BAr^F₄] and **3.4**[BPh₄] in CD₂Cl₂). This suggests that the nature of the non-coordinating anion does not significantly influence the electronics in these tris-carbene stabilized magnesium cations. The methyl protons in **3.3**[BAr^F₄] (δ -0.90 ppm) and **3**[BPh₄] (δ -0.86 ppm) are significantly upfield of **3.1** (δ -0.45 ppm), suggesting increased nucleophilicity from the neutral Grignard.

Scheme 3.3. Syntheses of tris(NHC)-stabilized Mg cations **3.3–3.4**



Suitable single crystals of **3.3**[BArF₄], **3.3**[BPh₄], **3.4**[BArF₄] and **3.4**[BPh₄] were obtained and analyzed by X-ray diffraction, revealing the expected mononuclear complexes (Figures 3.4, A3.9 and A3.11). Each structure maintains a distorted tetrahedral geometry around the magnesium cation, which is stabilized by three ⁱPrNHC ligands and one non-coordinating borate anion. The ^{NHC}C–Mg distances in **3.3-3.4** (see Table 3.1) are also comparable to **3.2** and the neutral bis-NHC complexes. The similarity in ^{NHC}C–Mg distances for **3.3**[BArF₄] [2.262(5), 2.276(6), 2.281(6) Å] reflects in the geometry around the magnesium atom, where the bond angles (103.6 – 112.2°) are only slightly deviated from the ideal 109.5° of a perfect tetrahedron. A detailed comparison of structural parameters for **3.2-3.5** are summarized in Table 1.

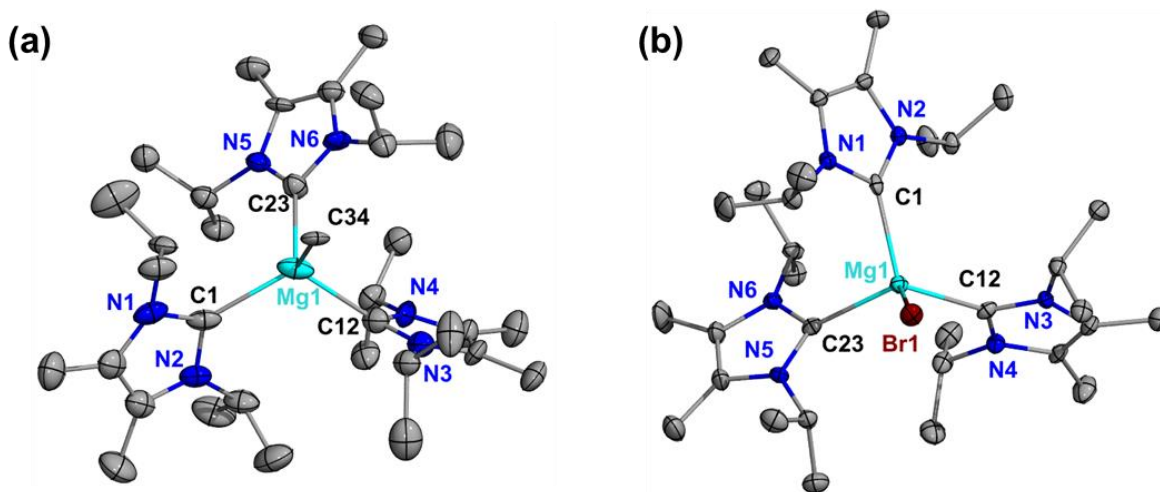


Figure 3.4. X-ray structures of BPh₄ salts for **3.3** (a) and **3.4** (b) (thermal ellipsoids are shown at 50% probability; H atoms and anions are hidden for clarity; only the major occupied positions are shown for the disordered C12 and C23 imidazole frameworks and *N*-isopropyl substituents in (a)). **3**[BAr^F₄] (Figure A3.9) and **4**[BAr^F₄] (Figure A3.11) are shown in Appendix III.

Compound **3.3** may also be prepared using THF, thus indicating that tris-NHC stabilization affords the electronic benefit of persistent carbene coordination which is competitive against donor solvents. Conversely, compound **3.4** is substantially more sensitive than **3.3** to adventitious moisture in THF despite considerable effort at rigorously drying the reaction solvents. Therefore, crystallization of hydrolysis products of the type [(ⁱPrNHC)H][BR₄]²¹⁶ (R = Ph or Ar^F) from THF solutions of **3.4** was consistently observed. Additionally, **3.3**[BPh₄] displays significantly improved solubility in arene solvents compared to **3.2**, thus rendering it a more practical alternative for synthetic applications where donor solvents should be avoided. Notably, compounds **3.2–3.4** are stable as solids in inert atmosphere for more than two months at room temperature, and up to two weeks in anhydrous arene solvents at -37 °C.

Table 3.1. Selected Bond Distances^a and Angles^b for Compounds **3.2-3.5** and **3.7-3.8**

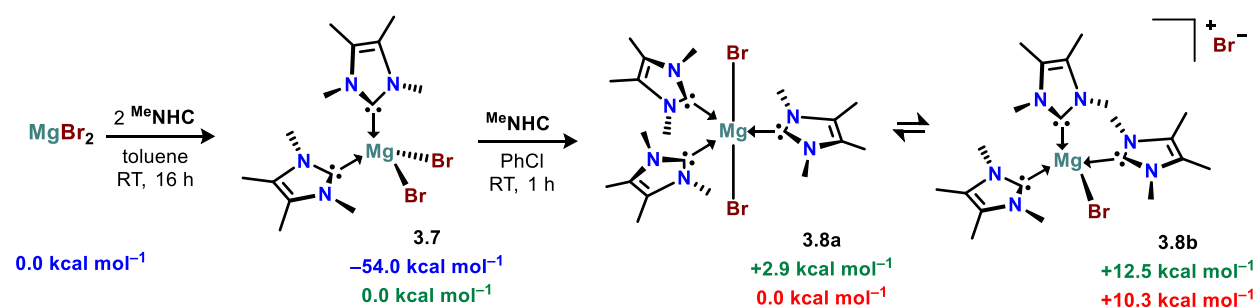
	3.2	3.3[BAr^F₄]	3.3[BPh₄]	3.4[BAr^F₄]	3.4[BPh₄]	3.5[BPh₄]	3.7	3.8a	3.8b
^{NHC} C–Mg	2.233(12) 2.209(10) 2.228(10) 2.212(11)	2.262(5) 2.276(6) 2.281(6)	2.277(2) 2.163(7) 2.271(2)	2.2360(18) 2.2554(18) 2.2434(18)	2.209(3) 2.210(3) 2.251(3)	2.260(2) 2.246(3)	2.234(13) 2.217(13)	2.214(5)	2.215(5)
Mg–X	2.223(11) 2.246(10) 2.215(10) 2.285(11)	2.154(5)	2.2557(19)	2.4934(6)	2.5195(9)	2.178(14)	2.487(3) 2.510(3)	2.883(3) 2.694(3)	2.513(3)
C1–N1	1.363(13)	1.364(7)	1.369(3)	1.360(2)	1.394(3)	1.365(3)	1.333(13)	1.361(7)	1.348(7) ^c
C1–N2	1.356(13)	1.376(6)	1.391(3)	1.360(2)	1.364(3)	1.360(3)	1.339(13)	1.361(7)	1.359(7) ^d
C1–Mg1– C12	100.1(4)	108.85(19)	114.5(3)	113.16(6)	115.3(11)	99.32(9)	108.9(4) ^e	119.77(3) <i>e</i>	109.70(15) ^f
C1–Mg1– C23		111.4(2)	108.76(7)	107.38(6)	101.59(10)	98.60(8) ^g			
C1–Mg1– X	115.7(4) 115.5(4)	109.8(2)	112.87(7)	107.99(5)	107.33(8)	107.1(4)	106.3(3) 108.0(3)	87.25(16) 92.75(16)	109.24(15) ^h
X ¹ –Mg–X ²	102.7(4) 101.7(4)						119.41(11)	180.00(6)	
N1–C1–N2	104.5(9)	103.2(4)	102.54(17)	103.94(14)	104.1(2)	103.51(19)	104.9(10)	102.6(4)	104.0(4)

^aAngstroms. ^bDegrees. ^cC8–N3, ^dC8–N4, ^fC8–Mg2–C8' and ^hC8–Mg2–Br3 were used for **3.8b**. ^eC8 (7) and C1' (**3.8a**) were used instead of C12. ^gO1 was used instead of C23 for **3.5[BPh₄]**.

3.5 NHC-mediated Heterolysis of MgBr₂

To further probe the electronic influence of multiple NHCs on magnesium complexes, we investigated the ionization of magnesium bromide in the absence of halide abstraction reagents. In order to maximize donor interactions with the metal center, the sterically unencumbered 1,3,4,5-tetramethylimidazol-2-ylidene (^{Me}NHC) ligand²¹⁷ was chosen for this investigation. Similar to **3.6**,¹⁰⁸ the neutral bis-NHC species (^{Me}NHC)₂MgBr₂ (**3.7**) was obtained as a colorless solid in 84% yield from the addition of two equivalents of ^{Me}NHC to MgBr₂ in toluene (Scheme 3.4). The X-ray structure of **3.7** (Figure 3.5 and Table 3.1) reveals metrical parameters comparable to **3.6**.

Scheme 3.2. NHC-mediated heterolysis of MgBr₂: syntheses and calculated reaction energetics^a



^aSMD- ω B97X-D// ω B97X-D/BS1 reaction energetics (ΔG) using implicit solvation models for toluene (blue values), chlorobenzene (green values), and bromobenzene (red values) solvents.

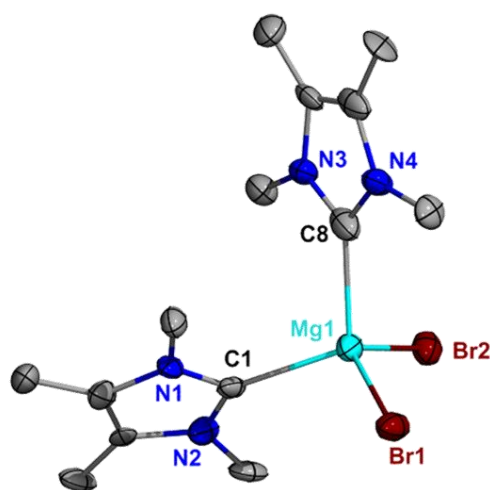


Figure 3.5. X-ray structure of **3.7** (thermal ellipsoids shown at 50% probability; H atoms are omitted for clarity).

Starting from a suspension of **3.7** in chlorobenzene, the addition of one or two equivalents of $\text{Me}^{\text{e}}\text{NHC}$ immediately yielded a colorless solution (Scheme 3.4). The ^1H NMR of the isolated product in $\text{C}_6\text{D}_5\text{Br}$ revealed a single NHC coordination environment (two singlets δ 3.55 ppm and 1.60 ppm) with the $\alpha\text{-CH}_3$ resonance (δ 3.55 ppm) significantly broadened. This suggests a possible dynamic equilibrium in solution, although the existence of more than one unique species in solution could not be resolved using variable temperature (VT) NMR experiments ($\text{C}_6\text{D}_5\text{Br}$, 373 – 248 K). Access to lower temperatures was limited by the freezing point of $\text{C}_6\text{D}_5\text{Br}$ (-30.7 °C) and the overall poor solubility of this compound in common organic solvents. However, single-crystal X-ray diffraction studies revealed that two distinct molecules, **3.8a** and **3.8b**, are co-crystallized in the solid-state in a 1:1 ratio (Figure 3.6).

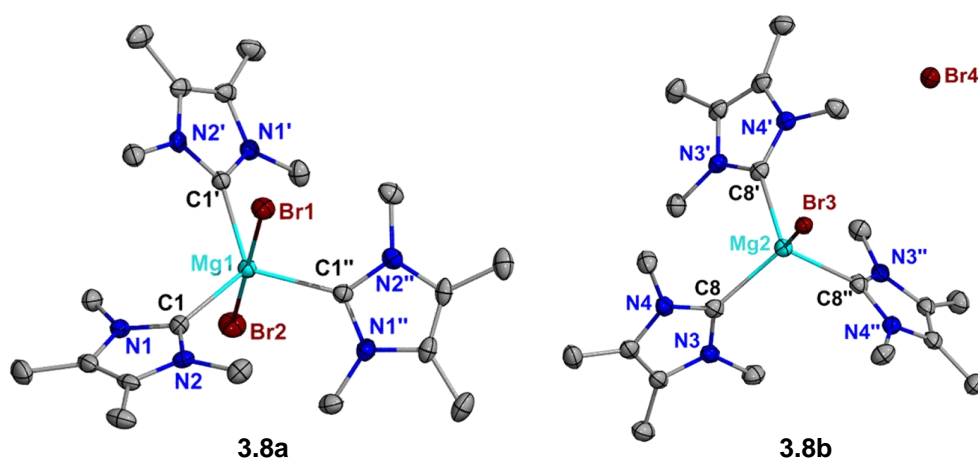


Figure 3.6. X-ray structure of **3.8a** and **3.8b** (thermal ellipsoids shown at 50% probability; H atoms omitted for clarity).

Complex **3.8a** is an unusual trigonal bipyramidal magnesium complex stabilized by three $\text{Me}^{\text{e}}\text{NHC}$ ligands in the equatorial plane and two Br ligands in the axial positions. The Mg–Br distances in **3.8a** (2.694(3) and 2.883(3) Å) are significantly elongated by 0.18 – 0.40 Å from the neutral bis-NHC complex, **3.7** (2.487(3) and 2.510(3) Å), as well as the expected additive

covalent radii between Mg and Br (2.53 Å).¹⁸⁴ Thus, **3.8a** may be considered as either a neutral L_3MgBr_2 complex or a cationic magnesium complex stabilized by a weakly coordinating bromide anion. Conversely, **3.8b** can only be described as an ionic $[L_3MgBr][Br]$ complex. The crystal structure of **3.8b** reveals a tetracoordinate magnesium cation stabilized by three carbenes and a bromide ligand, with the second bromide acting as a non-coordinating anion. The closest contact between Mg2 and the non-coordinating bromide, Br4, (6.374(2) Å) is nearly double the expected van der Waals separation between Mg and Br (3.56 Å).²¹⁸ The Mg2–Br3 bond length in **3.8b** (2.513(3) Å) is significantly shorter than those of **3.8a**, but comparable to **3.4** and **3.7** (see Table 3.1). In both **3.8a** and **3.8b**, a crystallographic three-fold rotation axis passes through the Mg–Br bond, and only one carbene is found in the asymmetric unit of each species. Thus, the $^{NHC}C-Mg$ bond distances for **3.8a** (2.214(5) Å) and **3.8b** (2.215(5) Å) are similarly identical. This results in a D_{3h} symmetry for **3.8a** where Br1–Mg–Br2 is exactly 180° and the $^{NHC}C-Mg-^{NHC}C$ angles are each 120°, as well as a C_{3v} symmetry for the cationic fragment in **3.8b**, which maintains a nearly perfect tetrahedral geometry (109.24 – 109.70(15)°) around the magnesium center.

Complexes **3.1** and **3.6** were found to be unreactive with ^{iPr}NHC under similar conditions as the reaction of **3.7** with ^{Me}NHC likely due to steric hindrance from the isopropyl groups. This indicates that the formation of **3.3-3.4** proceeded via initial halide abstraction followed by carbene coordination. SMD(chlorobenzene)- ω B97X-D// ω B97X-D/BS1 theoretical calculations suggest a small energy penalty of +2.9 kcal mol⁻¹ for the formation of **3.8a** by complexation of an additional NHC to **3.7**. Further displacement of a weakly coordinating bromide ligand to form **3.8b** is calculated to be endergonic by 9.6 kcal mol⁻¹, thus indicating a slight thermodynamic preference for **3.8a** in the suggested equilibrium. Nevertheless, the existence of **3.8a** and **3.8b** in the solid state indicates that multiple NHCs can easily ionize neutral magnesium complexes containing halides. The unique geometry of **3.8a**, owing to the

use of sterically unencumbered carbenes, indicates that the magnesium center may be able to accommodate additional carbenes to access further ionized or polarized species. Ionization of the remaining covalent Mg–Br interactions using excess carbenes, extended reaction times, or halide abstraction reagents have resulted in species spectroscopically dissimilar from **3.7** and **3.8**, but their poor solubility hindered successful crystallization attempts. Likewise, we explored an alternate route to **3.8** by the direct addition of 3 equivalents of ^{Me}NHC to a suspension of MgBr₂ in toluene. The resulting complex was spectroscopically comparable to **3.8** (δ 3.57 ppm (broad) and 1.60 ppm), thereby indicating that the direct heterolysis of polymeric MgBr₂ could be achieved without initial isolation of the neutral bis(NHC)-stabilized species.

3.6 Theoretical Analysis

In order to gain more insight into the structure and bonding of the bis- and tris-NHC magnesium systems, DFT geometry optimizations were performed at the ω B97X-D/BS1 level of theory. Overall, the Wiberg bond index (WBI) values computed for the ^{NHC}C–Mg bonds in the cationic complexes (Figure 3.7) are comparable to the neutral bis-NHC complexes,¹⁰⁸ with only slight increase in values most pronounced for **3.2⁺** (0.29 – 0.33) and **3.8b⁺** (0.32).

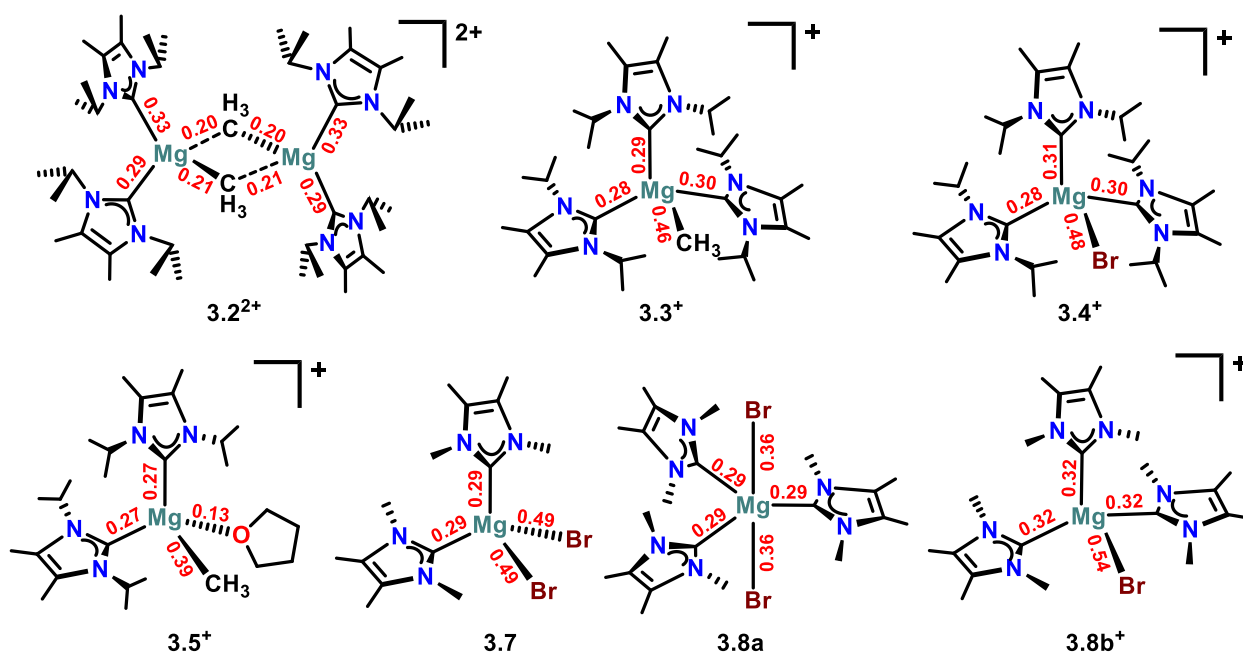


Figure 3.7. Comparison of NAO-Wiberg Bond Index (WBI) values for each reported compound.

Relative to their neutral precursors, higher Mg–X WBI values are generally observed for the cationic complexes. The Mg–Me bond in **3.3**⁺ (WBI 0.46) displays a greater degree of covalency than those in **3.1** (0.37) and **3.5**⁺ (0.39). The lower WBIs for the Mg–(μ -Me) bonds in **3.2**²⁺ (0.21, 0.20) relative to the terminal Mg–Me bonds in **3.1**, **3.3**⁺ and **3.5**⁺ suggest a significantly greater degree of charge separation between the Mg cations and bridging methyl anions. This observation is further supported by an inspection of the natural charges (Table A4.1) and Pipek-Mezey localized Molecular Orbitals for the Mg–(μ -Me) interactions in **3.2**⁺ (see Appendix IV). Expectedly, the WBI value for Mg–Br in (^{Me}NHC)₂MgBr₂ (**3.7**) is the same as previously reported for (^{iPr}NHC)₂MgBr₂.¹⁰⁸ However, the value for the Mg–Br bond in the ^{iPr}NHC-stabilized cation **3.4**⁺ (0.48) is lower than that of the ^{Me}NHC-stabilized cation **3.8b**⁺ (0.54) despite only slight differences in their ^{NHC}C–Mg WBI values (**3.4**⁺: 0.28, 0.30, 0.31 and **3.8b**⁺: 0.32). The larger difference in WBI values for the Mg–Br bonds in **3.8a** (0.36) and **3.8b**⁺ (0.54), which are on either side of **3.7** (0.49), corroborates the weakly coordinating nature of the bromide anions in **3.8a**.

3.7 Conclusion and Outlook

We have isolated the first examples of organomagnesium cations benefitting from untethered bis- and tris-carbene stabilization. The bis(NHC)-stabilized complexes exhibited solvent-dependent Schlenk-type ligand rearrangements to hitherto unknown organomagnesium complexes benefitting from unsupported tris-carbene stabilization. The facile and high yield syntheses of **3.3–3.4** demonstrate that tris-carbene-supported ionization using easily accessible halide abstraction reagents can be extended to other magnesium-halide systems. We further explored the electronic influence of tris-carbene stabilization in the NHC-mediated heterolysis of polymeric magnesium bromide. These types of solvent-free, base-saturated species are expected to have beneficial applications in molecular alkaline earth reduction chemistry^{219, 220} and small molecule activation.^{3, 89, 90, 221} Thus, investigations into the reactivity of these cations with hydride sources, small molecule substrates and reducing agents are reasonable extensions of this work.

Chapter Four: A Thermally Stable Magnesium Phosphaethynolate Grignard Complex

Contains work that was originally published in:

Obi, A. D.; Machost, H. R.; Dickie, D. A.; Gilliard, R. J., A Thermally Stable Magnesium
Phosphaethynolate Grignard Complex. *Inorg. Chem.* **2021**, *60*, 12481-12488

4.1 Overview of *s*-Block Phosphaethynolate Chemistry

During the last decade, the 2-phosphaethynolate (OCP) anion has developed into an important building block for the synthesis of phosphorus-containing molecules.^{222, 223} This nucleophile is isoelectronic to the cyanate ion, and can access two major resonance forms (i.e., $\text{O}^-\text{C}\equiv\text{P} \leftrightarrow \text{O}=\text{C}=\text{P}^-$) for ambidentate reactivity.²²⁴ Although the first structurally authenticated phosphaethynolate complex dates back nearly 30 years with the isolation of $[\text{Li}(\text{DME})_2][\text{OCP}]$,²²⁵ its thermal instability hampered extensive investigation. However, the emergence of stable $[\text{Na}(\text{ether})_x][\text{OCP}]$ complexes (ether = DME or dioxane) in 2011^{226, 227} enabled rapid development of the chemistry of the OCP anion.^{222, 223} Indeed, stable element–OCP/PCO complexes across the periodic table may be obtained by a simple salt metathesis reaction between $\text{Na}(\text{OCP})$ and ligand-stabilized element–halides.

In contrast to the stability and versatility of sodium and potassium phosphaethynolate complexes,²²⁶⁻²²⁹ their group 2 counterparts (Mg, Ca, Sr, Ba) are unstable in solution, thus difficult to study.^{230, 231} One rationale for their instability is the weak nature of the phosphaalkyne ($\text{C}\equiv\text{P}$) bond.^{229, 232} Since *s*-block elements are highly oxophilic, they favor the oxyphosphaalkyne isomer (i.e., $\text{O}^-\text{C}\equiv\text{P}$), whereby the OCP anion is prone to decomposition through oxidation and self-oligomerization.^{222, 229} The highly electropositive character of sodium and potassium cations allows for pronounced charge separation in their $\text{M}(\text{OCP})$ salts, which results in increased columbic repulsion between the OCP anions and discourages oligomerization.²²² The “free” OCP anion in these complexes is stabilized by delocalization of electron density from O to $\text{C}\equiv\text{P} \pi^*$, thereby reducing the bond order and consequent reactivity of the C–P bond and concomitantly increasing the bond order and thermodynamic stability of the C–O bond. Conversely, phosphaethynolate salts of the less electropositive group 2 elements are thus far prone to rapid decomposition in the same coordination environments as the alkali metal salts. Nevertheless, group 2 phosphaethynolate complexes are desirable reagents due to

their potential for Lewis acid reactivity profiles,² in contrast to the archetypal reactivity of group 1 organometallic reagents as strong nucleophiles.

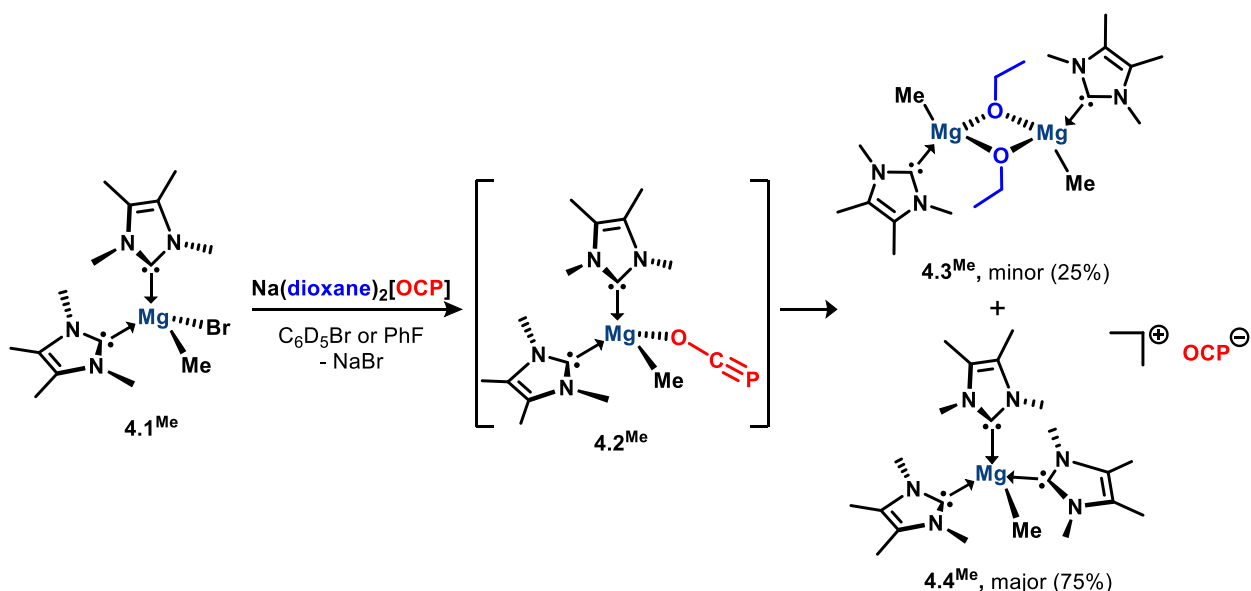
Being mindful of the critical importance of coordination environments in *s*-block phosphoethynolate chemistry, we hypothesized that the electronic influence of *N*-heterocyclic carbenes (NHCs) may enable the isolation of thermally stable alkaline earth phosphoethynolates. NHCs have become indispensable in *p*- and *d*-block organometallic chemistry as tunable donor-acceptor ligands.^{97, 98, 200, 233} However, they are relatively underexplored in *s*-block chemistry, partly because hard-soft acid-base effects can result in the destabilization of reactive species due to dynamic NHC coordination.⁹⁷ We recently discovered that such destabilizing effects can be mitigated by bis- or tris-NHC coordination in neutral and cationic magnesium complexes,^{107-109, 173} and were encouraged to apply similar principles towards magnesium phosphoethynolates. Herein, we report the isolation, characterization (NMR, IR, X-ray), and reactivity of structurally diverse NHC-stabilized magnesium phosphoethynolate complexes, including a novel phosphoethynolate-containing Grignard reagent. Unlike the majority of known *s*-block element phosphoethynolates, these complexes are remarkably soluble and thermally stable in aromatic hydrocarbon solvents. The influence of subtle changes in carbene stereoelectronics on their stability and reactivity is also evaluated.

4.2 Dioxane Activation via a Phosphoethynolate-containing Grignard Complex

As a starting point for this synthetic investigation, the carbene-stabilized Grignard reagent (^{Me}NHC)₂MgMeBr (**4.1^{Me}**, ^{Me}NHC = 1,3,4,5-tetramethylimidazol-2-ylidene) was prepared by the reaction of MeMgBr (3 M in Et₂O) and two equivalents of ^{Me}NHC in THF, and isolated as a colorless solid in 89% yield. Plate-like crystals of **4.1^{Me}** were analyzed by single-crystal X-ray diffraction (SC-XRD), which revealed a mononuclear complex (Figure A3.15) structurally analogous to our previously reported (^{iPr}NHC)₂MgMeBr (**4.1^{iPr}**; ^{iPr}NHC = 1,3-diisopropyl-4,5-dimethylimidazol-2-ylidene).¹⁰⁸ Compound **4.1^{Me}** is stable indefinitely under inert conditions

in the solid-state and up to 3 months in anhydrous aromatic or ethereal solvents, leading us to hypothesize that the electronic influence of two sterically unhindered NHCs may similarly stabilize a phosphaehtynolate-containing Grignard complex [e.g., (^{Me}NHC)₂MgMe(OCP), **4.2^{Me}**]. An NMR-monitored reaction between **4.1^{Me}** and [Na(dioxane)₂][OCP]²²⁶ in C₆D₅Br revealed an immediate conversion to new products, indicated by two new Mg–CH₃ singlets (3:1 ratio) in the ¹H NMR spectrum, and one singlet at -373.5 ppm in the ³¹P{¹H} NMR spectrum, downfield of [Na(dioxane)_x][OCP] (-392.0 ppm).²²⁶ The smaller Mg–CH₃ singlet is accompanied by downfield triplet and quartet (2:3) resonances consistent with an ethyl group. Indeed, X-ray diffraction studies on single-crystals obtained from preparative-scale reactions (Scheme 4.1) indicate that the observed signals are due to a methylmagnesium ethoxide [(^{Me}NHC)MgMe(μ-OEt)]₂ (**4.3^{Me}**, Figure 1a) and a magnesium phosphaehtynolate charge separated ion-pair [(^{Me}NHC)₃MgMe][OCP] (**4.4^{Me}**, Figure 4.1b).

Scheme 4.1. Dioxane activation in the attempted synthesis of a phosphaehtynolate-containing Grignard complex



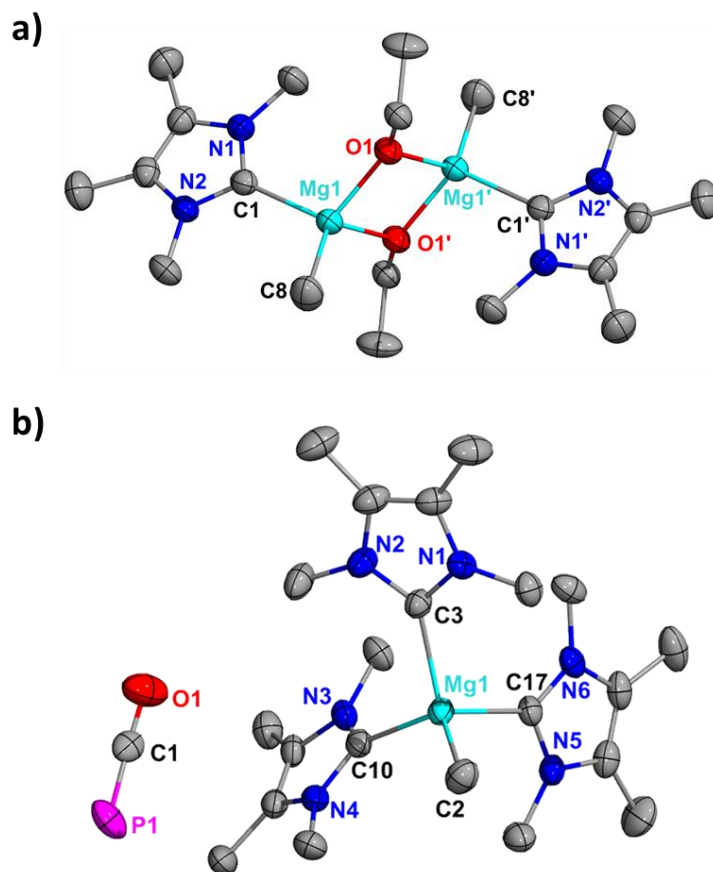


Figure 4.1. Molecular structures of **4.3^{Me}** (a) and **4.4^{Me}** (b). Thermal ellipsoids set at 50% probability. H atoms are omitted for clarity, and only major occupied positions for the disordered OCP anion in **4.4^{Me}** are shown. Selected bond distances (Å) and angles (deg): **4.3^{Me}**: Mg1–O1, 1.9659(13); Mg1–O1', 1.9868(13); Mg1–C1, 2.2649(18); Mg1–C8, 2.145(2), Mg1–Mg1', 2.9722(11); C1–N1, 1.354(2); O1–Mg1–O1', 82.48(5); O1–Mg1–C1, 109.72(6); O1–Mg1–C8, 119.67(8). **4.4^{Me}**: C1–P1, 1.574(14); O1–C1, 1.208(10); Mg1–C2, 2.156(4); Mg1–C3, 2.226(3); Mg1–C10, 2.230(4); Mg1–C17, 2.259(4); O1–C1–P1, 177.1(9); C2–Mg1–C17, 111.65(15); C2–Mg1–C10, 118.81(16).

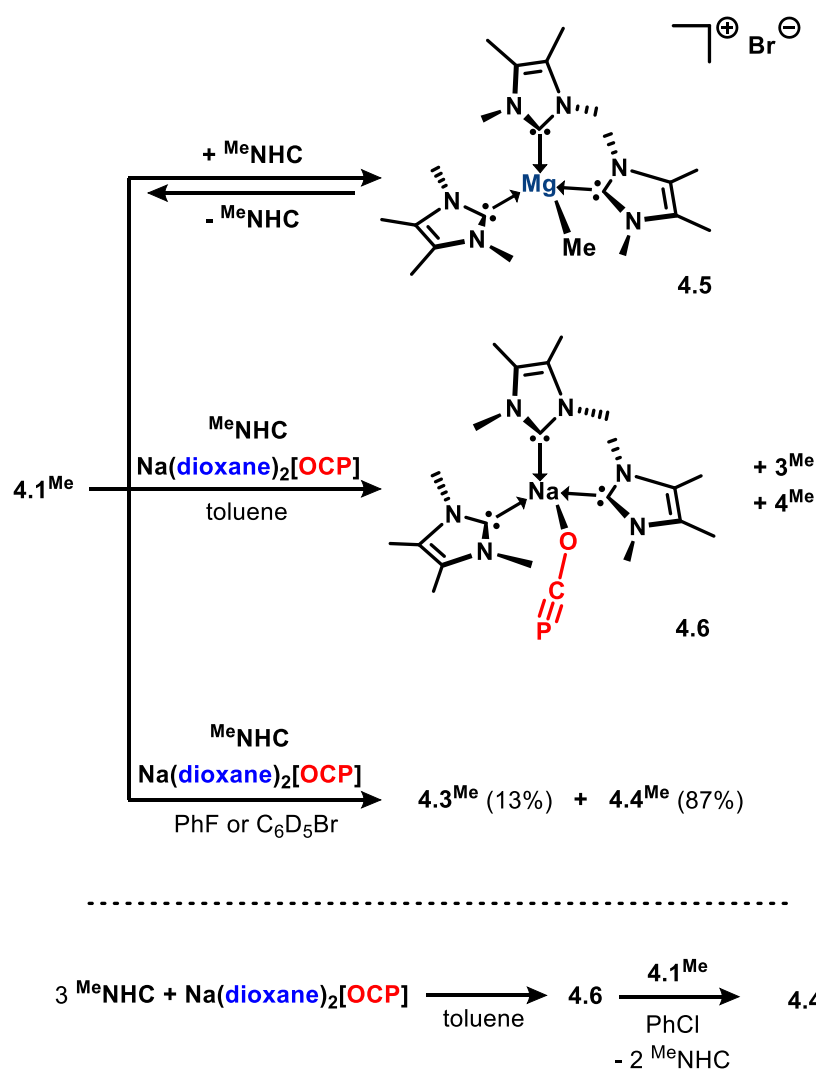
The metathetical exchange of a bromide ligand in **4.1^{Me}** to the softer OCP anion results in a more electrophilic Mg²⁺ cation in the transient phosphaehtynolate-containing Grignard reagent (**4.2^{Me}**). As we have previously observed in similar (NHC)₂MgRX complexes,¹⁰⁹ the increased electrophilicity results in a spontaneous NHC rearrangement to **4.4^{Me}**, enabling the formation

of an unobserved (^{Me}NHC)(dioxane)MgMe(OCP) intermediate, which decomposes to **4.3^{Me}** via dioxane activation. However, the ether activation mechanism is poorly understood.^{234, 235} The direct action of **4.2^{Me}** on dioxane is similarly likely, and the significantly higher yield of **4.4^{Me}** from this reaction (75% NMR conversion compared to 25% of **4.3^{Me}**) suggests that NHC rearrangement outcompetes dioxane activation. Indeed, **4.4^{Me}** is unreactive to ether cleavage, and no further conversion of dioxane to ethoxide was observed after the initial formation of **4.3^{Me}** and **4.4^{Me}** in the NMR experiment. Furthermore, the reaction of **4.1^{Me}** and [Na(dioxane)₂][OCP] in toluene (6 h, RT) afforded **4.3^{Me}** in 57% isolated yield, in contrast to a 25% NMR yield from the same reaction in C₆D₅Br. Hence, the influence of weakly coordinating halogenated solvents on the intermediary Lewis acidic species significantly attenuates their electrophilicity^{175, 236} and consequent reactivity.

In the direct synthesis of compound **4.4^{Me}**, equimolar amounts of **4.1^{Me}**, ^{Me}NHC and [Na(dioxane)₂][OCP] were sequentially combined in C₆D₅Br or fluorobenzene to yield the desired product (Scheme 4.2), albeit with minor amounts of **4.3^{Me}** (1:7 ratio of **4.3^{Me}**: **4.4^{Me}** in C₆D₅Br, Figure A2.46). After workup, **4.4^{Me}** was obtained as an off-white solid in 39% yield. NMR studies suggest that a dynamic equilibrium between multiple MeMg(OCP) species is present in solution. At room temperature, the ¹H NMR spectrum revealed two overlapping singlets in the Mg–CH₃ region, and one set of ^{Me}NHC peaks with the C(CH₃) singlet slightly broadened. In the ³¹P{¹H} NMR spectrum, the OCP singlet (δ -382.0 ppm) was also broadened, and shifted upfield (with further broadening) at lower temperatures but did not resolve into unique resonances (VT-NMR, 243 – 333 K, C₆D₅Br). The Mg–CH₃ singlets coalesced at 60 °C with equivalent intensities for the ^{Me}NHC singlets. At the same temperature, a previously unresolved C≡P doublet in the ¹³C{¹H} NMR spectrum was observed at 166.8 ppm (¹J_{CP} = 48.1 Hz), and the corresponding ³¹P{¹H} resonance (δ -378.3 ppm) is slightly shifted downfield. Notably, the observation of a ¹J(¹³C–³¹P) coupling information is without precedent

for group 2 phosphaaethynolate complexes due to rapid solution-state decomposition of previously reported complexes.^{230, 231} However, this coupling constant is smaller than reported values for “interaction free” OCP anions (range 62.0 – 63.2 Hz),^{228, 237, 238} and in the range of contacted OCP moieties in the s-block.^{225, 226} In the solid-state IR spectrum, two overlapping bands (vs) at 1800 cm⁻¹ and 1770 cm⁻¹ were attributed to the OCP asymmetric stretch, and are in the range of uncoordinated OCP anions.^{238, 239} Thus, **4.4**^{Me} is best described as a charge-separated ion-pair in the solid-state, although bound [Mg]–OCP forms may exist in solution.

Scheme 4.2. Dynamic carbene coordination and solvent effects in the direct synthesis of **4.4**^{Me}



The observed ether cleavage implicates **4.2**^{Me} as an intermediary species in the direct synthesis of **4.4**^{Me}, and motivated an investigation into the reaction of MeNHC and **4.1**^{Me} prior

to the formation of phosphaehtynolate complexes. The reaction of **4.1**^{Me} and ^{Me}NHC yielded a new product presumed to be [(^{Me}NHC)₃MgMe][Br] (**4.5**) based on a 3:1 ¹H NMR integral ratio for the characteristic ^{Me}NHC and Mg–CH₃ peaks (Scheme 4.2 and Figure A2.53). Attempts to obtain single crystals of **4.5** for structural elucidation by SC-XRD yielded **4.1**^{Me} instead, and VT-NMR studies on **4.5** (Figure A2.54) suggest a dynamic process between multiple Mg–CH₃-containing species. Theoretical studies suggest that while NHC complexation is facile, cationization is endergonic and favors neutral complexes in the equilibrium.¹⁰⁹ Having realized that the tris(NHC)-stabilized species **4.4**^{Me} and **4.5** are prone to dynamic ligand coordination in solution, we investigated solvent effects. The reaction of **4.1**^{Me}, ^{Me}NHC and [Na(dioxane)₂][OCP] in toluene yielded a complex mixture of products including **4.3**^{Me}, **4.4**^{Me} and (^{Me}NHC)₃Na(OCP) (**4.6**) (Figure 4.2). Clearly, the absence of weakly coordinating solvents resulted in pronounced ligand scrambling and loss of selectivity for the desired product. Nevertheless, the serendipitous isolation of **4.6** afforded a rare ether-free, hydrocarbon-soluble alkali metal phosphaehtynolate complex.

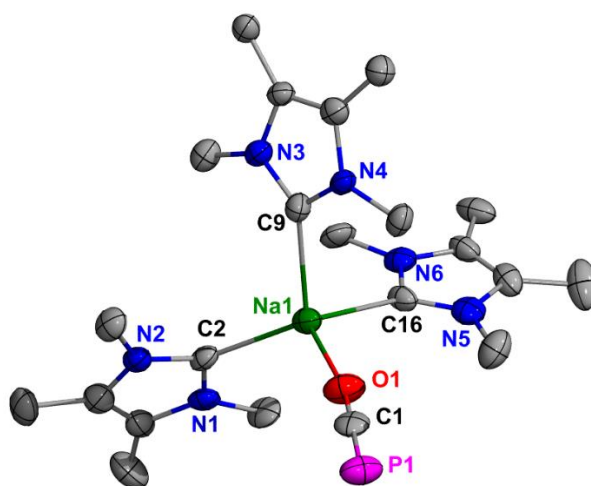


Figure 4.2. Molecular structure of **4.6** (thermal ellipsoids set at 50% probability; H atoms and co-crystallized toluene solvent are omitted for clarity). Only one of two crystallographically independent but chemically equivalent molecules in the asymmetric unit is represented. Selected bond distances (Å) and angles (deg): Na1–O1, 2.247(5); O1–C1, 1.215(5); C1–P1,

1.578(7); Na1–C2, 2.505(7); Na1–C9, 2.476(7); Na1–C16, 2.513(6); Na1–O1–C1, 167.2(5); O1–C1–P1, 179.2(6).

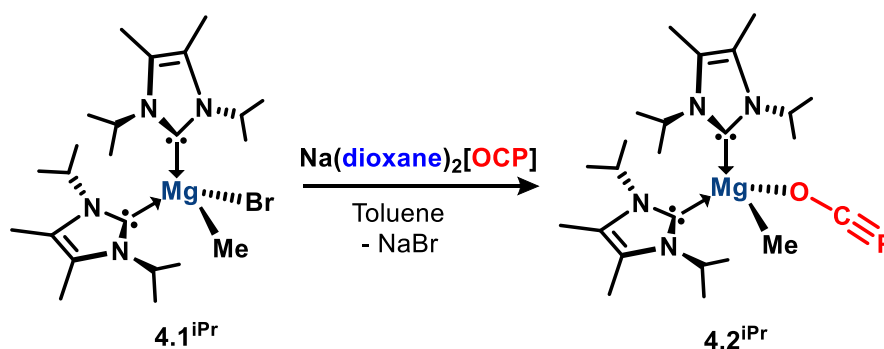
Compound **4.6** was directly prepared from the addition of three equivalents of ^{Me}NHC to [Na(dioxane)₂][OCP] in toluene, and isolated as a light yellow solid in 66% yield (Scheme 4.2, bottom). The OCP singlet resonance in the ³¹P{¹H} NMR spectrum (δ -388.4 ppm) is downfield of [Na(dioxane)_{2.5}][OCP] (δ -392.0 ppm).²²⁶ Single-crystal X-ray diffraction studies on **4.6** reveals a mononuclear molecule, whereby the terminal M–OCP bend angle (Na1–O1–C1: 167.2(5)°) is considerably wider than those of [(THF)Na(dibenzo-12-crown-6)][OCP] (138.1(2)°),²³⁰ but is comparable to [Li(DME)₂][OCP] (170.7°).²²⁵ The O–C≡P bond lengths in **4.6** (C–O, 1.215(8) Å; C≡P, 1.578(7) Å) are comparable to those of structurally authenticated Na(OCP) complexes,^{226, 230} but the Na–O bond distance (2.247(5) Å) is the shortest reported value to date, although only slightly shorter than [(THF)Na(dibenzo-12-crown-6)][OCP] (2.290(2) Å). Highlighting the practicality of **4.6** for ether-free synthesis, the reaction of **4.1**^{Me} and **4.6** in chlorobenzene cleanly affords **4.4**^{Me} in 58% isolated yield.

4.3 Isolation of a Stable Magnesium Phosphaethynolate Grignard Complex

On the basis of these observations, we turned our attention to the slightly more sterically encumbered 1,3-diisopropyl-4,5-dimethylimidazol-2-ylidene (^{iPr}NHC) to stabilize the desired Grignard complex. The reaction of (^{iPr}NHC)₂MgMeBr (**4.1**^{iPr})¹⁰⁸ and [Na(dioxane)₂][OCP] was monitored in C₆D₆, and the immediate formation of (^{iPr}NHC)₂MgMe(OCP) (**4.2**^{iPr}) followed by its slow conversion to [(^{iPr}NHC)MgMe(μ-OEt)]₂ (**4.3**^{iPr})¹⁷³ was observed. A preparative scale reaction in toluene affords **4.2**^{iPr} as a colorless crystalline solid in 70% yield (Scheme 4.3). In the ³¹P{¹H} NMR spectrum, the OCP singlet resonates at -366.8 ppm, which is comparable to (THF)₄Mg(OCP)₂ (δ -367.9 ppm).²³⁰ A doublet in the ¹³C{¹H} NMR spectrum (δ 162.4 ppm) is attributed to the OCP resonance, and the remarkably small ¹J(¹³C–³¹P) coupling constant (25.4 Hz) is outside the range for s-block OCP complexes (41.5 – 62 Hz),

and comparable to (salen)(THF)Al(OCP) (24.5 Hz).²⁴⁰ Notably, smaller coupling constants are indicative of more phosphalkyne (C≡P) than phosphaketene (C=P) bonding in solution, due to a greater contribution of the P 3s orbital to the C–P bond in the latter.²²² The solid-state IR spectrum of **4.2^{iPr}** provides further evidence for a phosphoethynolate anion with a very strong band at 1740 cm⁻¹ for the OCP asymmetric stretch, which is comparable to (THF)₄Mg(OCP)₂ (1759 cm⁻¹).²³⁰ In the ¹H NMR spectrum, the Mg–CH₃ resonance of **4.2^{iPr}** (δ -0.67 ppm) is upfield of **4.1^{iPr}** (δ -0.45 ppm), which suggests a more nucleophilic methyl group since the softer OCP anion results in increased cationic character for the Mg²⁺ center.¹⁰⁹

Scheme 4.3. Synthesis of a stable magnesium phosphoethynolate Grignard complex



The molecular structure of **4.2^{iPr}** was unambiguously determined by X-ray diffraction on a single-crystal obtained from a saturated toluene/hexanes (3:1) mixture at room temperature (Figure 4.3). The magnesium atom is contained within a tetrahedral coordination environment comprised of two NHCs, a terminal methyl group and an O-bound OCP moiety. The Mg1–O1–C1 angle (162.4(3)^o) is comparable to metal–OCP bend angles for rare earth complexes,^{241, 242} and significantly wider than those of group 2 and 13 (< 154^o).^{230, 231, 240, 243} The O1–C1 (1.232(5) Å) and C1–P1 (1.559(5) Å) bond distances are in the expected range for an ⁻O–C≡P anion,²²² and the Mg1–O1 bond (1.983(4) Å) is slightly shorter than those of (THF)₄Mg(OCP)₂ (2.024(16) Å).²³⁰

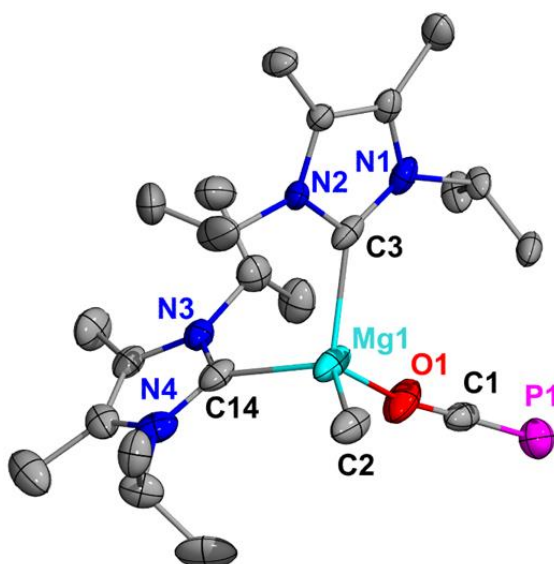


Figure 4.3. Molecular structure of **4.2^{iPr}** (thermal ellipsoids set at 50% probability; H atoms are omitted for clarity). Selected bond distances (Å) and angles (deg): Mg1–O1, 1.982(3); O1–C1, 1.232(5); C1–P1, 1.559(5); Mg1–C2, 2.143(5); Mg1–C3, 2.266(4); Mg1–C14, 2.261(4); Mg1–O1–C1, 162.4(3); O1–C1–P1, 178.7(4); O1–Mg1–C2, 113.28(17); O1–Mg1–C14, 96.16(15).

Compound **4.2^{iPr}** is highly soluble in non-polar solvents (e.g., toluene and benzene) and stable for several weeks under anhydrous conditions. In the solid-state, **4.2^{iPr}** can be stored in an inert atmosphere under ambient conditions for several months without noticeable decomposition. Compound **4.2^{iPr}** is also stable for several hours in refluxing benzene before decomposing to a light orange solution, which includes uncoordinated carbene and unidentified insoluble solids. Based on similar observations by others,²⁴⁴ these solids are presumed to be OCP oxidation products, as the OCP anion may be easily oxidized in the presence of electrophilic metals.^{222, 245, 246} Notably, **4.2^{iPr}** is stable in THF and does not activate the solvent under ambient conditions. The ³¹P{¹H} NMR resonance for the OCP singlet of **4.2^{iPr}** in THF-*d*₈ (δ -368.7 ppm) is comparable to the same in benzene-*d*₆ (δ -366.8 ppm), and in the ¹H NMR spectrum, integral ratios suggest the same coordination environment observed in the solid state.

Thus, the NHC-coordination in **4.2^{iPr}** is persistent even in the donor solvent, highlighting the vital role of steric protection from the ^{iPr}NHC ligands.

Table 4.1. Comparison of selected spectroscopic data and bond metrics^a for the isolated phosphoethynolate complexes.

	(^{iPr} NHC) ₂ Mg Me(OCP) (4.2^{iPr})	(^{Me} NHC) ₃ MgMe (OCP) (4.4^{Me})	(^{Me} NHC) ₃ Na(O CP) (4.6) ^a	(^{iPr} NHC) _n Mg(OEt) _n (OCP) (4.8/4.9)	(^{Me} NHC) ₃ Mg(OC P) ₂ (4.10)
δ ³¹ P (ppm)	-366.8	-378.2 ^b	-388.4	-364.9	-385.6
δ ¹³ C (C≡P) (ppm)	162.4	166.8 ^b	168.7	161.3	169.0
¹ J _{C-P} (Hz)	25.4	48.1 ^b	unresolved	unresolved	52.9
ν(OCP) (cm ⁻¹)	1740	1770, 1800	1761	1727	1744
M–O–C (°)	162.4(3)	N/A	167.2(5)	145.9(5) ^c	140.6(2), 147.5(3)
d(M–O) (Å)	1.982(3)	> 5.5	2.247(5)	1.938(4) ^c	2.143(2), 2.111(3)
d(O–C) (Å)	1.232(5)	1.208(10)	1.215(8)	1.254(7) ^c	1.199(5), 1.208(3)
d(C–P) (Å)	1.559(5)	1.574(14)	1.578(7)	1.545(6)	1.575(3), 1.584(6)
d(^{NHC} C–M) (Å)	2.266(4), 2.261(4)	2.226(3), 2.230(4), 2.259(4)	2.505(7), 2.476(7), 2.513(6)	2.192(6)	2.213(3), 2.216(3), 2.215(3)

^aValues reported for only one of two chemically equivalent but crystallographically unique molecules in the asymmetric unit. ^bData obtained at 60 °C. ^cM–OCP fragment.

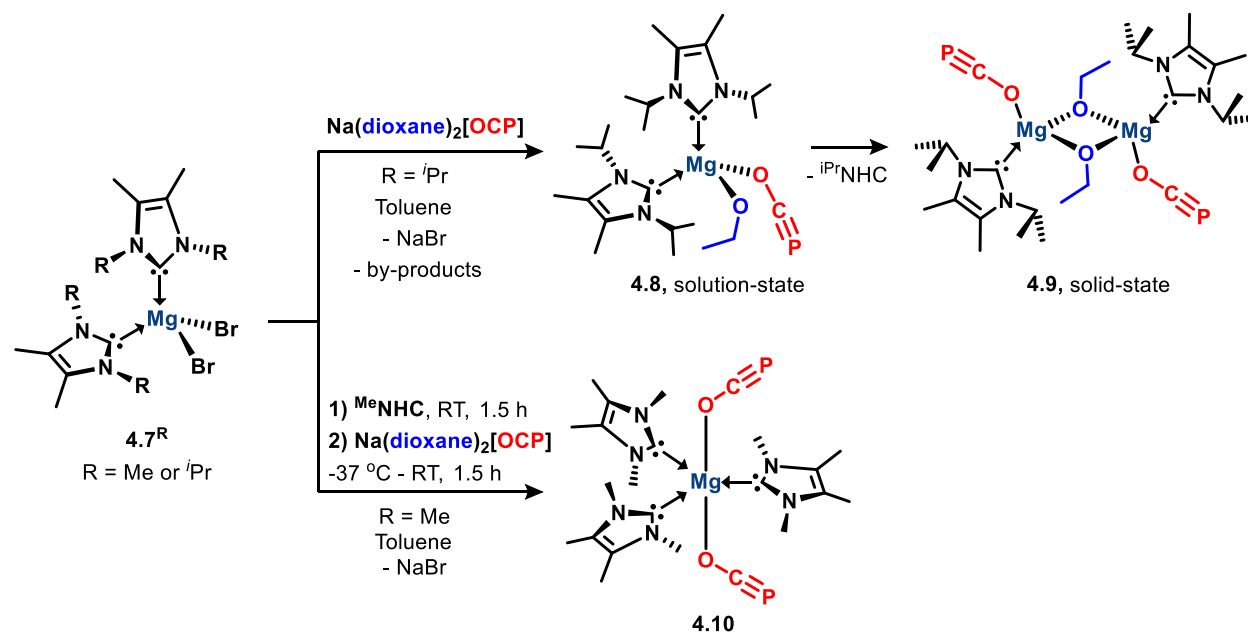
4.4 Isolation and Thermal Decarbonylation of a Carbene-Magnesium

Diphosphaethynolate

Upon the successful isolation of the Grignard complex (**4.2^{iPr}**), we explored the influence of NHCs in stabilizing the homoleptic magnesium diphosphaethynolate (Scheme 4.4). The reaction between (^{iPr}NHC)₂MgBr₂¹⁰⁸ (**4.7^{iPr}**) and two equivalents of [Na(dioxane)₂][OCP] yielded (^{iPr}NHC)₂Mg(OEt)(OCP) (**4.8**) as the only isolable product. The ³¹P{¹H} NMR

resonance (δ -364.9 ppm), and the OCP asymmetric stretch in the solid-state IR (vs, 1721 cm^{-1}) are comparable to **4.2**^{iPr} (Table 4.1).

Scheme 4.4. Role of carbene stereoelectronics in the stabilization of a magnesium bis(2-phosphaethynolate) complex



The structural assignment of **4.8** is based on ¹H NMR integral ratios, where the characteristic NHC and ethoxide resonances are in a 2:1 ratio. The ⁱPrNHC methine resonances are broadened in both the ¹H and ¹³C{¹H} NMR spectra, which may result from steric congestion or a potential dynamic process. Upon crystallization, **4.8** loses one equivalent of NHC to form [(ⁱPrNHC)Mg(μ-OEt)(OCP)]₂ (**4.9**), whose molecular structure was authenticated by SC-XRD (Figure 4.4a). The Mg–O contacts in **4.9** (1.930(5) – 1.953(4) Å) for both the ethoxide and OCP anions are remarkably short [covalent radius $R(\text{Mg}–\text{O}) = 2.02 \text{ \AA}^{184}$]. The Mg1–O1–C1 angle (145.9(5)°) is much smaller than in **4.2**^{iPr} (162.4(3)°), but is comparable to those of (THF)₄Mg(OCP)₂ (142.8(15)°).²³⁰ The C≡P bond (1.545(6) Å) in **4.9** is among the shortest reported values for metal-oxyphosphaalkyne complexes (see Table A2.1), and suggests a more substantial contribution of the O–C≡P resonance form in this compound than in **4.2**^{iPr} and (THF)₄Mg(OCP)₂. Notably, **4.9** was not observed in the NMR of the bulk material from this

reaction. Multiple crystallization attempts yielded a mixture of powdery and crystalline solids, from which the crystalline material is difficult to separate and independently analyze by NMR spectroscopy. Compound **4.8** is stable for several weeks in anhydrous benzene and toluene, and similar to **4.2^{iPr}**, decomposition is observed after several hours in refluxing benzene to afford free ^{iPr}NHC and unidentified solids.

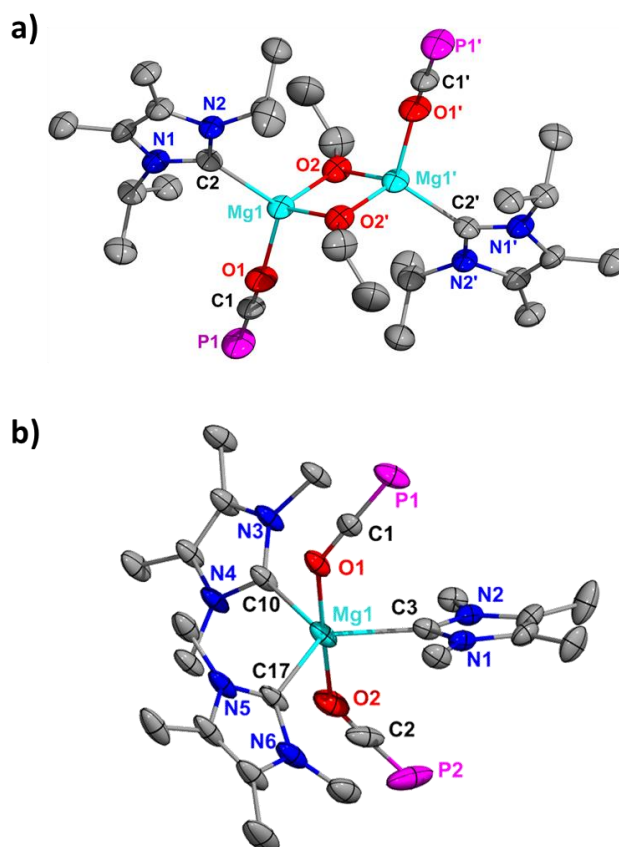


Figure 4.4. Molecular structure of **4.9** (a) and **4.10** (b). Co-crystallized solvent molecules for **4.10** and all H atoms are omitted for clarity. Thermal ellipsoids are shown at a probability level of 50% (**4.9**) and 30% (**4.10**). Selected bond distances (Å) and angles (deg): **9**: Mg1–O1, 1.938(4); Mg1–O2, 1.930(5), Mg1–O2', 1.953(4); O1–C1, 1.254(7); C1–P1, 1.545(6); Mg1–C2, 2.192(6); Mg1---Mg1, 2.885(4); Mg1–O1–C1, 145.9(5); O1–C1–P1, 179.3(6); O1–Mg1–C2, 112.6(2); O2–Mg1–O1, 115.2(2); O2–Mg1–O2', 84.04(19). **4.10**: Mg1–O1, 2.111(3); Mg1–O2, 2.143(2); Mg1–C3, 2.213(3); Mg1–C10, 2.216(3); Mg1–C17, 2.215(3); O1–C1, 1.208(3); O2–C2, 1.199(5); C1–P1, 1.575(3); C2–P2, 1.584(6); C1–O1–Mg1, 140.6(2); C2–O2–Mg1, 147.5(3); O1–Mg1–O2, 178.62(10); O2–Mg1–C3, 90.20(12); O1–Mg1–C3,

88.75(10); C17–Mg1–C3, 118.06(11); C10–Mg1–C3, 125.53(11); C17–Mg1–C10, 116.36(12).

Consistent with the reactivity profile for **4.4^{Me}**, we anticipated that base saturation via tris-NHC coordination may stabilize the target diphosphaethynolate complex and attenuate its Lewis acid reactivity or decomposition pathways. Indeed, the reaction of equimolar amounts of (^{Me}NHC)₂MgBr₂, ^{Me}NHC and [Na(dioxane)₂][OCP] in toluene yielded the desired product (^{Me}NHC)₃Mg(OCP)₂ (**4.10**) as a colorless crystalline solid in 35 % yield (Scheme 4.4). In the ³¹P{¹H} NMR spectrum, the OCP anion resonates at δ -385.6 ppm and is significantly upfield from those of (THF)₄Mg(OCP)₂, **4.2^{iPr}** and **4.8** (Table 4.1). The C≡P resonance (δ 169.0 ppm, ¹J_{CP} = 52.9 Hz) in the ¹³C{¹H} NMR spectrum is observed as a doublet with a much larger ¹³C–³¹P coupling constant than in **4.2^{iPr}**. Single crystal X-ray diffraction studies reveal that **4.10** is mononuclear (Figure 4.4b). The magnesium atom resides in a trigonal bipyramidal coordination environment with three ^{Me}NHC ligands on the equatorial positions (Σ ∠C–Mg–C = 359.95°). The axial OCP anions in **4.10** are *cis* to the OMgO plane, in contrast to (THF)₄Mg(OCP)₂ for which they are *trans*. Owing to the donor effects of tris(NHC)-stabilization, the Mg–O bond lengths in **4.10** are 0.09 – 0.21 Å longer than those of **4.2^{iPr}**, **4.9** and (THF)₄Mg(OCP)₂ (Table 1). The O–C≡P bond parameters in **4.10** are comparable to **4.6** and (THF)₄Mg(OCP)₂, with shorter O–C and longer C–P bond lengths than those of **4.2^{iPr}** and **4.9**. The isolation of **4.10** suggests that the difficulty in stabilizing the ^{iPr}NHC adduct results from unfavorable steric congestion, which may lead to carbene dissociation and enable a more electrophilic Mg²⁺ center for dioxane activation.

Compound **4.10** is stable in refluxing benzene for several hours. However, heating a colorless C₆D₆ solution of **4.10** in a J-Young NMR tube for 3 days at 105 °C yielded an orange solution, with the appearance of two new singlets in the ³¹P{¹H} NMR spectrum at δ -149.9 and -115.24 ppm. By layering this solution with hexanes, a few light yellow crystals were obtained and

characterized by X-ray diffraction as a charge-separated bis-NHC stabilized phosphorus(I) species $[(^{\text{Me}}\text{NHC})_2\text{P}^{\text{I}}][\text{OCP}]$ (**4.11**) (Scheme 4.5). The bond metrics in **4.11** (Figure 4.5) are comparable to reported $(\text{NHC})_2\text{P}^{\text{I}}$ cations,²⁴⁷⁻²⁵² and justify the structural depiction in Scheme 4.5. Similarly, the resonances in the $^{31}\text{P}\{^1\text{H}\}$ NMR spectrum are in agreement with known P^{I} cations (δ -115.24 ppm, range -93 to -127 ppm²⁴⁷⁻²⁵²) and a non-contacted OCP anion (δ -386.1 ppm).

Scheme 4.5. Thermal decomposition of a magnesium diphosphaethynolate complex

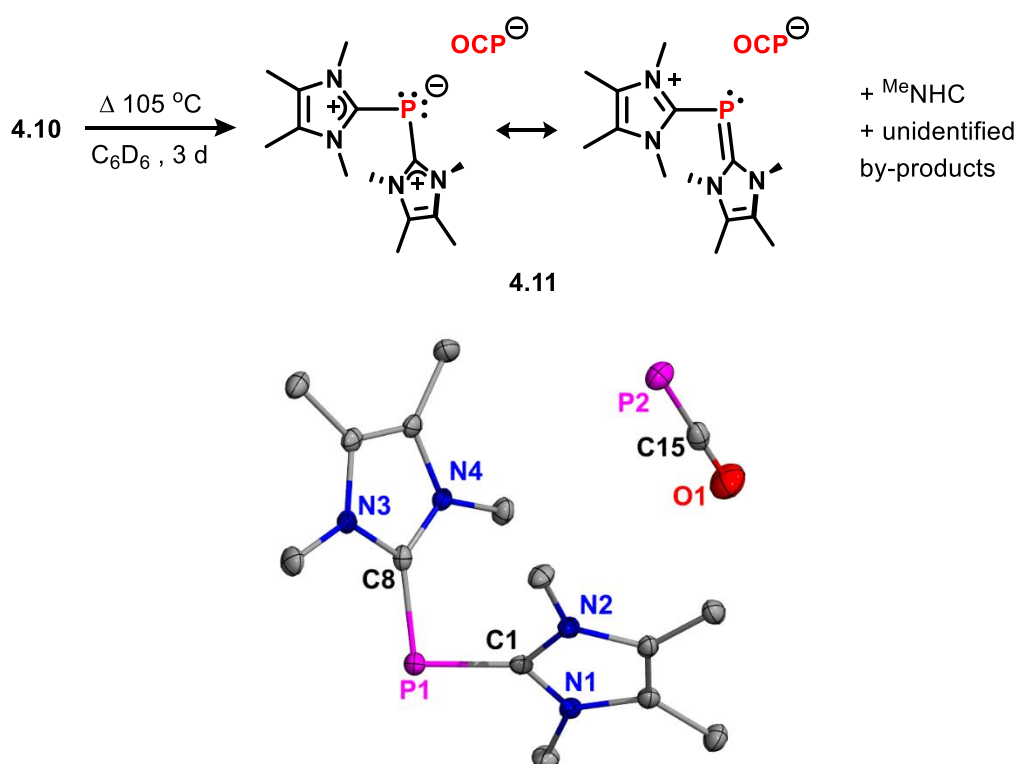


Figure 4.5. Molecular structure of **4.11** with H atoms omitted for clarity. Selected bond distances (Å) and angles (deg): P1–C1, 1.8045(18); P1–C8, 1.8055(18); C15–P2, 1.605(2); O1–C15, 1.196(2); C1–N1, 1.355(2); C1–N2, 1.390(2); C8–N3, 1.355(2); C8–N4, 1.351(2); C1–P1–C8, 96.63(8); O1–C15–P2, 179.00(17).

Upon its successful structural characterization, it becomes clear that **4.11** is a minor product of this transformation, and the major product remains unidentified (δ -149.9 ppm in the $^{31}\text{P}\{^1\text{H}\}$ NMR). Free $^{\text{Me}}\text{NHC}$ was identified as another by-product of this reaction, and the second major

set of $^{\text{Me}}\text{NHC}$ resonances in the ^1H NMR spectrum is presumably due to **4.11** but could not be confidently assigned (Figure A2.64). Attempts to independently isolate and spectroscopically characterize **4.11** were unsuccessful. Nevertheless, the observation of **4.11** suggests that a highly unusual decarbonylation of a phosphaehtynolate complex has occurred. Such reactivity is traditionally observed in the domain of phosphaketene ($\text{P}=\text{C}=\text{O}$) complexes.^{222, 223, 253-262} The $\text{P}^{\ominus}\leftarrow\text{C}=\text{O}$ resonance form is widely invoked to rationalize decarbonylation from OCP fragments, and lends credence to the intermediacy of a magnesium phosphide in this reaction. Literature precedence suggests that base transfer to the phosphorus atom or carbonyl carbon is a likely initial step in the observed decarbonylation.^{238, 261-265}

4.5 Conclusion and Outlook

Solvent-free, phosphaehtynolate-containing Grignard complexes have been isolated, and the stereoelectronic influence of 1,3-dialkyl substituted NHCs on their stabilization was explored. In contrast to known alkaline earth phosphaehtynolate salts which are ether-stabilized and rapidly decompose in solution, these NHC-stabilized complexes are highly soluble and thermally stable in common hydrocarbon solvents. The ability of some of these compounds to activate dioxane was attributed to enhanced metal Lewis acidity due to dynamic carbene coordination, which may render them promising reagents for bond activation at magnesium. In addition, the isolated carbene-saturated $\text{Na}(\text{OCP})$, which is soluble in non-polar solvents, may become a key reagent in situations where ethers must be avoided, or the solubility of ethereal solvent-coordinated $\text{Na}(\text{OCP})$ is problematic.

Chapter Five: N-Heterocyclic Carbene-Assisted Reversible Migratory Coupling of Aminoborane at Magnesium

Contains work that was originally published in:

Obi, A. D.; Frey, N. C.; Dickie, D. A.; Webster, C. E.; Gilliard, R. J., N-Heterocyclic Carbene-Assisted Reversible Migratory Coupling of Aminoborane at Magnesium. *Angew. Chem. Int. Ed.* **2022**, <https://doi.org/10.1002/anie.202211496>

5.1 Overview of *s*-block amidoboranes in hydrogen storage and catalysis

The promise of ammonia borane (NH_3BH_3) for hydrogen storage is punctuated by its slow dehydrogenation kinetics and formation of undesirable byproducts such as borazine (a fuel-cell poison) and ceramic boron nitride.²⁶⁶⁻²⁷⁴ As an alternative, saline *s*-block metal amidoboranes [$\text{M}(\text{NH}_2\text{BH}_3)_x$; $\text{M} = \text{Li}, \text{Na}, \text{K}, \text{Mg}, \text{Ca}, \text{Sr}$; $x = 1$ or 2] are capable of thermal dehydrogenation under much milder conditions than NH_3BH_3 , with little to no borazine release.²⁷⁵⁻²⁸⁵ In addition, their molecular complexes are competent for catalytic amine borane dehydrogenation (Figure 5.1a),^{55, 286-290} even under ambient conditions.²⁸⁸ The apparent catalytic activity trend for simple *s*-block $\text{M}(\text{N}(\text{SiMe}_3)_2)_x$ complexes is $\text{Mg} > \text{Li} \approx \text{Na} > \text{K} \approx \text{Ca}$,²⁸⁹ but highly variable activity can be achieved by rational modification of their coordination environments.²⁸⁶⁻²⁸⁸ Significantly, these molecular complexes are amenable to structural, electronic and mechanistic analyses,²⁷⁰ which complement solid-state mass or volumetric analysis techniques^{267, 272} for a holistic understanding of amine borane dehydrogenation.

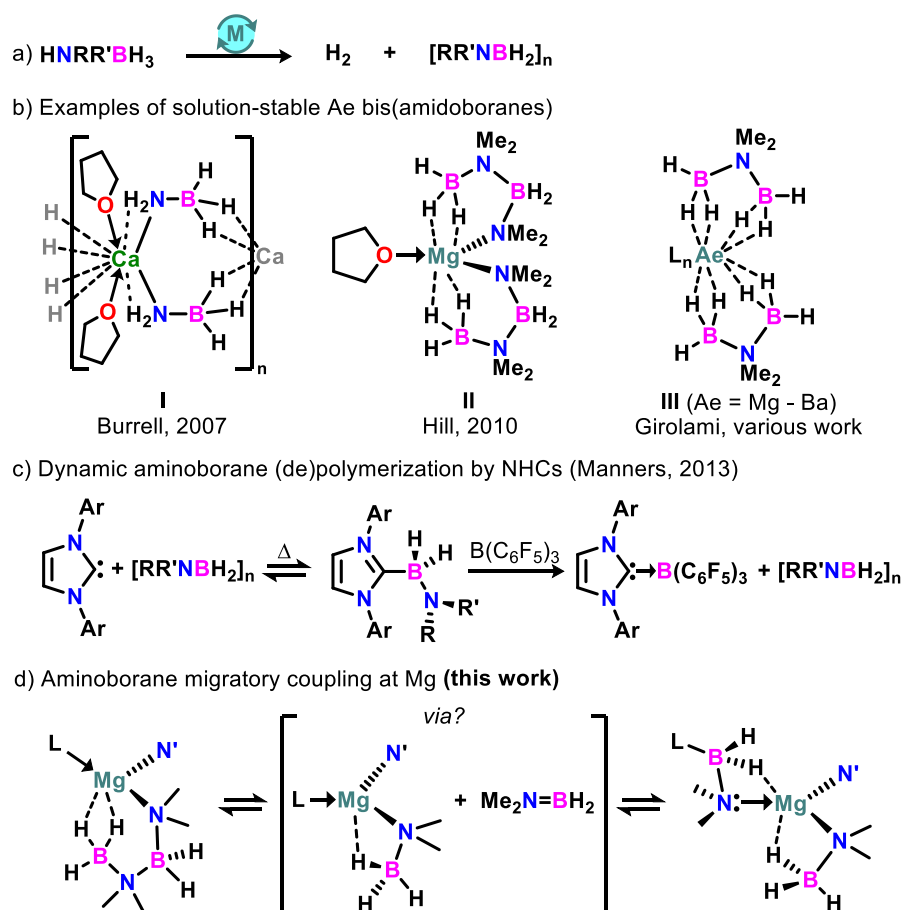


Figure 5.1. a) Simplified catalytic amine borane dehydrogenation by molecular species (R, R' = H, alkyl, aryl). b) Select examples of solution-stable group 2 bis(amidoboranes). c) Dynamic depolymerization of aminoboranes by N-heterocyclic carbenes (NHCs). d) This work: NHC-assisted reversible migratory insertion of aminoborane at magnesium (L = NHC, N' = silylamide or amidoborane).

Divalent group 2 metals are privileged to support a well-defined Ae–NR₂BH₃ unit (Ae = alkaline earth metal) kinetically stabilized by a persistent, monoanionic ligand with significant steric demand (e.g., β-diketiminato).^{55, 290-292} Consequently, they provide a molecular platform for probing metal–hydride polarizations, secondary interactions, and intermediates of thermal or catalytic dehydrogenation reactions through ¹¹B NMR spectroscopy and X-ray crystallography.^{55, 290-295} Conversely, solution-state investigations of homoleptic Ae(NR₂BH₃)₂ complexes are sparse. With the exception of [(THF)Ca(NH₂BH₃)₂]_n (I, Figure 5.1b),²⁷⁵ primary

alkaline earth bis(amidotrihydroborates) [i.e., Ae(NH₂BH₃)₂] are typically unstable in solution, and their syntheses require heterogenous or solid-state conditions.^{278, 279, 285} Compound **I** has poor solubility, and readily loses THF coordination under vacuum or in non-ethereal solvents, leading to polymeric or poorly-defined species. Employing more soluble secondary amine boranes, Hill and coworkers remarked that the formation of Ae(NR₂BH₃)₂ (R = alkyl, aryl) is complicated by incomplete aminolysis due to rapid catalytic dehydrogenation and/or dehydrocoupling reactions.^{296, 297} In the case for magnesium, the adduct (THF)Mg(NMe₂BH₂NMe₂BH₃)₂ (**II**) was isolated,⁵⁵ and the relevance of the complex ⁻{NMe₂BH₂NMe₂BH₃} anion for catalytic dehydrogenation of HNMe₂BH₃ to [Me₂NBH₂]₂ has been further evaluated in molecular species based on *d*⁰ metals.^{288-290, 298} Girolami has also reported a series of solution-stable alkaline earth bis(aminodiboranates) of the type LAe(NMe₂(BH₃)₂)₂ (**III**, Ae = Mg – Ba; L = Et₂O, THF, tmeda), although they were primarily investigated for chemical vapor deposition and not amine borane dehydrogenation.²⁹⁹⁻³⁰² However, these base-stabilized complexes are closer mimics of saline amidoboranes, and a more suitable choice of Lewis base may enhance their thermal stabilities for extensive molecular investigations.

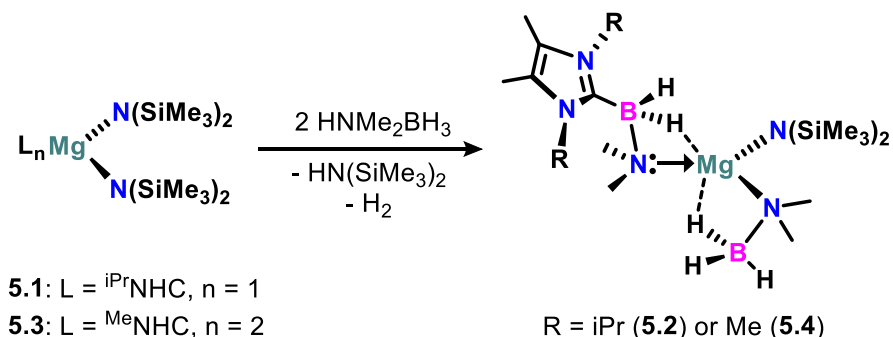
Given our established interest in the stabilization of unusual organoalkaline earth complexes using carbene ligands,^{28, 40, 106, 108, 109, 174, 205, 303} we anticipated that the persistent coordination and stereoelectronic tunability of N-heterocyclic carbenes (NHCs) may enable the stabilization of structurally diverse magnesium amidoborane complexes for molecular studies. Notably, NHCs can modulate the nuclearity of magnesium hydride clusters based on ligand size, as our laboratory and others have discovered.^{91, 104, 174} NHCs and cyclic (alkyl)(amino) carbenes (CAACs) are also active for the metal-free dehydropolymerization of amine boranes³⁰⁴ and phosphine boranes,³⁰⁵ with selective capture of dehydrogenation products (e.g., H₂, BH₂NR₂, BH₂NR₂BH₃) at the carbene C2 center. NHCs displayed significantly higher

activity than common strong bases such as 4-dimethylaminopyridine (DMAP), phosphines, and N-Heterocyclic olefins (NHOs) for the dynamic depolymerization of aminoboranes (Figure 5.1c).^{306, 307} Because these electronically flexible Lewis bases are, in their own right, active for amine borane dehydrocoupling reactions, the potential for non-innocent participation of NHCs in dehydrocoupling reactions involving magnesium amidoboranes is desirable for controlling amine borane dehydrogenation kinetics. We now report the syntheses, structural characterization, and spectroscopic studies of the first isolable, solution-stable magnesium bis(amidotrihydroborates) [LMg(NR₂BH₃)₂], and further evaluate the influence of NHCs in aminoborane coupling in structurally diverse magnesium amidoboranes. A dynamic insertion/elimination of Me₂N=BH₂ was observed in the ^{NHC}C–Mg and Mg–N bonds of compounds containing the ⁻{NMe₂BH₂NMe₂BH₃} anion, representing a rare example of reversible migratory insertion at a normal valent alkaline earth center. This fundamental organometallic process is unusual in the *s*-block,¹⁴⁹ and highlights the relevance of NHCs in understanding group 2 element-mediated amine borane dehydrocoupling.

5.2 Aminoborane Coupling at Carbene-Magnesium Centers

We have previously observed that 1,3-dialkyl-substituted NHCs are more suitable for the persistent stabilization of simple magnesium(II) complexes^{107-109, 173, 303} than conventional diaryl-substituted NHCs, wherein destabilizing ligand dissociation is common due to steric complications.^{198, 206} Therefore, the ligand 1,3-diisopropyl-4,5-dimethylimidazol-2-ylidene (^{iPr}NHC)²¹⁷ was chosen for our investigations for its ease of synthesis and the availability of methine protons as a convenient spectroscopic handle. The reaction of (^{iPr}NHC)Mg(N(SiMe₃)₂)₂ (**5.1**)¹⁷⁴ and two equivalents of dimethylamine borane in hexanes afforded the triamide complex (^{iPr}NHC–BN)Mg(NMe₂BH₃)(N(SiMe₃)₂) (**5.2**; ^{iPr}NHC–BN = ^{iPr}NHC–BH₂NMe₂) as a colorless crystalline solid in 67% yield (Scheme 5.1). The ¹¹B NMR spectrum of **2** features two well-defined quartet (δ –14.9 ppm; ¹J_{BH} = 90.2 Hz) and triplet (δ –

17.3 ppm; $^1J_{\text{BH}} = 85.4$ Hz) resonances ascribed to the $-\text{BH}_3$ and $-\text{BH}_2$ groups respectively. The heteroleptic configuration of **5.2** is retained in solution, and no evidence of Schlenk rearrangements was observed in the ^1H NMR spectrum.



Scheme 5.1. Dimethylamine borane dehydrocoupling in the synthesis of a heteroleptic magnesium amidoborane complex.

The molecular structure of **5.2** (Figure 5.2a) was unambiguously determined by single crystal X-ray diffraction,³⁰⁸ which reveals a monomeric magnesium amidoborane complex in a trigonal planar central geometry ($\Sigma \text{N-Mg-N} = 359.48^\circ$), albeit having $\text{Mg}\cdots\text{HB}$ agostic-type contacts from $^-\text{NMe}_2\text{BH}_3$ (Figure 5.2 caption). The B–N bond distances are relatively similar in the neutral and anionic amidoborane ligands, which suggests charge delocalization in $^{\text{iPr}}\text{NHC-BN}$. Hence, $^{\text{iPr}}\text{NHC-BN}$ may be considered a push-pull ligand ($\text{NHC}\rightarrow\text{BN}\rightarrow\text{Mg}$) similar to previous NHC-aminoborane adducts,^{304, 306} or a zwitterionic neutral donor ($\text{NHC}\rightarrow\text{BN}\rightarrow\text{Mg}$) in the coordination sphere of magnesium.

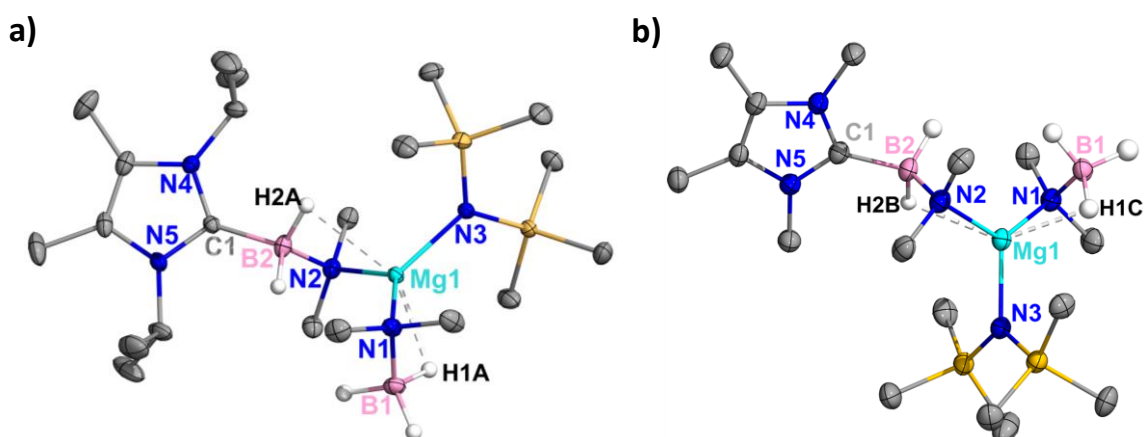


Figure 5.2. Molecular structures of **5.2** (a) and **5.4** (b). H atoms omitted for clarity, with the exception of B–H hydrides which were isotropically refined. Selected bond distances (Å) and angles (°) for **5.2** [and **5.4**]: Mg1–N1, 2.0944(8) [2.088(3)]; Mg1–N2, 2.1301(8) [2.116(3)]; Mg1–N3, 1.9964(8) [1.990(3)]; Mg1–H1A, 2.095(14) [Mg1–H1C, 2.14(4)]; Mg1–H2A, 2.373(13) [Mg1–H2B, 2.39(3)]; C1–B2, 1.6250(13) [1.625(5)]; B2–N2, 1.5653(13) [1.565(5)]; B1–N1, 1.5721(13) [1.560(5)]; N1–Mg1–N2, 131.96(3) [129.83(13)]; B2–N2–Mg1, 83.67(5) [90.1(2)]; H1A–Mg1–H2A, 147.3(5) [H1C–Mg1–H2B, 140.1(13)].

NMR-monitored stoichiometric reactions of **5.1** and HNMe_2BH_3 indicate the intermediacy of an $\text{Mg}(\text{NMe}_2\text{BH}_2\text{NMe}_2\text{BH}_3)$ unit ($\delta(\text{BH}_2)$ 2.53 ppm, $^1J_{\text{BH}} = 102.3$ Hz), as well as uncoordinated $^i\text{PrNHC-BN}$ ($\delta(\text{BH}_2)$ –13.4 ppm, $^1J_{\text{BH}} = 83.5$ Hz).³⁰⁹ Therefore, in addition to $\text{Me}_2\text{N}=\text{BH}_2$ capture at the $^{\text{NHC}}\text{C-Mg}$ bond in the formation of **5.2**, an NHC-mediated abstraction or migratory transfer of $\text{Me}_2\text{N}=\text{BH}_2$ from an $\text{Mg}(\text{NMe}_2\text{BH}_2\text{NMe}_2\text{BH}_3)$ unit cannot be discounted. In the absence of magnesium species, the reaction of $^i\text{PrNHC}$ and HNMe_2BH_3 yields the hydrogenated aminal $^i\text{PrNHC-H}_2$, $^i\text{PrNHC-BN}$ and amino borane oligomers, which is consistent with previous reports of reactions between carbenes and secondary amine boranes.^{304, 305, 310} However, in reactions of **5.1** and HNMe_2BH_3 , $^i\text{PrNHC-H}_2$ was only observed in minor quantities (ca. 6%), suggesting that the NHC-coordination in **5.1** is persistent, and the observed dehydrocoupling processes are primarily metal-mediated.

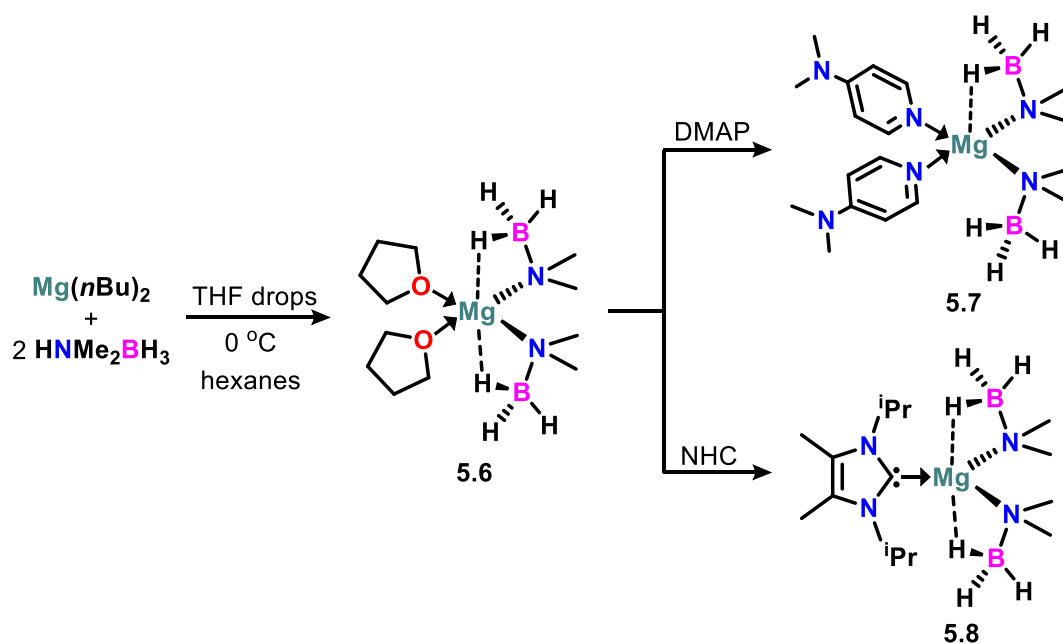
In further attempts to isolate an $\text{Mg}(\text{NMe}_2\text{BH}_3)_2$ carbene complex, we posited that the electronic influence of multiple carbenes may discourage rapid dehydrocoupling reactions by weakening agostic $\beta\text{-BH}$ interactions of the initial metathesis intermediate. Indeed, the coordination of multiple carbene ligands at divalent group 2 centers is known to modulate their electronic structures, even towards cationization in the absence of abstraction reagents.^{109, 111, 303} While **5.1** does not react with an additional $^i\text{PrNHC}$ ligand due to steric complications, the reaction of $\text{Mg}(\text{N}(\text{SiMe}_3)_2)_2$ and the less hindered 1,3,4,5-tetramethylimidazol-2-ylidene

(^{Me}NHC) affords (^{Me}NHC)₂Mg(N(SiMe₃)₂)₂ (**5.3**) as a colorless crystalline solid in 55% yield. The subsequent reaction of **5.3** and HNMe₂BH₃ yielded a mixture of products including (^{Me}NHC–BN)Mg(NMe₂BH₃)(N(SiMe₃)₂) (**5.4**) and uncoordinated ^{Me}NHC–BN due to the same dehydrocoupling processes observed in **5.1** (Scheme 5.1 and Figure A2.82). The molecular structure of **5.4** (Figure 5.2b) is structurally analogous to **5.2**, and their characteristic ¹¹B NMR resonances are nearly identical. Notwithstanding the unsuccessful isolation of a homoleptic Mg(NMe₂BH₃)₂ complex, these reactions highlight the facile nature of carbene-mediated Me₂N=BH₂ capture at magnesium. To elucidate the operative processes, the initial isolation of carbene-free Mg(NMe₂BH₃)₂ and Mg(NMe₂BH₂NMe₂BH₃)₂ species is necessary.

5.3 Synthesis of Homoleptic Mg(NMe₂BH₃)₂ Complexes

In addition to their thermal instability, the syntheses of Mg(NH₂BH₃)₂ salts require heterogenous or solid-state reaction conditions (e.g., ball milling) due to the poor nucleophilicity of the typical magnesium hydride starting material (compared to CaH₂ and alkali metal hydrides).^{279, 282} In contrast to MgH₂, hydrocarbon-soluble magnesium alkyls and amides are highly reactive and prone to rapid dehydrocoupling.^{55, 296, 297} In our initial attempts towards the selective isolation of Mg(NMe₂BH₃)₂, the reaction of Mg(*n*Bu)₂ and two equivalents of HNMe₂BH₃ in hexanes at 0 °C yielded a viscous oil from which a few colorless crystals were obtained by mechanical agitation using a glass pipette. Spectroscopic analysis suggest the presence of multiple species, but only Mg₄(μ-O)(NMe₂BH₃)₆ (**5.5**) was crystallographically identified (Figure 5.3a). Compound **5.5** presumably formed from the partial decomposition of Mg(NMe₂BH₃)₂ due to hydrolysis of trace moisture in the reaction solvent, and suggests that the target bis(amidoborane) may further benefit from Lewis base stabilization. In the presence of THF, the adduct (THF)₂Mg(NMe₂BH₃)₂ (**5.6**) was obtained as a sticky solid, which was difficult to purify due to its extremely high solubility (Scheme 5.2). However, addition of the stronger base DMAP precipitated (DMAP)₂Mg(NMe₂BH₃)₂ (**5.7**) as

a free-flowing white solid, which is easily purified by a hexanes or toluene wash. Likewise, in-situ NHC complexation to **5.6** afforded (^{iPr}NHC)Mg(NMe₂BH₃)₂ (**5.8**) as a colorless crystalline solid in 74% yield (Scheme 5.2). In contrast to the case for **5.5** and **5.6**, the identity and purity of **5.7** and **5.8** were also confirmed by heteronuclear (¹H, ¹¹B, ¹³C) NMR spectroscopy.



Scheme 5.2. Dimethylamine borane dehydrocoupling in the synthesis of a heteroleptic magnesium amidoborane complex.

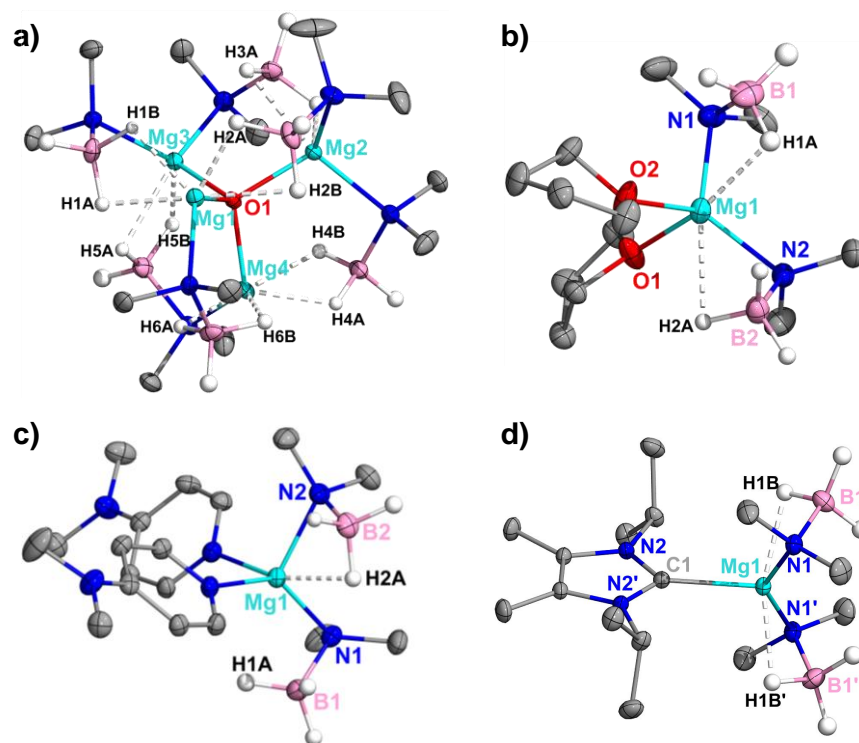


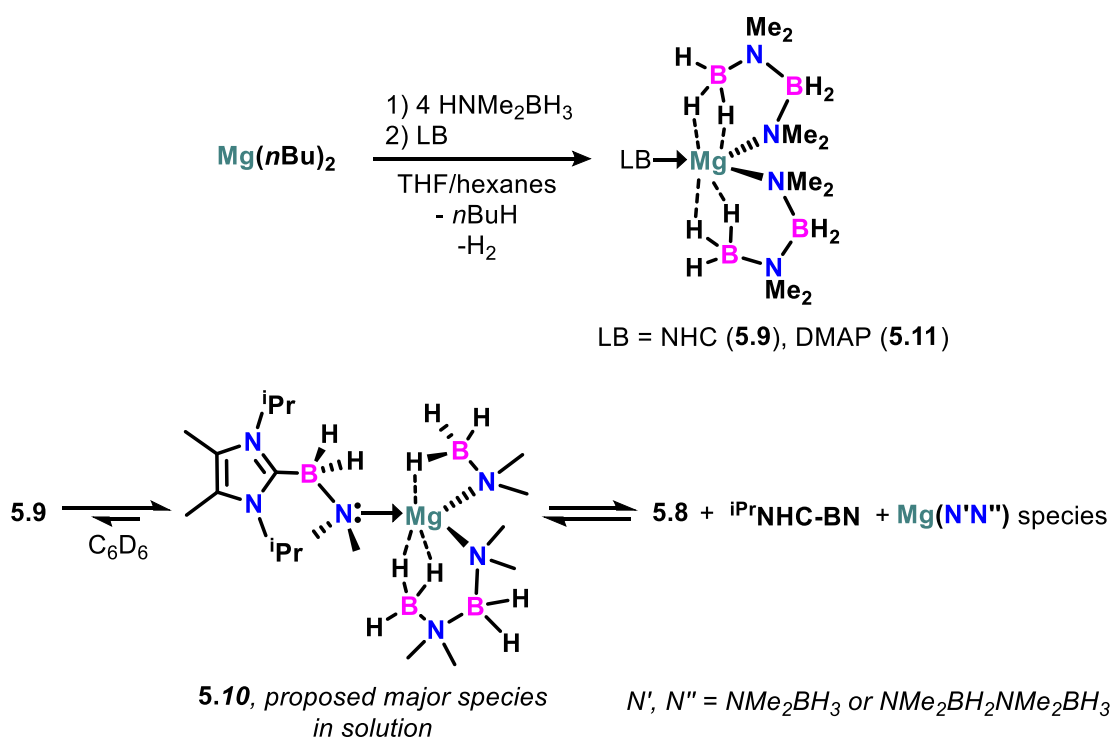
Figure 5.3. Molecular structures of **5.5** (a), **5.6** (b), **5.7** (c) and **5.8** (d). H atoms are omitted for clarity, with the exception of B–H hydrides which were isotropically refined. Selected bond distances (Å) and angles (°): **5.5**: Mg1–H1B, 1.975(15); Mg1–H2A, 1.949(17); Mg1–H1A, 2.132(16); Mg1–H2B, 2.254(17); Mg2–H3B, 1.960(17); Mg1–O1, 1.9718(9); Mg2–O1, 2.132(16); Mg1–N6, 2.0873(11); Mg1–O1–Mg2, 107.45(4); H3A–Mg2–H3B, 52.1(6); H1A–Mg1–H2B, 173.9(6). **5.6**: Mg1–N1, 2.1034(15); Mg1–H1A, 2.16(2); Mg1–H2A, 2.353(19); B1–N1, 1.578(2); N1–Mg1–N1', 113.79(6). **5.7**: Mg1–N1, 2.1099(14); Mg1–N2, 2.1147(14); Mg1–H2A, 2.210(18); Mg1···H1A, 2.477(21); B1–N1, 1.563(2); B2–N2, 1.581(2); N1–Mg1–N1', 113.18(6). **5.8**: Mg1–C1, 2.2062(10); Mg1–N1, 2.0848(7); Mg1–H1B, 2.104(13); B1–N1, 1.5707(11); N1–Mg1–N', 143.23(4); H1B–Mg1–H1B', 161.82(3). Symmetry transformations used to generate equivalent atoms (A') in **5.8**: $-x+1, y, -z+1/2$.

In contrast to the extensive network of multinuclear Mg···HB interactions in **5.5** and polymeric Mg(NH₂BH₃)₂ complexes,^{281, 282} Lewis base coordination in **5.6**, **5.7**, and **5.8** resulted in monomeric complexes (Figures 5.3b-d). The shortest Mg–H contacts in **5.6** (2.16(2)

and 2.353(19) Å) and **7** (2.210(18) Å) are elongated from those of **5.8** (both 2.104(13) Å). The ^{NHC}C–Mg bond in **5.8** (2.2062(10) Å) is comparable to the same for **5.1** and similar tricoordinate magnesium amides stabilized by ^{iPr}NHC (2.205(6) – 2.2120(19) Å).^{107, 174} Hence, the carbene coordination is expected to be persistent in solution. In the solid state, **5.7** and **5.8** are indefinitely stable in inert atmosphere under ambient conditions, and no decomposition was spectroscopically observed in their anhydrous benzene solutions over several weeks. Thus, the benefit of Lewis base stabilization of magnesium amidotrihydroborates for solution-state investigations is evident.

5.4 Dynamic Aminoborane Coupling in Complexes Containing the ⁻{NMe₂BH₂NMe₂BH₃} Anion

The reaction of Mg(*n*Bu)₂ and four equivalents of HNMe₂BH₃, followed by NHC complexation affords (^{iPr}NHC)Mg(NMe₂BH₂NMe₂BH₃)₂ (**5.9**) as a colorless crystalline solid (Scheme 5.3). The molecular structure of **5.9** is analogous to the THF adduct (**II**)⁵⁵ as a monomeric compound with four agostic Mg···HB contacts (Figure 5.4a). The ^{NHC}C–Mg bond in **5.9** (2.3450(16) Å) is significantly longer than that of **5.8** (2.2062(10) Å), and to the best of our knowledge, the longest known ^{carbene}C–Mg^{II} bond in the literature. Indeed, it closely compares with ^{carbene}C–Mg^I systems (2.312(3) – 2.341(2) Å),³³ whose elongated bonds are owed to the increased ionic radii of Mg(I). Similar to **II**, there are pronounced disparities in the B–N bond distances in **5.9** (Δ 0.024 – 0.051 Å) which suggests differing charge localization in the ⁻{NMe₂BH₂NMe₂BH₃} anion.



Scheme 5.3. Carbene-mediated shuttling of Me₂N=BH₂ in an Mg(NMe₂BH₂NMe₂BH₃)₂ complex.

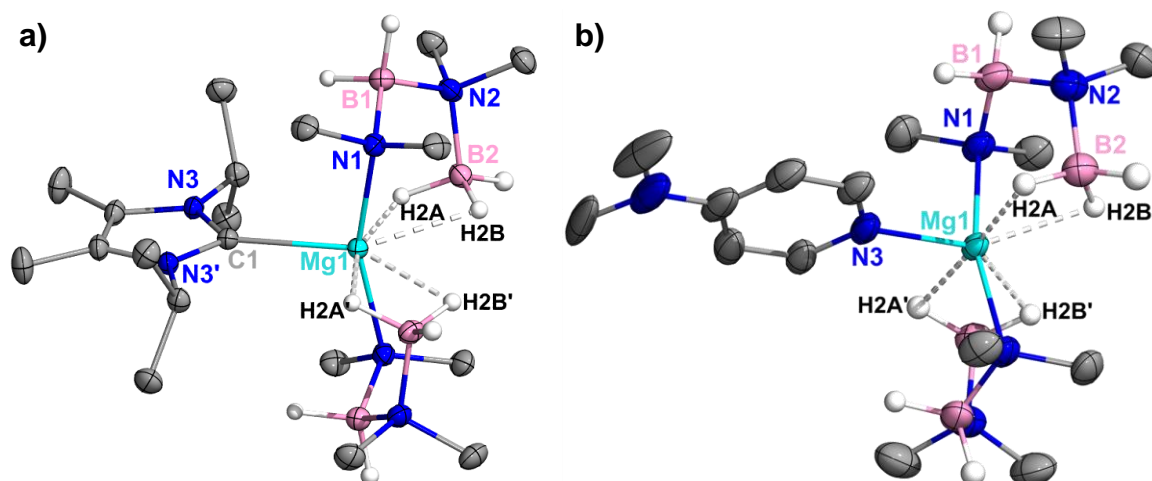
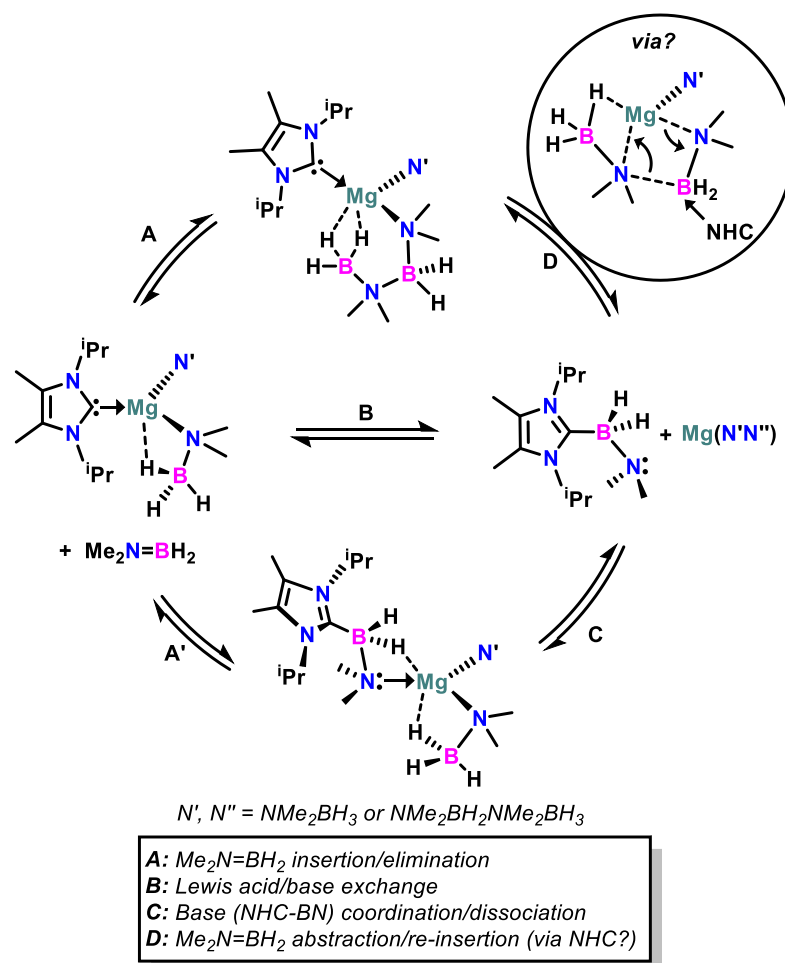


Figure 5.4. Molecular structures of 5.9 (a) and 5.11 (b). H atoms omitted for clarity, with the exception of B–H hydrides which were isotropically refined. Selected bond distances (Å) and angles (°) in 5.9 [and 5.11]: Mg1–C1, 2.3450(16) [Mg1–N3, 2.144(3)]; Mg1–N1, 2.1663(9) [2.1679(18)]; Mg1–H2A, 2.107(14) [2.18(3)]; Mg1–H2B, 2.295(15) [2.21(3)]; B1–N1, 1.5607(16) [1.547(4)]; B1–N2, 1.6115(16) [1.618(4)]; B2–N2, 1.5846(16) [1.580(3)]; N1–

Mg1–N1', 159.51(6) [163.16(12)]. Symmetry transformations used to generate equivalent atoms (A') in **5.9** [and **5.11**]: $-x+1, y, -z+1/2$ [$-x+1, y, -z+3/2$].

Despite crystallographic confirmation, **5.9** is unobserved by NMR but undergoes dynamic disproportionation in solution (C_6D_6) to several products including **5.8**, $iPrNHC-BN$, and a primary product presumed to be $(iPrNHC-BN)Mg(NMe_2BH_3)(NMe_2BH_2NMe_2BH_3)$ (**5.10**). Efforts to unambiguously identify **5.10** by X-ray crystallography only led to the isolation of **5.8**, **5.9**, or $iPrNHC-BN$, depending on solvent or temperature conditions. However, the assignment of **5.10** is based on several spectroscopic observations. The carbene methine protons in **5.10** (δ_H 4.89 ppm) are downfield from **5.8** (δ_H 4.57 ppm), which suggests $iPrNHC$ coordination to a more Lewis acidic fragment such as a borane, in contrast to the donor-rich environment of **5.9**. In the ^{11}B NMR spectrum, a prominent $Mg(NMe_2BH_2NMe_2BH_3)$ resonance (t, δ 2.89 ppm, $^1J_{BH}$ 101.8 Hz) was observed, but resonances due to $Mg(NMe_2BH_3)$ and $iPrNHC-BN$ units were overlapped. In variable temperature (VT) 1H NMR studies, the methine resonance for **5.10** decoalesced to two broad resonances at -55 °C (Figure A2.93), likely due to the heteroleptic nature of the proposed structure. Free NHC was also observed below -30 °C, which supports the likelihood of NHC dissociation and abstraction of aminoborane from $Mg(NMe_2BH_2NMe_2BH_3)$. At higher temperatures ($25 - 100$ °C), the increased formation of **5.8** and $iPrNHC-BN$, and concomitant decrease in **5.10** was observed (Figure A2.94). Nuclear Overhauser effect spectroscopy (NOESY) confirmed direct chemical exchange between **5.8**, $iPrNHC-BN$ and **5.10**, and in the latter, through-space interactions between the carbene methine protons and borane hydrides support the presence of an $iPrNHC-BN$ coordination adduct (Figure A2.98). Furthermore, we probed the relative molecular masses of the species in solution through diffusion ordered spectroscopy (DOSY) experiments, and the smallest diffusion coefficient was observed for **5.10**, which is expectedly the heaviest molecule.

Given the relative stability of **II**, it is clear that the dynamic disproportionation of **5.9** via aminoborane migration is carbene-mediated. The thermodynamic impetus for disproportionation seems to be the formation of a stable ^{iPr}NHC-BN unit, and the kinetic production of **5.8** is likely driven by presence of Lewis acidic magnesium species due to ^{iPr}NHC-BN dissociation and subsequent base substitution reactions from the borane (Me₂N=BH₂) to the base-free magnesium species (Scheme 5.4). Manners previously realized that NHC-BH₂NRR' complexes, stabilized by 1,3-diaryl-substituted NHCs, are labile via spontaneous dissociation in solution or carbene transfer to Lewis acids (e.g. B(C₆F₅)₃).³⁰⁶ In the case for ^{iPr}NHC-BN, no dynamic dissociation was observed at variable temperatures (203 – 353 K), but substitution reactions with B(C₆F₅)₃ or Mg(HMDS)₂ was facile (Figure A2.78). Strong bases such as DMAP and triphenylphosphine do not form adducts with Me₂N=BH₂ in their reactions with **II** or [Me₂N-BH₂]₂. Notably, (DMAP)Mg(NMe₂BH₂NMe₂BH₃)₂ (**5.11**) was subsequently isolated (Scheme 5.3 and Figure 5.4b), and no dynamic processes were observed in solution.



Scheme 5.4. Proposed mechanism for the disproportionation of carbene-stabilized $RMg(NMe_2BH_2NMe_2BH_3)$ complexes.

The impact of Lewis acidic magnesium species in the dynamic disproportionation of **5.9** was further evaluated in substitution reactions with Lewis bases. The 1H NMR spectrum of **5.9** in $THF-d_8$ revealed only one set of carbenic resonances due to uncoordinated $iPrNHC-BN$, whereas the magnesium species are solvated. Additionally, the reaction of **5.9** and two equivalents of $iPrNHC$ enabled complete abstraction of $Me_2N=BH_2$ from $Mg(NMe_2BH_2NMe_2BH_3)$ units to yield **5.8** and $iPrNHC-BN$ (Figure 5.5), and quench dynamic exchange processes. The persistence of **5.8** instead of $(iPrNHC-BN)-Mg$ adducts suggest that $iPrNHC-BN$ is a weaker base than NHCs for the stabilization of magnesium bis(amidoboranes), although it may serve as a mediator for aminoborane migration. Importantly, these observations

suggest competitive Lewis acidities between $\text{Me}_2\text{N}=\text{BH}_2$ and base-free magnesium amidoboranes, which may promote dynamic acid/base exchange processes as described in Scheme 5.4B.

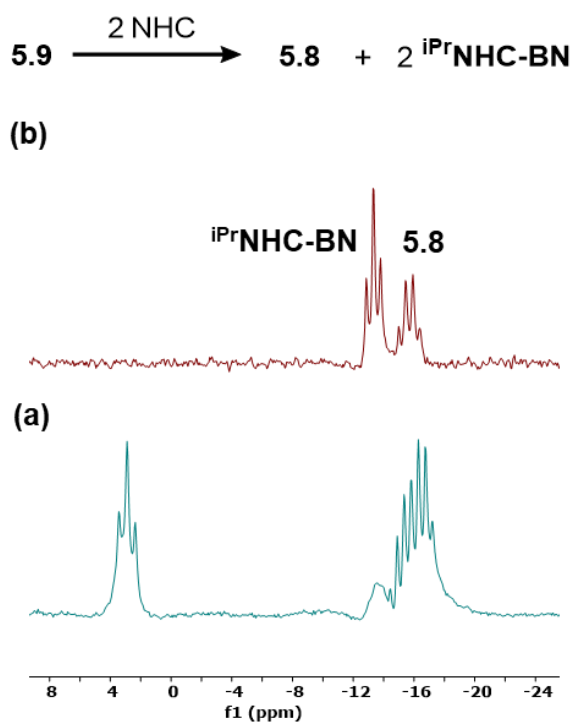
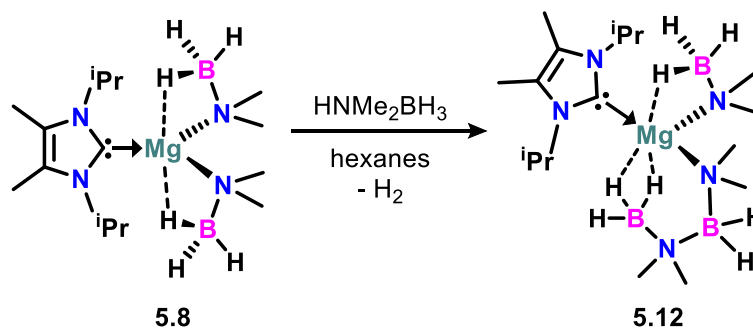


Figure 5.5. Stack plot of ^{11}B NMR spectra showing the presence of multiple species in **5.9** (a, bottom), and disappearance of $\text{Mg}(\text{NMe}_2\text{BH}_2\text{NMe}_2\text{BH}_3)$ units upon reaction with two equivalents of $^i\text{PrNHC}$ (b, top).

In these reactions, it is reasonable to expect $\text{Me}_2\text{N}=\text{BH}_2$ abstraction by the direct action of NHCs on $\text{Mg}(\text{NMe}_2\text{BH}_2\text{NMe}_2\text{BH}_3)$ units (Scheme 5.4D). However, the likelihood of varied charge localization in $^-\{\text{NMe}_2\text{BH}_2\text{NMe}_2\text{BH}_3\}$ supports spontaneous $\text{Me}_2\text{N}=\text{BH}_2$ elimination. The complex anion may be regarded as a donor-acceptor $(^-\text{NMe}_2\text{BH}_2\text{NMe}_2)(\text{BH}_3)$ adduct wherein BH_3 may be supported by either nitrogen base,^{292, 311} which permits the formation of $(^-\text{NMe}_2\text{BH}_3)$ and $\text{Me}_2\text{N}=\text{BH}_2$. In addition, β - and δ -BH elimination processes from $^-\{\text{NMe}_2\text{BH}_2\text{NMe}_2\text{BH}_3\}$ should be considered. The former yields $\text{HB}(\text{NMe}_2)_2$ and BH_3 or BH_4^- , which were not detected in **5.9** even at elevated temperatures, and the latter yields cyclic

tetramethylborazane ($[\text{Me}_2\text{N}-\text{BH}_2]_2$; t, 5.66 ppm, $^1J_{\text{BH}}$ 107.5 Hz), which was only observed above 100 °C in the VT ^{11}B NMR experiments, or partially accumulated during the sustained decomposition of **5.9** (65 °C, 16 h). However, the production of monomeric $\text{Me}_2\text{N}=\text{BH}_2$ is important to the dynamic processes because $^i\text{PrNHC}$ readily captures $\text{Me}_2\text{N}=\text{BH}_2$ at room temperature, but requires elevated temperatures (80 °C) to split the $[\text{Me}_2\text{N}-\text{BH}_2]_2$ dimer. Furthermore, metal hydride species due to unassisted β - or δ -BH elimination processes were not observed. A β -BH elimination in **5.8** should also yield $\text{Me}_2\text{N}=\text{BH}_2$, but this process is discounted by the compound's thermal stability in refluxing benzene (85 °C, 24 h) with no spectroscopic evidence of decomposition. Indeed, unassisted β - or δ -BH elimination from magnesium amidoboranes are known to be high energy processes,²⁹⁰ and unlikely to be predominant in the disproportionation of **5.9**.

In further efforts to elucidate some of the unobserved intermediates described in Scheme 5.4, we investigated the reaction of **5.8** and HNMe_2BH_3 , which yielded $(^i\text{PrNHC})\text{Mg}(\text{NMe}_2\text{BH}_3)(\text{NMe}_2\text{BH}_2\text{NMe}_2\text{BH}_3)$ (**5.12**) as a colorless crystalline solid (Scheme 5.5 and Figure 5/6). Owing to close Mg–H contacts from $\text{NMe}_2\text{BH}_2\text{NMe}_2\text{BH}_3$, the $^{\text{NHC}}\text{C}-\text{Mg}$ bond in **5.12** (2.2287(15) Å) is slightly elongated from **5.8** (2.2062(10) Å), and the geometry around the magnesium atom is modestly distorted from trigonal planar (sum of metal-ligand angles 354.9°). In contrast to **5.9** and **5.11**, the B–N bond distances within $\{\text{NMe}_2\text{BH}_2\text{NMe}_2\text{BH}_3\}$ in **5.12** are equivalent within standard deviation.



Scheme 5.5. Isolation of $(^i\text{PrNHC})\text{Mg}(\text{NMe}_2\text{BH}_3)(\text{NMe}_2\text{BH}_2\text{NMe}_2\text{BH}_3)$ (**5.12**).

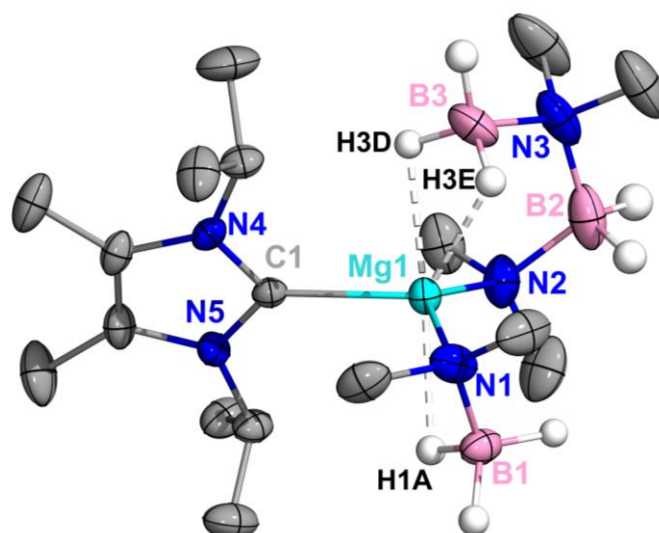


Figure 5.6. Molecular structure of **5.12**. H atoms are omitted for clarity, with the exception of B–H hydrides which were isotropically refined. Selected bond distances (Å) and angles (°): Mg1–C1, 2.2287(15); Mg1–N1, 2.0843(14); Mg1–N2, 2.1328(14); Mg1–H1A, 2.20(2); Mg1–H3D, 2.222(19); Mg1–H3E, 2.09(2); B1–N1, 1.512(3); B2–N2, 1.581(3); B3–N3, 1.574(3); N1–Mg1–C1, 107.28(6); N1–Mg1–N2, 132.89(7); H1A–Mg1–H3D, 168.4(7).

The isolation of **5.12** in the solid-state instead of (*i*PrNHC-BN)Mg(NMe₂BH₃)₂ contrasts the observed Me₂N=BH₂ capture at the ^{NHC}C–Mg bond in the formation of **5.2**, and indicates that small changes in the metal coordination environment [N(SiMe₃)₂ vs NMe₂BH₃] can substantially influence the nature of the thermodynamic product. As anticipated, **5.12** was not observed in solution, but is prone to the same dynamic processes observed for **5.9** (Scheme 5.4). Due to the heteroleptic nature of **5.12**, initial Schlenk type rearrangements in solution towards **5.8** and **5.9** cannot be discounted. Comparative dehydrocoupling reactions of **5.2** and HNMe₂BH₃ yielded (*i*PrNHC-BN)Mg(N(SiMe₃)₂)(NMe₂BH₂NMe₂BH₃) (**5.13**), and spectroscopic studies indicate disproportionation to **5.2**, **5.8**, **5.10**, and *i*PrNHC-BN, which likely involves Schlenk rearrangements (Figure A2.108).

5.5 Computational Studies

In order to gain additional insight into the aminoborane migratory coupling processes, density functional theory computations were performed at the ω B97X-D/cc-PVDZ level of theory.³¹²⁻³¹⁷ To minimize complications due to multiple metal-hydride interactions, only one amidoborane unit at the magnesium center was considered. Therefore, the conversion of **5.1** to **5.2** and **min-V** was selected as an appropriate thermodynamic model for the dehydrocoupling and migratory insertion processes (Figure 5.7). The corresponding electronic energies are described in Figure A4.8.

The metathetical reaction of **5.1** and HNMe_2BH_3 to form the mono-amidoborane (**int-1**) is exergonic by 8.2 kcal/mol. Subsequent amine borane dehydrogenation is anticipated to proceed via β -BH elimination processes that are unassisted (path A, black) or amine borane-assisted (path B, blue). In path A, an initial amidoborane rearrangement cleaves the Mg-N bond via **TS-2** in favor of hydride contacts in **int-2**. A formal hydride transfer to Mg incurs a $+13.0 \text{ kcal}\cdot\text{mol}^{-1}$ penalty in **TS-3**, but the resultant aminoborane remains coordinated to the metal center via BH contacts in **int-3**. The addition of a second HNMe_2BH_3 unit to **int-3** results in an $[\text{Mg}]\text{-H-H-NMe}_2\text{BH}_3$ species (**int-4**), which releases molecular H_2 towards the separated species $\text{LMg}(\text{NR}')(\text{NMe}_2\text{BH}_3) + \text{Me}_2\text{N}=\text{BH}_2$ (**int-5**).

Comparable unassisted β -hydride elimination has also been modelled in β -diketiminate magnesium systems,³¹⁸ and this mechanism is broadly accepted for rationalizing amine borane dehydrogenation at group 2 centers.²⁷⁰ However, recent studies have reconsidered the likelihood of this process.²⁹⁰ The anticipated metal-hydride intermediates were not observed in thermal studies of magnesium amidoboranes, and only identified in the presence of additional equivalents of amine borane. Therefore, an amine borane-assisted β -hydride elimination and dehydrocoupling rationale is increasingly adopted.^{288, 290}

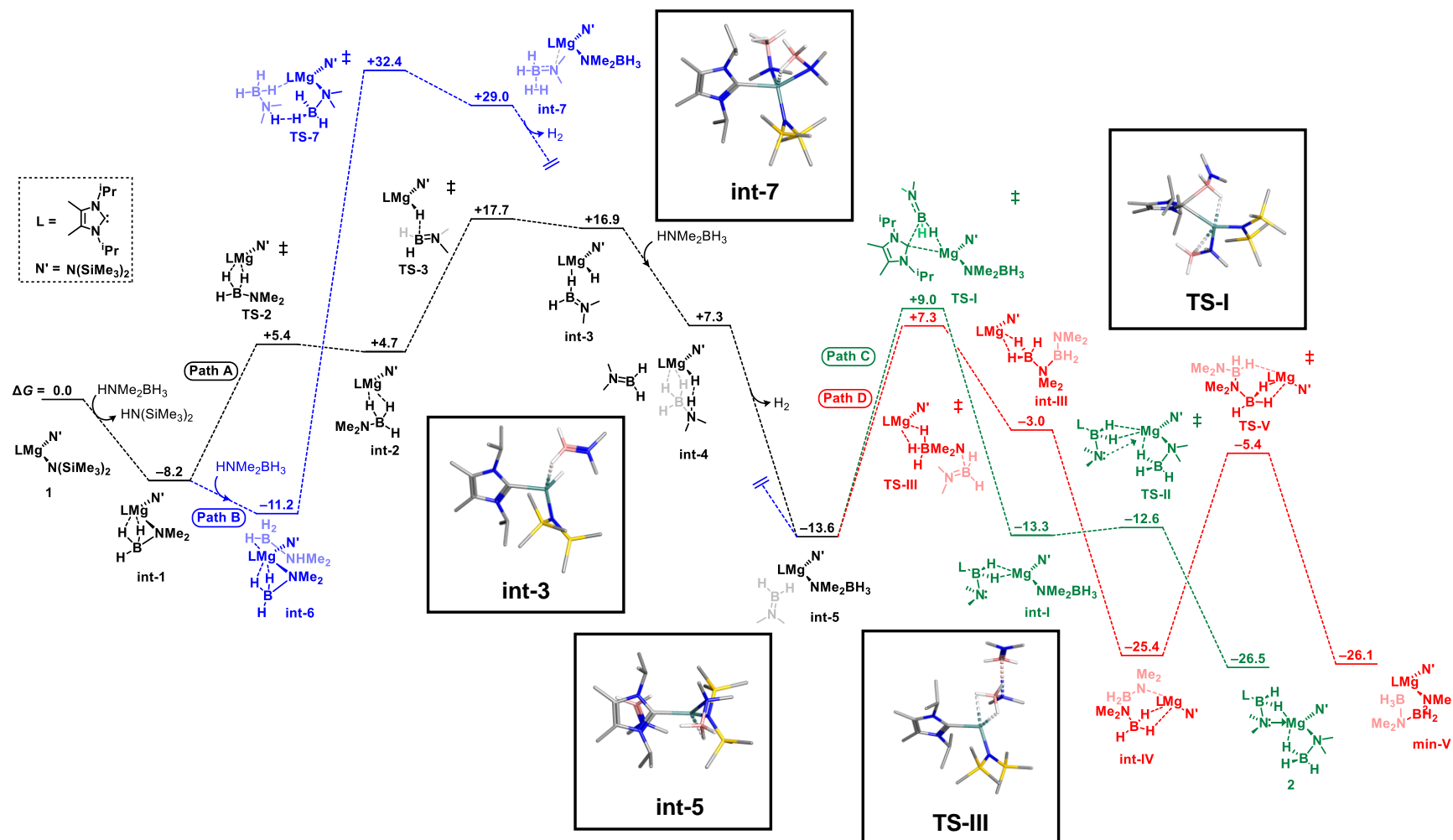


Figure 5.7. Calculated relative free energies (ΔG , $\text{kcal}\cdot\text{mol}^{-1}$) for the dehydrocoupling of **5.1** to **5.2** at the $\omega\text{B97X-D/cc-PVDZ}$ level of theory. Different models for H_2 elimination [path A (black) and path B (blue)] and $\text{Me}_2\text{N}=\text{BH}_2$ migratory coupling [path C (green) and path D (red)] were considered.

Path B (blue) provides a possible model for this process, beginning with an exergonic (+3.0 kcal/mol) coordination of HNMe₂BH₃ to the Mg center in **int-1** via hydride contacts (**int-6**). The interaction of amine proton and amidoborane hydride in **int-6** proceeds through a high energy transition state (**TS-7**, $\Delta\Delta G^\ddagger = +43.6 \text{ kcal}\cdot\text{mol}^{-1}$), resulting in **int-7**, which involves a loosely bound metal-aminoborane species with a σ -bound H₂ unit. Entropic release of molecular H₂ towards **int-5** ($\Delta\Delta G = -42.6 \text{ kcal}\cdot\text{mol}^{-1}$) is the thermodynamic driving force for this pathway, but the rate determining step (**TS-7**) suggests that it is less feasible than path A.

Following dehydrogenation, Me₂N=BH₂ coupling into the ^{NHC}C–Mg (path C, green) or Mg–N bond (path D, red) involves relatively low transformation energies. In path C, NHC migration from Mg to Me₂N=BH₂ (via **TS-I**, $\Delta\Delta G^\ddagger = +22.6 \text{ kcal}\cdot\text{mol}^{-1}$) forms a hydride-stabilized intermediate **int-I**. The formation of **5.2** through amide (:NMe₂–BH₂L) coordination to the Mg center is facile due to the low-lying nature of **TS-II** ($\Delta\Delta G^\ddagger = +0.7 \text{ kcal}\cdot\text{mol}^{-1}$). Notably, the free energy of dissociation of **5.2** into free ^{iPr}NHC–BN and Mg(N(SiMe₃)₂)(NMe₂BH₃) is +24.1 kcal·mol⁻¹ (Figure A4.7). In path D, the initial step (**TS-III**, +20.9 kcal·mol⁻¹) is comparable in energy to **TS-I** in path C and involves acid-base complexation of aminoborane and amidoborane to form **int-III**. In the latter, the ⁻{NMe₂BH₂NMe₂BH₃} anion is solely coordinated to Mg via BH₃, but subsequent amide coordination stabilizes the metal center to form **int-IV**. The local minimum **min-V** is structurally and thermodynamically comparable to **int-IV**, and results from further amide dissociation and rearrangement via **TS-V**. Although **min-V** was not observed in the solid state, there is ¹¹B NMR evidence for the rapid formation of the ⁻{NMe₂BH₂NMe₂BH₃} anion in the reaction of **5.1** and HNMe₂BH₃. The isolation of **5.12** also corroborates the accessibility of this pathway. Therefore, the low transformation energies between stationary points in paths C and D suggest that the thermal migratory coupling of Me₂N=BH₂ is feasible.

Compared to **min-V**, **5.2** is thermodynamically favored by $0.4 \text{ kcal}\cdot\text{mol}^{-1}$. In contrast to the **5.9** and **5.12** however, no dynamic aminoborane migration was experimentally observed for **5.2**. The facility of these processes for **5.9** and **5.12** may be due to the abundance of amidoborane units in their coordination sphere, whereby aminoborane coupling/decoupling results in bis(amidoborane) species capable of the same processes (i.e., **5.8** and **5.10**). Increased metal-hydride contacts in these bis(amidoborane) complexes may further stabilize their transition states for more facile transformations. The prevalence of stabilizing hydride contacts throughout the proposed mechanism is highlighted in selected stationary points in Figure A4.9. Indeed, the relative thermodynamic energies of **5.8–5.12** are partially correlated with the number of metal-hydride contacts and are in the order of $5.9 < 5.10 < 5.12 < 5.8$ (Figure 5.8). Additionally, Wiberg bond indices (WBI) and Mayer bond orders (MBO) support dissimilar N–B bond orders for the $\text{NMe}_2\text{BH}_2\text{NMe}_2\text{BH}_3$ anion (Table A4.3), as well as indicate significant bonding interactions between magnesium and amidoborane boron atoms (Table A4.4).

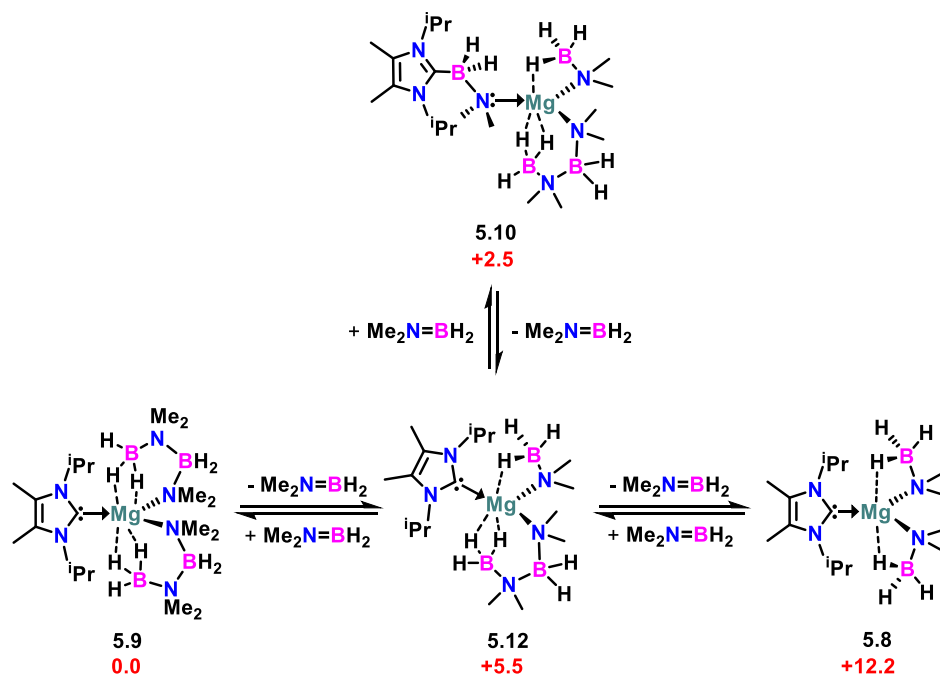


Figure 5.8. Relative free energies (ΔG , kcal·mol⁻¹) of aminoborane insertion/elimination between compounds **5.8**, **5.9**, **5.10**, and **5.12**.

5.6 Conclusion and Outlook

The dynamic migration of aminoborane units in the coordination sphere of magnesium has been investigated. It was determined that these dynamic processes are motivated by: (i) variable charge localization within $^{-}\{\text{NMe}_2\text{BH}_2\text{NMe}_2\text{BH}_3\}$, which results in the spontaneous elimination of $\text{Me}_2\text{N}=\text{BH}_2$; (ii) facile capture of $\text{Me}_2\text{N}=\text{BH}_2$ by NHC ligands, and thermodynamic stability of the subsequent $^{\text{iPr}}\text{NHC}-\text{BN}$ unit; (iii) and availability of base-free, Lewis acidic $\text{RMg}(\text{NMe}_2\text{BH}_3)$ units for an initial acid-base exchange with $^{\text{iPr}}\text{NHC}-\text{BN}$ to release $\text{Me}_2\text{N}=\text{BH}_2$, followed by aminoborane re-insertion into the $\text{Mg}-\text{N}$ bond. These processes are reminiscent of reversible 1,2-migratory insertion of unsaturated $2e^-$ ligands in transition metal chemistry, and to the best of our knowledge, unobserved in normal valent s -block element chemistry. Specifically, such NHC-mediated shuttling of aminoboranes at magnesium is anticipated to have significant implications for the development of reversible hydrogen storage materials based on magnesium amidoboranes.

Chapter Six: Carbene-Calcium Silylamides and Amidoboranes

Containing work that was originally published in:

Obi, A. D.; Freeman, L. A.; Coates, S.J.; Alexis, A.J.H.; Frey, N. C.; Dickie, D. A.; Webster, C. E.; Gilliard, R. J., Carbene-Calcium Silylamides and Amidoboranes. *Submitted*.

6.1 Overview of Calcium Bis(silylamide) Organometallic Chemistry

Recent advances in the organometallic chemistry of calcium have revitalized interest in the utility of this environmentally benign element for energy-relevant chemical transformations.^{2, 3, 16, 38, 99, 319} The potency of calcium is due in part to its central position among the alkaline earth elements, whereby the Ca^{2+} cation maintains high Lewis acidity (germane to the lighter elements Mg and Be) as well as enhanced Ca–R nucleophilicity (R = organic group) because of its high electropositivity and large ionic size.¹⁶ However, the development of organocalcium reagents is complicated by their poor kinetic stability due to weak metal-ligand bonds.^{49, 52, 320, 321} Degradation pathways such as Schlenk equilibrium, ether activation, and Wurtz coupling are much more pronounced in R_2Ca and RCaX complexes than in analogous magnesium and beryllium complexes.^{46, 49} To mitigate these challenges, the syntheses of simple organocalcium compounds often require specialized reagents, low temperatures, donor solvents, or even mechanochemical methods (e.g., ball milling).^{46, 62, 320, 322-324}

The landmark synthesis of $(\text{diox})_2\text{Ca}(\text{CH}(\text{SiMe}_3)_2)_2$ by Lappert *et al.*³²⁵ inspired subsequent exploitation of steric and electromeric effects of lipophilic silylalkyls towards ether-stable, hydrocarbon soluble and highly reactive calcium alkyls and amides,³²⁶⁻³³³ including the versatile calcium bis(trimethylsilyl)amide $[\text{Ca}(\text{N}(\text{SiMe}_3)_2)_2]$.³²⁴ Due to its ease of synthesis, high solubility, stability, and diverse reactivities, $\text{Ca}(\text{N}(\text{SiMe}_3)_2)_2$ has become the quintessential candidate for controlled investigations of calcium coordination chemistry. As a synthon, $\text{Ca}(\text{N}(\text{SiMe}_3)_2)_2$ has enabled access to diverse organocalcium reagents,³³⁴ including the modestly ether-stable dimethylcalcium whose difficult synthesis and purification puzzled organometallic chemists for more than six decades.⁵² Notably, Harder and coworkers realized that the silylamide group sufficiently stabilizes highly reducing calcium hydride clusters,³³⁵ which partially rationalizes the

high activity of $\text{Ca}(\text{N}(\text{SiMe}_3)_2)_2$ for catalytic hydrogenation,⁸²⁻⁸⁴ hydroelementation,^{336, 337} and dehydrocoupling reactions.^{3, 270, 338}

The rich coordination chemistry of $\text{Ca}(\text{N}(\text{SiMe}_3)_2)_2$ and its derivatives has been extensively studied using multidentate anionic spectator ligands (e.g., β -diketiminates), with illuminating insights into their bonding and reactivities.^{56, 61, 64, 333, 339-343} This kinetic stabilization strategy has also been extended towards the isolation of highly reactive molecular calcium hydrides,^{38, 70} alkyls,^{68, 188} aryls,³⁴⁴ and low-valent complexes.³⁰ Effective neutral donor ligands for comparative investigations are typically multidentate,^{88, 92, 93, 345} whereas monodentate bases are prone to dynamic dissociation and redistribution, which can be detrimental to the stability of organocalcium complexes.^{327, 346, 347} This is especially problematic for carbon-based donors such as N-heterocyclic carbenes (NHCs) and cyclic (alkyl)(amino) carbenes (CAACs), whose electronic flexibility (i.e., tunable σ -donor/ π -acceptor character) have resulted in new discoveries of fundamental bonding situations at beryllium and magnesium (e.g., low oxidation states, multiple bonding),^{26, 28, 39-41, 99, 100, 106, 170, 171, 348} but underexplored at calcium due to their significantly more challenging coordination chemistry.^{121, 347, 349} Considering the burgeoning influence of cyclic carbenes in group 2 chemistry,⁹⁸ it is pertinent to reconsider carbene-stabilization strategies at calcium by investigating their stereoelectronic effects at calcium silylamides.

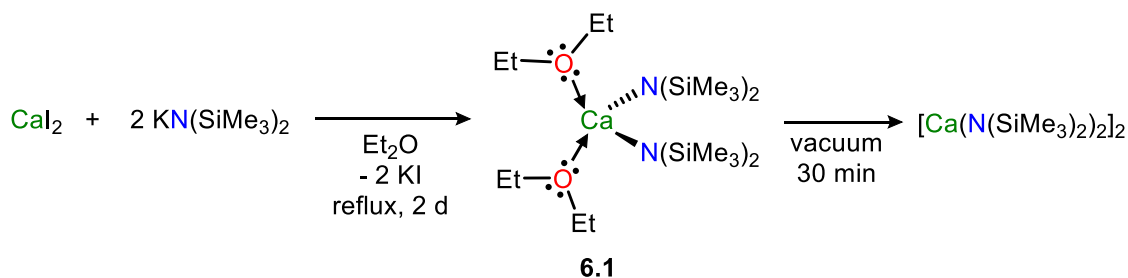
In previous efforts, we realized that dynamic electronic stabilization due to multiple sterically unencumbered NHCs at magnesium is often more beneficial than kinetic stabilization using bulkier NHCs.^{107-109, 173, 174, 303} Although the same strategy has not been elaborated at calcium, it was found that calcium silylalkyls and silylamides stabilized by two unencumbered NHCs are catalytically relevant,^{102, 103} whereas bulkier carbenes are prone to deleterious dissociation.^{121, 347, 349} Herein, we detail the syntheses and structural studies of a series of NHC- and CAAC-

coordinated calcium amides, and highlight marked disparities in their coordination chemistry due to steric, electronic and solvent effects. Further attempts to isolate catalytically-relevant carbene calcium hydrides were thwarted by their instability and high reactivity. However, the influence of carbenes in secondary calcium-hydride interactions were investigated using calcium amidoboranes, whereby unencumbered NHCs mediate the abstraction and migratory transfer of aminoborane ($\text{Me}_2\text{N}=\text{BH}_2$) towards a hydride-enriched calcium amidoborane complex.

6.2 Assessment of Steric and Solvent Effects in Carbene-Stabilized Silylamides.

The reaction of CaI_2 and two equivalents of $\text{K}(\text{HMDS})$ [HMDS = hexamethyldisilazide or $\text{N}(\text{SiMe}_3)_2$] in refluxing Et_2O , followed by removal of solvent in vacuo, and extraction into hexanes yielded the *bis*-ether-coordinated product $(\text{Et}_2\text{O})_2\text{Ca}(\text{HMDS})_2$ (**6.1**, Scheme 6.1).³⁵⁰ Colorless, single crystals of **6.1** were obtained from a concentrated hexanes solution at -37°C , and the molecular structure was confirmed by X-ray diffraction studies as the anticipated monomeric, tetracoordinate complex (Figure A3.35). Evacuation of the crystalline material afforded analytically pure $[\text{Ca}(\text{HMDS})_2]_2$ in 72% yield. The initial isolation of **6.1** minimizes the competitive formation of “-ate” complexes in the synthesis of $[\text{Ca}(\text{HMDS})_2]_2$,^{52, 351} and contrasts conventional strategies which require specialized reagents (e.g., $(\text{THF})\text{Ca}(\text{CH}_2\text{Ph})_2$) or strongly donating solvents (e.g., THF, dioxane) to ensure high purity material as Lewis-base adducts.^{324, 352}

Scheme 6.1. Synthesis of $(\text{Et}_2\text{O})_2\text{Ca}(\text{HMDS})_2$ (**6.1**)

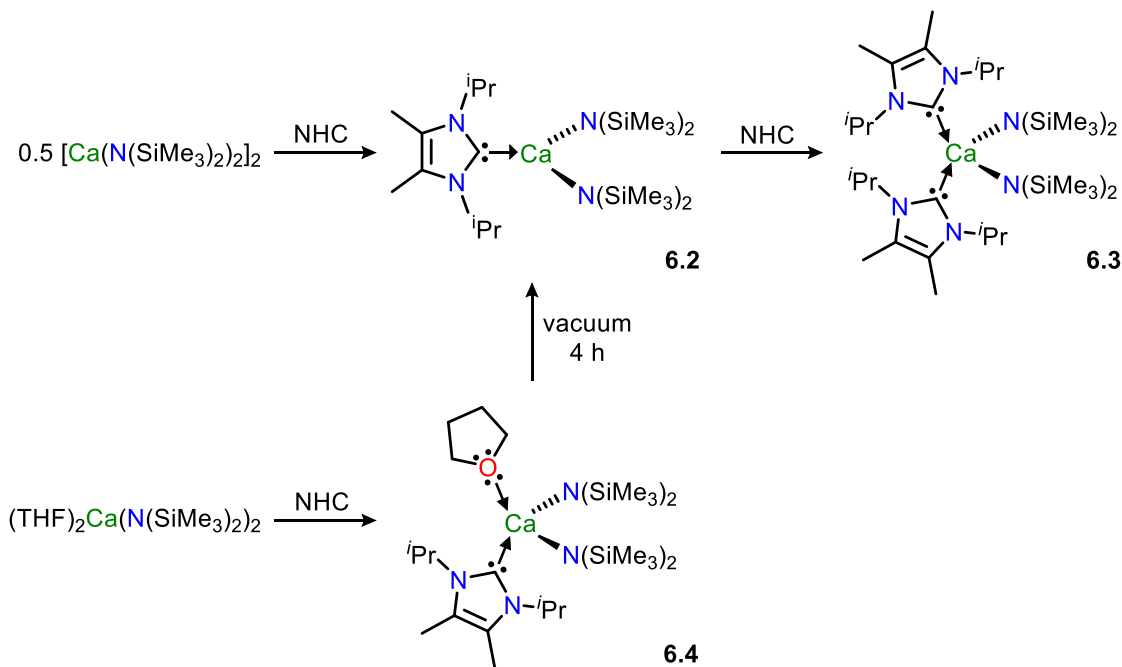


Hill and coworkers initially realized that bulky NHCs coordinate weakly to $\text{Ca}(\text{HMDS})_2$, whereby the ligand is labile in the presence of competitive donor solvents or bases (e.g., THF or $\text{O}=\text{PPh}_3$), and under catalytically-relevant conditions.³⁴⁷ However, Trifonov recently discovered that the coordination of two unencumbered NHCs to $(\text{THF})_2\text{Ca}(\text{HMDS})_2$ yielded highly active catalysts for chemoselective hydrophosphinations.¹⁰² The same bis(NHC)-stabilization strategy was successful for the catalytic cross-dehydrocoupling of amines and silanes using calcium silylalkyls.¹⁰³ We suspect that two NHCs were necessary to displace coordinated THF molecules in the starting material, and ensure persistent ligand coordination under catalytic conditions. Indeed, donor solvents can dramatically influence the electronics of alkaline earth centers stabilized by NHC ligands, as our laboratory and others have observed.^{107-109, 174, 303, 347} Therefore, upon isolation of **6.1**, we realized an opportunity to explicate the influence of solvation (or lack thereof) in the coordination chemistry of $\text{Ca}(\text{HMDS})_2$ and sterically unhindered NHCs.

The reaction of equimolar amounts of *N,N'*-diisopropyl-2,3-dimethylimidazol-2-ylidene and **6.1** or $\text{Ca}(\text{HMDS})_2$ in hexanes afforded the solvent-free carbene-metal complex $(\text{NHC})\text{Ca}(\text{HMDS})_2$ (**6.2**) as a crystalline white solid in 95% yield (Scheme 6.2). The 1:1 ratio of carbene to calcium was confirmed by the relative integration of carbene and silylamide resonances in the ^1H NMR spectrum, and the carbene methine resonance ($\delta_{\text{H}} = 4.20$ ppm) is slightly downfield from that of the bis(NHC) adduct (**6.3**, $\delta_{\text{H}} = 4.06$ ppm) previously reported by Trifonov.¹⁰² In contrast, the reaction of the solvated adduct $(\text{THF})_2\text{Ca}(\text{HMDS})_2$ and one equivalent of NHC yielded the mixed donor complex $(\text{NHC})(\text{THF})\text{Ca}(\text{HMDS})_2$ (**6.4**) as a hexanes-soluble, off-white solid. The ^1H NMR spectrum of **4** revealed a 1:1:2 ratio of THF, NHC and HMDS resonances, but the THF resonances of **4** ($\delta_{\text{H}} = 3.58, 1.37$ ppm) are not distinct from those of uncoordinated THF ($\delta_{\text{H}} = 3.57, 1.40$ ppm). Furthermore, the carbene resonances of **6.4** are broadened and the methine peak ($\delta_{\text{H}} = 4.22$ ppm)

is comparable to that of **6.2** ($\delta_{\text{H}} = 4.20$ ppm), suggesting that the electronic influence of THF coordination in **6.4** is likely negligible. Indeed, prolonged evacuation of **6.4** (RT, 4 h) under high vacuum cleanly affords **6.2**.

Scheme 6.2. Synthesis of N-heterocyclic carbene-stabilized calcium silylamides (6.2-6.4)



Colorless, single crystals of **6.2** and **6.4** were obtained from their respective hexanes solutions at -39 °C, and their molecular structures were unambiguously determined by X-ray diffraction (Figure 6.1). Complex **6.2** is a mononuclear tricoordinate calcium compound ligated by one NHC and two silylamide ligands. The additional coordination of THF in **6.4** resulted in a tetrahedral arrangement and metrical distortions towards elongated NHC-Ca and $\text{Ca-N}^{\text{amide}}$ bonds from those of **6.2** (see Figure 6.1 caption). The NHC-Ca bond in **6.2** ($2.547(6)$ Å) is significantly shortened from that of the isostructural $(\text{IPr})\text{Ca}(\text{HMDS})_2$ ($2.6285(16)$ Å; $\text{IPr} = 1,3\text{-bis}(2,6\text{-diisopropylphenyl})\text{imidazol-2-ylidene}$), indicating that reduced ligand bulk is beneficial for a more persistent carbene coordination. Among the tetrahedral complexes, the NHC-Ca bond in **6.4** ($2.617(2)$ Å) is expectedly shorter than those of **6.3** ($2.658(7)$ and $2.671(7)$ Å),¹⁰² which highlights

the pronounced donor effect of a second unencumbered NHC ligand on the Lewis acidity of the calcium center.

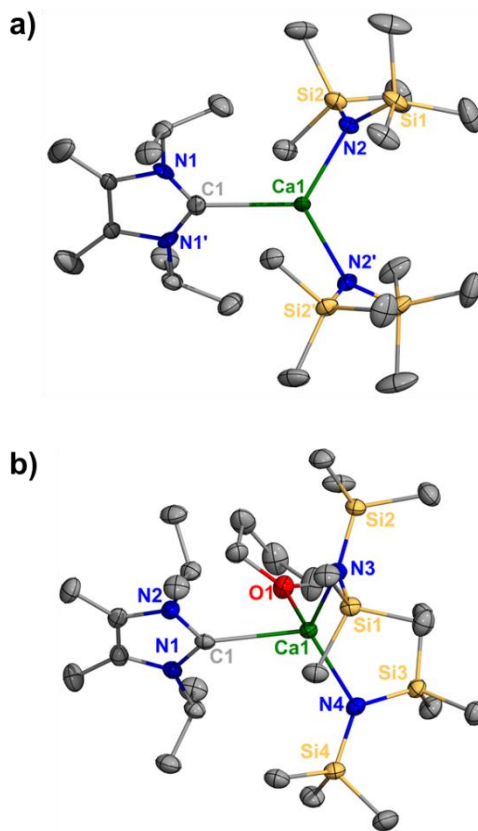


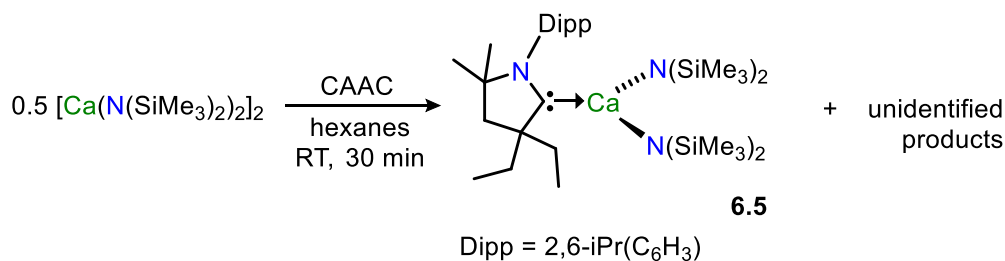
Figure 6.1. Molecular structures of **6.2** (a) and **6.4** (b). Thermal ellipsoids shown at 50% probability and H atoms omitted for clarity. Selected bond distances (Å) and angles (°): **6.2**: Ca1–N2: 2.280(3); Ca1–C1: 2.547(6); N1–C1: 1.350(7); N2–Ca1–N2: 122.3(2); N2–Ca1–C1: 118.83(12); N1–C1–N1: 113.9(6). **6.4**: Ca1–N4: 2.3239(19); Ca1–N3: 2.3482(18); Ca1–O1: 2.4294(17); Ca1–C1: 2.617(2); N1–C1: 1.364(3); N1–C2: 1.392(3); N4–Ca1–N3: 122.22(7); N4–Ca1–O1: 107.10(6); N4–Ca1–C1: 115.07(7); O1–Ca1–C1: 79.57(6).

6.3 Isolation of a cyclic (alkyl)(amino) carbene Calcium Complex

In contrast to the facile and high-yielding synthesis of NHC–Ca amides, the cyclic (alkyl)(amino) carbene (CAAC) adducts have remained elusive. Turner *et al.* reported that while

the preparation of (CAAC)Ae(HMDS)₂ was nearly quantitative for Ae = Mg, Sr and Ba, attempts to prepare the calcium analogue led to “intractable mixtures of products.”¹²¹ We similarly observed that the reaction of crystalline samples of CAAC and Ca(HMDS)₂ in equimolar amounts yielded multiple unidentified products in the crude mixture (Scheme 6.3 and Figure A2.117). Fortunately, recrystallization of this mixture from a saturated hexanes solution at –39 °C produced a few single crystals identified by X-ray diffraction studies as the desired coordination complex (CAAC)Ca(HMDS)₂ (**6.5**), which is to date, the first isolable CAAC–Ca complex (Figure 6.2). The ^{CAAC}C–Ca bond in **6.5** (2.700(5) Å) is much longer than those of the tricoordinate NHC complexes **6.2** (2.547(6) Å) and (IPr)Ca(HMDS)₂ (2.6285(16) Å). This disparity does not significantly influence the Ca–N^{amide} bonds, which are comparable for all the tricoordinate (carbene)Ca(HMDS)₂ complexes.

Scheme 6.3. Synthesis of CAAC-coordinated calcium amide 6.5



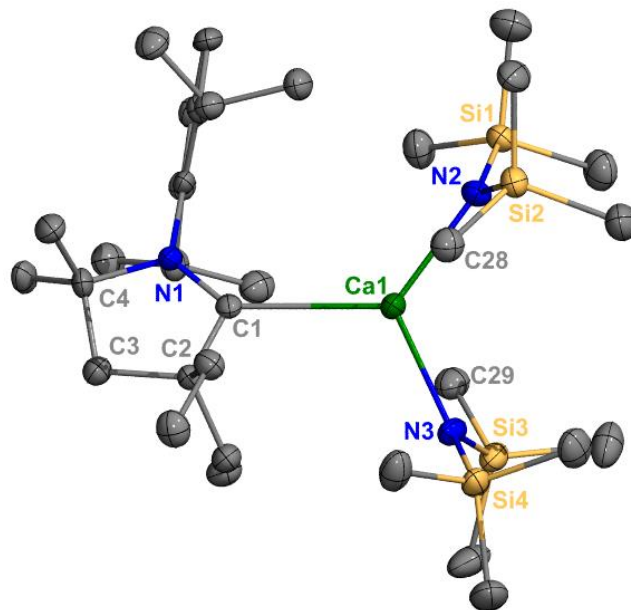


Figure 6.2. Molecular structure of **6.5**. Thermal ellipsoids shown at 50% and H atoms omitted for clarity. Only one of two crystallographically unique but chemically equivalent molecules in the unit cell is shown. Selected bond distances (Å) and angles (°): Ca1-C1: 2.700(5); Ca1-N2: 2.296(4); Ca1-N3: 2.321(4); C1-N1: 1.308(6); C1-C2: 1.512(7); N2-Ca1-C1: 126.31(15); N3-Ca1-C1: 115.35(15); N3-Ca1-N2: 118.10(16).

In an effort to minimize decomposition pathways in the formation of **6.5**, we attempted *in-situ* CAAC generation in the reaction of $\text{Ca}(\text{HMDS})_2$ and the CAAC aldiminium salt in a 2:1 ratio, but the observed products were spectroscopically identical to the direct complexation reaction. Conversely, the reaction of $\text{Ca}(\text{HMDS})_2$ and the carboxylate zwitterion CAAC-CO_2^{353} resulted in a quantitative liberation of free CAAC (assessed by ^1H NMR spectroscopy), and no carbene or carbene-carboxylate adducts of calcium were identified (Figure A2.118). The net reaction of $\text{Ca}(\text{HMDS})_2$ and CO_2 is assumed,³⁵⁴ and while the products remain unidentified, the subsequent calcium species clearly does not complex or degrade CAAC. The rapid decomposition of **6.5** is

therefore indicative of the high reactivity of $\text{Ca}(\text{HMDS})_2$ in the presence of electrophilic carbenes such as CAAC.

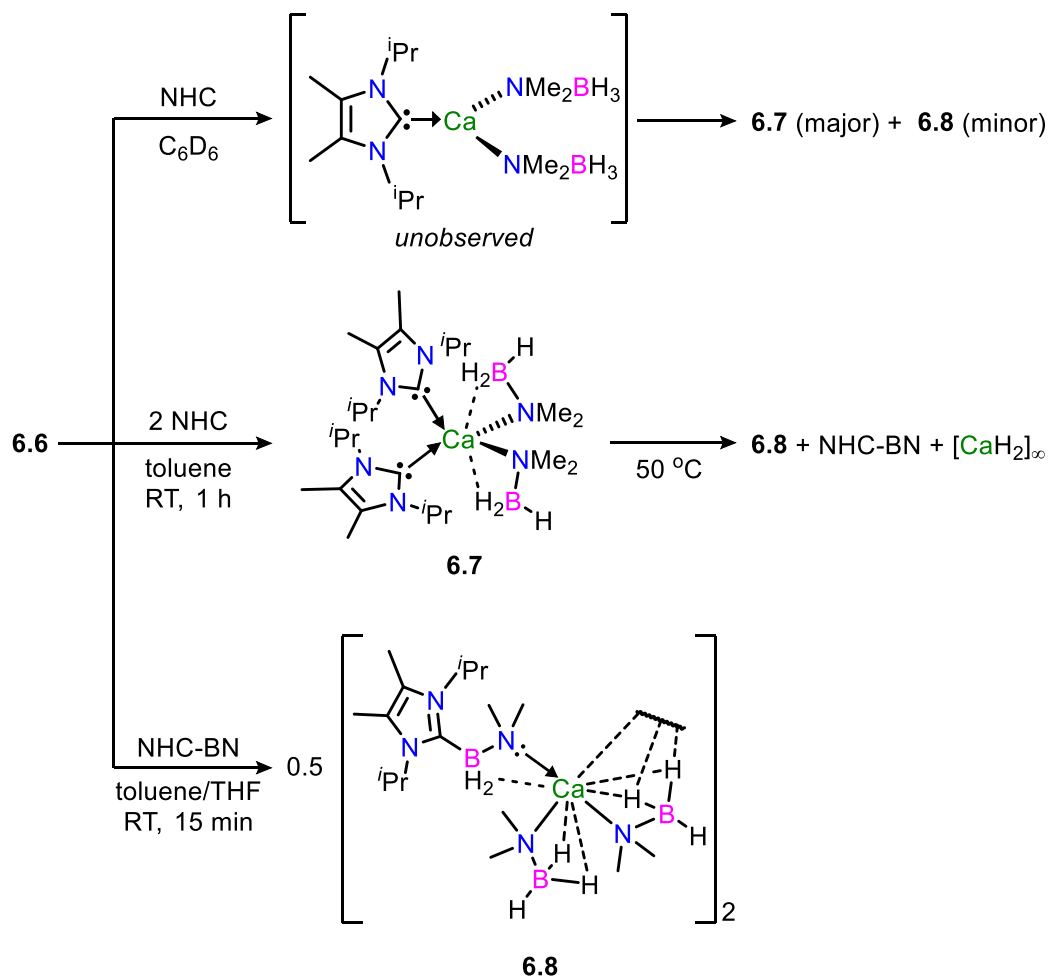
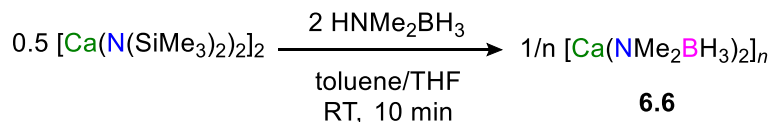
6.4 Involvement of Carbenes in Calcium-mediated Amine Borane Dehydrocoupling

Having realized that smaller NHCs are more suitable than larger carbenes for the stabilization of calcium amides, we were interested in their ability to stabilize calcium-based reducing agents such as hydrides and amidoboranes. Compound **6.2** readily reacts with PhSiH_3 under ambient conditions, but attempts at isolating the putative calcium hydride product have been unsuccessful. Therefore, we focused our attention on amidoboranes in an effort to evaluate the influence of carbene coordination on secondary calcium-hydride interactions. Notably, the parent calcium amidoborane $\text{Ca}(\text{NH}_2\text{BH}_3)_2$ has been identified as a potent hydrogen storage material, releasing about 90% of the anticipated H_2 weight percent at 170 °C.^{275, 280} As a result, there has been increased interest in understanding molecular processes relevant to hydrogen release from calcium amidoboranes.^{55, 270, 290, 293}

The reaction of $\text{Ca}(\text{HMDS})_2$ and two equivalents of dimethylamine borane in a THF/toluene mixture afforded solvent-free $\text{Ca}(\text{NMe}_2\text{BH}_3)_2$ (**6.6**) as a white solid in 93% yield after workup (Scheme 6.4). Efforts to isolate single crystals of **6.6** for structural determination were unsuccessful, but its elemental composition and purity are supported by heteronuclear NMR spectroscopy (^1H , ^{13}C , ^{11}B) and combustion microanalysis. The subsequent reaction of **6.6** and two equivalents of NHC in toluene afforded $(\text{NHC})_2\text{Ca}(\text{NMe}_2\text{BH}_3)_2$ (**6.7**) in 86% yield (Scheme 6.4). Notably, compound **6.6** does not react with IPr, presumably due to steric complications. Attempts to complex only one equivalent of the small NHC preferentially afforded **6.7**, as well as minor amounts of the amidoborane enriched complex $[(\text{NHC-BN})\text{Ca}(\text{NMe}_2\text{BH}_3)_2]_2$ (**6.8**, $\text{NHC-BN} = \text{NHC-BH}_2\text{NMe}_2$). The formation of **6.8** is presumably due to β -BH elimination from $\text{Ca}(\text{NMe}_2\text{BH}_3)$ and capture of the subsequent $\text{Me}_2\text{N}=\text{BH}_2$ unit by the NHC ligand. Evidence for

this process is found in the gentle (50 °C, 16 h) or rapid (80 °C, 5 h) thermal decomposition of **6.7** to **6.8**, $[\text{CaH}_2]_n$ and free NHC-BN. The subsequent reaction of **6.6** and NHC-BN¹⁰⁵ afforded **6.8** as a colorless solid in 73% crystalline yield. In contrast to **6.7**, compound **6.8** is stable in refluxing benzene (85 °C, 24 h) with no spectroscopic evidence of decomposition. Under similar conditions, **6.6** decomposes to $\text{HB}(\text{NMe}_2)_2$ and $[\text{CaH}_2]_n$ predominantly, albeit more sluggish than **6.7**. Therefore in addition to a metal-mediated β -BH elimination in the decomposition of **6.7**, NHC dissociation and abstraction of $\text{Me}_2\text{N}=\text{BH}_2$ from a $\text{Ca}(\text{NMe}_2\text{BH}_3)$ unit is also anticipated. This process is reminiscent of phosphine-mediated borane abstraction from beryllium borohydride in the synthesis of highly pure $[\text{BeH}_2]_n$,³⁵⁵ or NHC-mediated alane abstraction from LiAlH_4 in the synthesis of NHC-alane adducts.^{356, 357} Hence, a likewise process for the decomposition of NHC-stabilized calcium amidoboranes is plausible.

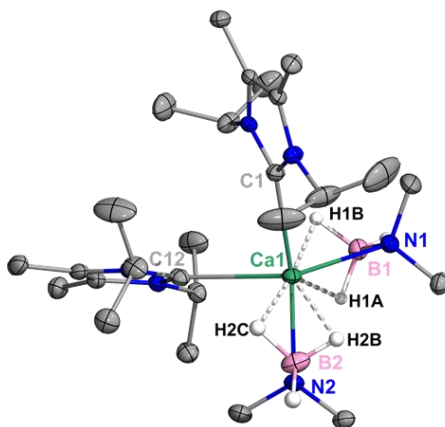
Scheme 6.4. Isolation and decomposition of an N-heterocyclic carbene-stabilized calcium amidoborane



The solid-state structures of **6.7** and **6.8** (Figure 6.3) were confirmed by X-ray crystallography on single crystals obtained from their respective saturated toluene solutions. Compound **6.7** is a monomeric, tetracoordinate calcium complex with four secondary Ca–H contacts (range 2.45(2) – 2.61(3) Å) from the boranes. The ^{NHC}C–Ca (2.631(2) Å and 2.672(3) Å) bonds are comparable to those of the bis(NHC) calcium silylamide **6.3**,¹⁰² and the Ca–N^{amide} bonds (2.4445(19) Å and 2.4492(17) Å) are within the highly diverse range of calcium-amidoborane contacts (2.069(7) – 2.582(2) Å).²⁷⁰ In the case for **6.8**, the absence of a second stabilizing Lewis base led to the

formation of a dimeric complex with up to eight Ca–H contacts (range 2.464(15) – 2.763(15) Å) per calcium atom. The hydride contacts in **6.8** are reminiscent of those of polymeric $[(\text{THF})_2\text{Ca}(\text{NH}_2\text{BH}_3)_2]_n$, whereby the combined protic ($\text{Ca}\cdots\text{HN}$) and hydridic ($\text{Ca}\cdots\text{HB}$) contacts similarly form “ CaH_8 ” units.²⁷⁵ Notably, a small amount of THF is required to ensure complete dissolution of **6.8** in non-polar solvents (e.g., benzene, toluene, hexanes), but the dimeric complex was repeatedly crystallized from these solutions without THF coordination. It is therefore assumed that the high thermal stability of **6.8** is due in part to thermodynamic stabilization from intermolecular Ca–H–B bonding interactions. Indeed, density functional theory (DFT) calculations ($\omega\text{B97X-D/cc-pVDZ}$ level of theory)³¹²⁻³¹⁷ corroborate a substantial thermodynamic stabilization due to dimerization ($\Delta G = -34.9$ kcal/mol).

a)



b)

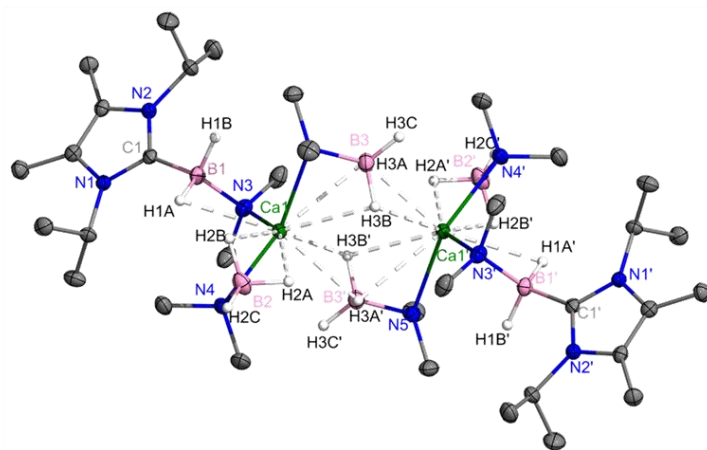
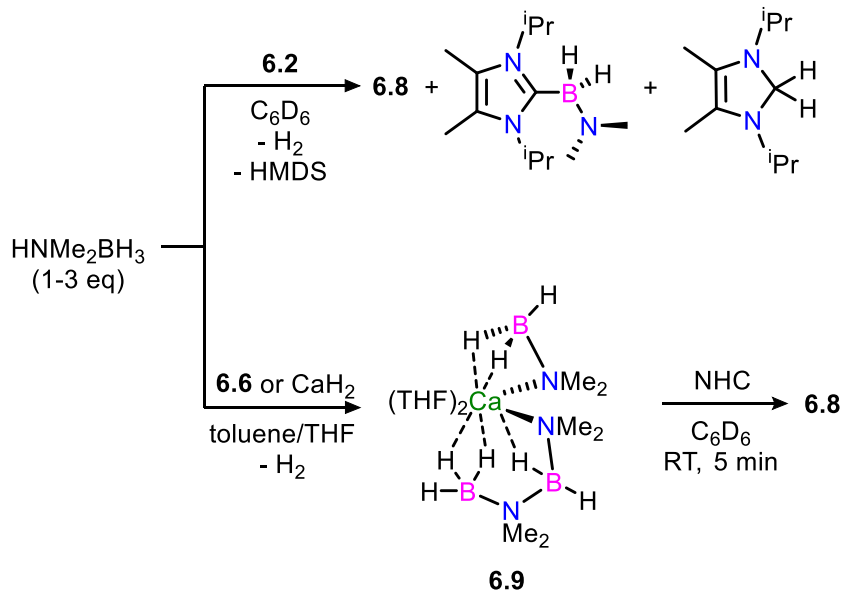


Figure 6.3. Molecular structures of **6.7** (a) and **6.8** (b). H atoms omitted for clarity, except for B–H hydrides, which were isotropically refined. Only one of two crystallographically unique but chemically equivalent molecules in the unit cell of **6.7** is shown. Selected bond distances (Å) and angles (°): **6.7**: Ca1–C1: 2.631(2); Ca1–C12: 2.672(3); Ca1–N1: 2.4445(19); Ca1–N2: 2.4492(17); B1–N1: 1.551(3); B2–N2: 1.539(3); N1–Ca1–N2: 108.29(6); C1–Ca1–N2: 145.71(6); C1–Ca1–C12: 90.33(6); H1B–Ca1–H2C: 174.2(9). **6.8**: Ca1–N3: 2.4788(12); Ca1–N4: 2.4654(12); Ca1–N5: 2.5105(11); Ca1–H1A: 2.672(14); Ca1–H1B: 2.681(15); Ca1–H2A: 2.464(15); Ca1–H2B: 2.476(16); Ca1–H3D: 2.559(15); Ca1–H3E: 2.763(15); B1–N3: 1.5532(18); B1–C1: 1.6289(19); B2–N4: 1.550(2); B3–N5: 1.5388(19); N4–Ca1–N3: 104.95(4); N4–Ca1–N4: 133.16(4); N5–Ca1–N3: 108.46(4).

To further probe the influence of NHCs in calcium-mediated amine borane dehydrocoupling, we investigated reactions of **6.2–6.4** and stoichiometric amounts of HNMe_2BH_3 (Scheme 6.5). The formation of **6.8** was observed in all cases and regardless of the equivalents (1–3) of HNMe_2BH_3 added, while **6.7** was unobserved. The absence of **6.7** support the rapid capture of the dehydrogenation product $\text{Me}_2\text{N}=\text{BH}_2$ by NHC ligands, without which dimerization to $[\text{Me}_2\text{N}-\text{BH}_2]_2$ or dehydrocoupling to $\text{RCa}(\text{NMe}_2\text{BH}_2\text{NMe}_2\text{BH}_3)$ is anticipated.^{55, 290, 296} Competitive dehydrogenation due to dissociated carbene ligands was also observed, leading to the formation of the hydrogenated aminal $\text{NHC}-\text{H}_2$ and free $\text{NHC}-\text{BN}$ in agreement with previous reports of carbene-mediated amine borane dehydrogenation.³⁰⁴⁻³⁰⁶

Scheme 6.5. Aminoborane capture at N-heterocyclic carbene-stabilized calcium amides



To prevent these competitive processes, reactions of **6.6** or $[\text{CaH}_2]_n$ and HNMe_2BH_3 were performed, with the goal of isolating the heteroleptic bis(amidoborane) $(\text{THF})_2\text{Ca}(\text{NMe}_2\text{BH}_3)(\text{NMe}_2\text{BH}_2\text{NMe}_2\text{BH}_3)$ (**6.9**, Scheme 6.5). Despite prolonged reaction times, full conversion of **6.6** to **6.9** was never achieved, and due to their comparable solubilities, **6.9** could not be completely separated from **6.6**. However, the molecular structure of **6.9** was confirmed by single-crystal X-ray diffraction (Figure 6.4), and the ^{11}B NMR spectrum features expected resonances for the $\text{NMe}_2\text{BH}_2\text{NMe}_2\text{BH}_3$ anion (Figure A2.128). The addition of one equivalent of NHC to a C_6D_6 solution of **6.9** at room temperature resulted in the rapid (< 10 min) and quantitative conversion to **6.8**. DFT calculations ($\omega\text{B97X-D/cc-pVDZ}$ level of theory) suggest that aminoborane migration from **6.9** is facile and dynamic ($\Delta\text{G} = +3.5$ kcal/mol for $\text{Me}_2\text{N}=\text{BH}_2$ elimination), and subsequent NHC-mediated capture of $\text{Me}_2\text{N}=\text{BH}_2$ towards the formation of **6.8** is highly exergonic ($\Delta\text{G} = -31.5$ kcal/mol, Figure A4.12). We recently observed that the comparative aminoborane migration in NHC-magnesium systems is reversible due to dynamic carbene transfer between Lewis acidic magnesium centers and aminoborane.¹⁰⁵ Conversely, $\text{Me}_2\text{N}=\text{BH}_2$ migration in the transformation of **6.9** to **6.8** is not reversible due to the poorer Lewis

acidity of Ca^{2+} (compared to Mg^{2+}), as well as the substantial stabilization influence of hydride contacts in **6.8**.

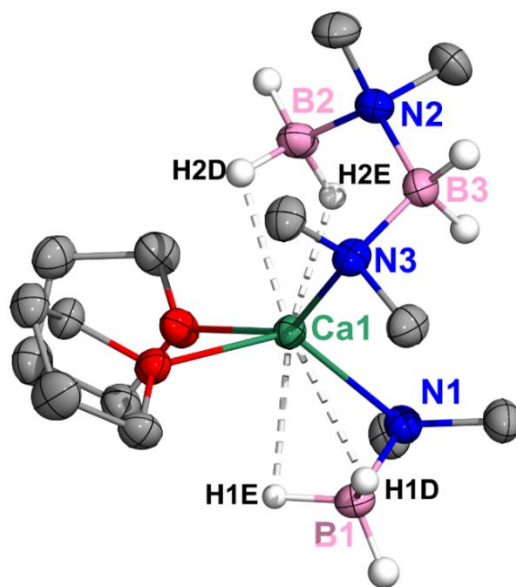


Figure 6.4. Molecular structure of **6.9**. H atoms omitted for clarity, except for B–H hydrides which were isotropically refined. Only one of two crystallographically independent but chemically equivalent molecules in the asymmetric unit is represented. Only major positions for disordered atoms are shown. Selected bond distances (Å) and angles (°): Ca1–N1: 2.4166(19); Ca1–N3: 2.4733(18); Ca1–H1D: 2.53(3); Ca1–H1E: 2.46(2); Ca1–H2D: 2.42(3); Ca1–H2E: 2.35(2); B1–N1: 1.540(3); B2–N2: 1.574(3); B2–N3: 1.602(3); B3–N3: 1.566(3); N1–Ca1–N3: 113.35(6); H2D–Ca1–H1D: 155.5(9); H1E–Ca1–H2E: 135.5(8).

6.5 Conclusion and Outlook

Comparative investigations of NHC- and CAAC-stabilized calcium amides reveal that sterically unencumbered NHCs form stronger and more persistent coordination adducts with calcium. Notably, the first CAAC-Ca complex (**6.5**) was structurally characterized, but this complex rapidly decomposes to intractable mixtures in solution. In their reactions with calcium amidoborane complexes, sterically unencumbered NHCs can abstract $\text{Me}_2\text{N}=\text{BH}_2$ from $\text{Ca}(\text{NMe}_2\text{BH}_3)$ or

Ca(NMe₂BH₂NMe₂BH₃) units to furnish a thermally stable amidoborane enriched calcium complex (**6.8**). Such participation of NHCs in calcium amidoborane dehydrocoupling is anticipated to have significant implications for tuning the reactivities of calcium amidoborane synthons, as well as improving our understanding of molecular hydrogen storage at calcium.

Chapter Seven: A Multi-Dimensional Carbodiphosphoranyl Approach to Bismuth Coordination Chemistry: Cationization, Redox-Flexibility, and Stabilization of a Crystalline Bismuth Hydridoborate.

Contains work that was originally published in:

Obi, A. D.; Dickie, D. A.; Tiznado, W.; Frenking, G.; Pan S.; Gilliard, R. J., A Multi-Dimensional Carbodiphosphoranyl Approach to Bismuth Coordination Chemistry: Cationization, Redox-Flexibility, and Stabilization of a Crystalline Bismuth Hydridoborate. *Submitted*.

7.1 Ligand Stabilization Strategies Towards Redox Active Organobismuth Reagents

In recent years, the organometallic chemistry of bismuth has re-emerged as a hot topic across multiple areas of synthetic chemistry and catalysis.³⁵⁸⁻³⁶² Bismuth is particularly appealing due to its non-toxic and environmentally benign nature, which may have future implications in the development of chemical transformations which do not rely on toxic or precious metals.³⁶³ Owing to high-lying, partially-filled orbitals, low-valent bismuth compounds are well-positioned to mimic the synergistic effect of *d*-orbitals in challenging bond activation events.^{19, 20, 364, 365} Despite these positive attributes, isolating well-defined bismuth complexes can be synthetically challenging due to the ease at which many compounds undergo thermal decomposition to bismuth metal or the corresponding oxy-salts. Indeed, the poor spatial overlap of atomic orbitals in bismuth compounds results in metastable Bi–X bonds (X = Bi, O, C, N, P, S, etc.) with low homolytic dissociation energies.³⁶³ However, this property can be harnessed by rational ligand stabilization strategies³⁶⁶⁻³⁶⁸ towards productive bond activations and radical redox transformations.^{358, 369-377} To this end, electronically-flexible pincer ligands are desirable for their redox-flexibility and tunable stereoelectronics.^{359, 366, 378} This strategy enabled the elucidation of monomeric Bi(II) radicals (e.g., **I-III**, Figure 7.1a) as transient or isolable intermediates in stoichiometric and catalytic transformations.^{369-374, 379-381} Chitnis exploited the redox noninnocence of a triamide ligand towards a “redox-confused” Bi(I/III) complex (**IV**, Figure 7.1b) with electromorphic reactivity, for example in its Lewis acidity towards pyridine oxide or basicity towards W(CO)₅.³⁸² Bi(I)/Bi(III) transformations are especially difficult,³⁸³ and the first implementation of such a redox cycle in catalysis was achieved by Cornella,³⁸⁴ enabled by an *NCN*-bismuthinidene introduced by Dostál (**V**, Figure 7.1c).³⁸⁵

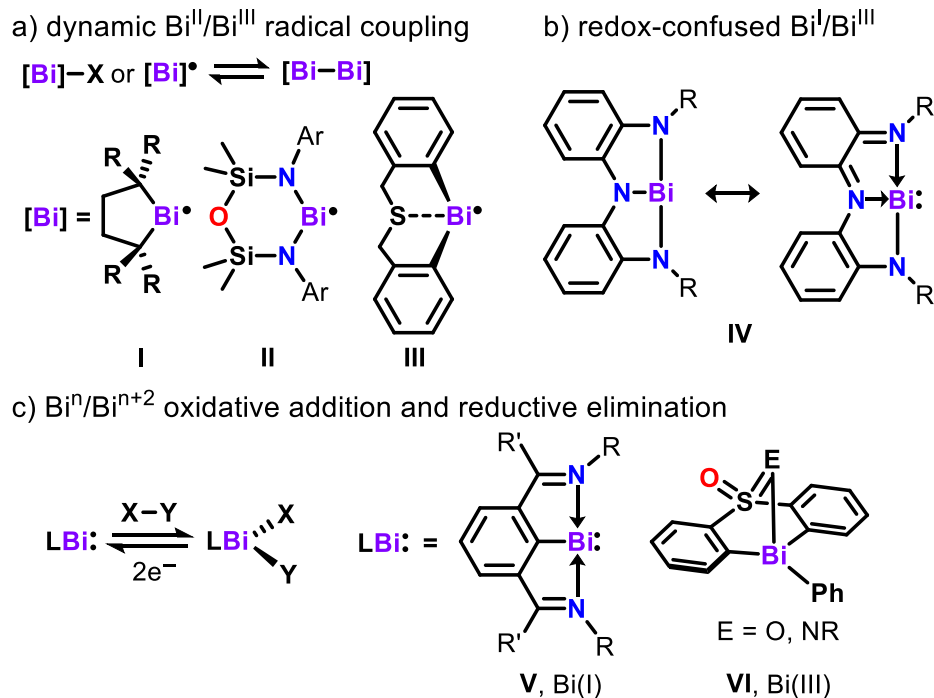


Figure 7.1. Selected examples of redox-flexible bismuth platforms highlighting design strategies based on pincer ligands and/or redox-flexible electronegative elements (R = alkyl, silyl, aryl).

Our interest concerns the paucity of bismuth-mediated transformations involving electronically-flexible, carbon-based donor ligands (i.e., carbenes and carbones). Despite the versatility of these ligands in light *p*-block element chemistry,⁹⁸ relevant studies concerning the heavier elements are comparatively rare.³⁸⁶ Coordination adducts of Bi(III) complexes and N-heterocyclic carbenes (NHCs) and cyclic(alkyl)(amino) carbenes (CAACs) are highly sensitive to small changes in their coordination environment, and prone to rapid decomposition in solution.^{143, 144, 150, 238, 387-389} For example, Bi(III) complexes of N-heterocyclic carbenes (NHC) bearing an unsaturated backbone (i.e., 1,3-bis(2,6-diisopropylphenyl)-imidazol-2-ylidene or IPr) are subject to thermal isomerization to abnormally bonded mesoionic complexes, while those involving the saturated NHC 1,3-bis(2,6-diisopropylphenyl)-4,5-dihydroimidazole-2-ylidene (SIPr) require THF-solvation for stabilization, without which they rapidly decompose to intractable mixtures.^{143,}

¹⁴⁴ Notably, the π -acidity of CAACs enabled the isolation and crystallographic elucidation of two-coordinate bismuthinidenes $[(\text{CAAC})\text{Bi}(\text{Ph})]^{150}$ and $[(\text{CAAC})_2\text{Bi}][\text{OTf}]^{389}$ involving partial $\text{C} \leftarrow \text{Bi}$ π -backbonding interactions. These complexes are also highly reactive and rapidly decompose under ambient conditions. Contrarily, carbenes such as carbodiphosphanes (CDPs)^{122, 123, 390} and carbodicarbenes (CDCs)^{126, 127, 130, 391} are four-electron σ , π -donors, and thus feature stronger $\text{carbone} \text{C} \equiv \text{Bi}$ multiple bonding interactions at Bi(III) centers (Figure 7.2a).¹⁴² The donor strength of carbenes permits isolation of stable low-coordinate monomeric Bi(III) complexes,^{142, 145, 392-394} whereas their carbene analogues mostly exist as dimeric complexes in coordinatively saturated octahedral geometries.^{143, 144, 387, 388} Notwithstanding their enhanced thermal stability, reported carbene-bismuth complexes are similarly disadvantaged by deleterious protonation,¹⁴⁵ and to the best of our knowledge, there are still no examples of productive bond activation events at bismuth centers stabilized by carbon donor ligands.^{360, 386}

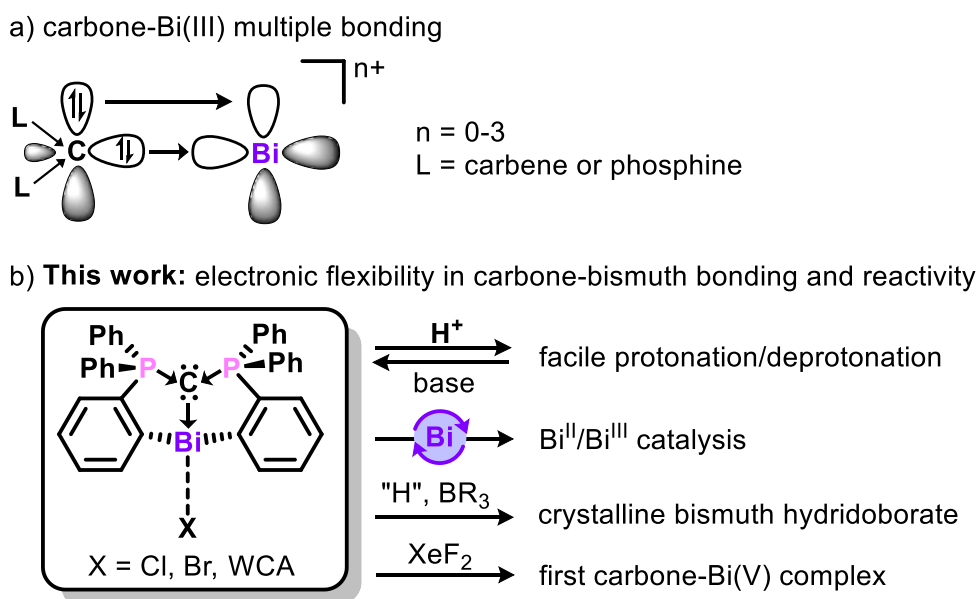


Figure 7.2. Electronic flexibility in carbene bismuth bonding highlighting (a) non-reductive carbene-Bi(III) multiple bonding via double dative interactions, and (b) redox flexibility within a

tethered, anionic carbodiphosphorane bismuth framework with multidimensional bonding and reactivity (WCA = weakly coordinating anion).

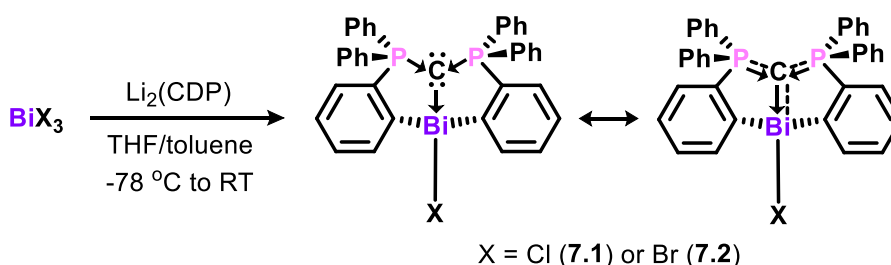
The recent dilithiation of hexaphenylcarbodiphosphorane¹²² by Sundermeyer afforded a dianionic, CCC-pincer ligand [Li₂(CDP)],³⁹⁵ which retains a four-electron σ,π -donor central carbone, and can be transferred to organometallic systems by simple halide metathesis reactions.³⁹ Inspired by the coordinative flexibility of this ligand, we were motivated to investigate its ability to stabilize redox-flexible bismuth reagents as part of our ongoing investigations into the electronic influence of carbones at heavy pnictogen complexes.¹⁴² We now report the isolation and reactivities of air-stable carbodiphosphoranyl (CDP)³⁹⁶ bismuth(III) halides (**7.1** and **7.2**), which can be easily ionized with highly tunable ^{carbone}C–Bi bonding in the monocations **7.3–7.10**. Herein, protolytic activation of the carbone center is reversible and maintains metal-ligand coordination, in contrast to the case for neutral carbone ligands whereby ligand protonation results in destabilized species.¹⁴⁵ Having established its robust coordination, we investigated the capacity of this framework for low valent redox transformations in the rapid catalytic silylation of 2,2,6,6-tetramethylpiperidin-1-oxyl (TEMPO), whereby **7.1** and **7.2** demonstrated higher or competitive activity compared to known Bi(II) platforms.^{370, 371, 381} The putative Bi–H intermediate in this transformation was captured using tris(pentafluorophenyl)borane to yield the first crystallographically characterized bismuth hydridoborate complex (**7.9**). Further redox flexibility of this framework was demonstrated in the oxidative fluorination of (CDP)BiX (X = Cl, SbF₆) to Bi(V) complexes (**7.11** and **7.12**), which are unprecedented examples of donor interactions between a carbone and high-valent heavy pnictogen.

7.2 Carbone Trans Influence in the Isolation of Carbodiphosphoranyl Bismuth(III) Halides

The reaction of equimolar amounts of Li₂(CDP) and BiCl₃ or BiBr₃ afforded the organobismuth(III) halides (CDP)BiCl (**7.1**) and (CDP)BiBr (**7.2**) respectively, in 70-80% yields

(Scheme 7.1). In contrast to the vibrant colors of monodentate CDP bismuth(III) halides,¹⁴⁵ compounds **7.1** and **7.2** are colorless solids. There is also little differentiation in the spectroscopic signatures of **7.1** and **7.2**. The CDP phosphorus resonance in **7.1** (δ_P 38.4 ppm) and the highly deshielded *ortho* CH–C_{Bi} doublet (δ_H 9.32 ppm) compare with the same for **7.2** (δ 38.6 ppm and 9.34 ppm respectively). In the $^{13}\text{C}\{^1\text{H}\}$ NMR spectra, the ylidic carbon resonances for **1** (δ_C 24.0 ppm, $^1J_{\text{PC}} = 98$ Hz) and **7.2** (δ_C 23.3 ppm, $^1J_{\text{PC}} = 98$ Hz) are significantly upfield from the monodentate (CDP)BiCl₃ adduct (δ_C 66.8 ppm, $^1J_{\text{PC}} = 72$ Hz),¹⁴⁵ due to the electron donating phenyl groups in their coordination sphere.

Scheme 7.1. Stabilization of bismuth halides at a dianionic carbodiphosphoranyl framework



Colorless, block-like single crystals of **7.1** and **7.2** were obtained from their respective saturated DCM/hexanes solutions at room temperature.³⁹⁷ Single crystal X-ray diffraction (SC-XRD) analysis revealed mononuclear structures, wherein the bismuth atom lies within a distorted see-saw geometry comprised of one tridentate CDP ligand and one halide atom (Figure 7.3). The metrical parameters for the CDP ligand in **7.1** and **7.2** are nearly identical within standard deviation (Figure 7.3 caption), with the exception of a slightly wider ligand bite angle in **7.2** (C3–Bi1–C21 is 98.32(16)^o in **7.1** and 102.12(11)^o in **7.2**). There are substantial intramolecular π -interactions between the *cis* “backbone” phenyl substituents [P1(Ph)---(Ph)P2 centroid distances: 3.646(3) Å (**7.1**) and 3.791(2) Å (**7.2**)], which may impose further rigidity on the ligand framework. However, the most remarkable feature in their molecular structures is an unprecedented *trans* carbone

influence for pnictogen complexes, whereby the donor carbone atom is *trans* to a functional group ($\text{C}^{\text{carbone}}\text{C}-\text{Bi}-\text{halide}$ is $163.30(12)^\circ$ in **7.1** and $165.31(8)^\circ$ in **7.2**). The anticipated contribution of σ - and π -symmetric lone pairs in the $\text{C}^{\text{carbone}}\text{C}-\text{Bi}$ bonding (see Figure 7.2 and Scheme 7.1)^{142, 145} imbues much greater *trans* influence than known *trans* donor-Bi-X examples,³⁹⁸⁻⁴⁰² resulting in highly elongated Bi-halide bonds in **7.1** [$3.0110(11)$ Å] and **7.2** [$3.0826(4)$ Å]. There is only a small difference between the Bi-Cl and Bi-Br bond lengths (Δ 0.072 Å), which are themselves more closely correlated with contacts between Bi and weakly-coordinated anions or halogenated solvents than those of typical covalent Bi-Cl ($\sum R_{\text{cov}} = 2.50$) and Bi-Br ($\sum R_{\text{cov}} = 2.65$) bonds.¹⁸⁴

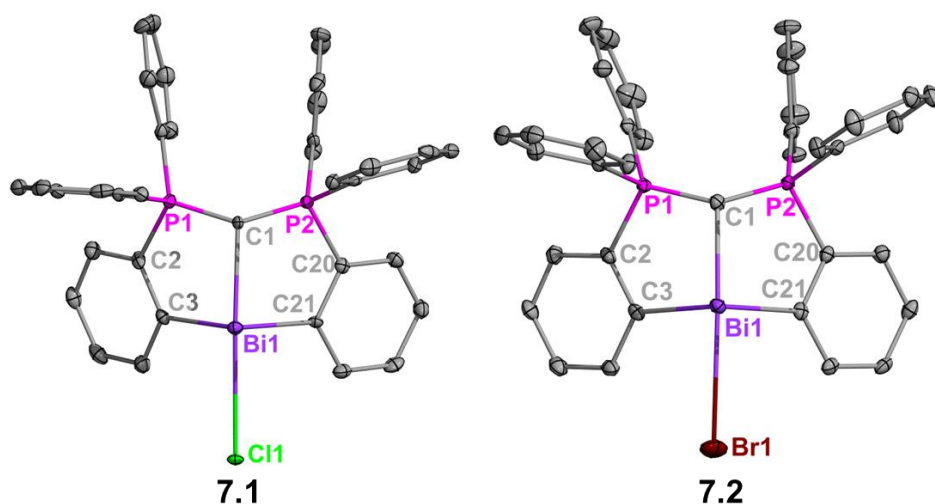


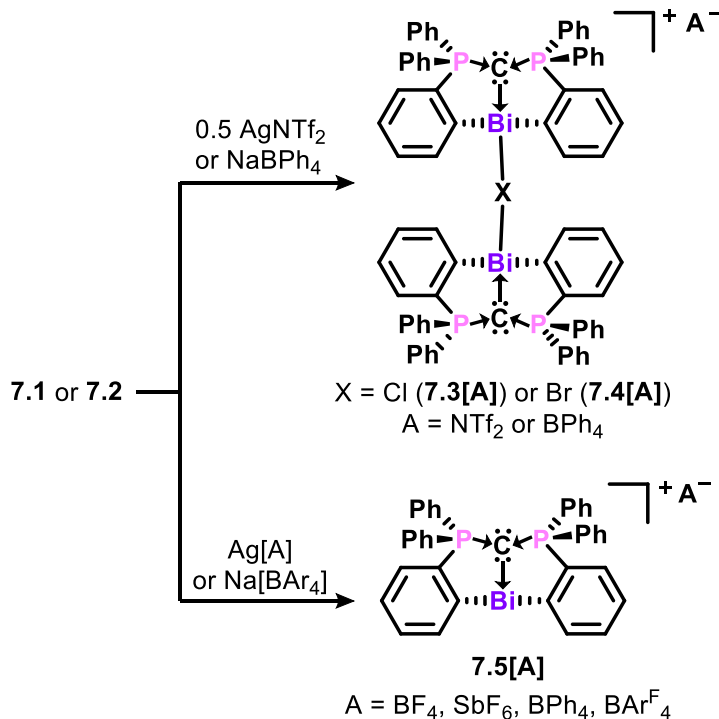
Figure 7.3. Molecular structures of **7.1** and **7.2**. Thermal ellipsoids set at 50% probability. Co-crystallized dichloromethane molecules and all H atoms are omitted for clarity. Selected bond distances (Å) and angles ($^\circ$) for **7.1** [and **7.2**]: Bi1-C1, 2.368(4) [2.346(3)]; Bi1-Cl1, 3.0110(11) [Bi1-Br1, 3.0826(4)]; Bi1-C3, 2.279(4) [2.273(3)]; Bi1-C21, 2.268(4) [2.275(3)]; C1-P1, 1.677(4) [1.680(3)]; C1-P2, 1.692(4) [1.686(3)]; C1-Bi1-Cl1, 163.30(12) [C1-Bi1-Br1, 165.31(8)]; C3-Bi1-C21, 98.32(16) [102.12(11)]; P1-C1-P2, 132.2(3) [134.9(2)].

Compounds **7.1** and **7.2** are highly soluble in dichloromethane (DCM) and chloroform, and indefinitely stable under anaerobic and anhydrous conditions in both solid- and solution-states. In contrast to the highly air- and moisture-sensitive monodentate carbone-bismuth(III) halides, **7.1** and **7.2** are bench-top-stable under air for at least one week. Furthermore, no degradation was spectroscopically observed when **7.1** and **7.2** were monitored for two months in hydrated CD_2Cl_2 , containing a stoichiometric amount of water. However, the addition of excess water to these solutions resulted in the precipitation of sticky solids presumed to be metal hydroxides.

7.3 Stabilization of Low-Coordinate Ionic Bismuth(III) Complexes

In an effort to isolate reactive, low coordinate complexes, we investigated the cationization of **7.1** and **7.2** using halide abstraction reagents. The reaction of **7.1** and $\text{Ag}[\text{NTf}_2]$ in THF or DCM resulted in incomplete halide abstraction to form the ionic complex $[\text{((CDP)Bi)}_2(\mu\text{-Cl})][\text{NTf}_2]$ (**7.3** $[\text{NTf}_2]$, Scheme 7.2). Notably, **7.3** $[\text{NTf}_2]$ may be considered a coordination adduct of **7.1** and the targeted ionic complex $[(\text{CDP)Bi}][\text{NTf}_2]$, which could not be isolated despite prolonged reaction times. The isostructural adducts **7.3** $[\text{BPh}_4]$ and $[\text{((CDP)Bi)}_2(\mu\text{-Br})][\text{BPh}_4]$ (**7.4** $[\text{BPh}_4]$) were isolated from reactions of NaBPh_4 with **7.1** and **7.2** respectively, but additional reaction times (16 - 48 h) enabled complete halide abstraction to obtain $[(\text{CDP)Bi}][\text{BPh}_4]$ (**7.5** $[\text{BPh}_4]$) in high yields (> 94%). The likewise reaction of **7.1** and $\text{Na}[\text{BAr}^{\text{F}}_4]$ ($\text{Ar}^{\text{F}} = 3,5\text{-(CF}_3)_2\text{C}_6\text{H}_3$) afforded **7.5** $[\text{BAr}^{\text{F}}_4]$, which exhibits improved solubility in common organic solvents (Et_2O , THF, CH_2Cl_2) in contrast to **7.5** $[\text{BPh}_4]$ which is highly soluble in DCM but poorly soluble in ethers. The utilization of fluoride-rich silver salts for cationization afforded **7.5** $[\text{BF}_4]$ and **7.5** $[\text{SbF}_6]$ in much shorter reaction times (30 min) (Scheme 7.2). The $^{31}\text{P}\{\text{H}\}$ resonances of **7.3-7.5** are downfield from those of **7.1** and **7.2**, and their chemical shifts increased with sequential halide abstraction (Table 7.1), which suggests electron deficiency at the phosphorus atoms due to increased carbone–bismuth interactions.

Scheme 7.2. Cationization of **7.1** and **7.2** towards stronger ^{carbonyl}C–Bi bonding



X-ray quality single crystals of **7.3-7.5** were obtained from their respective layered DCM/hexanes solutions at room temperature, and their molecular structures are described in Figure 7.4. Compounds **7.3[NTf₂]**, **7.3[BPh₄]** and **7.4[BPh₄]** are dimeric molecules with isostructural cationic units wherein the CDP-stabilized bismuth centers are symmetrically bridged by a single chloride halide, and balanced by a non-coordinating anion (Figure 7.4 and Figure A3.45). Their ^{carbonyl}C–Bi bonds are expectedly shortened from **7.1** and **7.2**, but their halide contacts are comparable, which further highlights the labile or weakly-coordinating nature of the halides. Notably, the Bi–X–Bi bond angles of 166.55°, 172.75(8)° and 167.49(6)° in **7.3[NTf₂]**, **7.3[BPh₄]** and **7.4[BPh₄]** respectively are on the wider end of reported values for (LBi)₂(μ-X) complexes (152 – 172°).^{380, 399} The molecular structures of **7.5[BF₄]** and **7.5[SbF₆]** each feature one Bi---F contact from the anion, which is shorter in **7.5[BF₄]** (2.891(3) Å) than **7.5[SbF₆]** (2.926(6) Å). In **7.5[BPh₄]**, a close Bi---Ph(BPh₃) centroid distance (3.870 Å) indicates non-negligible cation-

anion interactions, but similar interactions were not observed in **7.5**[BAr^F₄] likely owing to the π -electron deficient nature of the Ar^F groups, and the bismuth center is truly tricoordinate. The increased electrophilicity of the Bi³⁺ cation in **7.5**[BAr^F₄] is reflected in its ^{carbonyl}C–Bi bond (2.219(10) Å), which is significantly shorter than those of **7.5**[BF₄], **7.5**[SbF₆] and **7.5**[BPh₄] (2.269(8) – 2.275(4) Å), but comparable to that of the bis(triflate) Bi(III) complex stabilized by the neutral, monodentate CDP ligand (CDP)BiCl(OTf)₂ (^{carbonyl}C–Bi: 2.209(5) Å).¹⁴⁵

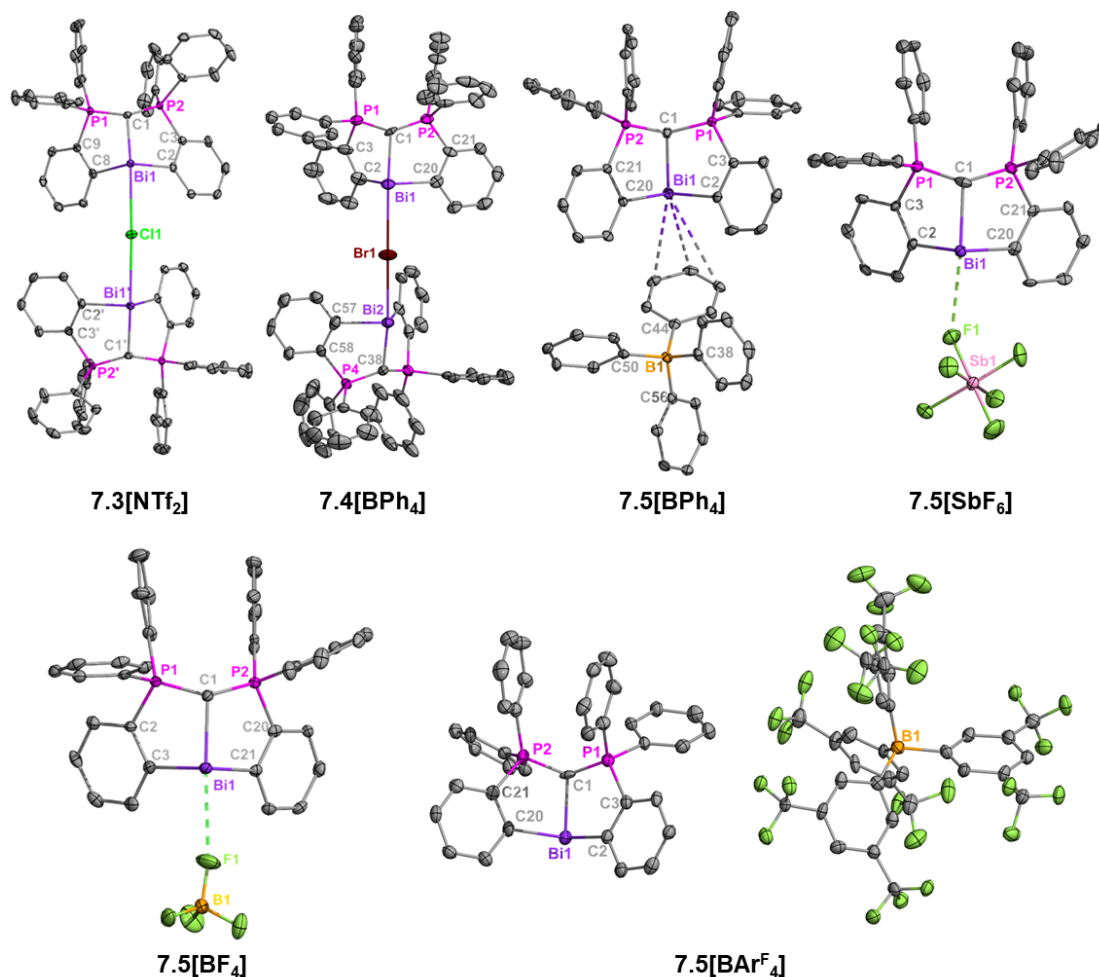


Figure 7.4. Molecular structures of **7.3**–**7.5**. A non-coordinating bis(triflimide) anion in **7.3**[NTf₂], tetraphenylborate anion in **7.4**[BPh₄], co-crystallized solvent molecules, and all H atoms are omitted for clarity. Selected bond distances (Å) and angles (°): **7.3**[NTf₂]: Bi1–C1, 2.295(2); Bi1–Cl1, 3.0939(3); Bi1–C2, 2.258(2); Bi1–C8, 2.290(2); C1–P1, 1.684(2); C1–P2, 1.691(2); C2–Bi1–

C8, 100.46(8); P1–C1–P2, 128.7(14). **7.4[BPh₄]**: Bi1–C1, 2.291(11); Bi1–Br1, 3.0947(15); Bi2–Br1, 3.1184(15); Bi1–C2, 2.286(11); Bi1–C20, 2.258(11); C1–P1, 1.691(12); C1–P2, 1.674(11); C2–Bi1–C8, 101.7(4); P1–C1–P2, 131.5(8). **7.5[BF₄]**: Bi1–C1, 2.275(4); Bi1–F1, 2.891(3); Bi1–C3, 2.260(5); Bi1–C21, 2.253(5); C1–P1, 1.704(5); C1–P2, 1.699(5); C3–Bi1–C21, 93.96(17); P1–C1–P2, 130.1(3). **7.5[SbF₆]**: Bi1–C1, 2.269(8); Bi1–F1, 2.926(6); Bi1–C2, 2.272(8); Bi1–C20, 2.257(8); C1–P1, 1.673(10); C1–P2, 1.712(9); C2–Bi1–C20, 96.4(3); P1–C1–P2, 131.3(5). **7.5[BPh₄]**: Bi1–C1, 2.275(3); Bi1–C2, 2.261(3); Bi1–C20, 2.252(3); C1–P1, 1.692(3); C1–P2, 1.698(3); C2–Bi1–C20, 96.95(10); P1–C1–P2, 132.33(18). **7.5[BAr^F₄]**: Bi1–C1, 2.219(10); Bi1–C2, 2.227(14); Bi1–C20, 2.290(13); C1–P1, 1.705(16); C1–P2, 1.684(15); C2–Bi1–C20, 102.3(6); P1–C1–P2, 132.6(7).

Table 7.1. Selected Spectroscopic and Structural Data for **7.1-7.6**

	$d(\text{carbonyl C–Bi})$ (Å)	$d(\text{Bi–X})$ (Å) ^a	$\delta^{31}\text{P}$ (ppm)	$\delta^{13}\text{C}$ (ppm) ^b	$^1J_{\text{PC}}$ (Hz) ^b
7.1	2.368(4)	3.0110(11)	38.4	24.0	98
7.2	2.346(3)	3.0826(4)	38.6	23.3	98
7.3[NTf₂]	2.295(2)	3.0939(3)	43.9	22.1	96
7.3[BPh₄]	2.303(6), 2.307(6)	2.9494(16), 2.9778(16)	47.0	20.8	94
7.4[BPh₄]	2.291(11), 2.300(12)	3.0947(15), 3.1184(15)	45.5	21.2	96
7.5[BF₄]	2.275(4)	2.891(3)	48.9	-	-
7.5[SbF₆]	2.269(8)	2.926(6)	51.5	18.8	92
7.5[BPh₄]	2.275(4)	3.870	50.4	19.2	93
7.5[BAr^F₄]	2.219(10)	-	53.3	18.7	93
7.6[BPh₄]	2.609(5)	2.6324(14)	28.1	18.6	71

^aX = halide except for **7.5[BPh₄]** (X = Bi–Ph(BPh₃) centroid). ^bYlidic carbon.

Compounds **7.3-7.5** are extremely moisture sensitive, yielding structurally similar ionic complexes of the type [(H-CDP)BiX][A] (**7.6-7.8**; X, A = halide and/or weakly coordinating anion) due to protonolysis of adventitious moisture in the reaction solvents (Figure 7.5). Remarkably, **7.6-7.8** are metalated complexes with tridentate CDP coordination to bismuth, which contrasts deleterious metal-ligand dissociation in the protonation of monodentate carbene-bismuth complexes.^{142, 145} In their molecular structures, an elongation of the ^{carbene}C–P bonds towards single bond regimes suggests elimination of the characteristic carbodiphosphorane C–P multiple bonds, and further reflects in the tetrahedral arrangement of the C1 carbon. Consequently, their P1–C1–P2 bond angles (range 120.4(3)° – 124.2(3)°) are contracted from those of **7.1-7.5** (128.7° – 134.9°). The Bi–halide bonds in **7.6** and **7.7** are comparable to typical terminal bismuth(III)-halide contacts in the literature, and significantly shortened from those of **7.1** and **7.2** (Table 7.1), as the *trans*-influence of the carbene is eliminated by protonation.

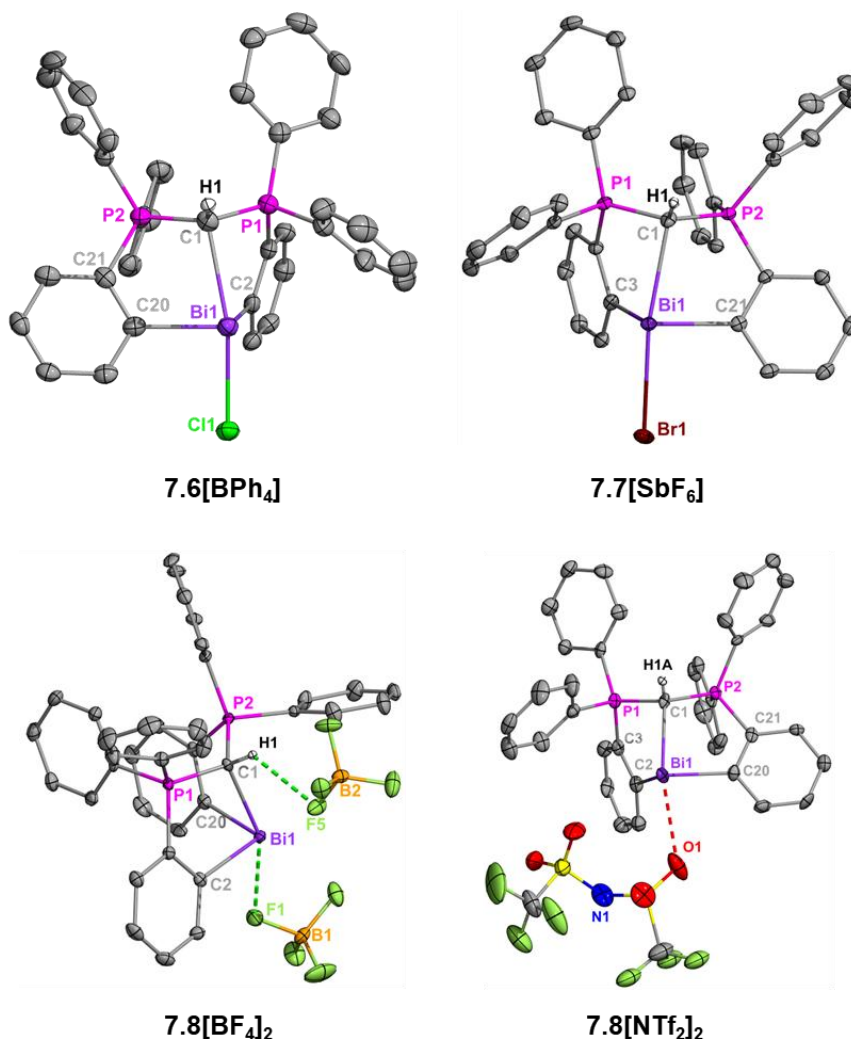
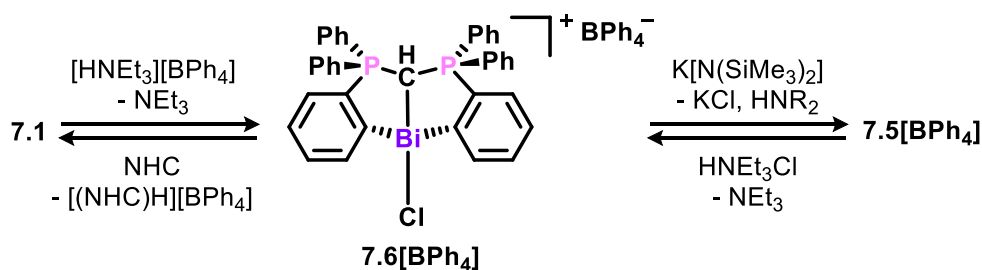


Figure 7.5. Molecular structures of **7.6-7.8**. Thermal ellipsoids shown at 50 % probability. Non-coordinating anions (for **7.6[BPh₄]**, **7.7[SbF₆]** and **7.8[NTf₂]₂**) and aromatic protons are omitted for clarity. Selected bond distances (Å) and angles (°): **7.6[BPh₄]**: Bi1–C1, 2.609(5); Bi1–Cl1, 2.6324(14); Bi1–C2, 2.281(5); Bi1–C20, 2.263(5); C1–P1, 1.739(5); C1–P2, 1.763(6); C2–Bi1–C20, 102.97(18); P1–C1–P2, 124.2(3). **7.7[SbF₆]**: Bi1–C1, 2.615(3); Bi1–Br1, 2.8461(4); Bi1–C3, 2.297(3); Bi1–C21, 2.281(3); C1–P1, 1.750(3); C1–P2, 1.765(3); C3–Bi1–C21, 100.22(9); P1–C1–P2, 122.07(16). **7.8[BF₄]₂**: Bi1–C1, 2.416(6); Bi1–F1, 2.657(3); Bi1–C2, 2.251(4); Bi1–C20, 2.285(5); C1–P1, 1.795(6); C1–P2, 1.781(4); C2–Bi1–C20, 95.45(15); P1–C1–P2, 120.4(3).

7.8[NTf₂]₂: Bi1–C1, 2.411(6); Bi1···O1, 2.841(7); Bi1–C2, 2.290(6); Bi1–C20, 2.244(7); C1–P1, 1.780(6); C1–P2, 1.793(7); C2–Bi1–C20, 98.3(2); P1–C1–P2, 120.6(3).

Although **7.6-7.8** were typically isolated in trace amounts as decomposition products, the intentional protonation of **7.1** using Evans' reagent [HNEt₃][BPh₄]⁴⁰³ afforded [(H-CDP)BiCl][BPh₄] (**7.6[BPh₄]**) in 84% yield, and permitted further spectroscopic analyses (Scheme 7.3). A prominent triplet resonance due to the C1 proton (δ_H 2.74 ppm, $^2J_{PH}$ 6.5 Hz) is observed in the ¹H NMR spectrum of **7.6[BPh₄]**, and the phosphorus resonance (δ_P 28.1 ppm) is significantly upfield from those of **7.1-7.5** (see Table 7.1). In the ¹³C{¹H} NMR spectrum, the central carbon (δ_C 18.6 ppm, $^1J_{PC}$ 71 Hz) extends a much smaller coupling constant with the neighboring phosphorus atoms than those of **7.1-7.5**, which suggests further deviation from carbene character and C–P multiple bonding. Notably, **7.6[BPh₄]** may be selectively and quantitatively deprotonated by dehydrohalogenation to **7.1** or **7.5[BPh₄]** using an unencumbered *N*-heterocyclic carbene (NHC = 1,3-diisopropyl-4,5-dimethylimidazol-2-ylidene) or potassium bis(trimethylsilyl)amide respectively (Scheme 7.3).

Scheme 7.3. Formation and dehydrohalogenation of **7.6[BPh₄]**



Notably, the bonding configuration in **7.6-7.8** is comparable to bis(iminophosphorane) methanide (BIPM) pnictogen complexes,^{392, 394} although the introduction of BIPM at bismuth resulted in intractable mixtures due in part to ^{ylide}C–H ↔ ^{imine}N–H tautomerization.³⁹² Thus, the

exclusion of chelating heteroatoms in this CDP framework discourages protonolysis of the pendant arms by carbene-heteroatom proton shuttling and enables robust ligand coordination.

7.4 Redox Catalysis and Isolation of a Bismuth Hydridoborate Complex

Having realized that the ionization of **7.1** and **7.2** involves facile tuning of ^{carbone}C–Bi interactions, we probed the impact of this donor interaction in redox transformations at bismuth. The reaction of **7.1** or **7.2** and stoichiometric equivalents of alkali-metal-based reducing agents (e.g., K₂C₈, Na, K[HBET₃] and Li[HBET₃]) resulted in slow decomposition (over 3 h) to an intractable mixture of products. We suspect that these reductions result in the formation of an unstable bismuth radical, as a combination of unfavorable sterics and carbene *trans* effect may hinder the stabilization of a Bi–Bi bond within this framework. The utilization of milder reducing agents (e.g., PhSiH₃, [Mg^I]⁹) yielded no reaction with **7.1** under ambient conditions, although the addition of excess PhSiH₃ (> 10 equiv.) resulted in partial decomposition with deposition of black solids presumed to be metallic bismuth. Spectroscopic analyses of the latter reaction indicate that **7.1** persists in solution even after one week, likely owing to a dynamic process between **7.1** and [Bi]–H (which is unobserved). Consequently, the accessibility of transient [Bi]–H and [Bi^{II}][•] species was probed via the addition of (2,2,6,6-tetramethylpiperidin-1-yl)oxyl (TEMPO).

Isolable [Bi^{II}–Bi^{II}] or [Bi^{II}][•] species have been shown to undergo thermal or photochemical Bi–O homolysis in their reactions with TEMPO, which enables catalytic dehydrocoupling of silanes and TEMPO via putative [Bi]–H intermediates.^{370, 371, 381} However, thermally activated dehydrocoupling reactions involving bismuth are typically sluggish in comparison to photochemical reactions as highlighted in recent studies by Lichtenberg.^{371, 381} Considering the unstable nature of the presumed radical and hydride intermediates within the (CDP)Bi framework, we hypothesized that, if accessible, their catalytic activity under thermal conditions may compete with established systems. Indeed, the addition of excess PhSiH₃ to a CD₂Cl₂ solution containing

7.1 and TEMPO in a 1:10 ratio resulted in a complete disappearance of the red color of TEMPO to yield a colorless solution after 3 d at room temperature (Table 7.2, entry 1). In contrast to our previous observations, metallic bismuth was not observed until TEMPO was completely consumed in this reaction. Spectroscopic analysis reveals the selective (> 95%) formation of PhH₂Si(OTEMP), as well as the persistence of **7.1** as the sole phosphorus-containing species.

Table 7.2. Reactions conditions and conversion data for catalysis experiments

$\text{TEMPO} + \text{PhSiH}_3 \xrightarrow[\text{5-10 mol \%}]{\text{cat.}} \text{PhH}_2\text{Si(OTEMP)}$					
entry	cat.	mol %	TEMPO/PhSiH ₃ (equiv)	condition	conversion ^a (%)
control	-	-	1/1	80 °C, 48 h	< 1
1	7.1	10	1/4	RT, 3 d	> 99 ^b
2	7.1	8	1/1	50 °C, 24 h	> 99 ^b
3	7.2	8	1/1	50 °C, 16 h	> 99 ^b
4	7.1	5	2/1	50 °C, 96 h	> 99 ^{b,c}

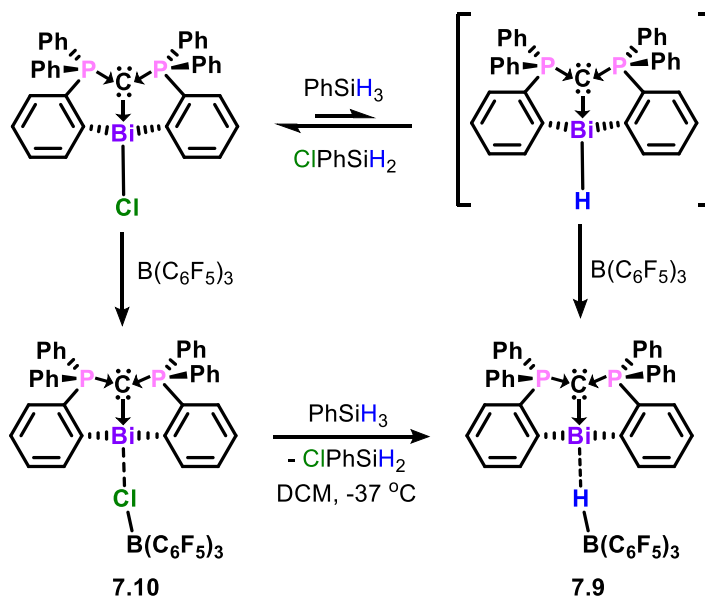
^aIn all cases, conversion was > 95% selective for PhH₂Si(OTEMP), and entries herein are based on ^bTEMPO consumption or ^csilane consumption.

The reaction of equimolar amounts of TEMPO and PhSiH₃ with 8 mol % **7.1** or **7.2** required mild heating (50 °C) for perceptible activity, but the complete consumption of TEMPO and plateaued production of PhH₂Si(OTEMP) was observed after 16 - 24 h (entries 2 and 3). Notably, PhSiH₃ was not consumed in this reaction, and H₂ was not detected in appreciable quantities in the ¹H NMR spectrum. In lieu of H₂ release, recent work by Lichtenberg suggests competitive processes whereby hydrogen abstraction from the putative [Bi]-H can occur on the surface of non-silanized glassware or via TEMPO to yield TEMPO-H or 2,2,6,6-tetramethylpiperidine and

water.³⁸¹ Indeed, the reaction of a 2:1 ratio of TEMPO and PhSiH₃ resulted in the complete consumption of PhSiH₃ and TEMPO (entry 4).

Because **7.1** and **7.2** are not consumed in these reactions, they are presumed the active catalysts, and a simplified catalytic cycle inspired by literature^{370, 371, 381} has been proposed in Figure A2.188. Unfortunately, none of the anticipated intermediates ([Bi]–H, [Bi^{II}]⁺, [Bi]–OTEMP) were spectroscopically observed or isolated. We hypothesized that the *trans* influence of the carbene contributes to their instability, which may rationalize their higher activity and selectivity in the thermal dehydrocoupling of TEMPO and PhSiH₃ than previously reported bismuth systems.^{370, 381} Therefore, we investigated the possible interception of the [Bi]–H intermediate by charge separation for thermodynamic stability. To this end, the Lewis acid tris(pentafluorophenyl)borane [B(C₆F₅)₃] has found versatile applications in frustrated Lewis pair (FLP) chemistry, and relevant to our investigations, as a hydride abstraction reagent.⁴⁰⁴ Indeed, the addition of B(C₆F₅)₃ to a mixture of (CDP)BiCl (**7.1**) and excess PhSiH₃ yielded the ionic complex [(CDP)Bi⁺⋯HB(C₆F₅)₃]⁻ (**7.9**) as a light-brown solid (Scheme 7.4). This reaction proceeds rapidly (15 min) at room temperature with significant deposition of bismuth metal, but can be controlled by reduced temperatures (-35 °C, 1 h) with improved yield (68 %). Upon isolation, **7.9** is thermally stable and amenable to spectroscopic investigations under ambient conditions.

Scheme 7.4. Synthesis of a bismuth hydridoborate complex



NMR analyses indicate that **7.9** is a charge-separated species in solution. The CDP phosphorus (δ_P 51.4 ppm) and carbonyl carbon (δ_C 18.7 ppm, $^1J_{PC}$ 91 Hz) resonances are comparable to those of **7.5**, and the ^{11}B NMR spectrum reveals a doublet (δ -25.5 ppm, $^1J_{\text{HB}}$ 98 Hz) in the expected range for the $\{\text{HB(C}_6\text{F}_5)_3\}^-$ anion. In the ^1H NMR spectrum, the B–H resonance is observed as a 1:1:1:1 quartet at δ 3.60 ppm ($^1J_{\text{BH}}$ 96 Hz). The B–H stretch (2310 cm^{-1}) in the solid-state IR spectrum is broadened (Figure A2.184), suggesting the possibility of secondary interactions with the cation.

The molecular structure of **7.9** was determined by X-ray diffraction on a single crystal obtained from a layered DCM/hexanes solution, and the anticipated Bi---H contact was unambiguously established in the tripodal coordination of $\{\text{HB(C}_6\text{F}_5)_3\}^-$ to the metal center (Figure 7.6a). Due to the high susceptibility of bismuth centers to deleterious reduction, isolable compounds involving any kind of bismuth-hydride contact are rare,⁴⁰⁵ and only one example has been crystallographically characterized as $(2,6\text{-Mes}_2\text{C}_6\text{H}_3)_2\text{BiH}$ (Mes = mesityl).⁴⁰⁶ The latter is a kinetically-stabilized bismuth hydride molecule with a short Bi–H bond (1.94(2) Å) and strong IR absorption band at 1759 cm^{-1} . Conversely, **7.9** features a much longer Bi–H interaction (3.14(3)

Å) as the hydride is expectedly localized on the boron atom. Gentle heating of **7.9** (50 °C, 1 h) yielded a colorless solid crystallographically identified as an isomorph (**7.9'**) whereby the Bi–H contact was labilized and no cation-anion interactions are present (Figure 7.6b). Instead, **7.9'** features unusual cation-cation interactions with Bi– π (aryl) interactions between neighboring cations (Figure 7.6c). In the absence of anion interactions, the ^{carbonyl}C–Bi bond is shortened from 2.2773(18) Å in **7.9** to 2.2499(13) Å in **7.9'**. It is therefore clear that this bismuth hydridoborate complex (**7.9**) benefits from thermodynamic stabilization due to charge-separation. Notably, attempts to stabilize smaller borohydrides (e.g., BH₄[−], HBEt₃[−]) at this framework are thus far unsuccessful, and likely requires additional steric protection to attenuate their disproportionation reactions (to [Bi⁰]_n, H₂ and BR₃).

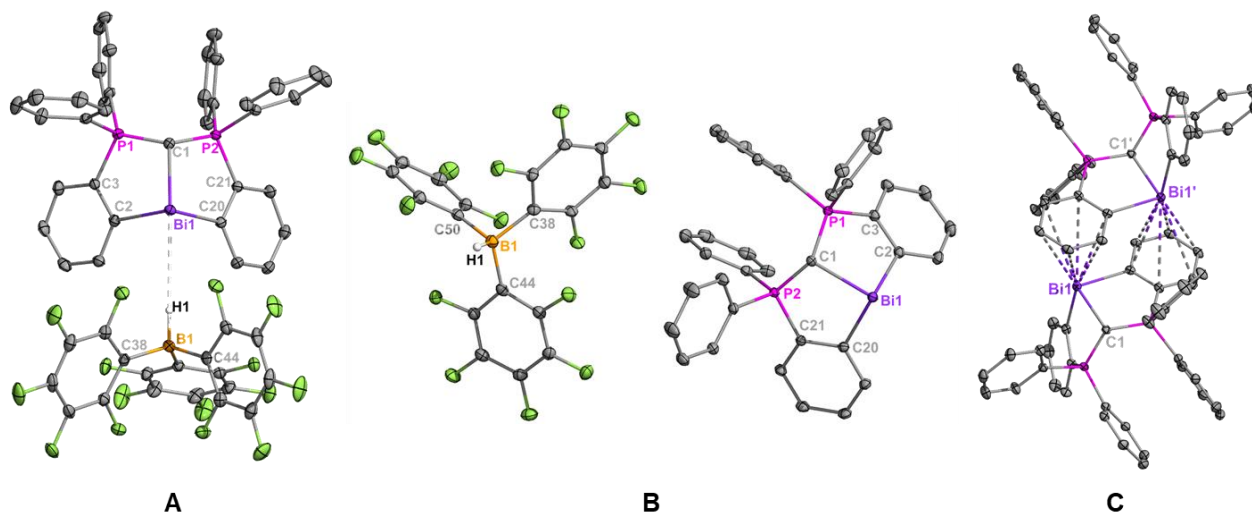


Figure 7.6. Molecular structures of **7.9** (A) and **7.9'** (B), showing cation-cation stacking in **7.9'** (C). Thermal ellipsoids are shown at 50 % probability, and aromatic protons omitted for clarity. B–H hydrides in **7.9** and **7.9'** were isotropically refined. Selected bond distances (Å) and angles (°) for **7.9** [and **7.9'**]: Bi1–C1, 2.2773(18) [2.2499(13)]; Bi1–C2, 2.2676(19) [2.2848(14)]; Bi1–C20, 2.2488(18) [2.2498(14)]; Bi1–H1, 3.14(3) [no contact]; C1–P1, 1.6959(19) [1.6993(14)]; C1–P2, 1.6994(19) [1.6998(14)]; C2–Bi1–C20, 95.42(6) [98.11(5)]; P1–C1–P2, 130.10(12) [128.26(8)].

Despite the facile isolation of **7.9**, a borane-mediated hydride abstraction from “(CDP)Bi–H” is difficult to substantiate due to the absence of spectroscopic evidence for the bismuth hydride. In the absence of $B(C_6F_5)_3$, the prolonged reaction of **7.1** and $PhSiH_3$ does not result in complete consumption of the reagents (despite evident decomposition to metallic bismuth). Therefore, a dynamic equilibrium which favors the formation of **7.1** via metathetical reaction of “(CDP)Bi–H” and $ClPhSiH_2$ is presumed (Scheme 7.4, top). Halide abstraction from **7.1** using $B(C_6F_5)_3$ is rapid (RT, < 5 min) and yields the ionic complex $[(CDP)Bi \cdots ClB(C_6F_5)_3]$ (**7.10**, Figure 7.7), which further reacts with $PhSiH_3$ to form **7.9** (Scheme 7.4). Although subsequent B–Cl/Si–H metathesis is probable, the intermediacy of a bismuth-centered hydride cannot be discounted as partial decomposition to metallic bismuth is also observed in this reaction, whereas **7.9** is thermally stable. Notably, no reaction was observed between $B(C_6F_5)_3$ and $PhSiH_3$ at room temperature, which discounts the initial formation of a silylium-hydridoborate,^{404, 407} and subsequent halide abstraction.^{408, 409}

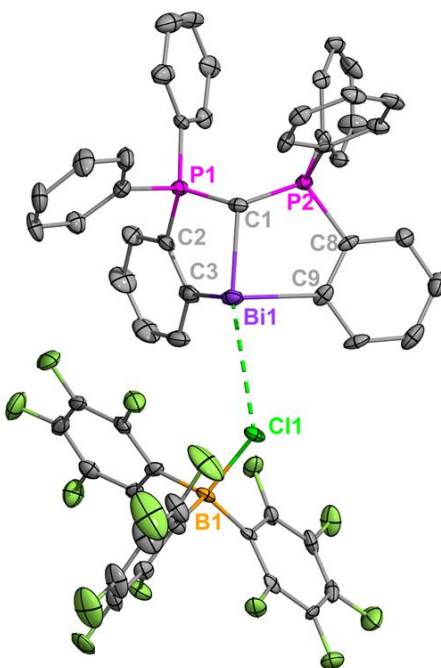
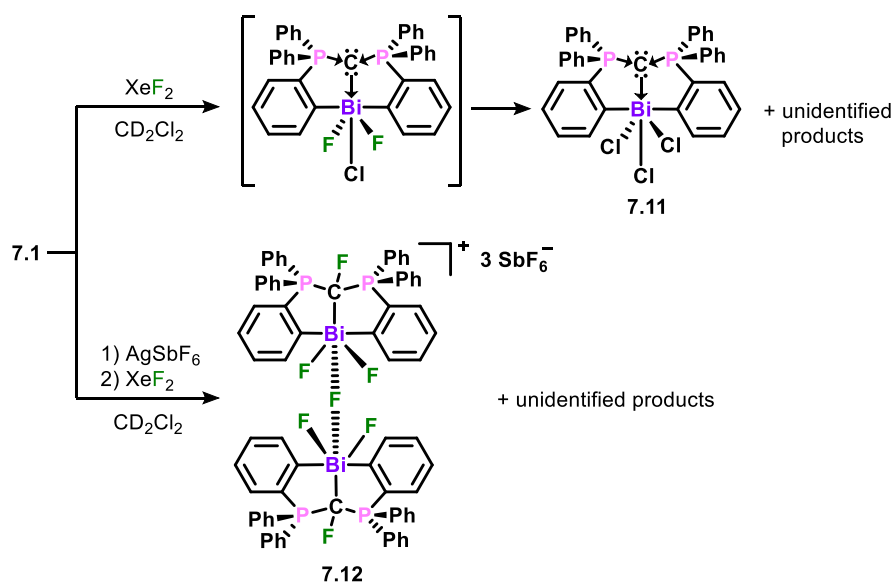


Figure 7.7. Molecular structure of **7.10**. Thermal ellipsoids are shown at 50 % probability, and aromatic protons omitted for clarity. Selected bond distances (Å) and angles (°): Bi1–C1, 2.259(5); Bi1–C11, 3.4142(18); B1–C11, 1.942(6); Bi1–C3, 2.293(6); Bi1–C9, 2.264(6); C1–P1, 1.695(6); C1–P2, 1.686(6); C3–Bi1–C9, 102.7(2); P1–C1–P2, 132.7(4).

7.5 Isolation of Bismuth(V) Complexes with Non-innocent Ligand Participation

Having established the capacity of this framework for low valent redox transformations, we were motivated by emerging opportunities in high valent bismuth catalysis,^{375,410} to investigate the stabilization of Bi(V) species. To the best of our knowledge, there are no examples of high valent heavy pnictogen complexes involving neutral carbon-based donors.⁴¹¹ We predicted that oxidation of the Bi(III) center will result in orbital perturbations towards an octahedral central geometry, which should planarize the CDP coordination and further enhance ^{carbone}C–Bi interactions. Notably, octahedral or hexacoordinate base-stabilized Pn(V) complexes are rare and of high synthetic interest due to their potential to access highly Lewis acidic acceptor orbitals.⁴¹¹⁻⁴¹³ Indeed, the reaction of **7.1** and XeF₂ yielded in a light brown solid containing a mixture of products (assessed via ³¹P NMR, see Supporting Information) from which the Bi(V) complex (CDP)Bi^VCl₃ (**7.11**) was isolated (Scheme 7.5).

Scheme 7.5. Isolation of carbodiphosphoranyl bismuth(V) complexes



The formation of **7.11** is attributed to ligand rearrangements from an intermediary heteroleptic adduct (CDP)BiClF₂. Intuitively, the perfluorinated adduct (CDP)BiF₃ should also result from this process, but attempts to unambiguously identify this product and other side products were unsuccessful due to the poor solubility of solids resulting from this reaction. However, single crystals of **7.11** were obtained from a layered DCM/hexanes solution of the reaction mixture, and the molecular structure was determined by X-ray crystallography (Figure 7.8). In the absence of chloride ions, the dimeric trication $[((F\text{-CDP})\text{BiF}_2)_2(\mu\text{-F})][\text{SbF}_6]_3$ (**7.12**) was isolated from the reaction of **7.5**[SbF₆] and XeF₂ (Scheme 7.5). Upon crystallization, compound **7.12** was also poorly soluble in organic solvents, but a weak phosphorus resonance (δ_P 15.0 ppm) could be identified in ³¹P{¹H} NMR spectrum in CD₂Cl₂. Surprisingly, the CDP ligands in **7.12** were fluorinated in likewise manner as the protonated CDP ligands in **7.6-7.8**. Therefore, a complex mechanism is likely, which presumably involves an initial oxidative fluorination to [(CDP)BiF₂][SbF₆]. In addition to their poor solubilities, the elusiveness of these fluorinated intermediates may be attributed to the poor spatial overlap of Bi–F bonds as well as the typical instability of diaryl Bi(V) complexes (Ar₂BiX₃, X = halide) complexes compared to the more

prevalent Ar_3BiX_2 complexes.^{368, 414} Nevertheless, the isolation of **7.11** and **7.12** highlights novel bonding modes for Bi(V) complexes, which involve tunable carbene-bismuth interactions.

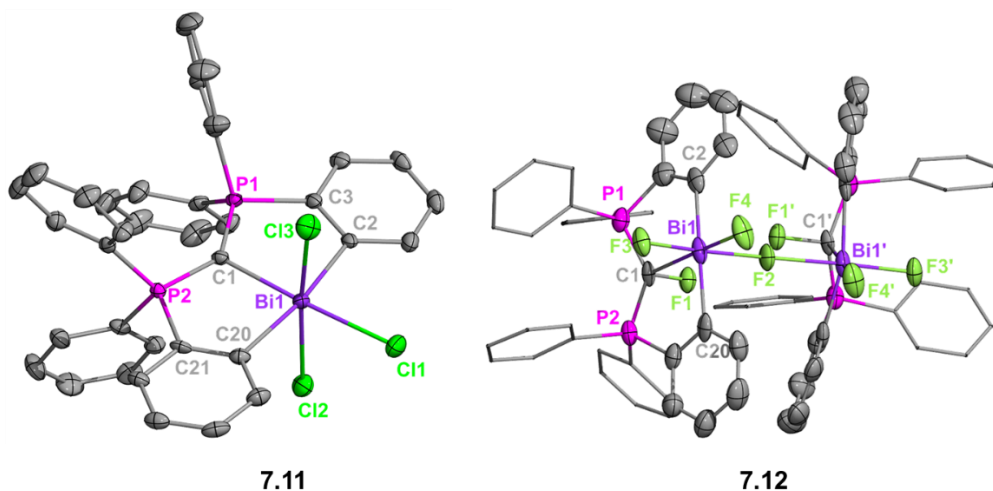


Figure 7.8. Molecular structure of **7.11** and **7.12**. Thermal ellipsoids shown at 50 % probability. Co-crystallized DCM molecules in **7.11**, three non-coordinating SbF_6^- anions in **7.12**, and all aromatic protons are omitted for clarity. A crystallographic two-fold rotational axis was found at F2 in **7.12**. Selected bond distances (\AA) and angles ($^\circ$): **7.11**: Bi1–C1, 2.227(3); Bi1–Cl1, 2.5867(10); Bi1–Cl2, 2.5912(10); Bi1–Cl3, 2.5538(11); Bi1–C2, 2.231(4); Bi1–C20, 2.224(4); C1–P1, 1.681(3); C1–P2, 1.675(3); C2–Bi1–C20, 170.63(13); P1–C1–P2, 133.1(2). **7.12**: Bi1–C1, 2.492(10); Bi1–F2, 2.2277(13); Bi1–F3, 2.057(6); Bi1–F4, 2.044(6); C1–F1, 1.440(11); Bi1–C2, 2.171(12); Bi1–C20, 2.182(13); C1–P1, 1.771(11); C1–P2, 1.791(11); C2–Bi1–C20, 162.4(4); P1–C1–P2, 135.8(6).

The molecular structure of **7.11** reveals a monomeric Bi(V) complex in the anticipated octahedral geometry (Figure 7.8). Two chloride ligands occupy apical positions, and the carbene coordination is in an equatorial position *trans* to a third chloride atom. Interestingly, the longest bismuth-chloride bond in **7.11** results from an axial chloride (Bi1–Cl2, 2.5912(10) \AA), although it closely compares with that of the equatorial chloride (Bi1–Cl1, 2.5867(10) \AA). The ^{carbone}C–Bi

interaction in **7.11** (C1–Bi1, 2.227(3) Å) is much shorter than those of **7.1** and **7.2** (see Table 7.1), owing to the enhanced electrophilicity of Bi(V) as well as the planarized CDP coordination. This donor interaction is unprecedented for Bi(V) complexes, but the ^{carbone}C–Bi bond is comparable to the covalent ^{Ph}C–Bi distances (2.231(4) and 2.224(4) Å). Intriguingly, theoretical bonding analysis (*vide infra*) suggest a predominantly electrostatic ^{carbone}C→Bi interaction, and **7.11** may benefit from cationization to permit empty symmetry correct orbitals for proper overlap with the carbone π -electrons. Thus far, our attempts to characterize such a complex have been unsuccessful due to poor solubility. Compound **7.12** also features an octahedral geometry around bismuth, but the carbone character of the C1 carbon was eliminated by fluorination. This reflected in elongated bonds between the C1 carbon and the bonded bismuth (both 2.492(10) Å) and phosphorus atoms (1.771(11), 1.791(11) Å).

7.6 Theoretical analysis

To shed light on the bonding situation of the new bismuth complexes, thermochemical calculations for **7.1**, **7.2**, **7.5⁺** and **7.11** were carried out at the BP86-D3(BJ)/def2-TZVPP level of theory. In the case of **7.5⁺**, the weakly interacting counteranion is not considered. Considering the crystal-packing effect in experimental structures and the accuracy of the level of theory, the computed geometrical parameters are in overall good agreement with experimental values. However, there are notable disparities in the ^{CDP}C–Bi and Bi–X (X = Cl, Br) bond distances for the halido complexes. Compared to experimental values, the calculated ^{CDP}C–Bi bond distances in **7.1**, **7.2** and **7.11** are slightly longer, and the Bi–halide bonds in **7.1** and **7.2** are significantly shorter (Figure A4.13). The differences in Bi–halide bonds are partially attributed to solvent (DCM) interactions with the halide ligands through H-bonding in crystals. Therefore, we considered the effect of solvation (DCM) in the geometries by employing polarizable continuum model (PCM) as an implicit solvation model. The corresponding structures with geometrical parameters given in

Figure A4.14 show much improved agreement with experimental values, and were thus considered for bonding analysis. Notably, *trans* effect also plays a role in the elongation of Bi–X bonds in **7.1** and **7.2** since CDP σ -donation populates the Bi–X σ^* anti-bonding orbital. Indeed, these Bi–X bond distances are significantly longer than the typical covalent bond distances computed from their covalent radii (Bi–Cl: 2.50 Å, Bi–Br: 2.65 Å)¹⁸⁴ or the parent salts BiCl₃ (2.455 Å) and BiBr₃ (2.613 Å) calculated at the same level.

Furthermore, we performed a quantum theory of atoms-in-molecules (QTAIM) analysis to gain insight into the topology of the electron density in these complexes.⁴¹⁵ Figure 7.9 displays the contour plots of Laplacian of electron density ($\nabla^2\rho(r)$) at the ^{CDP}C–Bi–^{Ph}C plane where red dotted regions show the electron density accumulated region ($\nabla^2\rho(r) < 0$) and blue solid lines indicate electron density depleted region ($\nabla^2\rho(r) > 0$). The large electron density around both ^{CDP}C and ^{Ph}C is polarized towards the Bi center, although the bond critical point (BCP) is located at $\nabla^2\rho(r) > 0$ region, which is very common for polar covalent bonds and bonds involving heavy elements. This is because $\nabla^2\rho(r_c)$ value is derived from the sum of the three curvature values (λ_1 , λ_2 and λ_3), wherein the curvature (λ_3) along the bond axis is always positive and the other two perpendicular to it are negative. Therefore, the criterion of a negative $\nabla^2\rho(r_c)$ value at the BCP for a covalent bond would depend on the condition $\lambda_1 + \lambda_2 > \lambda_3$. However, this is not always the case, especially with respect to bonds involving heavy elements or polar bonds (including a simple F₂ molecule).⁴¹⁶ The energy density $H(r_c)$, proposed by Kraka and Cremer, is a more effective descriptor in these cases.⁴¹⁶ It is negative at the BCP for covalent bonds and positive for non-covalent bonds. In the present cases, $H(r_c)$ is negative for both ^{CDP}C–Bi and ^{Ph}C–Bi bonds, which indicates covalent character, which is expectedly larger in the latter bond than in the former. For all the systems, irrespective of the charge and oxidation states of Bi, the ^{Ph}C–Bi bonds have similar $H(r_c)$ values.

However, the covalent character for the ${}^{\text{CDP}}\text{C-Bi}$ bonds is larger in **7.5⁺** and **7.11**, than in **7.1** and **7.2**.

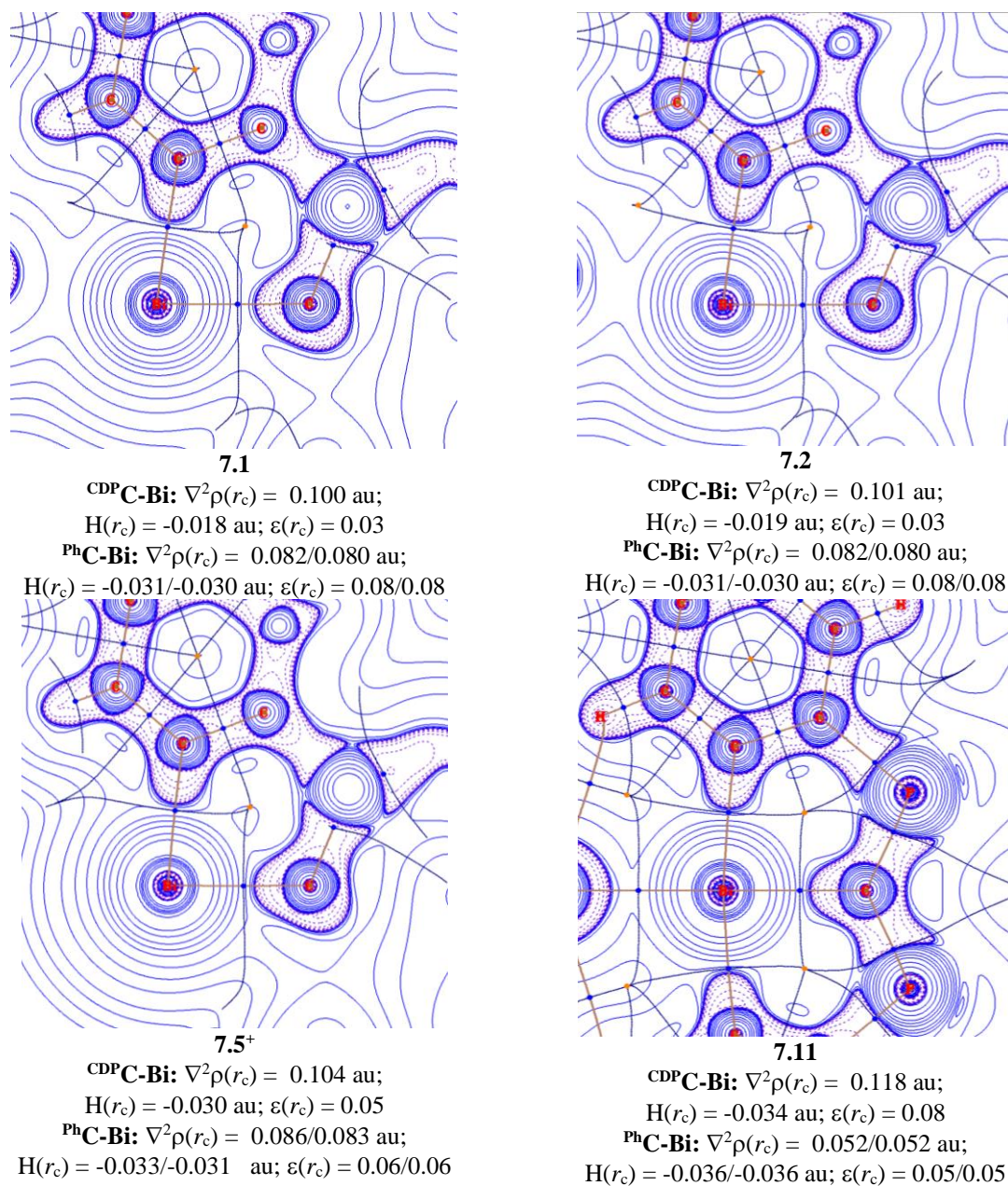


Figure 7.9. The contour plots of Laplacian of electron density at the plane of ${}^{\text{CDP}}\text{C-Bi-PhC}$ of the studied complexes at the BP86-D3(BJ)/def2-TZVPP level including solvation effect where blue solid lines show $\nabla^2\rho(r) > 0$ and red dotted lines show $\nabla^2\rho(r) < 0$.

The ellipticity values ($\varepsilon(r_c)$) at the BCP of $^{\text{CDP}}\text{C}-\text{Bi}$ and $^{\text{Ph}}\text{C}-\text{Bi}$ bonds are also given in Figure 7.10. In single and triple bonds, $\varepsilon(r_c)$ is close to zero because of the cylindrical contour of electron density, whereas in double bonds the asymmetrical electron distribution perpendicular to the bond path results in an elliptical contour of electron density ($\varepsilon(r_c) > 0$). It is well-known that CDP is a strong σ -donor and weak π -donor, and its π -donating ability depends on the correct symmetry and orientation of the acceptor orbital as well as the electrophilicity of that fragment.⁴¹⁷⁻

⁴¹⁹ In the present cases, $\varepsilon(r_c)$ values for $^{\text{CDP}}\text{C}-\text{Bi}$ bonds are nearly zero (0.03 - 0.08) which indicates the absence of any effective double dative bond between $^{\text{CDP}}\text{C}$ and Bi. Natural bond orbital (NBO) analyses corroborate these observations, wherein only one $2c-2e$ $^{\text{CDP}}\text{C}-\text{Bi}$ σ -bond is identified, whereas the two π electrons on $^{\text{CDP}}\text{C}$ are identified as a lone pair (LP), except for **7.11** (see Table A4.5). In **7.11**, two σ electrons on $^{\text{CDP}}\text{C}$ are also described as a LP, albeit with low occupation number (1.44 e) which indicates that the use of a tighter cut-off value for LP isolation would result in a $2c-2e$ $^{\text{CDP}}\text{C}-\text{Bi}$ σ -bond. The Mayer bond order (MBO) for $^{\text{CDP}}\text{C}-\text{Bi}$ bonds range from 0.58 (**7.1**) – 0.81 (**7.5**⁺), indicating $^{\text{CDP}}\text{C}\rightarrow\text{Bi}$ dative bond character. On the other hand, $^{\text{Ph}}\text{C}-\text{Bi}$ bond orders are very close to the ideal single bond for Bi(III) complexes, whereas it is slightly smaller in the Bi(V) complex. Minimal $^{\text{CDP}}\text{C}\rightarrow\text{Bi}$ π dative interaction is also evident upon inspection of the frontier molecular orbitals (Figure 7.10). The acceptor orbital of Bi is sd hybridized with minor p -orbital contribution, but it is not properly oriented to engage with the π lone pair on CDP.

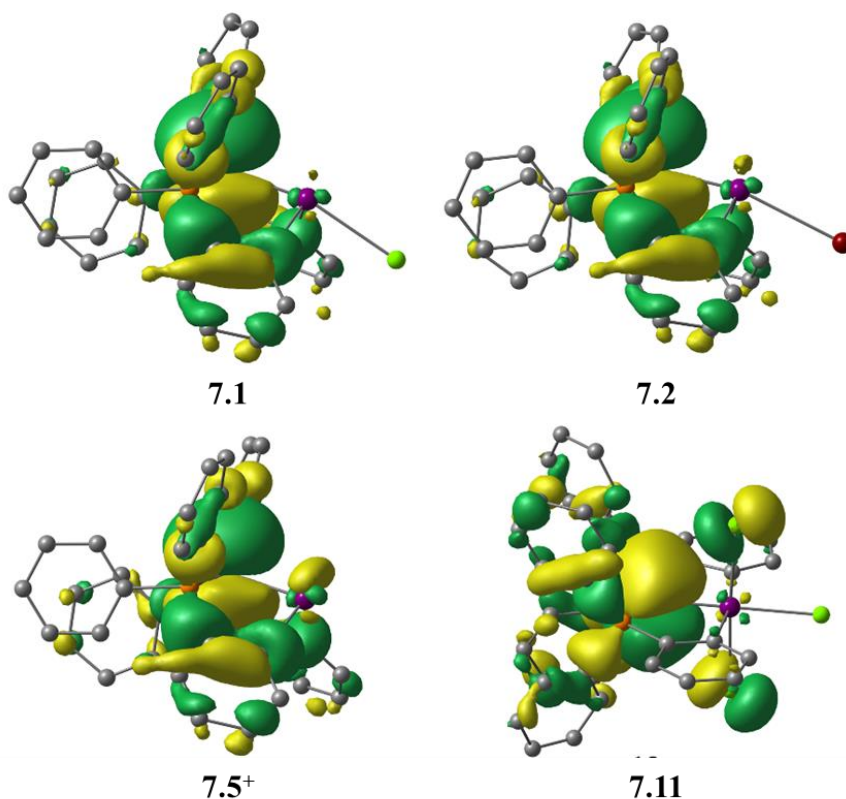


Figure 7.10. The highest occupied molecular orbital (HOMO) showing π lone-pair on CDP in the studied complexes. A low isovalue of 0.02 au is used to visualize the small MO coefficient on Bi center.

7.7 Conclusion and Outlook

The dianionic carbodiphosphoranyl ligand framework enabled multi-dimensional bonding and reactivity at bismuth centers featuring a carbon donor ligand, as well as redox-flexibility at both metal and ligand. In contrast to known carbene-bismuth complexes which are highly prone to deleterious ligand protonation under air or moisture, compounds **7.1** and **7.2** are air stable and the carbene center can be reversibly protonated while retaining metal-ligand coordination. The latter feature is desirable for developing productive bond activation processes involving proton shuttling or ligand cooperativity. Compounds **7.1** and **7.2** also feature carbene *trans* effect, which is unprecedented among the heavy pnictogens, and partially responsible for their remarkable

activity for catalytic TEMPO silylation. Such bismuth-mediated thermal dehydrocoupling reactions are typically slow, but we have observed high activities under mild conditions (50 °C) and low catalyst loadings (5-10 mol%), which compete with or even rival, known Bi^{II}/Bi^{III} systems. The putative [Bi]–H intermediate in the redox process was captured using B(C₆F₅)₃ to yield the first isolable bismuth hydridoborate benefiting from thermodynamic stabilization due to charge separation. Furthermore, high valent Bi(V) complexes (**7.11** and **7.12**) were isolated by oxidative fluorination, and **7.11** represents the first example of carbene coordination to a high valent heavy pnictogen. Bonding analyses suggest predominantly ^{carbene}C→Bi interaction through the CDP σ-lone-pair with little involvement of the π-lone-pair. However, the ability to selectively tune the strength of the ^{carbene}C→Bi interaction by ionization or oxidation is desirable for modulating the reactivity of bismuth complexes stabilized by this ligand framework.

Appendix I: Experimental

General Considerations.

All manipulations were carried out under an atmosphere of purified argon using standard Schlenk techniques or in an MBRAUN LABmaster glovebox equipped with a $-37\text{ }^{\circ}\text{C}$ freezer and operating at $< 0.1\text{ ppm H}_2\text{O}$ and O_2 . Glassware were oven-dried at $190\text{ }^{\circ}\text{C}$ overnight. Solvents (hexanes, toluene and benzene) were distilled over sodium/benzophenone under an argon atmosphere, and stored over 3 \AA molecular sieves. Deuterated solvents were purchased from Acros Organics and Cambridge Isotope Laboratories dried the same way as their protic analogues. The NMR spectra were recorded at room temperature on a Varian Inova 500 MHz (^1H : 500 MHz) and a Bruker Avance 600 MHz (^1H : 600 MHz, ^{13}C : 150.90 MHz). Proton and carbon chemical shifts are reported in ppm and are referenced to SiMe_4 using the residual proton and carbon signals of the deuterated solvent.⁴²⁰ Data are ordered as follows: chemical shift, multiplicity (s = singlet, d = doublet, t = triplet, q = quartet, sept = septet, m = multiplet, br = broad), coupling constants (J/Hz) and integration. DOSY experiments were carried out using the PFGSE (Pulsed-Field Gradient Spin-Echo) NMR Diffusion methods and analyzed with the software implemented by Bruker on an NMR AVIII600 spectrometer. A detailed description of methods implemented is available in the Supporting Information. IR spectra were recorded on an Agilent Cary 630 FT-IR equipped with a diamond ATR unit in an argon filled glovebox.

General Considerations for DOSY experiments. DOSY experiments were carried out using the PFGSE (Pulsed-Field Gradient Spin-Echo) NMR Diffusion methods and analyzed with the software implemented by Bruker on an NMR AVIII600 spectrometer. The signal intensity variation (integral) in the ^1H NMR spectrum (I) is related to the strength of the gradient (G) by the following equation: $\text{Ln}(I/I_0) = -\gamma^2\delta^2G^2(\Delta-\delta/3) D$, where γ = gyromagnetic ratio of the proton, δ

= length of the gradient pulse, G_i = gradient strength, Δ = delay between the midpoints of the gradients, and D = diffusion coefficient.^{421, 422} Before recording the DOSY experiment, the values of δ (small delta) and Δ (big delta) were optimized for each complex by using the 1D sequence for diffusion measurements (stebpgp1s1d, δ (2 x P30) and Δ (d20), Bruker's software). These values provided considerable reduction of the intensity of the signal, but remained strong enough to be integrated. The bidimensional DOSY experiment (stebpgp1s sequence) was recorded with the optimized δ and Δ values, varying G along 12 spectra. The data were analyzed with the Bruker software, which provided directly the diffusion coefficient (D). Hydrodynamic radii (r_H) were calculated from the Stokes–Einstein equation: $r_H = (k \cdot T) / (6 \cdot \pi \cdot \eta \cdot D)$ (where T is absolute temperature, k is the Boltzmann constant, η is the solvent viscosity and D is the coefficient of diffusion).

Synthetic Procedures.

Chapter Two:

Additional Considerations. Anhydrous $MgBr_2$ (98%, Strem Chemicals) was used as received. Free ^{iPr}NHC (1,3-diisopropyl-4,5-dimethylimidazol-2-ylidene)²⁷ and diimines²⁸ were prepared using literature procedures and recrystallized before use. Compound **2.1** was prepared as previously reported using toluene instead of THF,¹³ and new crystal structures of $(^{iPr}NHC)_2MgBr_2$ (**2.1** and **2.1'**) containing solvent molecules in the unit cell are described in Table A3.1. Elemental analyses (EA) were performed at Midwest Microlab, Indianapolis, IN, USA. Satisfactory EA results could not be obtained for **2.4**, **2.5** and **2.8**, which decomposed rapidly during the shipping and handling processes due to their extreme air and moisture sensitivity. NMR and FTIR spectra for all complexes have been provided in the Supporting Information as further evidence of bulk purity.

Synthesis of (iPrNHC)₂Mg(MesDAB^{Me}) (2.2). In a 100 mL round bottomed flask, MesDAB^{Me} (147 mg, 0.459 mmol) was dissolved in toluene (40 mL) and KC₈ flakes (136 mg, 1.01 mmol) were added to the light-yellow solution at room temperature and stirred for 3 h at room temperature. The dirty green suspension observed was added dropwise without filtering to a suspension of (iPrNHC)₂MgBr₂ (**2.1**, 250 mg, 0.459 mmol) and stirred at room temperature for 15 h. A red-orange filtrate was recovered over a Celite pad, and reduced to incipient recrystallization with vacuum, yielding yellow plate-like X-ray quality single crystals after 2 days at room temperature. Following decantation of the mother liquor and removal of volatiles with vacuum, compound **2.2** was recovered as an air- and moisture- sensitive, light orange solid (256 mg, 79% yield). ¹H NMR (600 MHz, C₆D₆, 298K): δ 7.03 (s, 4H, Ar(*m*-H)), 4.77 (sept, 4H, *J* = 7.0 Hz, CH-*i*Pr), 2.50 (s, 12H, Ar(*o*-CH₃)), 2.44 (s, 6H, Ar(*p*-CH₃)), 2.11(s, 6H, C(CH₃)-DAB backbone), 1.58 (s, 12H, C(CH₃)-Im), 1.08 (d, *J* = 7.0 Hz, 24H, CH₃-*i*Pr). ¹³C {¹H} NMR (150.9 MHz, C₆D₆, 298K): δ 188.7 (C_{Im}), 184.7 (C_{Im}), 154.8, 131.8, 125.7, 125.0, 123.1, 121.1, 53.2, 22.6, 21.6, 21.2, 18.1, 10.2. FTIR (solid state): ν 2979 (m), 2928 (m), 2893 (m), 2837 (m), 1632 (w), 1602 (m), 1461 (s), 1412 (m), 1354 (s), 1293 (s), 1256 (s), 1160 (m), 1071 (m), 1002 (m), 961 (w), 932 (w), 853 (s), 732 (s). Anal. Calc'd for C₄₄H₆₈MgN₆ (MW: 705.38 g/mol): C, 74.92; H, 9.72; N, 11.91. Found: C, 74.75; H, 9.62; N, 11.33.

Synthesis of (iPrNHC)₂Mg(MesDAB^H) (2.3). Procedure followed for the preparation of **2.2**, using MesDAB^H (134 mg, 0.459 mmol) instead of MesDAB^{Me}, and corresponding molar equivalents of **2.1** (250 mg, 0.459 mmol) and KC₈ (136 mg, 1.01 mmol). Similarly, a red-orange filtrate was recovered and concentrated with vacuum, yielding yellow block-like X-ray quality single crystals after 3 days at room temperature. Following decantation of the mother liquor and removal of volatiles with vacuum, compound **2.3** was recovered as an air and moisture sensitive orange solid

(235 mg, 76% yield). ^1H NMR (600 MHz, C_6D_6 , 298K): δ 7.02 (s, 4H, Ar(*m*-H)), 5.98 (s, 2H, CH-DAB backbone), 4.90 (sept, 4H, $J = 7.0$ Hz, CH-*i*Pr), 2.56 (s, 12H, Ar(*o*-CH₃)), 2.43 (s, 6H, Ar(*p*-CH₃)), 1.59 (s, 12H, C(CH₃)-Im), 1.12 (d, $J = 7.0$ Hz, 24H, CH₃-*i*Pr). $^{13}\text{C}\{^1\text{H}\}$ NMR (150.9 MHz, C_6D_6 , 298K): δ 184.2 (*C*_{Im}), 155.9, 130.2, 129.6, 125.2, 122.8, 122.5, 53.5, 22.5, 22.3, 21.3, 10.3. FTIR (solid state): ν 2975 (m), 2925 (m), 2852 (m), 1630 (w), 1602 (w), 1580 (m), 1463 (s), 1414 (m), 1356 (s), 1293 (s), 1260 (s), 1220 (s), 1161 (m), 1096 (s), 1071 (m), 1006 (m), 907 (w), 853 (m), 714 (m). Anal. for $\text{C}_{42}\text{H}_{64}\text{MgN}_6$ (MW: 677.32) calculated to include one toluene per two molecules of **2.3** in unit cell $\text{C}_{91}\text{H}_{136}\text{Mg}_2\text{N}_{12}$: C, 75.55; H, 9.48; N, 11.62. Found: C, 75.22; H, 9.39; N, 11.38.

*Synthesis of (*i*PrNHC)₂Mg(*Dipp*DAB^{Me}) (2.4).* In a 20 mL scintillation vial, compound **2.1** (50 mg, 0.0918 mmol) and *Dipp*DAB^{Me} (37 mg, 0.0918 mmol) were combined in toluene (12 mL) yielding a light-yellow mixture. Then KC_8 flakes (27 mg, 0.202 mmol) were added slowly with vigorous stirring. After 16 h, the mixture was filtered through a 0.45 μm pore syringe filter. The orange filtrate recovered was concentrated in a 3:1 hexanes/toluene mixture, and stored at -37°C yielding red-orange plate-like single crystals suitable for X-ray diffraction. After removing the mother liquor and drying under vacuum, **2.4** was recovered as an air and moisture sensitive orange solid (52 mg, 60% yield). ^1H NMR (600 MHz, C_6D_6 , 298K): δ 7.30 (d, $J = 7.5$ Hz, 4H, Ar(*m*-H)), 7.11 (t, $J = 7.3$ Hz, 2H, Ar(*p*-H)), 4.69 (br. s, 4H, CH-*i*Pr(Im)), 4.29 (sept, $J = 6.9$ Hz, 4H, CH-*i*Pr(*Dipp*)), 2.13 (s, 6H C(CH₃)-DAB backbone), 1.61 (s, 12H, C(CH₃)-Im), 1.47 (d, $J = 6.7$ Hz, 12H, CH₃-*i*Pr(DAB)), 1.22 (d, $J = 6.9$ Hz, 12H, CH₃-*i*Pr(DAB)), 1.09 (d, $J = 6.8$ Hz, 24H, CH₃-*i*Pr(Im)). $^{13}\text{C}\{^1\text{H}\}$ NMR (150.9 MHz, C_6D_6 , 298K): δ 185.1 (*C*_{Im}), 155.2, 145.4, 128.6, 125.3, 123.6, 121.7, 118.5, 53.4, 32.0, 26.9, 26.3, 26.1, 23.3, 23.1, 18.8, 14.4, 10.4. FTIR (solid state): ν 3036 (w), 2925 (s), 2861 (s), 1638 (w), 1582 (m), 1463 (m), 1416 (s), 1343 (s), 1310 (s), 1239 (s),

1112 (m), 1070 (m), 935 (s), 777 (s), 749 (m). Satisfactory elemental analysis results could not be obtained for this compound due to rapid decomposition during shipping and handling.

Synthesis of $(iPrNHC)_2Mg(DippDAB^H)$ (2.5). Procedure followed for the preparation of **2.4**, using $DippDAB^H$ (35 mg, 0.0918 mmol) instead of $DippDAB^{Me}$ and corresponding molar equivalents of **2.1** (50 mg, 0.0918 mmol) and KC_8 (27 mg, 0.202 mmol). After 16 h, the reaction mixture was filtered through a 0.45 μm pore syringe filter, and the yellow-orange filtrate was concentrated under vacuum to a slurry of solids, which was further precipitated with hexanes (3 mL). The precipitates were collected by filtration, and evacuated to dryness to obtain compound **2.5** as a yellow solid (44 mg, 63% yield). 1H NMR (500 MHz, C_6D_6 , 298K): δ 7.28 – 7.32 (m, 4H, Ar(*m*-H)), 7.09 (m, 2H, Ar(*p*-H)), 6.01 (s, 2H, CH-DAB backbone), 4.85 (sept, 4H, $J = 8.6$ Hz, CH-*iPr*(Im)), 4.20 (sept, 4H, $J_{HH} = 8.1$ Hz, CH-*iPr*(Dipp)), 1.62 (s, 12H, C(CH₃)-Im), 1.37 (d, $J = 6.8$ Hz, 24H, CH₃-*iPr*(Im)), 1.12 (d, $J = 6.8$ Hz, 24H, CH₃-*iPr*(Im)). $^{13}C\{^1H\}$ NMR (150.9 MHz, C_6D_6 , 298K): δ 184.4 (C_{Im}), 156.4, 144.3, 125.4, 123.8, 123.7, 118.3, 53.6, 27.5, 26.5, 22.9, 10.3. FTIR (solid state): ν 2938 (m), 2860 (m), 1633 (w), 1585 (m), 1461 (m), 1420 (s), 1360 (s), 1311 (s), 1248 (s), 1218 (m), 1086 (s), 1019 (m), 922 (m), 823 (m), 751 (s), 685 (m). Combustion analysis on an NMR pure sample of **2.5** yielded unsatisfactory results. Notably, dynamic ligand rearrangements were observed during the crystallization and purification of this compound (see below).

Isolation of $[(iPrNHC)Mg(\mu-DippDAB^H)]_2$ (2.6) and $Mg(DippDAB^H)_2$ (2.7). A concentrated toluene solution of **2.5** precipitated few X-ray quality crystals of **2.6** after 2 days at -37 °C. The supernatant was stored at room temperature, and yielded crystals of **2.7** in trace yields, hence spectroscopic data (IR or EPR) for **2.7** was not obtained. Notably, single crystals of **2.6** were also obtained in extremely poor yield. Sustained efforted (prolonged crystallization times and different solvent

mixtures) yielded powdery solids after the initial deposition of few single crystals. The ^1H NMR yielded resonances corresponding to **2.5** and a yet unidentified solid (Figure A2.11). As a result, combustion microanalysis on a verified sample of **2.6** could not be performed.

Preparation of 2.6 from in situ ($i^{\text{Pr}}\text{NHC}$)MgBr₂. To a colorless toluene (15 mL) solution of $i^{\text{Pr}}\text{NHC}$ (50 mg, 0.277 mmol) was added anhydrous MgBr₂ powder (51 mg, 0.277 mmol), and stirred at room temperature. After 16 h, $\text{DippDAB}^{\text{H}}$ (104 mg, 0.277 mmol), followed by golden KC₈ flakes (82 mg, 0.610 mmol), was added to the cloudy bronze solution. Additional toluene (20 mL) was added, and the mixture was stirred for an additional 16 h. A yellow-orange solution was recovered via filtration and dried under vacuum to reveal an orange solid, which was further recrystallized from a 3:1 hexanes/toluene solution. X-ray diffraction identified the crystals as the expected dinuclear complex, **2.6**, and NMR studies identified the bulk product as **2.5**, and the same unknown product observed in the earlier reaction.

*Synthesis of ($i^{\text{Pr}}\text{NHC}$)Mg($\text{DippDAB}^{\text{Me}}$)-KBr (**2.8**).* In a 100 mL round bottomed flask, anhydrous brown MgBr₂ powder (51 mg, 0.277 mmol) and $i^{\text{Pr}}\text{NHC}$ (50 mg, 0.277 mmol) were combined in toluene (15 mL) and stirred. After 6 h, a dirty orange toluene suspension of K₂($\text{DippDAB}^{\text{Me}}$) (prepared *in situ* by stirring $\text{DippDAB}^{\text{Me}}$ (112 mg, 0.277 mmol) and KC₈ (82 mg, 0.610 mmol) in toluene for 6 h) was added to the cloudy bronze [$(i^{\text{Pr}}\text{NHC})\text{MgBr}_2$] solution, and stirred for 3 days. The resulting mixture was filtered over a celite pad and the dark orange filtrate recovered was concentrated to 3 mL under vacuum, yielding yellow blocklike crystals after a few hours at room temperature. A second crop of crystals was obtained from the mother liquor at -37 °C. After removal of volatiles, compound **2.8** was recovered as an orange-yellow powder (40 mg, 20 % crystalline yield). ^1H NMR (600 MHz, C₆D₆, 298 K) δ 7.32 – 7.28 (m, 4H, Ar(*m*-H)), 7.11 (t, J = 7.5 Hz, 2H, Ar(*p*-H)), 4.50 (sept, J = 6.9 Hz, 2H, CH-*i*Pr(Im)), 3.96 – 3.85 (m, 4H, CH-*i*Pr(Dipp)),

1.72 (s, 6H), 1.64 (d, $J = 6.8$ Hz, 6H), 1.57 (d, $J = 6.9$ Hz, 6H), 1.39 (s, 6H), 1.21 (d, $J = 6.8$ Hz, 6H), 1.11 (d, $J = 7.0$ Hz, 6H). $^{13}\text{C}\{^1\text{H}\}$ NMR (150.9 MHz, C_6D_6 , 298K): δ 181.9, 153.0, 145.8, 143.6, 125.1, 124.2, 122.5, 119.9, 119.7, 54.4, 27.9, 27.4, 27.0, 25.7, 24.2, 22.7, 16.7, 10.0. FTIR (solid state): ν 3055 (w), 2954 (s), 2923 (s), 2863 (s), 1587 (m), 1459 (m), 1423 (s), 1358 (m), 1309 (m), 1243 (s), 1162 (m), 1120 (m), 1075 (m), 943 (s), 866 (w), 771 (s), 753 (m).

Chapter Three:

Additional Considerations. Anhydrous MgBr_2 (98%, Strem Chemicals) and $\text{Na}[\text{BPh}_4]$ (> 99.5%, Sigma Aldrich) were used as received. $\text{Na}[\text{BAr}^{\text{F}}_4]$,⁴²³ $i\text{PrNHC}^{217}$ and $\text{MeNHC}^{217, 424}$ were prepared according to literature and recrystallized before use. $(i\text{PrNHC})_2\text{MgMeBr}$ (**3.1**) and $(i\text{PrNHC})_2\text{MgBr}_2$ (**3.6**) were prepared as previously reported.¹⁰⁸ Elemental analyses yielded overall unsatisfactory results due to the extreme air and moisture sensitivity of these compounds. Similar challenges with determining the purity of group 2 complexes using combustion microanalysis are well documented.^{78, 159, 206, 425} Therefore, NMR spectroscopy was used to determine bulk purity, and the spectra of all compounds are provided in the Appendix II.

*Synthesis of $[\{(i\text{PrNHC})_2\text{Mg}\}_2(\mu\text{-Me})_2][(\text{BAr}^{\text{F}}_4)_2]$, (**3.2**).* In a 20 mL scintillation vial, a chlorobenzene solution (5 mL) of $\text{Na}[\text{BAr}^{\text{F}}_4]$ (93 mg, 0.105 mmol) was added dropwise to a stirring solution of **3.1** (50 mg, 0.104 mmol) in the same solvent. After 3 h, trace solids presumed to be NaBr were removed via filtration. The recovered light bronze solution was concentrated under reduced pressure before addition of hexanes (3 mL) to precipitate the product as a white solid, which was further washed with hexanes (1 x 5 mL) and dried under vacuum (83 mg, 63%). X-ray quality single crystals were grown from a concentrated $\text{C}_6\text{H}_5\text{Cl}$ /hexanes solution of **3.2** at -37 °C freezer. Notably, **3.2** may also be prepared using the ether solvate $\text{Na}[\text{BAr}^{\text{F}}_4]\cdot(\text{Et}_2\text{O})_{3.5}$. ^1H NMR (500 MHz, $\text{C}_6\text{D}_5\text{Br}$, 398K): δ 8.07 (s, 8H, Ar(*o*-H)), 7.61 (s, 4H, Ar(*p*-H)), 4.30 (br. s, 4H,

CH-*i*Pr), 1.86 (s, 12H, C(CH₃)), 1.21 (d, *J* = 7.0 Hz, 24H), -1.02 (s, 3H, Mg(CH₃)). ¹¹B NMR (192.55 MHz, C₆D₅Br, 398K): δ -6.02. Due to poor solubility, a sufficiently resolved ¹³C NMR spectrum could not be obtained.

Synthesis of [(ⁱPrNHC)₃MgMe][BAr^F₄], (3.3[BAr^F₄]). In a 20 mL scintillation vial, free ⁱPrNHC (19 mg, 0.104 mmol) and **3.1** (50 mg, 0.104 mmol) were dissolved in toluene (15 mL) and stirred. Then Na[BAr^F₄] (93 mg, 0.105 mmol) was added slowly to the cloudy mixture and stirred for 6 h at room temperature. A clear solution was recovered via filtration and the remaining solids were extracted with additional toluene (5 mL) leaving behind trace off-white solids presumed to be NaBr. The filtrate was concentrated under vacuum and stored at room temperature, yielding large colorless plate-like crystals suitable for single-crystal X-ray diffraction. After drying under vacuum, **3.3[BAr^F₄]** was recovered as a crystalline white solid (120 mg, 80%). Notably, **3.3[BAr^F₄]** may also be prepared using THF without the formation of solvated products. ¹H NMR (600 MHz, C₆D₆, 298 K): δ 8.33 (s, 8H, Ar(*o*-H)), 7.68 (s, 4H, Ar(*p*-H)), 4.72 (br. s, 6H, CH-*i*Pr), 1.63 (s, 18H, C(CH₃)), 1.01 (br. s, 36H, CH₃-*i*Pr), -0.90 (s, 3H, Mg(CH₃)). Due to poor solubility, a sufficiently resolved ¹³C{¹H} NMR could not be obtained in C₆D₆. Although successfully characterized in CD₂Cl₂, complexes **3.3-3.4** slowly convert into unidentified products after 2 h in the solvent. ¹H NMR (600 MHz, CD₂Cl₂, 298 K): δ 7.71 (s, 8H, Ar(*o*-H)), 7.56 (s, 4H, Ar(*p*-H)), 4.84 (sept, *J* = 7.0 Hz, 6H, CH-*i*Pr), 2.20 (s, 18H, C(CH₃)), 1.32 (d, *J* = 7.7 Hz, 36H, CH₃-*i*Pr), -1.35 (s, 3H, Mg(CH₃)). ¹³C NMR (150.90 MHz, CD₂Cl₂, 298 K): 186.2, 182.6, 135.2, 129.2, 126.3, 125.9, 124.1, 117.9, 22.6, 10.7, -8.9. ¹¹B NMR (192.55 MHz, CD₂Cl₂, 298K): δ -6.67.

Synthesis of [(ⁱPrNHC)₃MgMe][BPh₄], (3.3[BPh₄]). In a 100 mL round-bottomed flask, ⁱPrNHC (39 mg, 0.219 mmol) and **3.1** (102 mg, 0.213 mmol) were dissolved in toluene (50 mL) and stirred at room temperature before Na[BPh₄] (80 mg, 0.233 mmol) was added to the cloudy mixture. After

16 h, a colorless solution was recovered via filtration and reduced to incipient recrystallization, yielding large block-like colorless crystals suitable for X-ray diffraction at room temperature. Solids recovered from filtration were further extracted with toluene (15 mL). After removal of volatiles, **3.3[BPh₄]** was recovered as a crystalline white solid (135 mg, 71% yield). ¹H NMR (600 MHz, C₆D₆, 298 K): δ 8.12 (m, 8H, Ar(*m*-H)), 7.36 (t, *J* = 7.3 Hz, 8H, Ar(*o*-H)), 7.21 (t, *J* = 7.3 Hz, 4H, Ar(*p*-H)), 4.73 (sept, *J* = 7.0 Hz, 6H, CH-*i*Pr), 1.66 (s, 18H, C(CH₃)), 1.04 (d, *J* = 7.1 Hz, 36H, CH₃-*i*Pr), -0.86 (s, 3H, Mg(CH₃)). ¹³C {¹H} NMR (150.9 MHz, C₆D₆, 298 K): δ 182.2, 137.5, 126.1, 122.1, 53.2, 22.4, 10.3. ¹H NMR (600 MHz, CD₂Cl₂, 298 K): δ 7.31 (m, 8H, Ar(*m*-H)), 7.02 (t, *J* = 7.5 Hz, 8H, Ar(*o*-H)), 6.87 (t, *J* = 7.2 Hz, 4H, Ar(*p*-H)), 4.84 (sept, *J* = 7.0 Hz, 6H, CH-*i*Pr), 2.21 (s, 18H, C(CH₃)), 1.34 (d, *J* = 8.1 Hz, 36H, CH₃-*i*Pr), -1.34 (s, 3H, Mg(CH₃)). ¹³C {¹H} NMR (150.9 MHz, CD₂Cl₂, 298 K): δ 182.4, 164.7, 136.3, 126.3, 126.0, 122.1, 22.6, 10.8, -8.96. ¹¹B NMR (192.55 MHz, CD₂Cl₂, 298K): δ -6.44.

*Synthesis of [(ⁱPrNHC)₃MgBr][BAr^F₄], (**3.4[BAr^F₄]**). Procedure followed for the preparation of **3.3[BAr^F₄]**, using (ⁱPrNHC)₂MgBr₂ (57 mg, 0.104 mmol) and corresponding molar equivalents of ⁱPrNHC (19 mg, 0.104 mmol) and Na[BAr^F₄] (93 mg, 0.105 mmol) in toluene. After 6 h, a light bronze solution was recovered via filtration and the expected product further extracted from the precipitated solids using chlorobenzene (5 mL). The solutions recovered were concentrated under vacuum, and upon light agitation, precipitated colorless block-like crystals, which were further dried under vacuum to obtain **3.4[BAr^F₄]** a colorless solid (76 mg, 49% yield). ¹H NMR (600 MHz, CD₂Cl₂, 298K): δ 7.71 (s, 8H, Ar(*o*-H)), 7.56 (s, 4H, Ar(*p*-H)), 4.90 (sept, *J* = 7.0 Hz, 6H, CH-*i*Pr), 2.22 (s, 18H, C(CH₃)), 1.36 (d, *J* = 7.1 Hz, 36H, CH₃-*i*Pr). ¹³C NMR (150.9 MHz, CD₂Cl₂, 298K): δ 177.7, 162.7, 162.3, 162.0, 161.7, 135.2, 129.4, 129.2, 127.7, 127.1, 125.9, 124.1, 117.9, 54.1, 22.6, 10.7. ¹¹B NMR (192.55 MHz, CD₂Cl₂, 298K): δ -6.67.*

Synthesis of [(ⁱPrNHC)₃MgBr][BPh₄], (3.4[BPh₄]). Procedure followed for the preparation of **3.3[BAr^F₄]**, using Na[BPh₄] (36 mg, 0.104 mmol) and corresponding molar equivalents of (ⁱPrNHC)₂MgBr₂ and ⁱPrNHC in toluene. After 3 days, colorless precipitates were collected over a fritted Buchner funnel and dried under vacuum. Due to poor solubility of the product, NaBr was not removed prior to yield (111 mg, quantitative) and NMR analyses, the latter revealing a single pure product (Figure A2.25). An aliquot of the product was concentrated in C₆H₅Br and layered with hexanes, yielding X-ray quality single crystals of **3.4[BPh₄]** at -37 °C. NOTE: Despite rigorous efforts at drying the reaction solvents, the hydrolysis product [(ⁱPrNHC)H][BPh₄]²¹⁶ was regularly obtained alongside **3.4[BPh₄]** during crystallization. ¹H NMR (600 MHz, CD₂Cl₂, 298K): δ 7.31 (m, 8H, Ar(*m*-H)), 7.02 (t, *J* = 7.4 Hz, 8H, Ar(*o*-H)), 6.87 (t, *J* = 7.3 Hz, 4H, Ar(*p*-H)), 4.90 (sept, *J* = 7.0 Hz, 6H, CH-*i*Pr), 2.23 (s, 18H, C(CH₃)), 1.37 (d, *J* = 7.1 Hz, 36H, CH₃-*i*Pr). ¹³C NMR (150.9 MHz, CD₂Cl₂, 298K): δ 186.2, 177.7, 165.0, 136.3, 127.11, 125.99, 125.98, 122.1, 54.1, 22.6, 10.8. ¹¹B NMR (192.55 MHz, CD₂Cl₂, 298K): δ -6.60.

Synthesis of [(ⁱPrNHC)₂(THF)Mg(Me)][BAr^F₄], (3.5[BAr^F₄]). A THF (5 mL) solution of Na[BAr^F₄]·(Et₂O)_{3.5} (60 mg, 0.0524 mmol) was added dropwise to a stirring colorless THF (5 mL) solution of **3.1** (25 mg, 0.0521 mmol) in a 20 mL scintillation vial. After 12 h, a colorless solution was recovered over a 0.45 μm pore syringe filter, and volatiles were removed under vacuum with trituration/wash using hexanes (4 x 5 mL). After initial spectroscopic analysis, the off-white solid recovered was concentrated in toluene/THF and crystallized as the tris-carbene adduct **3.3[BAr^F₄]**. Notably, the THF coordination in the bulk sample **3.5[BAr^F₄]** was found to be persistent against evacuation over several hours. ¹H NMR (600 MHz, C₆D₆, 298K): δ 8.33 (s, 8H, Ar(*o*-H)), 7.68 (s, 4H, Ar(*p*-H)), 4.31 (br. s, 4H, CH-*i*Pr), 3.46 (s, O(CH₂)-THF), 1.57 (s, 12H, C(CH₃)), 1.36(s,

CH₂(CH₂)-THF), 0.98 (m, 24H, CH₃-*i*Pr), -1.04 (s, 3H, Mg(CH₃)). Due to poor solubility, a sufficiently resolved ¹³C NMR spectrum could not be obtained.

Synthesis of [(ⁱPrNHC)₂(THF)MgMe][BPh₄], (3.5[BPh₄]). Procedure followed for the preparation of **3.5[BAr^F₄]** using Na[BPh₄] (35 mg, 0.104 mmol) instead of Na[BAr^F₄]. Colorless single crystals suitable for X-ray diffraction were obtained from a C₆H₅Br/hexanes solution. ¹H NMR revealed a complex mixture of **3.5[BPh₄]** and ligand rearrangement products **3.3[BPh₄]** and **3.4[BPh₄]**, and the corresponding resonances were all identified (Figure A2.38). Notably, this reaction yielded similar results when performed using THF/toluene mixtures instead of pure THF. ¹H NMR (600 MHz, CD₂Cl₂, 298K): δ 7.30 (m, 8H, Ar(*m*-H)), 7.02 (t, *J* = 7.4 Hz, 8H, Ar(*o*-H)), 6.87 (t, *J* = 7.2 Hz, 4H, Ar(*p*-H)), 4.64 (sept, *J* = 7.1 Hz, 4H, CH-*i*Pr), 3.87 (m, 4H, O(CH₂)-THF), 2.19 (s, 12H, C(CH₃)), 1.96 (m, CH₂(CH₂)-THF), 1.40 (d, *J* = 7.1 Hz, 24H, CH₃-*i*Pr), -1.42 (s, 3H, Mg(CH₃)). Due to unsuccessful attempts to isolate pure samples of **3.5[BPh₄]** from the ligand rearrangement minor products, ¹³C{¹H} NMR and yield analyses were not performed.

Synthesis of (^{Me}NHC)₂MgBr₂, (3.7). Free ^{Me}NHC (70 mg, 0.564 mmol) was added to a stirring toluene (15 mL) suspension of MgBr₂ (52 mg, 0.282 mmol). After 16 h, white precipitates were recovered via filtration and dried under vacuum to obtain compound **3.7** as a white solid (102 mg, 84% yield). This reaction was similarly successful when performed using THF instead of toluene. Single crystals suitable for X-ray diffraction were obtained from a C₆H₅Br/hexanes solution of **3.7**. ¹H NMR (600 MHz, C₆D₅Br, 298 K): δ 3.57 (br. s, 6H, N(CH₃)), 1.55 (s, 6H, C(CH₃)). ¹³C{¹H} NMR (200 MHz, C₆D₅Br, 298K): δ 178.1, 124.6, 34.6, 8.2.

Synthesis of (^{Me}NHC)₃MgBr₂ (3.8a) and [(^{Me}NHC)₃MgBr][Br] (3.8b). Free ^{Me}NHC (29 mg, 0.232 mmol) was added to a stirring suspension of **3.7** (50 mg, 0.116 mmol) in C₆H₅Cl (5 mL). A clear solution was observed after 5 min and allowed to stir for 1 h at room temperature. After

filtration of trace solids, a layer of hexanes was added to the filtrate, precipitating colorless prism-like co-crystallized (1:1) adducts of **3.8a** and **3.8b** at room temperature after 1 day. After removal of the supernatant and drying under vacuum, the product was isolated as an off-white solid (33 mg, 41% yield). An alternative procedure involves the addition of ^{Me}NHC (70 mg, 0.564 mmol) and to a stirring toluene solution of MgBr₂ (30 mg, 0.161 mmol). After 24 h, white solids were recovered via filtration dried under vacuum (73 mg, 82% yield). Notably, VT-NMR (C₆D₅Br, 248 K – 373 K) experiments could not resolve more than one unique product in solution. ¹H NMR (600 MHz, C₆D₅Br, 298 K): δ 3.55 (br. s, 6H, N(CH₃)), 1.60 (s, 6H, C(CH₃)). ¹³C{¹H} NMR (200 MHz, C₆D₅Br, 298K): δ 124.2, 34.6, 8.3. Due to poor solubility, the carbene carbon resonance was not observed.

Chapter Four:

Additional Considerations. 1,3,4,5-tetramethylimidazol-2-ylidene (^{Me}NHC),²¹⁷ **1^{iPr}**,¹⁰⁸ **7^{iPr}**,¹⁰⁷ **7^{Me}**,¹⁰⁹ and [Na(dioxane)₂][OCP]²²⁶ were synthesized according to the literature. A new crystal structure for **7^{iPr}** containing bromobenzene solvent in the unit cell is described in Table A3.4. Combustion microanalyses on the new compounds yielded overall unsatisfactory results because the extreme air and moisture sensitivity of these compounds resulted in rapid decomposition during handling. NMR and FTIR spectra for all complexes have been provided as further evidence of bulk purity.

*Synthesis of (^{Me}NHC)₂MgMeBr (**4.1^{Me}**)* – A procedure similar to the previously reported (^{iPr}NHC)₂MgMeBr (**4.1^{iPr}**) was followed.¹⁰⁸ MeMgBr (3 M in Et₂O, 0.7 mL) was added dropwise to a stirring solution of ^{Me}NHC (520 mg, 4.19 mmol) in freshly distilled THF (~10 mL) and stirred at room temperature. The colorless THF solution gradually became turbid, and within minutes, colorless precipitates began to form. The mixture was stirred for 16 h and the volume was reduced

under vacuum to 5 mL. Hexanes (~ 5 mL) was added, and the mixture was stirred for an additional 30 min to aid further precipitation. The solids were collected via filtration and washed with a mixture of hexanes and toluene. After drying under vacuum, compound **4.1^{Me}** was then recovered as a colorless solid (684 mg, 89% yield). Single crystals suitable for X-ray diffraction were obtained by layering a concentrated chlorobenzene solution with hexanes at room temperature, and the molecular structure is described in Figure A3.15. Notably, this compound is sparingly soluble in toluene, benzene and THF, but readily dissolves in halogenated benzenes. ¹H NMR (600 MHz, C₆D₆, 298 K): δ 3.47 (s, 12H, NCH₃), 1.30 (s, 12H, CCH₃), -0.29 (s, 3H, MgCH₃). ¹H NMR (600 MHz, C₆D₅Br, 298 K): δ 3.54 (s, 12H, NCH₃), 1.58 (s, 12H, CCH₃), -0.67 (s, 3H, MgCH₃). ¹³C{¹H} NMR (150.9 MHz, C₆D₅Br, 298 K): δ 187.7 (s, C_{carbene}), 124.1 (s, CCH₃), 34.3 (s, NCH₃), 8.3 (s, CCH₃), -9.3 (s, MgCH₃). M.p.: decomposed at 182 °C.

Synthesis of (i^{Pr}NHC)₂MgMe(OCP) (4.2^{iPr}). [Na(dioxane)₂][OCP] (162 mg, 0.626 mmol) was added in one portion to a cloudy toluene solution (~ 8 mL) of **4.1^{iPr}** (300 mg, 0.625 mmol) at room temperature. The mixture was stirred for 5 min and a homogenous light green solution was observed with traces of undissolved solid presumed to be NaBr. After 10 min, the solution was filtered and reduced under vacuum to 1 mL. Then, hexanes (~ 1 mL) was added, and the solution was allowed to sit undisturbed at room temperature, yielding colorless single crystals of **4.2^{iPr}** overnight (200 mg, 70 % yield). Note: After the isolation of crystalline material, ¹H NMR analysis of the crude product from the mother liquor identified [(^{iPr}NHC)MgMe(μ-OEt)]₂ (**4.3^{iPr}**)¹⁷³ as a minor product due to dioxane activation. Prolonged reaction times increase the yield of this product as well as the quantity of insoluble solids attributed to OCP oxidation, and consequently reduce the yield of **4.2^{iPr}** (42% yield of **4.2^{iPr}** and 10% yield of **4.3^{iPr}** after 16 h). ¹H NMR (600 MHz, C₆D₆, 298 K): δ 5.11 (m, 4H, CH-*iPr*), 1.65 (s, 12H, C(CH₃)₂), 1.30 (d, *J* = 14.5 Hz, 24H, CH₃-

*i*Pr), -0.67 (s, 3H, Mg(CH₃)). ¹H NMR (600 MHz, THF-*d*₈, 298 K): δ 4.50 (br. s, 4H, CH-*i*Pr), 2.10 (s, 12H, C(CH₃)₂), 1.41 (d, *J* = 6.7 Hz, 24H, CH₃-*i*Pr), -1.68 (s, 3H, MgCH₃). ³¹P NMR (243 MHz, C₆D₆, 298K): δ -366.8. ³¹P NMR (243 MHz, THF-*d*₈, 298K): δ -368.7. ¹³C{¹H} NMR (150.9 MHz, C₆D₆, 298 K): δ 183.3 (s, C_{carbene}), 162.4 (d, ¹*J*_{CP} = 25.4 Hz, OCP), 129.3 (s, CCH₃), 124.8 (s, CCH₃), 52.9 (s, NCH(CH₃)), 22.7 (s, NCH(CH₃)), 10.1 (s, CCH₃), -11.9 (s, MgCH₃). FTIR (solid state): ν 2979 (m), 2932 (m), 2882 (m), 2779 (w), 1798 (w), 1740 (vs, OCP), 1641 (w), 1451 (m), 1354 (s), 1325(m), 1286 (w), 1222 (w), 1200 (w), 1135 (w), 1099 (m), 1071 (w), 904 (w), 855 (m), 740 (m). M.p.: 138–142 °C.

Isolation of [(^{Me}NHC)₂MgMe(μ-OEt)]₂ (4.3^{Me}). In the attempted synthesis of (^{Me}NHC)₂MgMe(OCP) (4.2^{Me}), the same procedure for the synthesis of 4.2^{*i*Pr} was followed by reacting 4.1^{Me} (200 mg, 0.544 mmol) and [Na(dioxane)₂][OCP] (140 mg, 0.544 mmol) in toluene (~ 8 mL). After 6 h, the mixture was filtered, and a clear solution was recovered. This solution was concentrated to 3 mL under vacuum, then 1 mL of hexanes was added, and colorless crystals precipitated overnight at -37 °C. The colorless solid recovered was characterized by ¹H NMR as the dioxane activation product 4.3^{Me} (40 mg, 57% yield), and the molecular structure (Figure 3.1a) was confirmed by X-ray diffraction on a suitable single crystal. ¹H NMR (600 MHz, C₆D₆, 298 K): δ 4.24 (q, *J* = 6.9 Hz, 2H, O(CH₂)), 3.62 (s, 6H, N(CH₃)), 1.50 (t, *J* = 6.9 Hz, 3H, O(CH₂CH₃)), 1.32 (s, 6H, C(CH₃)), -0.56 (s, 3H, Mg(CH₃)). ¹³C{¹H} NMR (150.9 MHz, C₆D₆, 298 K): δ 193.8 (s, C_{carbene}), 184.4 (s, C_{carbene}), 128.6 (s, CCH₃), 125.7 (s, CCH₃), 58.3 (s, OCH₂), 34.4 (s, NCM_e), 22.9 (s, OCH₂CH₃), 8.1 (s, CCH₃), -12.5 (s, MgCH₃). FTIR (solid state): ν 2956 (m), 2883 (m), 1653 (w), 1435 (m), 1373 (s), 1125 (vs), 1070 (s), 898 (m), 842 (m), 729 (s). M.p.: decomposed at 142 °C.

Synthesis of [(^{Me}NHC)₃MgMe][OCP] (4.4^{Me}).

Method A: **4.1^{Me}** (50 mg, 0.136 mmol) and ^{Me}NHC (17 mg, 0.137 mmol) were stirred in fluorobenzene for 30 min, then [Na(dioxane)₂][OCP] (35 mg, 0.136 mmol) was added slowly. After 5 min, trace solids were removed by filtration using a 0.45 μm pore syringe filter. The solution was concentrated and stored at -37 °C, yielding colorless needle-like crystals suitable for X-ray diffraction. These crystals were then washed with toluene to yield **4.4^{Me}** as an off-white solid (25 mg, 39% yield). Notably, **4.3^{Me}** was formed as a minor product (ca. 13% NMR yield in C₆D₅Br). As a result, the solids obtained must be thoroughly washed with toluene to obtain a pure sample of **4.4^{Me}**.

Method B: **4.1^{Me}** (65 mg, 0.177 mmol) and (^{Me}NHC)₃Na(OCP) (80 mg, 0.177 mmol, see below for synthesis) were combined in chlorobenzene and stirred for 15 minutes at RT. The mixture was filtered, concentrated under vacuum, and layered with hexanes to obtain colorless needle-like crystals of **4.4^{Me}** at room temperature (48 mg, 58% yield).

¹H NMR (800 MHz, C₆D₅Br, 333 K) δ 3.49 (s, 18H, NCH₃), 1.73 (s, 18H, CCH₃), -0.94 (s, 3H, MgCH₃). ¹³C NMR (201 MHz, C₆D₅Br, 333 K): δ 186.9 (s, C_{carbene}), 166.8 (d, ¹J_{CP} = 48.1 Hz, OCP), 124.4 (s, CCH₃), 34.4 (s, NCM_e), 8.4 (s, CCH₃), -10.76 (s, MgCH₃). ³¹P NMR (243 MHz, C₆D₅Br, 298K): δ -382.0 (s, OCP). FTIR (solid state): ν 2919 (m), 1800 (vs, OCP), 1770 (vs, OCP), 1653 (m), 1435 (s), 1371 (vs), 1157 (w), 1093 (m), 1023 (w), 969 (w), 843 (s), 732 (vs), 690 (m).

Synthesis of (^{Me}NHC)₃MgMeBr (4.5). ^{Me}NHC (21 mg, 0.124 mmol) was added in one portion to a chlorobenzene (5 mL) suspension of **4.1^{Me}** (50 mg, 0.136 mmol), and a clear solution was observed. After stirring for 3 h at RT, the solution was evaporated under vacuum, and the clathrate residue was triturated several times with hexanes and toluene until a powdery solid was obtained. This solid was further washed with hexanes to recover **4.5** as an off-white solid (45 mg, 70%

yield). ^1H NMR (600 MHz, C_6D_6 , 298 K) δ 3.52 (s, 18H, N(CH_3)), 1.62 (s, 18H, C(CH_3)), -0.69 (s, 3H, Mg(CH_3)). Notably, **4.1**^{Me} crystallizes from a concentrated chlorobenzene/hexanes solution of **4.5** at room temperature. ^1H VT-NMR studies probing dynamic carbene coordination in **4.5** is described in Figure A2.54.

Synthesis of (^{Me}NHC)₃Na(OCP) (4.6). [Na(dioxane)₂][OCP] (173 mg, 0.672 mmol) and ^{Me}NHC (250 mg, 2.02 mmol) were combined in a scintillation vial and stirred in freshly distilled toluene (~12 mL) at room temperature. The relatively insoluble [Na(dioxane)₂][OCP] solids gradually solubilized upon carbene complexation. After 3 h, trace solids were removed by filtration. The filtrate was dried under vacuum and washed with hexanes (3 x 5 mL) to obtain **4.6** as a light-yellow solid (200 mg, 66 % yield). Single crystals suitable for X-ray diffraction were obtained from a concentrated toluene solution at -37 °C. ^1H NMR (600 MHz, C_6D_6 , 298 K): δ 3.52 (s, 6H, NCH₃), 1.51 (s, 6H, CCH₃). $^{13}\text{C}\{^1\text{H}\}$ NMR (150.9 MHz, C_6D_6 , 298 K): δ 188.8 (C_{carbene}), 123.1 (s, CCH₃), 35.3 (s, NCM_e), 8.6 (s, CCH₃). ^{31}P NMR (243 MHz, C_6D_6 , 298K): δ -388.4 (s, OCP). FTIR (solid state): ν 2923 (m), 1761 (vs, OCP), 1653 (w), 1576 (w), 1451 (m), 1399 (m), 1368 (s), 1211 (w), 1130 (w), 1094 (w), 961 (w), 840 (s), 719 (s). M.p.: 104-110 °C. Compound **4.6** is thermally stable, and shows no decomposition after 4 days in refluxing benzene.

Isolation of (^{iPr}NHC)₂Mg(OEt)(OCP) (4.8) and [^{iPr}NHC]Mg(μ -OEt)(OCP)₂ (4.9). In the attempted synthesis of (^{iPr}NHC)₂Mg(OCP)₂, a toluene suspension of [Na(dioxane)₂][OCP] (100 mg, 0.386 mmol) was added dropwise to a toluene (10 mL) solution of (^{iPr}NHC)₂MgBr₂ (100 mg, 0.186 mmol), which had been cooled for 30 minutes in the glovebox freezer (-37 °C). The mixture was stirred for 4 h at room temperature and then filtered through a 0.45 μm syringe filter. The clear, light-tan solution was concentrated under vacuum to 2 mL, and slow diffusion of hexanes into this solution at room temperature yielded a white solid identified as **4.8** by solution-state ^1H

NMR spectroscopy. A few colorless single crystals were also obtained from the same solution and characterized by X-ray diffraction as **4.9**. However, enough single crystals of **4.9** could not be obtained for spectroscopic analysis. Notably, the products of this reaction were only isolated by crystallization. The filtrate reduces to a viscous oil under vacuum, and several attempts to obtain a solid by trituration using hexanes were unsuccessful.

Yield: 15 mg (16% based on **4.8** and 28% based on **4.9**). ^1H NMR (600 MHz, C_6D_6 , 298 K): δ 4.53 (br. s, 4H, $\text{CH-}i\text{Pr}$), 3.89 (q, $J = 6.9$ Hz, 2H, OCH_2), 1.65 (s, 12H, $\text{C}(\text{CH}_3)_2$), 1.50 (d, $J = 6.8$ Hz, 24H, CH_3-iPr), 1.32 (t, $J = 6.9$ Hz, 3H, OCH_2CH_3). ^{31}P NMR (243 MHz, C_6D_6 , 298K): δ -364.9 (s, OCP). $^{13}\text{C}\{^1\text{H}\}$ NMR (150.9 MHz, C_6D_6 , 298 K): δ 188.7 (s, $\text{C}_{\text{carbene}}$), 161.3 (s, OCP), 58.3 (s, OCH_2), 51.3 (br. s, $\text{NCH}(\text{CH}_3)$), 23.7 (s, OCH_2CH_3), 22.4 (s, $\text{NCH}(\text{CH}_3)$), 9.4 (s, CCH_3). Sufficiently resolved ^{13}C - ^{31}P coupling information could not be obtained in the $^{13}\text{C}\{^1\text{H}\}$ NMR spectrum for the $\text{C}\equiv\text{P}$ resonance (δ 161.3 ppm). FTIR (solid state): ν 2971 (m), 2930 (m), 2865 (w), 2712 (w), 1727 (vs, OCP), 1634 (w), 1453 (m), 1348 (s), 1310(m), 1220 (m), 1107 (s), 1064 (s), 889 (m), 848 (m), 751 (m), 721 (w).

*Synthesis of $(^{\text{Me}}\text{NHC})_3\text{Mg}(\text{OCP})_2$ (**4.10**).* $^{\text{Me}}\text{NHC}$ (32 mg, 0.254 mmol) and $(^{\text{Me}}\text{NHC})_2\text{MgBr}_2$ (100 mg, 0.231 mmol) were combined in toluene (15 mL) and stirred for 1.5 h at room temperature. The reaction mixture was cooled to -37 °C, and a pre-cooled suspension of $[\text{Na}(\text{dioxane})_2][\text{OCP}]$ (125 mg, 0.486 mmol) in toluene (10 mL) was added dropwise. After 1.5 h, the mixture was filtered over a Buchner funnel, and the filtrate was stored at -37 °C yielding colorless crystals of **4.10** (41 mg, 35% yield). ^1H NMR (600 MHz, C_6D_6 , 298 K): δ 3.51 (s, 6H, NCH_3), 1.47 (s, 6H, CCH_3). $^{13}\text{C}\{^1\text{H}\}$ NMR (150.9 MHz, C_6D_6 , 298 K): δ 189.4 (s, $\text{C}_{\text{carbene}}$), 168.97 (d, $^1J_{\text{CP}} = 52.9$ Hz, OCP), 129.3 (s, CCH_3), 128.6 (s, CCH_3), 125.7 (s, CCH_3), 34.9 (s, NCMe), 8.4 (s, CCH_3). ^{31}P NMR (243 MHz, C_6D_6 , 298K): δ -385.6 (s, OCP). FTIR (solid state): ν 2951 (m), 2930 (m), 2860 (w), 2705

(w), 2556 (w), 1744 (vs, OCP), 1632 (w), 1576 (m), 1440 (m), 1368 (s), 1211 (m), 1131 (m), 1066 (m), 963 (w), 894 (w), 840 (m), 812 (m), 719 (m).

Isolation of [(^{Me}NHC)₂P^I][OCP] (4.11). In a J-Young NMR tube, a 20 mg sample of **4.10** in C₆D₆ was heated at 105 °C for three days. During this time, the colorless solution gradually became orange, and a yellow paste formed on the walls of the NMR tube. In one instance light yellow crystals of **4.11** were obtained at room temperature by layering the orange solution with hexanes. In the ¹H NMR, resonances corresponding to **4.11** and free ^{Me}NHC were identified. However, the ³¹P NMR indicates that a phosphorus-containing species, which is yet unidentified, is likely the major product of this reaction.

Chapter Five:

Additional Considerations. HNMe₂BH₃ (sublimed before use, 27-30 °C, high vacuum) and Mg(*n*Bu)₂ were purchased from Sigma Aldrich. 1,3-diisopropyl-4,5-dimethylimidazol-2-ylidene (^{iPr}NHC),²¹⁷ 1,3,4,5-tetramethylimidazol-2-ylidene (^{Me}NHC),²¹⁷ Mg(N(SiMe₃)₂)₂, (^{iPr}NHC)Mg(N(SiMe₃)₂)₂ (**5.1**),¹⁷⁴ and (THF)Mg(NMe₂BH₂NMe₂BH₃)₂⁵⁵ were synthesized according to the literature and recrystallized prior to use. Satisfactory combustion microanalyses could not be obtained for the isolated complexes due to their high air and moisture sensitive nature. NMR spectra have been provided as further evidence of bulk purity.

Synthesis of (^{iPr}NHC-BN)Mg(NMe₂BH₃)(N(SiMe₃)₂) (5.2). To a stirring solution of (^{iPr}NHC)Mg(N(SiMe₃)₂)₂ (300 mg, 0.571 mmol) in hexanes (~ 5 mL) was added solid HNMe₂BH₃ (85 mg, 1.14 mmol) slowly. After 1 h, the colorless solution was concentrated under vacuum, and stored at -37 °C yielding colorless crystals of the title product. After removal of the supernatant and drying under vacuum, **5.2** was obtained as a white solid (160 mg, 67% yield). ¹H NMR (600 MHz, C₆D₆, 298 K): δ 5.37 (hept., *J* = 7.1 Hz, 2H, *CH-iPr*), 2.75 (s, 6H, N(CH₃)₂), 2.44 (s, 6H,

$\text{N}(\text{CH}_3)_2$), 1.42 (s, 6H, $\text{C}(\text{CH}_3)_2$), 0.93 (d, $J = 7.1$ Hz, 12H, CH_3 -*i*Pr), 0.58 (s, 18H, $\text{Si}(\text{CH}_3)_3$). ^{11}B NMR (192 MHz, C_6D_6 , 298 K): -14.89 (q, $J = 90.2$ Hz, BH_3), -17.33 (t, $J = 85.4$ Hz, BH_2). $^{13}\text{C}\{^1\text{H}\}$ NMR (151 MHz, C_6D_6 , 298 K): δ 188.8 ($\text{C}_{\text{carbene}}$), 125.6 ($\text{C}(\text{CH}_3)$), 50.9 (CH -*i*Pr), 48.3 ($\text{N}(\text{CH}_3)_2$), 46.5 ($\text{N}(\text{CH}_3)_2$), 21.0 ($\text{C}(\text{CH}_3)$), 10.0 (CH_3 -*i*Pr), 6.19 ($\text{Si}(\text{CH}_3)_3$).

Synthesis of $i\text{PrNHC-BN}$

Method 1: In a 100 mL Schlenk flask, HNMe_2BH_3 (50 mg, 0.849 mmol) and 10 mol% $\text{Mg}(\text{N}(\text{SiMe}_3)_2)_2$ (30 mg, 0.087 mmol) were stirred in toluene (~ 8 mL), and heat to 60 °C under constant argon flow. Formation of $[\text{Me}_2\text{NBH}_2]_2$ ($\delta_{\text{B}} = 5.02$ ppm) was monitored by ^{11}B NMR. After 24 h, $i\text{PrNHC}$ (150 mg, 0.831 mmol) was added to the solution and heat for 2 h at 80 °C. Volatiles were evaporated under vacuum and the resultant solid was washed using hexanes (2 x 3 mL) to afford the title compound as a white solid (90 mg, 46% yield). Note that $i\text{PrNHC-BN}$ is moderately soluble in hexanes, but the solvent is necessary to remove the more soluble unreacted carbene and Mg-based products. ^1H NMR (600 MHz, C_6D_6 , 298 K): δ 6.26 (br. s, 2H, CH -*i*Pr), 2.97 (q, $J = 90$ Hz, 2H, BH_2), 2.79 (s, 6H, $\text{N}(\text{CH}_3)_2$), 1.59 (s, 6H, $\text{C}(\text{CH}_3)$), 1.17 (d, $J = 7.0$ Hz, 12H, CH_3 -*i*Pr). ^{11}B NMR (192 MHz, C_6D_6 , 298 K): -13.4 (t, $J = 89.3$ Hz, BH_2). $^{13}\text{C}\{^1\text{H}\}$ NMR (201 MHz, C_6D_6 , 298 K): δ 123.7 ($\text{C}(\text{CH}_3)$), 48.2 (CH -*i*Pr), 48.1 ($\text{N}(\text{CH}_3)_2$), 21.4 ($\text{C}(\text{CH}_3)$), 10.0 (CH_3 -*i*Pr).

Method 2: The same procedure for the synthesis of **5.9** (*vide infra*) was followed except 3 equivalents of $i\text{PrNHC}$ (270 mg, 1.5 mmol) was added. $i\text{PrNHC-BN}$ was extracted from the mixture using hexanes (15 mL) and recrystallized at room temperature (85 mg, 36% yield). After initial extraction, the leftover solids contained $i\text{PrNHC-BN}$ (minor) and **5.8** (major) as the only products in the ^1H and ^{11}B NMR spectra.

*Synthesis of $(^{\text{Me}}\text{NHC})_2\text{Mg}(\text{N}(\text{SiMe}_3)_2)_2$ (**5.3**).* To a solution of $\text{Mg}(\text{N}(\text{SiMe}_3)_2)_2$ (264 mg, 0.765 mmol) in toluene (~10 mL) was added $^{\text{Me}}\text{NHC}$ (200 mg, 1.61 mmol) in one portion and stirred for

16 h at room temperature. The clear solution was concentrated under vacuum to incipient crystallization of solids, and colorless block-like crystals were obtained after a few hours at room temperature. After removal of the supernatant, the crystals were washed with hexanes (1 x 3 mL) and dried under vacuum to obtain **5.3** as a colorless solid (250 mg, 55%). ^1H NMR (600 MHz, C_6D_6 , 298 K): δ 3.53 (s, 6H, N(CH₃)), 1.45 (s, 6H, C(CH₃)), 0.38 (s, 18H, Si(CH₃)₃). $^{13}\text{C}\{^1\text{H}\}$ NMR (151 MHz, C_6D_6 , 298 K): δ 188.9 (*C_{carbene}*), 124.36 (C(CH₃)), 35.4 (N(CH₃)), 8.3 (C(CH₃)), 6.9 (Si(CH₃)₃).

*Isolation of $(^{\text{Me}}\text{NHC-BN})\text{Mg}(\text{NMe}_2\text{BH}_3)(\text{N}(\text{SiMe}_3)_2)$ (**5.4**).* HNMe₂BH₃ (20 mg, 0.356 mmol) was added in one portion to a toluene solution of **5.3** (100 mg, 0.169 mmol). Vigorous bubbling was immediately observed, indicating rapid dehydrocoupling, but the reaction was allowed to stir for 6 h at room temperature. The resultant colorless solution was concentrated to ~1.5 mL and stored at -37 °C, yielding colorless crystals. Spectroscopic (^1H and ^{11}B NMR) analysis indicate the presence of multiple co-crystallized species including **5.4** and uncoordinated $^{\text{Me}}\text{NHC-BN}$ and the title product could not be isolated as a pure compound.

*Isolation of $\text{Mg}_4(\mu\text{-O})(\text{NMe}_2\text{BH}_3)_6$ (**5.5**) and $(\text{THF})_2\text{Mg}(\text{NMe}_2\text{BH}_3)_2$ (**5.6**).* A hexanes solution (~10 mL) of HNMe₂BH₃ (112 mg, 1.90 mmol) in a 100 mL Schlenk flask was cooled to 0 °C in an ice bath, then Mg(*n*Bu)₂ (1M in hexanes, 1 mL, 1.00 mmol) was added dropwise to the stirring solution. The colorless solution was slowly warmed to room temperature and stirred for 1.5 h, after which all volatiles were evaporated and a sticky oil was recovered. The product was redissolved in minimal hexanes (~ 0.5 mL) and mechanically agitated using a glass pipette, resulting in the immediate precipitation of colorless crystals from which **5.5** was identified by X-ray crystallography. Spectroscopic studies and combustion microanalysis on the isolated crystals suggest they are not analytically pure. Multiple attempts at identifying the co-crystallized solids

were inhibited by rapid decomposition by polymerization of the X-ray paratone oil. Notably, the THF adduct (**5.6**) was crystallized from a concentrated hexanes/THF (100/1) solution of **5.5**, but likewise attempts to purify **5.6** was inhibited by its high solubility in organic solvents.

Synthesis of (DMAP)₂Mg(NMe₂BH₃)₂ (5.7). DMAP (50 mg, 0.422 mmol) was dissolved in minimal toluene and added to a hexanes solution of **5.6** (68 mg) with vigorous stirring. A homogenous colorless solution was initially observed after addition, but continued stirring resulted in the precipitation of white solids, which were collected by filtration after 15 minutes. Further wash using hexanes (1 x 5 mL) yielded the title product as an analytically pure white solid (62 mg, 77 % yield). Notably, the toluene/hexanes filtrate contained (DMAP)Mg(NMe₂BH₂NMe₂BH₃)₂ (**5.11**, *vide infra*) due to the presence of the THF adduct in the starting material. Colorless crystals of **7** suitable for X-ray diffraction were obtained from a toluene sample which was concentrated at 80 °C, and slowly cooled to room temperature. ¹H NMR (800 MHz, C₆D₆, 298 K): δ 8.53 (m, 2H, ArH), 5.89 (d, *J* = 7.0 Hz, 2H, ArH), 2.60 (m, 9H, N(CH₃)₂ + BH₃), 2.11 (s, 6H, N(CH₃)₂). ¹¹B NMR (192 MHz, C₆D₆, 298 K) δ -13.8 (q, *J* = 89.6 Hz, BH₃). ¹³C {¹H} NMR (201 MHz, C₆D₆, 323 K): δ 154.9 (ArC), 150.1 (ArC), 106.7 (ArC), 106.3 (ArC), 49.6 (br. s, N(CH₃)₂), 38.1 (q, *J* = 64.0 Hz, N(CH₃)₂).

Synthesis of (ⁱPrNHC)Mg(NMe₂BH₃)₂ (5.8). A few drops of THF were added to a hexanes solution (~10 mL) of HNMe₂BH₃ (112 mg, 1.90 mmol) in a 100 mL Schlenk flask, and the solution was cooled to 0 °C in an ice bath. Then, Mg(*n*Bu)₂ (1M in heptanes, 1 mL, 1.00 mmol) was added dropwise via syringe to the stirring solution. The colorless solution was slowly warmed to room temperature and stirred for 1.5 h, after which all volatiles were evaporated under vacuum. The sticky solid recovered was redissolved in toluene, and ⁱPrNHC (177 mg, 0.982 mmol) was added. After stirring for 1.5 h at room temperature, the colorless solution was filtered, concentrated, and

stored at -37 °C yielding colorless crystals of the title product after two days. After isolation of initial product, repeated concentration and recrystallizations of the supernatant, followed by hexanes wash (2 x 2 mL), afforded **5.8** as a colorless solid (237 mg, 74% yield). ¹H NMR (600 MHz, C₆D₆, 298 K): δ 4.57 (hept, *J* = 7.0 Hz, 2H, *CH*-*i*Pr), 2.52 (s, 12H, N(CH₃)₂), 1.52 (s, 6H, C(CH₃)₂), 1.14 (d, *J* = 7.0 Hz, 12H, CH₃-*i*Pr). ¹¹B NMR (192 MHz, C₆D₆, 298 K): -15.5 (q, *J* = 87.3 Hz, BH₃). ¹³C{¹H} NMR (151 MHz, C₆D₆, 298 K): δ 188.4 (*C*_{carbene}), 179.1 (*C*_{carbene}), 129.3 (*C*(CH₃)), 125.3 (*C*(CH₃)), 54.1 (*CH*-*i*Pr), 48.1 (N(CH₃)₂), 22.2 (*C*(CH₃)), 9.8 (CH₃-*i*Pr).

Synthesis of (ⁱPrNHC)Mg(NMe₂BH₂NMe₂BH₃)₂ (5.9). A few drops of THF were added to a hexanes solution (~10 mL) of HNMe₂BH₃ (112 mg, 1.90 mmol) in a 100 mL Schlenk flask, then Mg(*n*Bu)₂ (1M in heptanes, 0.5 mL, 0.500 mmol) was added dropwise via syringe with vigorous stirring at room temperature. After 16 h, volatiles were removed using vacuum and a white solid (~140 mg) was recovered. In the glovebox, the solid was redissolved in hexanes, and sub-stoichiometric ⁱPrNHC (77 mg, 0.427 mmol) was added in one portion, resulting in immediate precipitation of white solids, which were further redissolved in toluene. Colorless single crystals were obtained from the concentrated toluene solution at room temperature and confirmed by X-ray diffraction as the title compound. Yield: 90 mg (49%). Anal. Calc'd (Found) for C₁₉H₅₄B₄MgN₆ (MW: 434.23 g/mol): C 52.56 (51.82), H 12.54 (12.39), N 19.35 (18.03). NMR studies suggest dynamic disproportionation reactions, and **5.9** is not observed (Figures A2.93 and A2.94).

Synthesis of (DMAP)Mg(NMe₂BH₂NMe₂BH₃)₂ (5.11). DMAP (19 mg, 0.153 mmol) was dissolved in minimal toluene (~3 mL), then (THF)Mg(NMe₂BH₂NMe₂BH₃)₂ (50 mg, 0.153 mmol) was added in one portion and shaken together. As soon as a homogenous solution was formed, the reaction was left undisturbed and colorless, X-ray quality crystals of **5.11** rapidly precipitated from the concentrated solution at room temperature (40 mg, 70% yield). ¹H NMR (600 MHz, C₆D₆, 298

K) δ 8.52 (d, $J = 7.1$ Hz, 2H), 5.82 (d, $J = 7.3$ Hz, 2H), 2.57 – 2.01 (m, 40H, overlapped $N(CH_3)_2$, BH_2 and BH_3 resonances). ^{11}B NMR (192 MHz, C_6D_6 , 298 K) δ 3.0 (m, BH_2), -15.7 (q, $J = 81.6$, 77.7 Hz, BH_3). ^{13}C NMR (151 MHz, C_6D_6 , 298 K) δ 154.7 (ArC), 149.4 (ArC), 106.2 (ArC), 53.5 ($N(CH_3)_2$), 51.9 ($N(CH_3)_2$), 47.1 ($N(CH_3)_2$), 44.9 ($N(CH_3)_2$), 38.0 ($N(CH_3)_2$).

Isolation of (ⁱPrNHC)Mg(NMe₂BH₃)(NMe₂BH₂NMe₂BH₃) (5.12). Compound **5.8** (30 mg, 0.0936 mmol) and HNMe₂BH₃ (5 mg, 0.0894 mmol) were combined in a 1:1 toluene/hexanes mixture and stirred for 1 h. The colorless solution was evacuated to dryness and 1H NMR (C_6D_6 , 298 K) was obtained, which indicated the presence of **5.8** and **5.10**. Prolonged reaction times (3 days) did not result in further changes in the integral ratios of the carbenic products. Recrystallization of the solids from a concentrated hexanes/toluene mixture afforded single crystals of the title product (25 mg, 76 %). VT-NMR studies confirm the dynamic disproportionation of **5.12**.

Isolation of (ⁱPrNHC)Mg(N(SiMe₃)₂)(NMe₂BH₂NMe₂BH₃) (5.13). Compound **5.2** (15 mg, 0.0354 mmol) and HNMe₂BH₃ (4 mg, 0.0708 mmol) were combined in hexanes and vigorous bubbling was immediately observed. After stirring overnight, the colorless solution was concentrated and stored at -37 °C yielding colorless crystals of the title compound. 1H and ^{11}B NMR studies show the presence of **5.2**, **5.8**, **5.10**, and ⁱPrNHC-BN, which may be due to competitive silylamide protonolysis or Schlenk-type rearrangements of **5.13**, followed by the same dynamic disproportionation of **5.10** observed in **5.9** and **5.12**. Notably, a 1:2 stoichiometric ratio of **5.2**/HNMe₂BH₃ was necessary to obtain crystals of **5.13**. Repeated attempts using a 1:1 ratio yielded crystals of **5.2** instead, despite evidence for the consumption of HNMe₂BH₃. This was ascribed to Schlenk-type rearrangements in **5.13**, resulting in bis(silylamide) species that may further react with HNMe₂BH₃ to yield **5.2** (Figure A2.108). Furthermore, in VT studies (Figures

A2.111 and A2.112), **5.2** appear unchanged suggesting that the dynamic disproportionation processes are due to **5.10**.

Chapter Six:

Additional Considerations. Diethyl-substituted cyclic (alkyl)(amino) carbene (CAAC)¹¹⁵ and *N,N'*-diisopropyl-2,3-dimethylimidazol-2-ylidene (NHC)²¹⁷ were prepared according to the literature and recrystallized from hexanes before use. CAAC-CO₂³⁵³ and NHC-BN¹⁰⁵ were prepared according to the literature. KN(SiMe₃)₂ (Millipore Sigma) and CaI₂ (Strem Chemical Inc) were purchased from commercial sources and without further purification. Dimethylamine borane (Millipore Sigma) was purified by sublimation.

*Synthesis of [Ca(N(SiMe₃)₂)₂]₂ via (Et₂O)₂Ca(N(SiMe₃)₂)₂ (**6.1**)* – Calcium iodide (2.000 g, 6.81 mmol) and potassium hexamethyldisilazane (2.715 g, 13.61 mmol) were combined in a 250 mL Schlenk pressure tube and suspended in diethyl ether (approx. 80 mL). The resulting white suspension was stirred vigorously at 40 °C for 2 d. All volatiles were removed under vacuum until a white solid was obtained. The solid was extracted with hexanes (approx. 80 mL) and dried completely under reduced pressure to yield a bright white solid which was determined to be the solvent-free dimer (1.756 g, 72% yield). ¹H NMR data of this product matched those reported in the literature. NOTE: due to the ease with which coordinated diethyl ether can be removed from **6.1**, complete characterization data could not be obtained for that species. To obtain single crystals of **6.1** for X-ray diffraction studies, the initial removal of Et₂O and other volatiles from the reaction mixture was stopped once a sticky white residue was obtained (instead of evaporating to dryness). This residue was extracted with hexanes, and the filtrate concentrated to yield single crystals of the ether-coordinated species at -39 °C. Keeping these crystals under reduced pressure for any period of time resulted in conversion to the solvent-free species.

Synthesis of (NHC)Ca(N(SiMe₃)₂)₂ (6.2) – Free NHC (1.000 g, 2.77 mmol) and Ca(N(SiMe₃)₂)₂ (0.500 g, 2.77 mmol) were combined in a 100 mL Schlenk flask and dissolved in minimal hexanes (approx. 50 mL). The resulting colorless solution was stirred for 1 h at RT and dried completely under reduced vacuum. The resulting off-white solid was collected and determined to be the product, **6.2**, (1.43 g, 95%). Single crystals suitable for X-ray diffraction studies were obtained from keeping a saturated solution of **6.2** in hexanes at –39 °C. ¹H NMR (600 MHz, C₆D₆) δ 4.20 (hept, 2H, *J* = 7.1 Hz, (CH₃)₂CH), 1.50 (s, 6H, C(CH₃)), 1.31 (d, 12H, *J* = 6.8 Hz, (CH₃)CH), 0.38 (s, 36H, Si(CH₃)₃); ¹³C NMR (150.90 MHz, C₆D₆) δ 124.2 (C(CH₃)), 51.4 (NCH(CH₃)₂), 23.8 (C(CH₃)), 9.3 ((CH₃)₂CH), 6.0 (Si(CH₃)₃); m.p.: 150-154 °C.

Synthesis of (NHC)₂Ca(N(SiMe₃)₂)₂ (6.3) – Procedure followed exactly from **6.2** using the following amounts: NHC (0.200 g, 1.11 mmol); Ca(N(SiMe₃)₂)₂ (0.200 g, 0.554 mmol). Yield: 0.363 g, 91%. Spectroscopic data matched those previously reported.¹⁰²

Synthesis of (NHC)(THF)Ca(N(SiMe₃)₂)₂ (6.4) – The procedure for synthesis of **2** was followed using NHC (0.350 g, 1.94 mmol) and (THF)₂Ca(HMDS)₂ (0.980 mg, 1.94 mmol). Compound **6.4** was isolated via the same method as **6.2** and **6.3** as an off-white hydrocarbon-soluble solid (1.17 g, 98%). ¹H NMR (600 MHz, C₆D₆) δ 4.22 (br. s, 2H, (CH₃)₂CH), 3.58 (m, 4H, THF) 1.48 (s, 6H, C(CH₃)), 1.37 (m, 4H, THF) 1.31 (br. s, 12H, (CH₃)CH), 0.39 (s, 36H, Si(CH₃)₃); ¹³C NMR (150.90 MHz, C₆D₆) δ 100.4 (C(CH₃)), 68.4 (THF), 51.5 (NCH(CH₃)₂), 25.6 (THF), 23.7 (C(CH₃)), 9.2 ((CH₃)₂CH), 6.0 (Si(CH₃)₃); m.p.: decomp. 97 °C.

Isolation of (CAAC)Ca(N(SiMe₃)₂)₂ (6.5) – Crystalline Ca(N(SiMe₃)₂)₂ (50 mg, 0.139 mmol) and diethyl-substituted CAAC (43 mg, 0.139 mmol) were combined in a 20 mL scintillation vial and dissolved in minimal hexanes (approx. 10 mL). The resulting solution was concentrated to saturation and kept at -39 °C, yielding colorless single crystals of **6.5** suitable for X-ray diffraction.

Due to extreme instability of the compound, attempts to characterize **6.5** in solution were unsuccessful. A representative ^1H NMR spectrum is shown in Figure A2.117.

*Synthesis of $\text{Ca}(\text{NMe}_2\text{BH}_3)_2$ (**6.6**)* – $(\text{THF})_2\text{Ca}(\text{N}(\text{SiMe}_3)_2)_2$ (430 mg, 0.851 mmol) and HNMe_2BH_3 (100 mg, 1.70 mmol) were combined in a scintillation vial containing a toluene/THF (100/1, ca. 8 mL) mixture. All solids dissolved and the colorless solution was allowed to sit undisturbed for 30 min, then volatiles were evacuated under vacuum. The sticky white residue was triturated and washed using hexanes to yield the title compound as a white solid (120 mg, 92% yield). NOTE: This compound readily loses any coordinated THF under vacuum, and the solvent-free species is sparingly soluble in non-polar or aromatic solvents. For well-resolved NMR resonances, one pipette drop of THF- d_8 was added to the C_6D_6 suspension, resulting in complete dissolution of **6.6**. ^1H NMR (600 MHz, C_6D_6) δ 2.52 (s, 6H, $\text{N}(\text{CH}_3)_2$), 1.95 (q, $J = 87.0$ Hz, 3H, BH_3). ^{11}B NMR (192 MHz, C_6D_6) -13.3 (q, $J = 87.3$ Hz, BH_3). ^{13}C NMR (201 MHz, C_6D_6) δ 47.8 ($\text{N}(\text{CH}_3)_2$). Anal. Calc'd (Found) for $\text{C}_4\text{H}_{18}\text{B}_2\text{CaN}_2$ (MW: 155.90 g/mol): C, 30.82 (30.95); H, 11.64 (11.59); N, 17.97 (16.96). m.p.: > 250 °C.

*Synthesis of $(\text{NHC})_2\text{Ca}(\text{NMe}_2\text{BH}_3)_2$ (**6.7**)* – $\text{Ca}(\text{NMe}_2\text{BH}_3)_2$ (50 mg, 0.321 mmol) was dissolved in a toluene/THF (100/1) solution, then added dropwise to a concentrated solution of NHC (116 mg, 0.642 mmol) in toluene. After 30 min, volatiles were evacuated under vacuum and the residue triturated using hexanes to afford the title compound as a white solid (138 mg, 83% yield). ^1H NMR (800 MHz, C_6D_6) δ 5.04 (br. s, 2H, $(\text{CH}_3)_2\text{CH}$), 2.69 (s, 6H, $\text{N}(\text{CH}_3)_2$), 2.31 (q, $J = 86.7$ Hz, 3H), 1.65 (s, 6H, $\text{C}(\text{CH}_3)$), 1.24 (br. s, 12H, $(\text{CH}_3)\text{CH}$). ^{11}B NMR (192 MHz, C_6D_6) -16.1 (q, $J = 88.3$ Hz, BH_3). ^{13}C NMR (201 MHz, C_6D_6) δ 123.8 ($\text{C}(\text{CH}_3)$), 52.6 ($\text{NCH}(\text{CH}_3)_2$), 48.7 ($\text{N}(\text{CH}_3)_2\text{BH}_3$), 22.6 ($\text{C}(\text{CH}_3)$), 10.0 ($\text{NCH}(\text{CH}_3)_2$). m.p.: 127-132 °C.

Synthesis of [(NHC-BN)Ca(NMe₂BH₃)₂]₂ (6.8) – In a 20 mL scintillation vial, NHC–BN (25 mg, 0.105 mmol)¹⁰⁵ and Ca(NMe₂BH₃)₂ (17 mg, 0.109 mmol) were combined in a hexanes/THF 100/4 mixture and shaken until clear. The colorless solution was concentrated to incipient crystallization of solids and stored undisturbed at room temperature, yielding colorless crystals of **6.8** within two hours (30 mg, 73 % yield). ¹H NMR (600 MHz, C₆D₆) δ 5.81 (br. s, 2H, (CH₃)₂CH), 2.68 (s, 12H, N(CH₃)₂BH₃), 2.59 (s, 6H, N(CH₃)₂BH₂), 2.11 (q, *J* = 86.5 Hz, 6H, BH₃), 1.60 (s, 6H, C(CH₃)), 1.11 (d, *J* = 7.1 Hz, 12H, (CH₃)CH). ¹¹B NMR (192 MHz, C₆D₆) -13.4 (q, *J* = 89.8 Hz, BH₃), -15.5 (br. t, *J* = 88.3 Hz, BH₂). ¹³C NMR (151 MHz, C₆D₆) δ 124.7 (C(CH₃)), 50.1 (NCH(CH₃)₂), 48.6 (N(CH₃)₂BH₃), 47.1 (N(CH₃)₂BH₂), 21.3 (C(CH₃)), 10.1 (NCH(CH₃)₂). Anal. Calc'd (Found) for C₁₇H₄₇B₃CaN₅ (MW: 394.11 g/mol): C, 51.81 (51.56); H, 12.02 (11.94); N, 17.77 (17.29). m.p: 178-180 °C.

Isolation of (THF)₂Ca(NMe₂BH₃)(NMe₂BH₂NMe₂BH₃) (6.9)

Method A: CaH₂ (50 mg, 1.19 mmol) was stirred in THF (~ 8 mL) overnight to yield a fine gray powder, then HNMe₂BH₃ (210 mg, 3.56 mmol) was added in one portion and the reaction was stirred for 4 d at room temperature. Filtering the reaction mixture afforded colorless filtrate, which was concentrated to an oil under vacuum. Addition of minimal hexanes resulted in the precipitation of crystalline solids from which **6.9** was identified by single-crystal X-ray diffraction, but the presence of **7** among the solids was confirmed by ¹¹B NMR spectroscopy (approx. 3:4 ratio of **6.6**:**6.9**), and the compounds could not be separated by fractional crystallization.

Method B: (THF)₂Ca(N(SiMe₃)₂)₂ (356 mg, 0.705 mmol) and HNMe₂BH₃ (124 mg, 2.11 mmol) were combined in a toluene/THF mixture (100/1) and stirred at room temperature for 3 days, but similar observations as method A were observed after workup. NMR-monitored stoichiometric reactions of **6.6** (15 mg, 0.064 mmol) and HNMe₂BH₃ (5.7 mg, 0.064 mmol) with moderate

heating (30 °C) for 6 days suggest a catalytic process due to the persistence of **6.6**, as well as formation of $[\text{Me}_2\text{NBH}_2]_2$ and $\text{HB}(\text{NMe}_2)_2$ in congruence with previous reports.^{55, 296}

Chapter Seven:

Additional Considerations. BiBr_3 , $\text{Ag}(\text{SbF}_6)$, $\text{Ag}(\text{BF}_4)$, $\text{Ag}(\text{NTf}_2)$, XeF_2 , PhSiH_3 , and TEMPO were purchased from commercial sources and used as received. BiCl_3 (Sigma Aldrich) was purified by extraction into refluxing toluene to yield crystalline (toluene) BiCl_3 . Di(*ortho*)lithiated carbodiphosphorane $\text{Li}_2(\text{CDP})$,³⁹⁵ $\text{Na}[\text{BAR}^{\text{F}}_4]$ ⁴²³ and $[\text{HNEt}_3][\text{BPh}_4]$ ⁴⁰³ were synthesized according to the literature. Combustion microanalysis was performed using a PerkinElmer Series 2400 II CHNS/O Analyzer. NMR spectra for all complexes have been provided as further evidence of bulk purity.

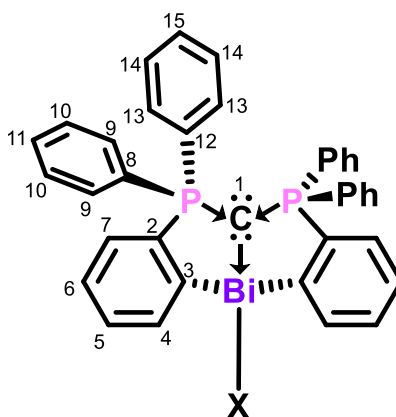


Figure A1.1. To simplify assignment of proton and carbon resonances, the numbering scheme above has been adopted.

General procedure for the synthesis of 7.1 and 7.2. In a 50 mL Schlenk flask $\text{Li}_2(\text{CDP})$ (300 mg, 0.547 mmol) was dissolved in toluene (~ 10 mL) and cooled to $-78\text{ }^\circ\text{C}$. Then, an equimolar amount of BiCl_3 or BiBr_3 in THF (~5 mL) was added via cannula through the Schlenk flask sidearm. An orange-yellow solution was immediately observed, and was stirred at $-78\text{ }^\circ\text{C}$ for 30-45 min. Upon warming to room temperature, precipitation of light brown solids was observed, and discoloration to white (after > 24 h) indicated reaction completion. Solvents were removed via vacuum, and the

crude material was washed with toluene before the product was extracted using copious amounts of DCM (40-60 mL). Evaporation to dryness yielded analytically pure colorless solids. Typical yields range from 70-80%, but can be increased with prolonged reaction times (48 – 72 h) and/or multiple DCM extractions of the crude material. X-ray quality single crystals were obtained from a layered DCM/hexanes solution at room temperature.

(CDP)BiCl (7.1). Yield: 77 %. $^1\text{H NMR}$ (800 MHz, CD_2Cl_2 , 298 K): δ 9.32 (d, $^1J_{\text{HH}}$ 7.6 Hz, 2H, H_4), 8.06–8.00 (m, 4H, $H_6 + H_7$), 7.69–7.66 (m, 2H, H_5), 7.54 (t, $^1J_{\text{HH}}$ 7.3 Hz, 2H, H_{11}), 7.50 (t, $^1J_{\text{HH}}$ 7.9 Hz, 4H, H_{10}), 7.47 (m, 4H, H_9), 7.22 (t, $^1J_{\text{HH}}$ 8.1 Hz, 2H, H_{15}), 6.94 (t, $^1J_{\text{HH}}$ 6.6 Hz, 4H, H_{14}), 6.89–6.87 (m, 4H, H_{13}). $^{31}\text{P}\{^1\text{H}\}$ NMR (243 MHz, CD_2Cl_2 , 298 K): δ 38.4. $^{13}\text{C}\{^1\text{H}\}$ NMR (201 MHz, CD_2Cl_2 , 298 K): δ 179.7 (t, $^3J_{\text{PC}} = 13.2$ Hz, C_3), 147.6 (m, C_2), 140.2 (t, $^3J_{\text{PC}} = 7.7$ Hz, C_4), 135.5 (t, $J_{\text{PC}} = 7.6$ Hz, C_9), 134.8 (m, C_8/C_{12}), 133.0 (t, $J_{\text{PC}} = 5.3$ Hz, C_{13}), 132.3 (m, $C_5 + C_6$), 131.9 (C_{11}), 131.8 (C_{15}), 131.1 (m, C_8/C_{12}), 130.2 (dd, $J_{\text{PC}} = 147$ Hz, C_7), 129.1 (dt, $J_{\text{PC}} = 22.2$ Hz, $J_{\text{PC}} = 6.2$ Hz, $C_{10} + C_{14}$), 127.3 (t, $J_{\text{PC}} = 5.3$ Hz, C_9), 24.0 (t, $^1J_{\text{PC}} = 98.0$ Hz, C_1)

(CDP)BiBr (7.2). Yield: 91 %. $^1\text{H NMR}$ (800 MHz, CD_2Cl_2 , 298 K): δ 9.34 (d, $^1J_{\text{HH}}$ 7.6 Hz, 2H, H_4), 7.99 (q, $^1J_{\text{HH}} = 7.4$ Hz, 4H, $H_6 + H_7$), 7.63 (m, $^1J_{\text{HH}} = 7.1$ Hz, 2H, H_5), 7.51 (t, $^1J_{\text{HH}} = 7.4$ Hz, 2H, H_{11}), 7.48 – 7.41 (m, 8H, $H_9 + H_{10}$), 7.19 (t, $^1J_{\text{HH}} = 7.4$ Hz, 2H, H_{15}), 6.91 (t, $^1J_{\text{HH}} = 7.1$ Hz, 4H, H_{14}), 6.86–6.83 (m, 4H, H_{13}). $^{31}\text{P}\{^1\text{H}\}$ NMR (243 MHz, CD_2Cl_2 , 298 K): δ 38.7. $^{13}\text{C}\{^1\text{H}\}$ NMR (201 MHz, CD_2Cl_2 , 298 K): δ 178.6 (t, $^3J_{\text{PC}} = 13.1$ Hz, C_3), 147.8 (m, C_2), 141.1 (t, $^3J_{\text{PC}} = 7.9$ Hz, C_4), 135.5 (t, $J_{\text{PC}} = 7.5$ Hz, C_9), 134.6 (m, C_8/C_{12}), 133.1 (t, $J_{\text{PC}} = 5.2$ Hz, C_{13}), 132.4 (C_5), 132.3 (t, $J_{\text{PC}} = 5.3$ Hz, C_6), 132.0 (C_{11}), 131.9 (C_{15}), 130.8 (m, C_8/C_{12}), 129.1 (dt, $J_{\text{PC}} = 21.1$ Hz, $J_{\text{PC}} = 5.9$ Hz, $C_{10} + C_{14}$), 127.4 (t, $J_{\text{PC}} = 5.6$ Hz, C_9), 23.3 (t, $^1J_{\text{PC}} = 98.0$ Hz, C_1)

Synthesis of $(((CDP)Bi)_2(\mu-Cl))[NTf_2]$ (**7.3[NTf₂]**) – Compound **7.1** (50 mg, 0.0642 mmol) and AgNTf₂ (25 mg, 0.0642 mmol) were combined in DCM (~ 8 mL) and stirred in the dark for 30 min. The resulting mixture was filtered to recover a colorless solution, which was then concentrated and layered with hexanes to yield colorless crystals of **7.3[NTf₂]** (41 mg, 71 % yield). **¹H NMR** (800 MHz, CD₂Cl₂, 298 K) δ 8.95 (d, ¹J_{HH} = 7.5 Hz, 2H, H₄), 8.09 – 7.97 (m, 4H, H₅ + H₆), 7.64 (t, ¹J_{HH} = 7.1 Hz, 2H, H₇), 7.60 (t, ¹J_{HH} = 7.4 Hz, 2H, H₁₁), 7.56 – 7.48 (m, 8H, H₉ + H₁₀), 7.29 (t, ¹J_{HH} = 7.4 Hz, 2H, H₁₅), 7.00 (t, ¹J_{HH} = 6.9 Hz, 4H, H₁₄), 6.94 – 6.87 (m, 4H, H₁₃). **³¹P{¹H} NMR** (243 MHz, CD₂Cl₂, 298 K): δ 43.9. **¹³C{¹H} NMR** (201 MHz, CD₂Cl₂, 298 K): **¹³C NMR** (201 MHz, CD₂Cl₂) δ 178.7 (m, C₃), 147.7 (m, C₂), 139.4 (m, C₄), 136.0 (m, C₉), 134.1 (m, C₈/C₁₂), 133.2 (m, C₁₃), 132.4 (m, C₅ + C₆), 132.2(C₁₁), 130.2 (m, C₈/C₁₂), 129.4 (d, J_{PC} = 28.1 Hz, C₁₀ + C₁₄), 127.7 (m, C₉), 120.5 (t, ¹J_{CF} = 322 Hz, CF₃), 22.1 (t, ¹J_{PC} = 96.0 Hz, C₁). Anal. (C₇₆H₅₆Bi₂ClF₆NO₄P₄S₂; MW: 1802.70) Calc'd (Found): C 50.64 (50.48); H 3.13 (3.18); N 0.78 (0.89).

Synthesis of $(((CDP)Bi)_2(\mu-Cl))[BPh_4]$ (**7.3[BPh₄]**) – Compound **7.1** (50 mg, 0.0642 mmol) and NaBPh₄ (11 mg, 0.0321 mmol) were combined in DCM (~ 8 mL) and stirred overnight. The resulting colorless mixture was filtered and evacuated under vacuum to yield **7.3[BPh₄]** as a colorless solid (48 mg, 81 % yield). Single crystals of **7.3[BPh₄]** suitable for X-ray diffraction was obtained at room temperature from a DCM/hexanes layered solution. **¹H NMR** (800 MHz, CD₂Cl₂, 298 K) δ 8.60 (d, ¹J_{HH} = 7.4 Hz, 2H, H₄), 8.01 (dd, J = 12.7, 7.6 Hz, 4H, H₅ + H₆), 7.66 (t, ¹J_{HH} = 7.3 Hz, 2H, H₇), 7.60 (t, ¹J_{HH} = 6.8 Hz, 2H, H₁₁), 7.56 – 7.48 (m, 8H, H₉ + H₁₀), 7.32 – 7.26 (m, 8H, H₁₅ + H_{BPh₄}), 6.98 (m, 10H, H₁₄ + H_{BPh₄}), 6.91 – 6.87 (m, 4H, H₁₃), 6.82 (t, J = 7.4 Hz, 3H, H_{BPh₄}). NOTE: proton integrations suggest a slight excess of **7.5[BPh₄]** in the isolated solids. **³¹P{¹H} NMR** (243 MHz, CD₂Cl₂, 298 K): δ 46.9. **¹³C{¹H} NMR** (201 MHz, CD₂Cl₂, 298 K): **¹³C**

NMR (201 MHz, CD₂Cl₂) δ 177.8 (t, ¹J_{PC} = 14.1 Hz, C₃), 164.5 (q, ¹J_{BC} = 50.3 Hz, C_{ipso}(BPh₄)), 147.6 (m, C₂), 138.7 (t, ¹J_{PC} = 8.0 Hz, C₄), 136.3 (m, C_{aryl}), 133.4 (m, C₈/C₁₂), 133.3 (t, ¹J_{PC} = 6.0, C₁₃), 132.7 (C₅ + C_{BPh₄}), 132.2 (t, ¹J_{PC} = 5.3 Hz, C₆), 130.6 (dd, J_{PC} 161, 12.6 Hz, C₇), 129.8 – 129.3 (m, C₈/C₁₂), 129.5 (dt, J_{PC} = 22.6, 6.2 Hz, C₁₀ + C₁₄), 128.0 (t, ¹J_{PC} = 5.3 Hz, C₉), 126.0 (C_{aryl}), 122.1 (C_{BPh₄}), 20.8 (t, ¹J_{PC} = 93.9 Hz, C₁). An alternate procedure whereby **7.1** (10 mg, 0.0128 mmol) and **7.5[BPh₄]** (14 mg, 0.0128 mmol) were combined in CD₂Cl₂ also yielded **7.3[BPh₄]** as the sole product in the NMR spectra (¹H and ³¹P).

Synthesis of [((CDP)Bi)₂(μ-Br)][BPh₄] (7.4[BPh₄]) – Compound **7.2** (10 mg, 0.0121 mmol) and **7.5[BPh₄]** (*vide infra*; 13 mg, 0.0121 mmol) were combined in DCM (~ 2 mL), and after all the solids were dissolved, the concentrated solution was layered with hexanes to obtain colorless crystals of **7.4[BPh₄]**. ¹H NMR (800 MHz, CD₂Cl₂, 298 K) δ 8.86 (d, ¹J_{HH} = 7.5 Hz, 2H, H₄), 8.03 – 8.01 (m, 4H, H₅ + H₆), 7.59 (q, ¹J_{HH} = 7.7 Hz, 4H, H₇ + H₁₁), 7.55 – 7.47 (m, 8H, H₉ + H₁₀), 7.31 (m, 5H, H_{BPh₄}), 7.27 (m, 2H, H₁₅), 6.98 (m, 9H, H₁₄ + H_{BPh₄}), 6.91 – 6.88 (m, 4H, H₁₃), 6.83 (t, J = 7.3 Hz, 2H, H_{BPh₄}). ³¹P{¹H} NMR (243 MHz, CD₂Cl₂, 298 K): δ 45.5. ¹³C{¹H} NMR (201 MHz, CD₂Cl₂, 298 K): ¹³C NMR (201 MHz, CD₂Cl₂) δ 177.8 (m, C₃), 164.5 (q, ¹J_{BC} = 49.1 Hz, C_{ipso}(BPh₄)), 147.7 (m, C₂), 139.6 (m, C₄), 136.3 (s, C_{BPh₄}), 136.1 (m, C₉), 133.7 (m, C₈/C₁₂), 133.2 (t, ¹J_{PC} = 5.4, C₁₃), 132.6 (C₅ + C_{BPh₄}), 132.2 (t, ¹J_{PC} = 5.3 Hz, C₆), 130.5 (dd, J_{PC} 149.5, 12.7 Hz, C₇), 130.0 – 129.7 (m, C₈/C₁₂), 129.4 (dt, J_{PC} = 23.7, 6.1 Hz, C₁₀ + C₁₄), 127.9 (t, ¹J_{PC} = 5.3 Hz, C₉), 126.0 (C_{aryl}), 122.1 (C_{BPh₄}), 21.2 (t, ¹J_{PC} = 95.7 Hz, C₁).

General procedure for the synthesis of 7.5[BAr₄] – In a 20 mL scintillation vial, equimolar amounts of **7.1** (75 mg, 0.0963 mmol) or **7.2** (79 mg, 0.0963 mmol) and Na[BAr₄] (Ar = Ph or 3,5-(CF₃)₂C₆H₃) were combined in DCM (~ 3 mL) and stirred for 16 – 48 h. The colorless solution

was filtered, concentrated and layered with hexanes to afford colorless crystals of **7.5[BAr^F4]** at room temperature.

7.5[BAr^F4] (Ar^F = 3,5-(CF₃)₂C₆H₃). Yield: 145 mg, 94 %. ¹H NMR (800 MHz, CD₂Cl₂, 298 K): δ 8.10 (d, *J* = 7.4 Hz, 2H, *H*₄), 8.03 (d, *J* = 5.1 Hz, 4H, *H*₅ + *H*₆), 7.80 (t, *J* = 7.3 Hz, 2H, *H*₇), 7.74 (s, 8H, *o*-H_{BAr^F}), 7.65 – 7.54 (m, 14H, *p*-H_{BAr^F} + *H*₉₋₁₁), 7.32 (t, *J* = 7.5 Hz, 2H, *H*₁₅), 7.03 (t, *J* = 6.7 Hz, 4H, *H*₁₄), 6.96 – 6.92 (m, 4H, *H*₁₃). ³¹P NMR (243 MHz, CD₂Cl₂, 298 K) δ 53.3. ¹³C{¹H} NMR (201 MHz, CD₂Cl₂, 298 K) δ 175.3 (m, *C*₃), 162.2 (q, ¹*J*_{BC} = 49.6 Hz, *C*_{BAr^F}), 147.3 (m, *C*₂), 137.3 (m, *C*₄), 136.8 (m, *C*₉), 135.2 (*C*_{BAr^F}), 133.5 (t, *J*_{PC} = 5.4 Hz, *C*₆), 133.3 (*C*₁₁), 133.1 (m, *C*₇), 132.6 (m, *C*₈/*C*₁₂), 132.2 (m, *C*₁₃), 129.8 (dt, *J*_{PC} = 23.2, 6.2 Hz, *C*₁₀ + *C*₁₄), 129.2 (qq, ²*J*_{FC} = 34.2, 2.8 Hz, *C*(CF₃)), 128.5 (m, *C*₉ + *C*₈/*C*₁₂), 125.01 (q, ¹*J*_{FC} = 272.3 Hz, CF₃), 117.9 (*C*_{BAr^F}), 18.7 (t, ¹*J*_{PC} = 93.0 Hz, *C*₁). Satisfactory microanalysis data could not be obtained.

7.5[BPh₄]. Here, prolonged reaction times (typically 48 h) is important for complete conversion and improved yield (106 mg, 99 %). ¹H NMR (800 MHz, CD₂Cl₂, 298 K): δ 8.02 (m, 6H, *H*₄₋₆), 7.79 (t, *J* = 7.3 Hz, 2H, *H*₇), 7.68 – 7.62 (m, 2H, *H*₁₁), 7.62 – 7.51 (m, 8H, *H*₉ + *H*₁₀), 7.33 (m, 10H, *H*_{BPh₄}), 7.00 (m, 12H, *H*₁₅ + *H*_{BPh₄}), 6.95 – 6.88 (m, 4H, *H*₁₄), 6.82 (t, *J* = 7.2 Hz, 4H, *H*₁₃). ³¹P NMR (243 MHz, CD₂Cl₂, 298 K) δ 50.4. ¹³C{¹H} NMR (201 MHz, CD₂Cl₂, 298 K) δ 176.8 (*C*₃), 164.5 (q, ¹*J*_{BC} = 49.5 Hz, *C*_{BPh₄}), 147.4 (m, *C*₂), 138.9, 137.5 (m, *C*₄), 136.7 (m, *C*₉), 136.4 (*C*_{BPh₄}), 133.4 (m, *C*₁₃), 133.2 (*C*₁₁), 133.1 (m, *C*₇), 132.1 (m, *C*₆), 129.7 (m, *C*₁₀ + *C*₁₄), 128.8 (m, *C*₈/*C*₁₂), 128.3 (m, *C*₉), 127.8, 126.0 (m, *C*_{BPh₄}), 122.1 (*C*_{BPh₄}), 19.2 (t, ¹*J*_{PC} = 93.0 Hz, *C*₁). Anal. (C₆₁H₄₈BBiP₂, MW: 1062.79) Calc'd (Found): C 68.94 (68.07); H 4.55 (4.54). **Method 2:** **7.8[BPh₄]** (*vide infra*, 57 mg, 0.0519 mmol) and K[N(SiMe₃)₂] (12 mg, 0.0622 mmol) were combined in THF and stirred for 2 d at room temperature. The colorless solution was filtered and completely dried under vacuum to yield a colorless flaky solid (55 mg, > 99 % yield).

General procedure for the syntheses of 7.5[BF₄] and 7.5[SbF₆] – In a 20 mL scintillation vial, equimolar amounts of **7.1** or **7.2** and the appropriate silver salt were combined in DCM or THF (~ 3 mL) and stirred in the dark for 30 min. The mixture was filtered to recover a colorless solution, which was then concentrated and layered with hexanes to afford colorless crystals of **7.5[A]** at room temperature.

7.5[BF₄]. Amounts: **7.1** (50 mg, 0.0642 mmol) and AgBF₄ (13 mg, 0.0642 mmol). Yield: 30 mg, 57 %. **¹H NMR** (600 MHz, CD₂Cl₂, 298 K): δ 8.10 (d, *J* = 7.4 Hz, 2H, *H*₄), 8.06 – 8.02 (m, 4H, *H*₅ + *H*₆), 7.80 (t, *J* = 7.3 Hz, 2H, *H*₇), 7.66 – 7.51 (m, 10H, *H*₉₋₁₁), 7.32 (t, *J* = 7.5 Hz, 2H, *H*₁₅), 7.03 (t, *J* = 6.7 Hz, 4H, *H*₁₄), 6.96 – 6.92 (m, 4H, *H*₁₃). **³¹P NMR** (243 MHz, CD₂Cl₂, 298 K) δ 49.0. **¹⁹F NMR** (564 MHz, CD₂Cl₂, 298 K) δ -151.7, -151.8. **¹¹B NMR** (192 MHz, CD₂Cl₂, 298 K) δ -1.25. **¹³C{¹H} NMR** (150 MHz, CD₂Cl₂, 298 K) δ 177.7 (m, *C*₃), 147.5 (m, *C*₂), 138.0 (m, *C*₄), 136.4 (m, *C*₁₃), 135.1 (m, *C*₈/*C*₁₂), 133.4 (t, *J*_{PC} = 5.5 Hz, *C*₆), 133.2 (*C*₇), 132.8, (*C*₁₁), 132.8 (*C*₁₅), 132.2 (t, *J*_{PC} = 5.7 Hz, *C*₁₃), 129.6 (dt, *J*_{PC} = 16.5, 6.2 Hz, *C*₁₀ + *C*₁₄), 128.1 (t, *J*_{PC} = 5.2 Hz, *C*₉/*C*₁₀). The *C*₁ resonance was not observed. Despite sustained effort, reaction solvents (hexanes, DCM) were not completely evacuated from the crystalline material, and as a result, satisfactory microanalysis data could not be obtained.

7.5[SbF₆]. Amounts: **7.1** (78 mg, 0.100 mmol) and AgSbF₆ (34 mg, 0.100 mmol). Yield: 89 mg, 91 %. **¹H NMR** (800 MHz, CD₂Cl₂, 298 K): 8.16 (d, *J* = 7.4 Hz, 2H, *H*₄), 8.02 (dd, *J* = 12.7, 8.0 Hz, 4H, *H*₅ + *H*₆), 7.81 (t, *J* = 7.1 Hz, 2H, *H*₇), 7.63 (t, *J* = 6.8 Hz, 2H, *H*₉), 7.58 (m, 8H, *H*₉ + *H*₁₀), 7.33 (t, *J* = 7.4 Hz, 2H, *H*₁₅), 7.03 (t, *J* = 7.7 Hz, 4H, *H*₁₄), 6.95 – 6.91 (m, 4H, *H*₁₃). **³¹P NMR** (201 MHz, CD₂Cl₂, 298 K) δ 51.5. **¹⁹F NMR** (564 MHz, CD₂Cl₂, 298 K) δ -62.9. **¹³C{¹H} NMR** (201 MHz, CD₂Cl₂, 298 K) δ 176.0 (m, *C*₃), 147.4 (m, *C*₂), 137.5 (t, *J*_{PC} = 8.0 Hz, *C*₄), 136.7 (t, *J*_{PC} = 7.8 Hz, *C*₉), 136.0, 133.5 (t, *J*_{PC} = 5.0 Hz, *C*₆), 133.2 (*C*₅), 133.1 (m, *C*₇ + *C*₁₁), 132.5, 132.2

(m, C₁₃), 131.3 (d, $J_{PC} = 126.9$ Hz, C₈/C₁₂), 129.7 (dt, $J_{PC} = 23.3, 6.2$ Hz, C₁₀ + C₁₄), 128.7 (m, C₈/C₁₂), 128.4 (m, C₉/C₁₀), 18.8 (t, $^1J_{PC} = 93.7$ Hz, C₁). Anal. Calc'd (Found) for C₃₇H₂₈BiF₆P₂Sb·CH₂Cl₂: C 42.89 (42.56); H 2.84 (2.61).

Synthesis of [(H-CDP)Bi][BPh₄] (7.6[BPh₄]) – In a 20 mL scintillation vial, **1** (70 mg, 0.0899 mmol) and [HNEt₃][BPh₄]⁴⁰³ (38 mg, 0.0902 mmol) were combined in DCM or THF (~ 2 mL) and stirred for 15 min. The colorless solution was completely dried under vacuum to obtain the title product as a colorless solid (82 mg, 84 % yield). Colorless single crystals of **7.6[BPh₄]** suitable for X-ray diffraction was obtained from a layered DCM/hexanes solution at room temperature. An alternative procedure was found whereby **7.5[BPh₄]** (15 mg, 0.0141 mmol) and NEt₃·HCl (2 mg, 0.0145 mmol) were combined in CD₂Cl₂ and immediately examined by ¹H and ³¹P NMR, which identified **7.6[BPh₄]** as the primary product. **¹H NMR** (600 MHz, CD₂Cl₂, 298 K): δ 9.25 (d, $J = 7.6$ Hz, 2H, H₄), 7.97 (tdd, $J = 7.5, 2.5, 1.3$ Hz, 2H), 7.74 (t, $J = 7.5$ Hz, 2H), 7.58 (td, $J = 8.0, 3.6$ Hz, 4H), 7.54 – 7.46 (m, 8H), 7.30 (m, 8H, H_{BPh₄}), 7.24 – 7.16 (m, 6H), 6.97 – 6.88 (m, 12H), 6.80 (t, $J = 7.3$ Hz, 4H), 2.74 (t, $^2J_{PH} = 6.5$ Hz, 1H, H₁). **³¹P NMR** (243 MHz, CD₂Cl₂, 298 K) δ 28.1. **¹¹B NMR** (192 MHz, CD₂Cl₂, 298 K) δ -6.6. **¹³C NMR** (201 MHz, CD₂Cl₂, 298 K) δ 180.4 (d, $J_{PC} = 19.8$ Hz), 164.5 (q, $J_{BC} = 49.4$ Hz, B-C_{ipso}(BPh₄)), 140.2 (d, $J_{PC} = 16.0$ Hz, C₄), 138.6 (d, $J_{PC} = 15.9$ Hz), 137.5 (d, $J_{PC} = 104.9$ Hz), 136.9 (s), 136.3 (s, C_{BPh₄}), 134.0 (s), 134.8 (s), 133.4 (d, $J_{PC} = 11.2$ Hz), 132.0 (d, $J_{PC} = 9.9$ Hz), 131.1 (d, $J_{PC} = 12.4$ Hz), 130.3 (d, $J_{PC} = 12.6$ Hz), 129.6 (d, $J_{PC} = 12.7$ Hz), 126.0 (s, C_{BPh₄}), 125.7 (s), 124.3 (s), 123.9 (s), 122.1 (s, C_{BPh₄}), 18.6 (t, $^1J_{PC} = 70.7$ Hz). Due to difficulties in completely evacuating reaction solvents from this compound, satisfactory microanalysis data could not be obtained. However, the purity is evident by NMR.

Isolation of [(H-CDP)BiBr][SbF₆] (7.7[SbF₆]) – During the synthesis of **7.5[SbF₆]** (*vide supra*), the presence of adventitious moisture in one instance led to the decomposition product **7.7[SbF₆]**

due to hydrolysis. Fortunately, fractional crystallization enabled separation of the ionic products and isolation of a small amount of **7.5**[SbF₆] (10 mg) for spectroscopic and crystallographic characterization. ¹H NMR (600 MHz, CD₂Cl₂, 298 K): δ 9.38 (ddd, *J* = 7.7, 2.4, 1.0 Hz, 2H, *H*₄), 7.92 (tdd, *J* = 7.5, 2.5, 1.3 Hz, 2H), 7.80 – 7.76 (m, 2H), 7.71 – 7.65 (m, 8H), 7.60 – 7.53 (m, 4H), 7.28 – 7.21 (m, 6H), 7.01 – 6.95 (m, 4H), 3.24 (t, ²*J*_{PH} = 6.8 Hz, 1H, *H*₁). ³¹P NMR (243 MHz, CD₂Cl₂, 298 K): δ 29.0 ¹³C NMR (150 MHz, CD₂Cl₂, 298 K): δ 177.5 (*C*₃), 142.2 (d, *J*_{PC} = 16.1 Hz), 138.5, 138.4 (m), 137.7 (m), 137.1 (d, *J*_{PC} = 4.2 Hz), 135.0 (m), 134.7 (m), 134.5 (d, *J*_{PC} = 11.0 Hz), 132.1 (d, *J*_{PC} = 10.4 Hz), 131.0 (d, *J*_{PC} = 12.6 Hz), 130.3 (d, *J*_{PC} = 12.8 Hz), 129.6 (d, *J*_{PC} = 12.9 Hz), 18.6 (m, *C*₁).

Synthesis of [(CDP)Bi]·[HB(C₆F₅)₃] (7.9) – B(C₆F₅)₃ (48 mg, 0.0937 mmol) was added to a colorless DCM solution of **7.1** (73 mg, 0.0937 mmol) stirred for 5 min at room temperature, then cooled to -37 °C in the glovebox freezer. Then a cooled solution (-37 °C) of excess PhSiH₃ (ca. 2 pipette drops) in DCM (~ 2 mL) was added dropwise to the colorless solution with vigorous stirring, and immediately stored at -37 °C. After 45 min, the solution was removed from the freezer and sat undisturbed for 20 min, during which it slowly warmed to room temperature, and the initially colorless mixture turned light yellow with visible deposition of black solids presumed to be metallic bismuth. Mixture was filtered and dried completely under vacuum (with multiple trituration/wash sequences using hexanes) until a freely flowing yellow powder was obtained, which is the title product (80 mg, 68% yield). Single crystals suitable for X-ray diffraction were obtained from a layered DCM/hexanes mixture at -37 °C. Gentle heating (50 °C, 1 h) of **7.9** afforded a colorless solution from which the fully charge separated isomorph [(CDP)Bi][HB(C₆F₅)₃] (**7.9'**) was isolated (crystals obtained from DCM/hexanes layer at room temperature). However, no reasonable distinctions in the NMR spectra of **7.9** and **7.9'** were

observed. **¹H NMR** (800 MHz, CD₂Cl₂, 298 K) δ 8.09 (d, *J* = 7.4 Hz, 2H, *H*₄), 8.02 (m, 4H, *H*₅ + *H*₆), 7.80 (t, *J* = 7.3 Hz, 2H, *H*₇), 7.63 (t, *J* = 8.1 Hz, 2H, *H*₁₁), 7.60 – 7.55 (m, 8H, *H*₉ + *H*₁₀), 7.31 (t, *J* = 6.8 Hz, 2H, *H*₁₅), 7.04 – 7.00 (m, 4H, *H*₁₄), 6.95 – 6.90 (m, 4H, *H*₁₃), 3.60 (q, *J*_{BH} = 91.9 Hz, 1H, BH). **³¹P NMR** (243 MHz, CD₂Cl₂, 298 K) δ 51.4. **¹¹B NMR** (192 MHz, CD₂Cl₂, 298 K) δ -25.5 (d, *J*_{HB} = 97.9 Hz). **¹³C NMR** (201 MHz, CD₂Cl₂, 298 K) δ 175.3 (m, *C*₃), 149.2 (m, HBAr₃), 148.0 (m, HBAr₃), 147.3 (m, *C*₂), 138.8 (m, HBAr₃), 137.3 (t, *J*_{PC} = 8.0 Hz, *C*₄), 136.8, (t, *J*_{PC} = 8.0 Hz, *C*₉), 136.2 (m, HBAr₃), 133.5 (t, *J*_{PC} = 5.6 Hz, *C*₁₃), 133.3 (m, *C*₅), 133.1 (m, *C*₇), 132.6 (m, *C*₈/*C*₁₂), 132.2 (t, *J*_{PC} = 5.6 Hz), 129.7 (dt, *J*_{PC} = 25.3, 6.3 Hz, *C*₁₀ + *C*₁₄), 128.5 (t, *J*_{PC} = 5.2 Hz, *C*₉), 128.6 (m, *C*₈/*C*₁₂), 18.7 (t, ¹*J*_{PC} = 91.4 Hz, *C*₁). Anal. Calc'd (Found) for C₅₅H₂₉BBiF₁₅P₂·(CH₂Cl₂)_{0.5}: C 51.32 (51.61); H 2.33 (2.86).

Isolation of [(CDP)Bi···ClB(C₆F₅)₃] (10) – In a J-Young tap NMR tube, **1** (15 mg, 0.0193 mmol) and B(C₆F₅)₃ (10 mg, 0.0196 mmol) were combined in CD₂Cl₂ and immediately (ca. 5 min) analyzed by NMR (¹H, ³¹P and ¹¹B), which indicated conversion to the anticipated ionic adduct. Layering this solution with hexanes afforded colorless single crystals of the title product for X-ray diffraction analysis (yield: 13 mg, 54%). **¹H NMR** (600 MHz, CD₂Cl₂, 298 K): δ 8.13 (d, *J* = 7.4 Hz, 2H, *H*₄), 8.06 – 7.99 (m, 4H, *H*₅ + *H*₆), 7.78 (t, *J* = 7.1 Hz, 2H, *H*₇), 7.63 (t, *J* = 7.4 Hz, 2H, *H*₁₁), 7.60 – 7.55 (m, 8H, *H*₉ + *H*₁₀), 7.31 (td, *J* = 7.4, 1.4 Hz, 2H, *H*₁₅), 7.02 (t, *J* = 7.8 Hz, 4H, *H*₁₄), 6.96 – 6.89 (m, 4H, *H*₁₃). **³¹P NMR** (243 MHz, CD₂Cl₂, 298 K): δ 51.1. **¹¹B NMR** (192 MHz, CD₂Cl₂, 298 K): No resonance detected. **¹³C NMR** (201 MHz, CD₂Cl₂, 298 K) δ 175.6 (m, *C*₃), 148.5 (m, ArC), 147.4 (m, *C*₂), 137.6 (m, *C*₄), 136.7, (m, *C*₉), 134.9 (m, ArC), 133.5 (m, *C*₁₃), 133.2 (m, *C*₅), 133.1 (m, *C*₇), 132.4 (m, *C*₈/*C*₁₂), 132.2 (m, ArC), 132.0 (m, ArC), 131.0 (m, ArC), 130.3 (m, ArC), 129.7 (d, *J*_{PC} = 22.4 Hz, *C*₁₀ + *C*₁₄), 128.9 (m, *C*₉), 128.5 (m, *C*₈/*C*₁₂), 18.8 (t, ¹*J*_{PC} = 93.4 Hz, *C*₁).

Isolation of (CDP)BiCl₃ (7.11) – In separate scintillation vials, colorless DCM solutions (ca. 2 mL) of **7.1** (28 mg, 0.0359 mmol) and XeF₂ (9 mg, 0.0539 mmol) were cooled to -35 °C in the glovebox freezer. With vigorous stirring, the XeF₂ solution was added dropwise to **7.1**, and then left to stand at -35 °C for 1 h during the colorless solution turned light brown. The solution was concentrated under vacuum and layered with hexanes, yielding a few single crystals of the title product. After crystallization, **7.11** is insoluble in common organic solvents, which hampered characterization by NMR spectroscopy. Prior to crystallization, an aliquot of the reaction solvent was inspected by ³¹P NMR (Figure A2.190).

Isolation of [(F-CDP)BiF₂)₂(μ-F)][SbF₆]₃ (7.12) – In a J-Young NMR tube, **7.5[SbF₆]** (15 mg, 0.0153 mmol) and XeF₂ (8 mg, 0.0460) were combined in CD₂Cl₂. Due to the poor solubility of solids, attempted NMR analysis gave unintelligible spectra. The solution was filtered and layered with hexanes to yield a few single crystals of **7.12** suitable for X-ray diffraction analysis.

Appendix II: Spectral Data

Chapter Two:

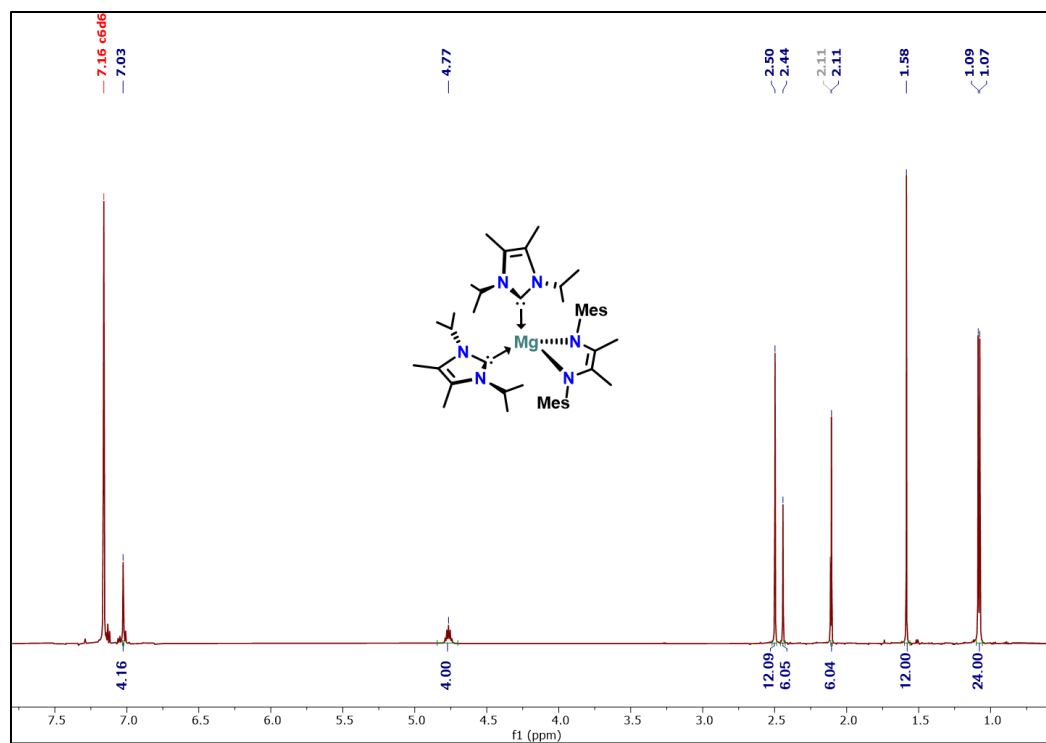


Figure A2.1. ¹H NMR spectrum (600.13 MHz, C₆D₆, 298 K) of compound 2.2.

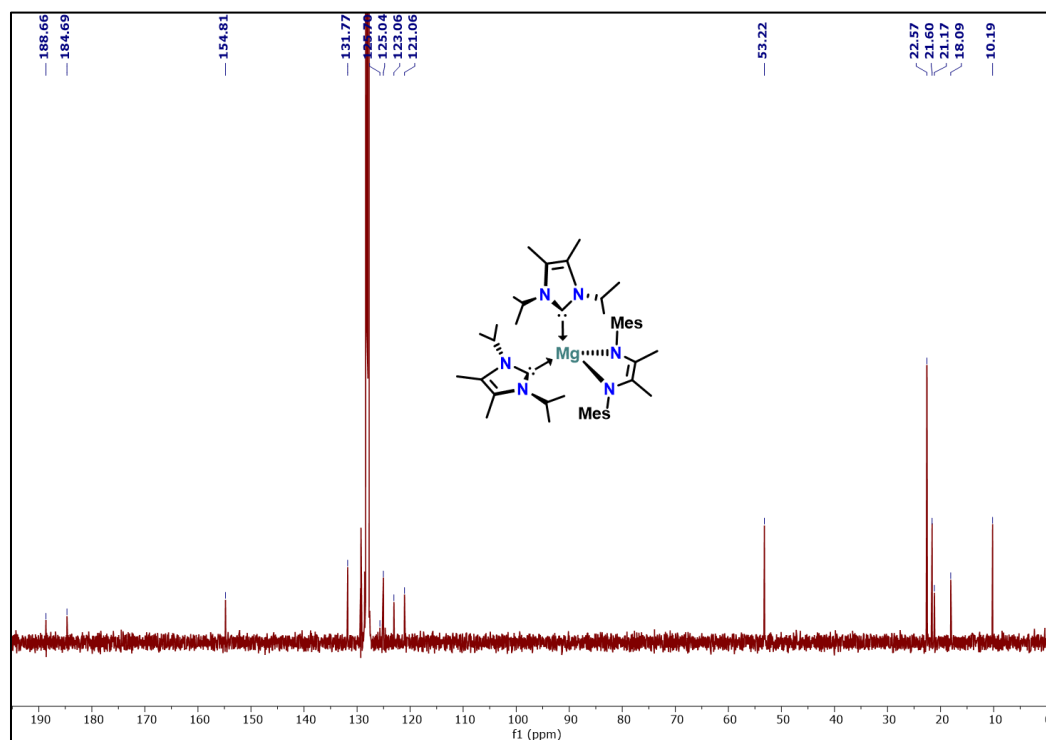


Figure A2.2 $^{13}\text{C}\{^1\text{H}\}$ NMR (150.9 MHz, C_6D_6 , 298 K) of compound **2.2**.

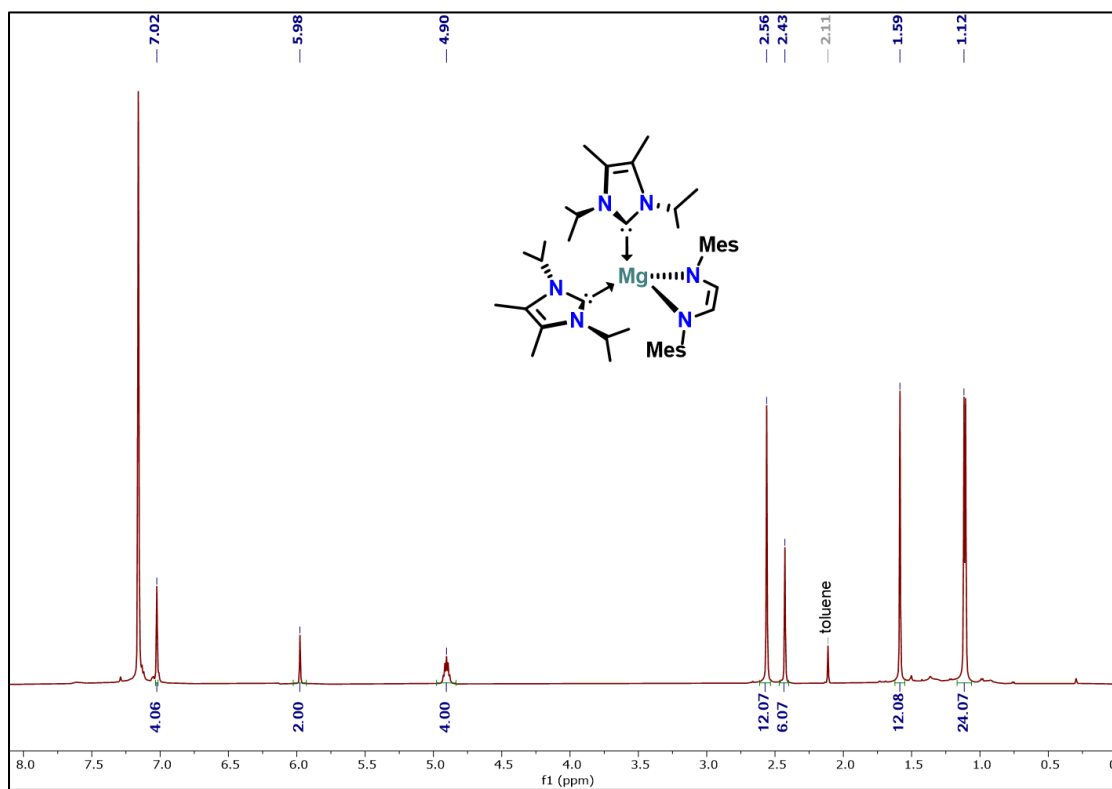


Figure A2.3 ^1H NMR spectrum (600.13 MHz, C_6D_6 , 298 K) of compound **2.3**.

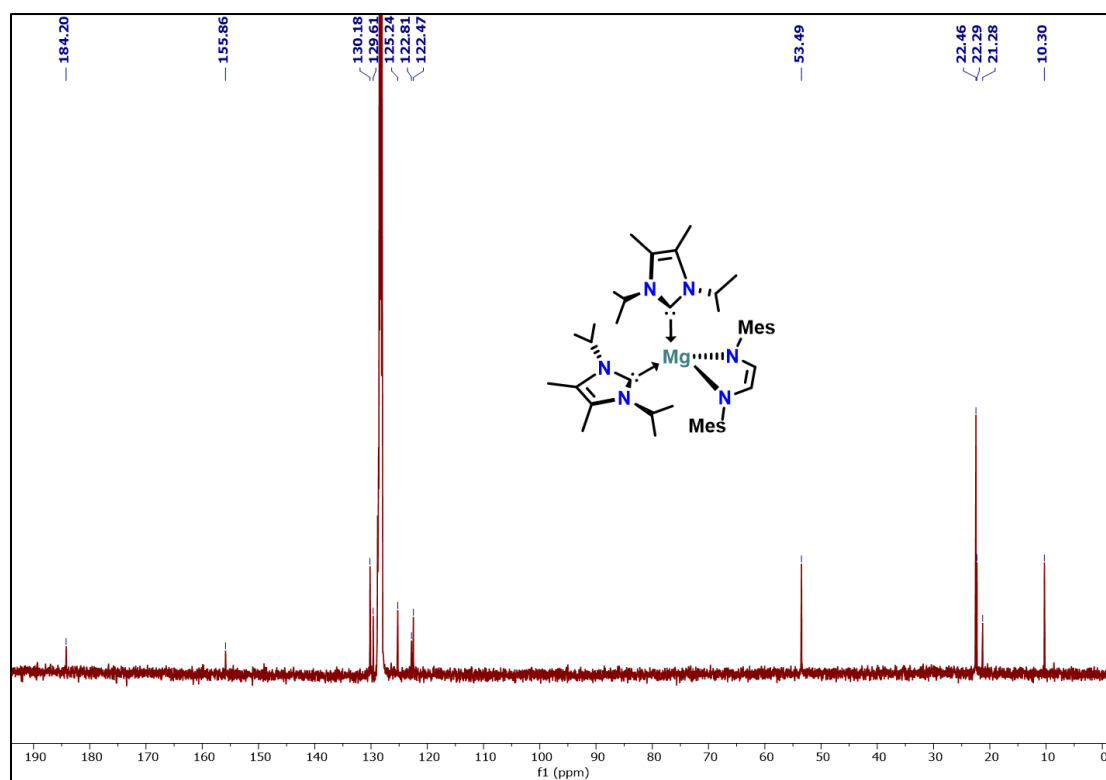


Figure A2.4. $^{13}\text{C}\{^1\text{H}\}$ NMR (150.9 MHz, C_6D_6 , 298 K) of compound **2.3**.

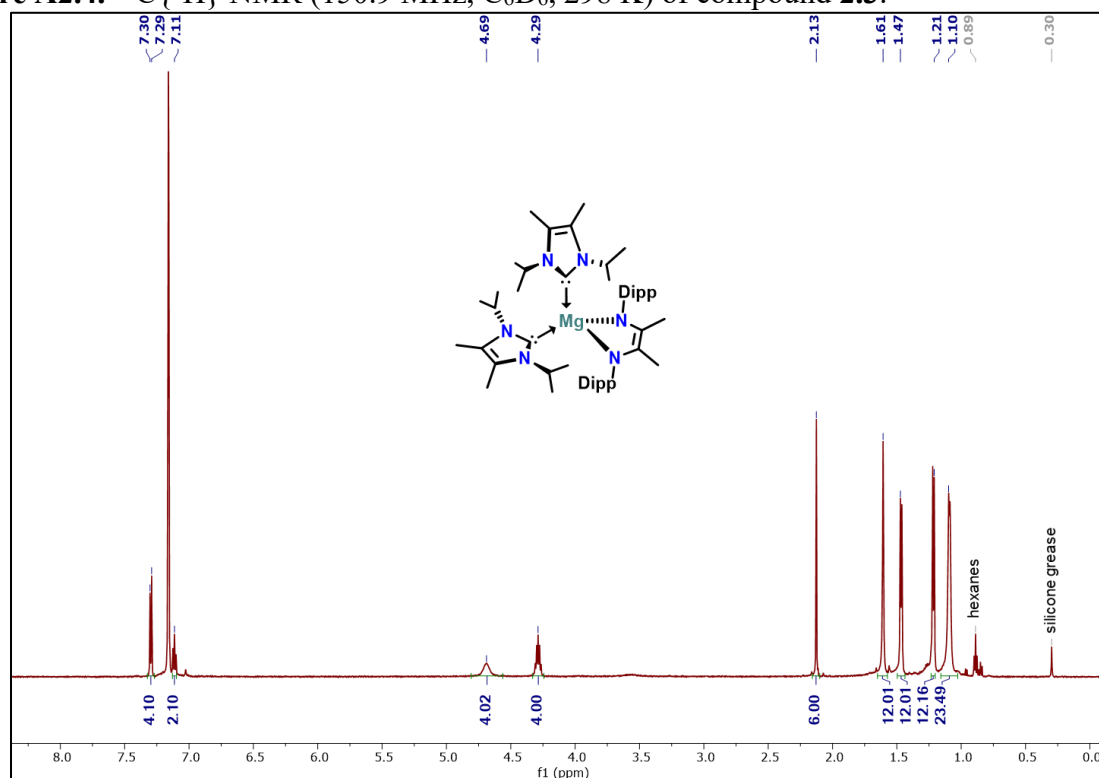


Figure A2.5. ^1H NMR spectrum (600.13 MHz, C_6D_6 , 298 K) of compound **2.4**.

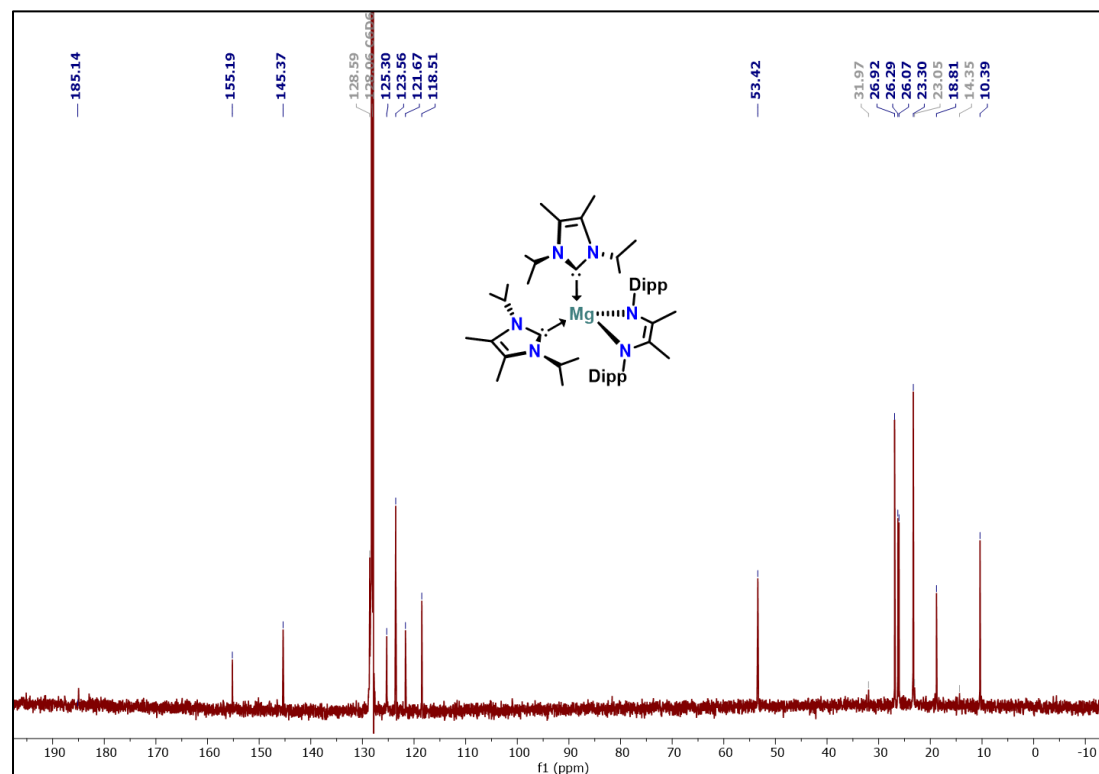


Figure A2.6. $^{13}\text{C}\{^1\text{H}\}$ NMR (150.9 MHz, C_6D_6 , 298 K) of compound **2.4**.

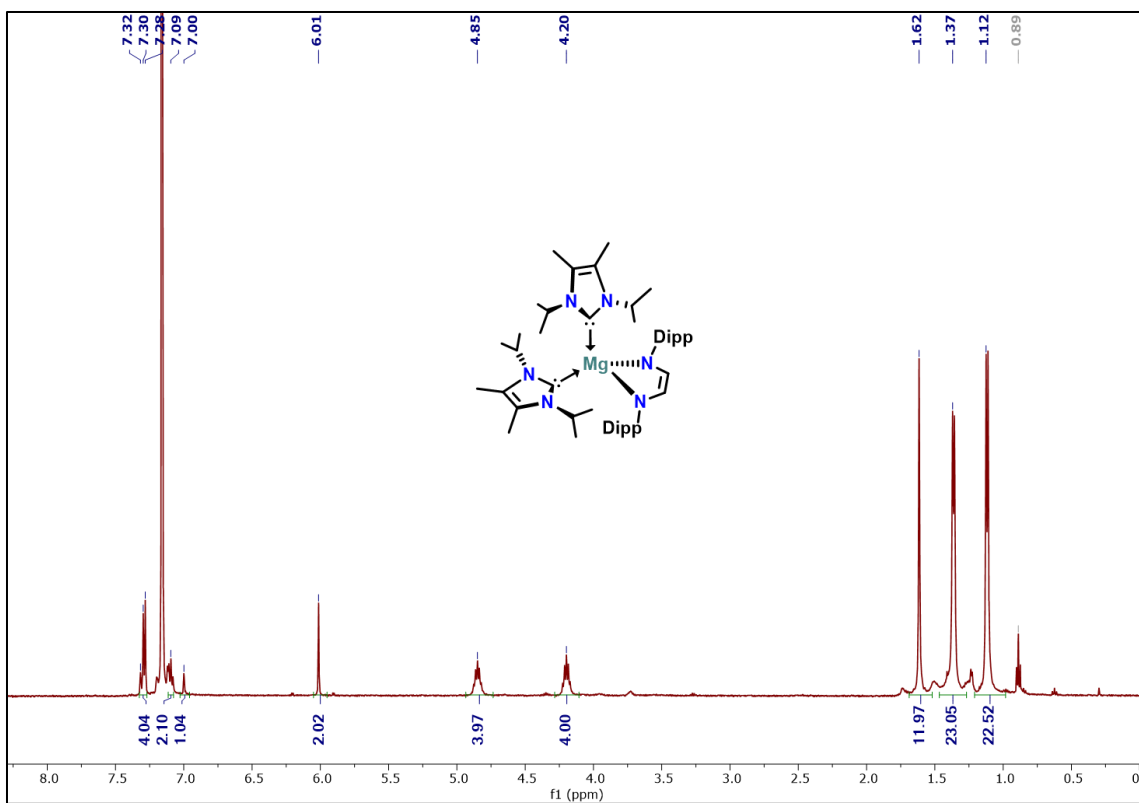


Figure A2.7. ^1H NMR spectrum (600.13 MHz, C_6D_6 , 298 K) of compound 2.5.

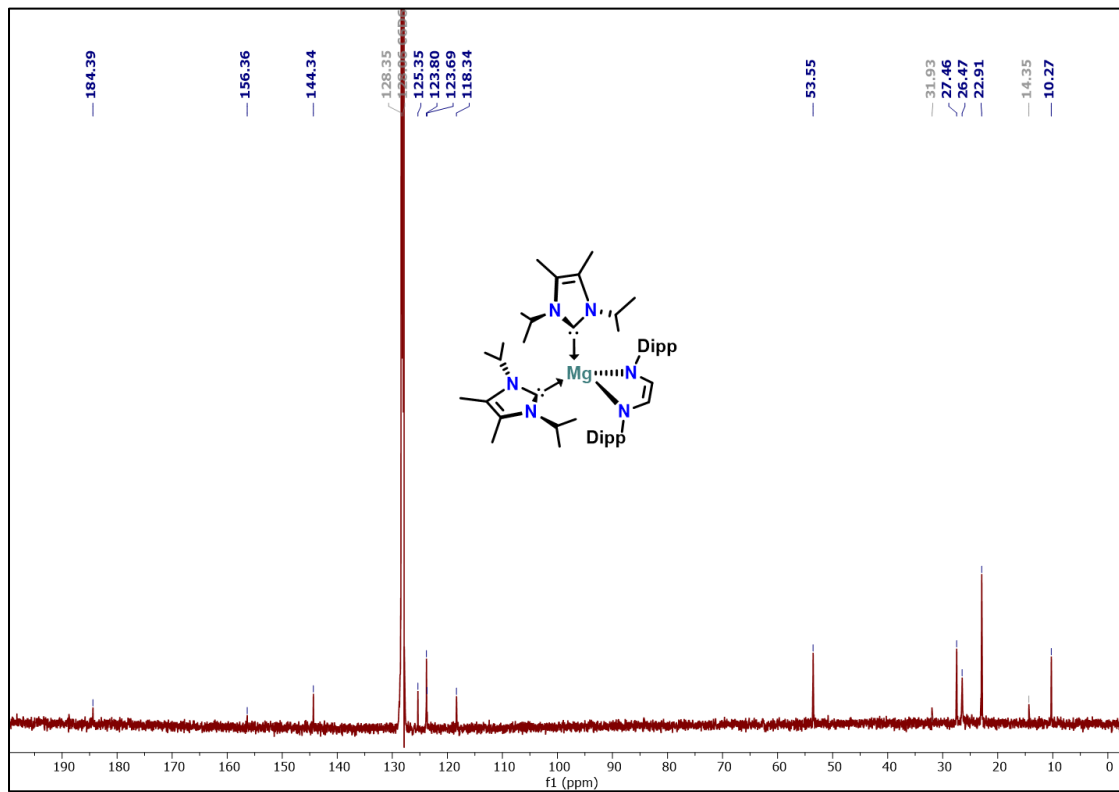


Figure A2.8. $^{13}\text{C}\{^1\text{H}\}$ NMR (150.9 MHz, C_6D_6 , 298 K) of compound 2.5.

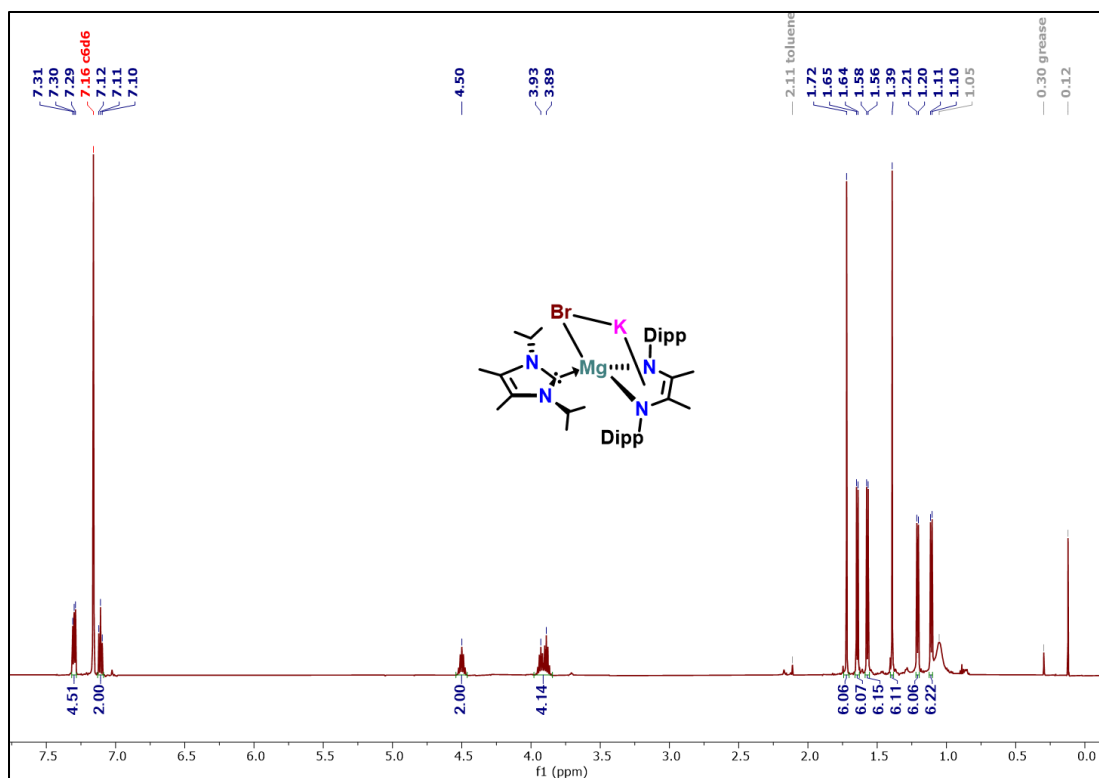


Figure A2.9. ^1H NMR spectrum (600.13 MHz, C_6D_6 , 298 K) of compound 2.8.

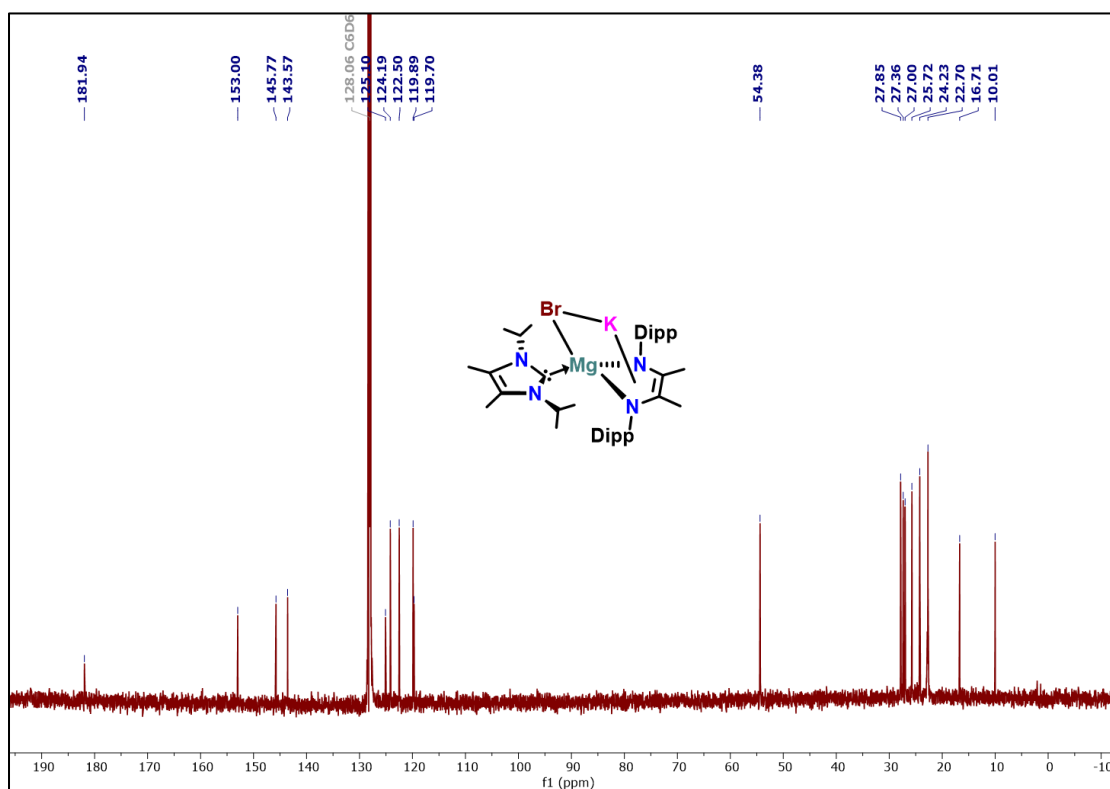


Figure A2.10. $^{13}\text{C}\{^1\text{H}\}$ NMR (150.9 MHz, C_6D_6 , 298 K) of compound 2.8.

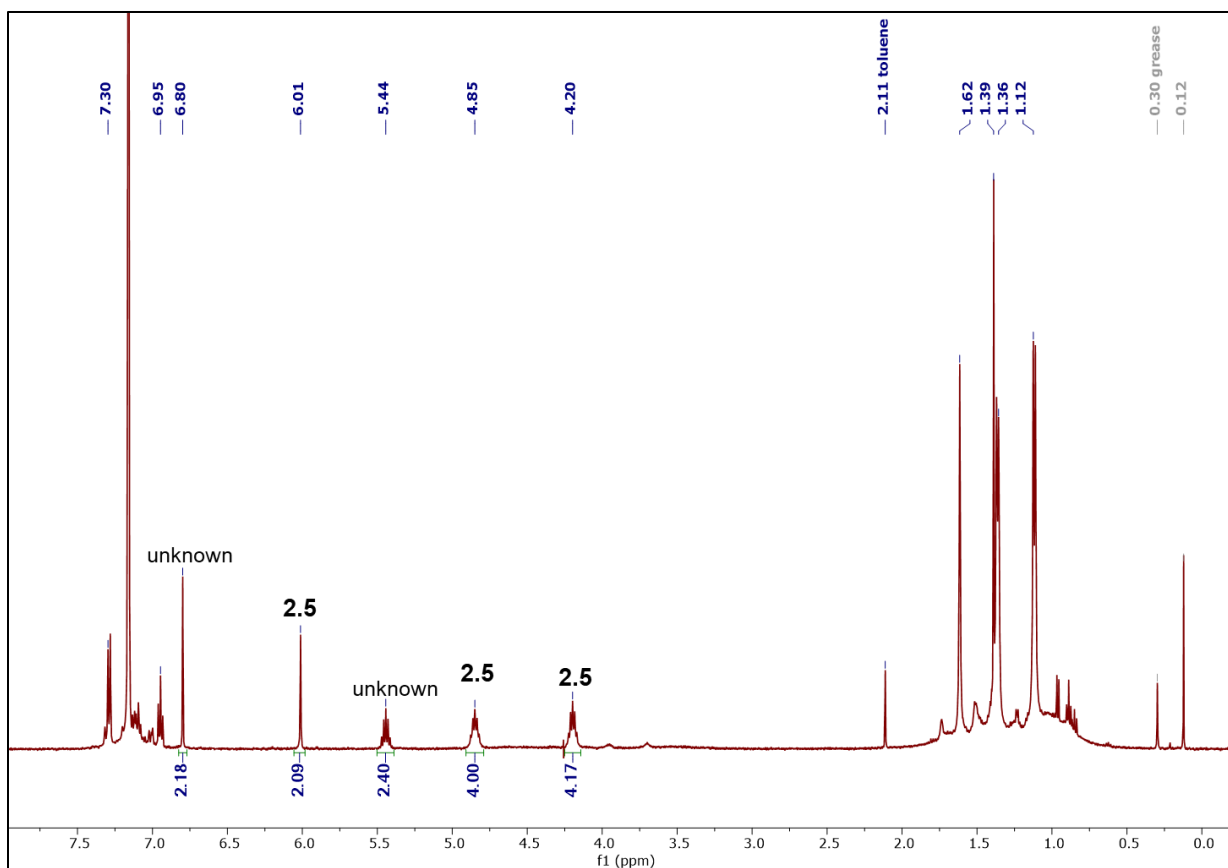


Figure A2.11. ^1H NMR of crystallized product from a toluene solution of **2.5/2.6**. Efforts to structurally identify the unknown product were unsuccessful. This product was regularly obtained in the ratios shown in the peak integrations. The broadened baseline in the alkyl region is expected to be due to the presence of the NMR silent diradical, **2.7**.

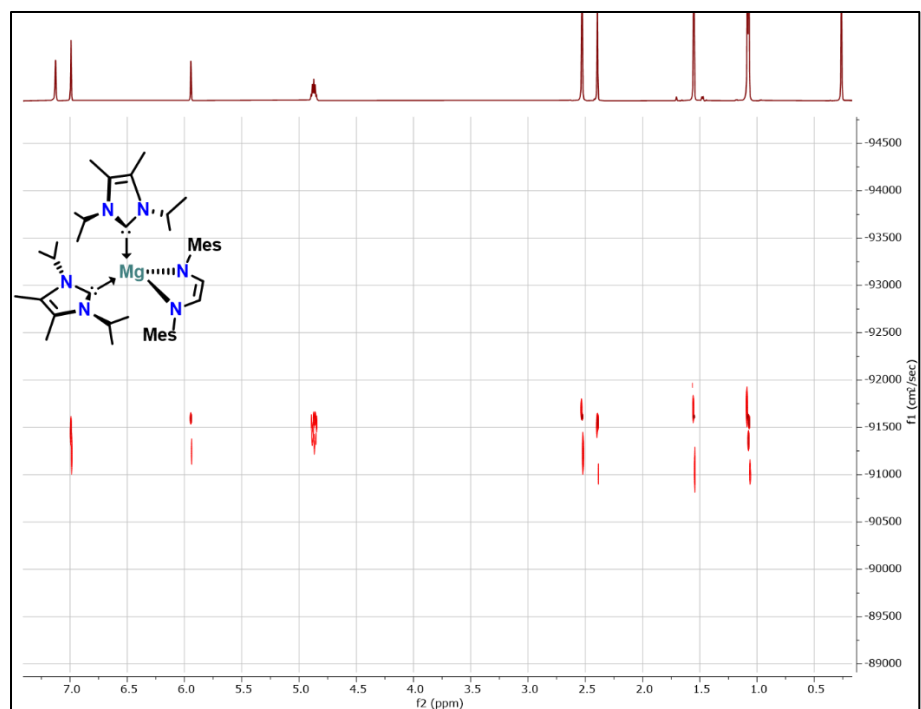


Figure A2.12. DOSY NMR of **2.3** (600 MHz, C₆D₆, 298 K). Based on the diffusion constant ($D = 6.97 \times 10^{-10} \text{ m}^2/\text{s}$), the hydrodynamic radius and volume were estimated to be 5.11 Å and 560 Å³ respectively.

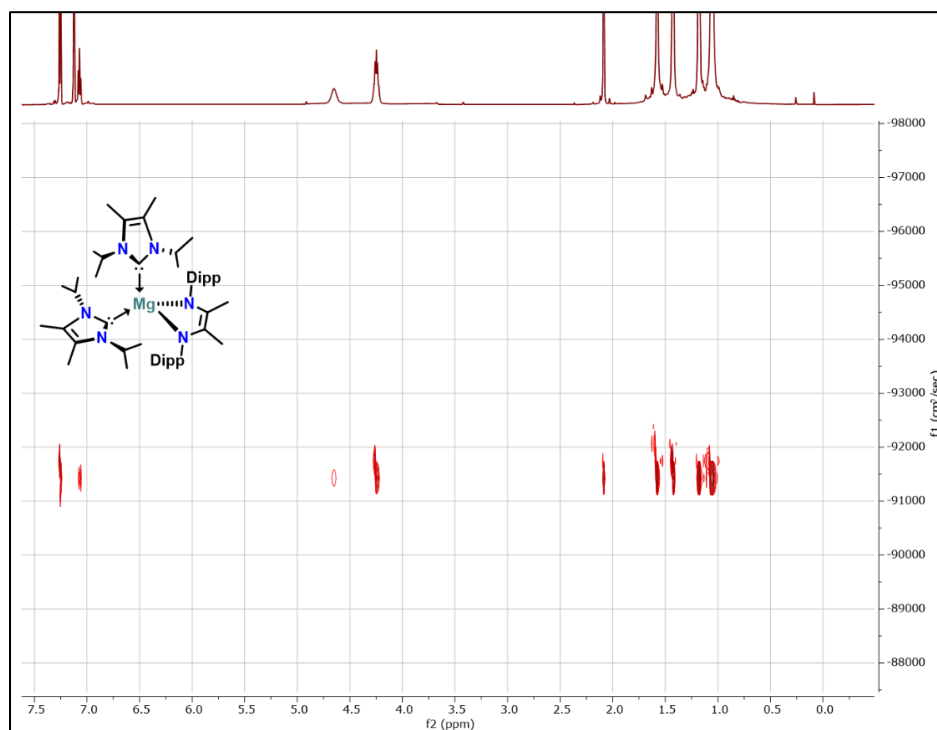


Figure A2.13. DOSY NMR of **2.4** (600 MHz, C₆D₆, 298 K). Based on the diffusion constant ($D = 7.11 \times 10^{-10} \text{ m}^2/\text{s}$), the hydrodynamic radius and volume were estimated to be 5.01 Å and 526 Å³ respectively.

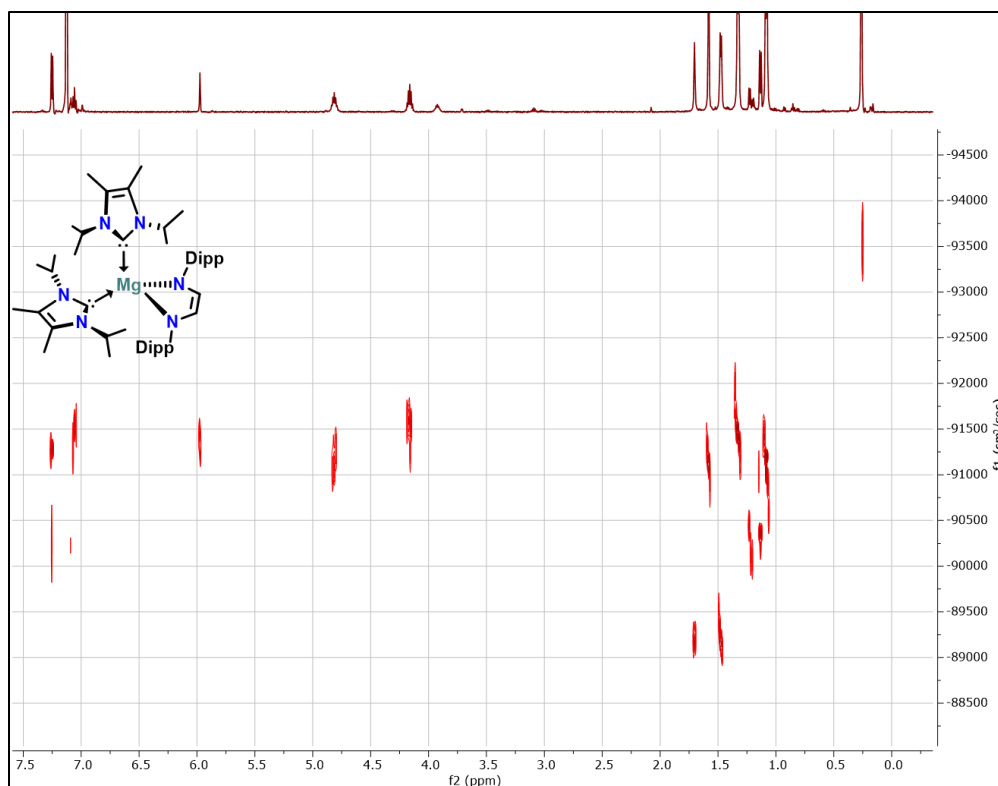


Figure A2.14. DOSY NMR of **2.5** (600 MHz, C₆D₆, 298 K). Based on the diffusion constant ($D = 7.19 \times 10^{-10} \text{ m}^2/\text{s}$), the hydrodynamic radius and volume were estimated to be 4.95 Å and 508 Å³ respectively.

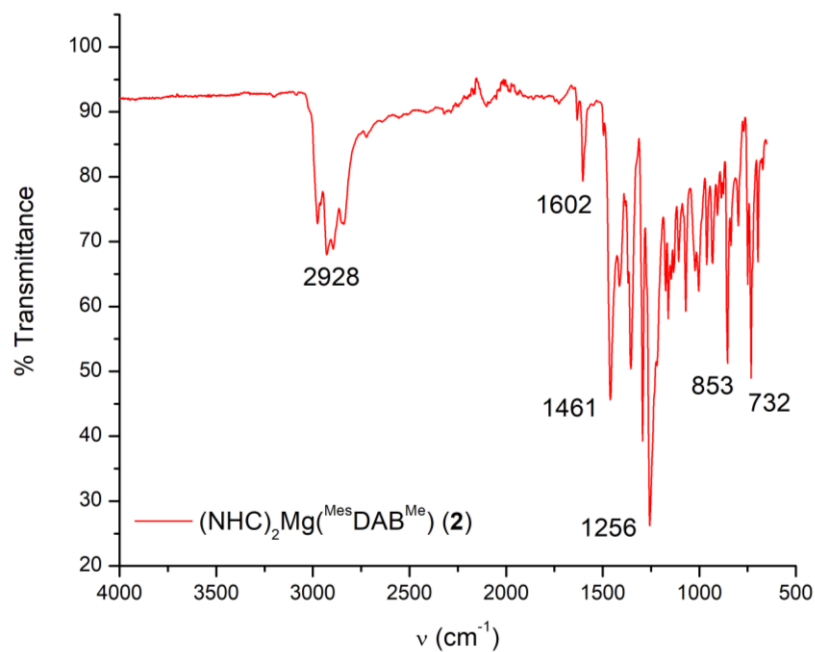


Figure A2.15. FTIR spectrum of compound **2.2**.

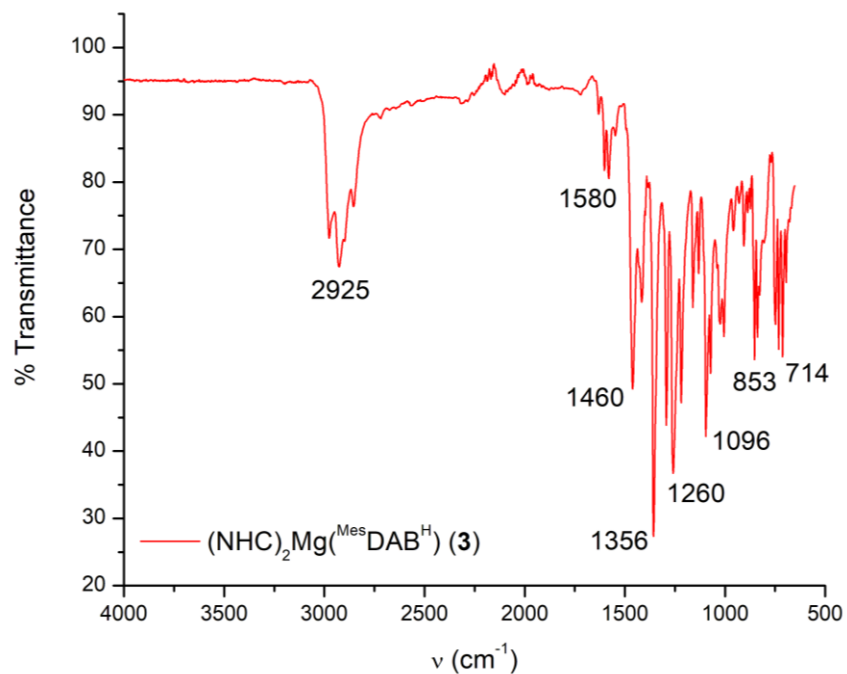


Figure A2.16. FTIR spectrum of compound **2.3**.

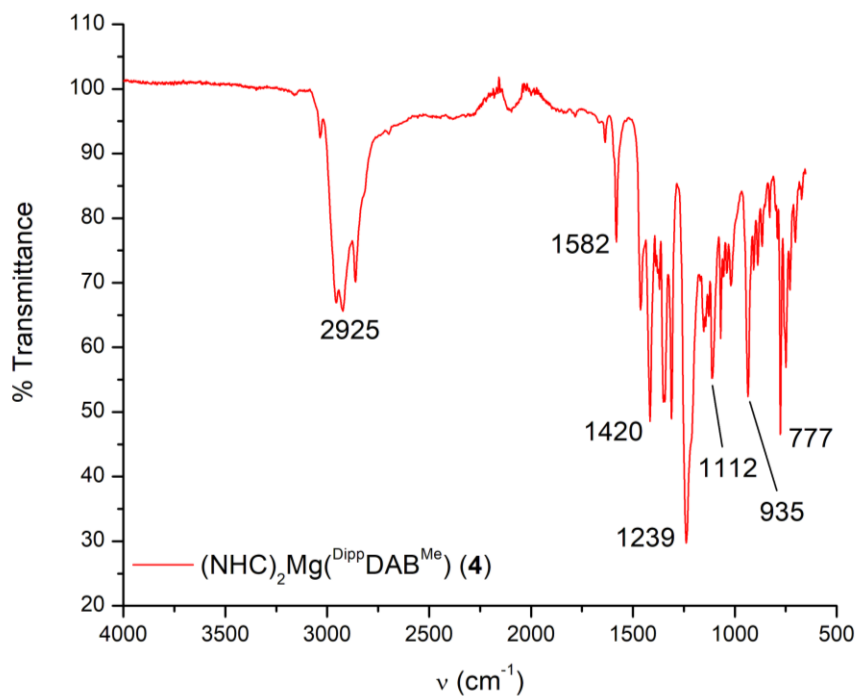


Figure A2.17. FTIR spectrum of compound **2.4**.

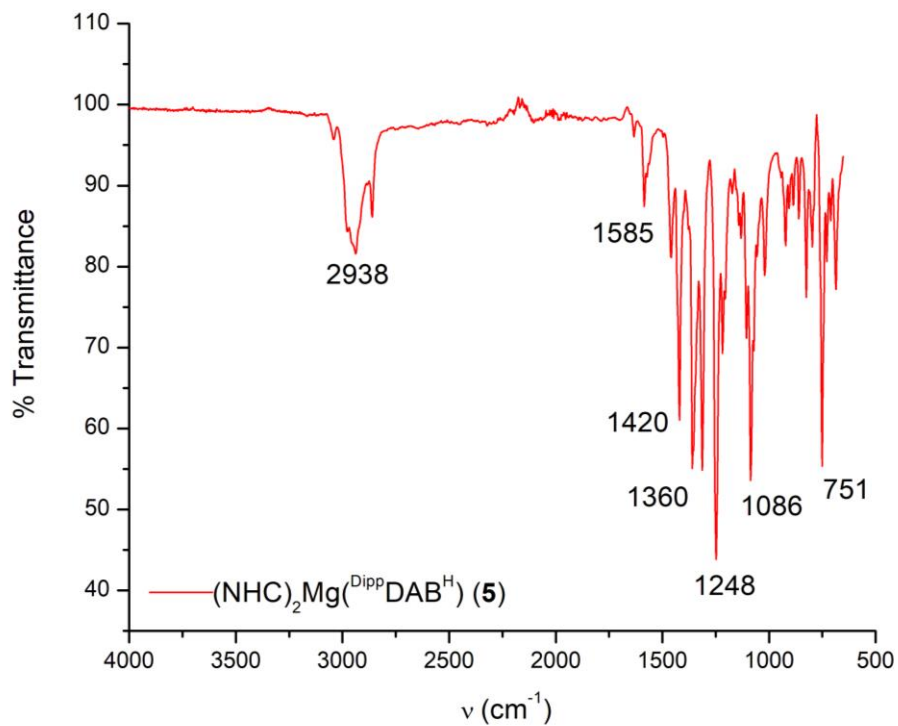


Figure A2.18. FTIR spectrum of compound **2.5**.

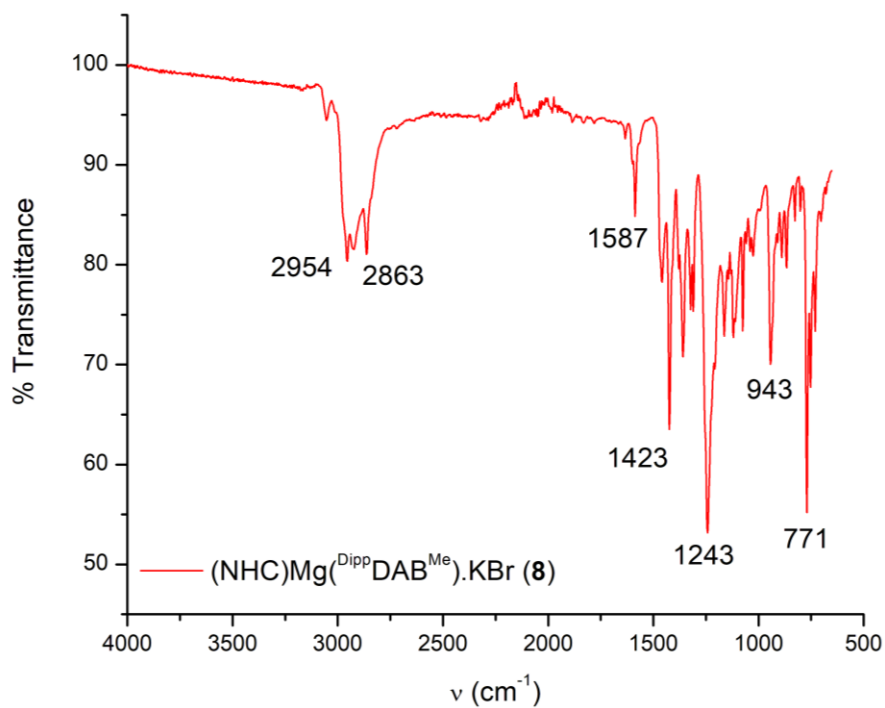


Figure A2.19. FTIR spectrum of compound **2.8**.

Chapter Three:

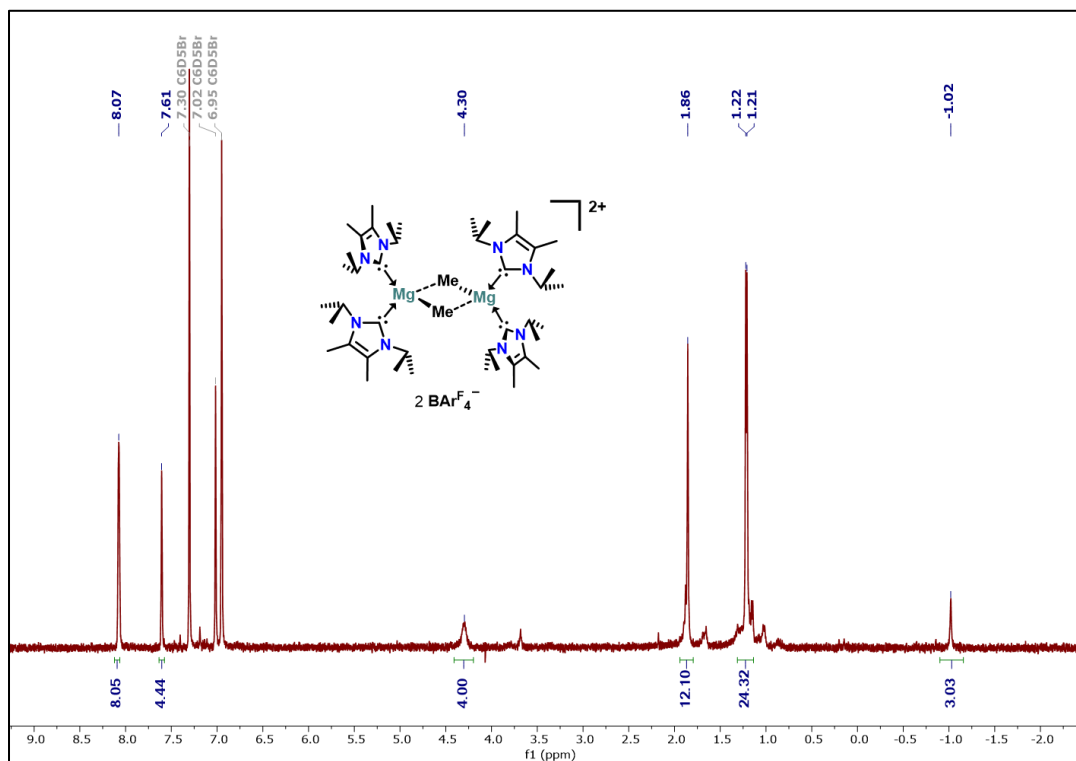


Figure A2.20: ^1H NMR spectrum (500 MHz, $\text{C}_6\text{D}_5\text{Br}$, 398 K) of **3.2**.

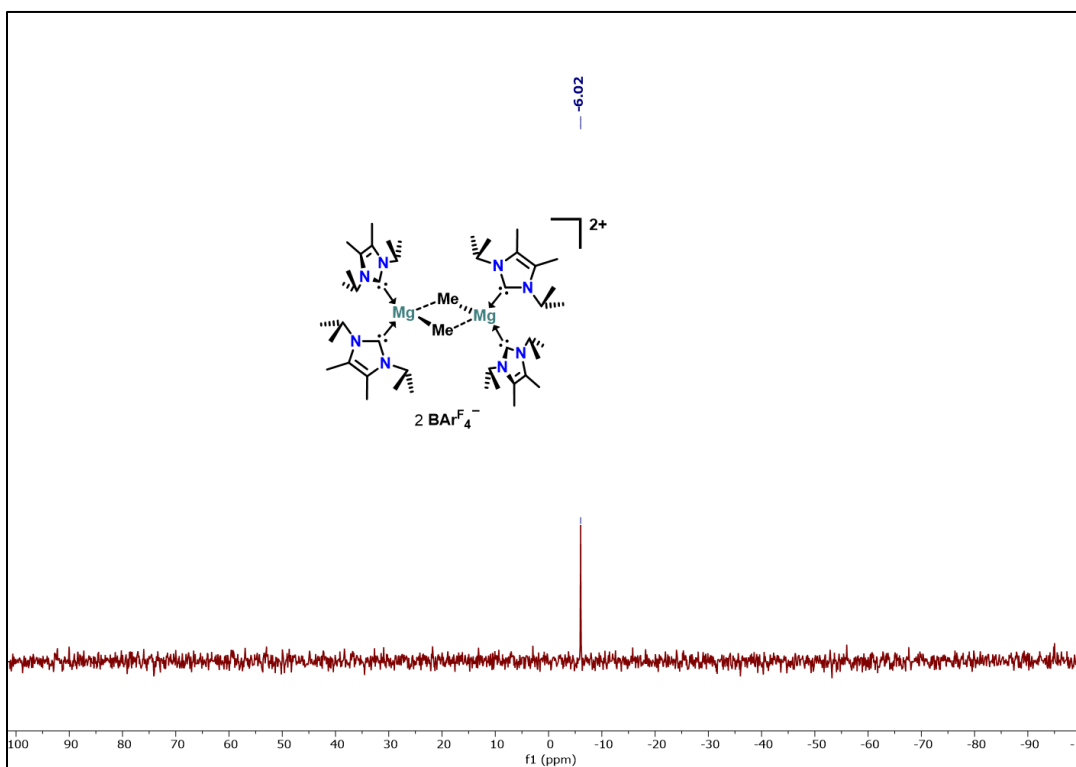


Figure A2.21: ^{11}B NMR spectrum (192.55 MHz, $\text{C}_6\text{D}_5\text{Br}$, 298 K) of **3.2**.

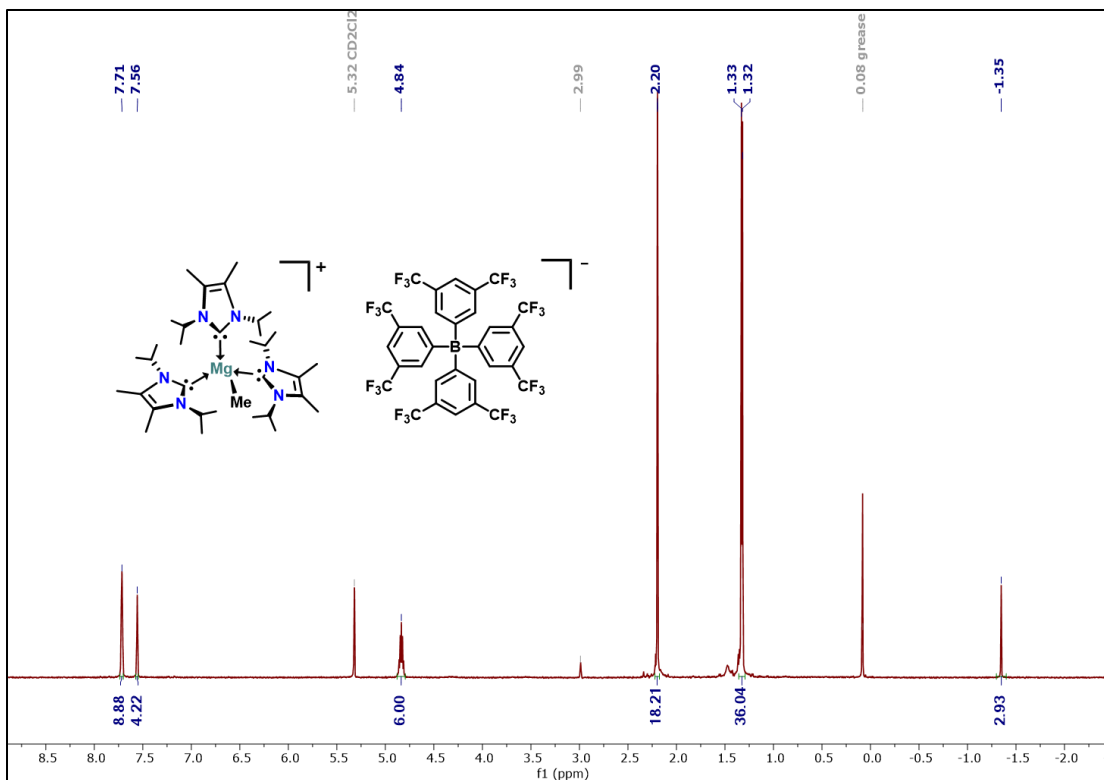


Figure A2.22: ^1H NMR spectrum (600 MHz, CD_2Cl_2 , 298 K) of $3.3[\text{BAr}^{\text{F}}_4]$.

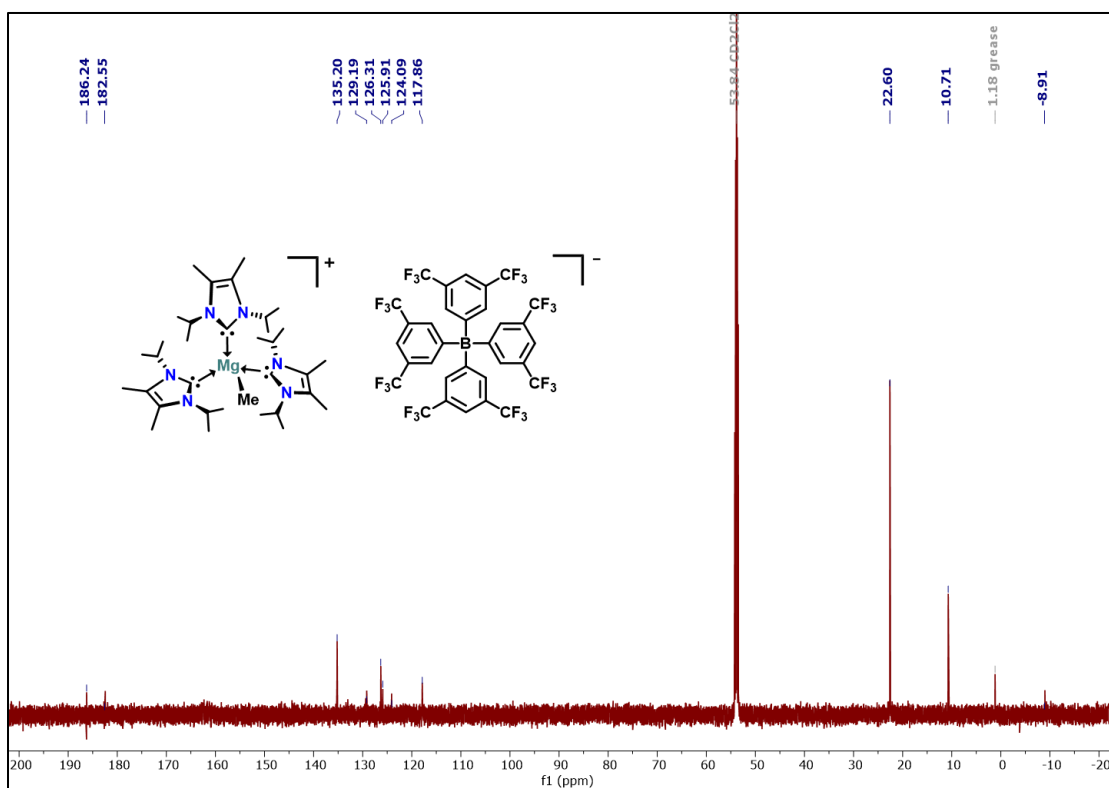


Figure A2.23: $^{13}\text{C}\{^1\text{H}\}$ NMR spectrum (151 MHz, CD_2Cl_2 , 298 K) of $3.3[\text{BAr}^{\text{F}}_4]$.

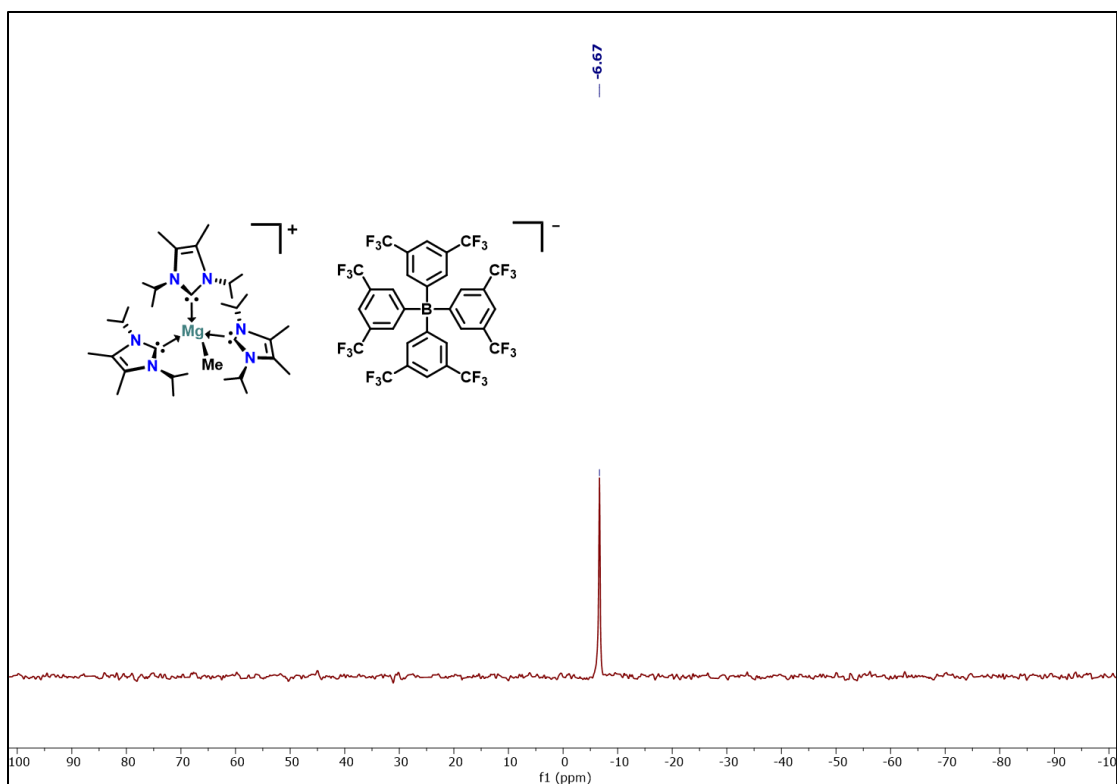


Figure A2.24: ^{11}B NMR spectrum (192.55 MHz, CD_2Cl_2 , 298 K) of $3.3[\text{BarF}_4]$.

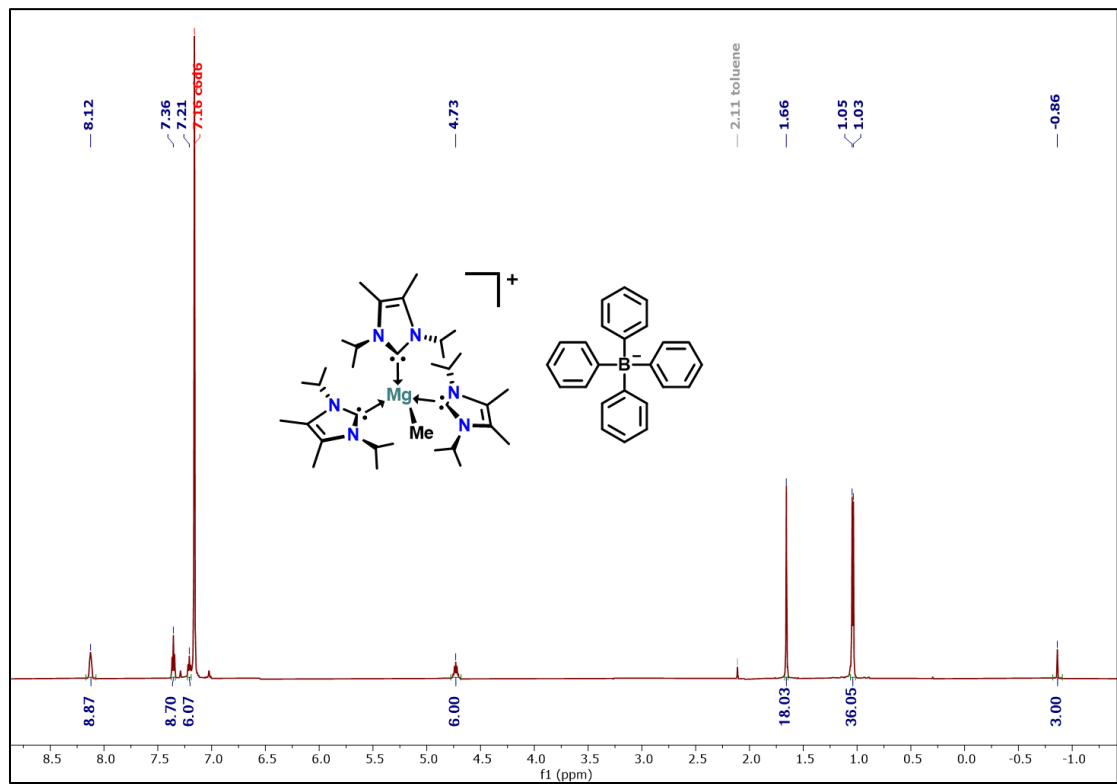


Figure A2.25: ^1H NMR spectrum (600 MHz, C_6D_6 , 298 K) of $3.3[\text{BPh}_4]$.

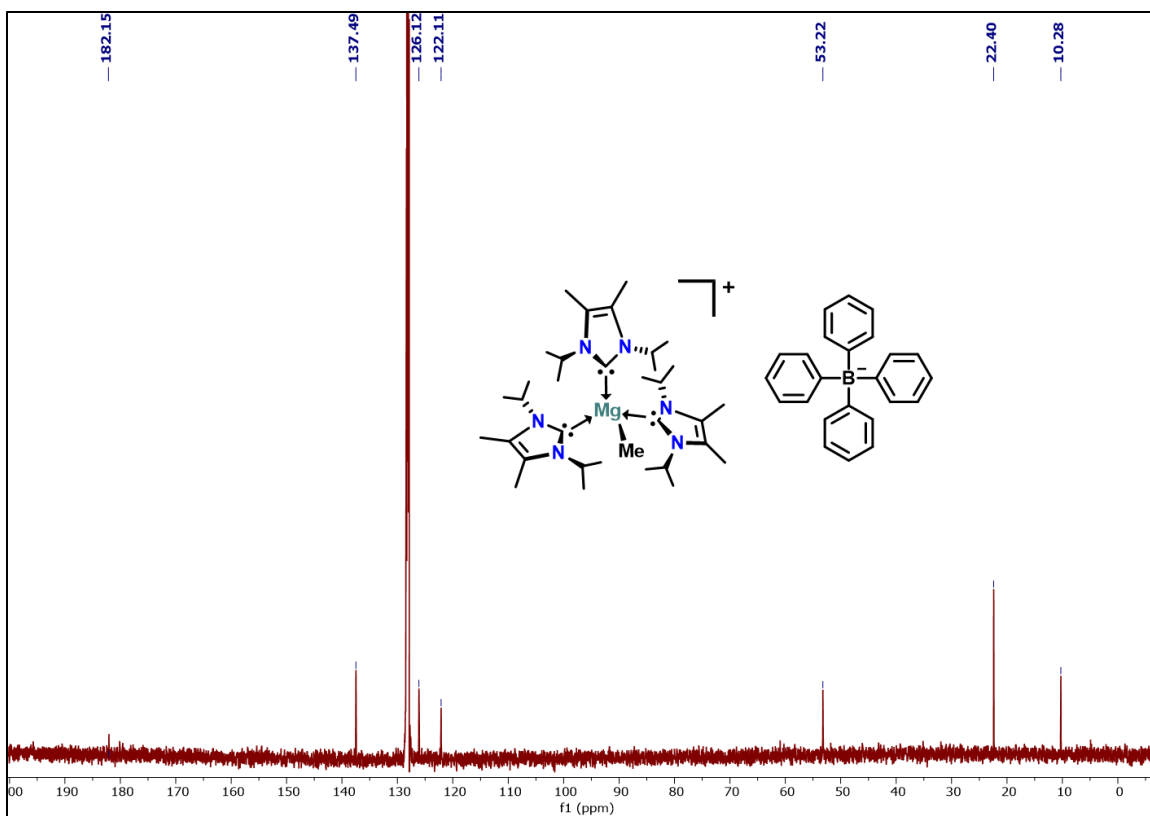


Figure A2.26: $^{13}C\{^1H\}$ NMR spectrum (151 MHz, C_6D_6 , 298 K) of **3.3**[BPh₄].

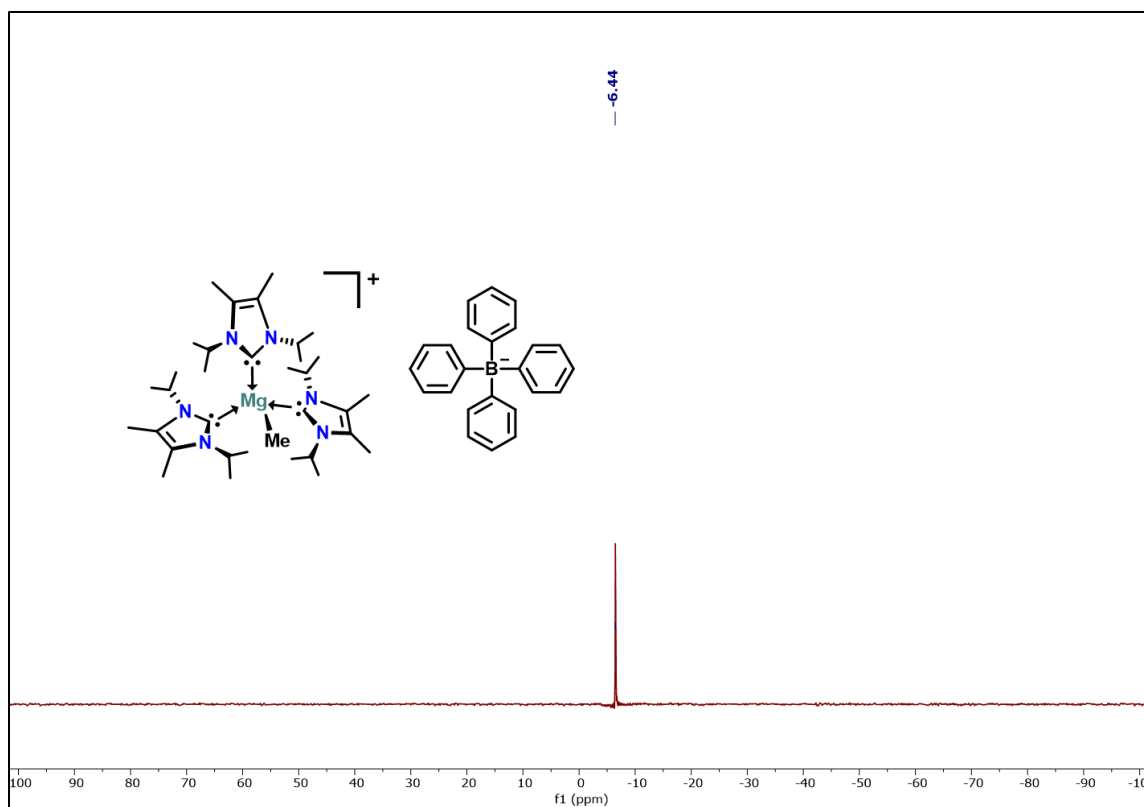


Figure A2.27: ^{11}B NMR spectrum (192.55 MHz, CD_2Cl_2 , 298 K) of **3.3**[BPh₄].

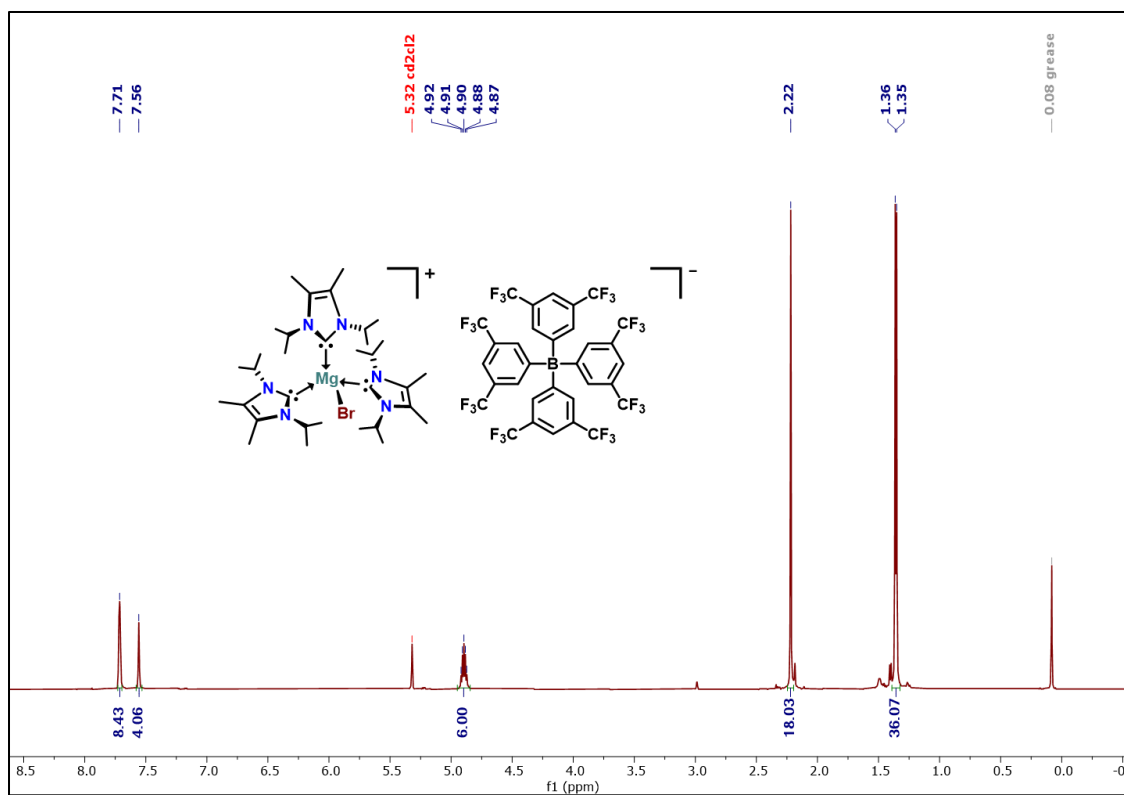


Figure A2.28: ^1H NMR spectrum (600 MHz, CD_2Cl_2 , 298 K) of $3.4[\text{BAr}^{\text{F}}_4]$.

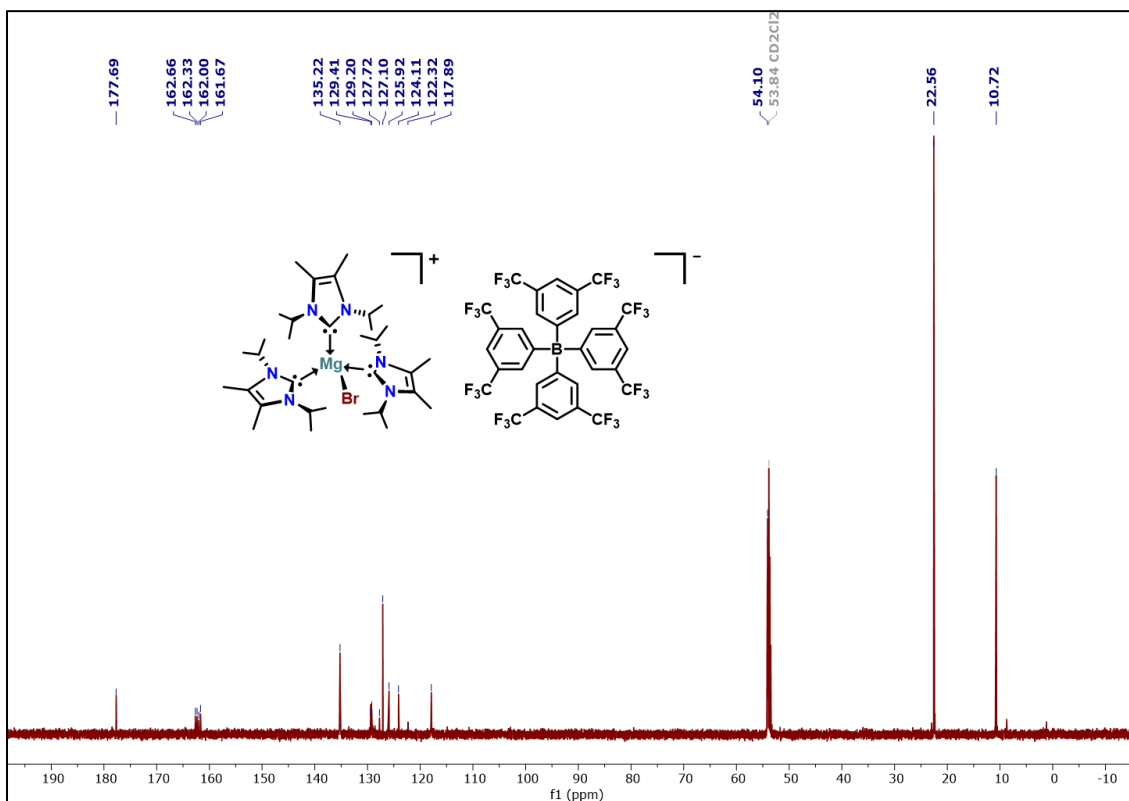


Figure A2.28: $^{13}\text{C}\{^1\text{H}\}$ NMR spectrum (151 MHz, CD_2Cl_2 , 298 K) of $3.4[\text{BAr}^{\text{F}}_4]$.

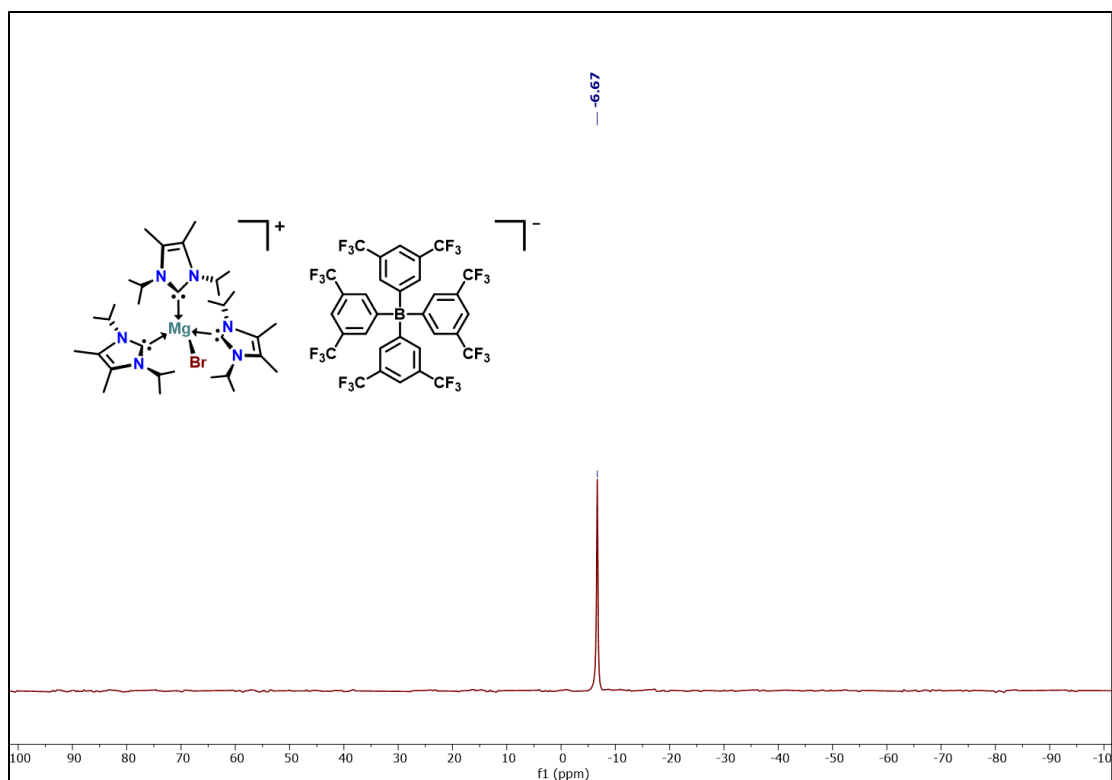


Figure A2.29: ^{11}B NMR spectrum (192.55 MHz, CD_2Cl_2 , 298 K) of $3.4[\text{BAr}^{\text{F}}_4]$.

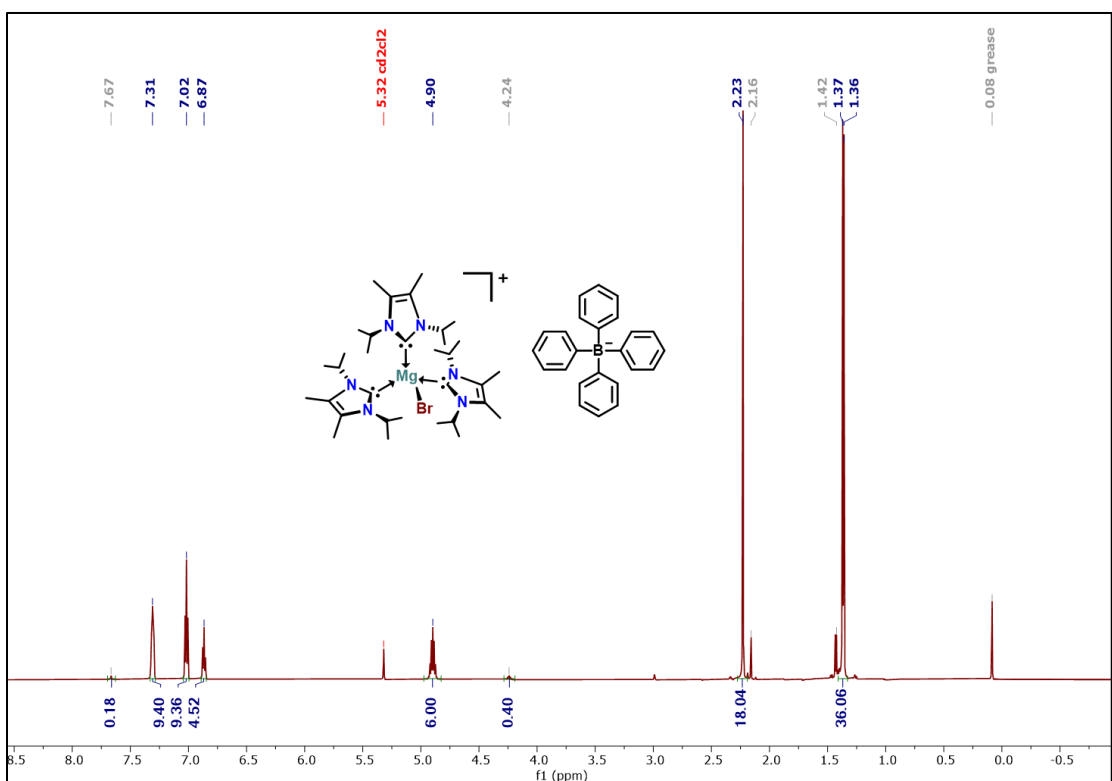


Figure A2.30: ^1H NMR spectrum (600 MHz, CD_2Cl_2 , 298 K) of $3.4[\text{BPh}_4]$. Unlabeled peaks in grey represent hydrolysis product.

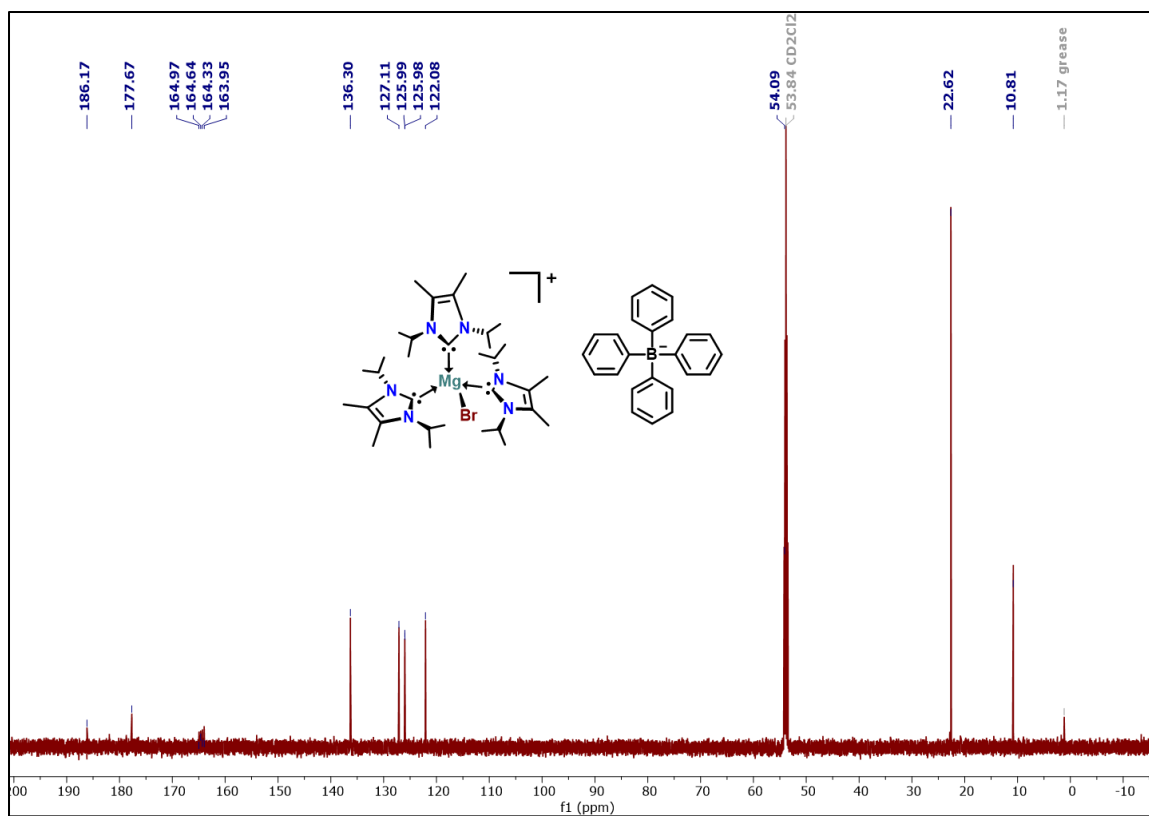


Figure A2.31: $^{13}\text{C}\{^1\text{H}\}$ NMR (151 MHz, CD_2Cl_2 , 298 K) of **3.4**[BPh₄].

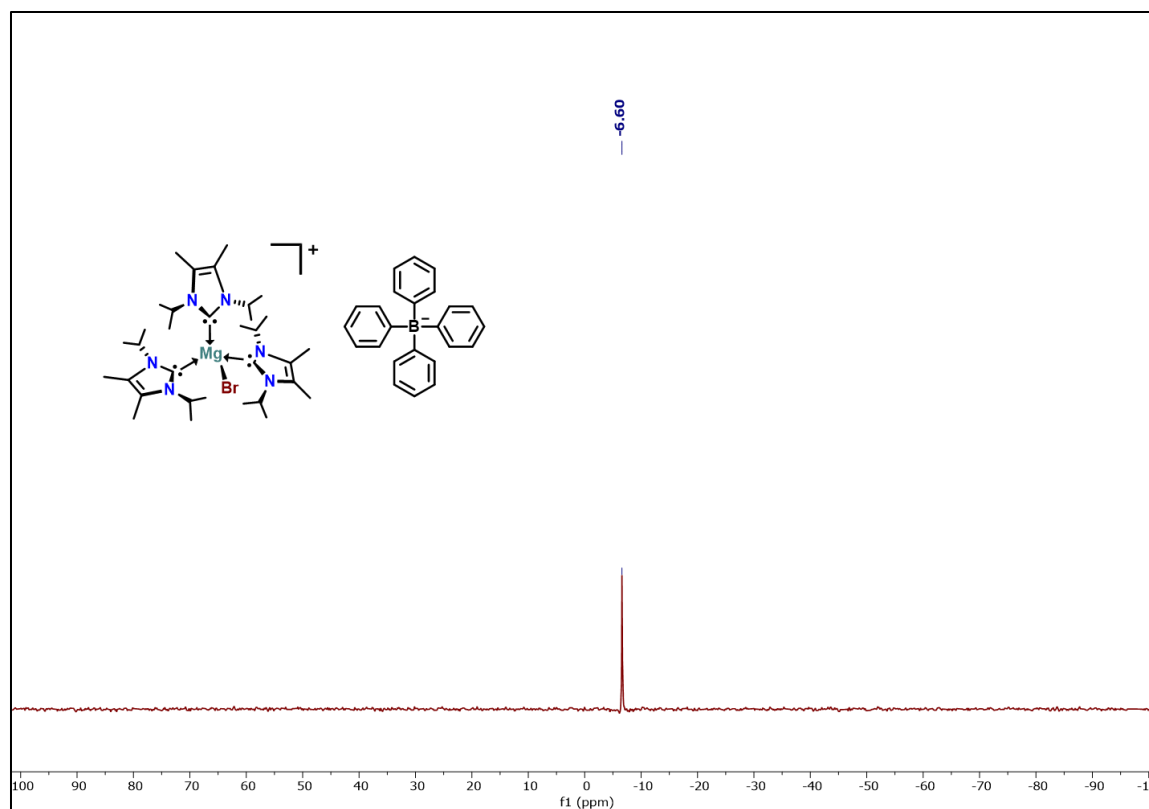


Figure A2.32: ^{11}B NMR spectrum (192.55 MHz, CD_2Cl_2 , 298 K) of **3.4**[BPh₄].

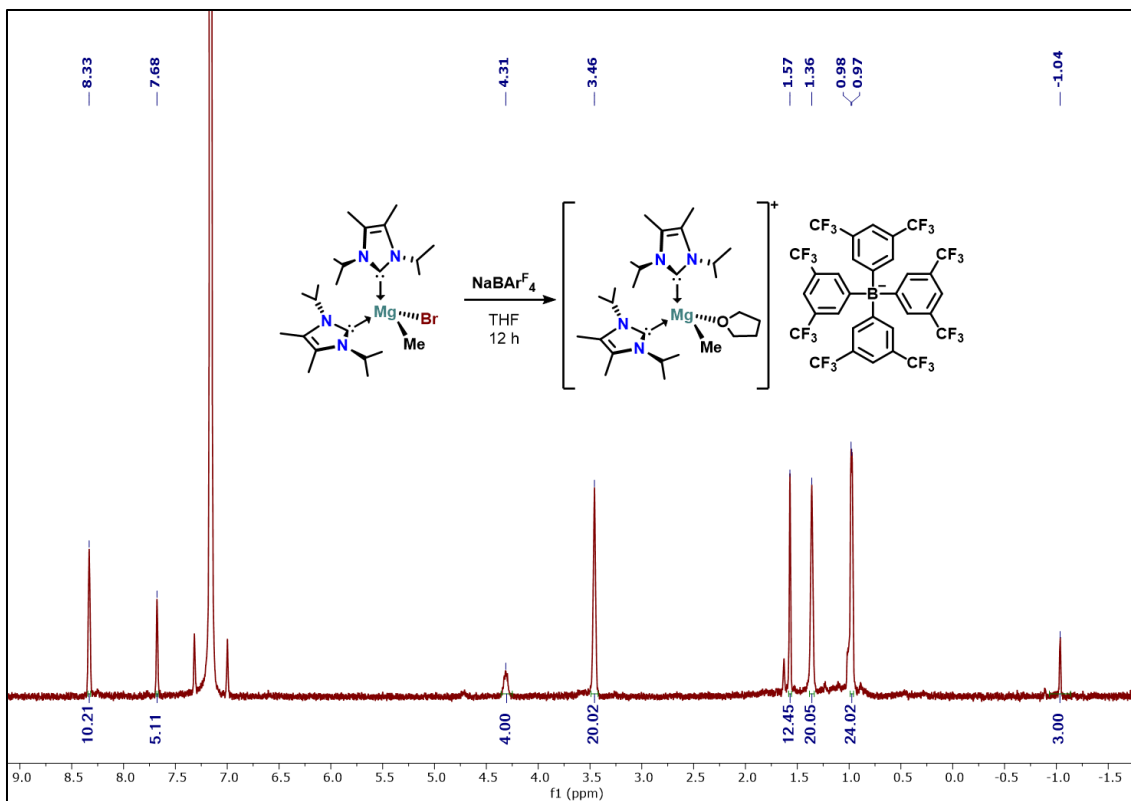


Figure A2.33: ^1H NMR spectrum (600.13 MHz, C_6D_6 , 298 K) of $3.5[\text{BAr}^{\text{F}}_4]$.

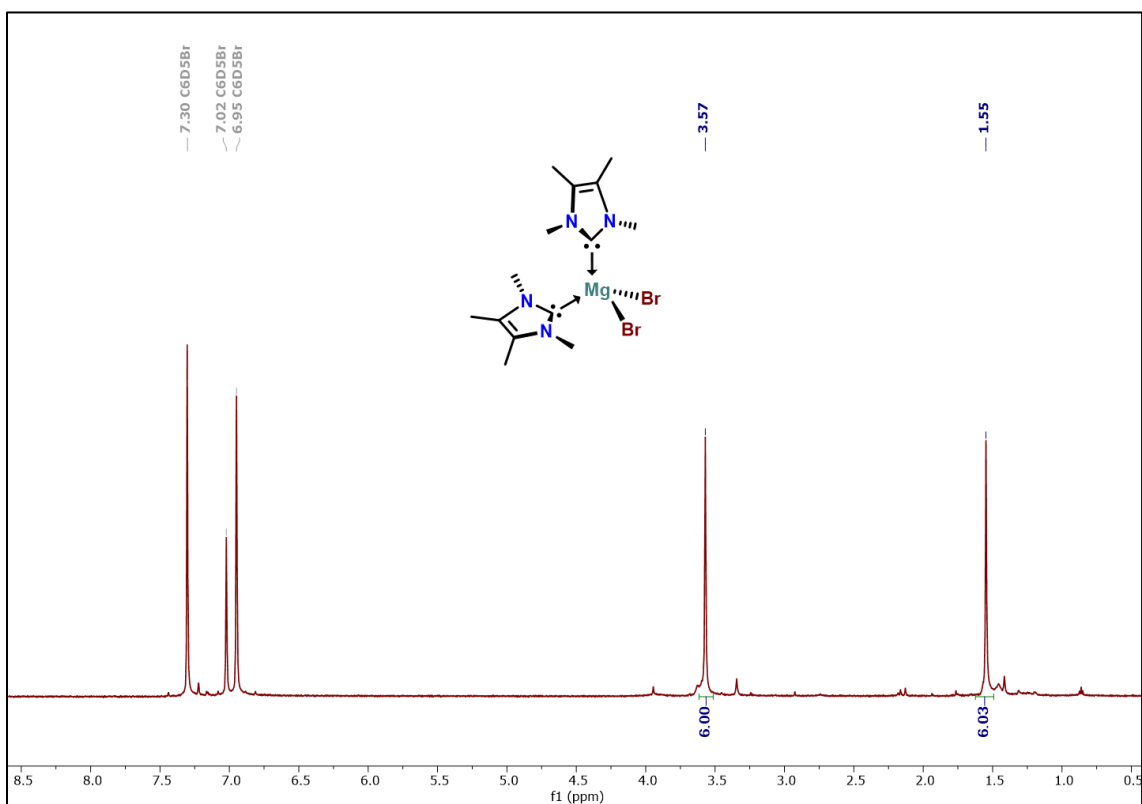


Figure A2.34: ^1H NMR spectrum (600.13 MHz, $\text{C}_6\text{D}_5\text{Br}$, 298 K) of 3.7 .

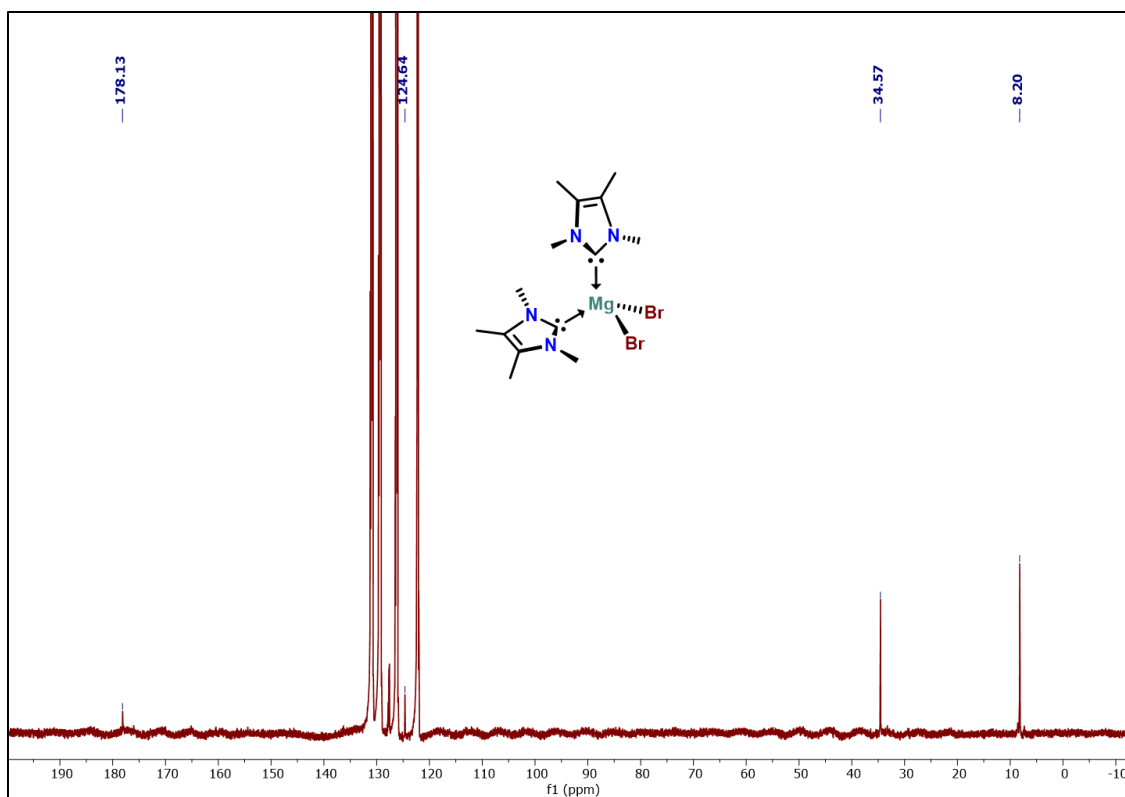


Figure A2.35: $^{13}\text{C}\{^1\text{H}\}$ NMR spectrum (200 MHz, $\text{C}_6\text{D}_5\text{Br}$, 298 K) of 3.7.

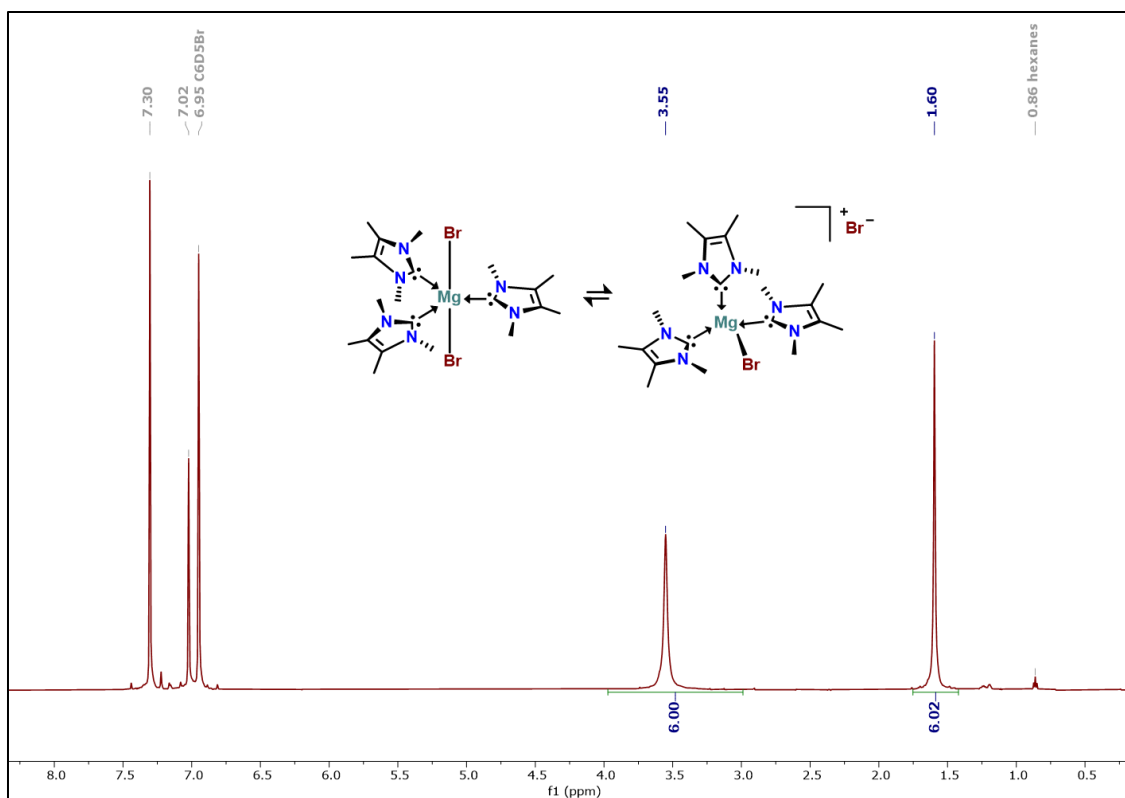


Figure A2.36: ^1H NMR spectrum (600.13 MHz, $\text{C}_6\text{D}_5\text{Br}$, 298 K) of 3.8.

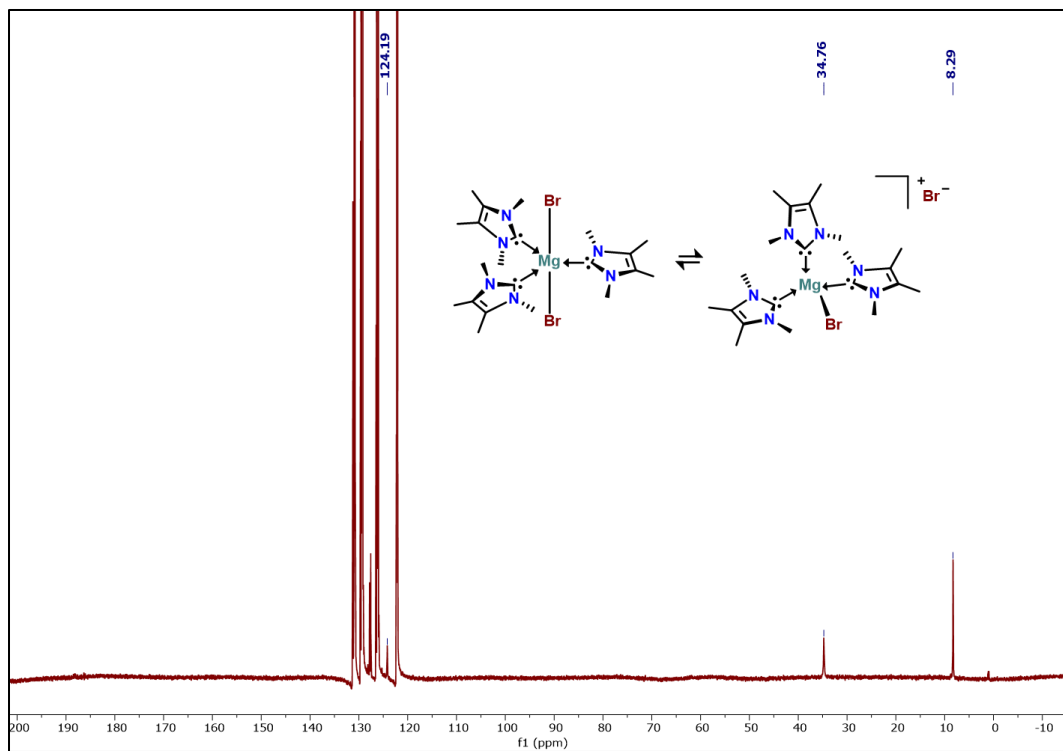


Figure A2.37: $^{13}\text{C}\{^1\text{H}\}$ NMR spectrum (200 MHz, $\text{C}_6\text{D}_5\text{Br}$, 298 K) of **3.8**.

Reactions involving Ligand rearrangement products. ^1H NMR spectrum (600 MHz, CD_2Cl_2 , 298 K) described unless otherwise indicated.

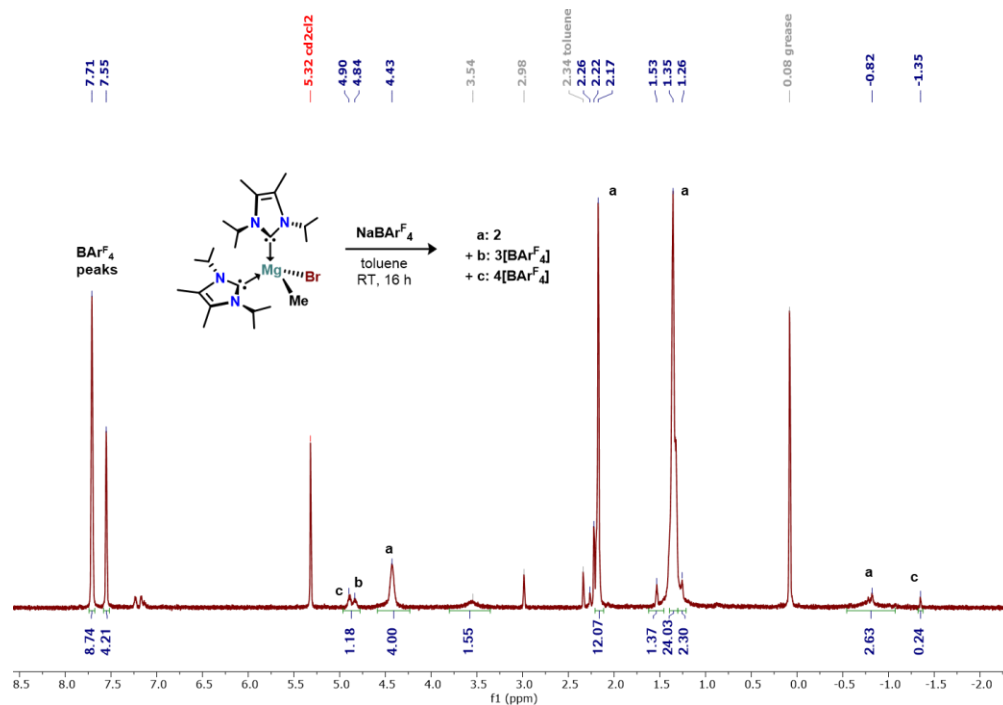


Figure A2.38: Reaction of **3.1** and $\text{Na}[\text{BArF}_4]$ in toluene.

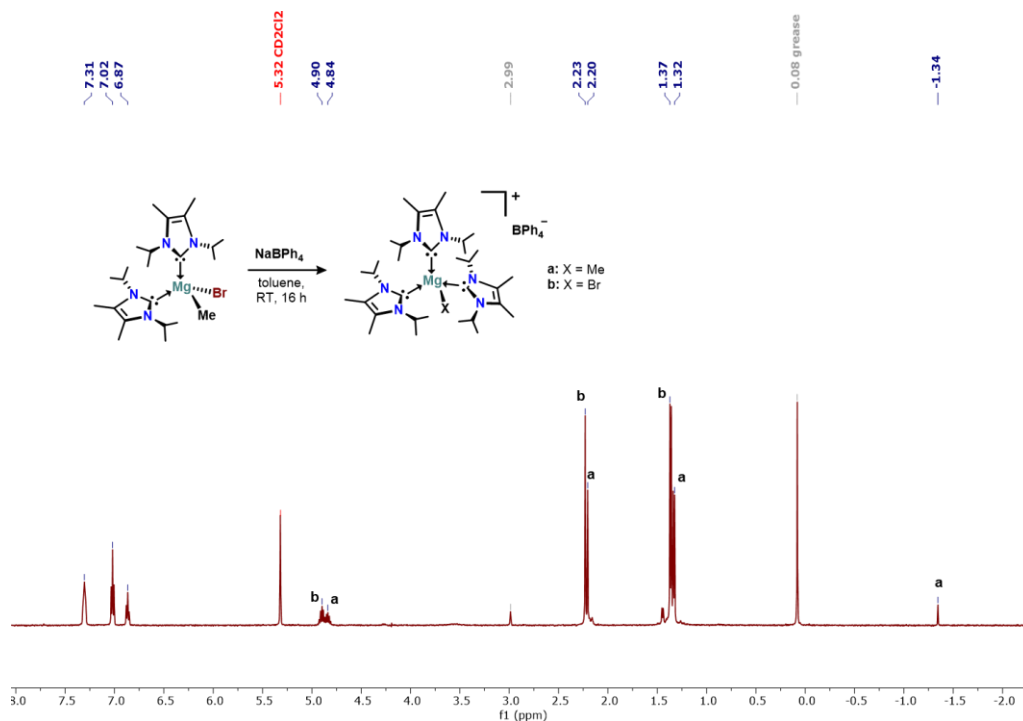


Figure A2.39: Reaction of **3.1** and $\text{Na}[\text{BPh}_4]$ in toluene.

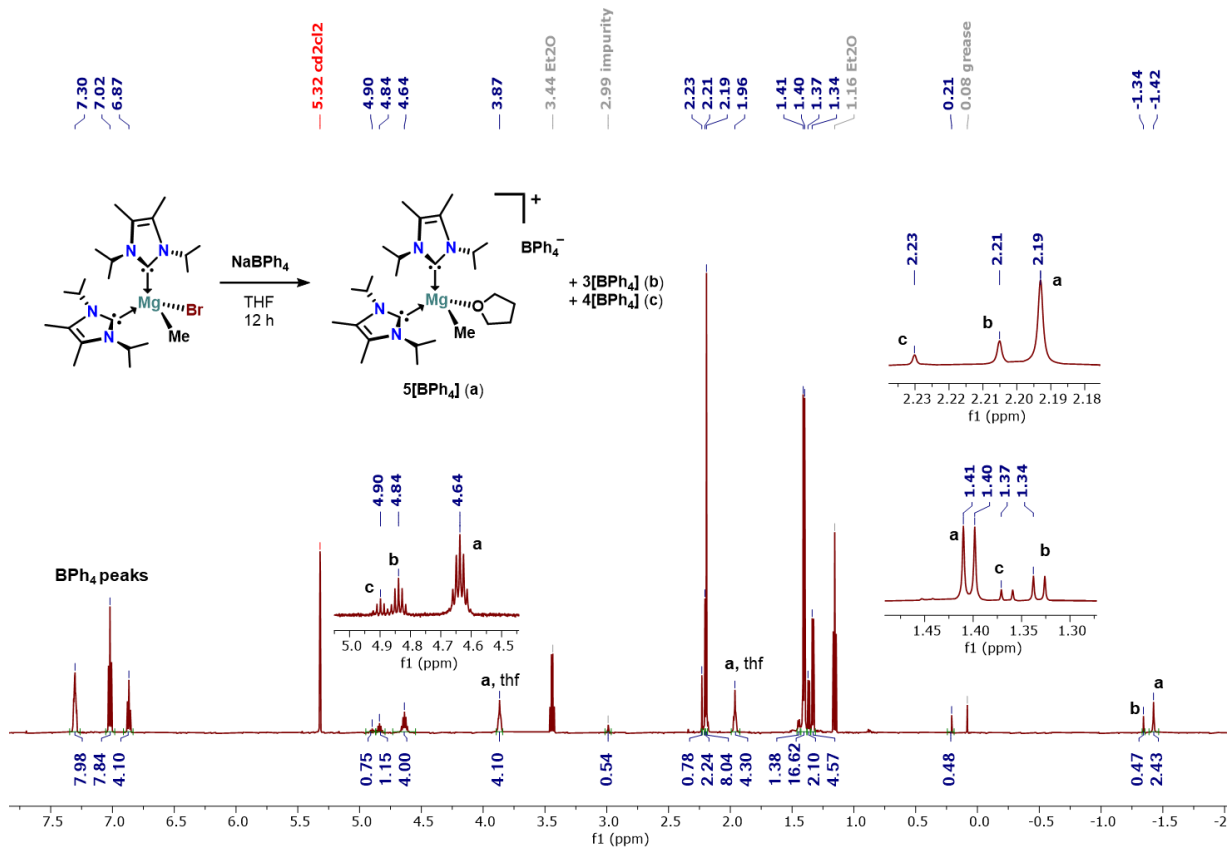


Figure A2.40: Synthesis of 3.5[BPh₄].

Chapter Four:

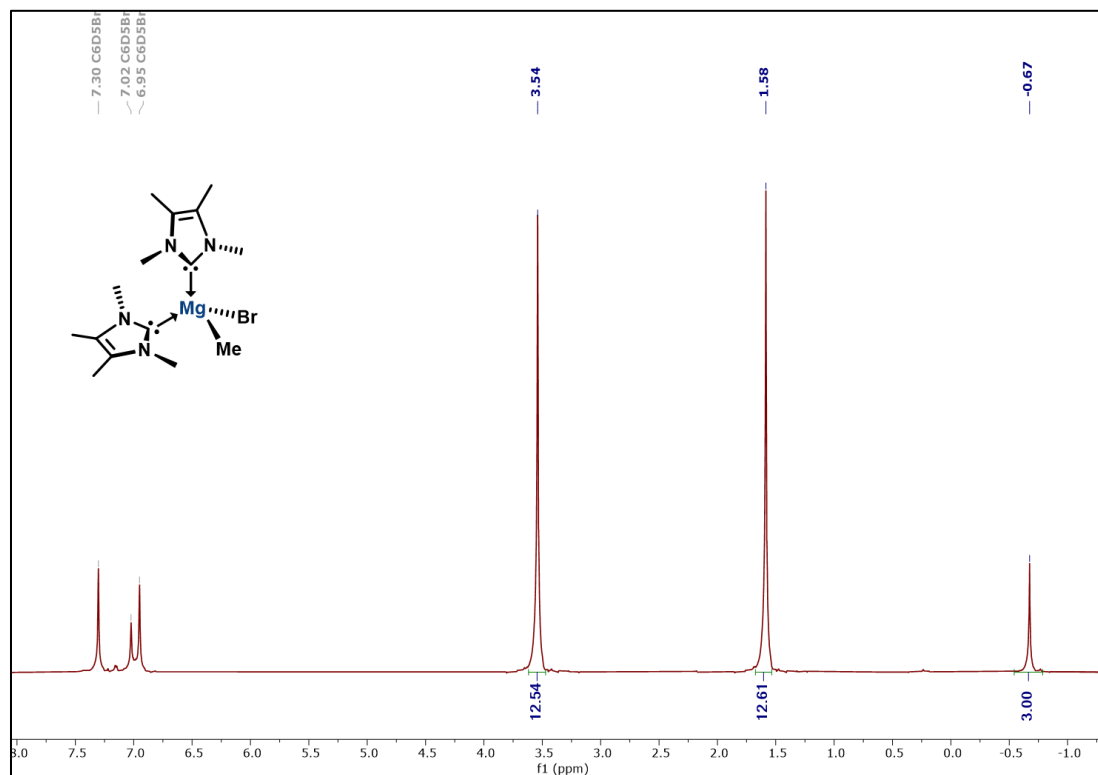


Figure A2.41. ^1H NMR spectrum (600.13 MHz, $\text{C}_6\text{D}_5\text{Br}$, 298 K) of **4.1^{Me}**.

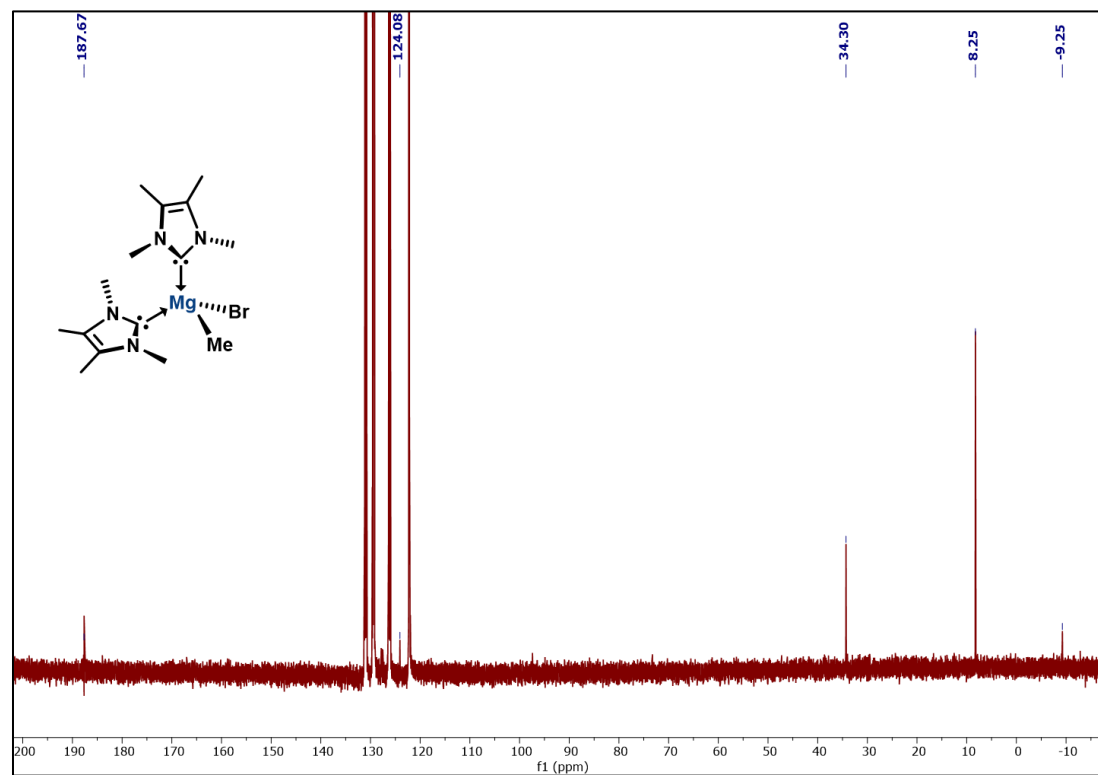


Figure A2.42. ^{13}C NMR spectrum (150.90 MHz, $\text{C}_6\text{D}_5\text{Br}$, 298 K) of **4.1^{Me}**.

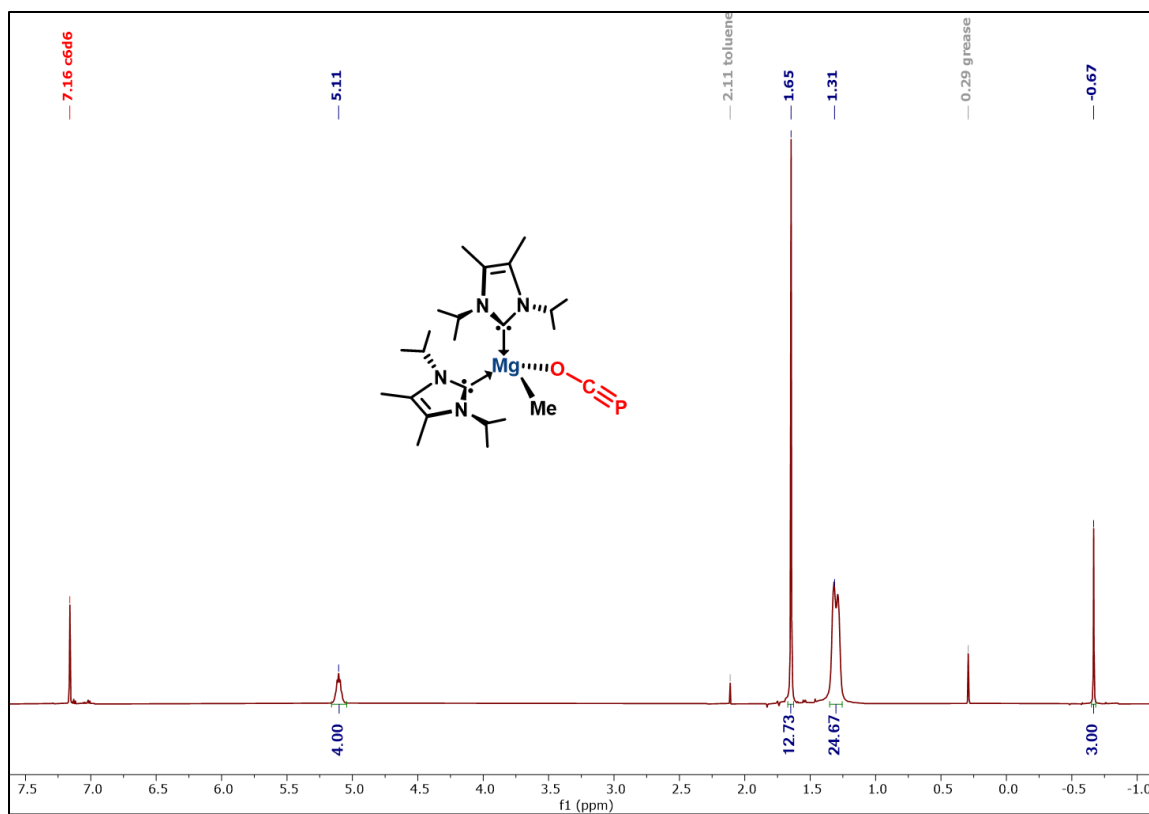


Figure A2.43. ^1H NMR spectrum (600.13 MHz, C_6D_6 , 298 K) of 4.2ⁱPr.

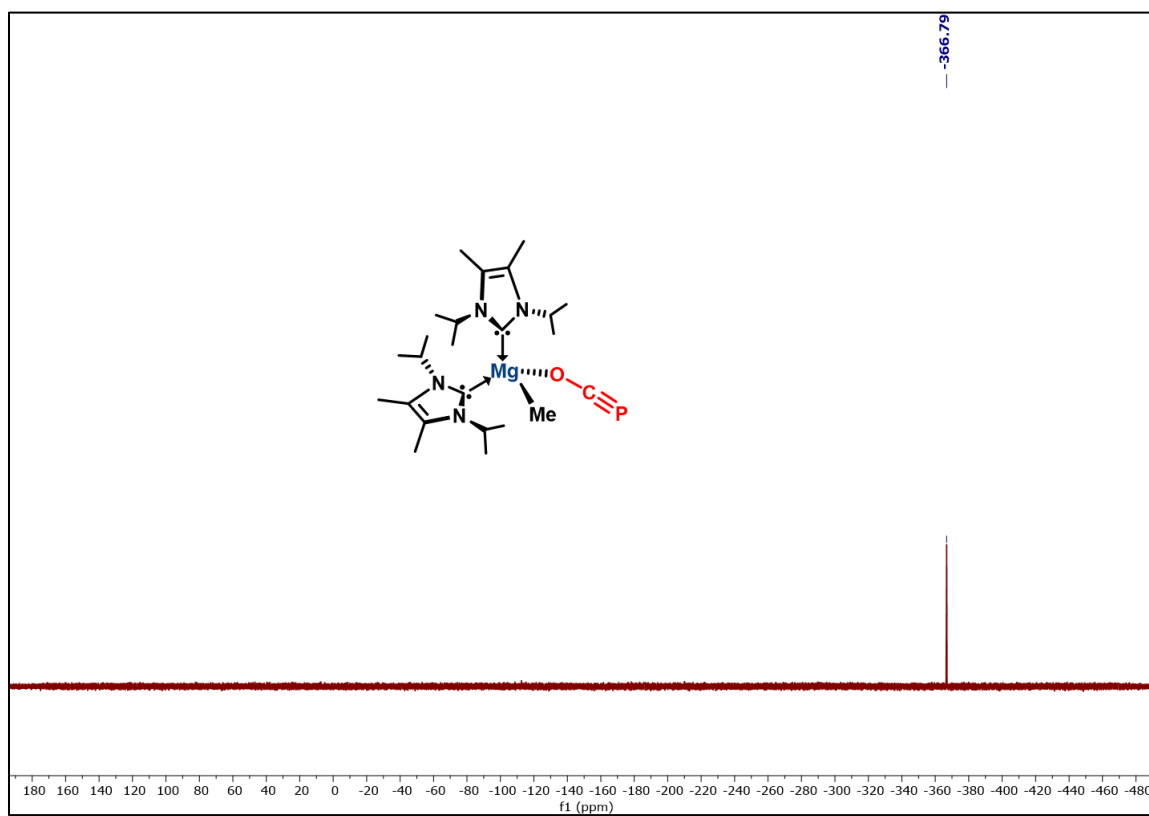


Figure A2.44. ^{31}P NMR spectrum (243 MHz, C_6D_6 , 298 K) of 4.2ⁱPr.

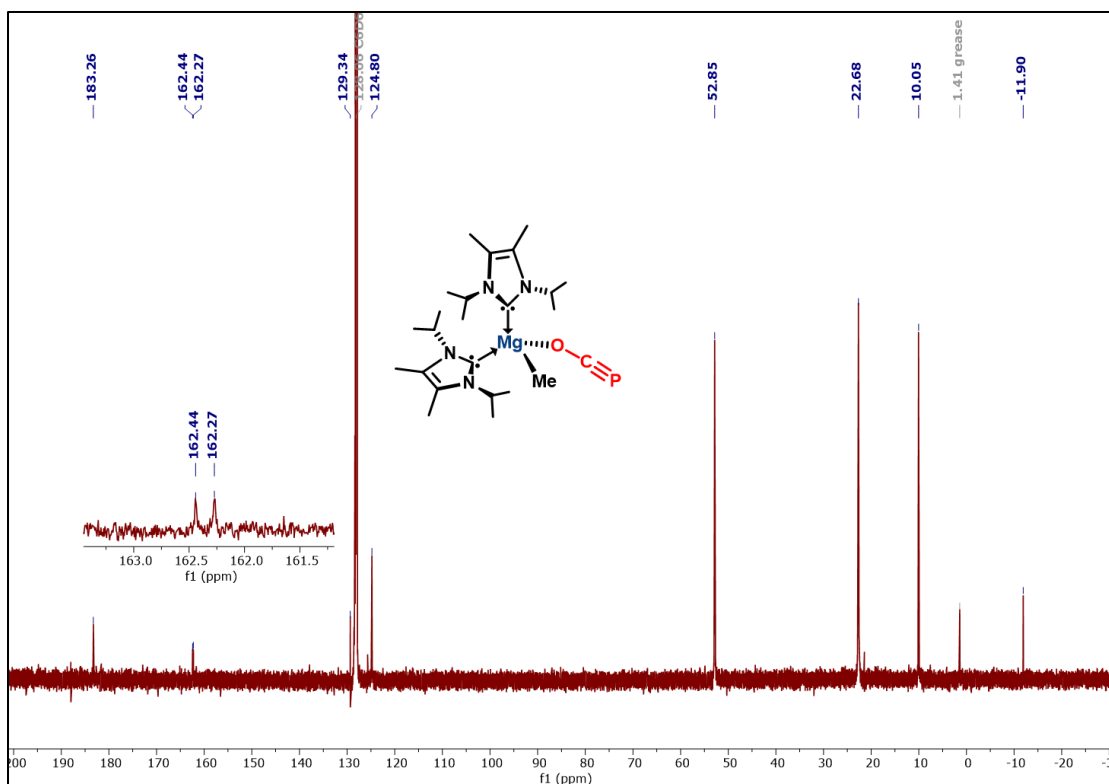


Figure A2.45. ^{13}C NMR spectrum (150.90 MHz, C_6D_6 , 298 K) of 4.2^{iPr} .

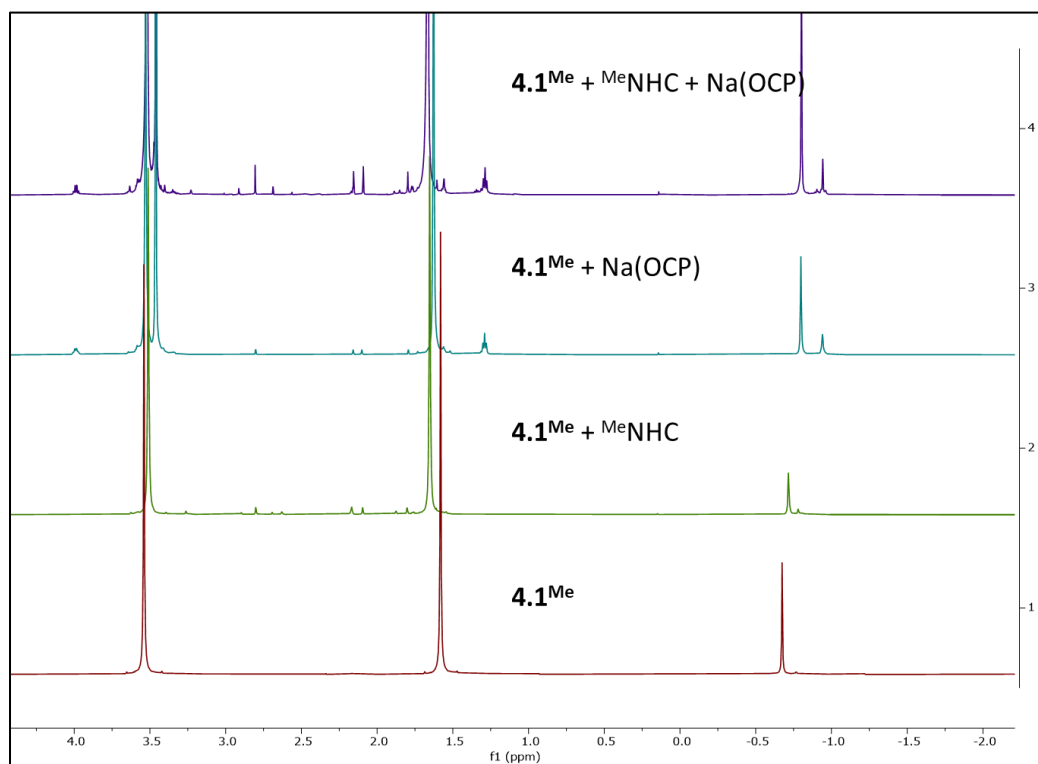


Figure A2.46. Stacked ^1H NMR spectrum ($\text{C}_6\text{D}_5\text{Br}$, 298 K) showing dioxane activation in the reaction of 4.1^{Me} and $[\text{Na}(\text{dioxane})_2][\text{OCP}]$. Each spectrum was obtained after 5 min reaction time.

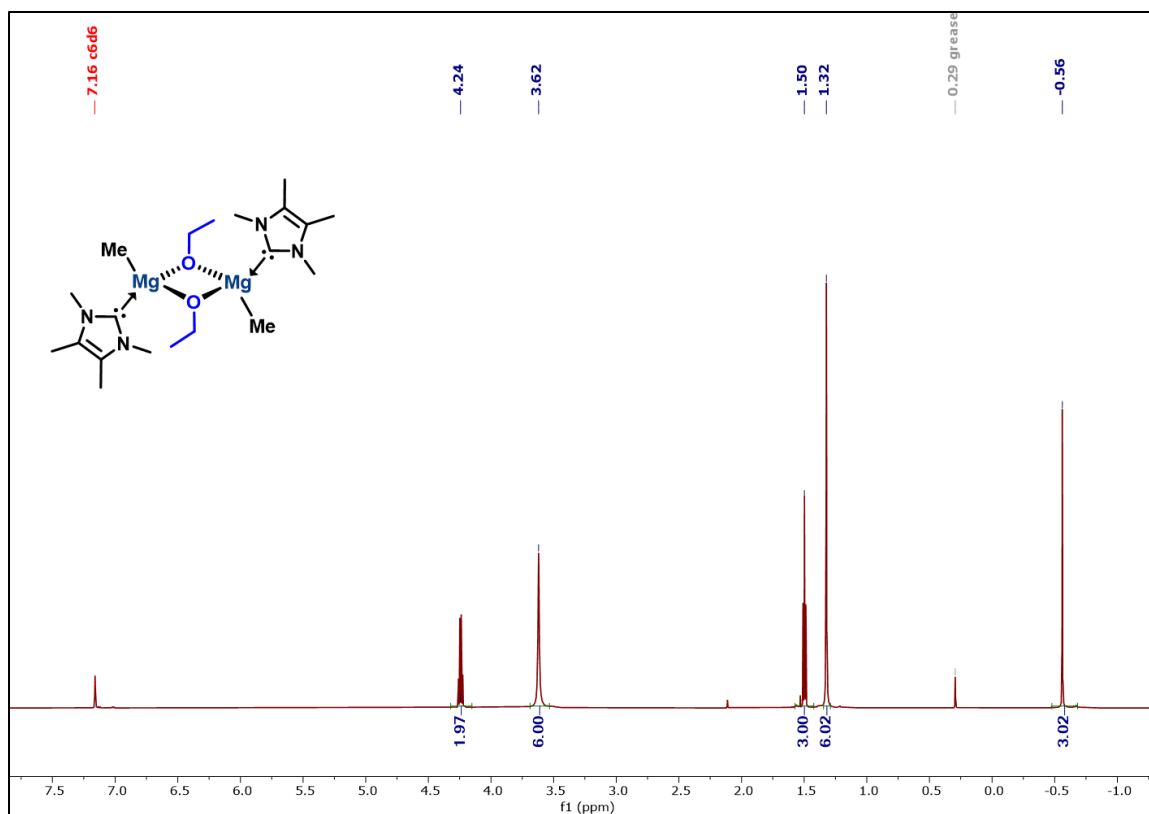


Figure A2.47. ¹H NMR spectrum (600.13 MHz, C₆D₆, 298 K) of 4.3^{Me}.

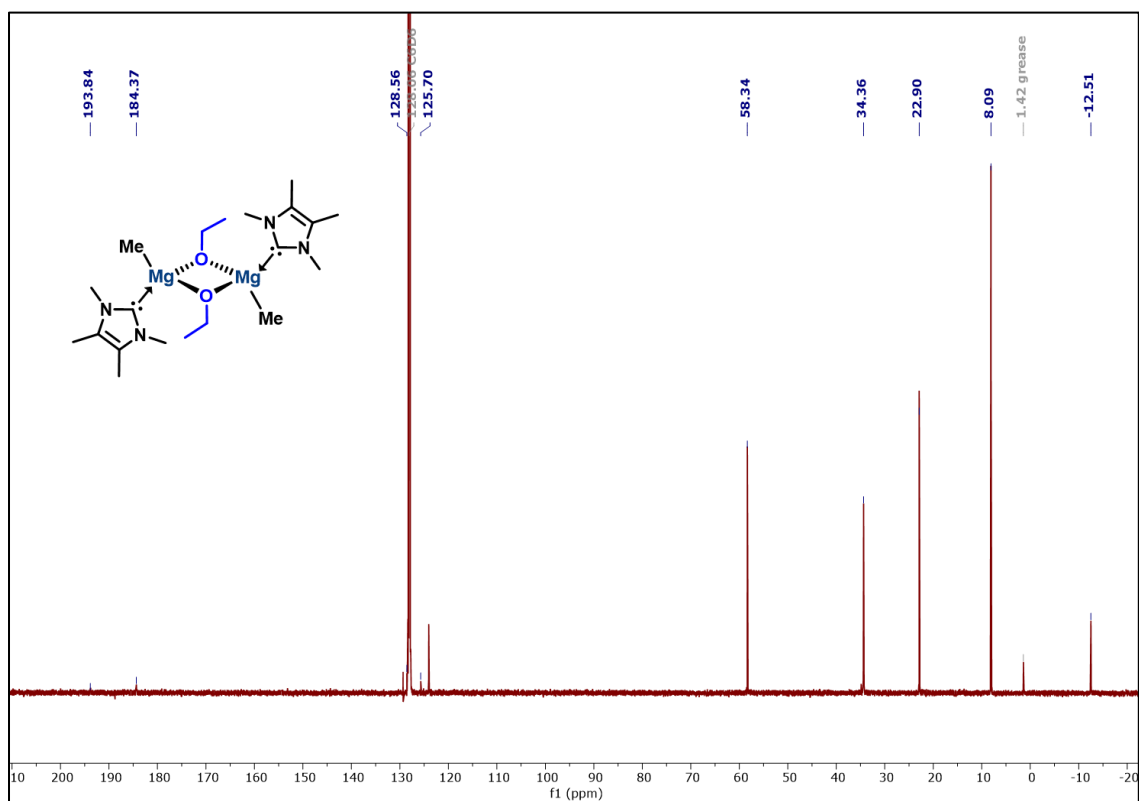


Figure A2.48. ¹³C NMR spectrum (150.90 MHz, C₆D₆, 298 K) of 4.3^{Me}.

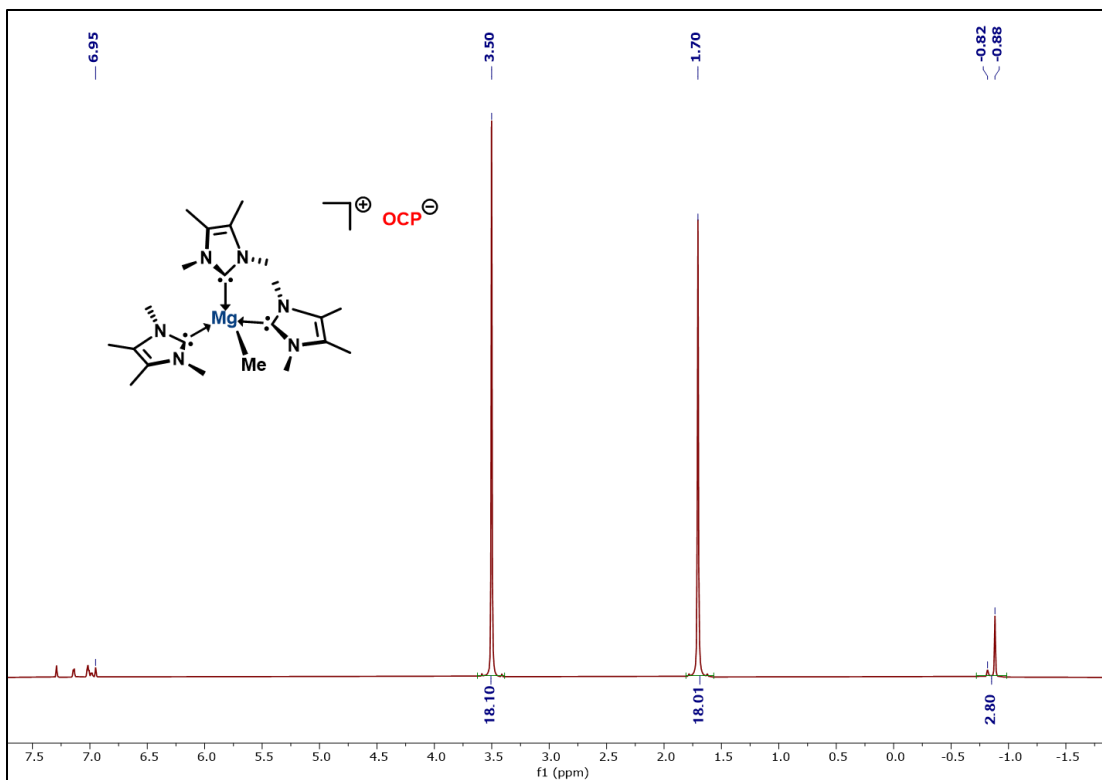


Figure A2.49. ^1H NMR spectrum (800 MHz, $\text{C}_6\text{D}_5\text{Br}$, 298 K) of 4.4^{Me} .

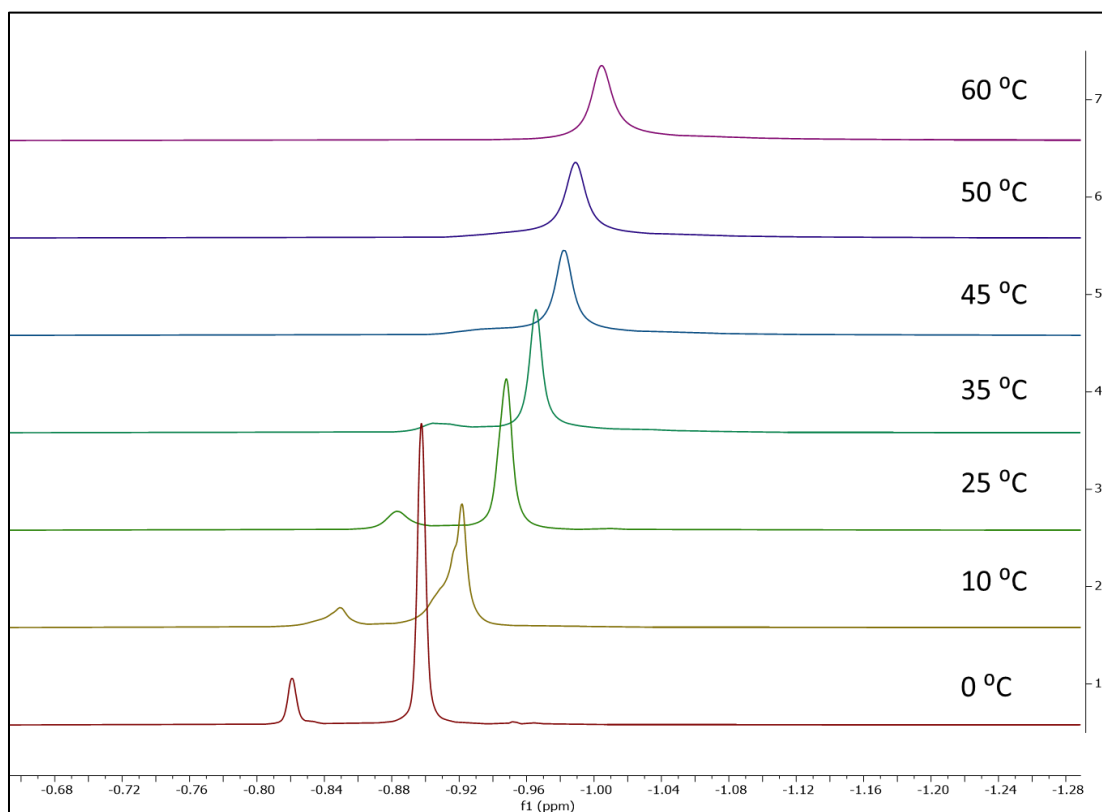


Figure A2.50. ^1H VT-NMR spectrum of 4.4^{Me} highlighting the $\text{Mg}(\text{CH}_3)$ region.

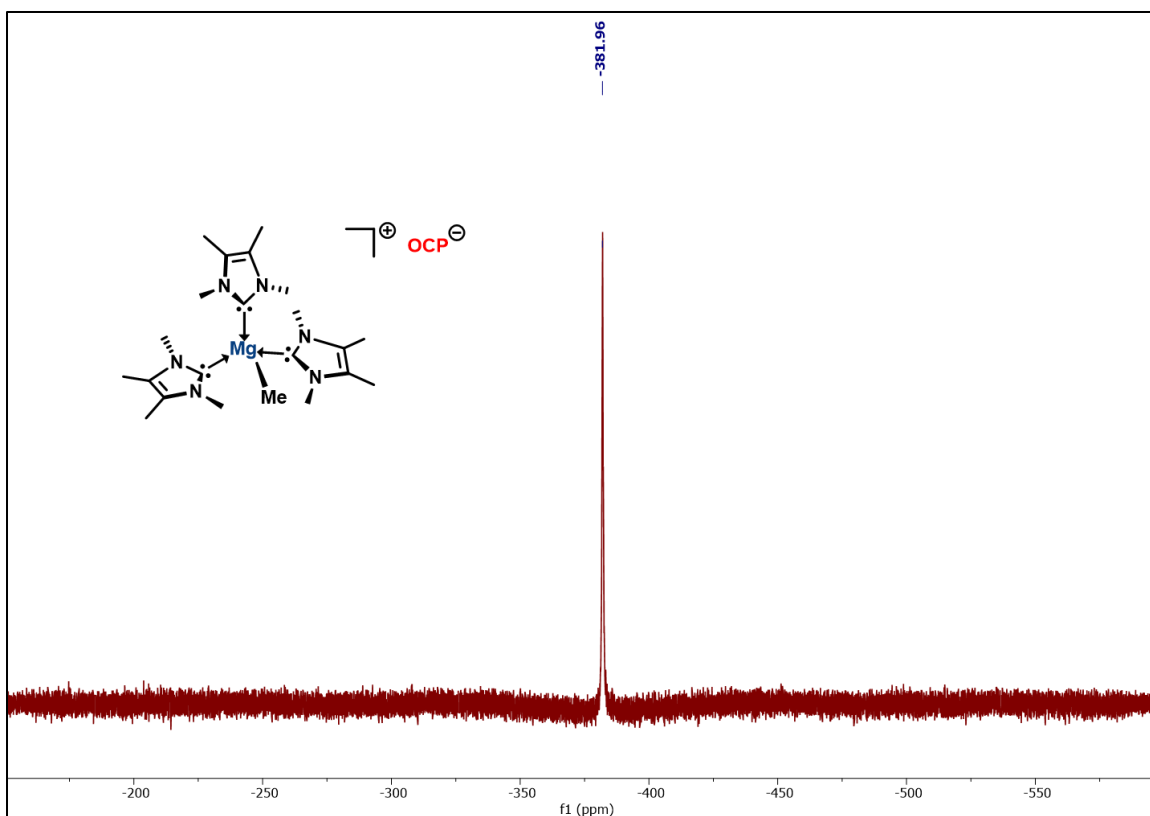


Figure A2.51. ^{31}P NMR spectrum (243 MHz, $\text{C}_6\text{D}_5\text{Br}$, 298 K) of 4.4^{Me} .

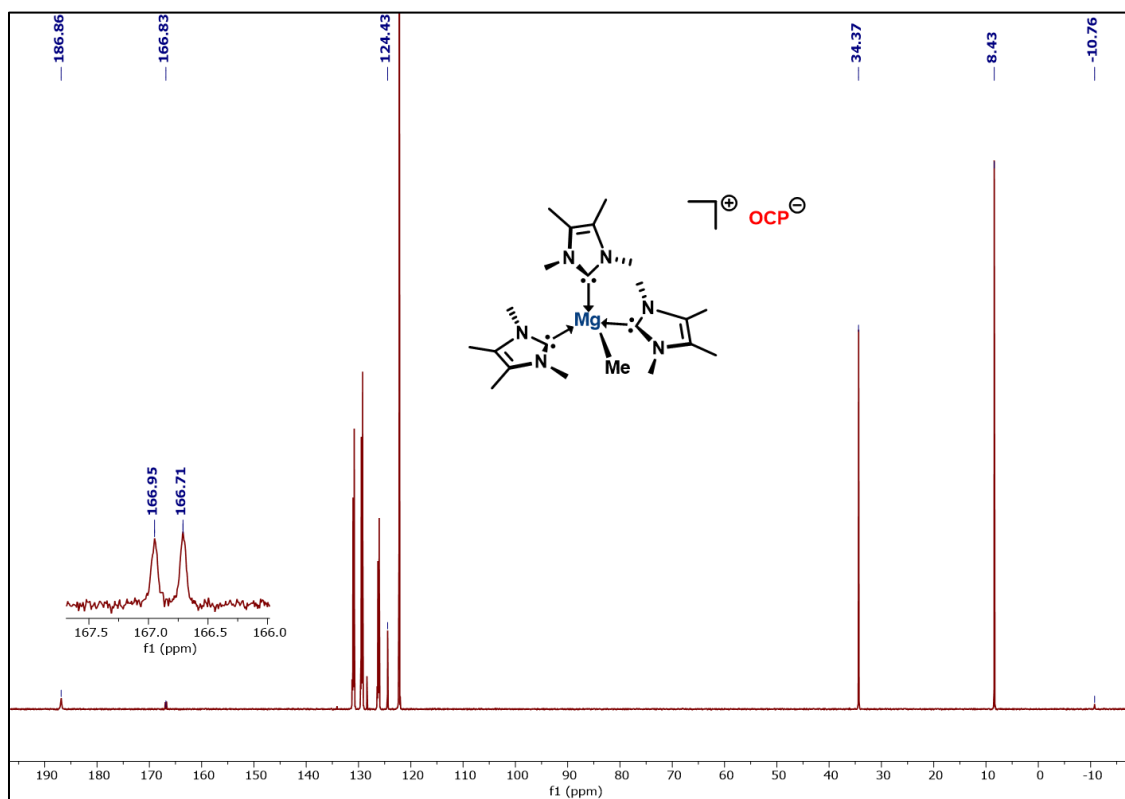


Figure A2.52. ^{13}C NMR spectrum (200 MHz, $\text{C}_6\text{D}_5\text{Br}$, 333 K) of 4.4^{Me} .

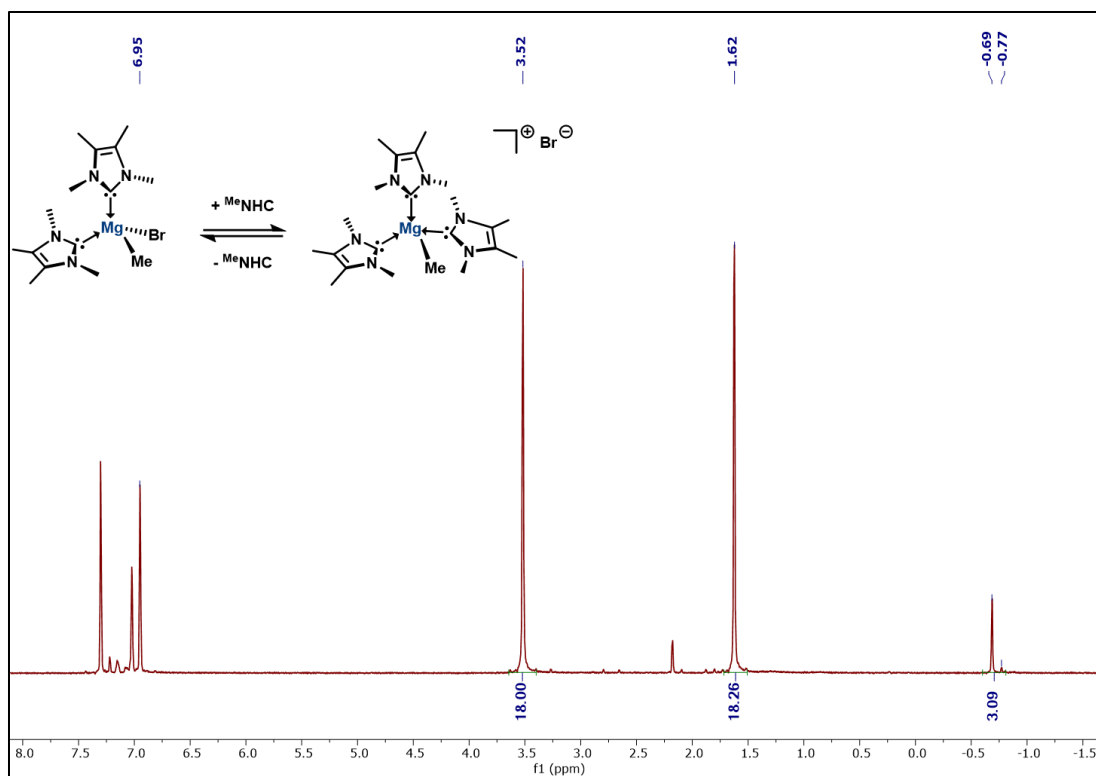


Figure A2.53. ^1H NMR spectrum (600 MHz, $\text{C}_6\text{D}_5\text{Br}$, 298 K) of **4.5**.

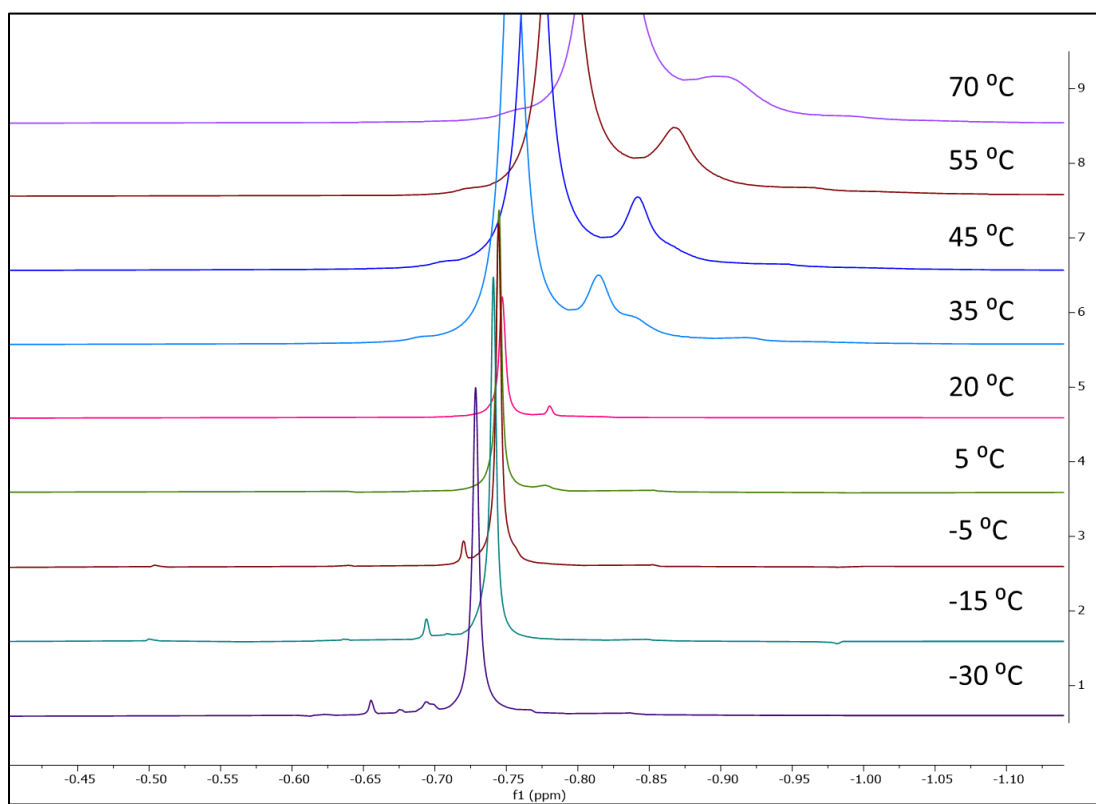


Figure A2.54. ^1H VT-NMR spectrum of **4.5** showing the $\text{Mg}-\text{CH}_3$ region.

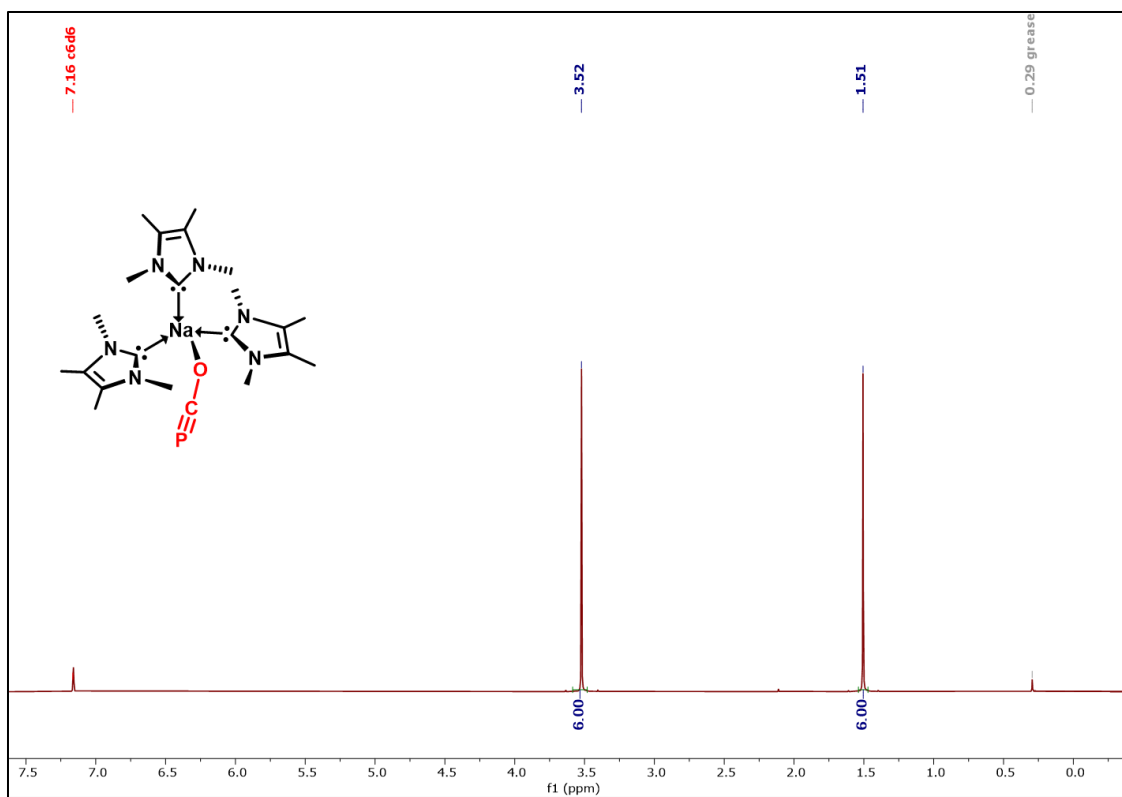


Figure A2.55. ^1H NMR spectrum (600.13 MHz, C_6D_6 , 298 K) of **4.6**.

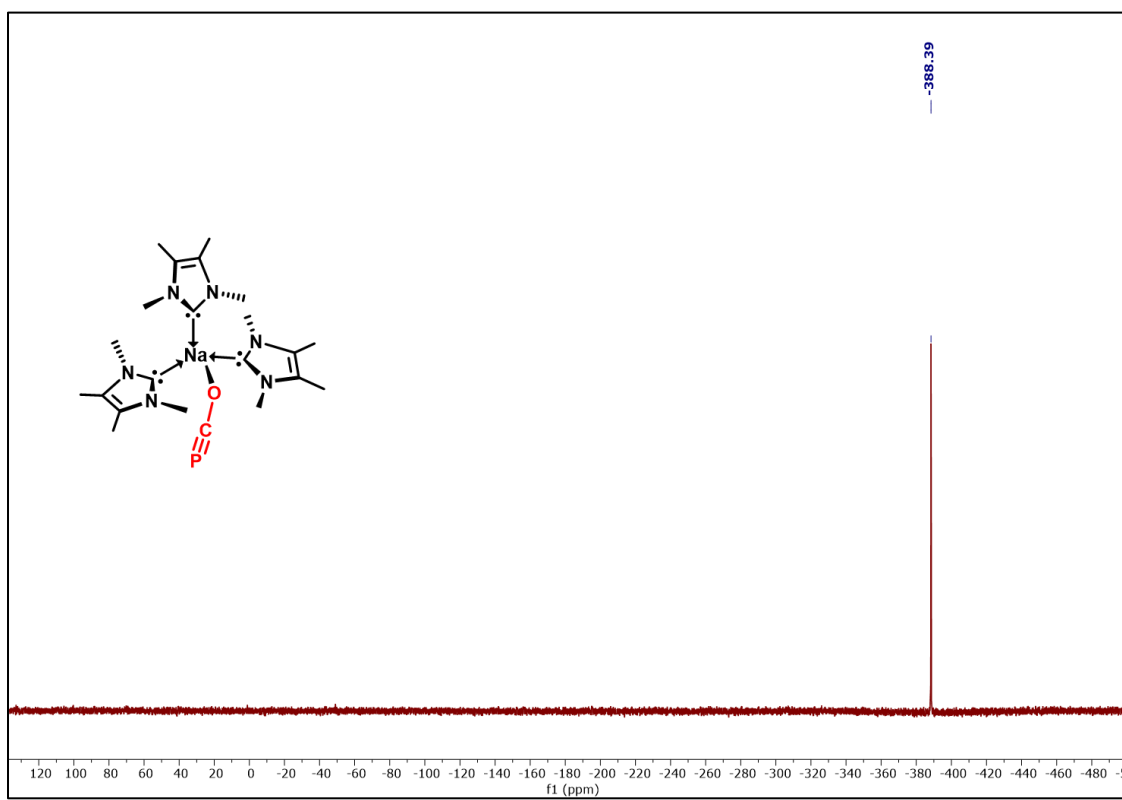


Figure A2.56. ^{31}P NMR spectrum (243 MHz, C_6D_6 , 298 K) of **4.6**.

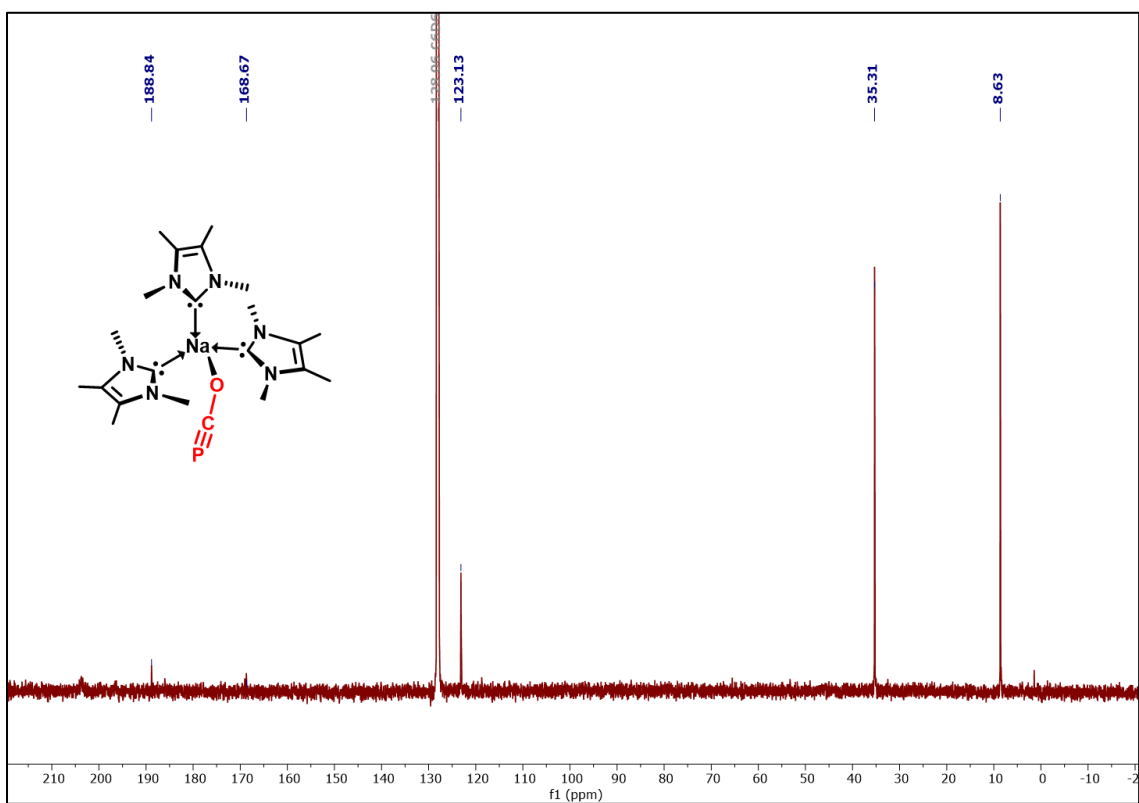


Figure A2.57. ¹³C NMR spectrum (150.90 MHz, C₆D₆, 298 K) of 4.6.

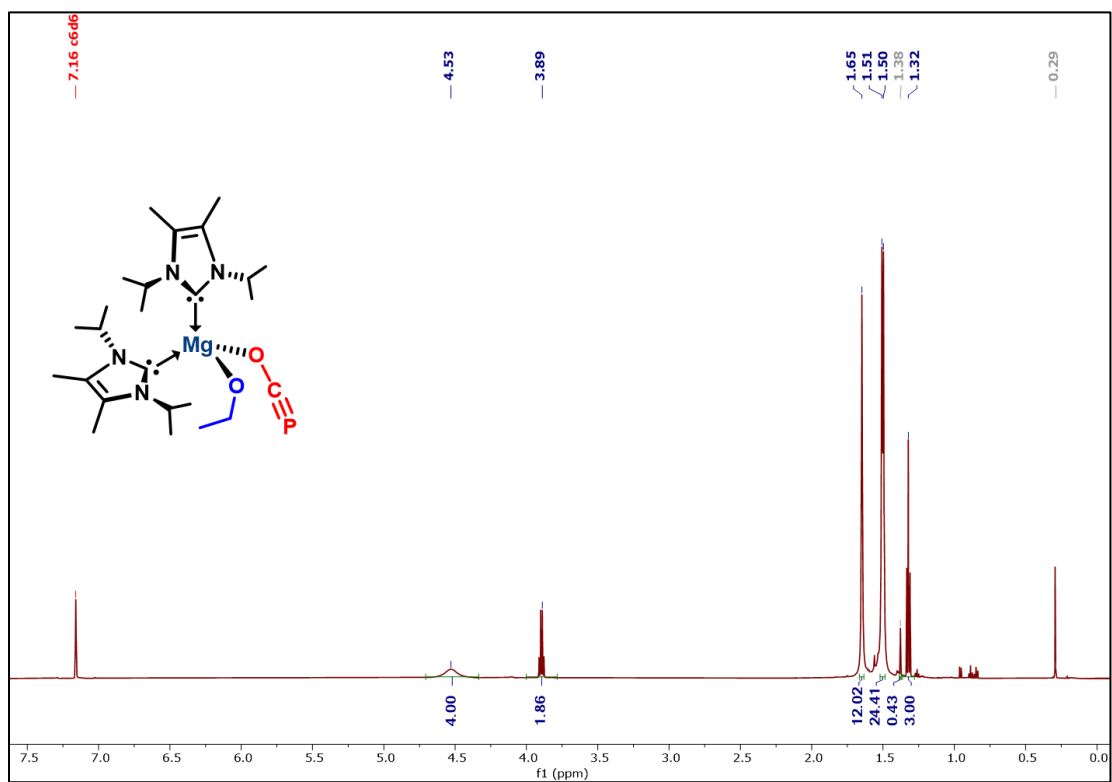


Figure A2.58. ¹H NMR spectrum (600.13 MHz, C₆D₆, 298 K) of 4.8.

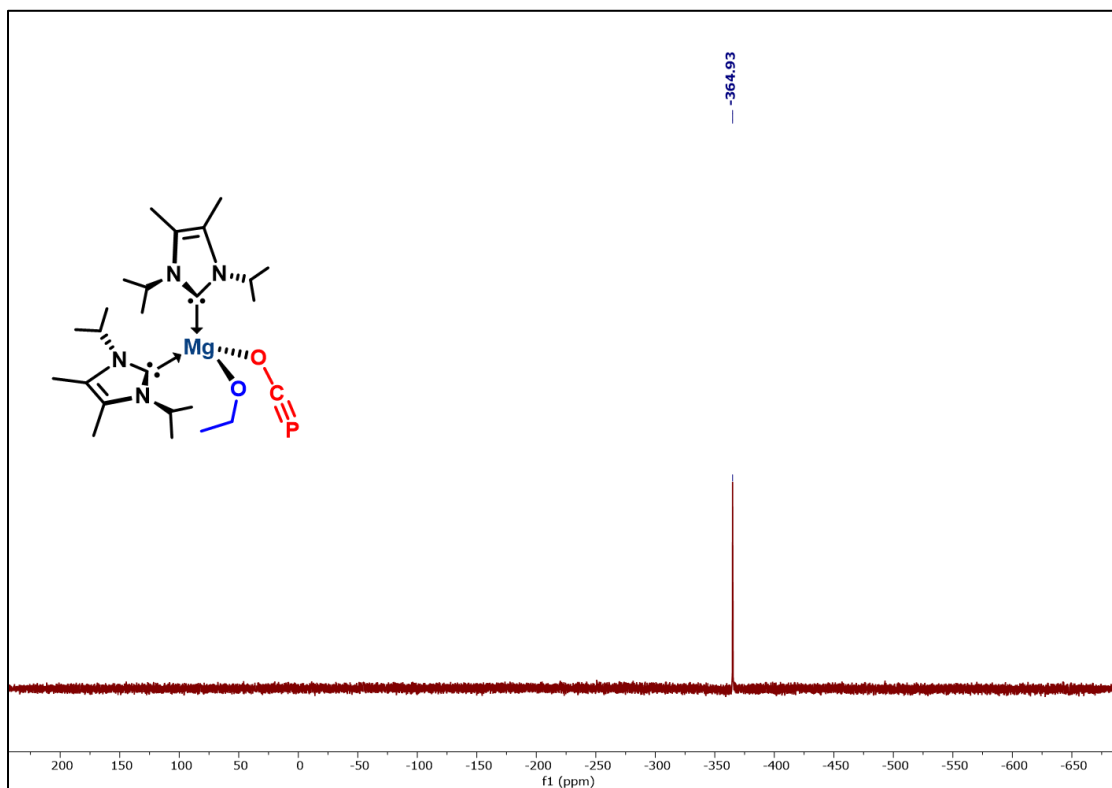


Figure A2.59. ^{31}P NMR spectrum (243 MHz, C_6D_6 , 298 K) of **4.8**.

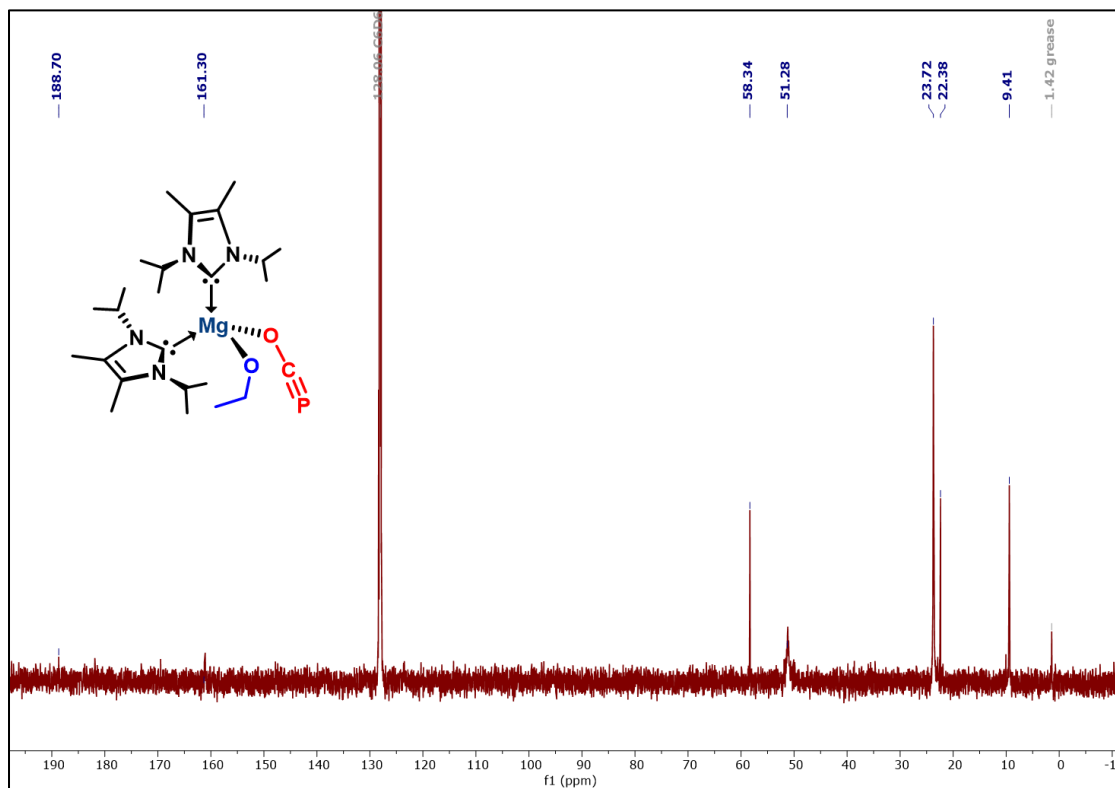


Figure A2.60. ^{13}C NMR spectrum (150.90 MHz, C_6D_6 , 298 K) of **4.8**.

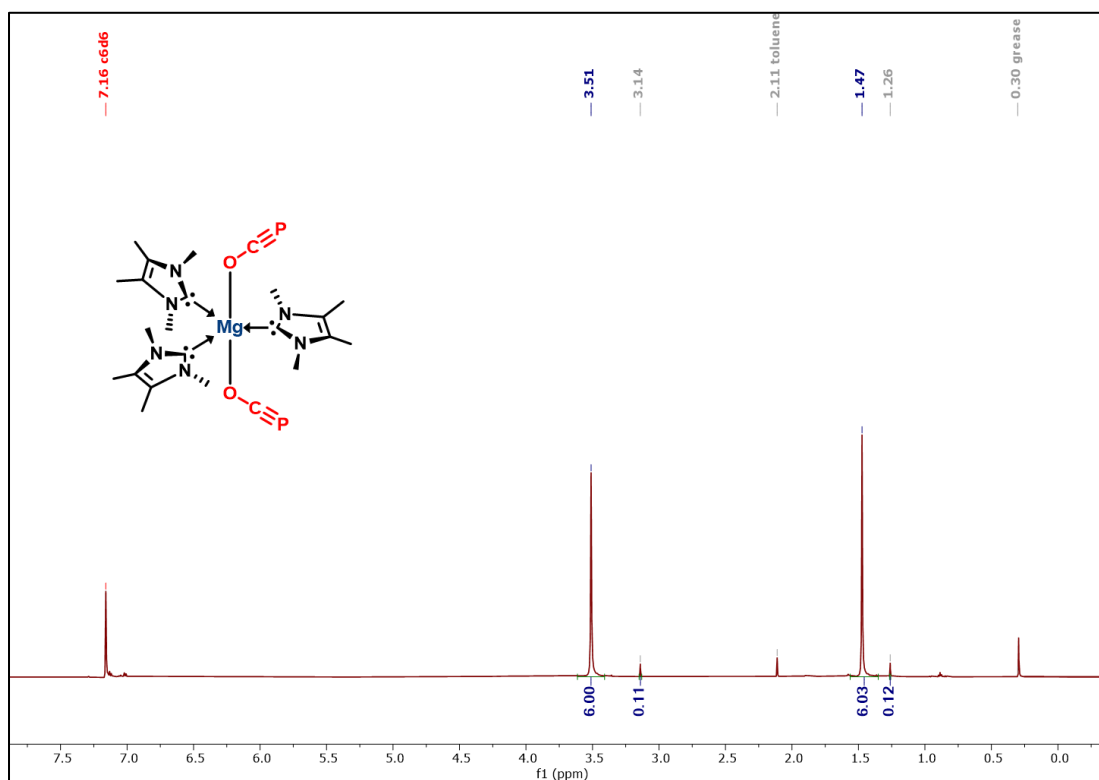


Figure A2.61. ^1H NMR spectrum (600.13 MHz, C_6D_6 , 298 K) of **4.10**.

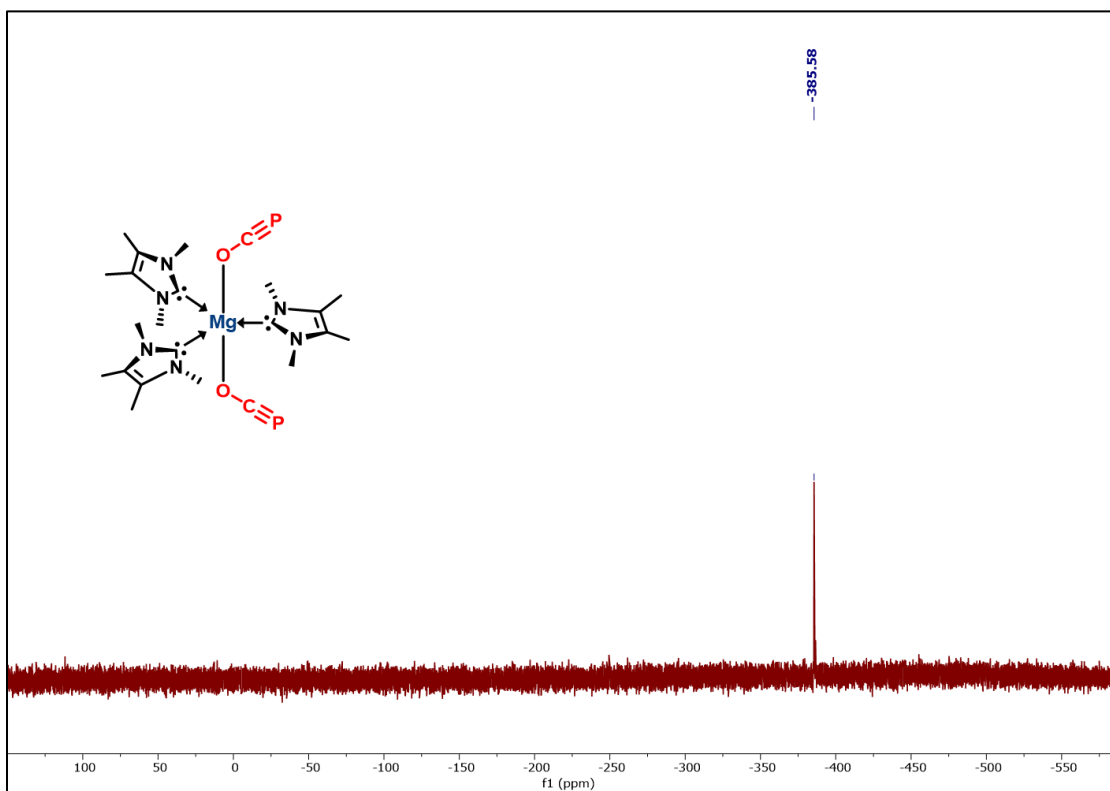


Figure A2.62 ^{31}P NMR spectrum (243 MHz, C_6D_6 , 298 K) of **4.10**.

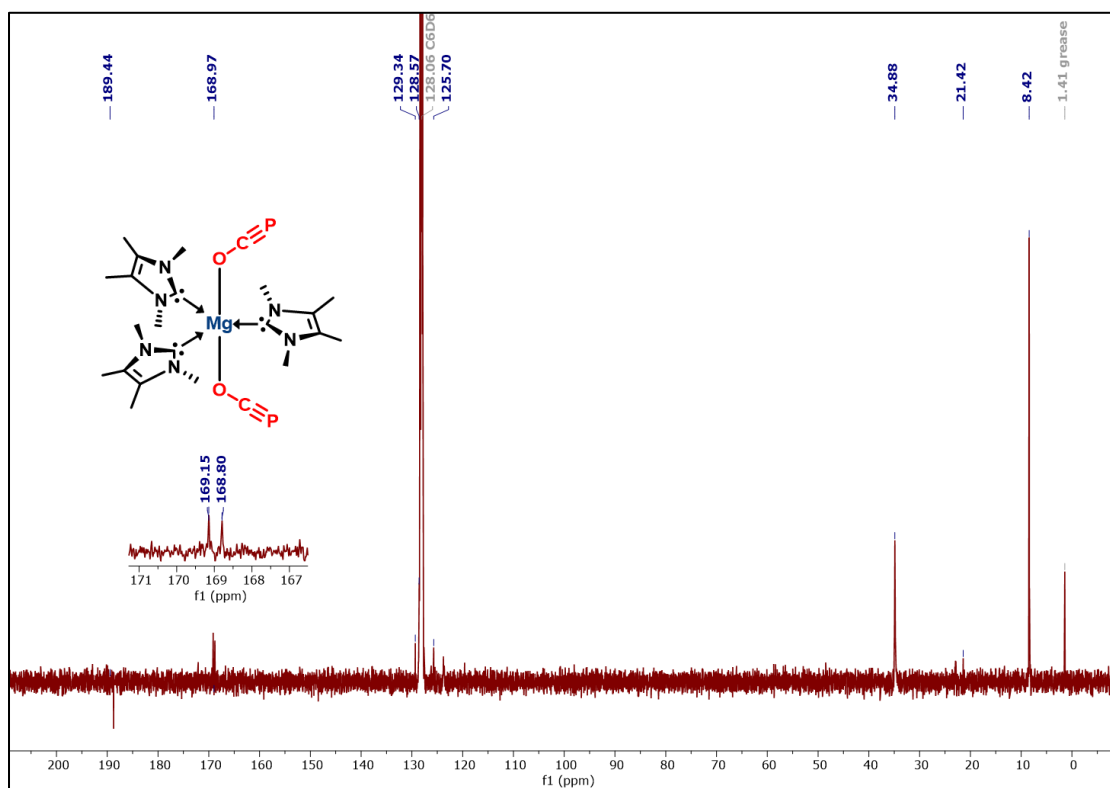


Figure A2.63. ^{13}C NMR spectrum (150.90 MHz, C_6D_6 , 298 K) of **4.10**.

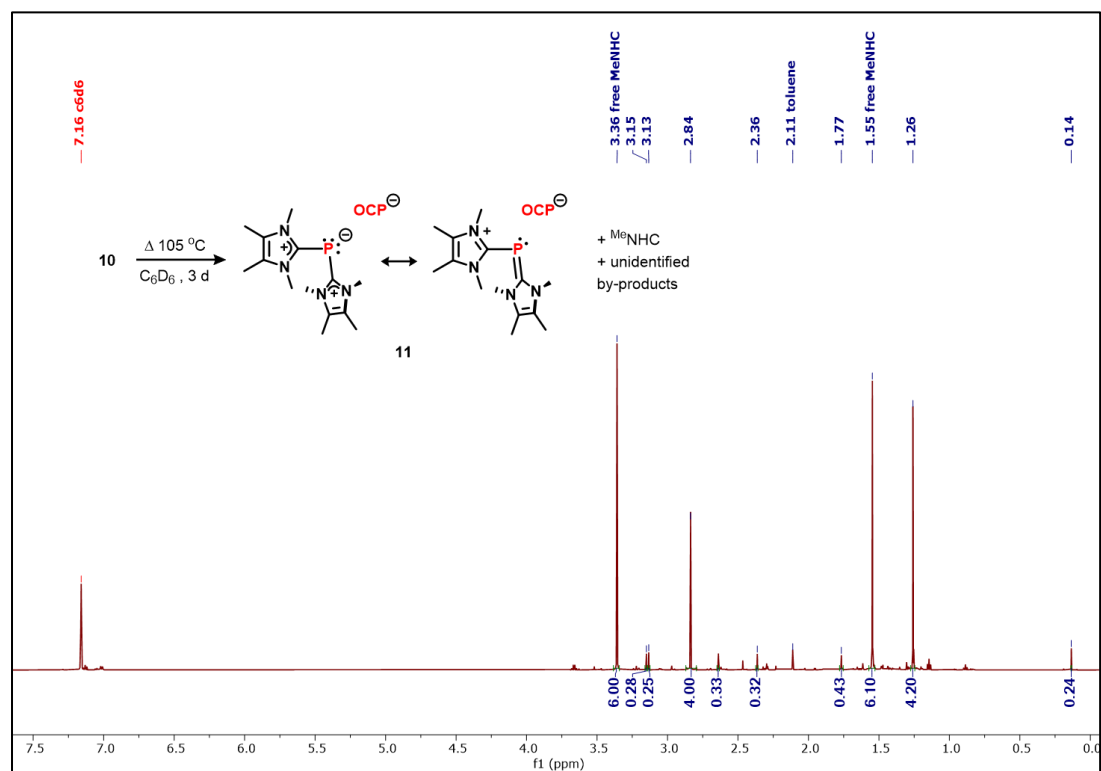


Figure A2.64. ^1H NMR spectrum showing the thermal decomposition of **4.10**.

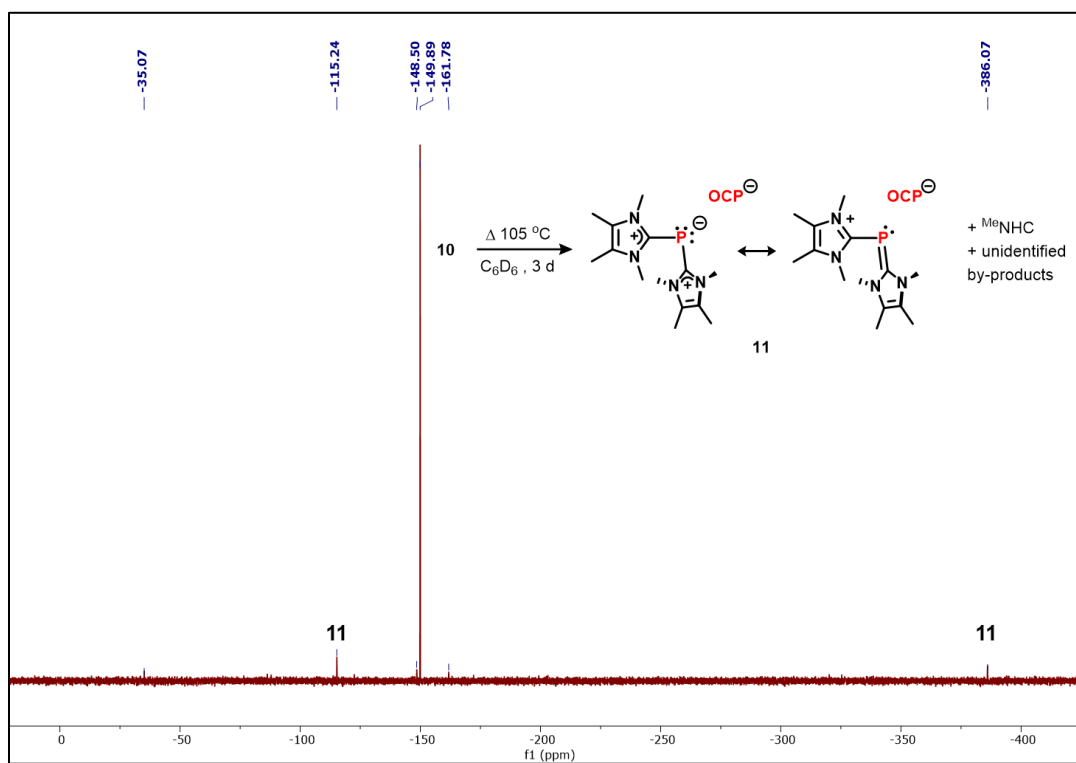


Figure A2.65. ^{31}P NMR spectrum showing the thermal decomposition of **4.10**.

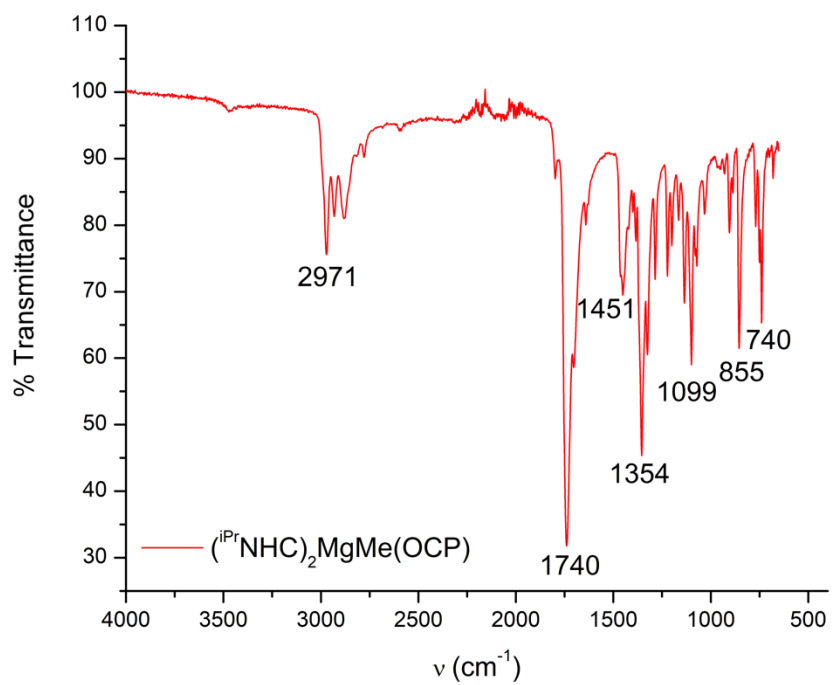


Figure A2.66. Solid state FTIR spectrum of compound **4.2^{iPr}**.

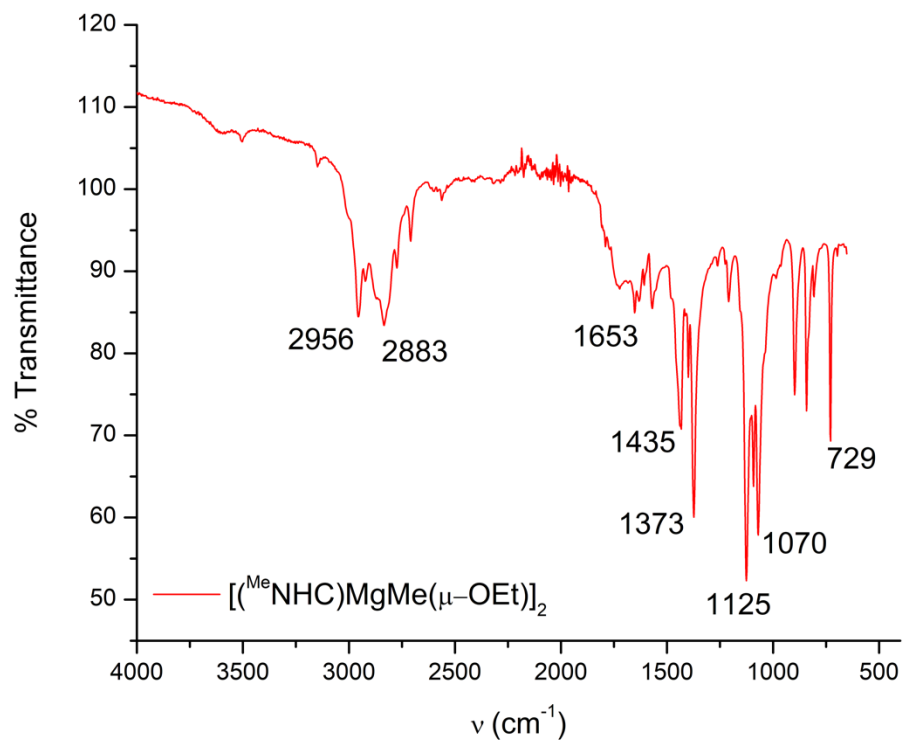


Figure A2.67. Solid state FTIR spectrum of compound 4.3^{Me} .

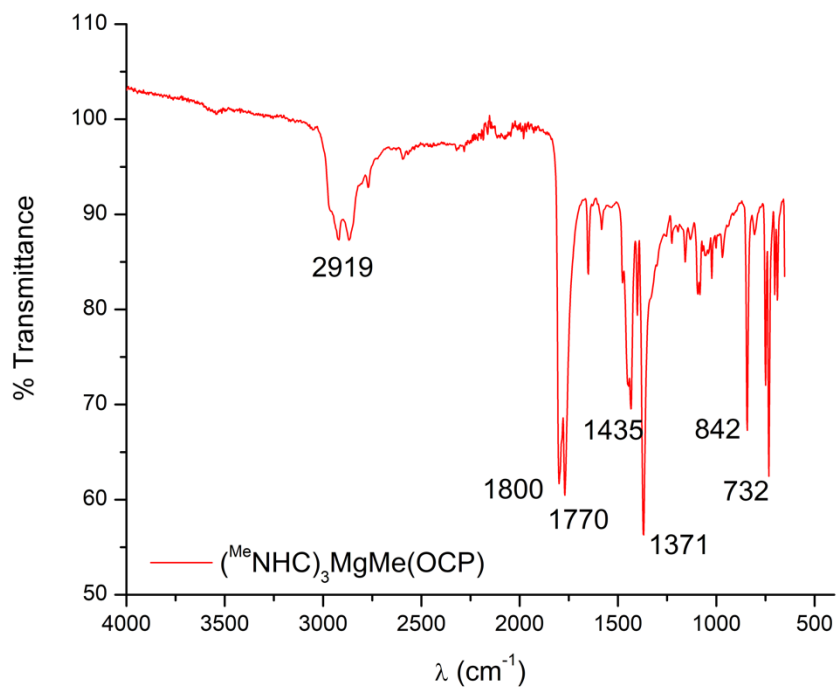


Figure A2.68. Solid state FTIR spectrum of compound 4.4^{Me} .

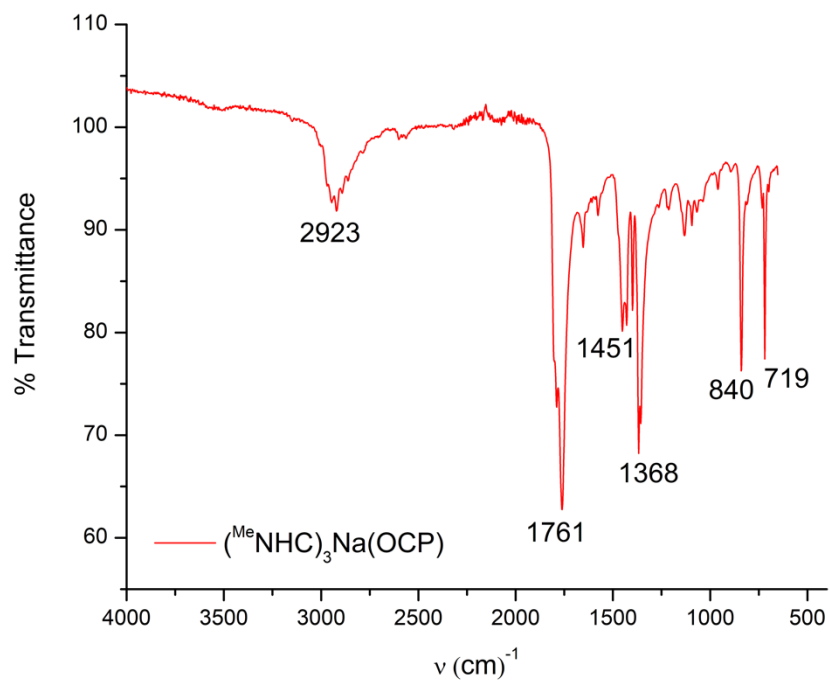


Figure A2.69. Solid state FTIR spectrum of compound 4.6.

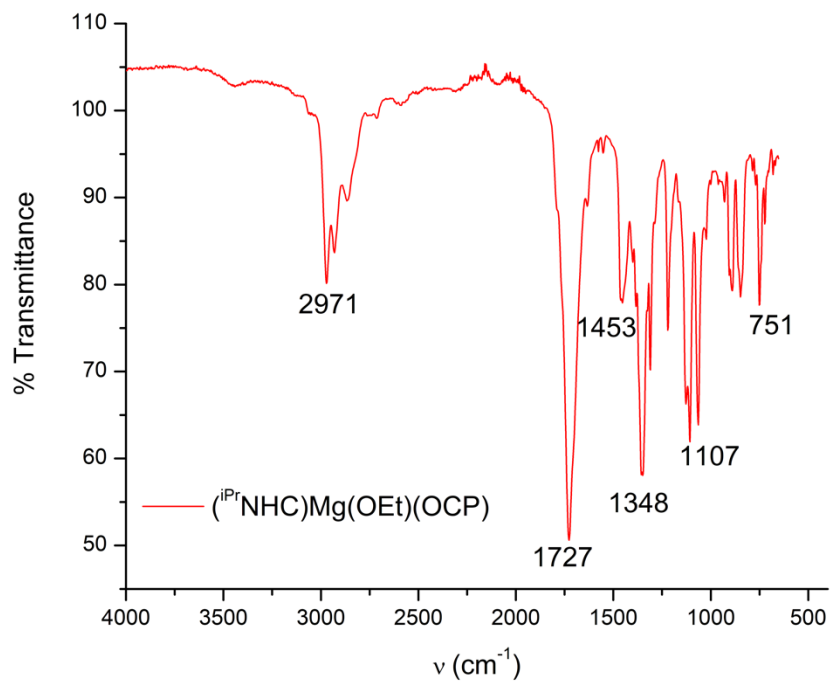


Figure A2.70. Solid state FTIR spectrum of 4.8/4.9.

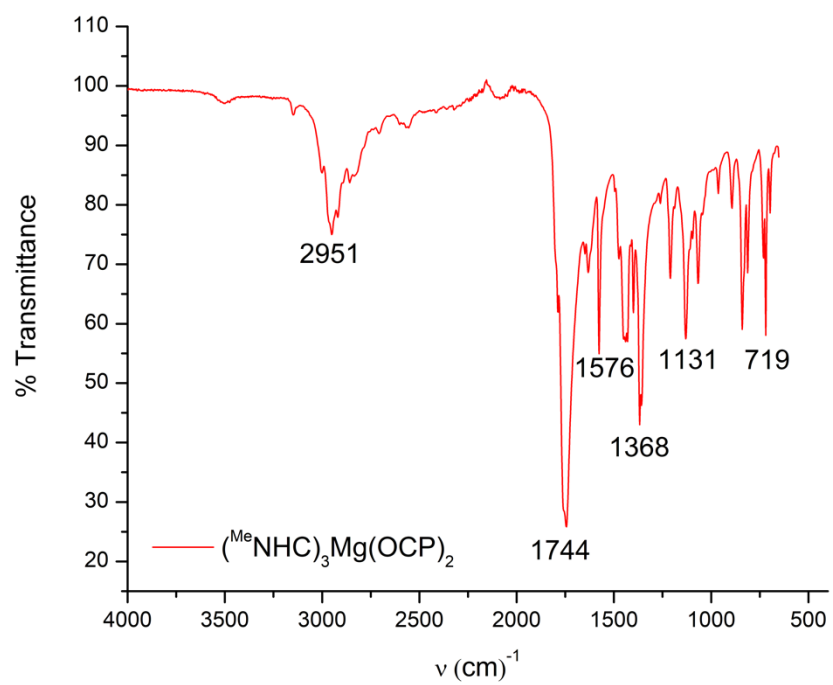


Figure A2.71. Solid state FTIR spectrum of **4.10**.

Table A2.1. Comparison of structural and spectroscopic data for reported metal oxyphosphaalkyne complexes

<i>Compound</i>	<i>CSD Database ID</i>	<i>Ref.</i>	<i>M–O (Å)</i> <i>[R_{cov}]</i>	<i>O–C (Å)</i>	<i>C–P (Å)</i>	<i>M–O–C (°)</i>	<i>ν(OCP)</i> <i>(cm⁻¹)</i>	<i>δ^{31P}</i> <i>(ppm)</i>	<i>δ^{13C}</i> <i>(ppm)</i>	<i>¹J_{CP}</i> <i>(Hz)</i>
Li(DME) ₂ (OCP)	YADTIG	²²⁵	1.878(5) [1.96]	1.198(4)	1.555(3)	170.7	n/a	-384.2	166.6	41.5
[Na(DME) ₂ (OCP) ₂	EYELAW	²²⁶	2.349(3) 2.336(3) [2.18]	1.203(4) 1.213(4)	1.589(3) 1.575(3)	132.1(3) 133.0(3)	1780	n/a	n/a	n/a
[Na(dioxane) _x (OCP) _∞		²²⁶	n/a	1.163(4)	1.634(3)	n/a	1755	-392	166.3	46.5
(THF)Na(dibenzo-12-c-6)(OCP)	LELSED	²³⁰	2.290(2)	1.207(4)	1.582(3)	138.1(2)	1765	n/a	n/a	n/a
(NHC) ₃ Na(OCP)		this work	2.247(5)	1.215(8)	1.578(7)	167.2(5)	1761	-388.4	168.7	n/a
[K(18-c-6)][OCP]	UFUPOC	²²⁸	2.901(2) [2.59]	1.212(4)	1.579(3)	110.1(2)	1730	-396.8	170.3	62
(THF) ₄ Mg(OCP) ₂	LELSAZ	²³⁰	2.024(16) [2.02]	1.196(3)	1.572(3)	142.8(15)	1759	-367.9	n/a	n/a
(NHC) ₃ Mg(OCP) ₂		this work	2.143(2) 2.111(3)	1.199(5) 1.208(3)	1.575(3) 1.584(6)	140.6(2) 147.5(3)	1744	-385.6	169.0	52.9
[(NHC) ₃ MgMe][OCP]		this work	n/a	1.208(10)	1.574(14)	n/a	1770, 1800	-378.2	166.8	48.1

(NHC) ₂ MgMe(OCP)		this work	1.982(3)	1.232(4)	1.559(5)	162.4(3)	1740	-366.8	162.4	25.4
[(NHC)Mg(μ-OEt)(OCP)] ₂		this work	1.938(4)	1.254(7)	1.545(6)	145.9(5)	1727	-364.9	161.3	n/a
(DME) ₃ Ca(OCP) ₂	MOBTOM	²³¹	2.358(2) 2.335(2) [2.34]	1.207(3) 1.199(3)	1.575(2)	154.6(2) 165.1(2)	n/a	n/a	n/a	n/a
NHB(OCP)	ZEWLUL	²⁴³	1.425(2) [1.48]	1.269(2)	1.545(2)	126.16(11)	1649	-285.9	140.3	17.6
(salen)Al(OCP)	VOBBOG	²⁴⁰	1.8206(7) [1.89]	1.2538(10)	1.5646(9)	131.38(6)	1692	-336.8	155.1	4.7
(salen)(THF)Al(OCP)	VOBCAT	²⁴⁰	1.920(3)	1.228(5)	1.587(5)	137.5(2)	n/a	-353.9	161.3	24.6
[U]-OCP	ADURID	⁴²⁶	2.345(4) [2.33]	1.237(6)	1.559(6)	164.5	1688	-300	n/a	n/a
(amid) ₃ U(OCP)	RUHKOW	²⁴²	2.297(3)	1.219(6)	1.576(5)	170.9(3)	1685	-285.2	n/a	n/a
(amid) ₃ Th(OCP)	RUHKUC	²⁴²	2.3118(2) [2.38]	1.246(4)	1.561(4)	176.4(3)	1683	-334.4	n/a	n/a
(amid) ₂ (THF)Y(OCP)	YUCLAM	²⁴¹	2.1562(12) [2.26]	1.250(2)	1.559(2)	167.7	1691	-346.9	156	7.3
[(18-c-6)Na(THF) ₂] [(amid) ₂ (THF)Y(OCP) ₂]]	YUCLIU	²⁴¹	2.221(2) 2.225(2)	1.227(3) 1.229(3)	1.570(3)	164.2(2) 162.5(2)	1771 (w)	-368.7	160.4 (dd)	18.0
[(amid) ₂ Nd(μ-OCP)] ₂	YUCLUG	²⁴¹	2.352(3) [2.37]	1.234(5)	1.582(4)	173.0	1748 (m)	-278.1	n/a	n/a

[(18-c-6)Na(THF) ₂][(amid) ₂ (THF)Nd(OCP) ₂]	YUCLOA	²⁴¹	2.3106(15) 2.3263(15)	1.234(3) 1.214(3)	1.562(3) 1.562(2)	164.1	1683	-289.7	n/a	n/a
(amid) ₂ (THF)Nd(OCP)	YUCLEQ	²⁴¹	2.224(3)	1.252(6)	1.557(6)	117.6	1685	-292.2	n/a	n/a
(amid)(18-c-6)Sm(OCP)	YUCMER	²⁴¹	2.610(3) [2.35]	1.219(5)	1.586(4)	133.9	1758	-391.7	n/a	n/a
[(12-c-6)Na(THF) ₂][(amid) ₂ (THF)Sm(OCP) ₂]	YUCMIV	²⁴¹	2.299(2) 2.286(2)	1.218(4) 1.234(4)	1.576(3) 1.563(4)	162.1	n/a	n/a	n/a	n/a
(2,2,2-crypt)Sm(OCP) ₂	YUCMUH	²⁴¹	2.568(6) 2.613(6)	1.212(10) 1.205(11)	1.580(8) 1.591(9)	145.0(5) 140.0(6)	1763, 1749	-374	183.9	48.4

Chapter Five:

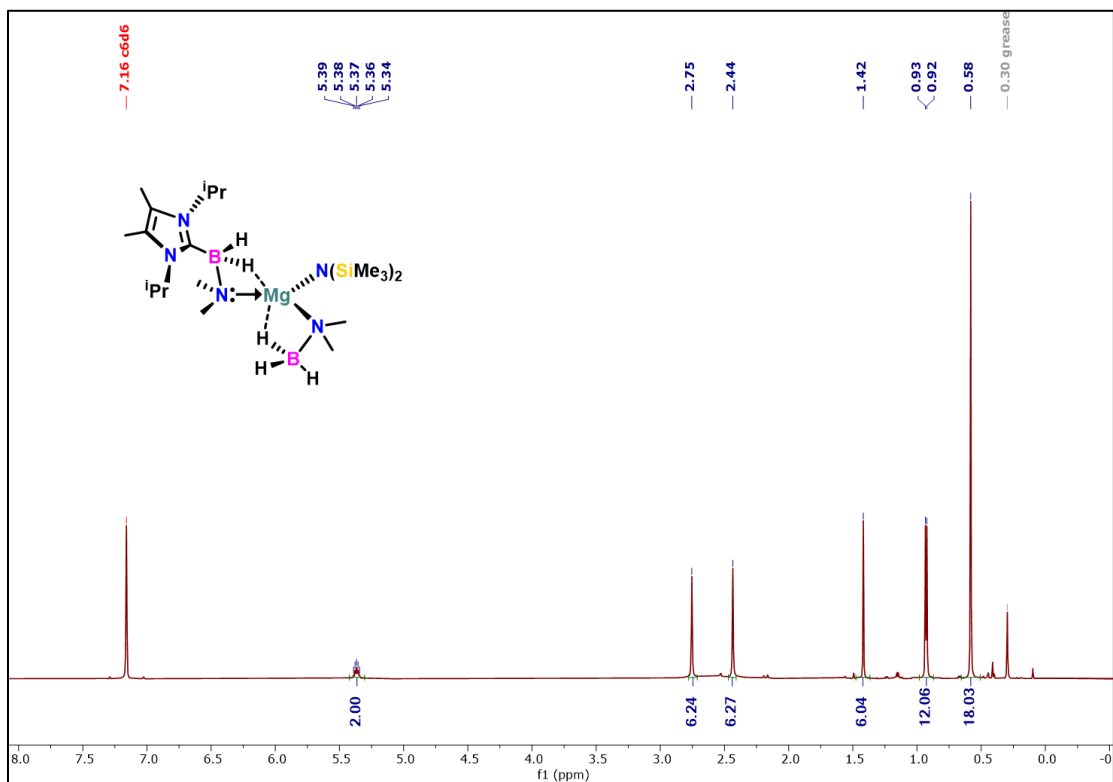


Figure A2.72. ^1H NMR spectrum (600 MHz, C_6D_6 , 298 K) of **5.2**.

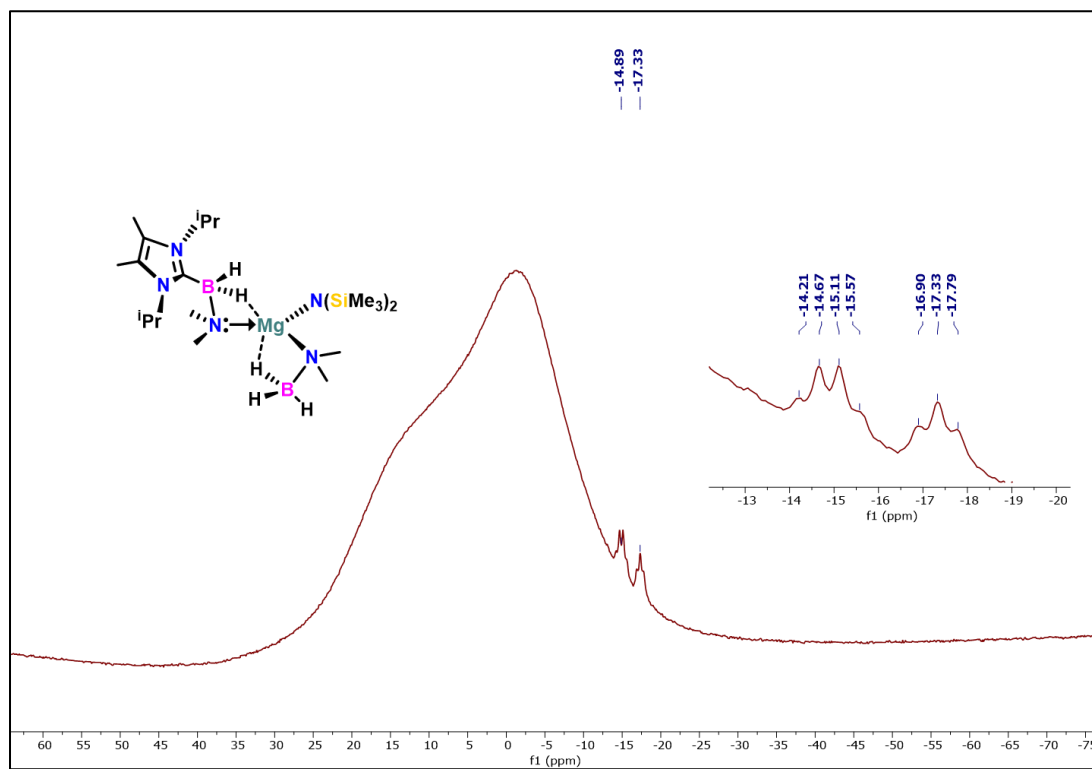


Figure A2.73. ^{11}B NMR spectrum (192 MHz, C_6D_6 , 298 K) of **5.2**.

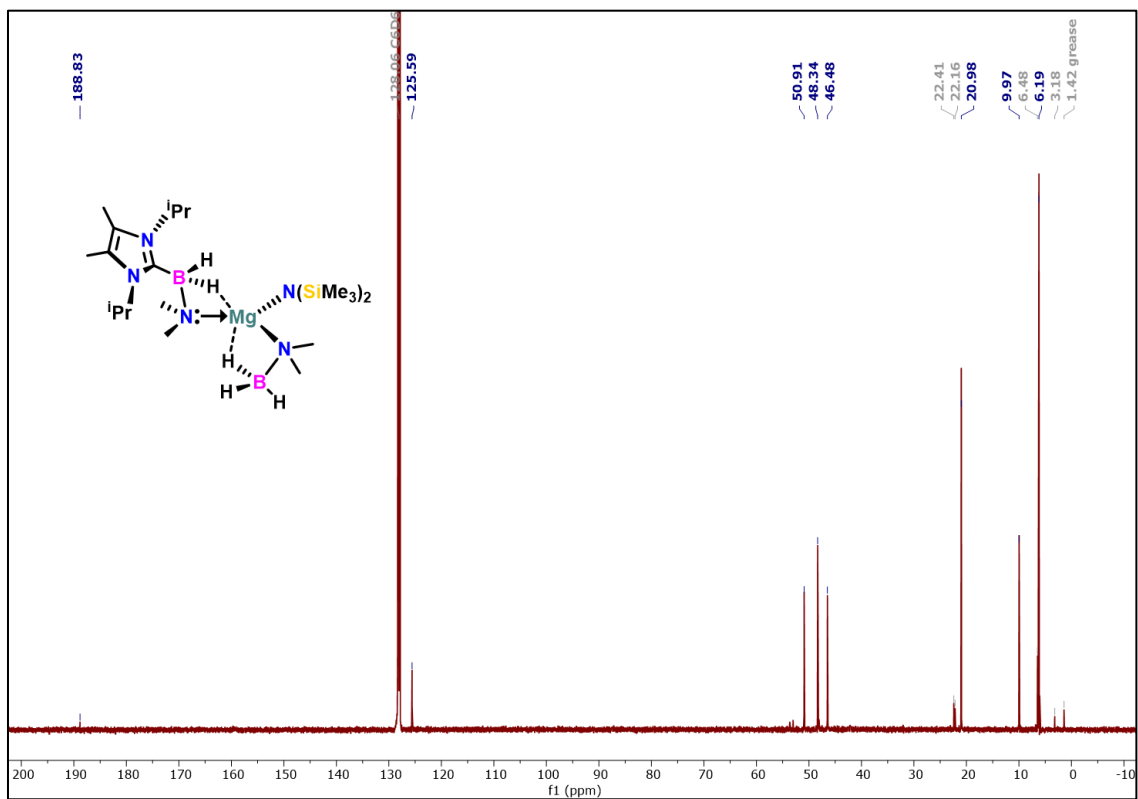


Figure A2.74. $^{13}\text{C}\{^1\text{H}\}$ NMR spectrum (151 MHz, C_6D_6 , 298 K) of **5.2**. Peaks in grey are unidentified impurities.

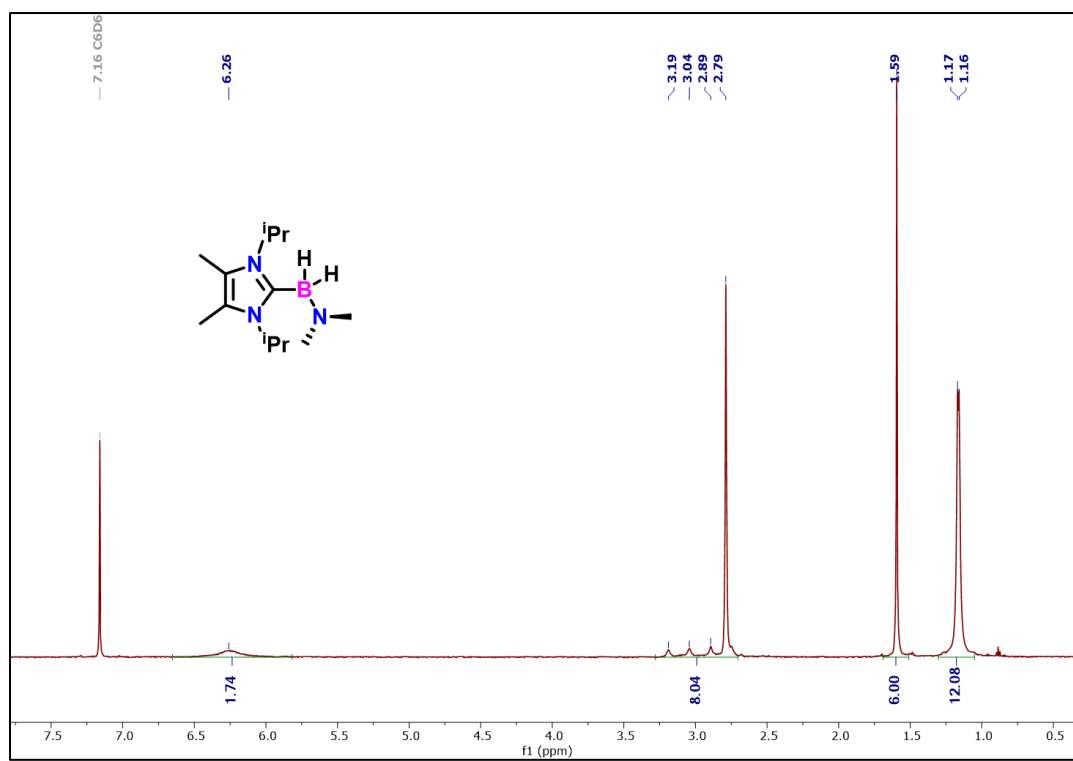


Figure A2.75. ^1H NMR spectrum (600 MHz, C_6D_6 , 298 K) of *i*PrNHC-BN.

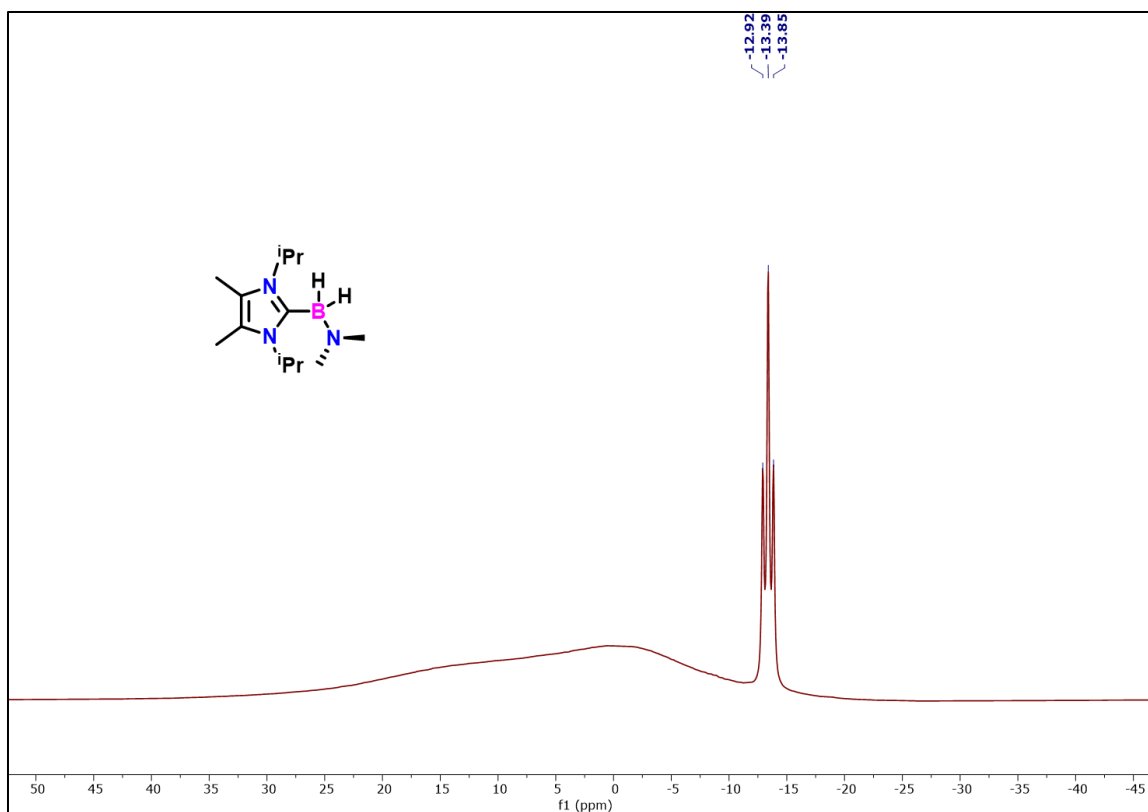


Figure A2.76. ^{11}B NMR spectrum (192 MHz, C_6D_6 , 298 K) of $i\text{PrNHC-BN}$.

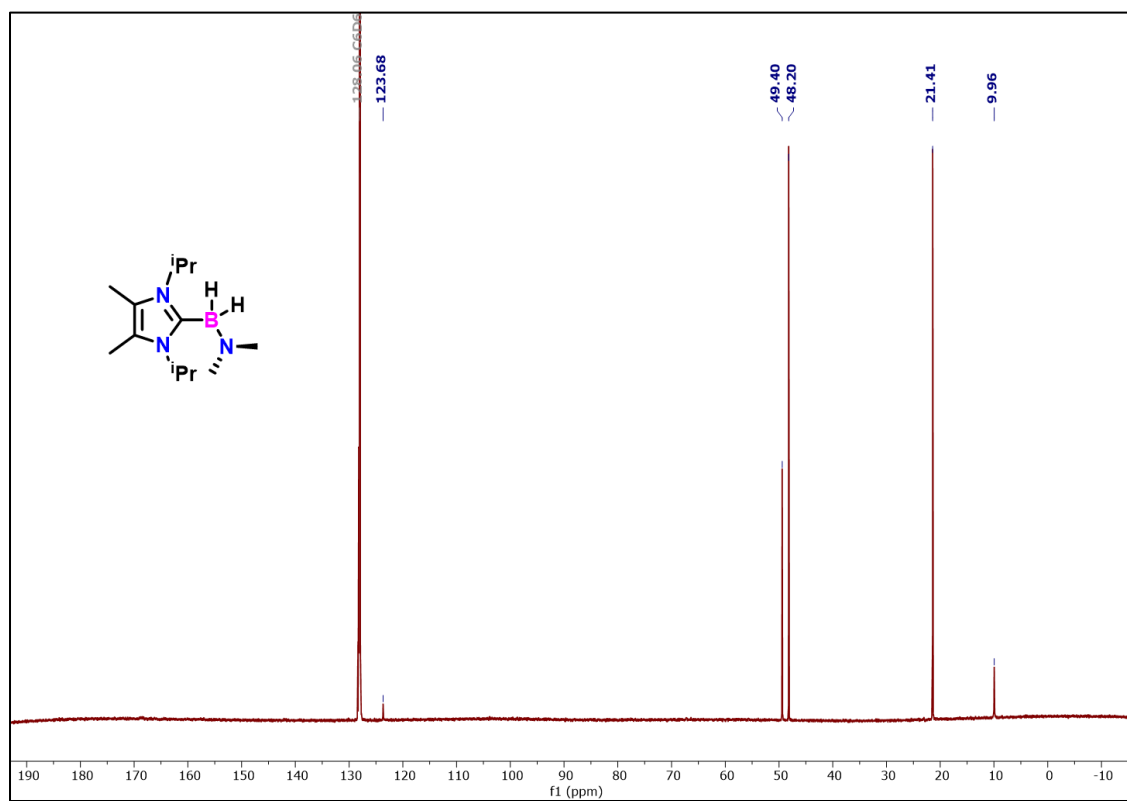


Figure A2.77. $^{13}\text{C}\{^1\text{H}\}$ NMR spectrum (151 MHz, C_6D_6 , 298 K) of $i\text{PrNHC-BN}$.

Reaction of *i*PrNHC-BN and Mg(N(SiMe₃)₂)₂

In a J-Young tap NMR tube, *i*PrNHC-BN (8 mg, 0.0338 mmol) and Mg(N(SiMe₃)₂)₂ (12 mg, 0.0348 mmol) were combined in C₆D₆ and monitored by ¹H and ¹¹B NMR spectroscopy.

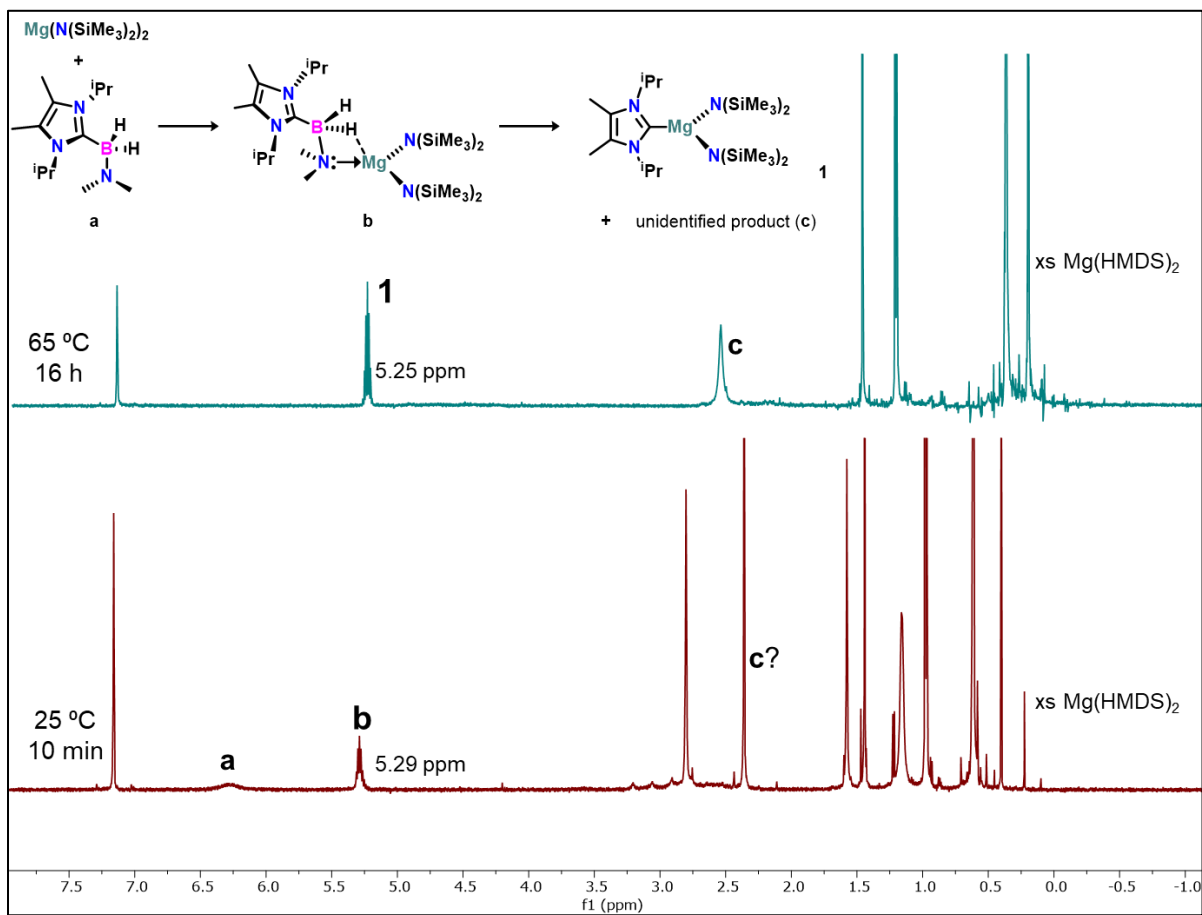


Figure A2.78. Stack plot of ¹H NMR spectra for the reaction of *i*PrNHC-BN and Mg(N(SiMe₃)₂)₂.

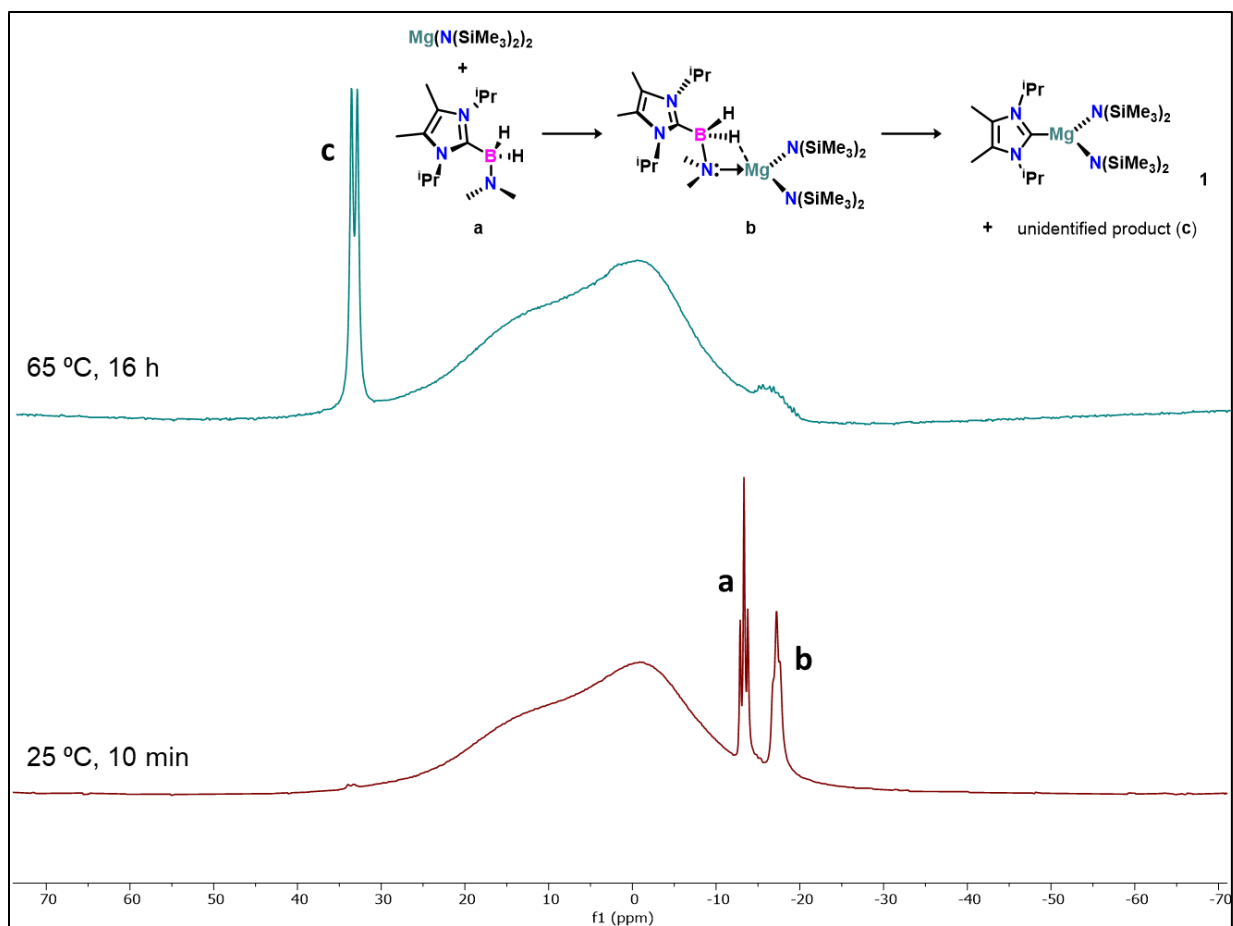


Figure A2.79. Stack plot of ^1H NMR spectra for the reaction of $i\text{PrNHC-BN}$ and $\text{Mg}(\text{N}(\text{SiMe}_3)_2)_2$. C (33.6 ppm) is compared to $\text{HB}(\text{NMe}_2)_2$ (28.7 ppm)^{55, 286} but cannot be confidently assigned.

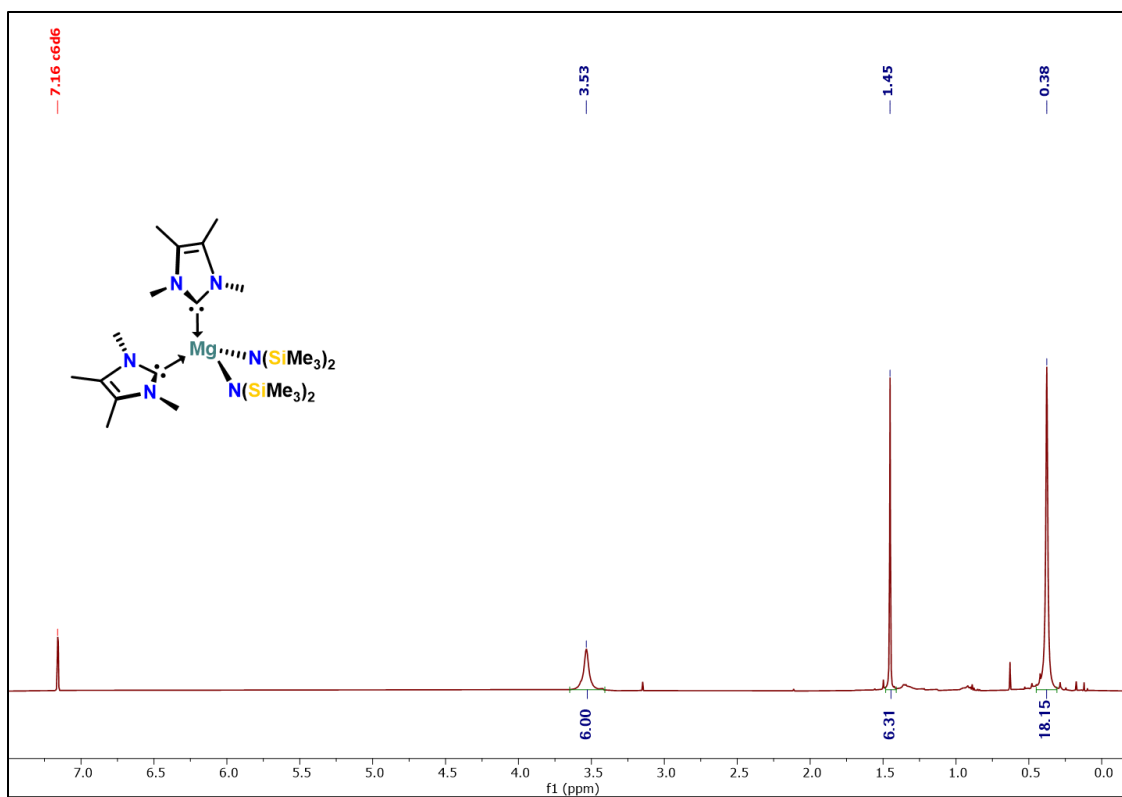


Figure A2.80. ^1H NMR spectrum (600 MHz, C_6D_6 , 298 K) of **5.3**.

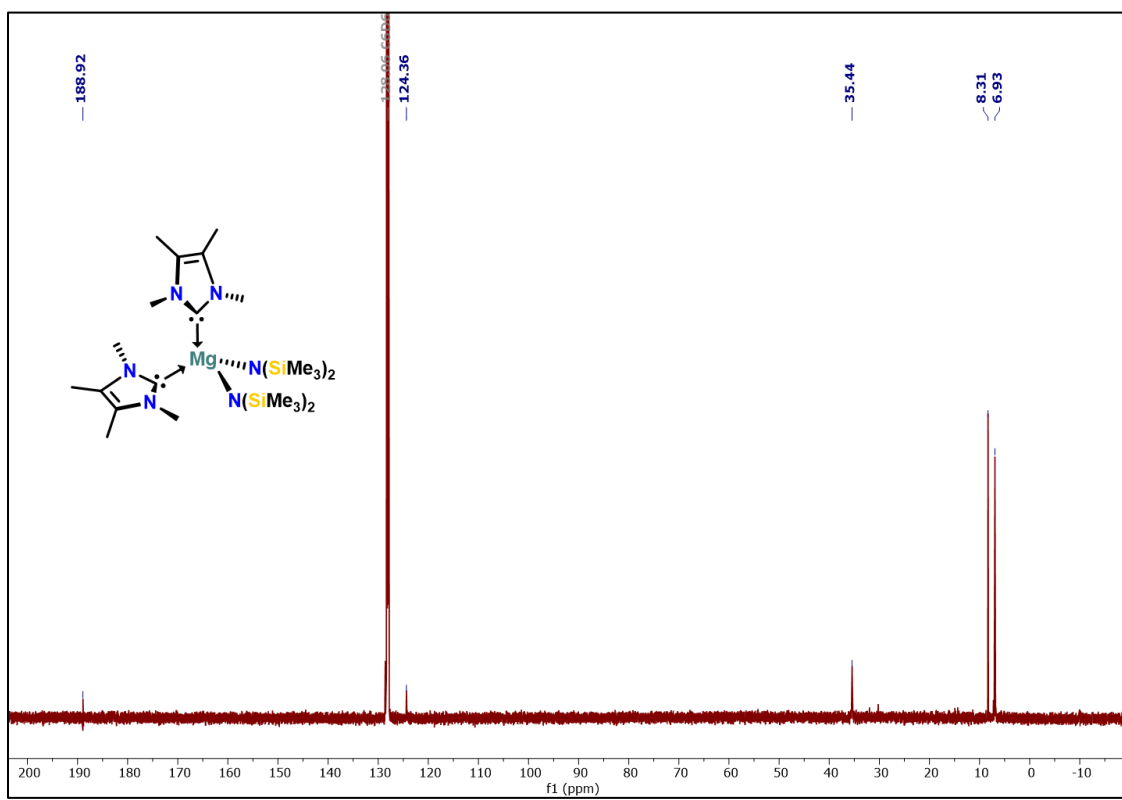


Figure A2.81. $^{13}\text{C}\{^1\text{H}\}$ NMR spectrum (151 MHz, C_6D_6 , 298 K) of **5.3**.

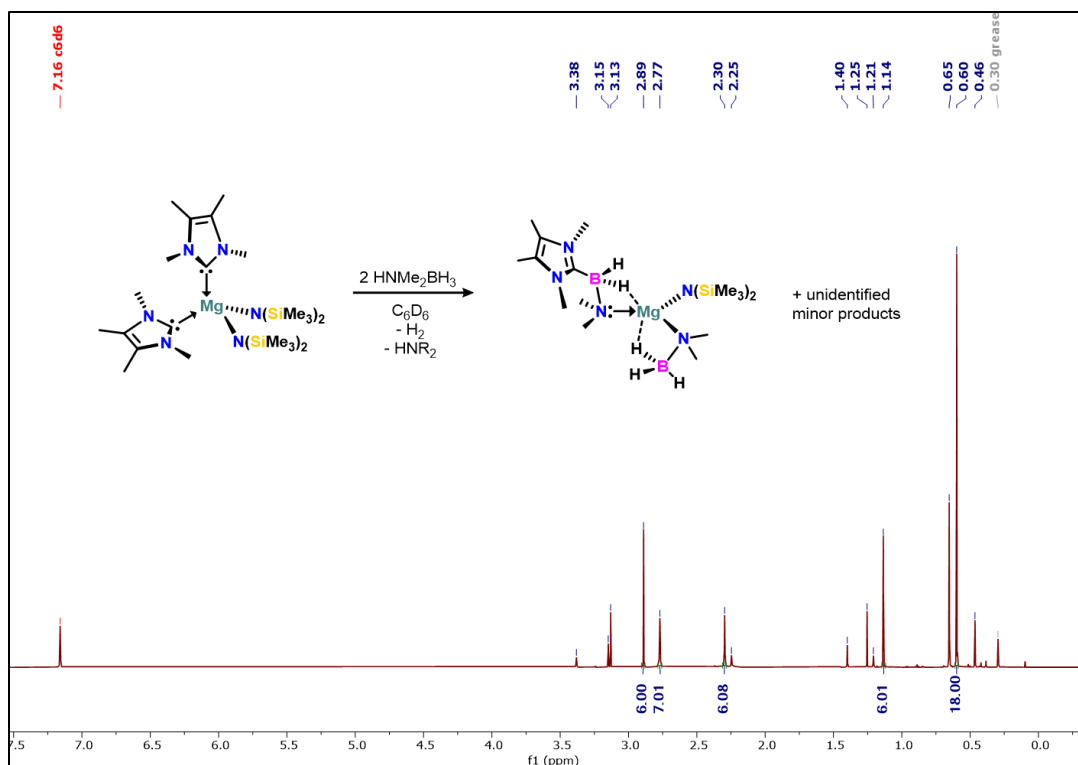


Figure A2.82. ^1H NMR spectrum highlighting the presence of **5.4** as major product in the reaction of **5.3** and HNMe_2BH_3 .

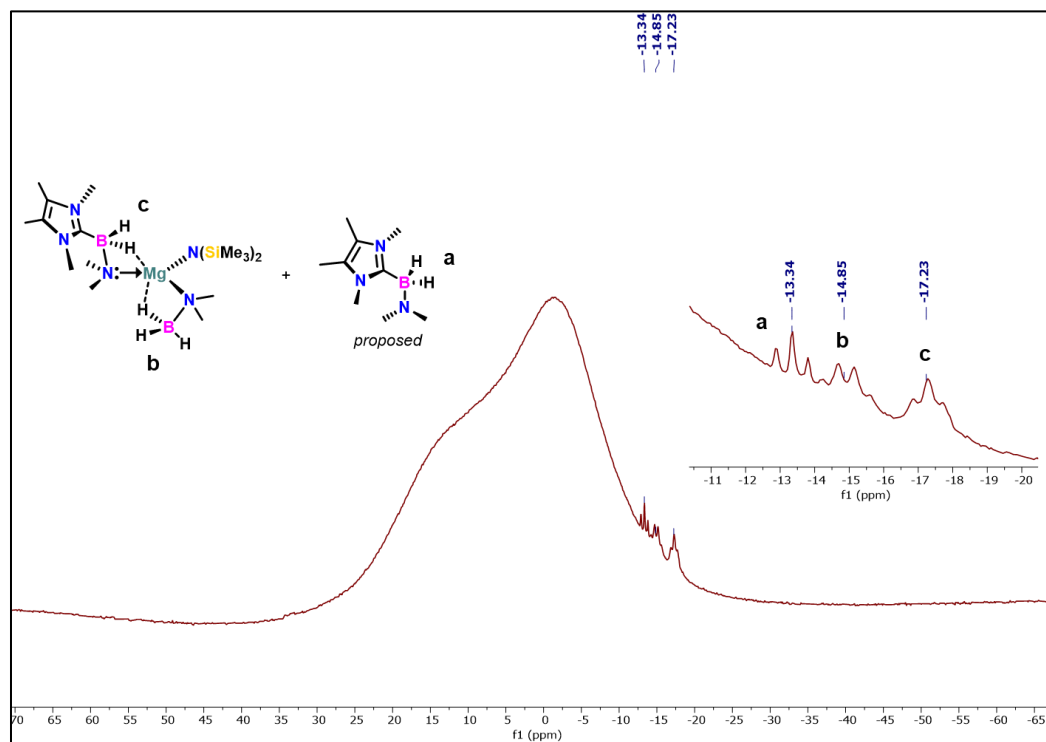


Figure A2.83. ^{11}B NMR spectrum (192 MHz, C_6D_6 , 298 K) showing the boron containing products from the reaction **5.3** and HNMe_2BH_3 .

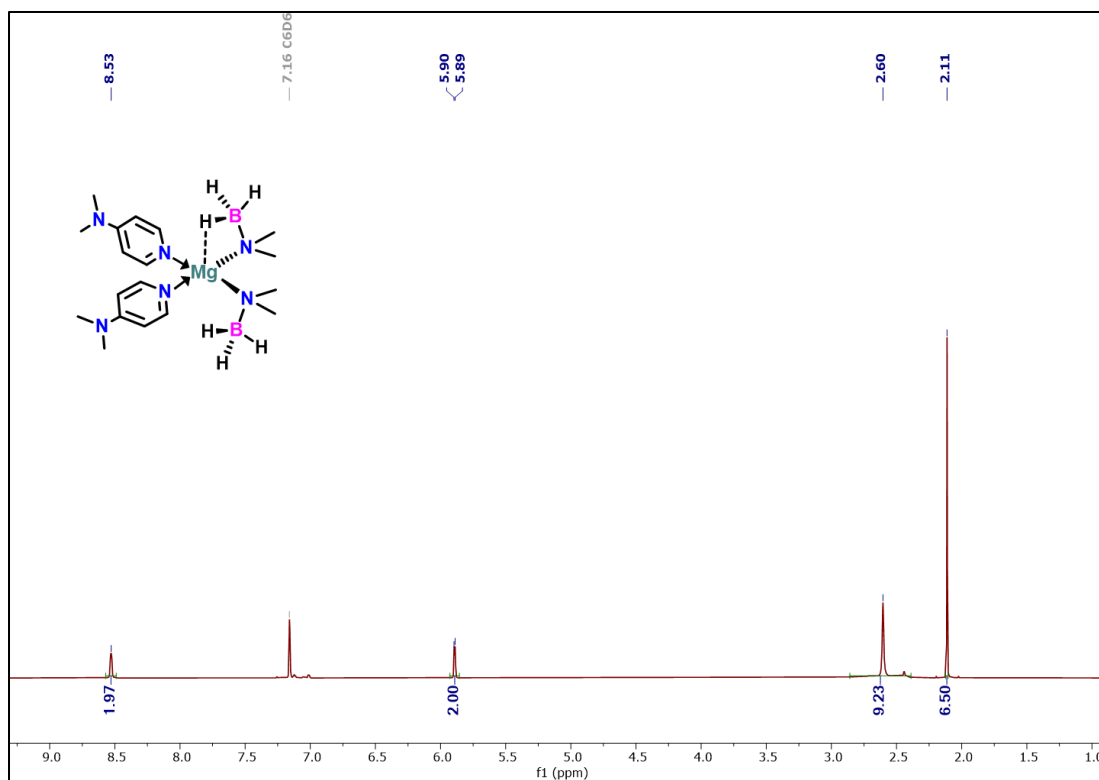


Figure A2.84. ^1H NMR spectrum (800 MHz, C_6D_6 , 298 K) of **5.7**.

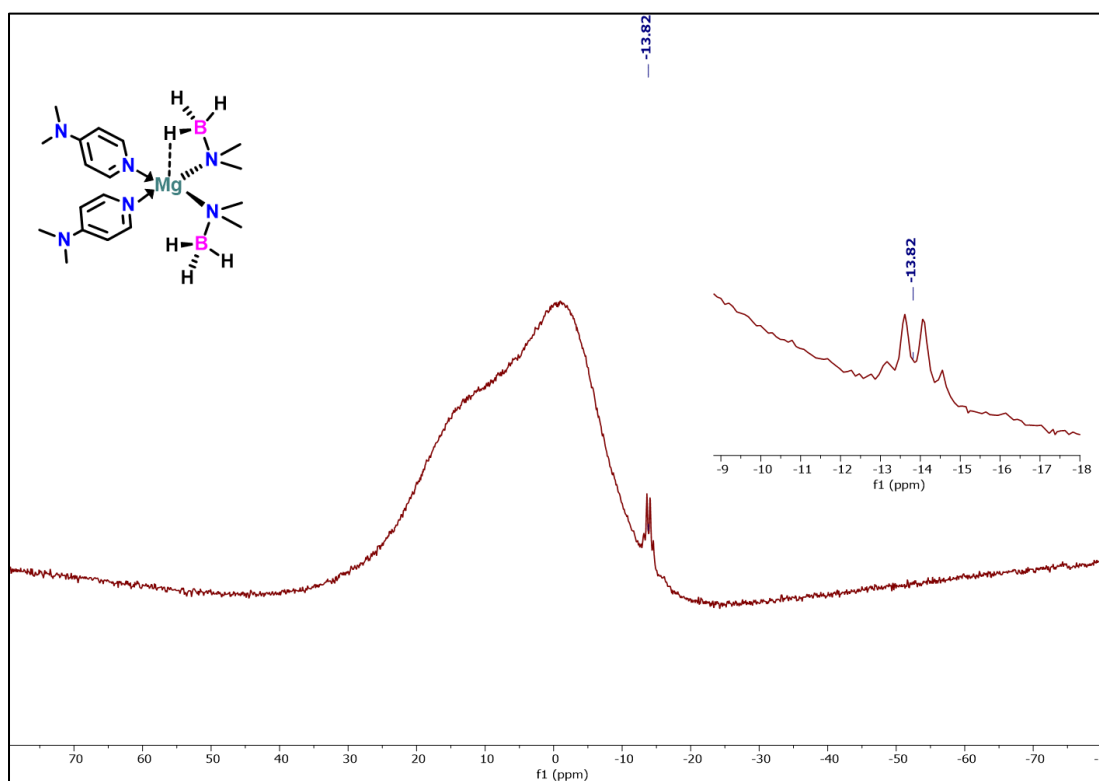


Figure A2.85. ^{11}B NMR spectrum (192 MHz, C_6D_6 , 298 K) of **5.7**.

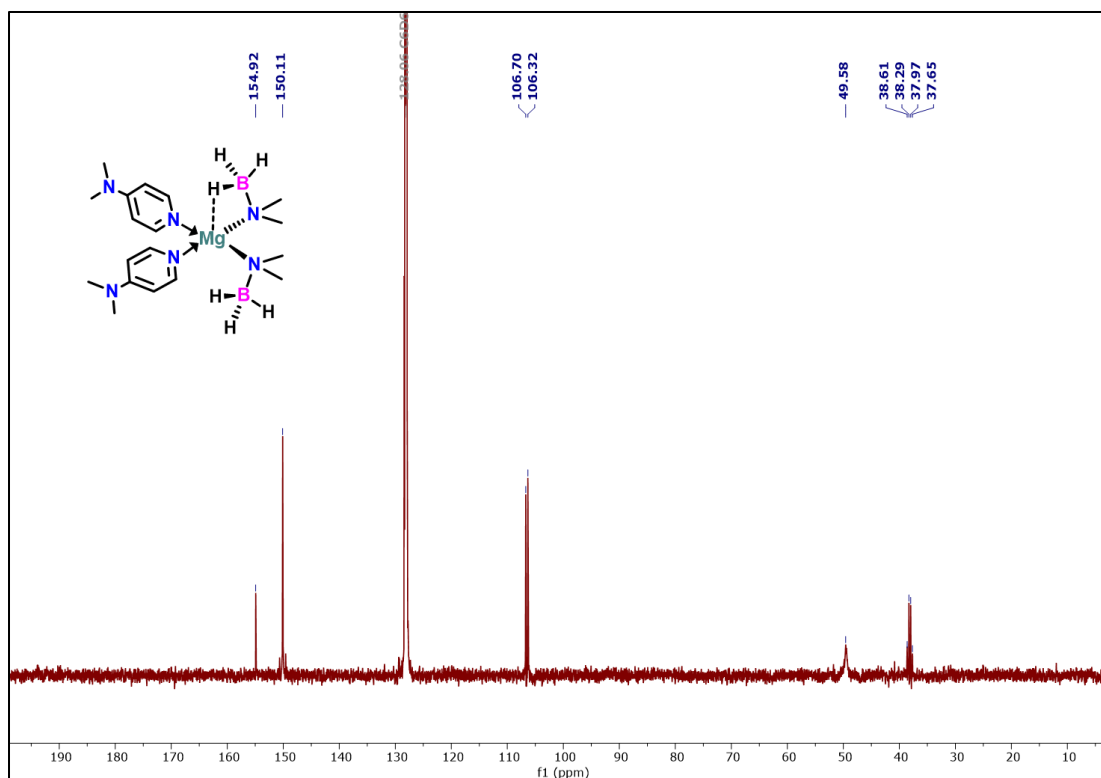


Figure A2.86. $^{13}\text{C}\{^1\text{H}\}$ NMR spectrum (200 MHz, C_6D_6 , 323 K) of 5.7.

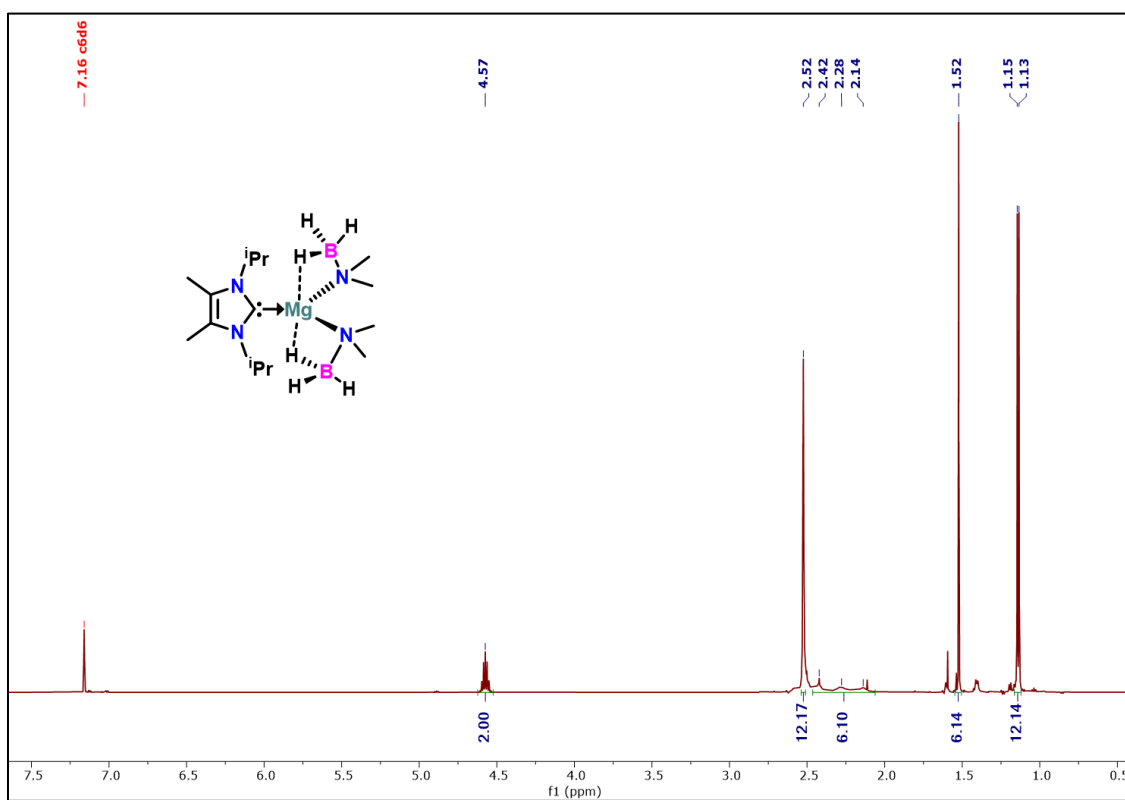


Figure A2.87. ^1H NMR spectrum (600 MHz, C_6D_6 , 298 K) of 5.8.

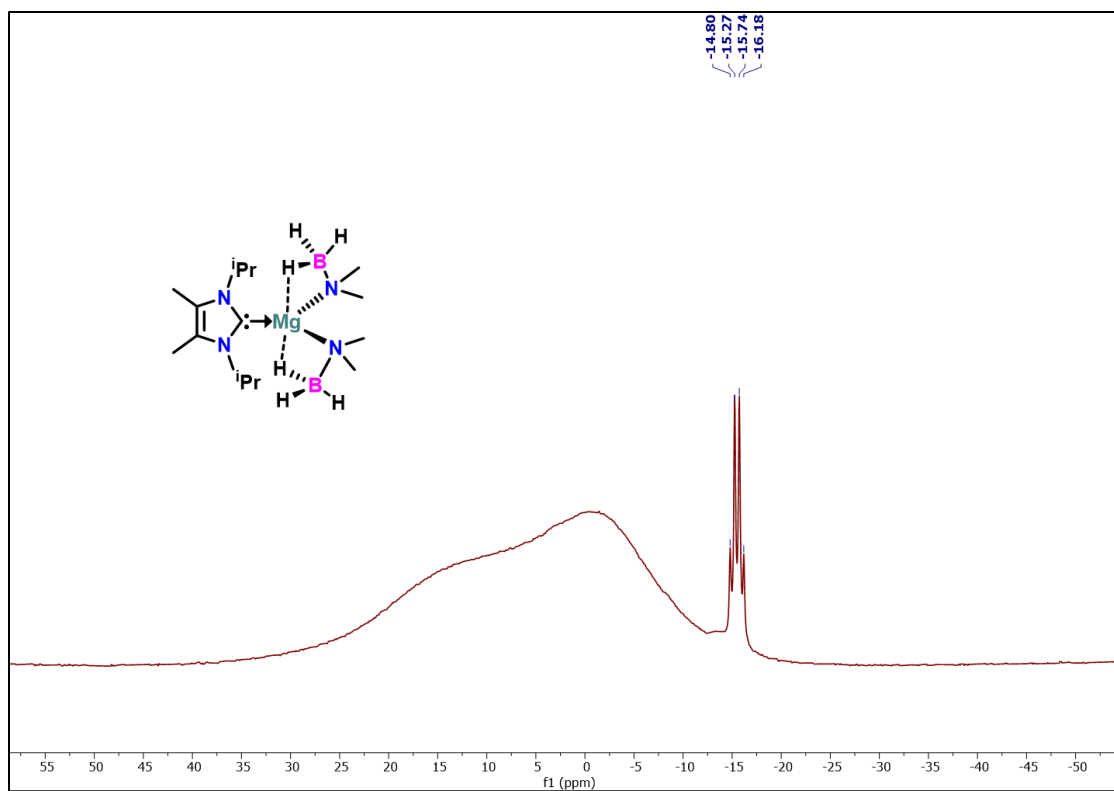


Figure A2.89. ^{11}B NMR spectrum (192 MHz, C_6D_6 , 298 K) of 5.8.

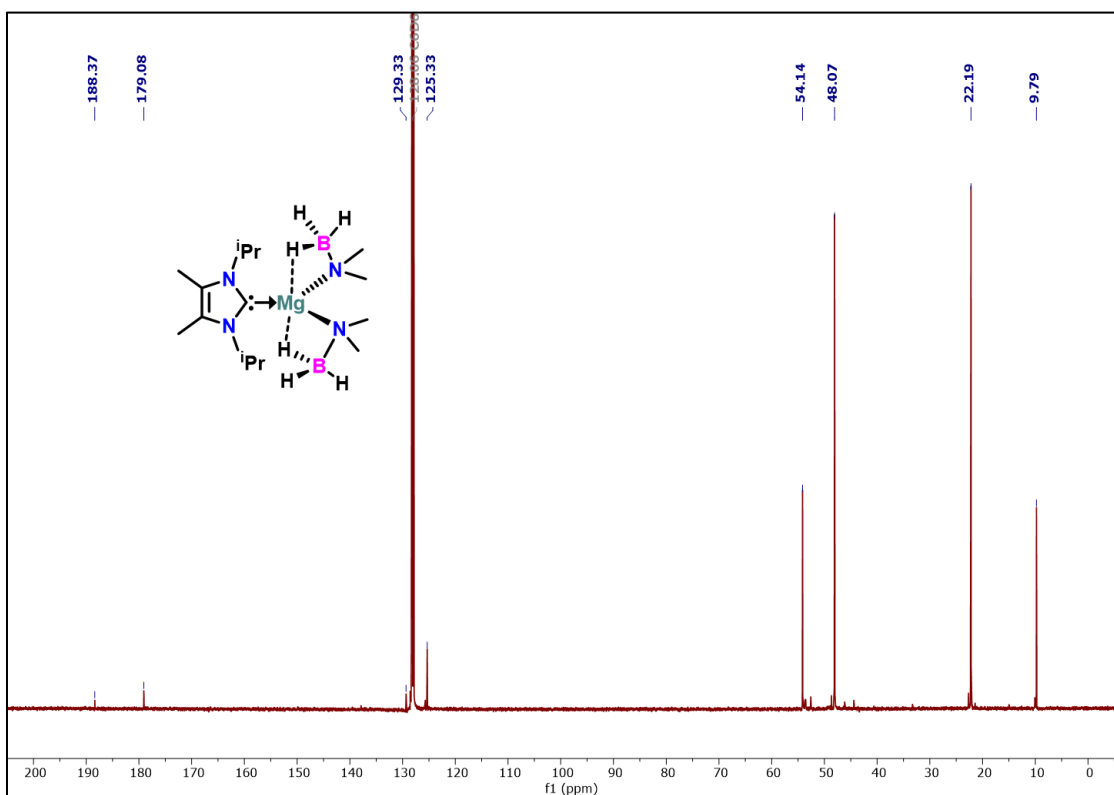


Figure A2.90. $^{13}\text{C}\{^1\text{H}\}$ NMR spectrum (151 MHz, C_6D_6 , 298 K) of 5.8.

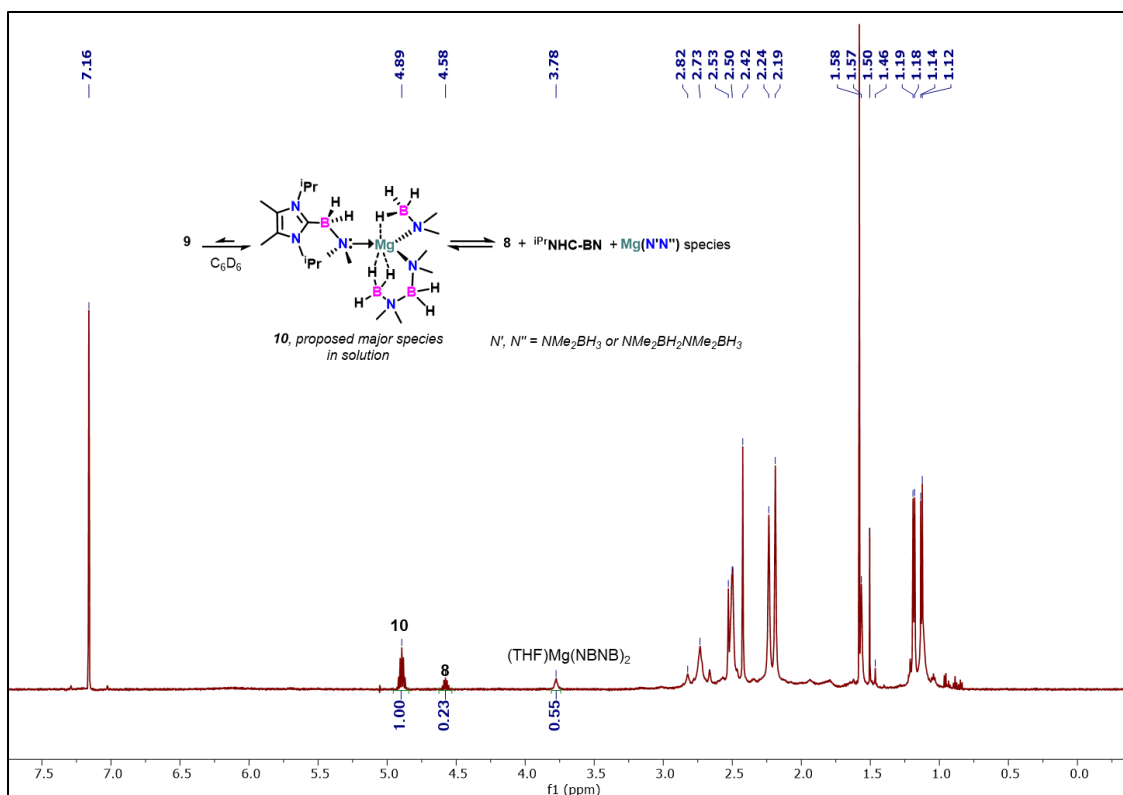


Figure A2.91. ^1H NMR spectrum of **5.9** (600 MHz, C_6D_6 , 298 K) showing disproportionation to **5.8** and **5.10**.

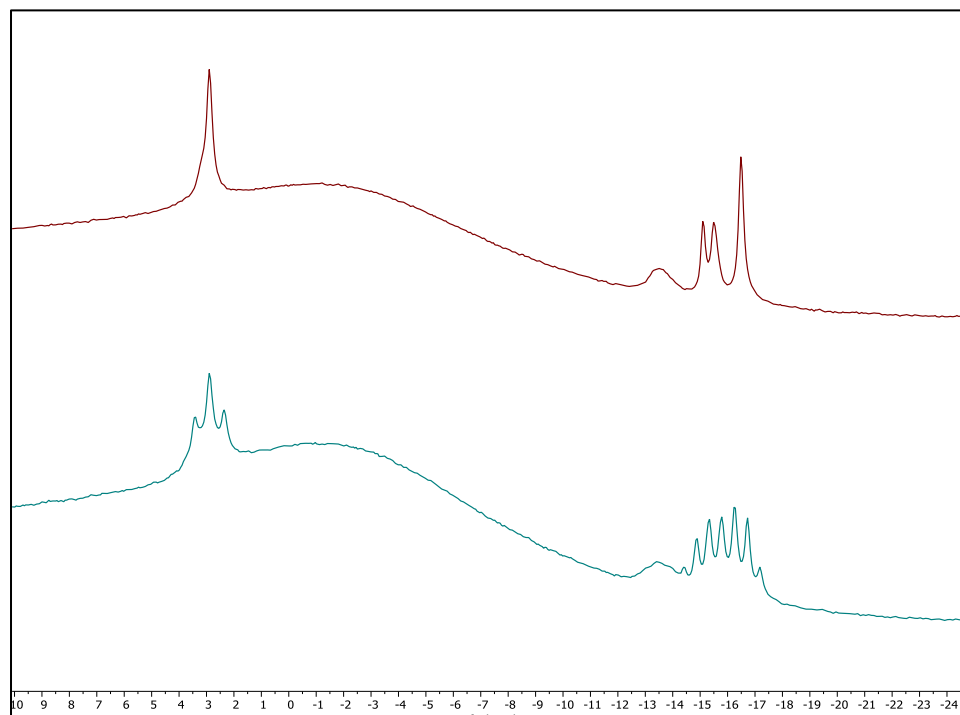


Figure A2.92. Stack plot of ^{11}B (bottom) and $^{11}\text{B}\{^1\text{H}\}$ (top) NMR spectra of **5.9** highlighting the presence of multiple boron containing-products including **5.8**, **5.10**, and $i\text{PrNHC-BN}$.

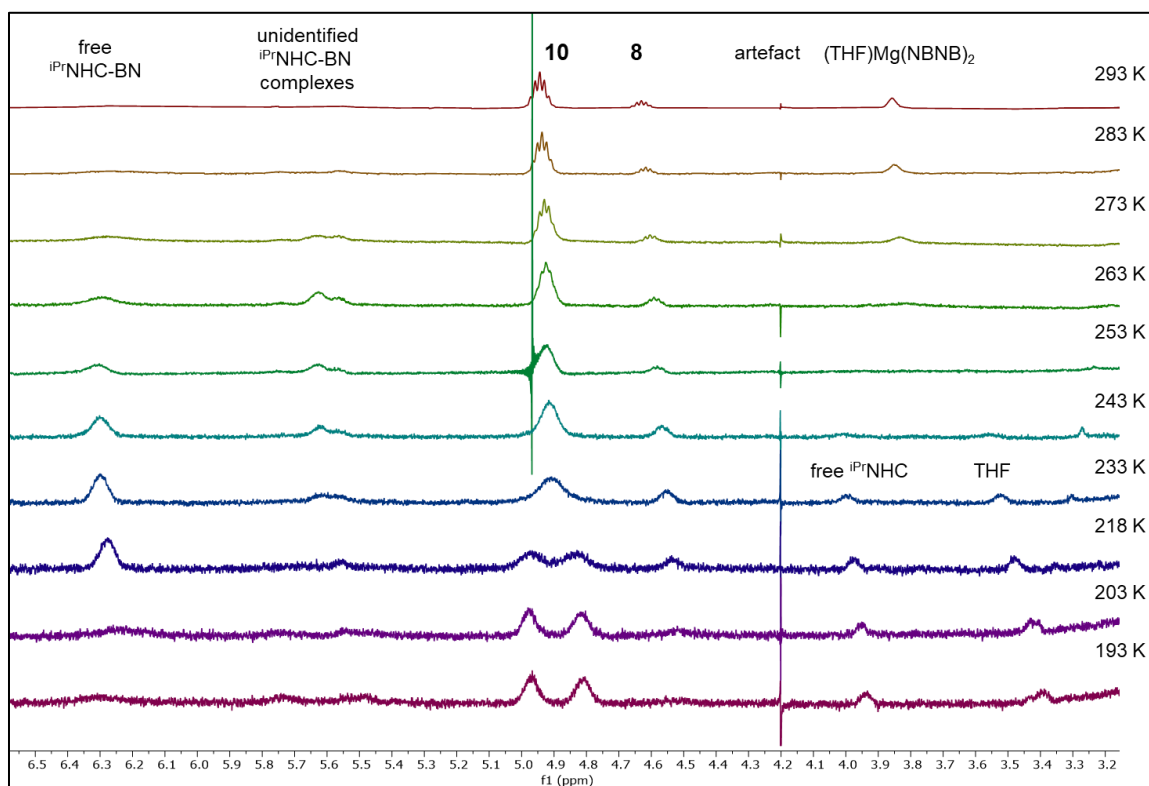


Figure A2.93. Stack plot of VT-NMR spectra of **5.9** in toluene- d_8 (193 – 293 K).

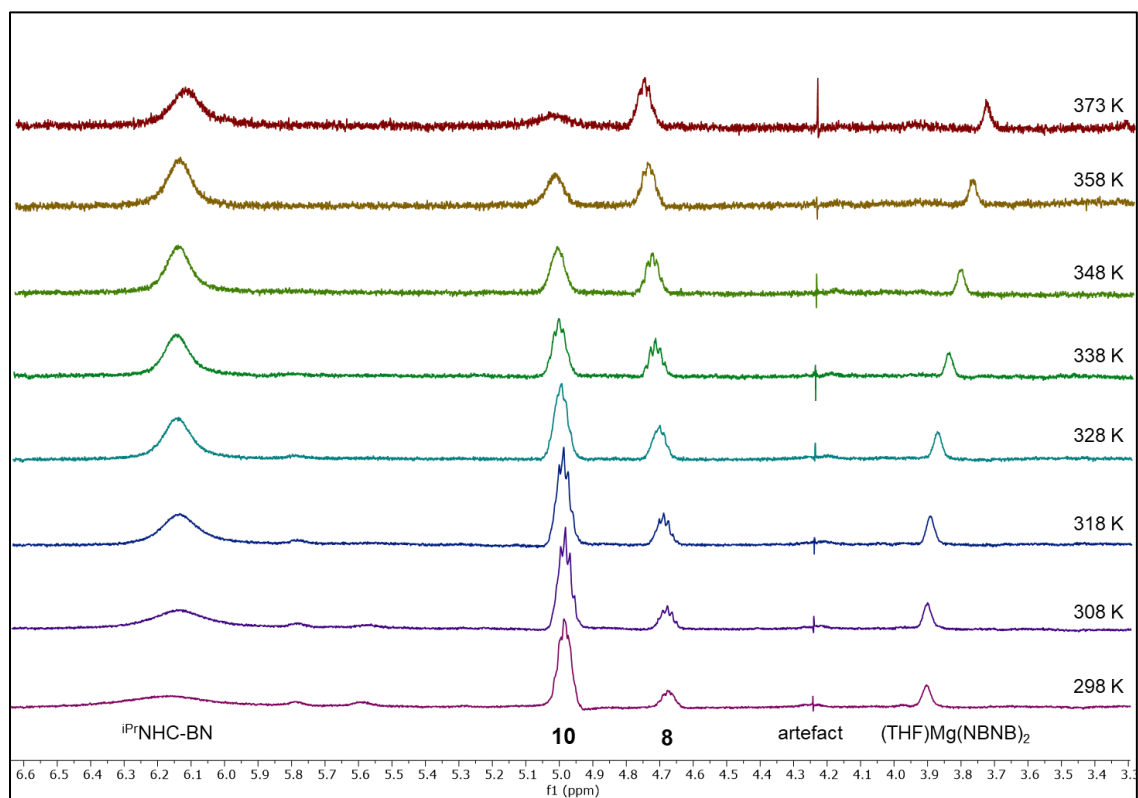


Figure A2.94. Stack plot of VT-NMR spectra of **5.9** in toluene- d_8 (298 – 373 K).

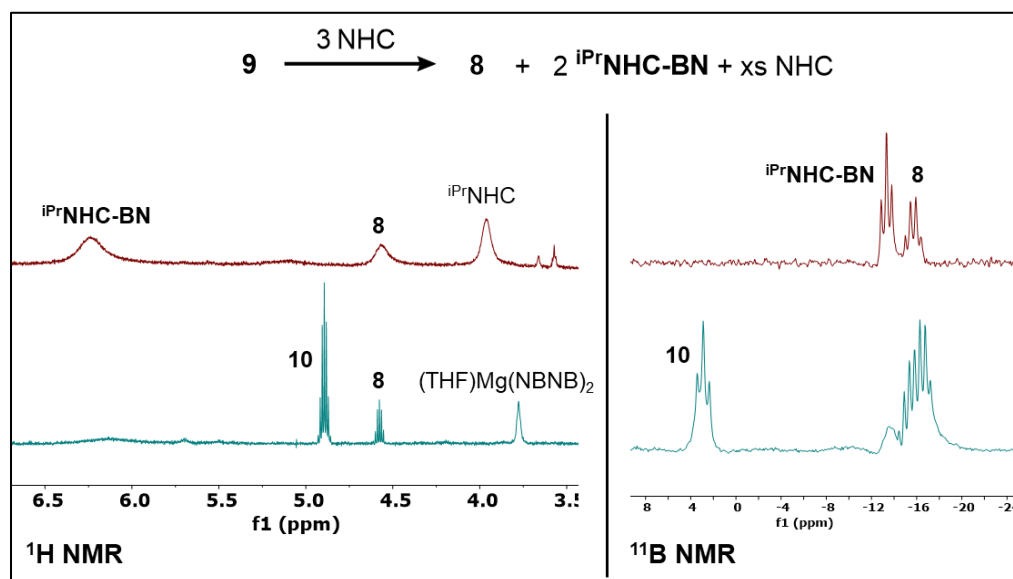


Figure A2.95. Reaction of **5.9** with NHC, highlighting conversion to **iPrNHC-BN** and **5.8** as the sole boron-containing products. The ¹¹B NMR spectra was processed to remove signals due to the ¹¹B probe.

NMR monitored formation of 5.9 and NOESY NMR studies

Equimolar amounts of (THF)Mg(NMe₂BH₂NMe₂BH₃)₂ (9 mg, 0.0276 mmol) and NHC (5 mg, 0.0276 mmol) were combined in C₆D₆ and heteronuclear 1D and 2D NMR were collected.

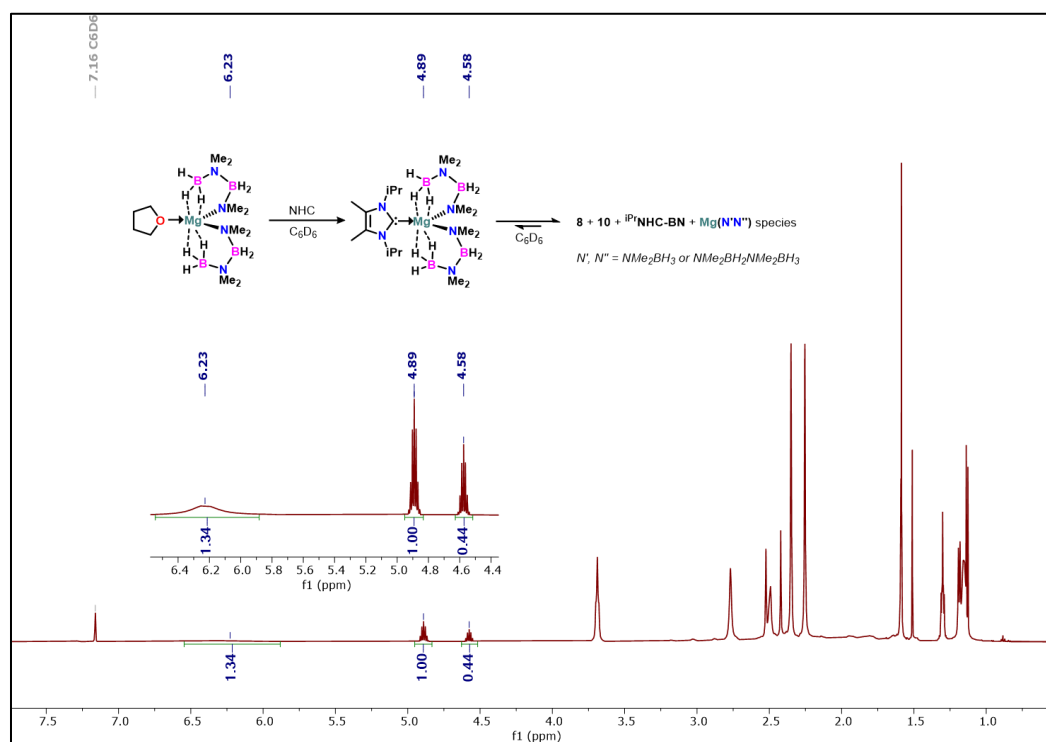


Figure A2.96. ¹H NMR spectrum (600 MHz, C₆D₆, 298 K).

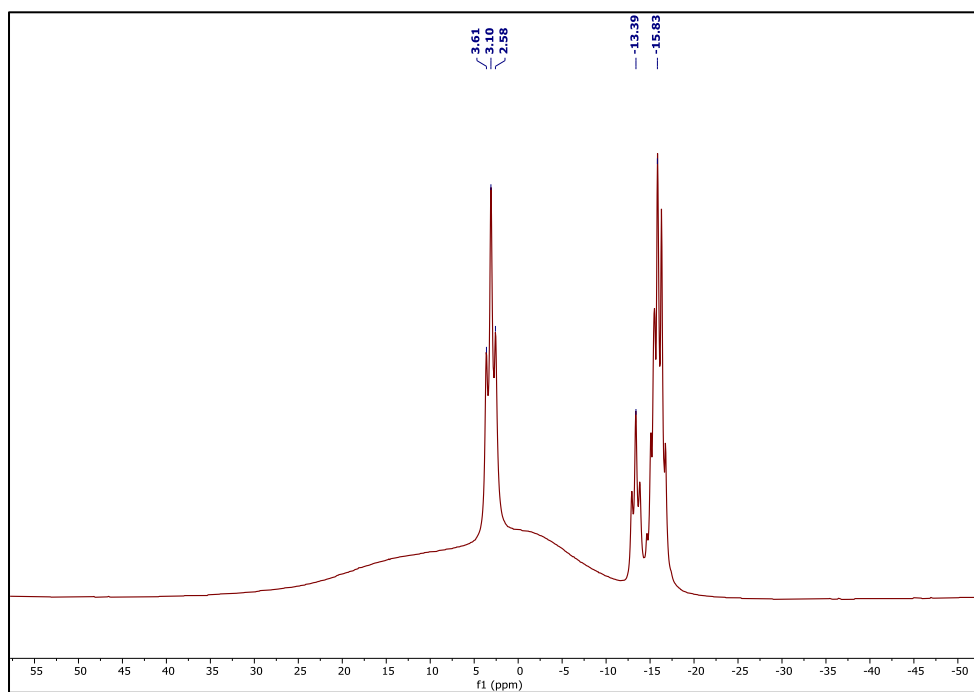


Figure A2.97. ^{11}B NMR spectrum (192 MHz, C_6D_6 , 298 K).

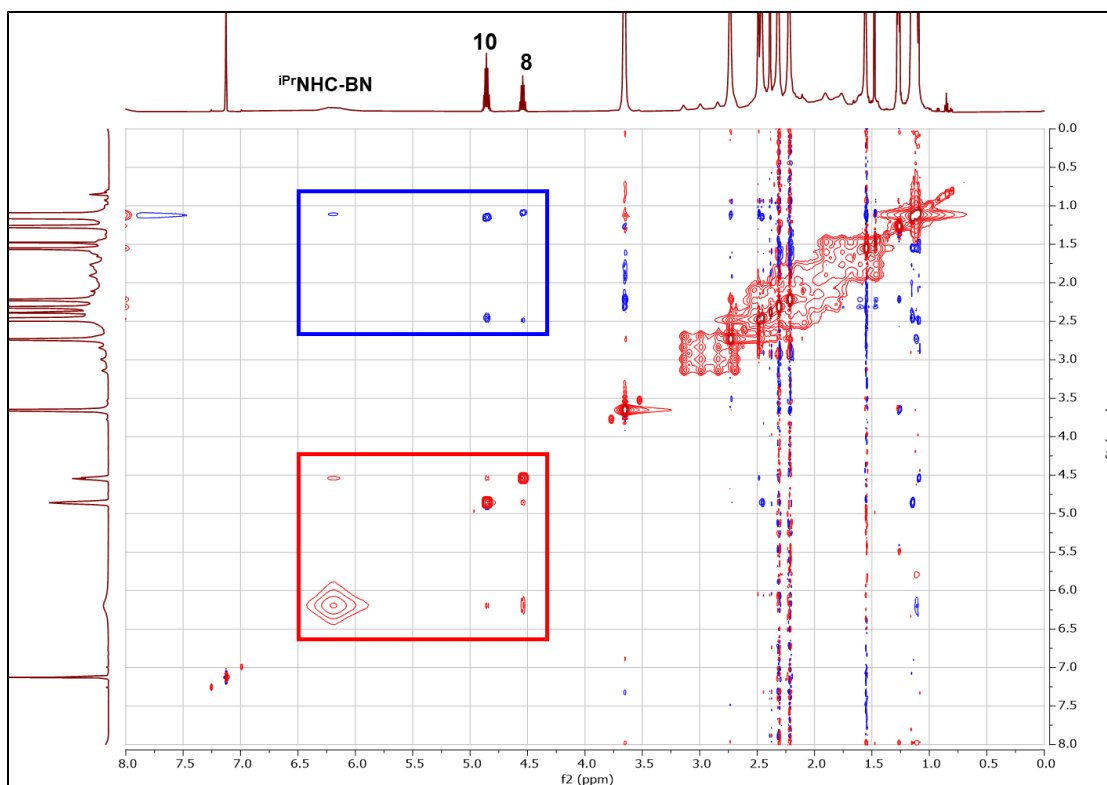


Figure A2.98. NOESY NMR spectrum of **5.9** (C_6D_6 , 298 K) highlighting in phase cross-peaks (red) between resonances in direct chemical exchange, and out of phase cross peaks (blue) for through-space interactions.

DOSY NMR of 5.9

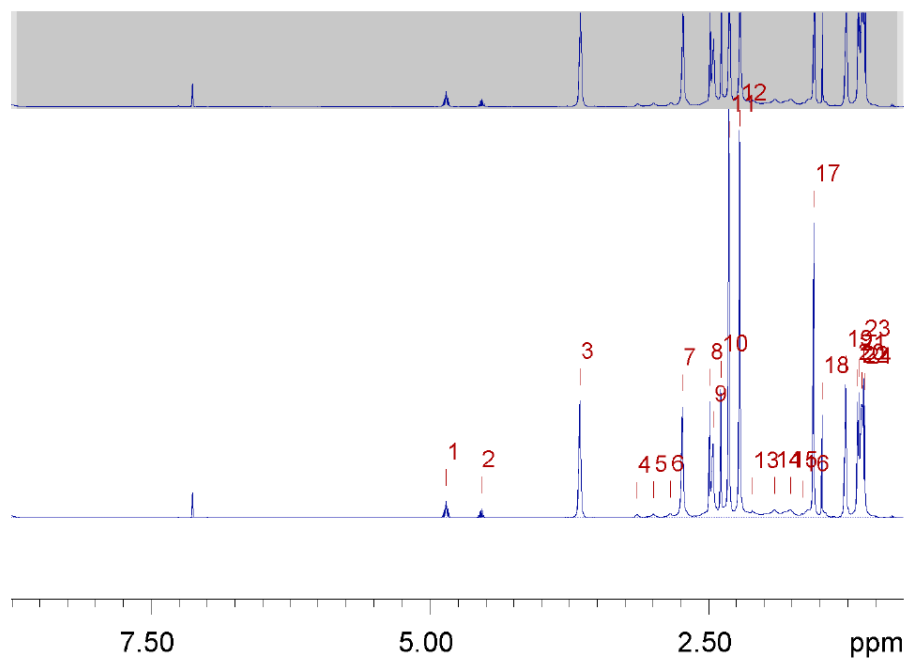


Figure A2.99. Peak selections

Table A2.2. Diffusion data and hydrodynamic radii for selected peaks in Figure A2.99.

peak	ppm	D (m ² /s)	error	rH
1	4.859	8.64E-10	9.68E-12	4.12E-10
2	4.543	9.17E-10	1.53E-11	3.88E-10
3	3.658	1.69E-09	1.03E-11	2.11E-10
4	3.144	1.10E-09	3.60E-11	3.24E-10
5	2.996	1.09E-09	2.09E-11	3.27E-10
6	2.845	1.10E-09	1.85E-11	3.24E-10
7	2.737	1.09E-09	4.60E-12	3.27E-10
8	2.491	9.30E-10	5.93E-12	3.83E-10
9	2.461	8.95E-10	4.60E-12	3.98E-10
10	2.389	8.69E-10	9.90E-12	4.10E-10
11	2.318	9.94E-10	9.17E-12	3.58E-10
12	2.222	9.96E-10	7.87E-12	3.58E-10
13	2.109	9.88E-10	1.22E-11	3.61E-10
14	1.909	1.00E-09	1.46E-11	3.56E-10
15	1.766	1.02E-09	1.31E-11	3.49E-10
16	1.66	1.00E-09	2.47E-11	3.56E-10
17	1.556	9.82E-10	6.25E-12	3.63E-10
18	1.48	8.89E-10	2.27E-11	4.01E-10
19	1.27	1.66E-09	1.26E-11	2.15E-10

20	1.161	8.90E-10	5.68E-12	4.00E-10
21	1.15	9.05E-10	9.01E-12	3.94E-10
22	1.125	1.10E-09	1.96E-12	3.24E-10
23	1.107	9.73E-10	1.24E-11	3.66E-10
24	1.095	9.43E-10	1.27E-11	3.78E-10

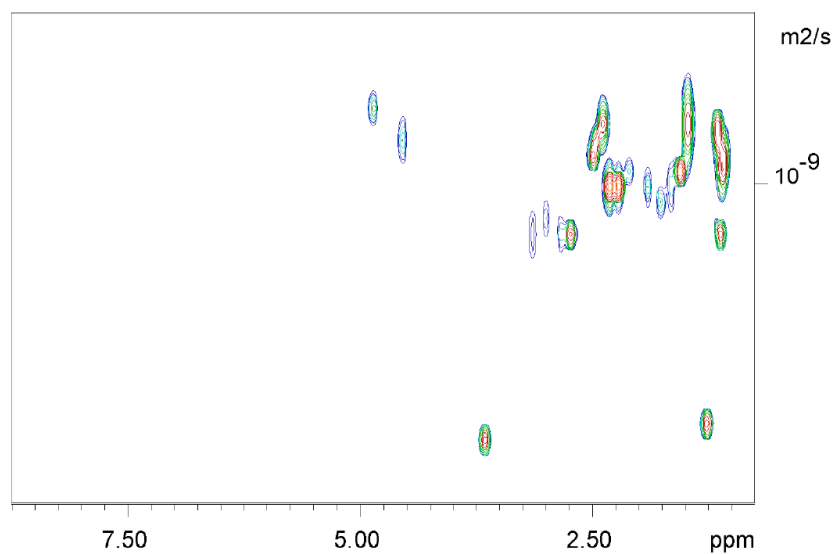


Figure A2.100. DOSY fit

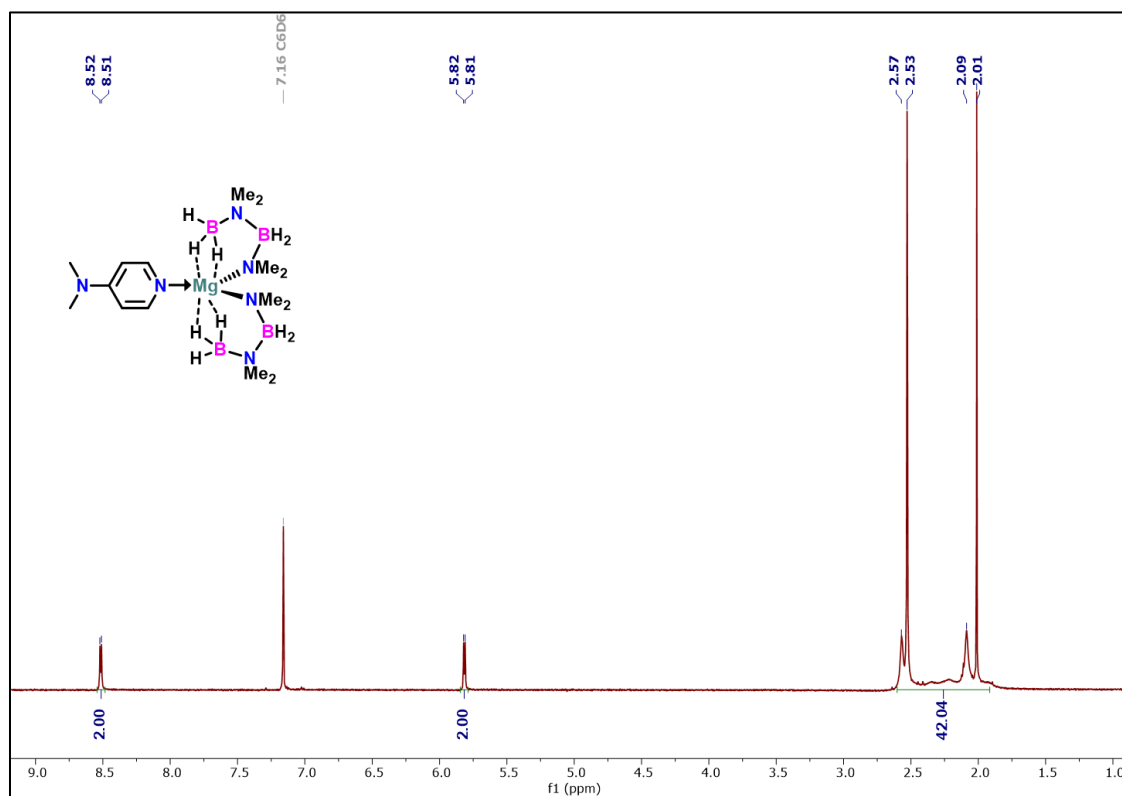


Figure A2.101. ¹H NMR spectrum (600 MHz, C₆D₆, 298 K) of **5.11**.

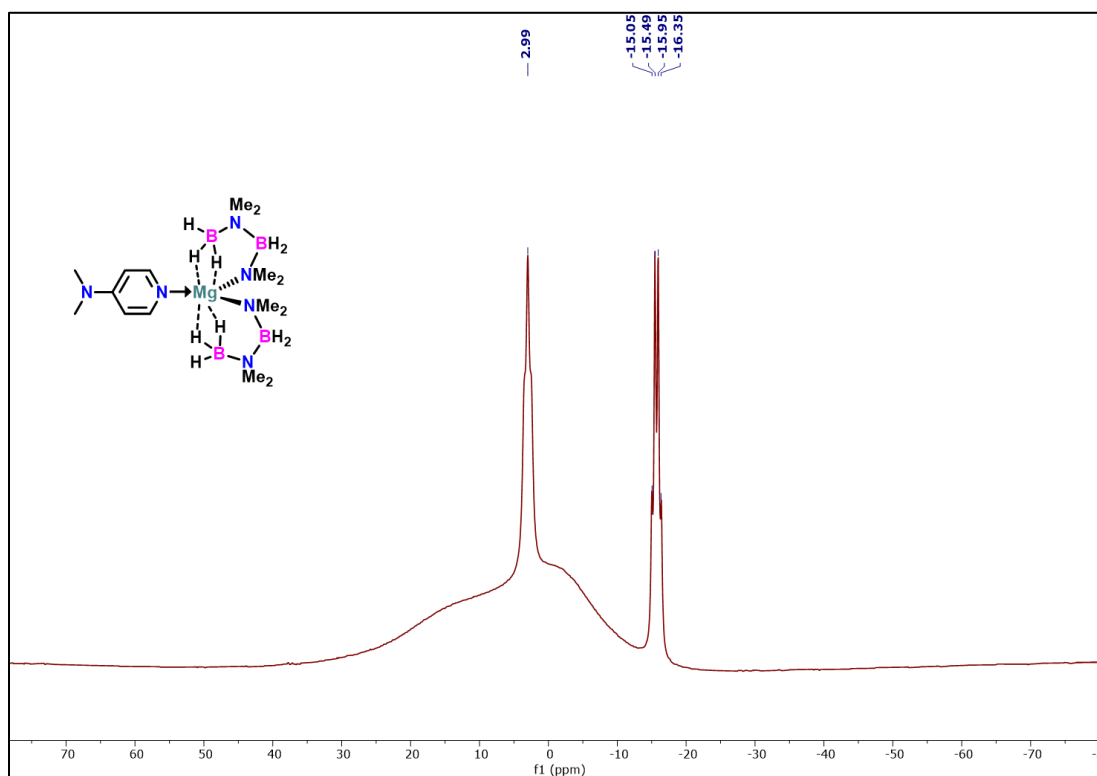


Figure A2.102. ^{11}B NMR spectrum (192 MHz, C_6D_6 , 298 K) of **5.11**.

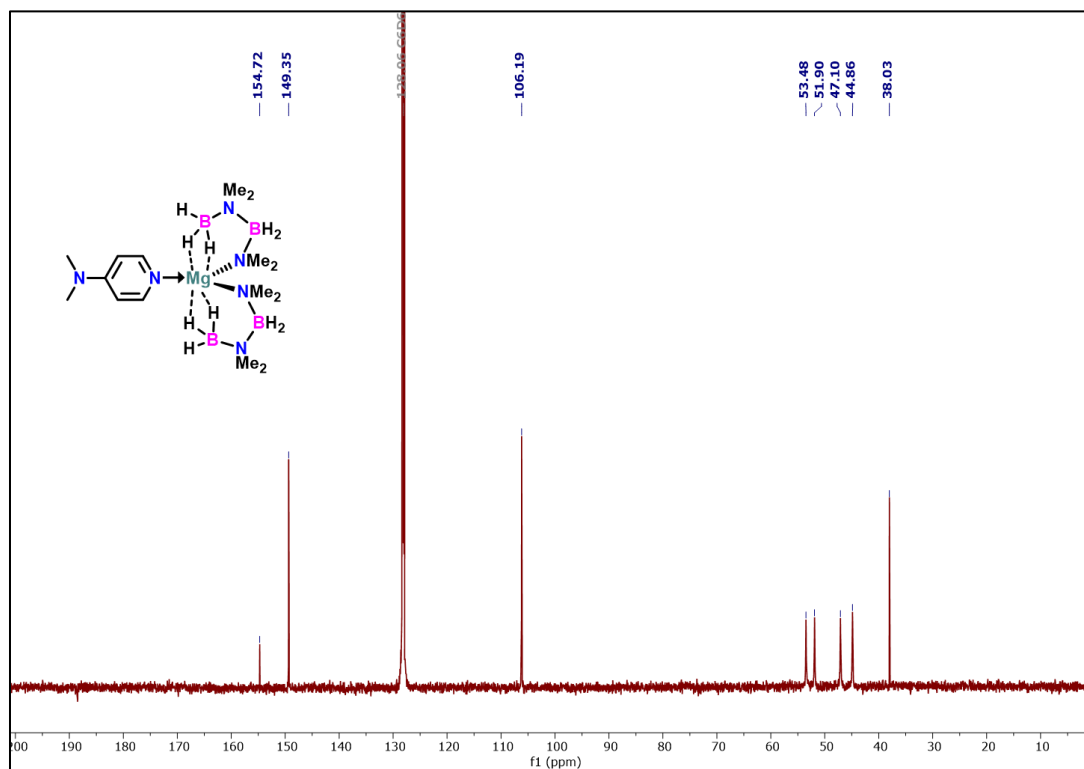


Figure A2.103. $^{13}\text{C}\{^1\text{H}\}$ NMR spectrum (151 MHz, C_6D_6 , 298 K) of **5.11**.

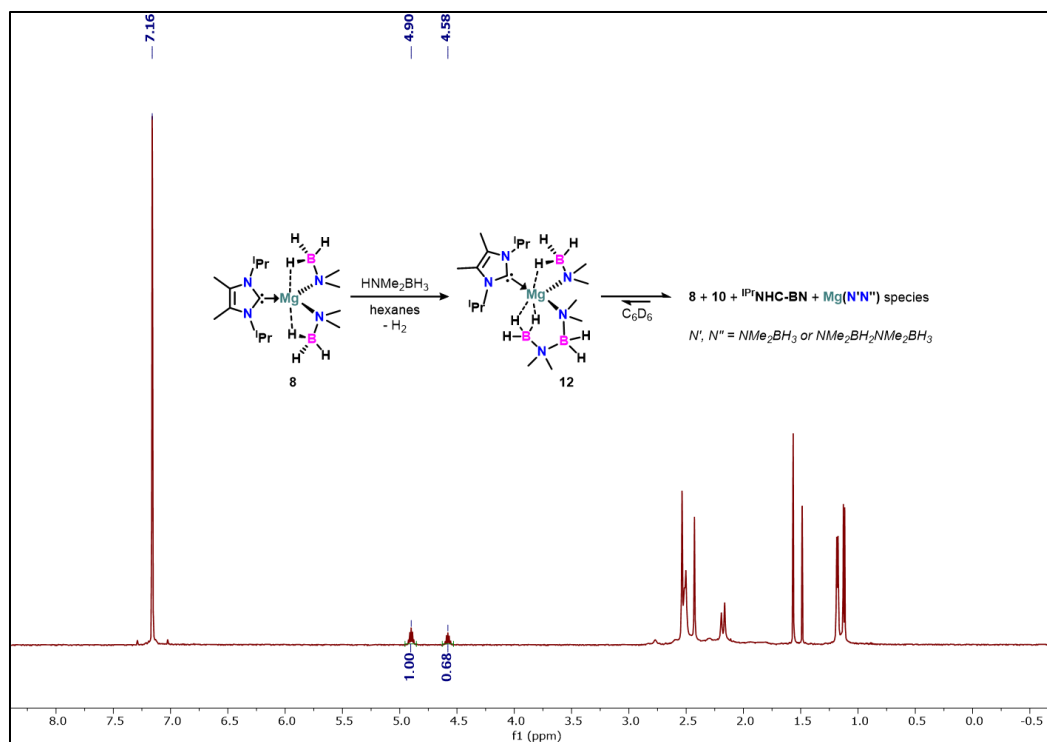


Figure A2.104. ^1H NMR spectrum of **5.12** showing disproportionation products.

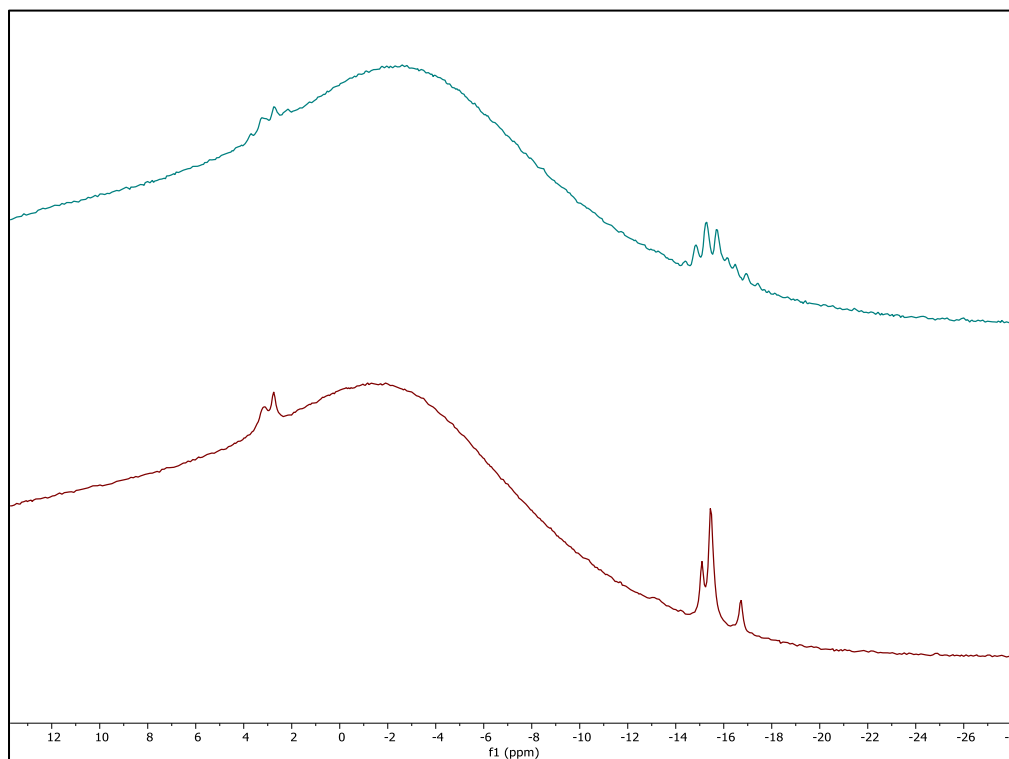


Figure A2.105. Stack plot of ^{11}B (top) and $^{11}\text{B}\{^1\text{H}\}$ (bottom) NMR spectra of **5.12** highlighting the presence of multiple boron containing-products.

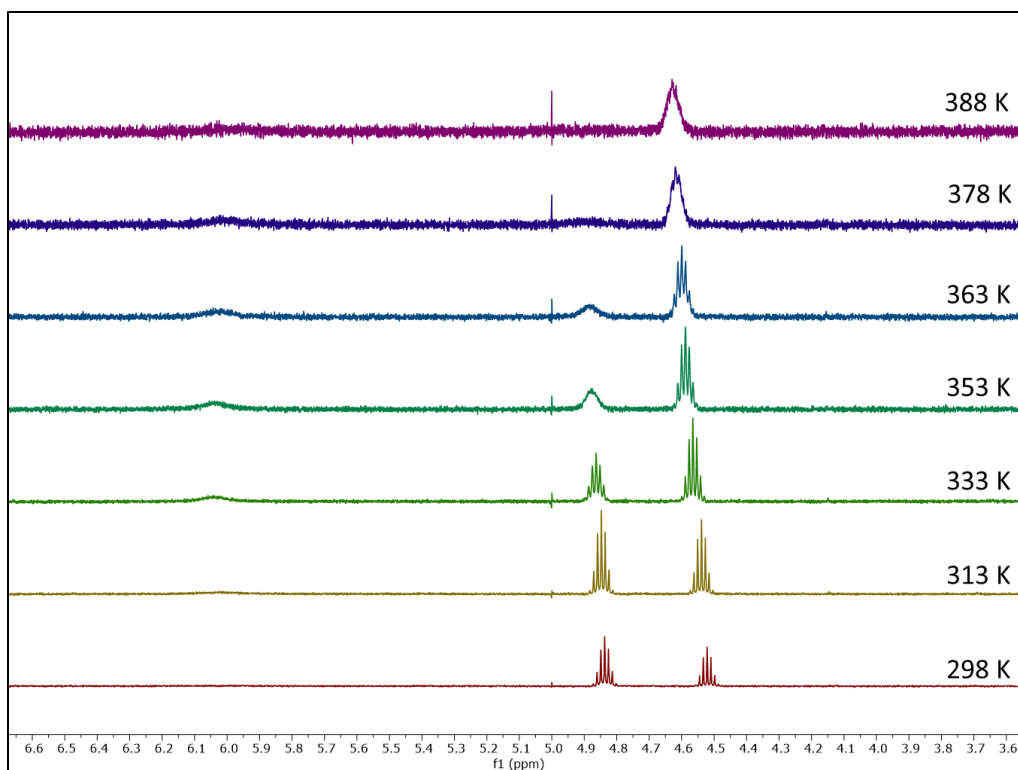


Figure A2.106. VT ^1H NMR (C_6D_6 , 298 – 388 K) of **5.12** highlighting the carbenic methine protons.

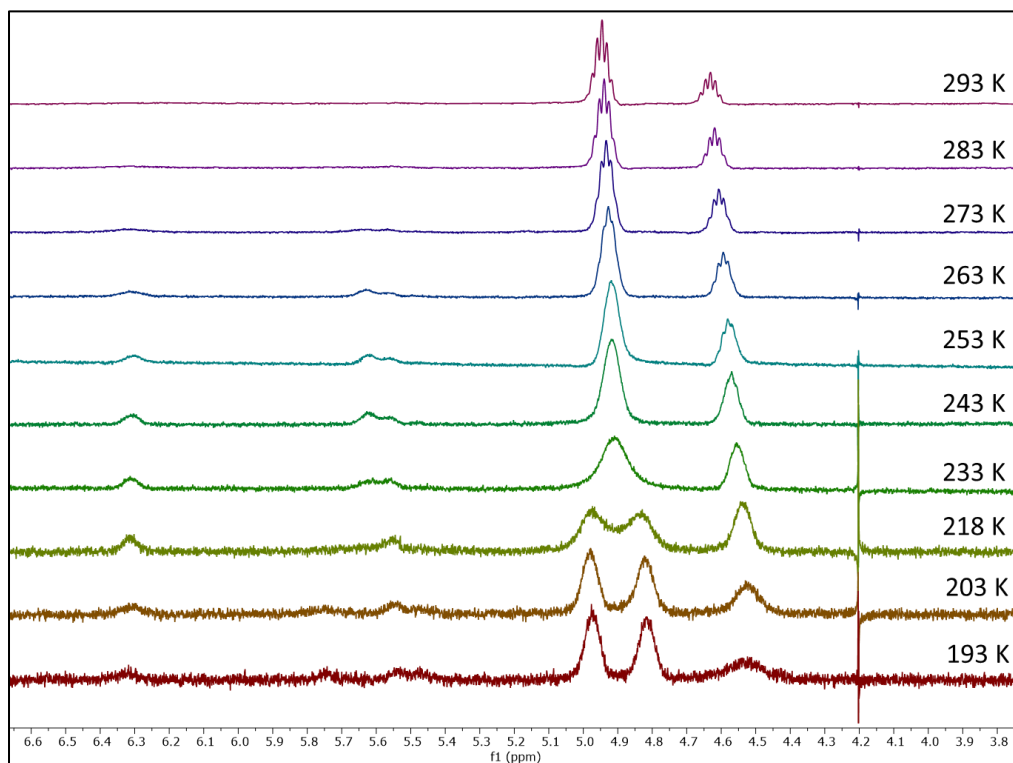


Figure A2.107. VT ^1H NMR (C_7D_8 , 193 – 293 K) of **5.12** highlighting the carbenic methine protons.

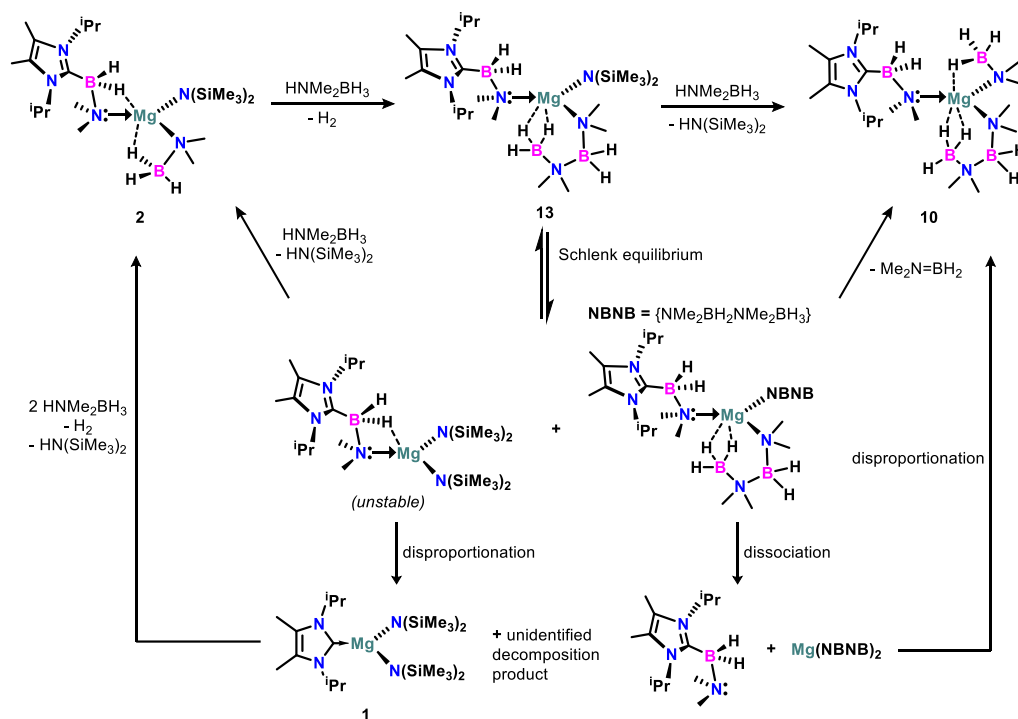


Figure A2.108. Proposed disproportionation of **5.13** via Schlenk rearrangements and competitive reactions of HNMe_2BH_3 , ultimately resulting in **5.2** and **5.10**, with **5.10** undergoing dynamic disproportionation to **5.8** and $i\text{PrNHC-BN}$ complexes.

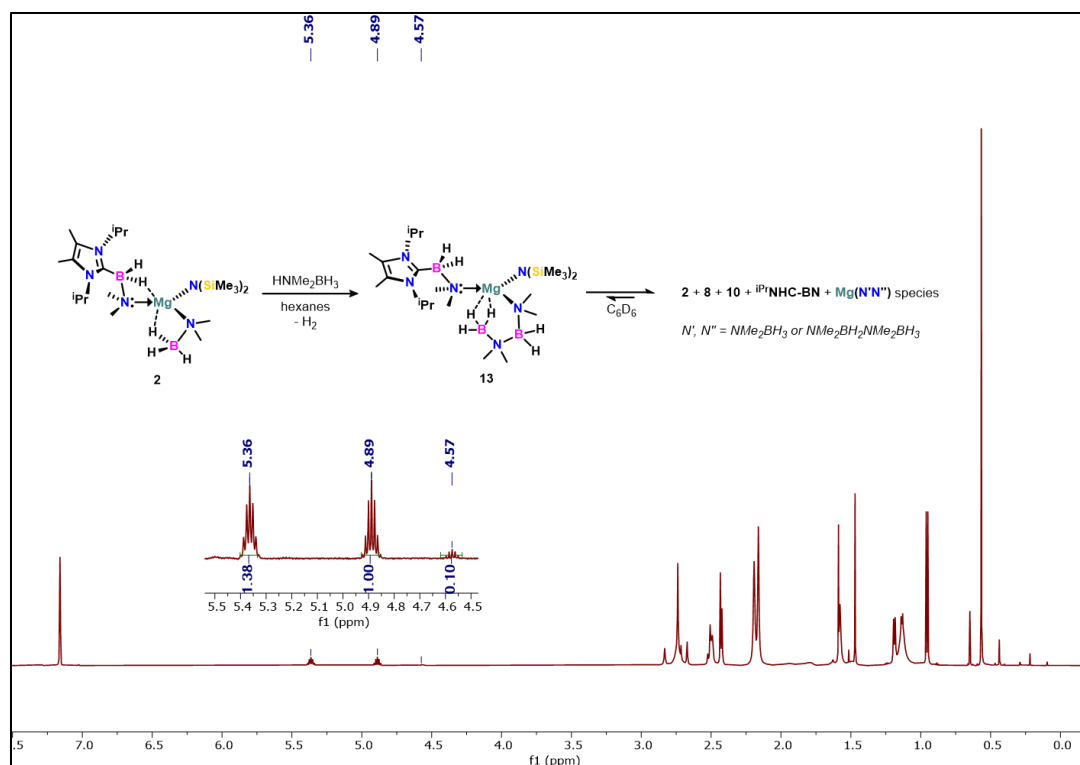


Figure A2.109. ^1H NMR spectrum of **5.13** showing disproportionation to **5.2** and **5.8**.

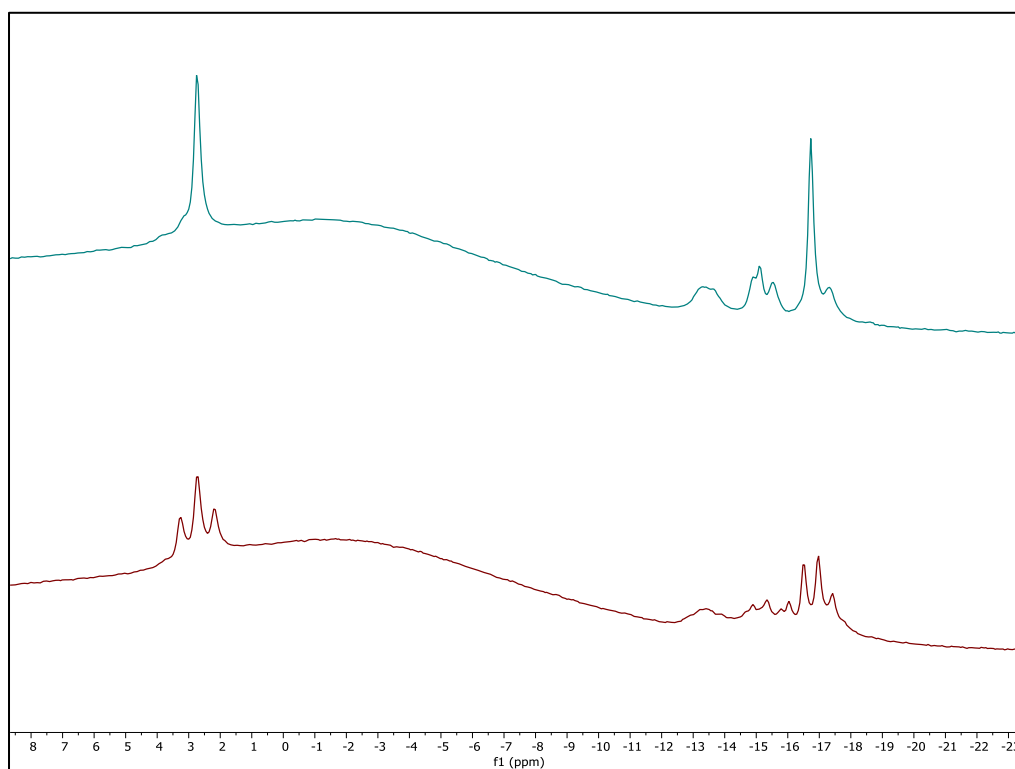


Figure A2.110. Stacked ^{11}B (bottom) and $^{11}\text{B}\{^1\text{H}\}$ (top) NMR spectra of **5.13** highlighting the presence of multiple boron containing-products.

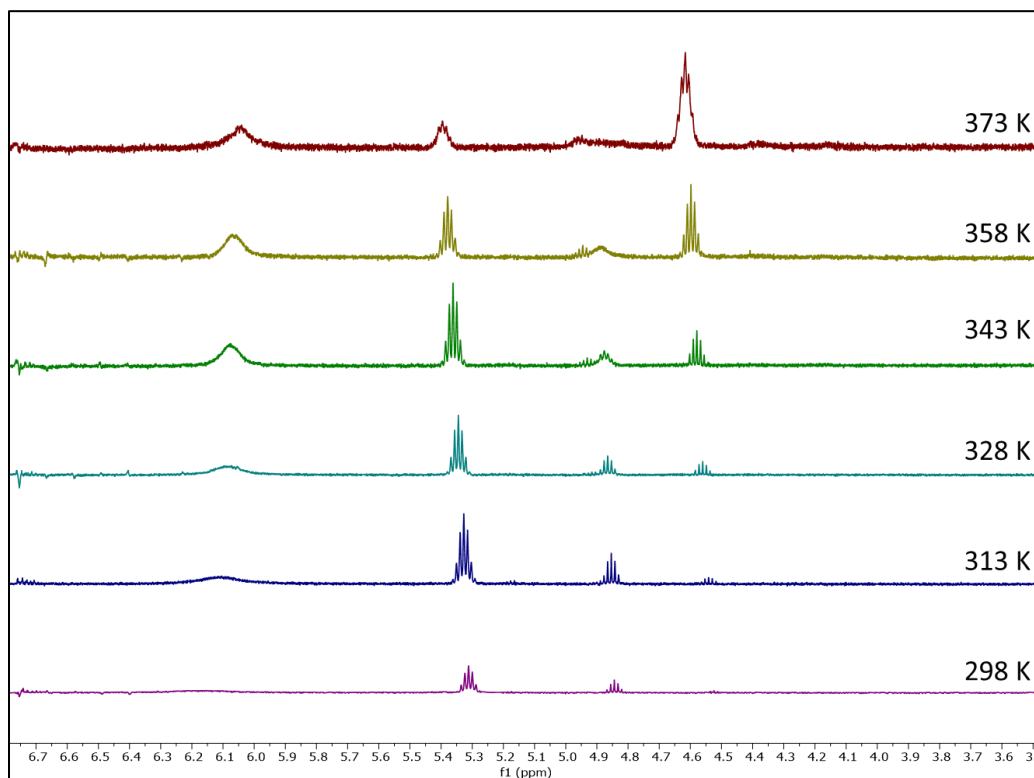


Figure A2.111. VT ^1H NMR (C_6D_6 , 298 – 373 K) of **5.13** highlighting carbene methine region.

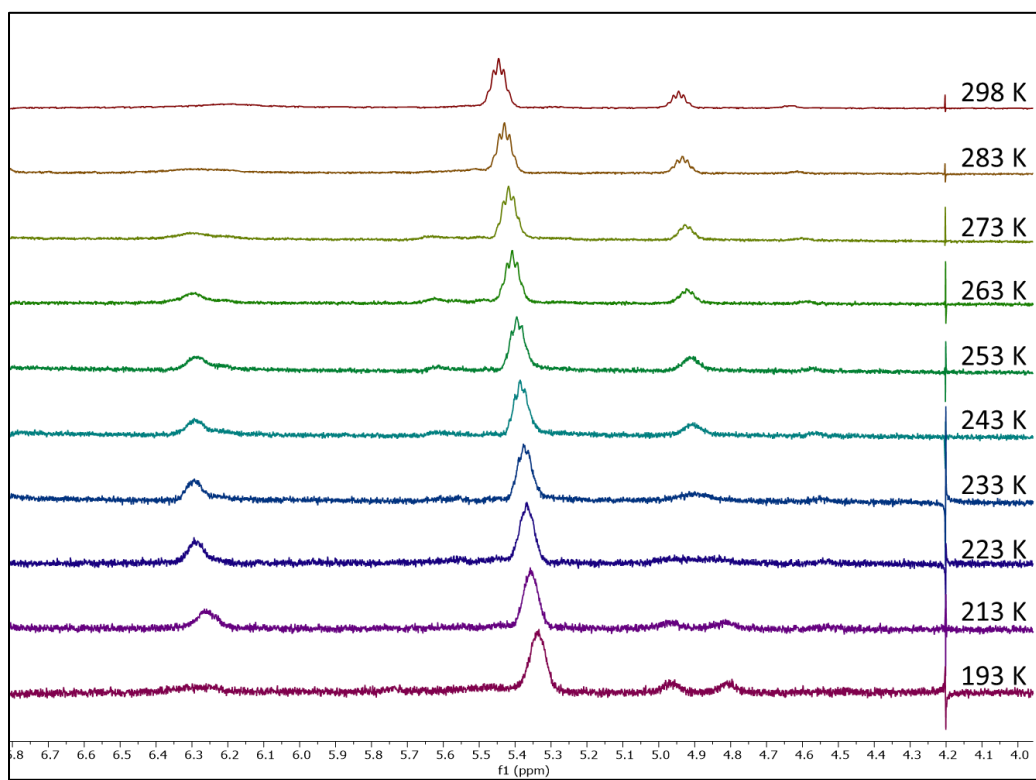


Figure A2.112. VT ¹H NMR (C₇D₈, 193 – 298 K) of **5.13** highlighting the carbene methine region.

Chapter Six:

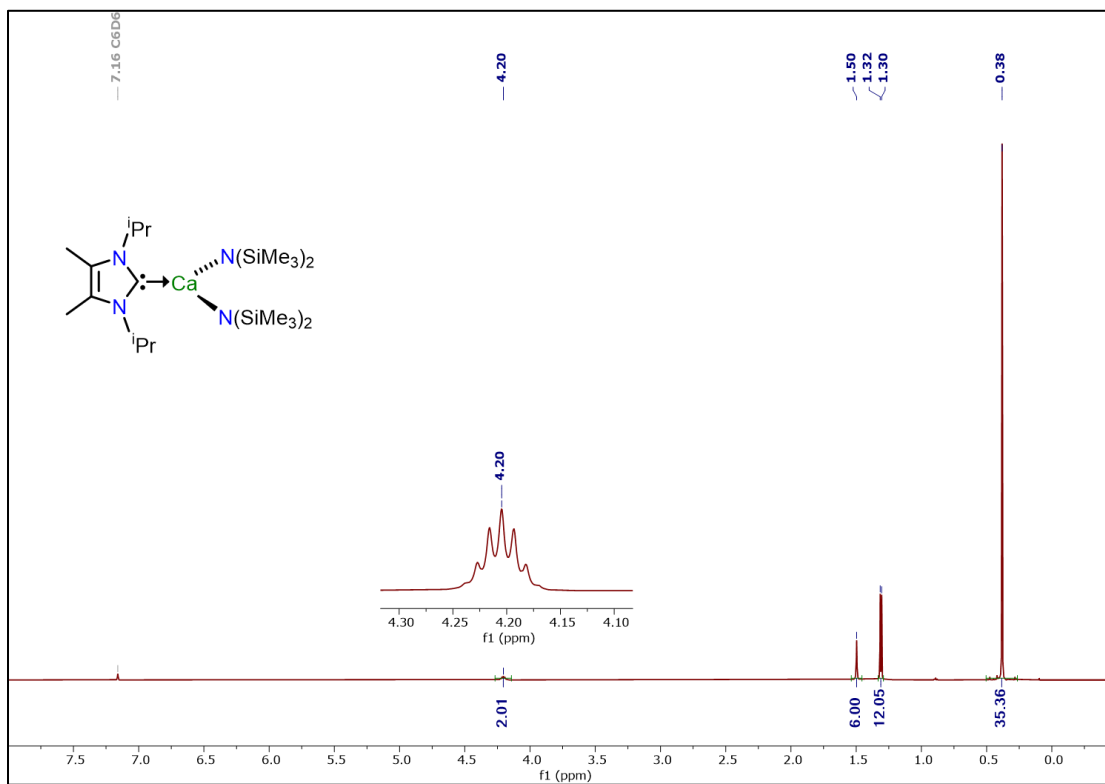


Figure A2.113. ^1H NMR spectrum of **6.2** in C_6D_6 at 298 K.

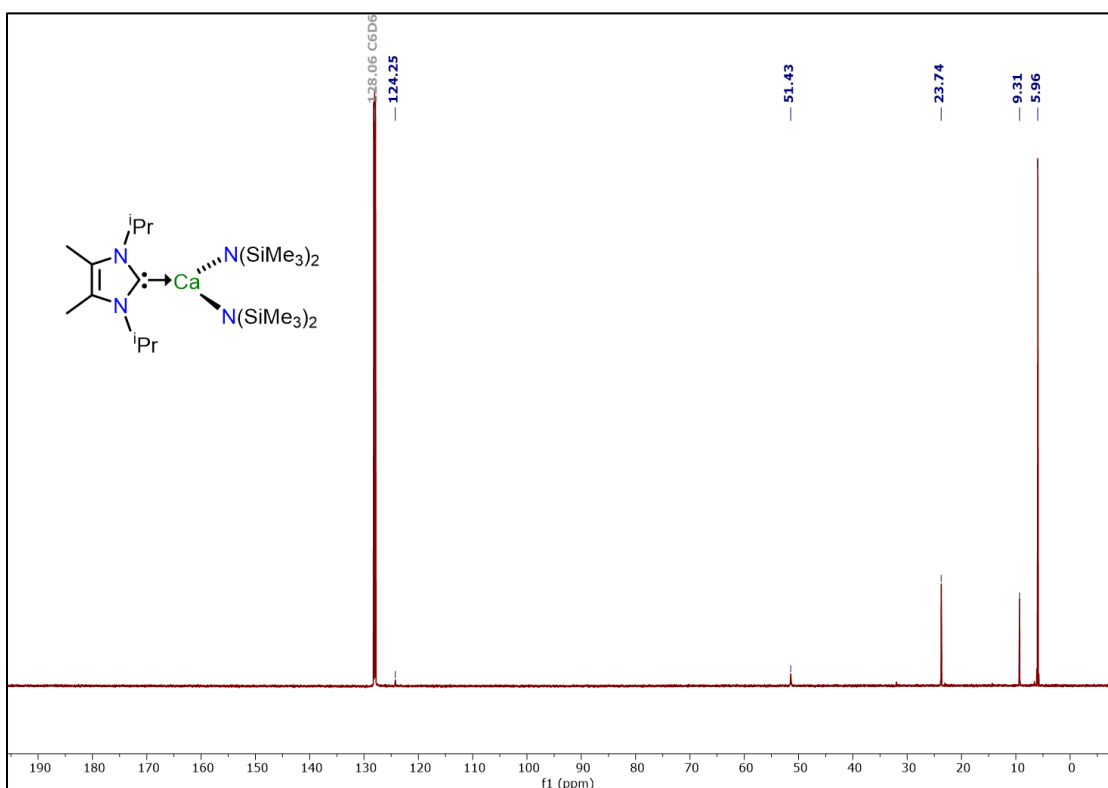


Figure A2.114. ^{13}C NMR spectrum of **6.2** in C_6D_6 at 298 K.

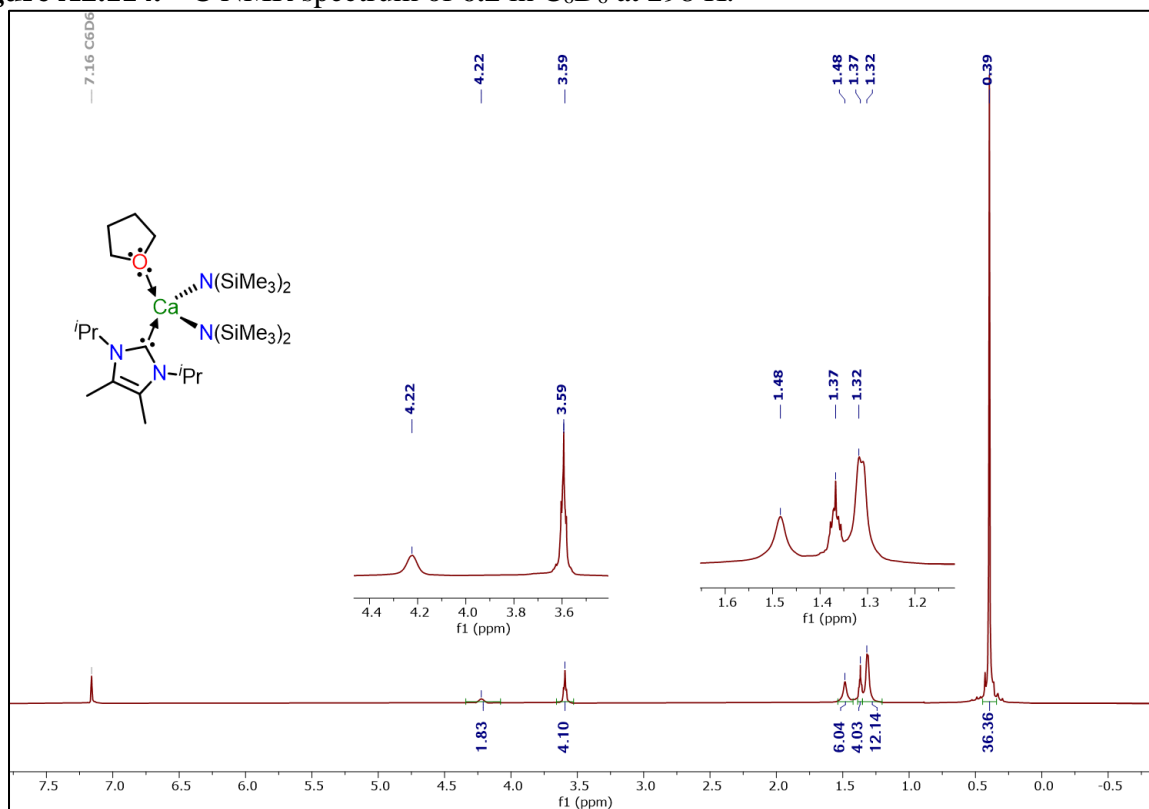


Figure A2.115. ^1H NMR spectrum of **6.4** in C_6D_6 at 298 K.

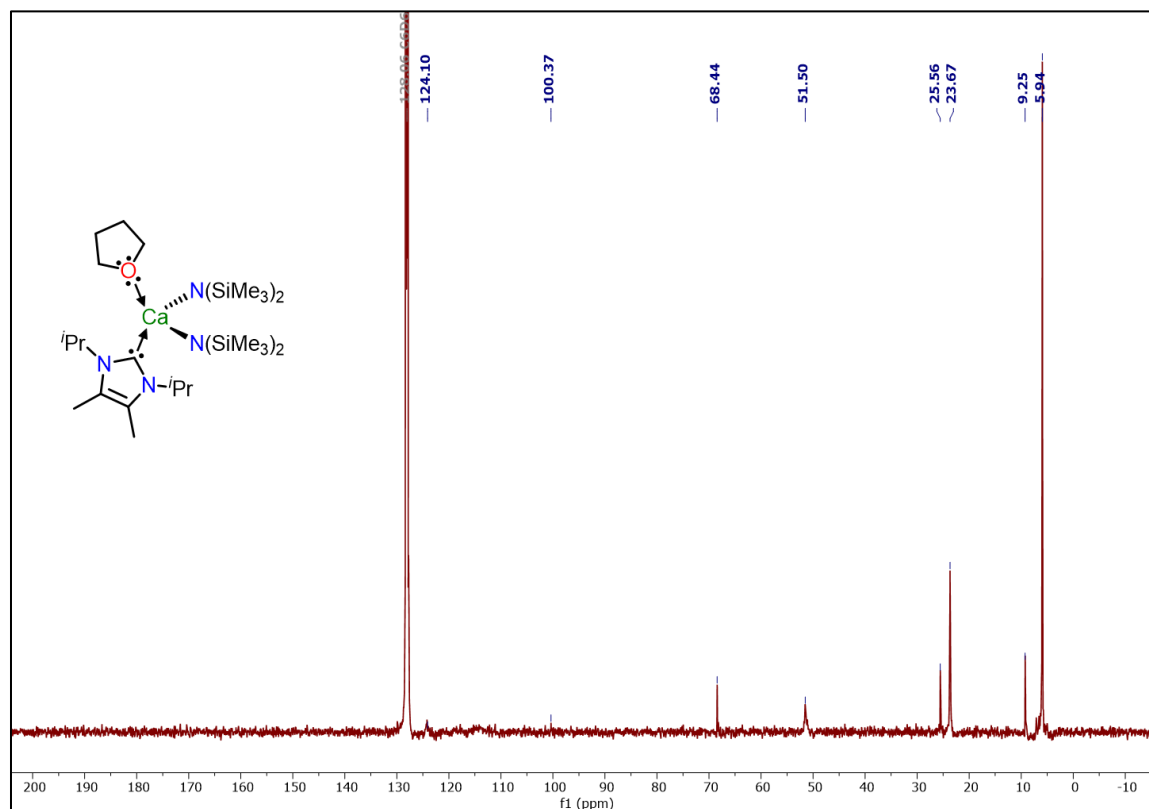


Figure A2.116. ^{13}C NMR spectrum of **6.4** in C_6D_6 at 298 K.

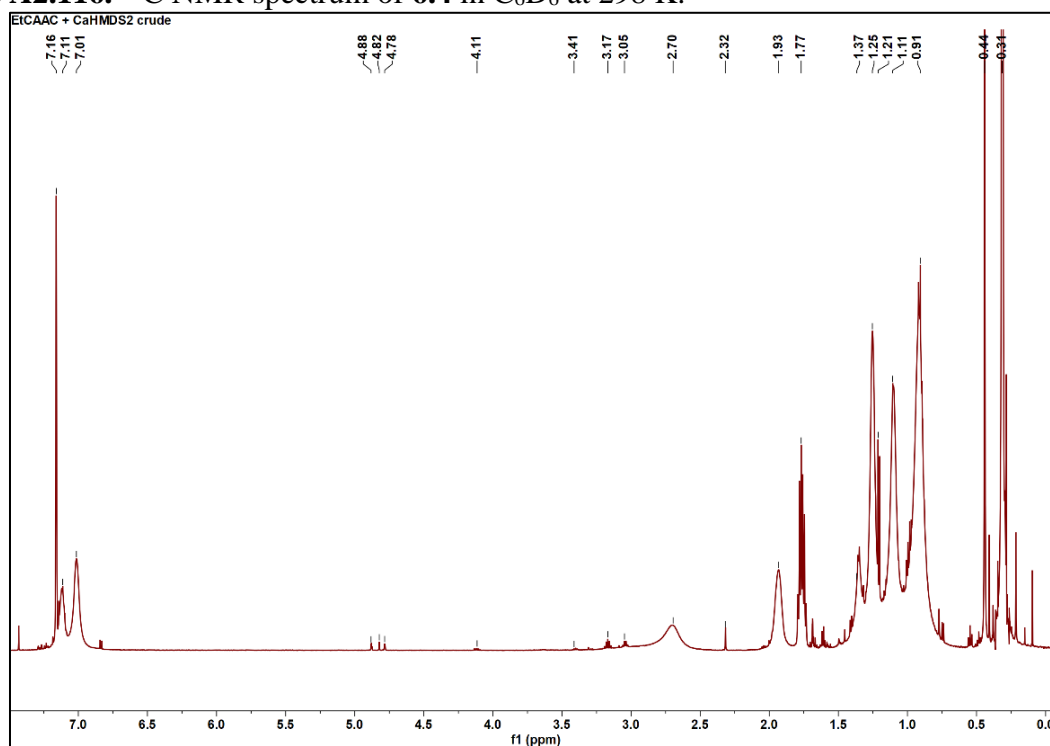


Figure A2.117. Example of a crude ^1H NMR spectrum of a mixture of CAAC and solvent-free $\text{Ca}(\text{HMDS})_2$ in C_6D_6 at 298 K.

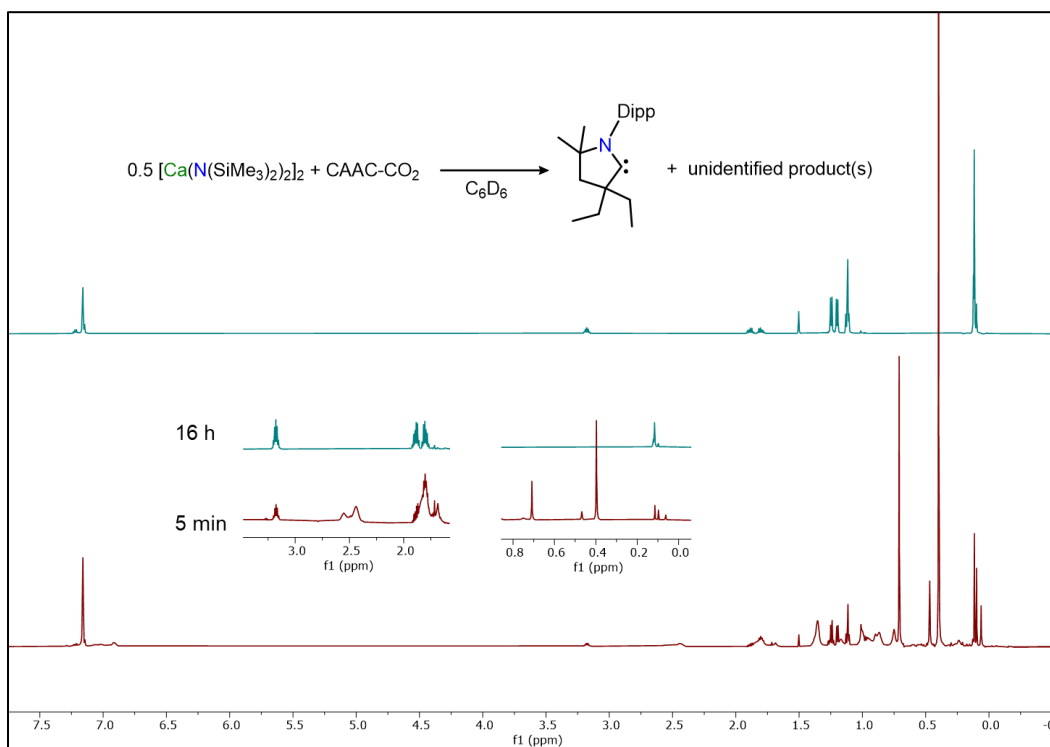


Figure A2.118. Stacked ^1H NMR spectra of the reaction of CAAC- CO_2 and $\text{Ca}(\text{N}(\text{SiMe}_3)_2)_2$ after 5 min (bottom) and 16 h (top) at room temperature, highlighting the liberation of free CAAC.

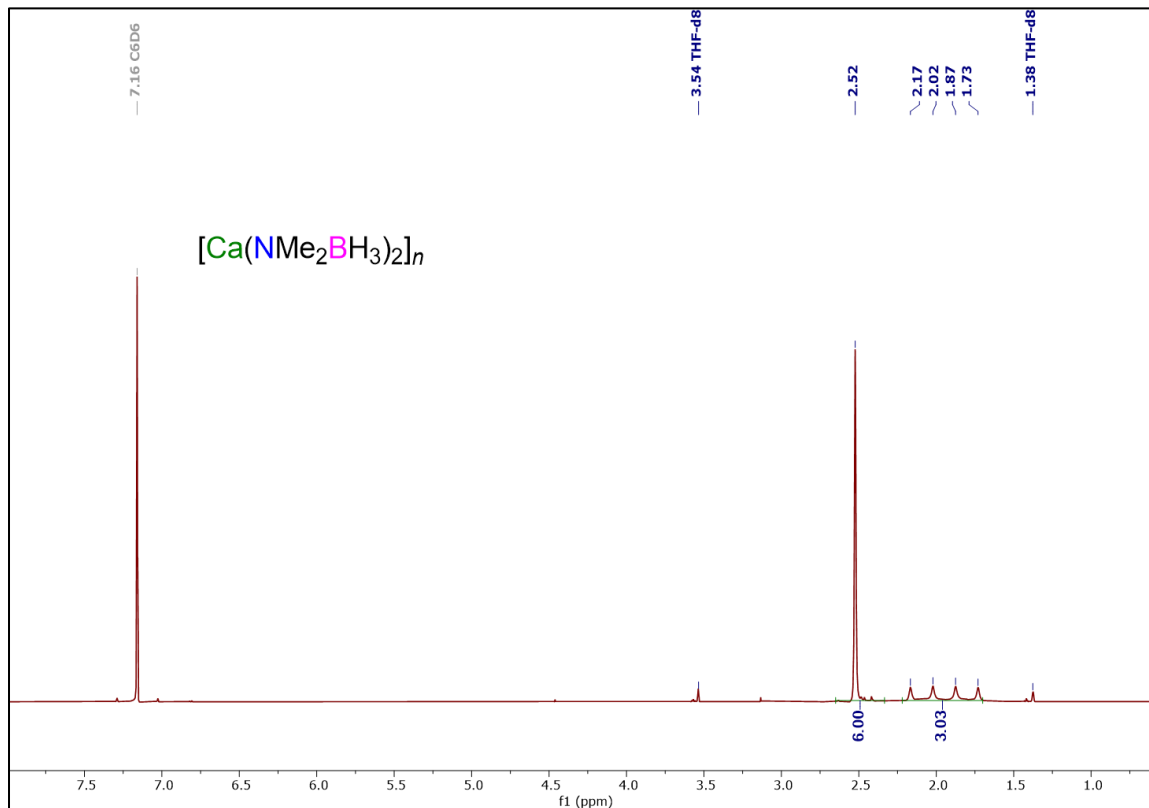


Figure A2.119. ^1H NMR spectrum of **6.6** in C_6D_6 at 298 K.

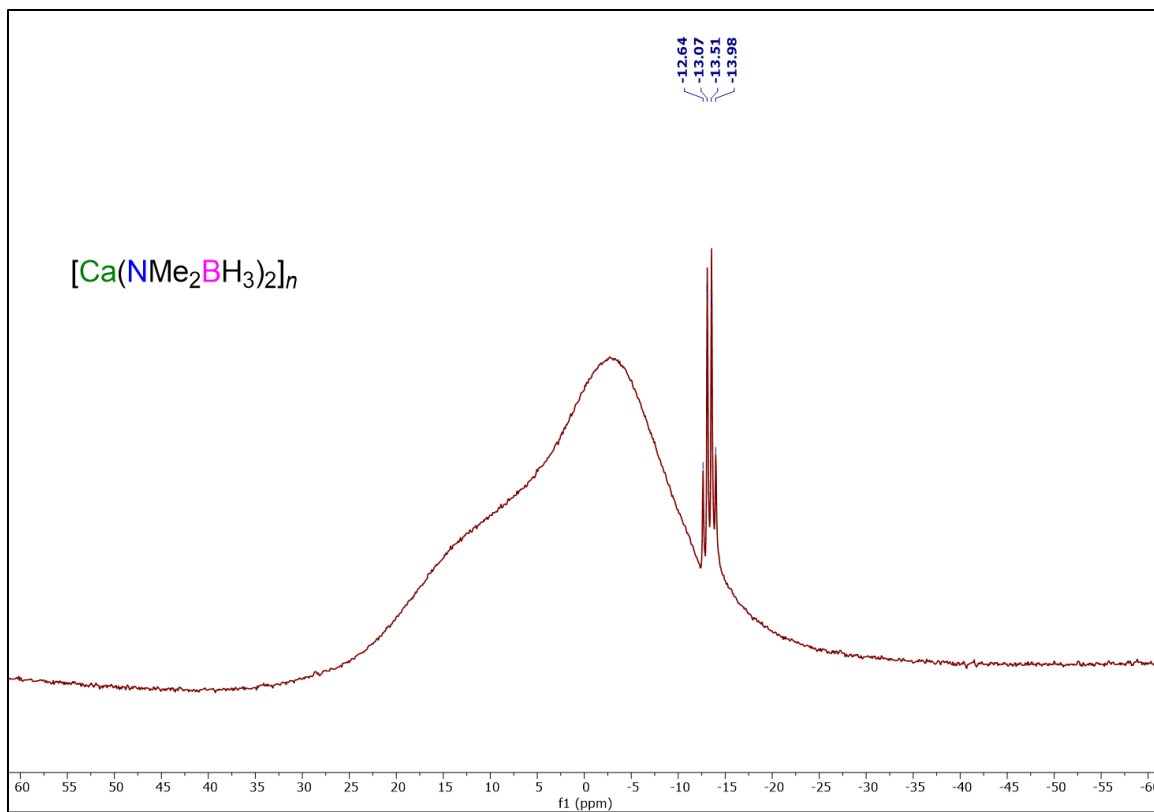


Figure A2.120. ^{11}B NMR spectrum of **6.6** in C_6D_6 at 298 K.

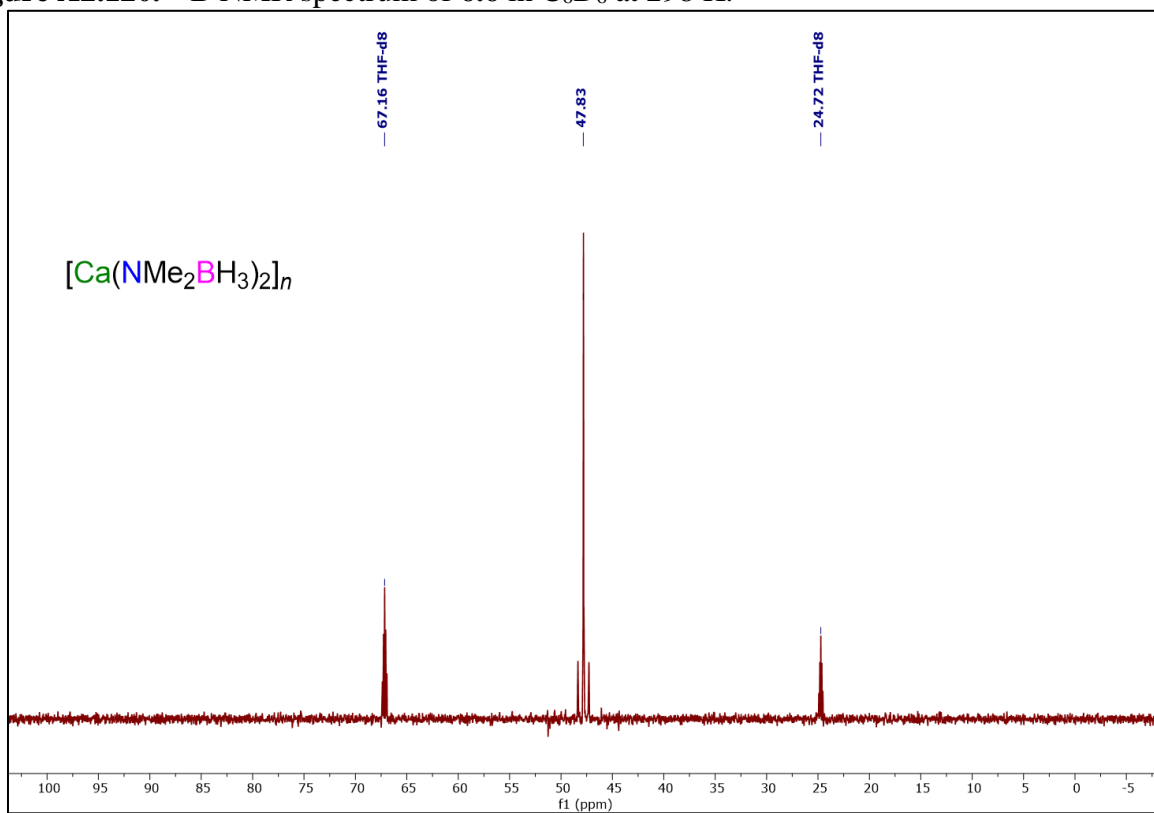


Figure A2.121. ^{13}C NMR spectrum of **6.6** in C_6D_6 at 298 K.

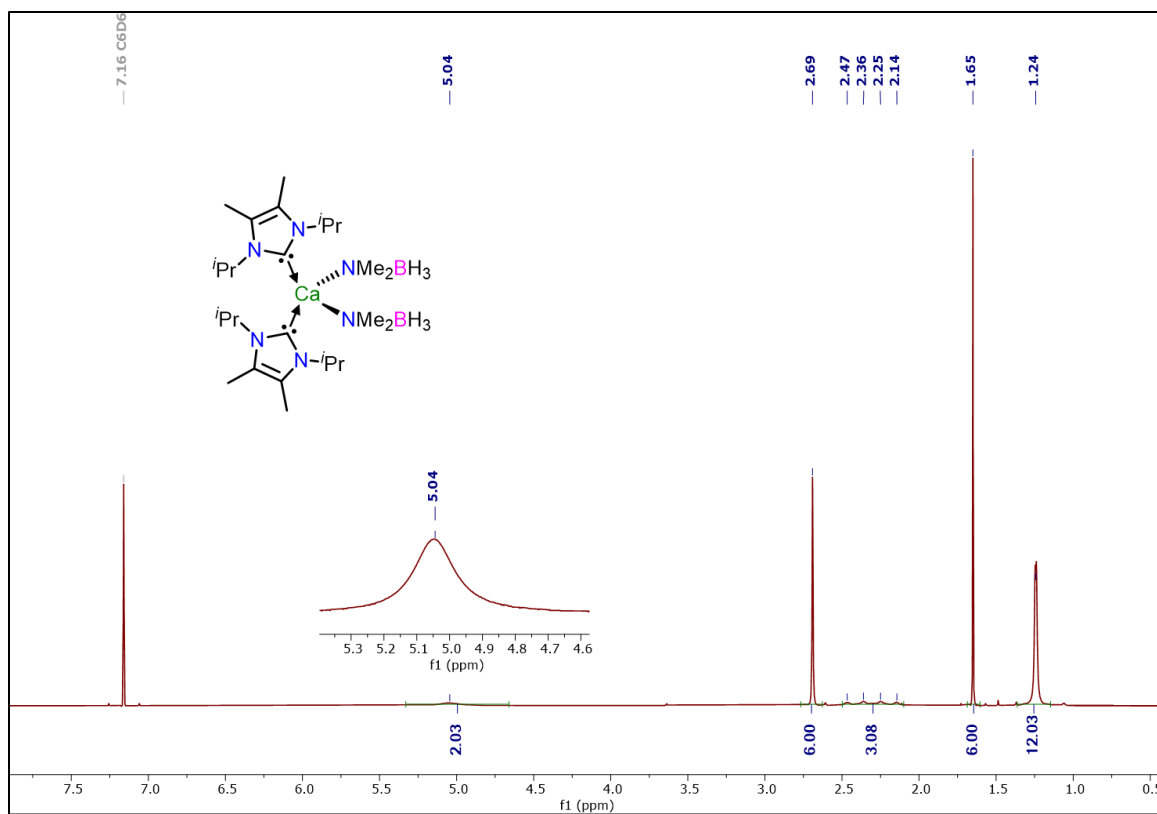


Figure A2.122. ^1H NMR spectrum of **6.7** in C_6D_6 at 298 K.

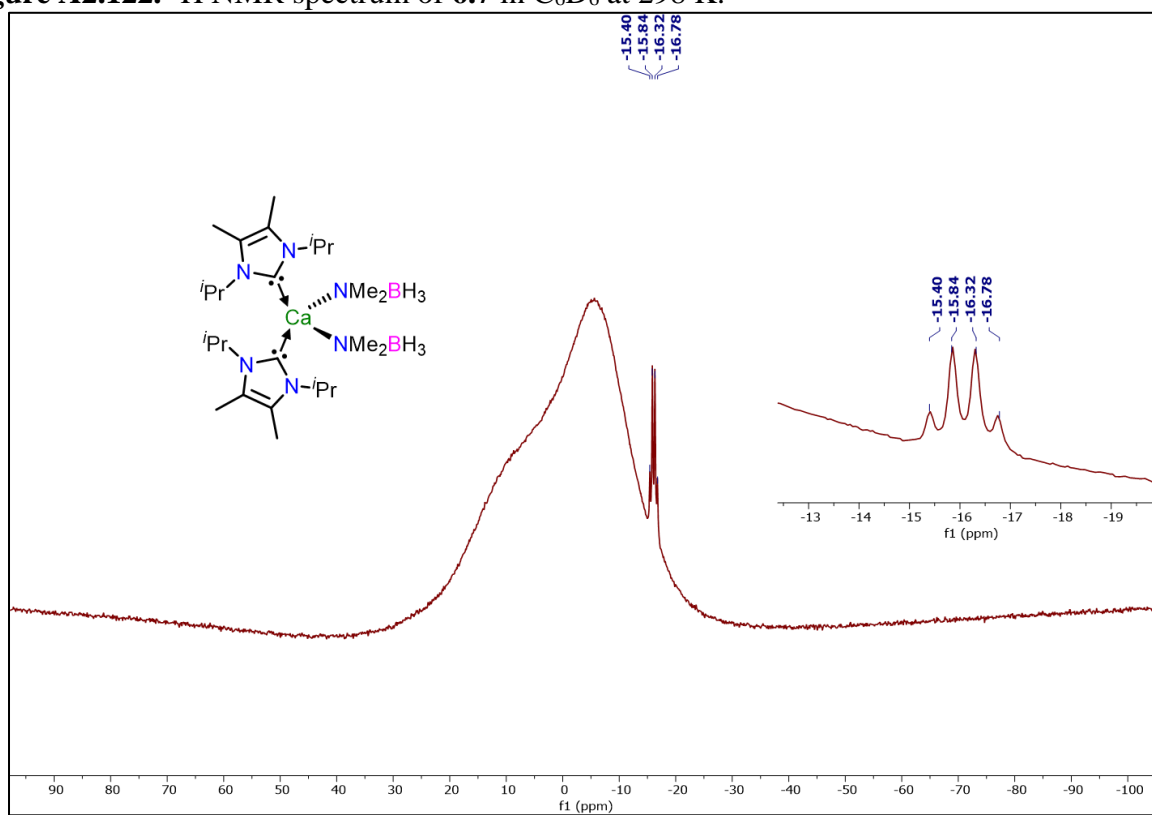


Figure A2.123. ^{11}B NMR spectrum of **6.7** in C_6D_6 at 298 K.

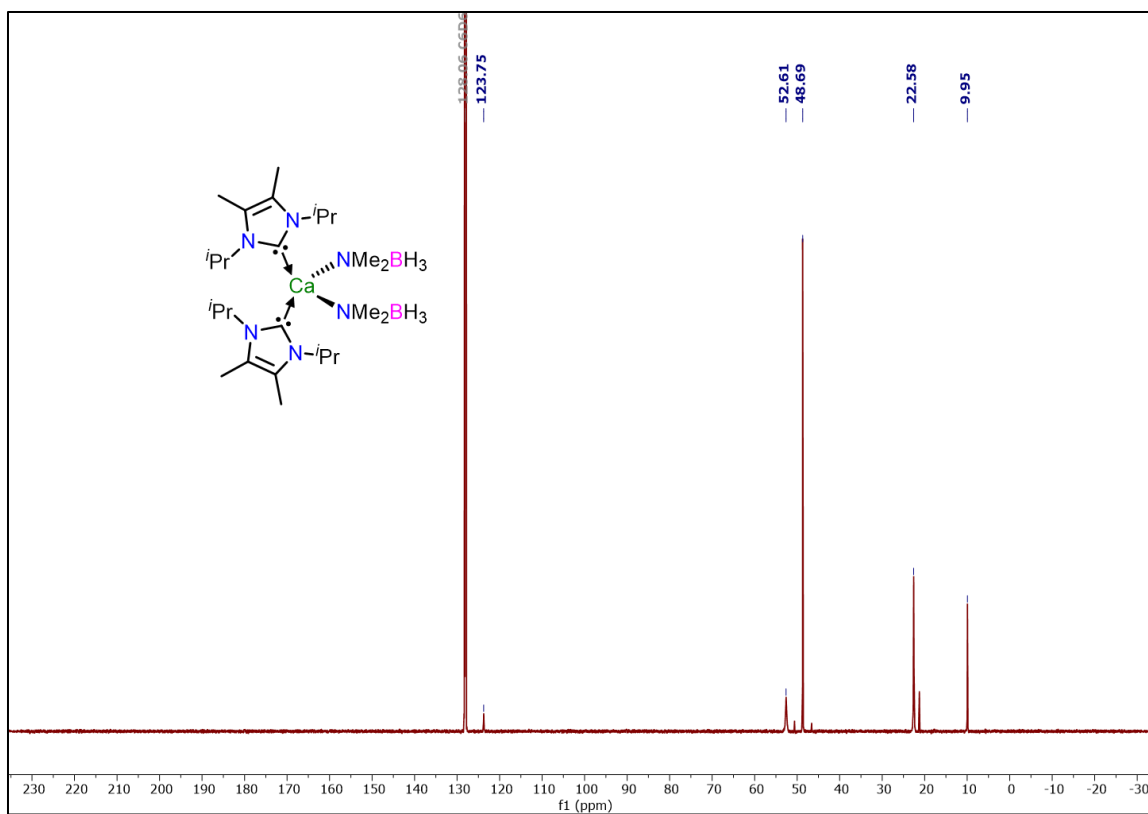


Figure A2.124. ^{13}C NMR spectrum of **6.7** in C_6D_6 at 298 K.

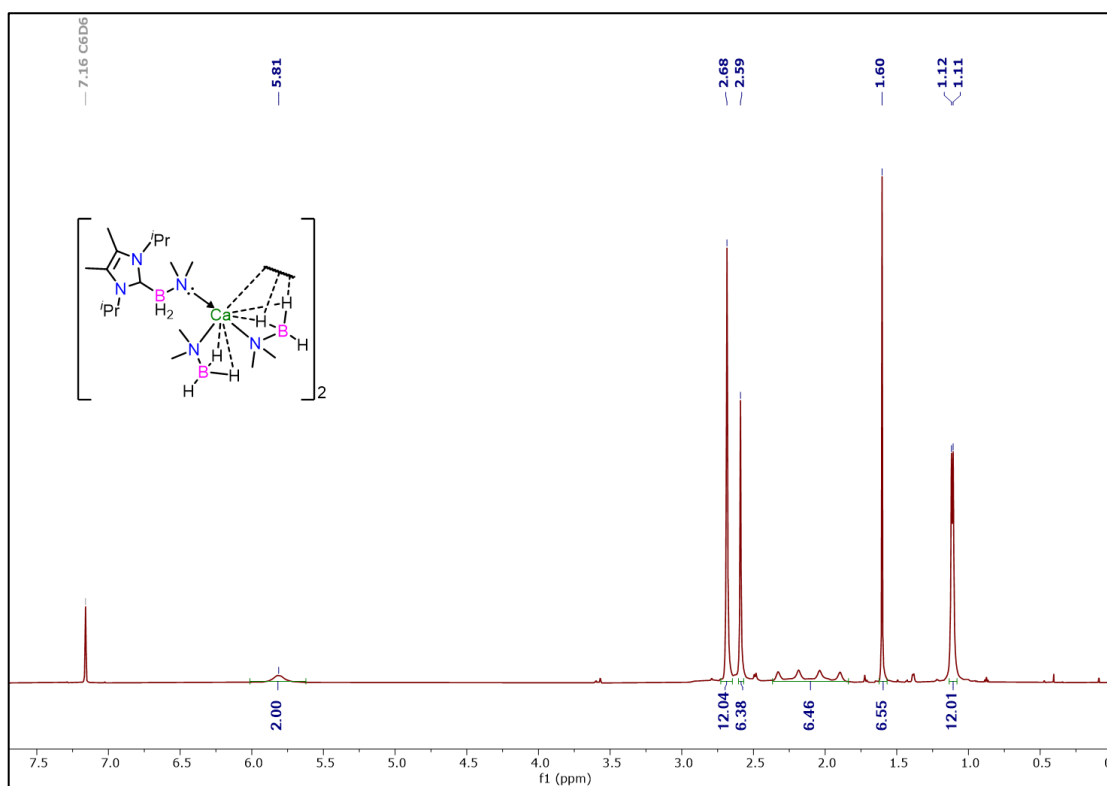


Figure A2.125. ^1H NMR spectrum of **6.8** in C_6D_6 at 298 K.

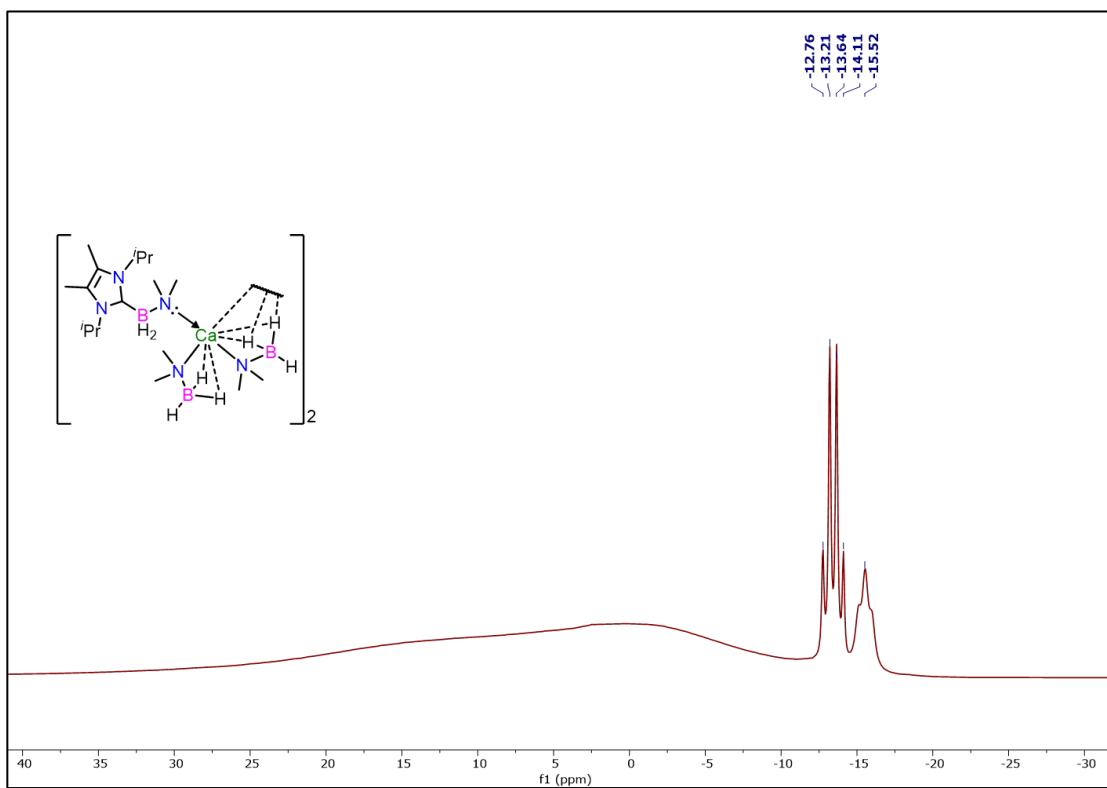


Figure A2.126. ^{11}B NMR spectrum of **6.8** in C_6D_6 at 298 K.

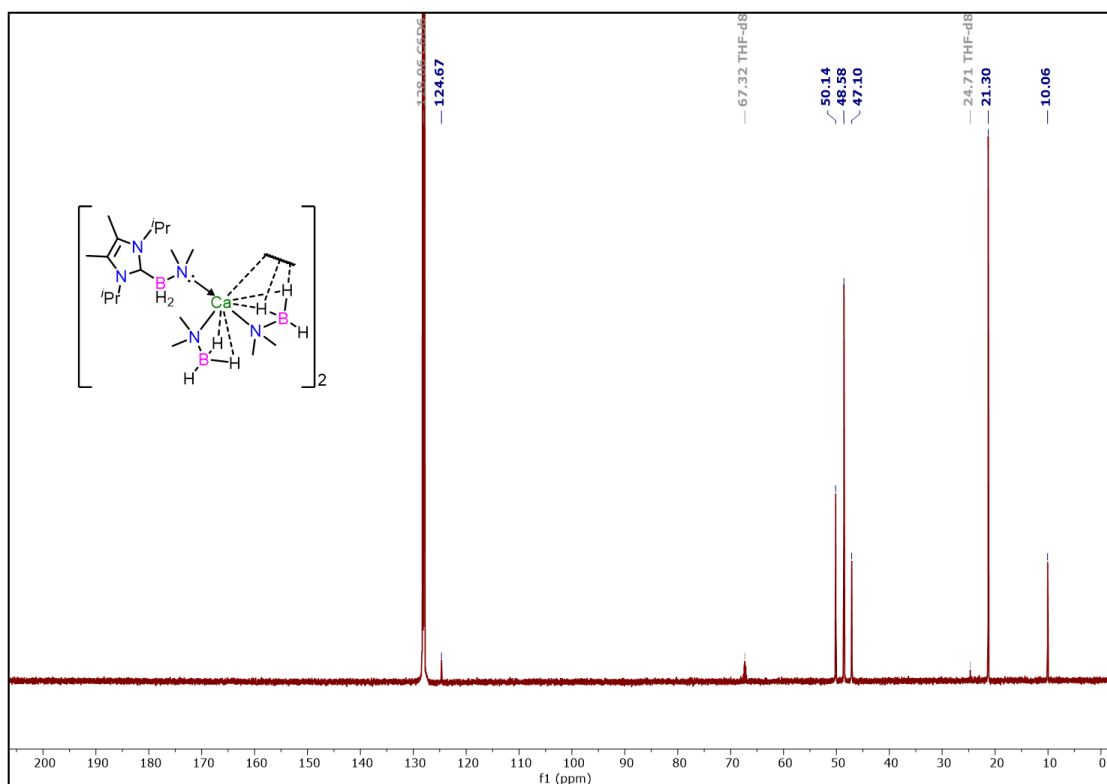


Figure A2.127. ^{13}C NMR spectrum of **6.8** in C_6D_6 at 298 K.

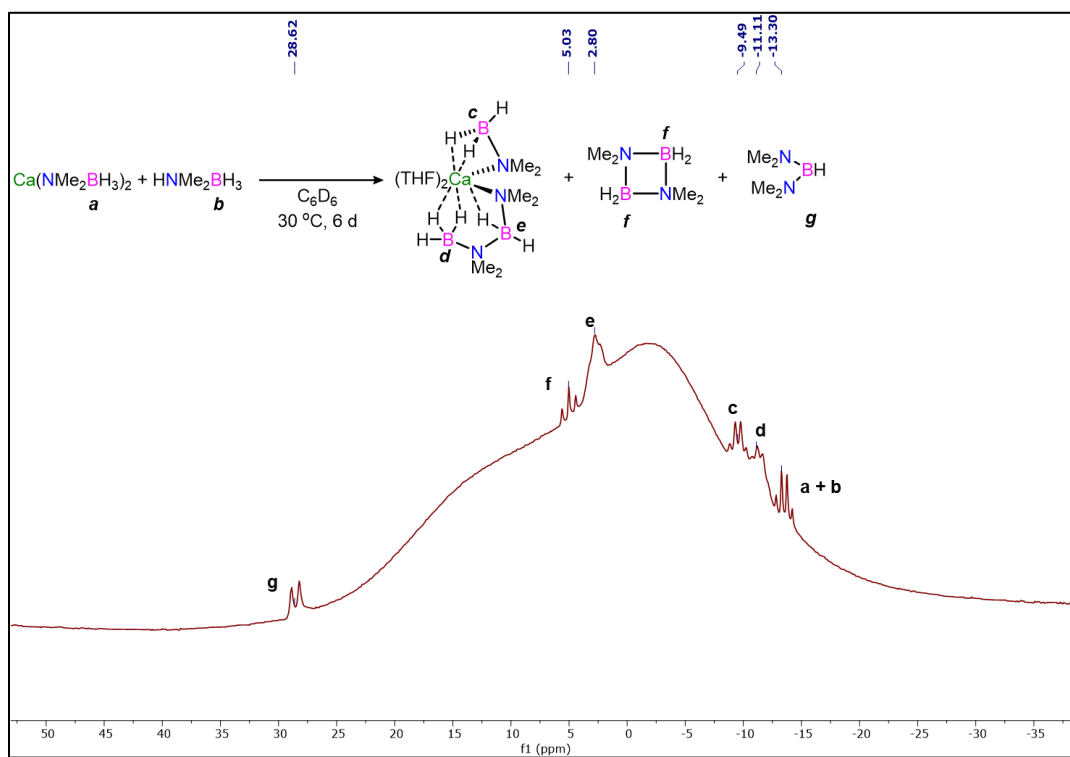


Figure A2.128. ^{11}B NMR spectrum showing the incomplete consumption of **6.7** in the formation of **6.9**.

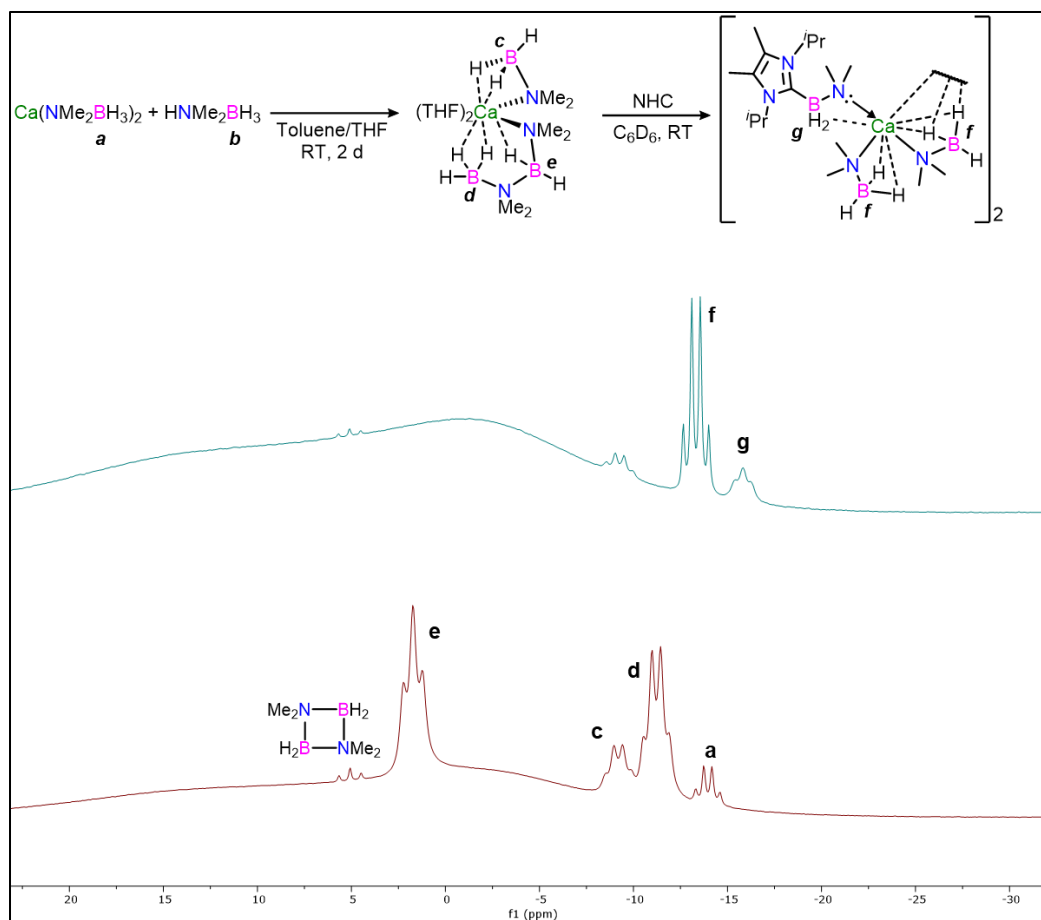


Figure A2.129. Stacked ^{11}B NMR spectrum showing the ^{11}B NMR spectrum of **6.7** (bottom), and its subsequent reaction with NHC (top).

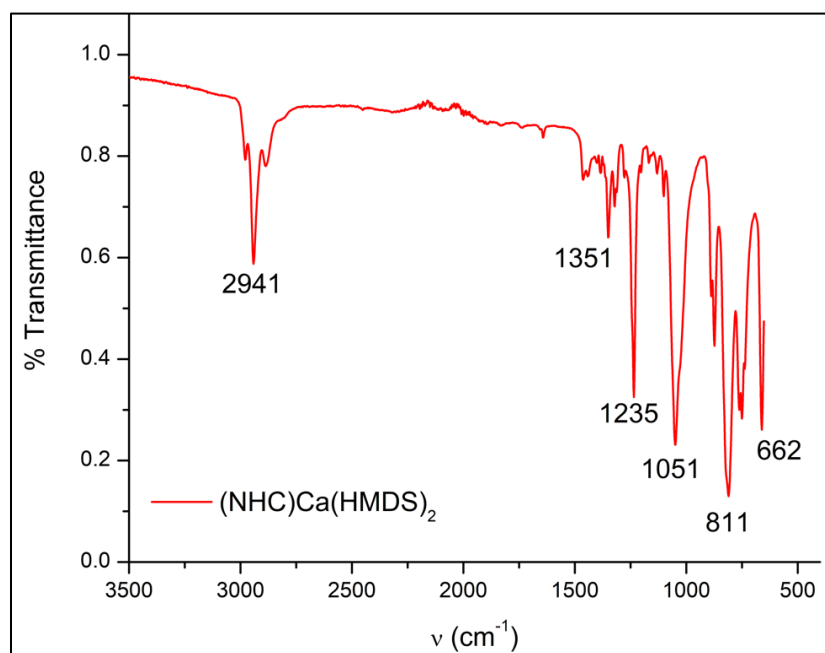


Figure A2.130. Solid-state FTIR spectrum of compound **6.2**.

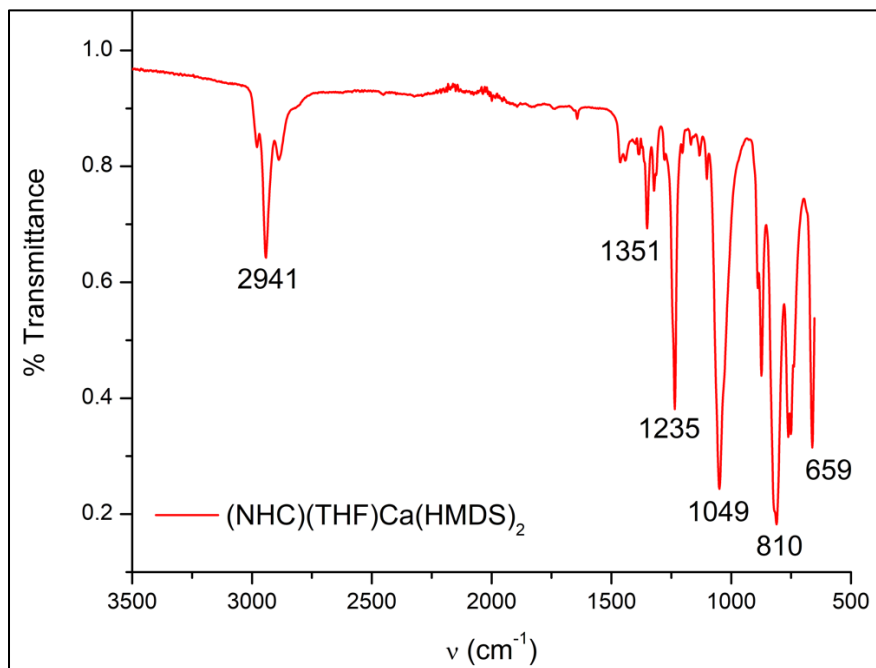


Figure A2.131. Solid-state FTIR spectrum of compound **6.4**.

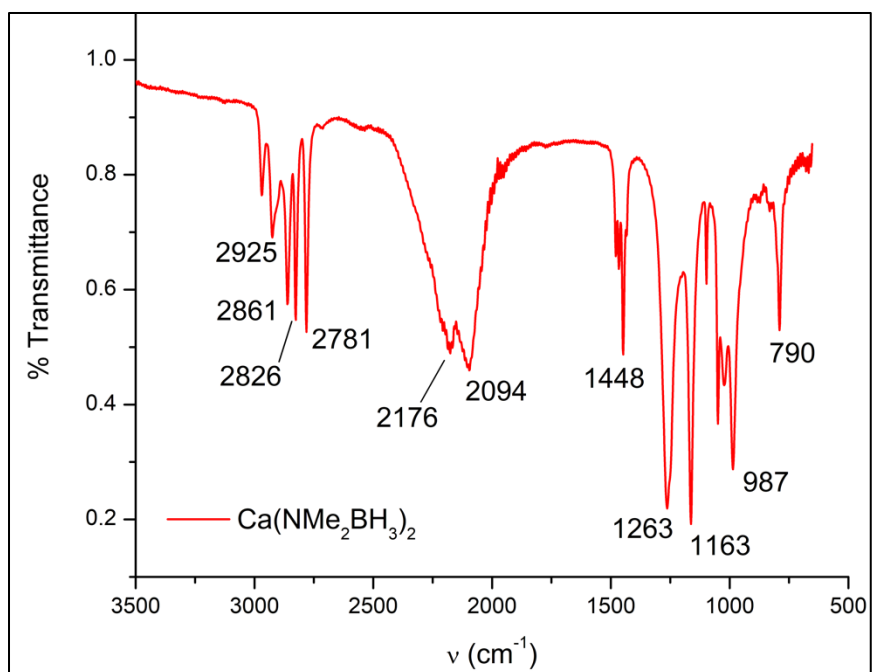


Figure A2.132. Solid-state FTIR spectrum of compound **6.6**.

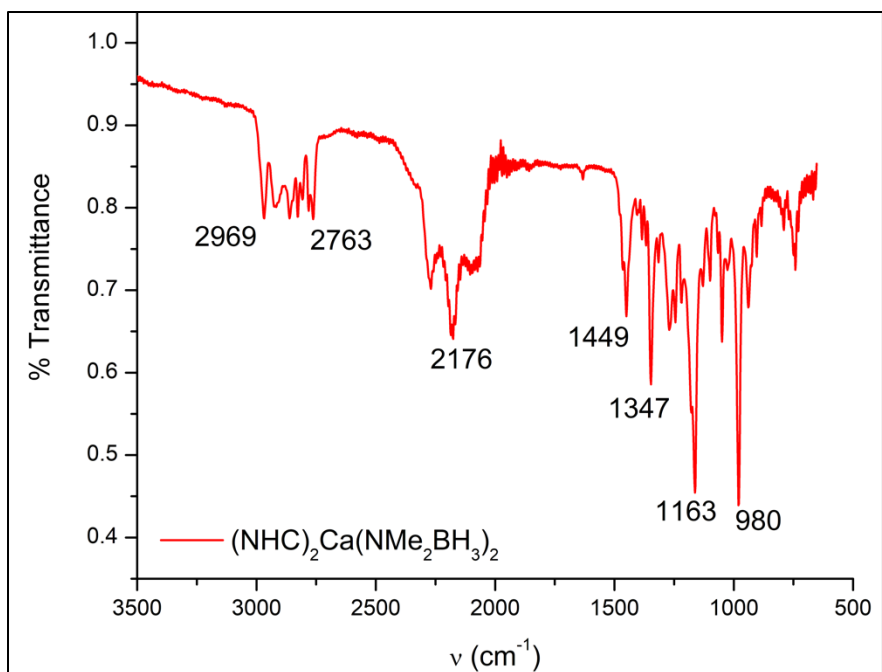


Figure A2.133. Solid-state FTIR spectrum of compound **6.7**.

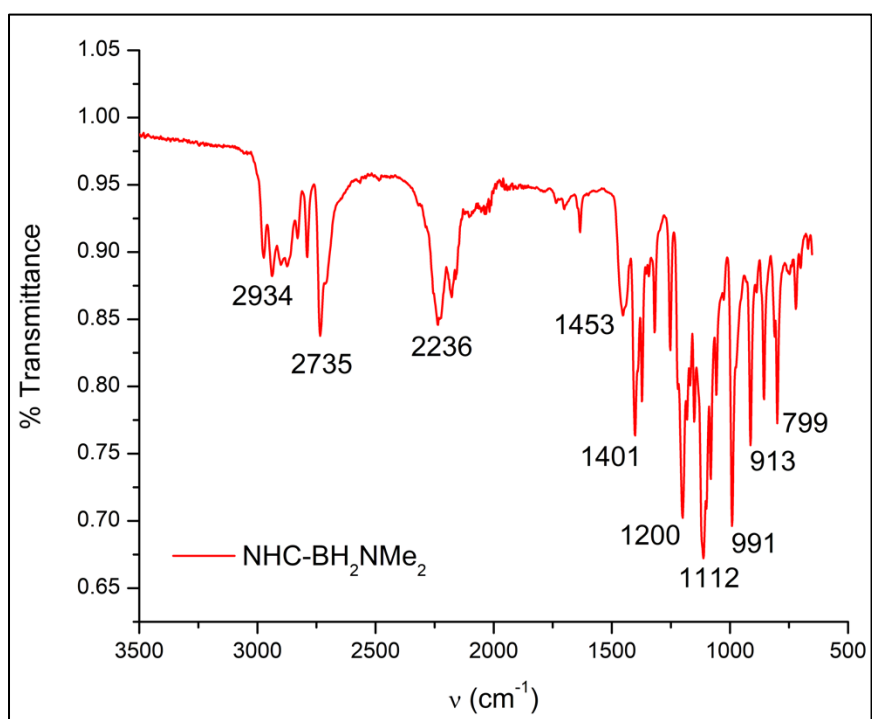


Figure A2.134. Solid-state FTIR spectrum of **NHC-BN**.

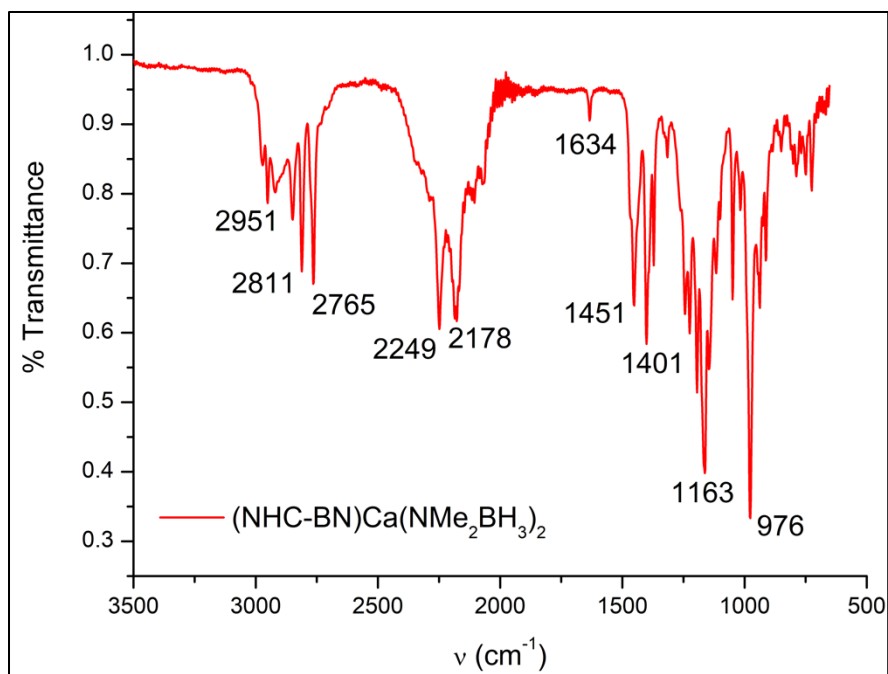


Figure A2.135. Solid-state FTIR spectrum of **6.8**.

Chapter Seven:

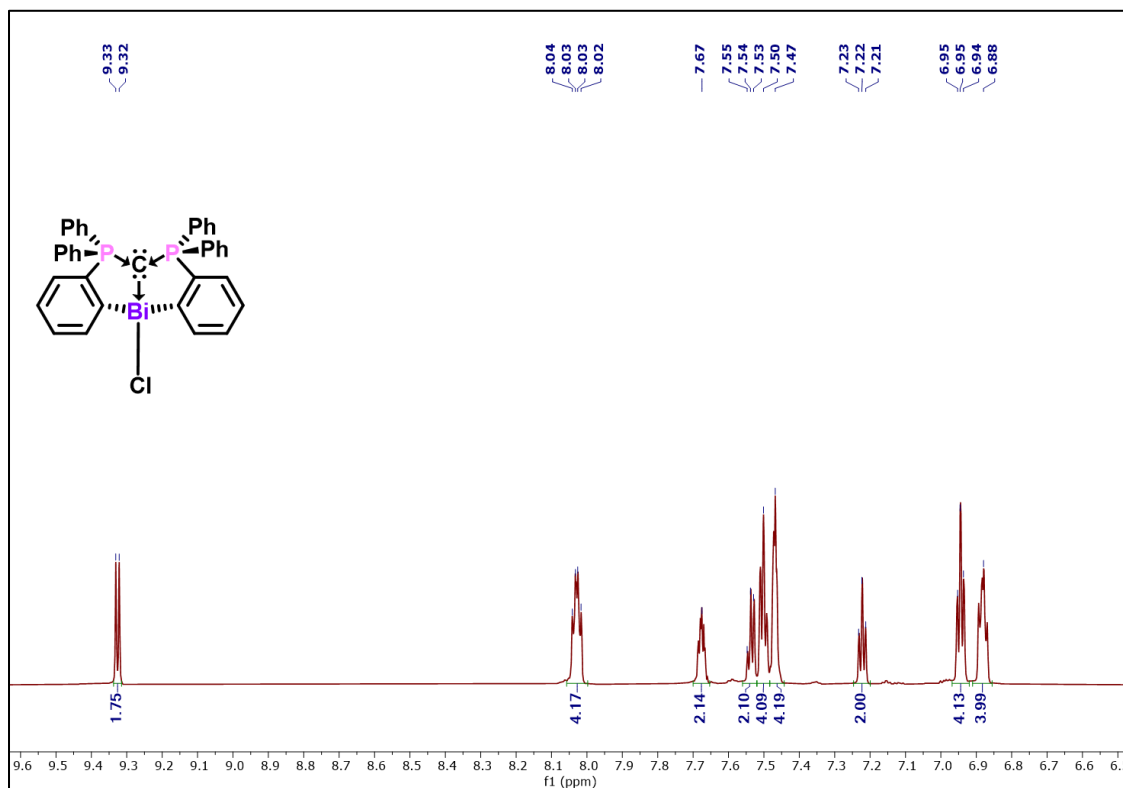


Figure A2.136. ^1H NMR spectrum of **7.1** (800 MHz, CD_2Cl_2 , 298 K).

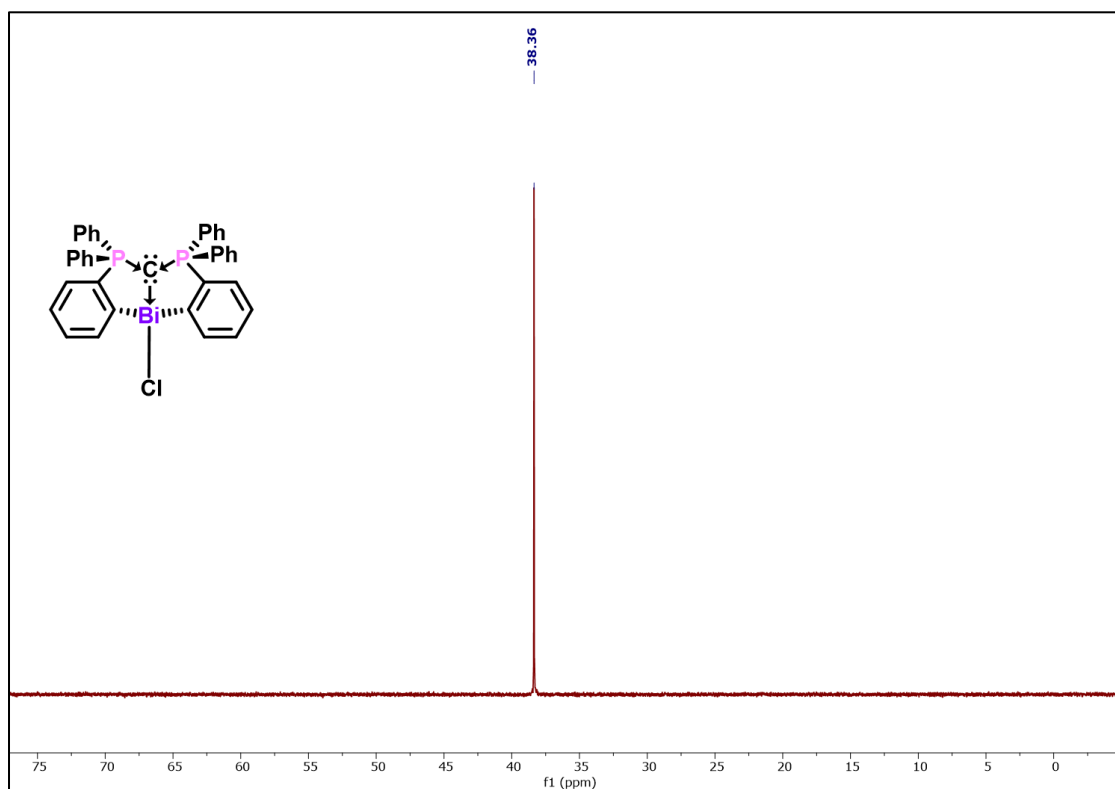


Figure A2.137. ^{31}P NMR spectrum of **7.1** (243 MHz, CD_2Cl_2 , 298 K).

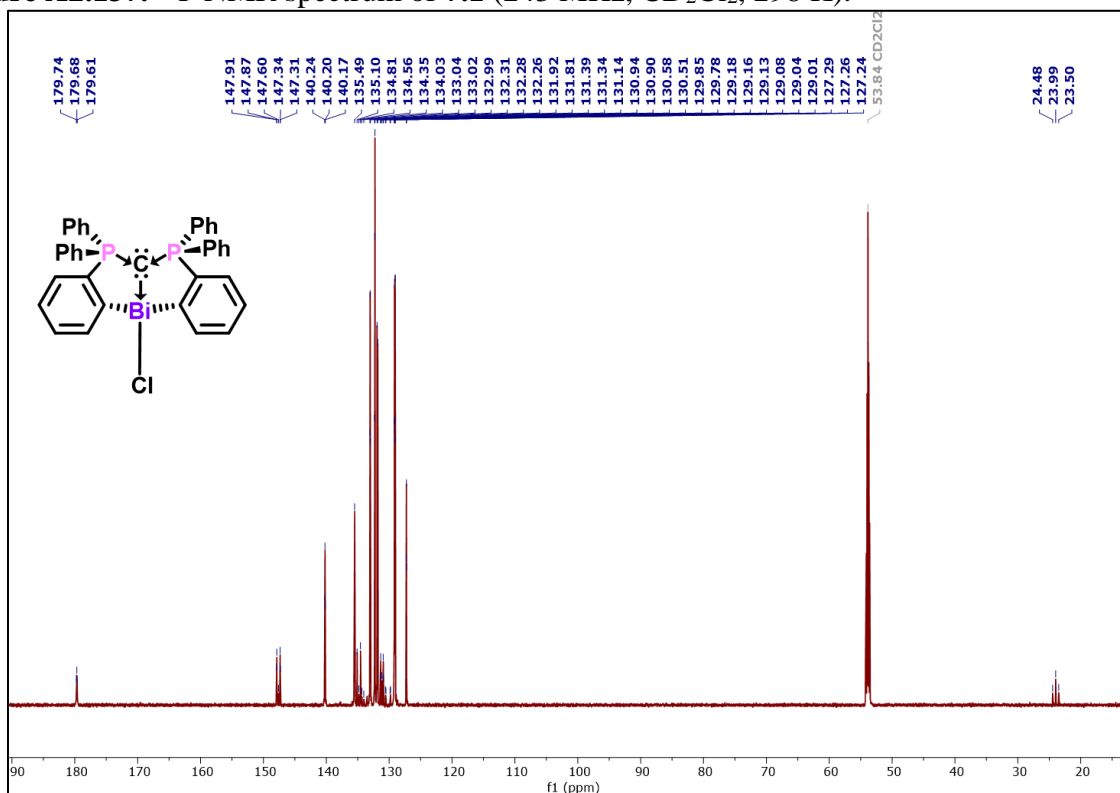


Figure A2.138. ^{13}C NMR spectrum of **7.1** (201 MHz, CD_2Cl_2 , 298 K).

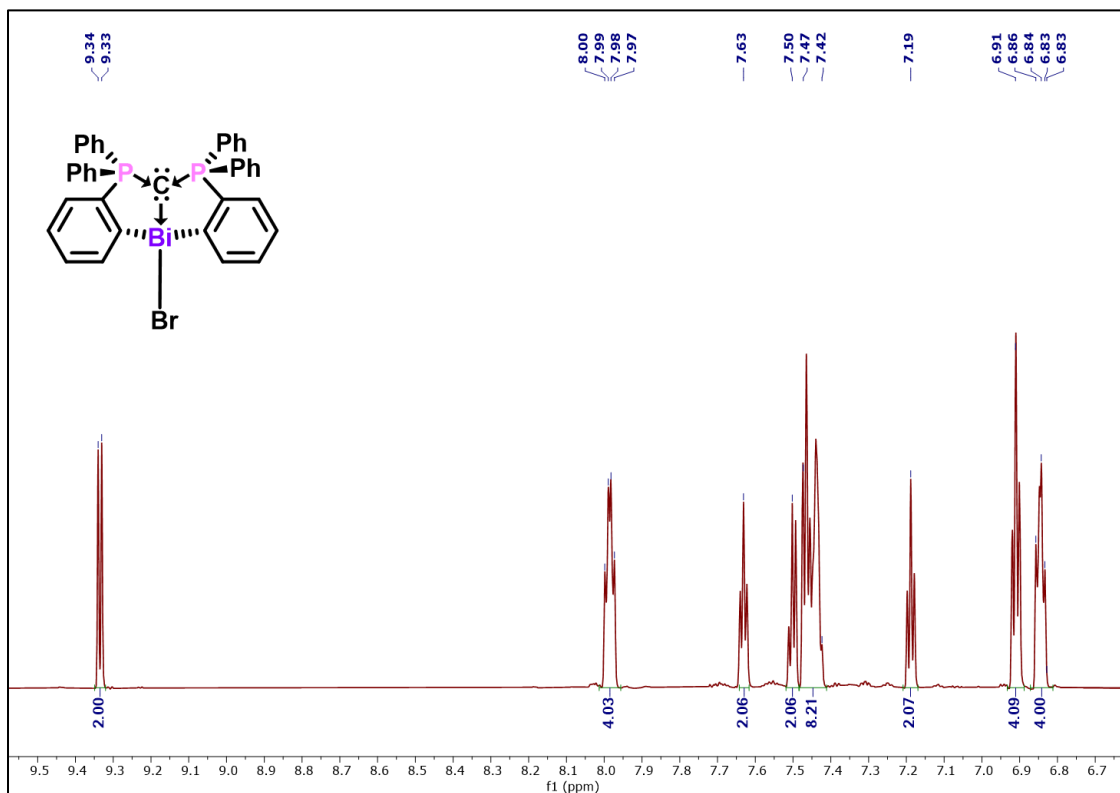


Figure A2.139. ^1H NMR spectrum of **7.2** (800 MHz, CD_2Cl_2 , 298 K).

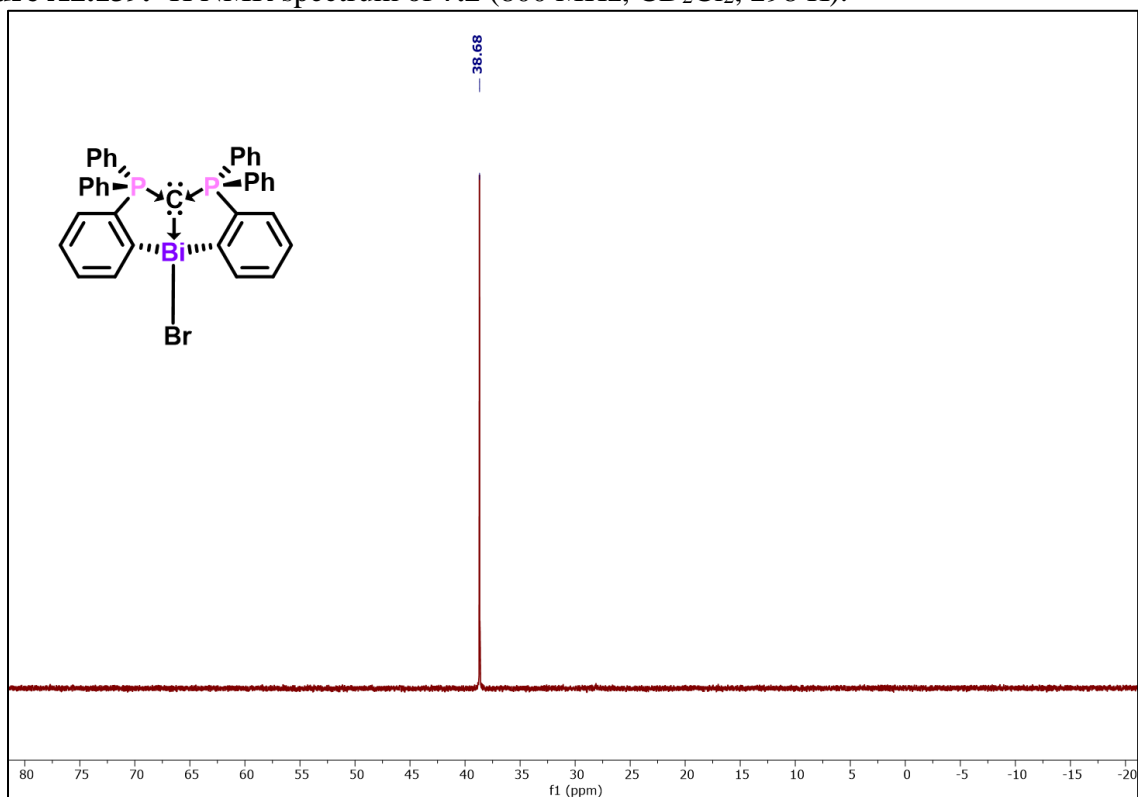


Figure A2.140. ^{31}P NMR spectrum of **7.2** (243 MHz, CD_2Cl_2 , 298 K).

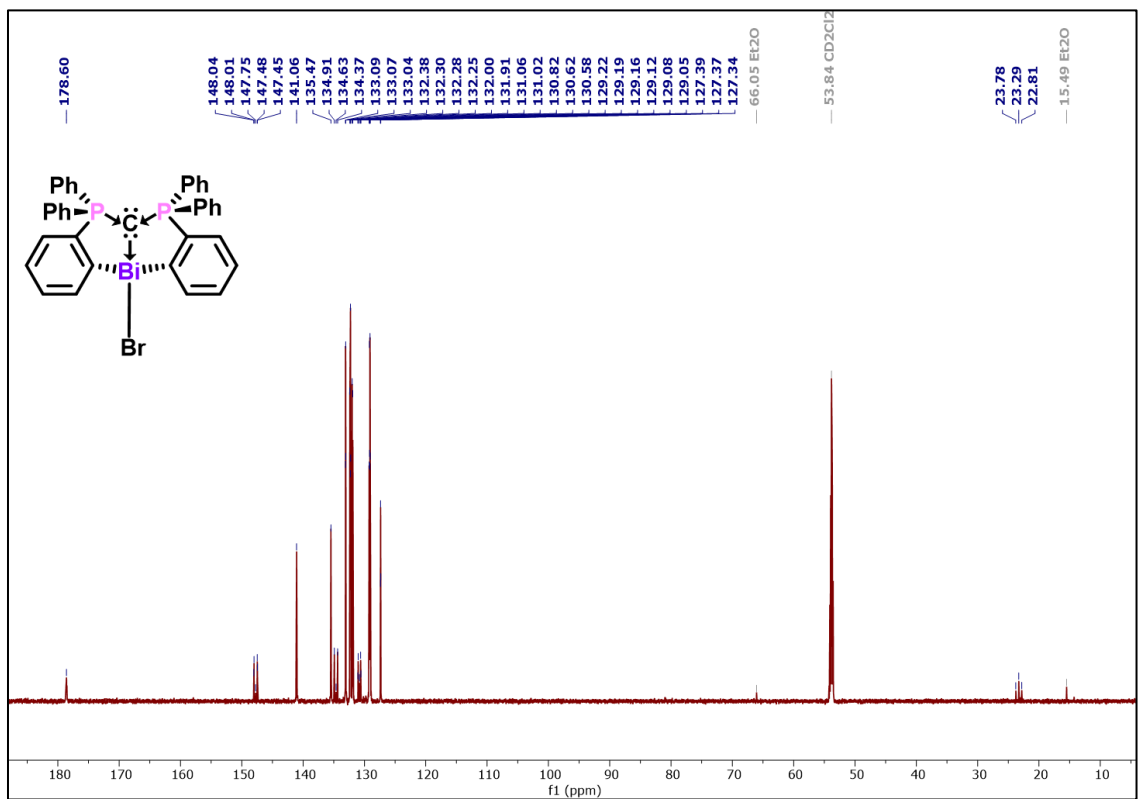


Figure A2.141. ^{13}C NMR spectrum of **7.2** (201 MHz, CD_2Cl_2 , 298 K).

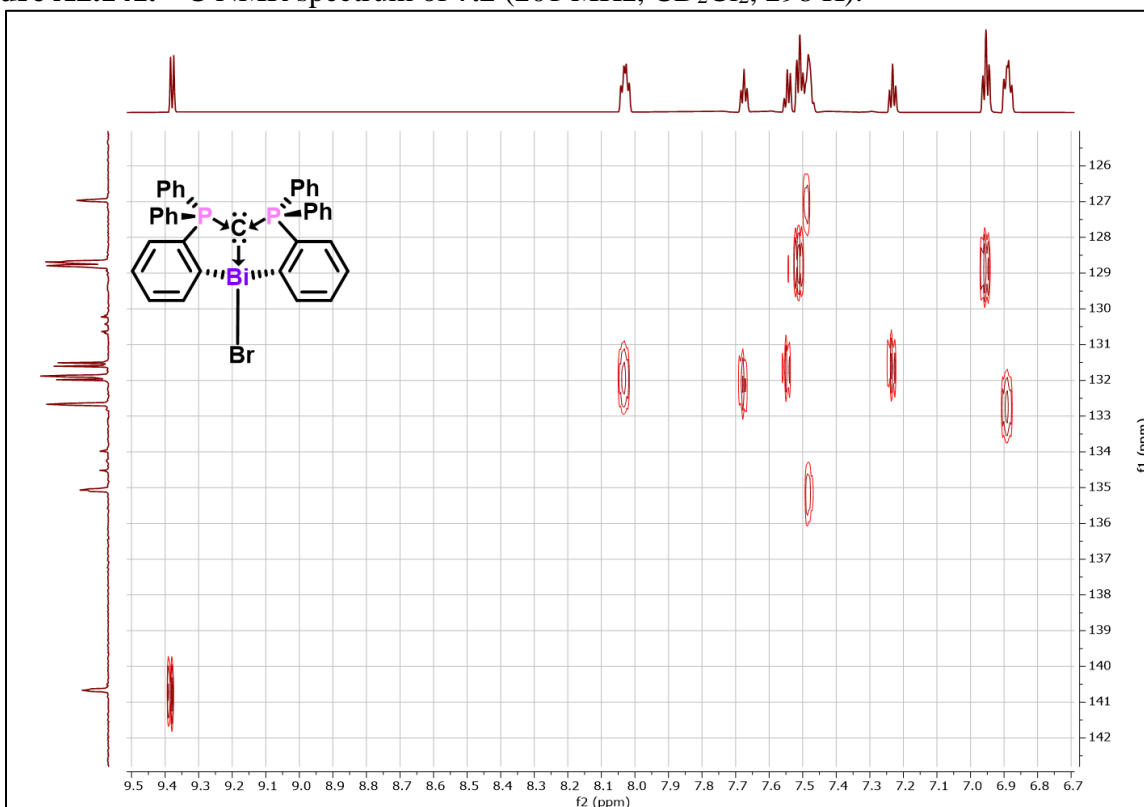


Figure A2.142. ^1H - ^{13}C HSQC NMR spectrum of **7.2**.

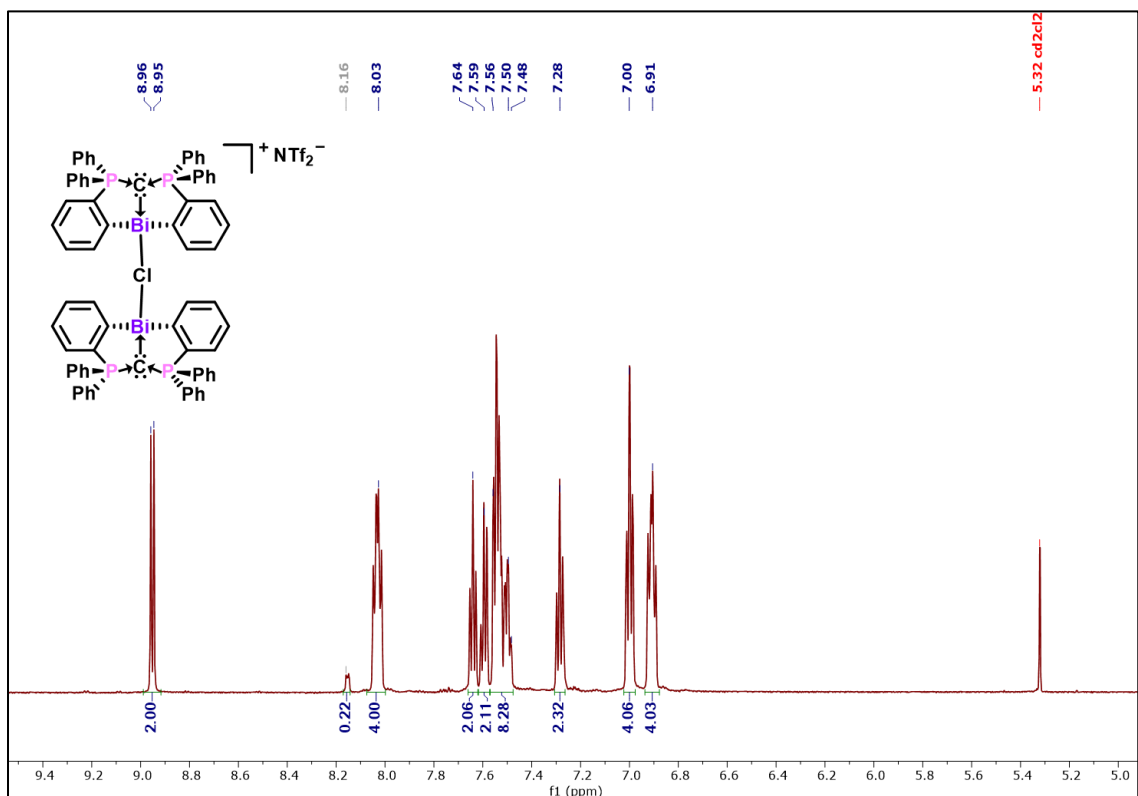


Figure A2.143. ^1H NMR spectrum of **7.3** $[\text{NTf}_2]$ (800 MHz, CD_2Cl_2 , 298 K).

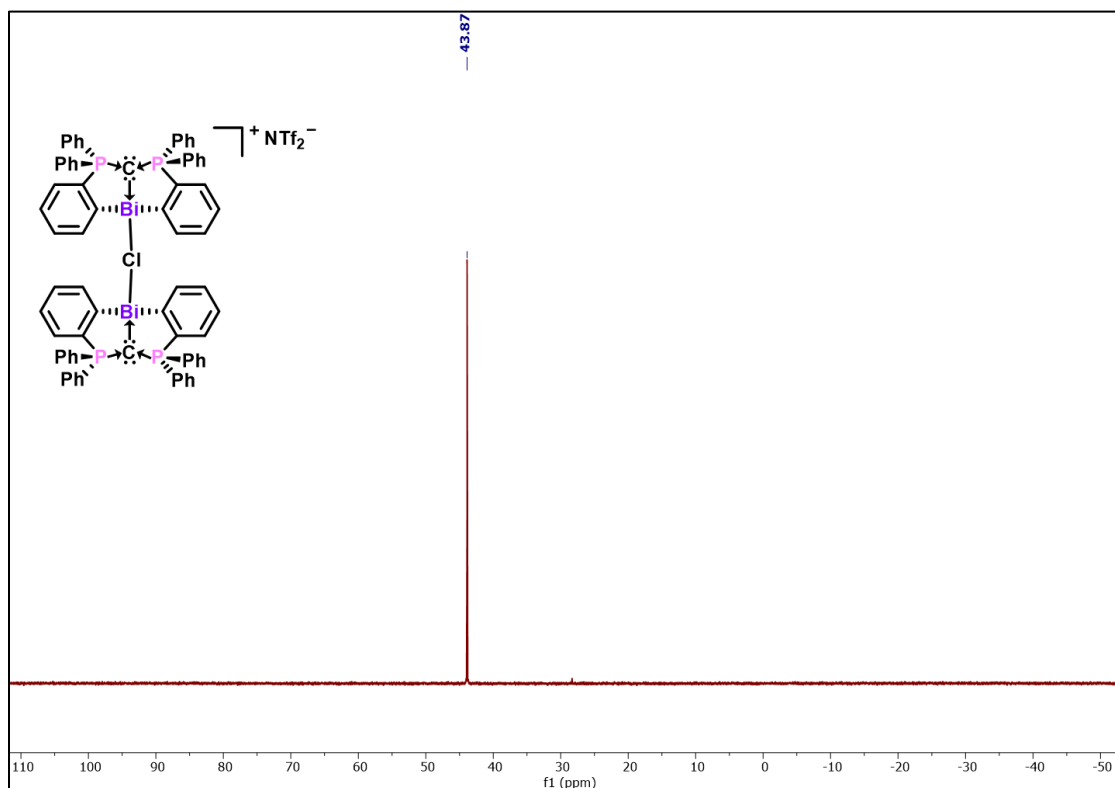


Figure A2.144. ^{31}P NMR spectrum of **7.3** $[\text{NTf}_2]$ (243 MHz, CD_2Cl_2 , 298 K).

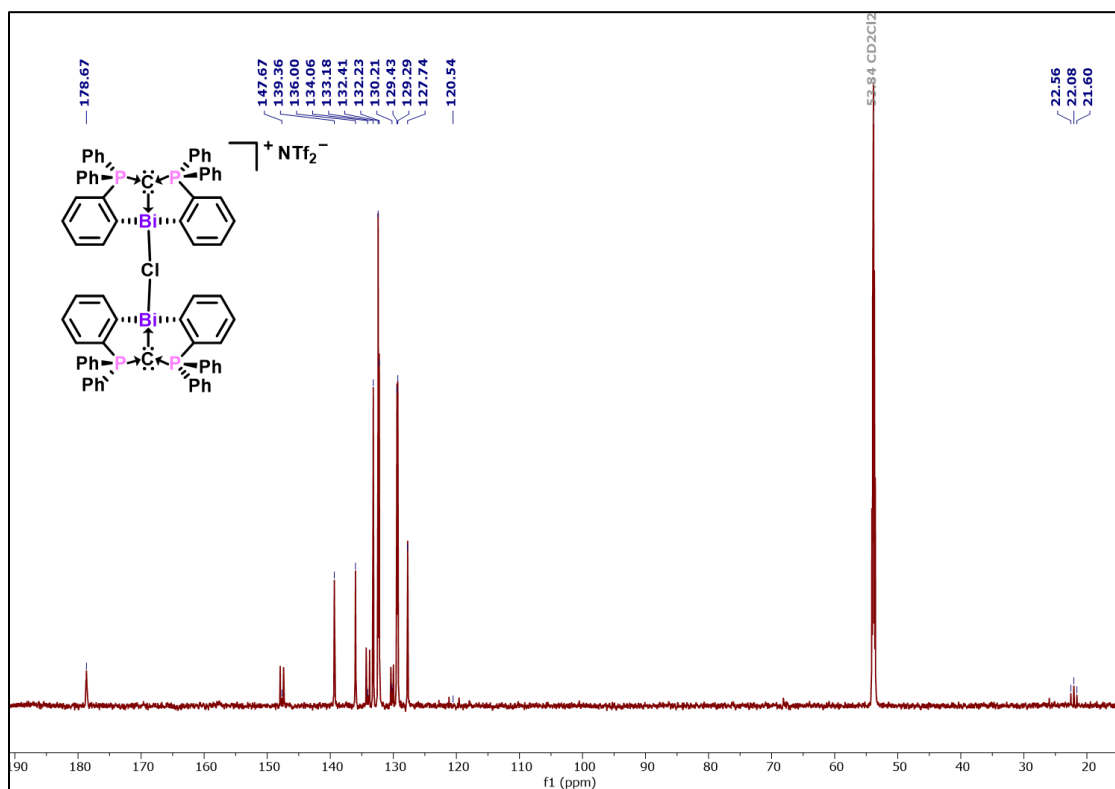


Figure A2.145. ^{13}C NMR spectrum of $7.3[\text{NTf}_2]$ (201 MHz, CD_2Cl_2 , 298 K).

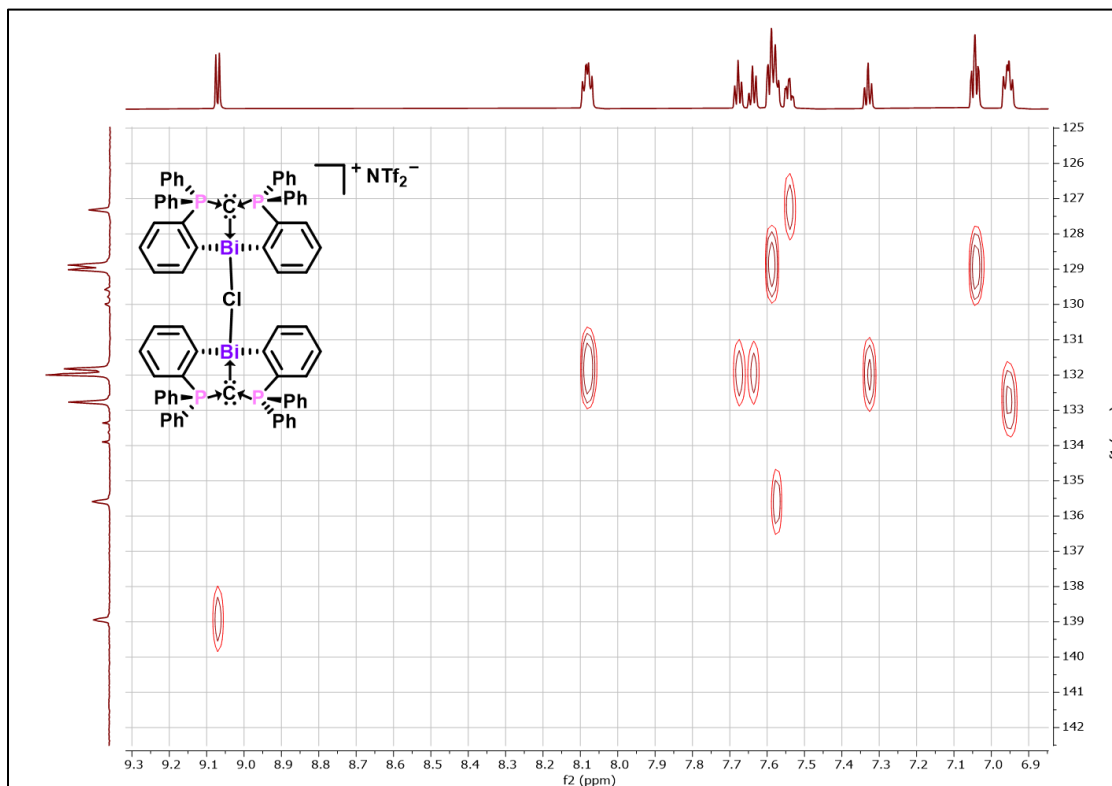


Figure A2.146. ^1H - ^{13}C HSQC NMR spectrum of $7.3[\text{NTf}_2]$.

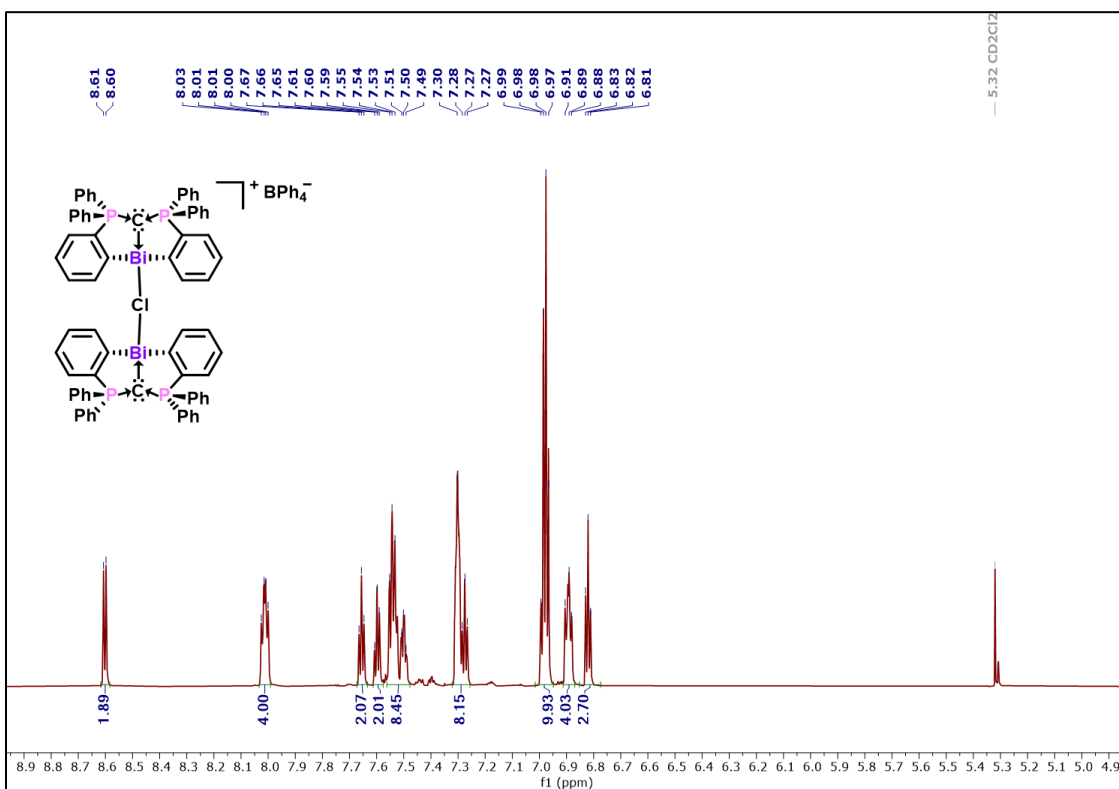


Figure A2.147. ^1H NMR spectrum of **7.3**[BPh $_4$] (800 MHz, CD $_2$ Cl $_2$, 298 K).

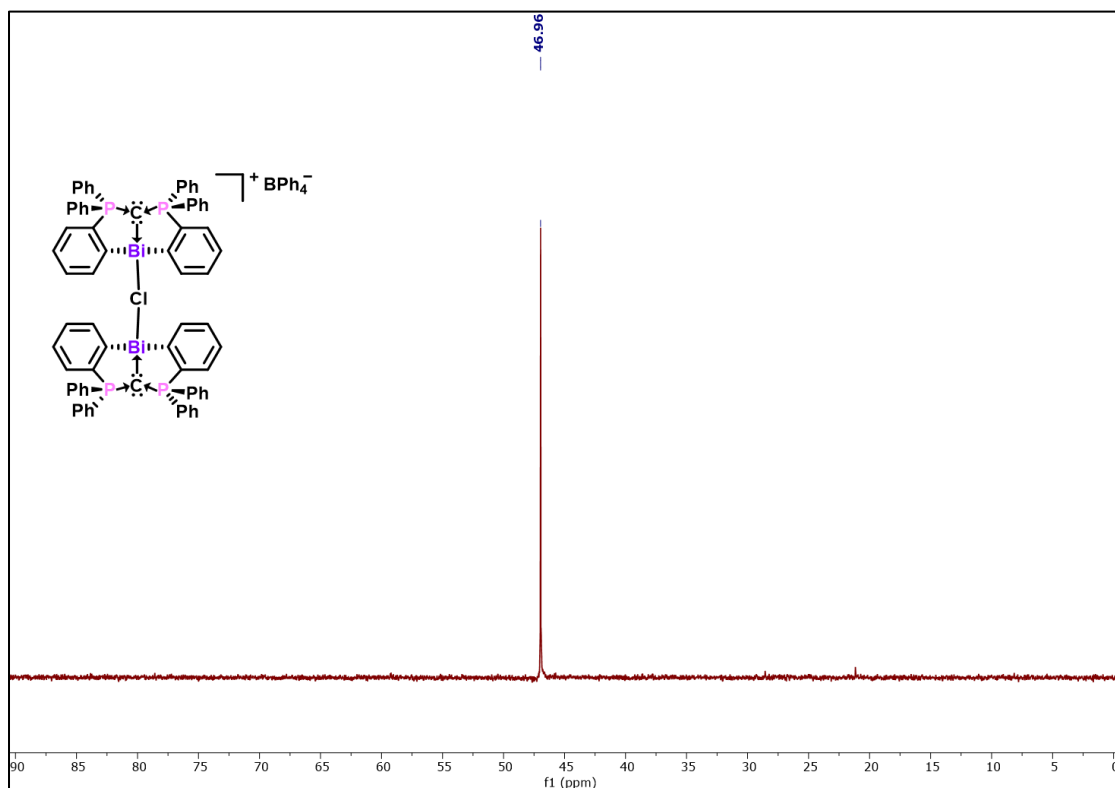


Figure A2.148. ^{31}P NMR spectrum of **7.3**[BPh $_4$] (243 MHz, CD $_2$ Cl $_2$, 298 K).

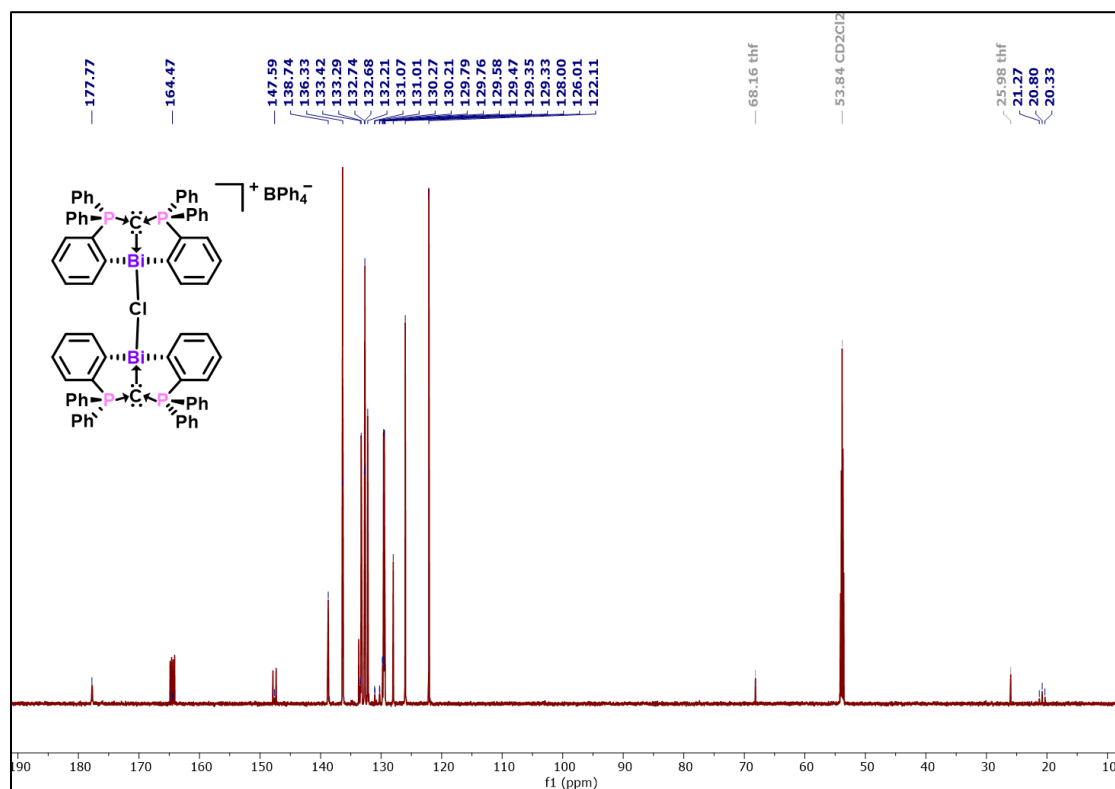


Figure A2.149. ^{13}C NMR spectrum of **7.3**[BPh $_4$] (201 MHz, CD $_2$ Cl $_2$, 298 K).

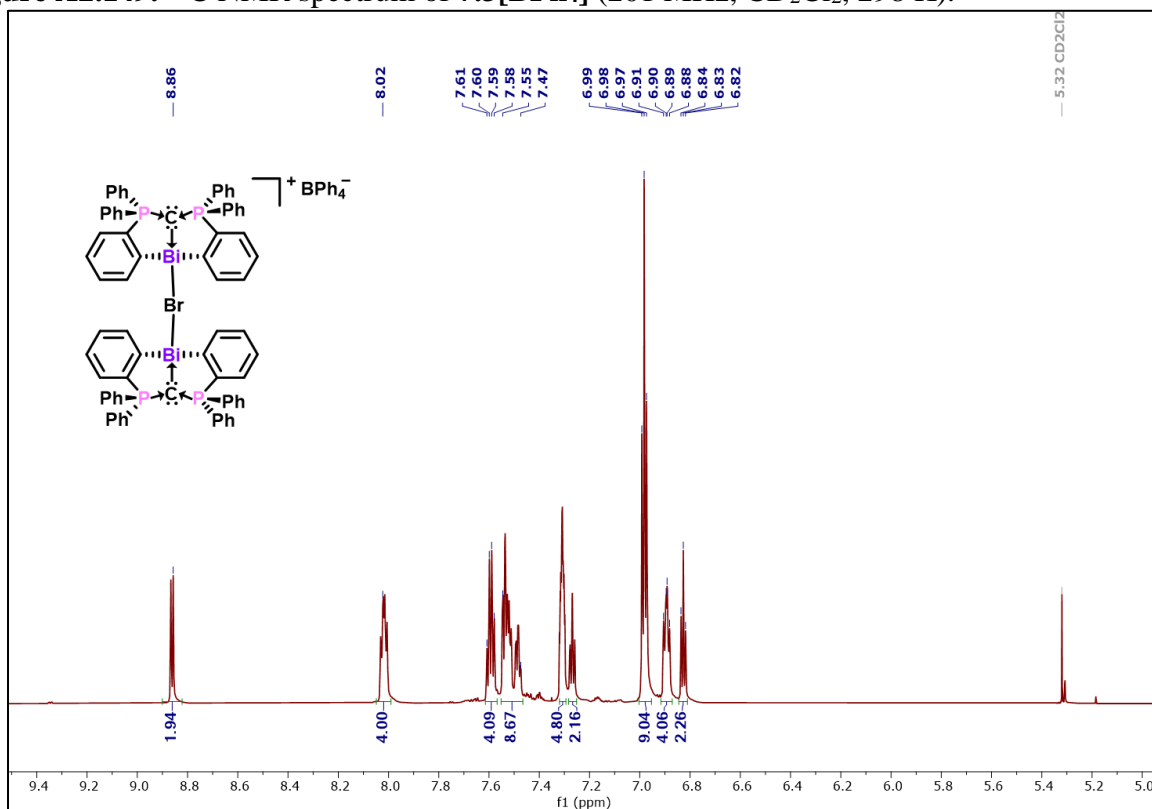


Figure A2.150. ^1H NMR spectrum of **7.4**[BPh $_4$] (800 MHz, CD $_2$ Cl $_2$, 298 K).

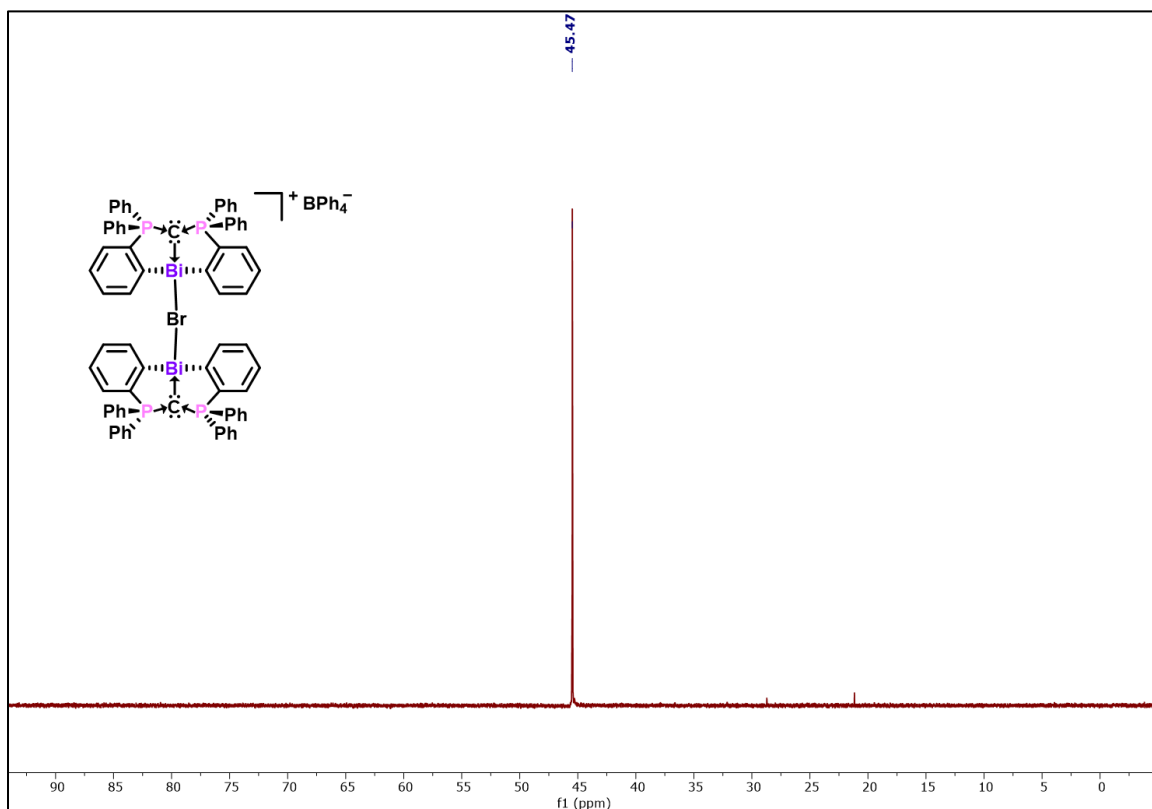


Figure A2.151. ^{31}P NMR spectrum of **7.4**[BPh $_4$] (243 MHz, CD $_2$ Cl $_2$, 298 K).

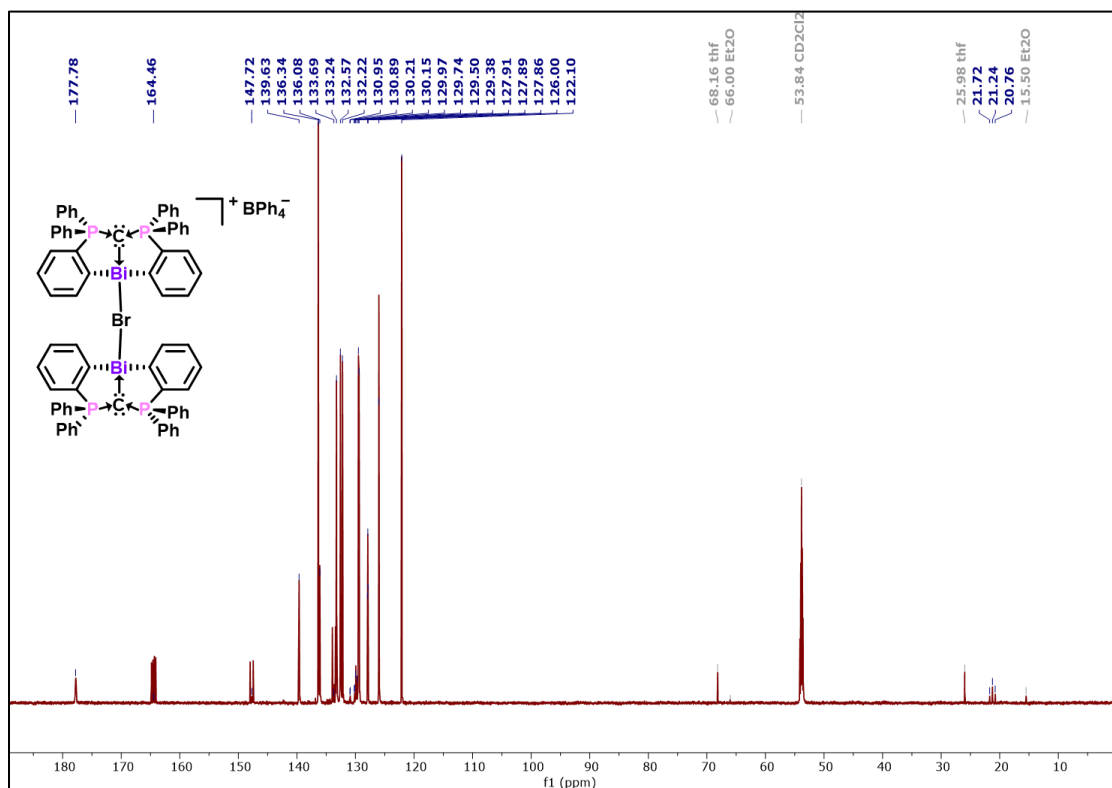


Figure A2.152. ^{13}C NMR spectrum of **7.4**[BPh $_4$] (201 MHz, CD $_2$ Cl $_2$, 298 K).

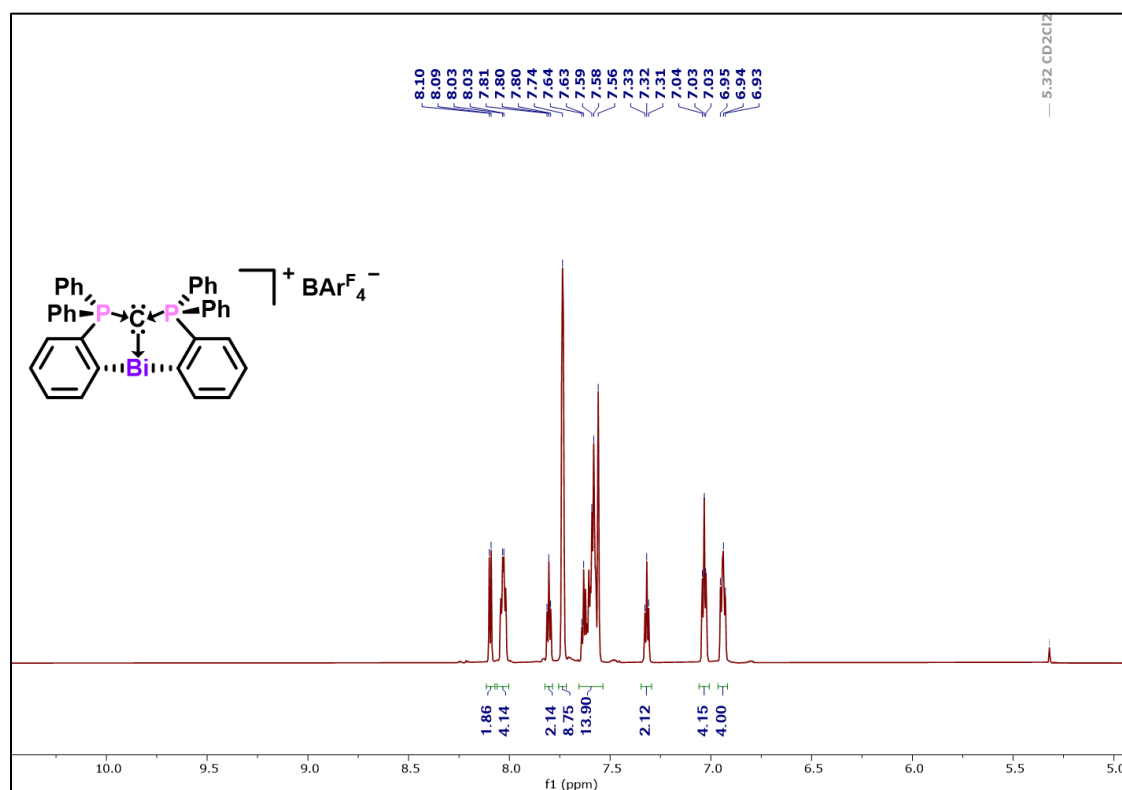


Figure A2.153. ^1H NMR spectrum of $7.5[\text{BAr}^{\text{F}}_4]$ (800 MHz, CD_2Cl_2 , 298 K).

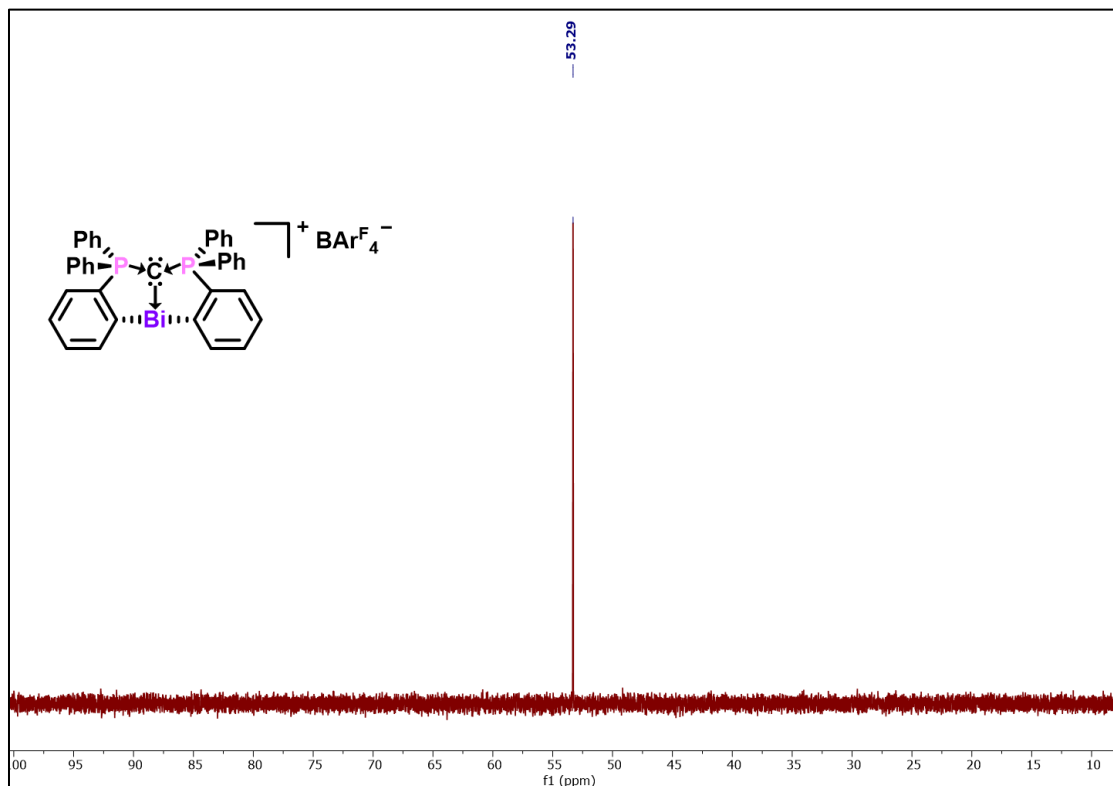


Figure A2.154. ^{31}P NMR spectrum of $7.5[\text{BAr}^{\text{F}}_4]$ (243 MHz, CD_2Cl_2 , 298 K).

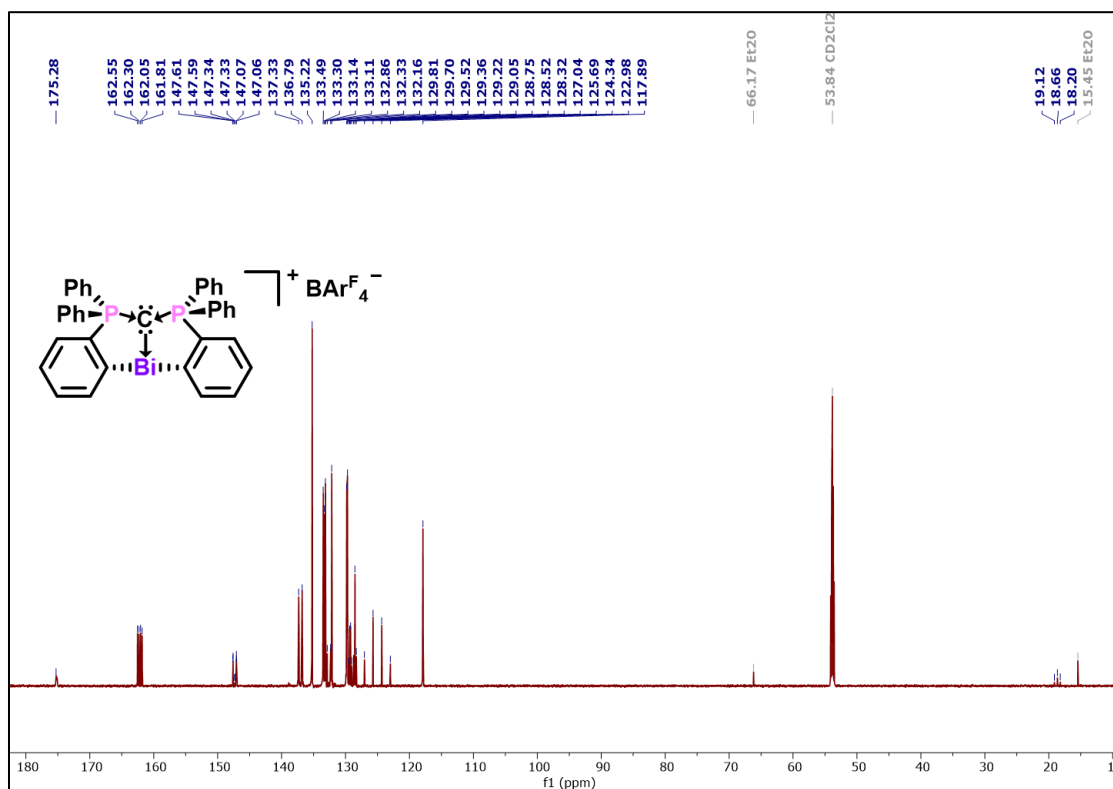


Figure A2.155. ^{13}C NMR spectrum of $7.5[\text{BAr}^{\text{F}}_4]$ (201 MHz, CD_2Cl_2 , 298 K).

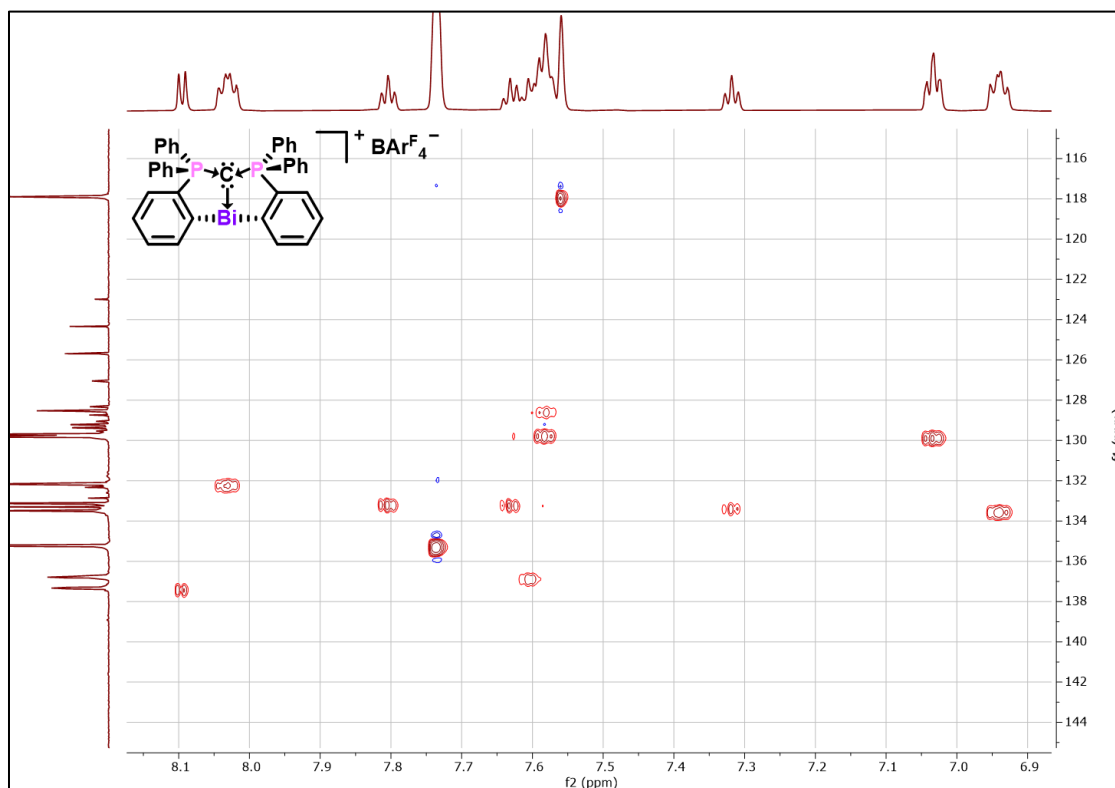


Figure A2.156. ^1H - ^{13}C HSQC NMR spectrum of $7.5[\text{BAr}^{\text{F}}_4]$.

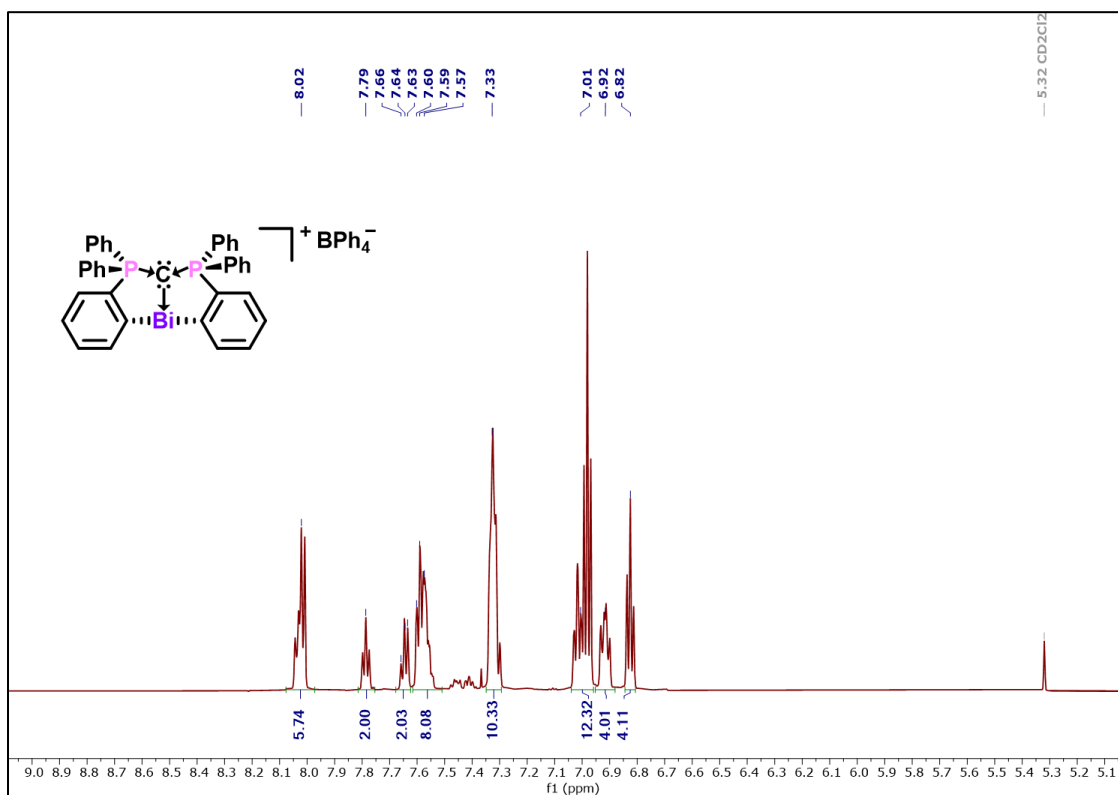


Figure A2.157. ^1H NMR spectrum of $7.5[\text{BPh}_4]$ (800 MHz, CD_2Cl_2 , 298 K).

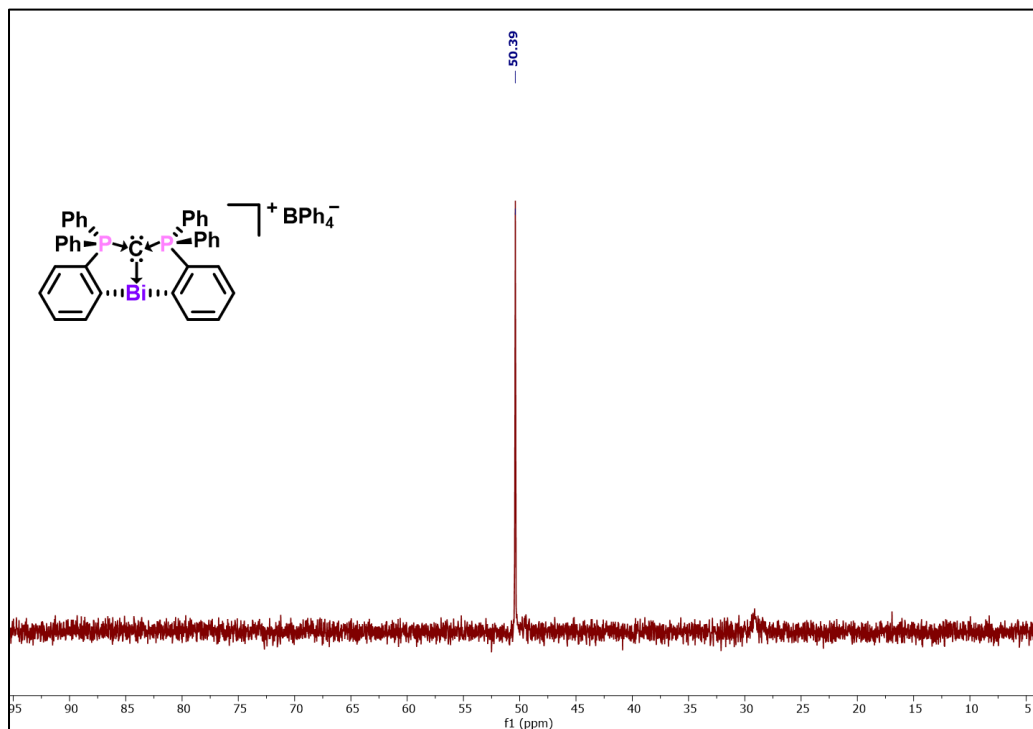


Figure A2.158. ^{31}P NMR spectrum of $7.5[\text{BPh}_4]$ (243 MHz, CD_2Cl_2 , 298 K).

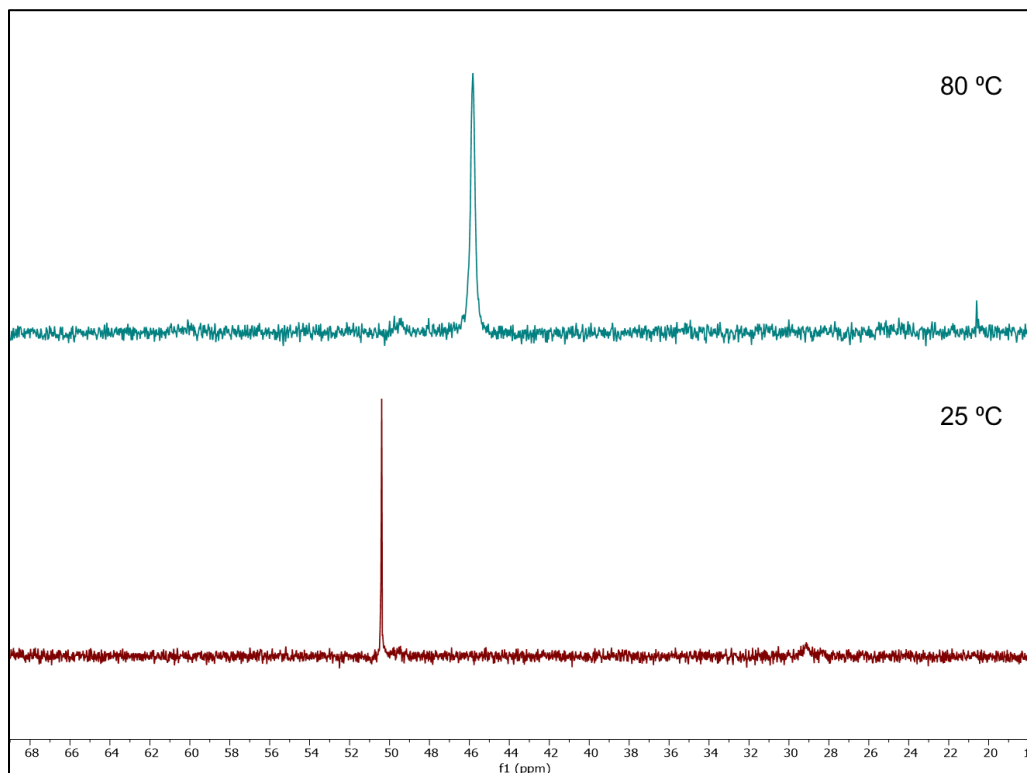


Figure A2.159. Stack plot of ^{31}P NMR spectra of $7.5[\text{BPh}_4]$ in $\text{THF-}d_8$ showing upfield shifts at higher temperatures. Notably, $7.5[\text{BPh}_4]$ was recovered from this experiment without THF coordination.

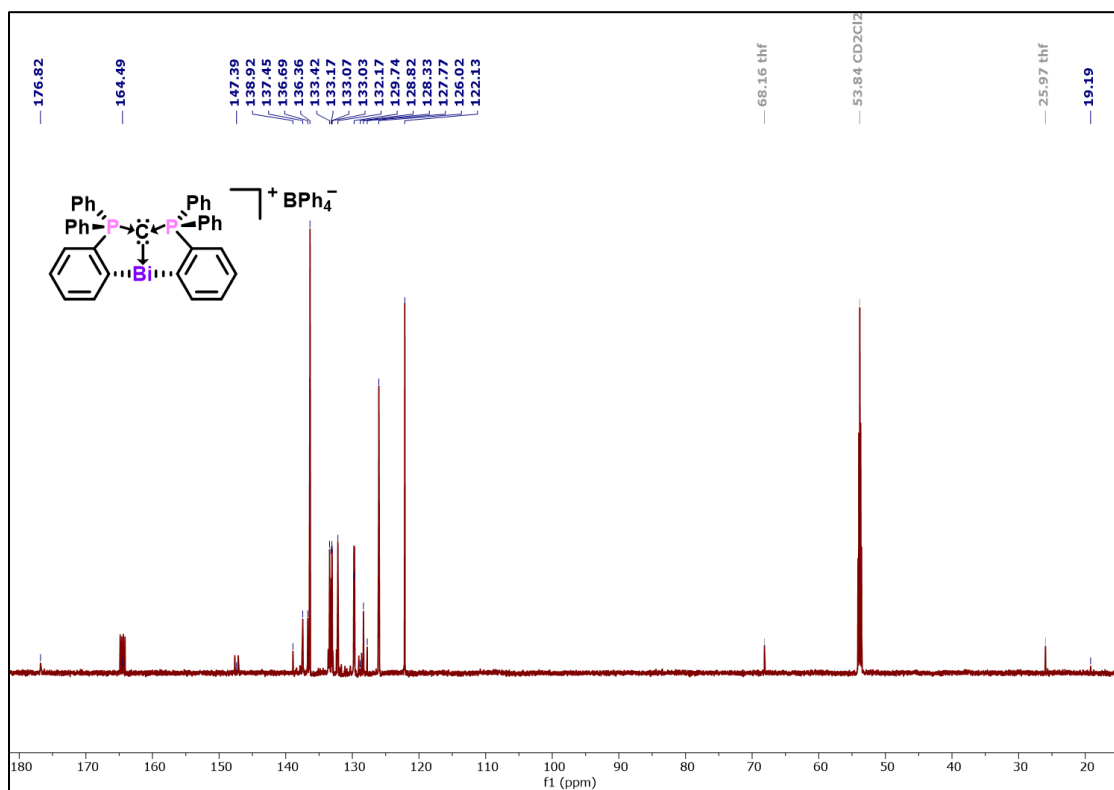


Figure A2.160. ^{13}C NMR spectrum of $7.5[\text{BPh}_4]$ (201 MHz, CD_2Cl_2 , 298 K).

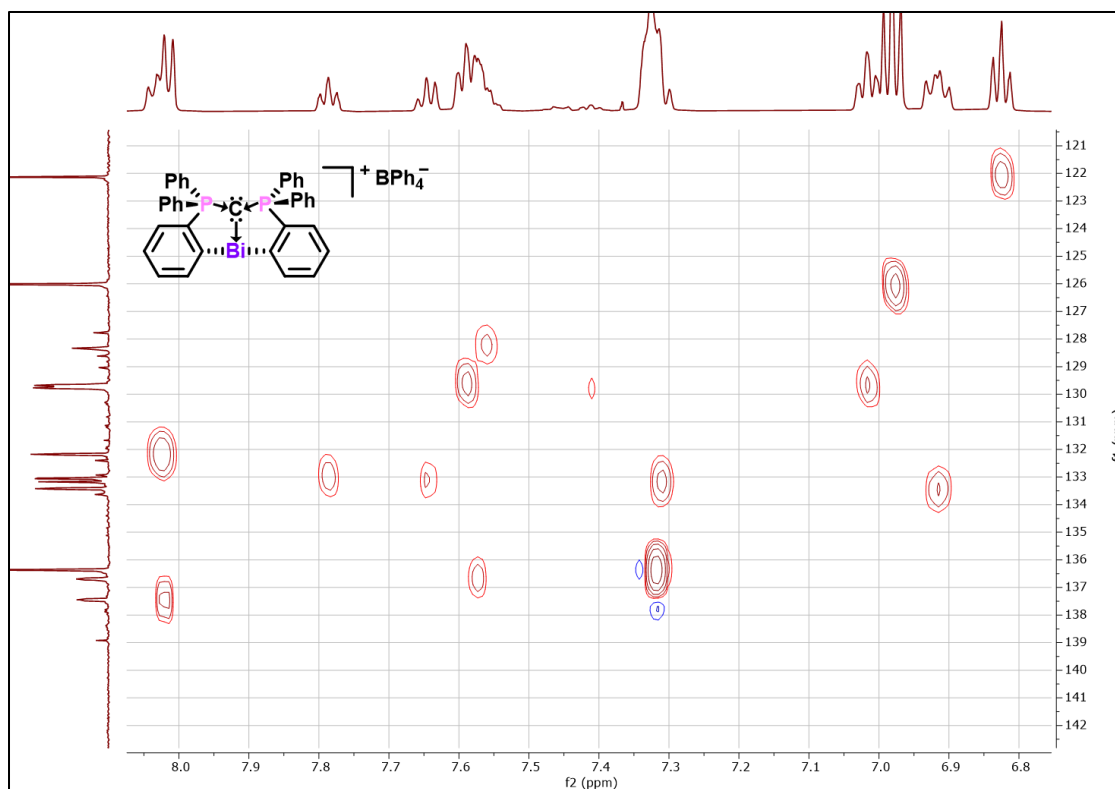


Figure A2.161. ^1H - ^{13}C HSQC spectrum of **7.5**[BPh $_4$].

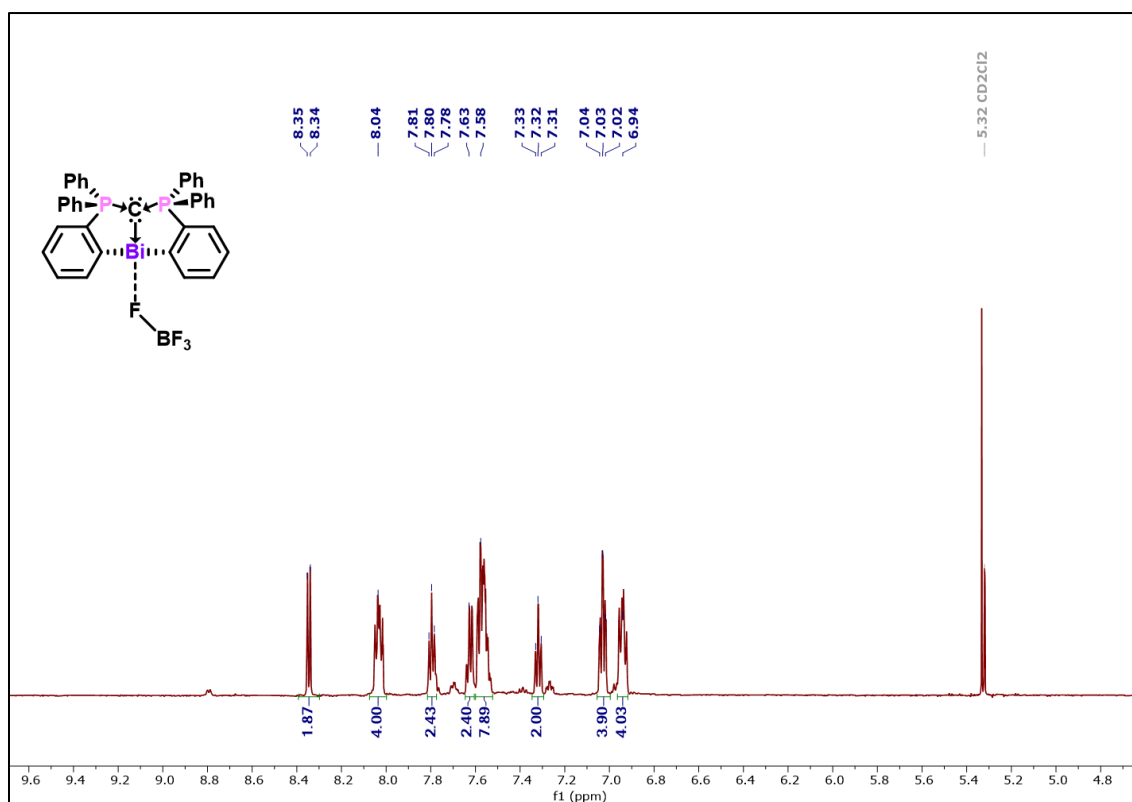


Figure A2.162. ^1H NMR spectrum of **7.5**[BF $_4$] (600 MHz, CD $_2$ Cl $_2$, 298 K).

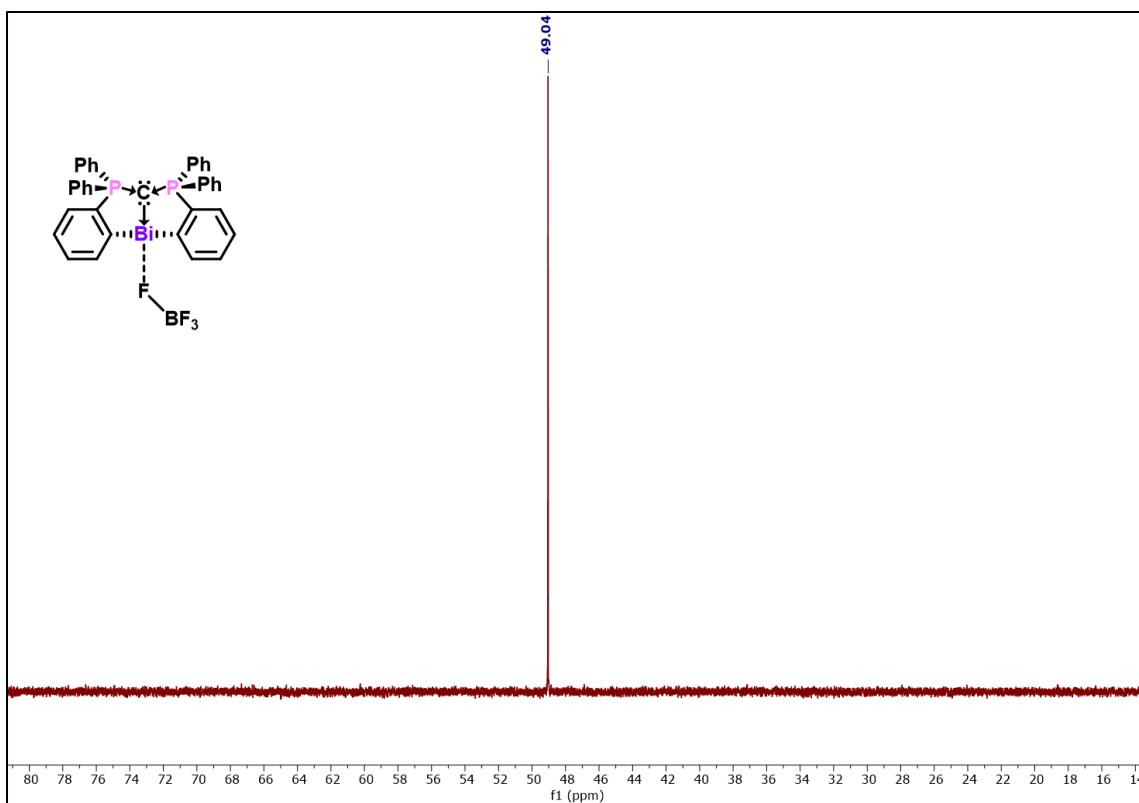


Figure A2.163. ^{31}P NMR spectrum of $7.5[\text{BF}_4]$ (243 MHz, CD_2Cl_2 , 298 K).

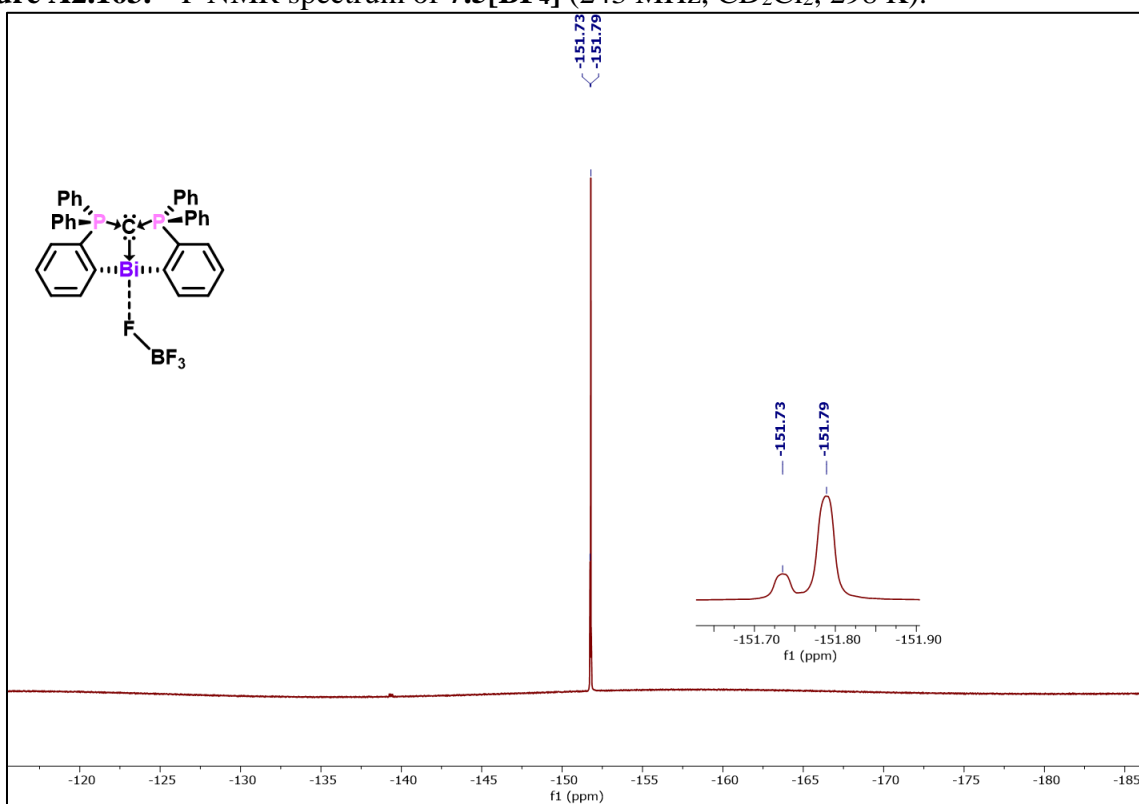


Figure A2.164. ^{19}F NMR spectrum of $7.5[\text{BF}_4]$ (564 MHz, CD_2Cl_2 , 298 K).

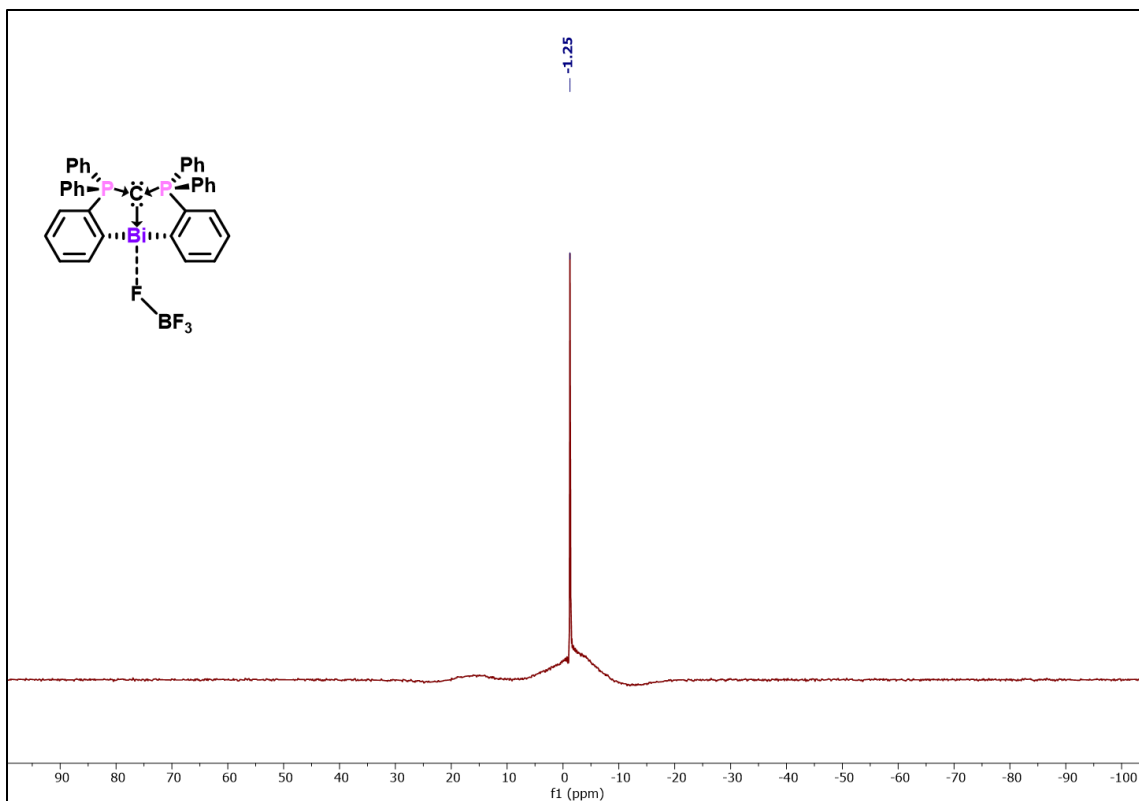


Figure A2.165. ^{11}B NMR spectrum of $7.5[\text{BF}_4]$ (192 MHz, CD_2Cl_2 , 298 K).

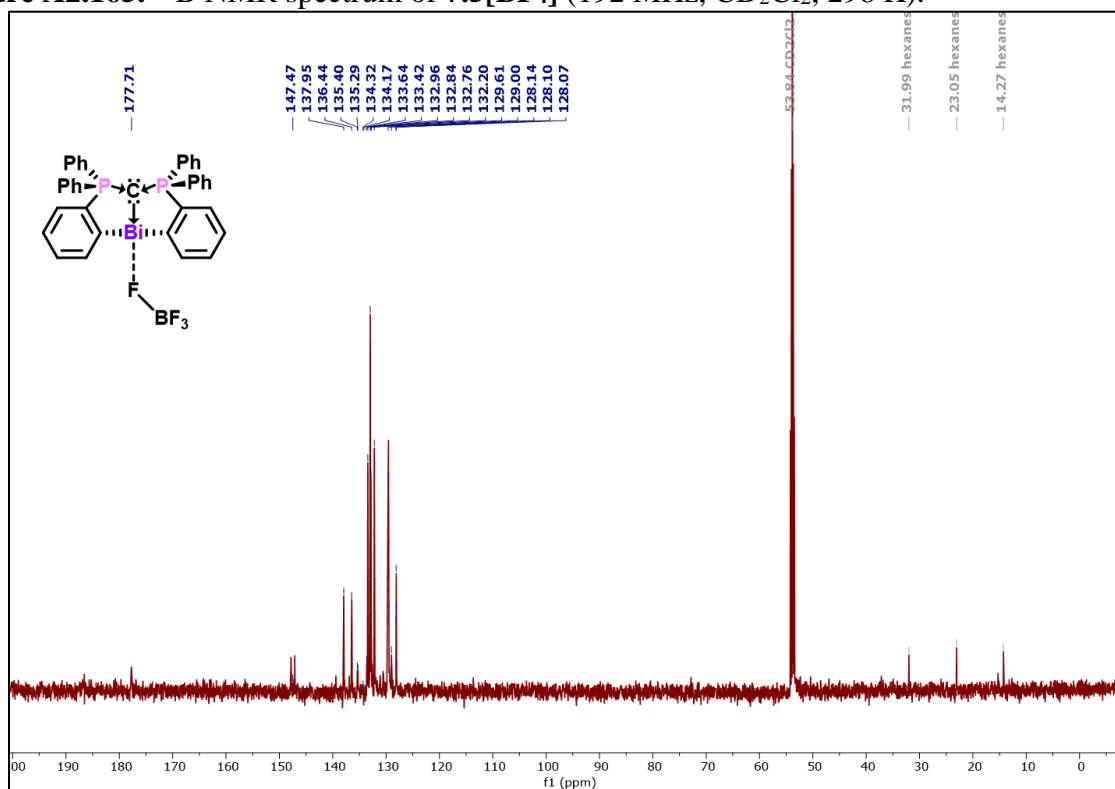


Figure A2.166. $^{13}\text{C}\{^1\text{H}\}$ NMR spectrum of $7.5[\text{BF}_4]$ (150 MHz, CD_2Cl_2 , 298 K).

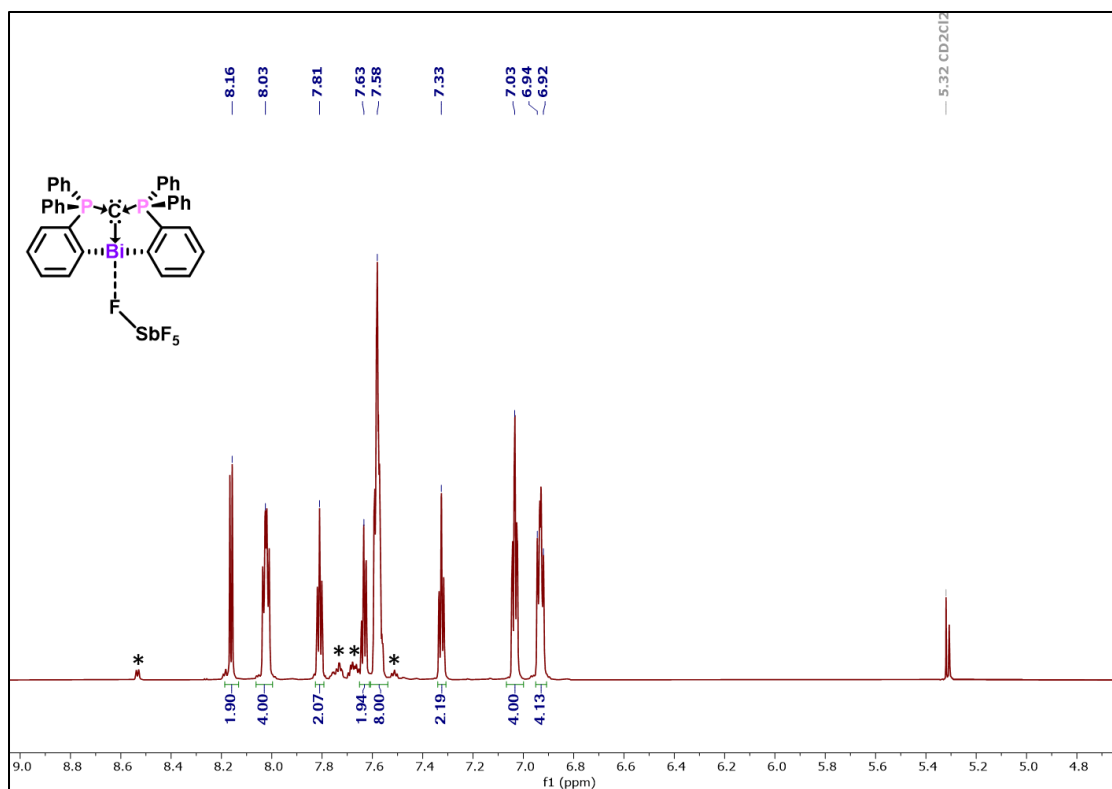


Figure A2.167. ¹H NMR spectrum of **7.5**[SbF₆] (800 MHz, CD₂Cl₂, 298 K). *Unidentified impurities.

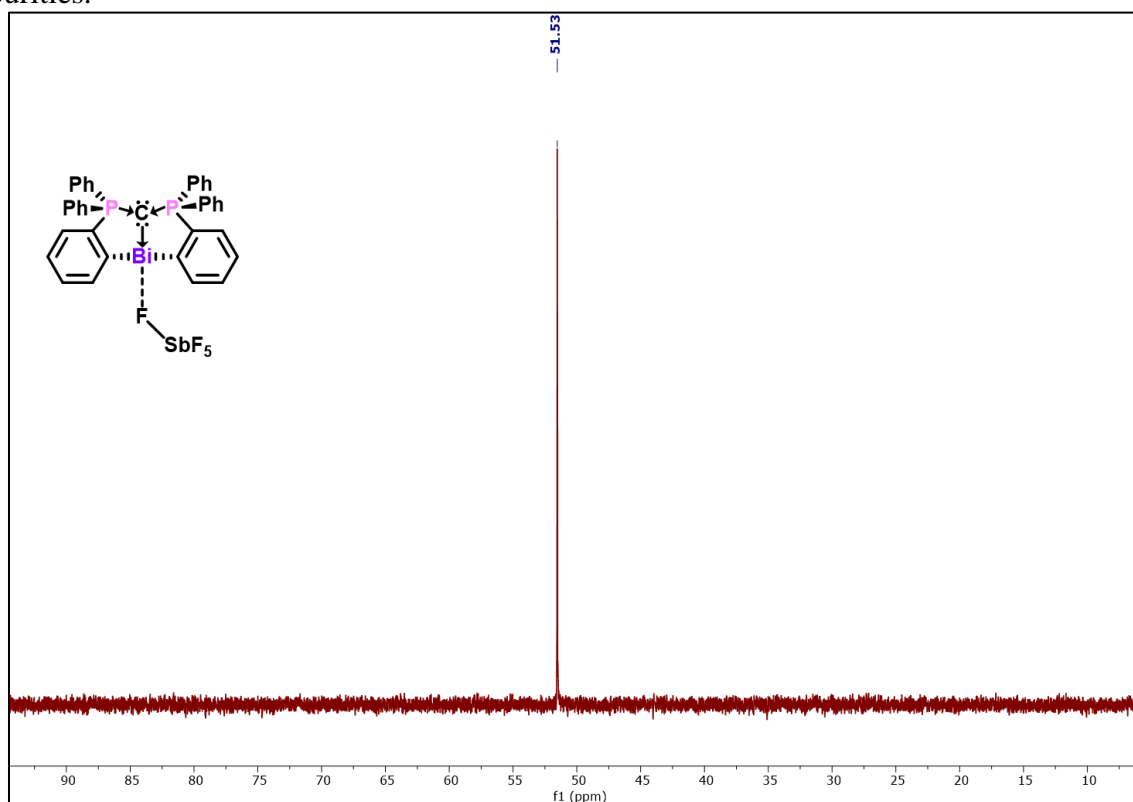


Figure A2.168. ³¹P NMR spectrum of **7.5**[SbF₆] (201 MHz, CD₂Cl₂, 298 K).

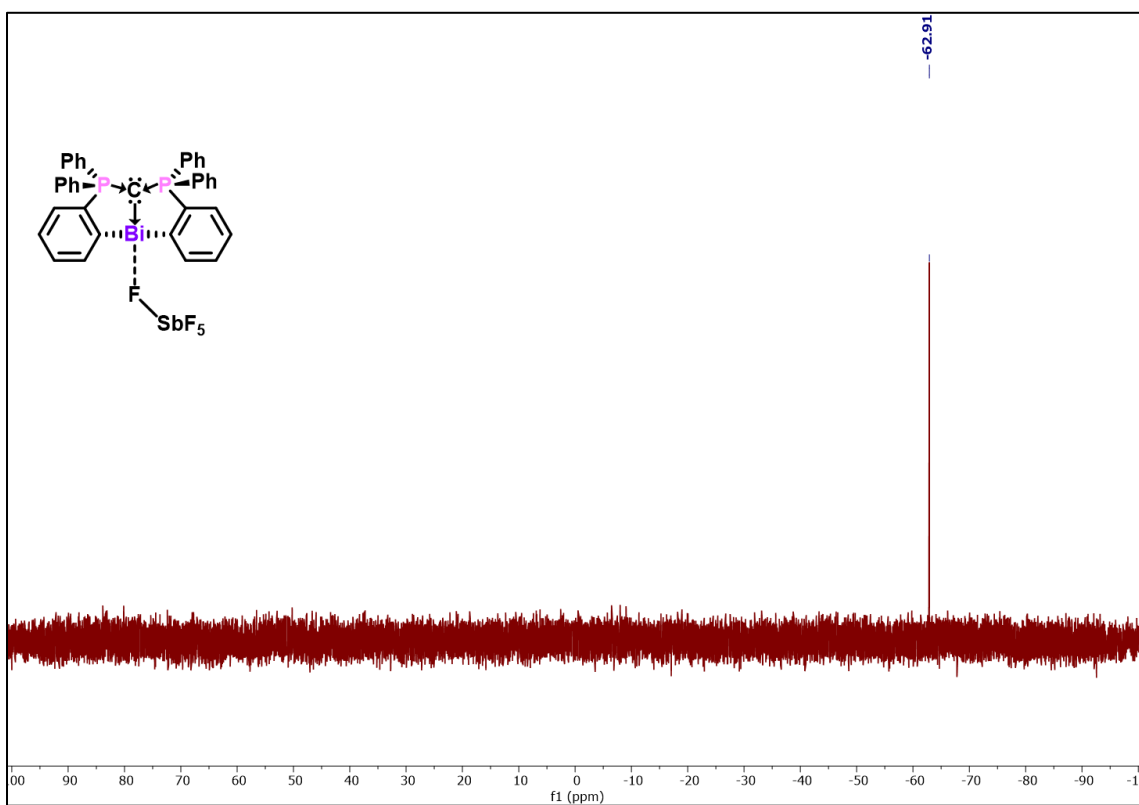


Figure A2.169. ^{19}F NMR spectrum of $7.5[\text{SbF}_6]$ (564 MHz, CD_2Cl_2 , 298 K).

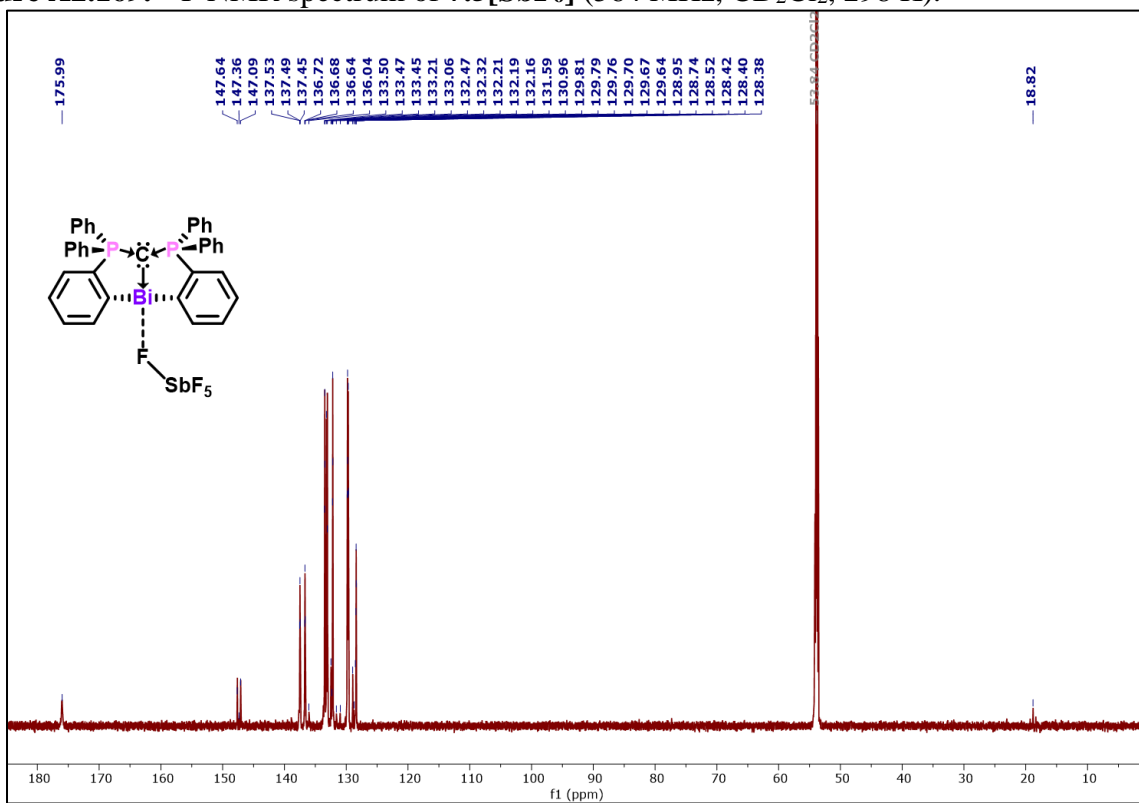


Figure A2.170. $^{13}\text{C}\{^1\text{H}\}$ NMR spectrum of $7.5[\text{SbF}_6]$ (201 MHz, CD_2Cl_2 , 298 K).

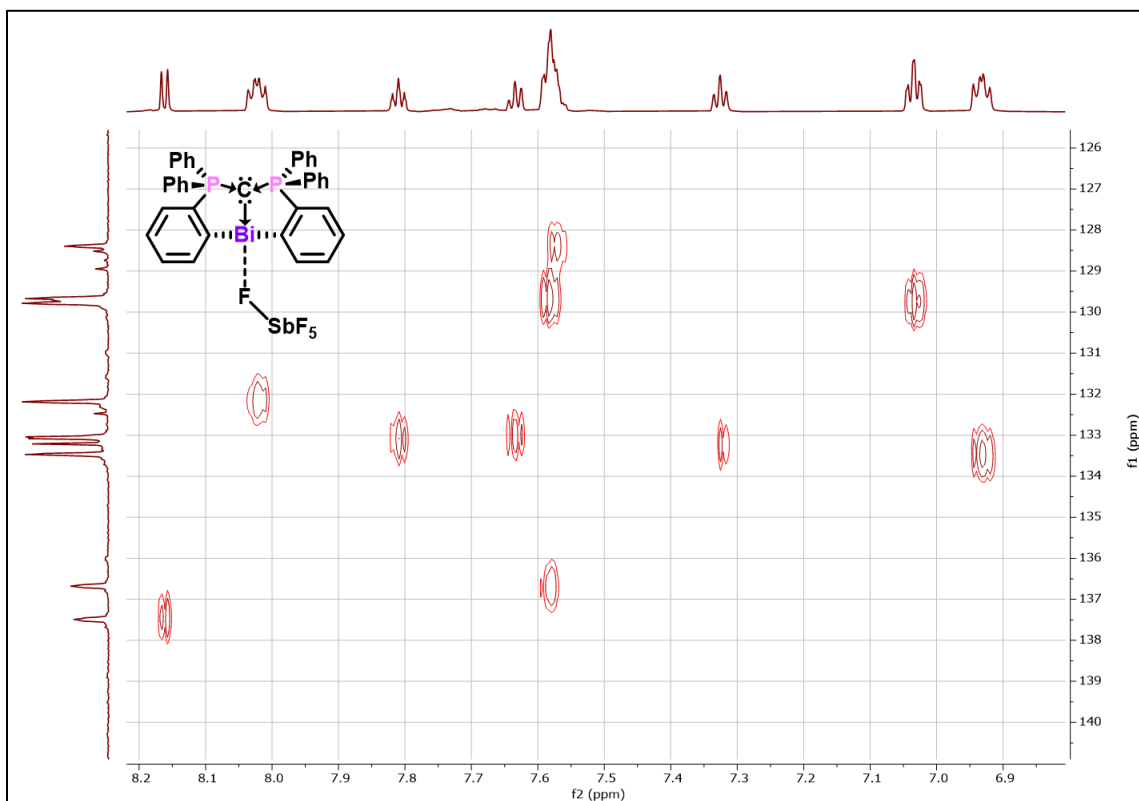


Figure A2.171. ^1H - ^{13}C HSQC spectrum of **7.5**[SbF_6].

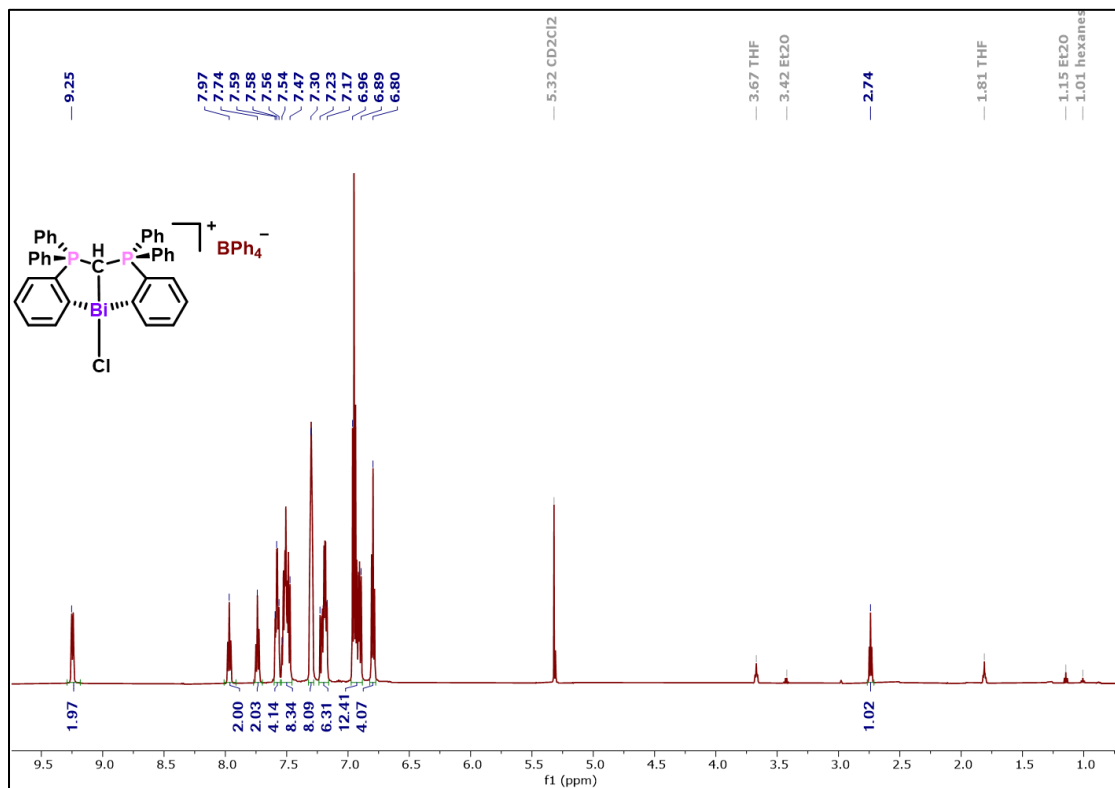


Figure A2.172. ^1H NMR spectrum of **7.6**[BPh_4] (600 MHz, CD_2Cl_2 , 298 K).

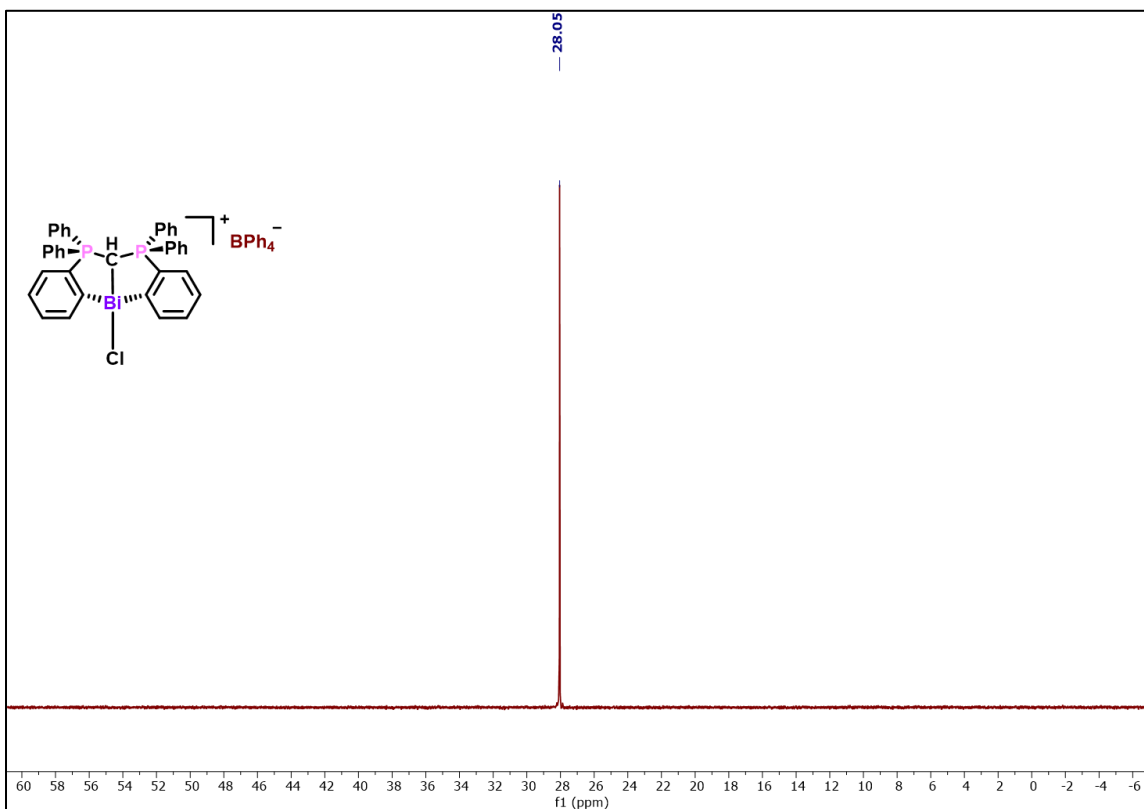


Figure A2.173. ^{31}P NMR spectrum of $7.6[\text{BPh}_4]$ (243 MHz, CD_2Cl_2 , 298 K).

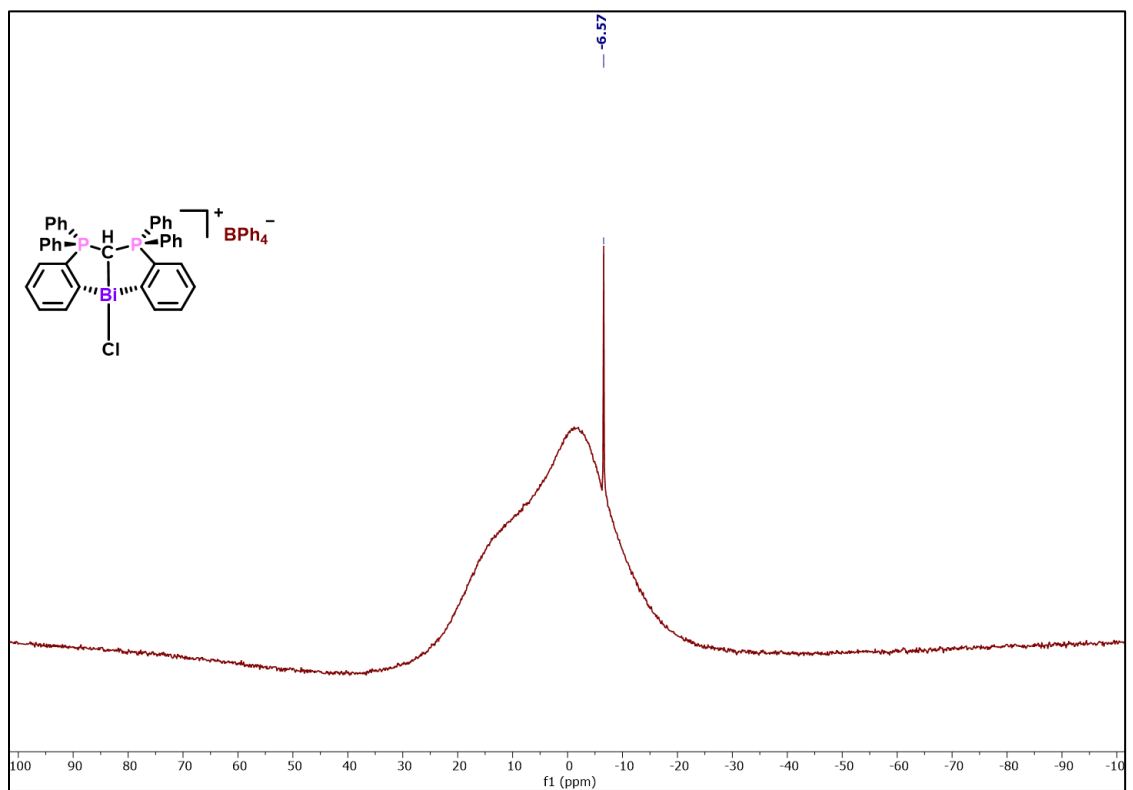


Figure A2.174. ^{11}B NMR spectrum of **7.6**[BPh $_4$] (192 MHz, CD $_2$ Cl $_2$, 298 K).

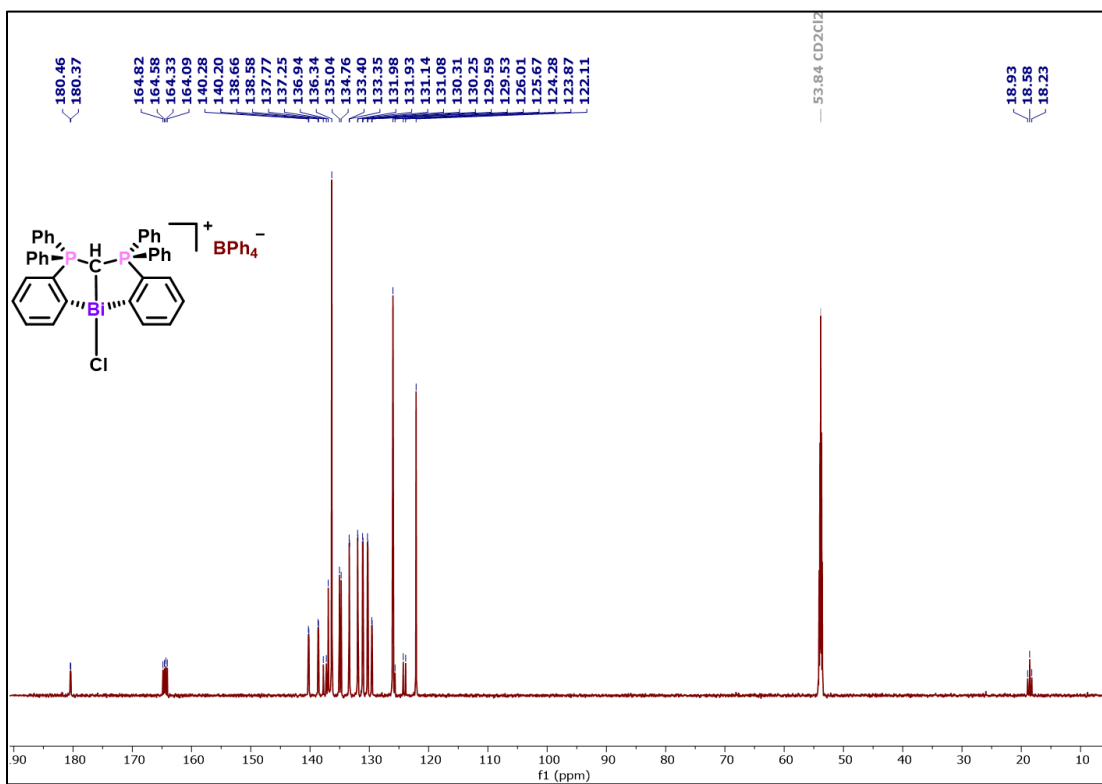


Figure A2.175. $^{13}\text{C}\{^1\text{H}\}$ NMR spectrum of **7.6**[BPh $_4$] (201 MHz, CD $_2$ Cl $_2$, 298 K).

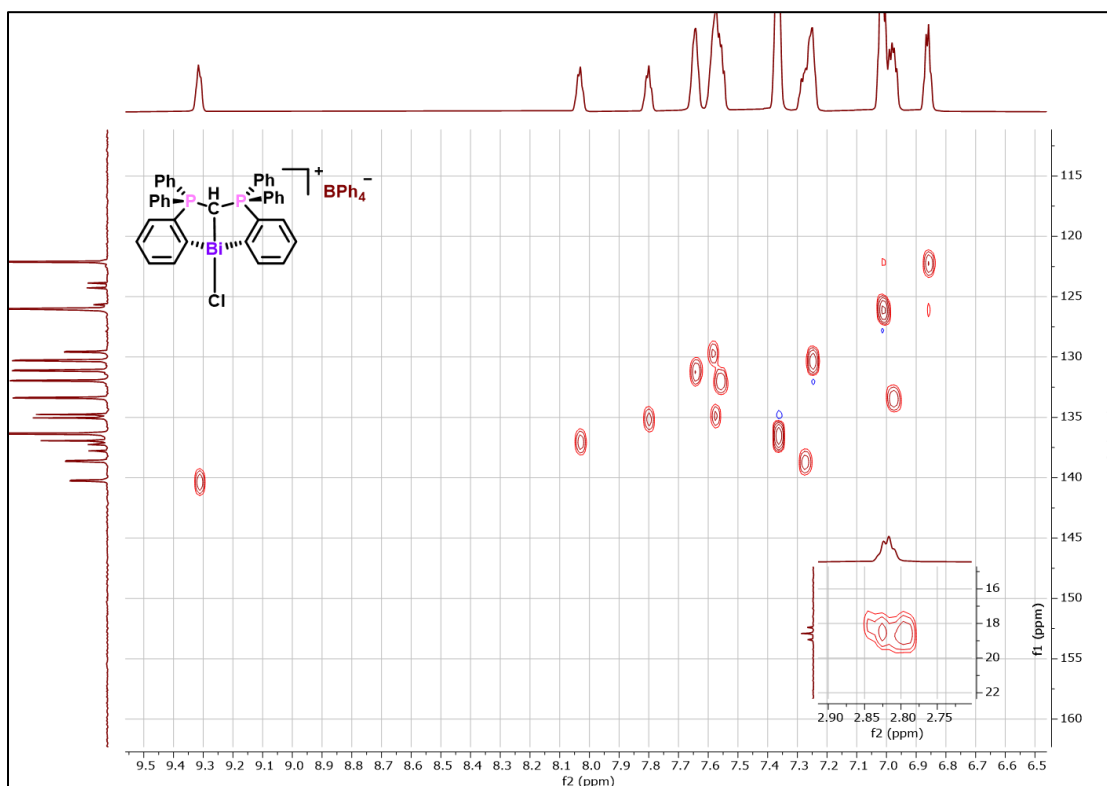


Figure A2.176. ^1H - ^{13}C HSQC NMR spectrum of **7.6**[BPh₄].

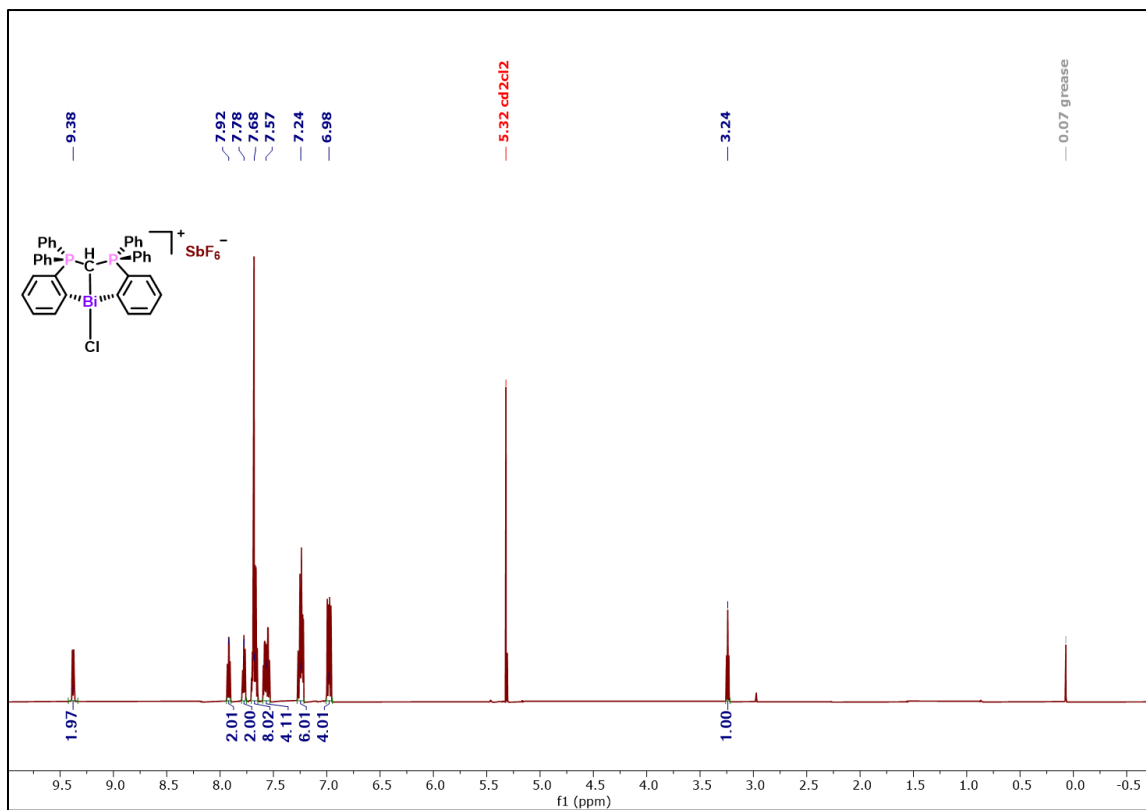


Figure A2.177. ^1H NMR spectrum of **7.7**[SbF₆] (600 MHz, CD₂Cl₂, 298 K).

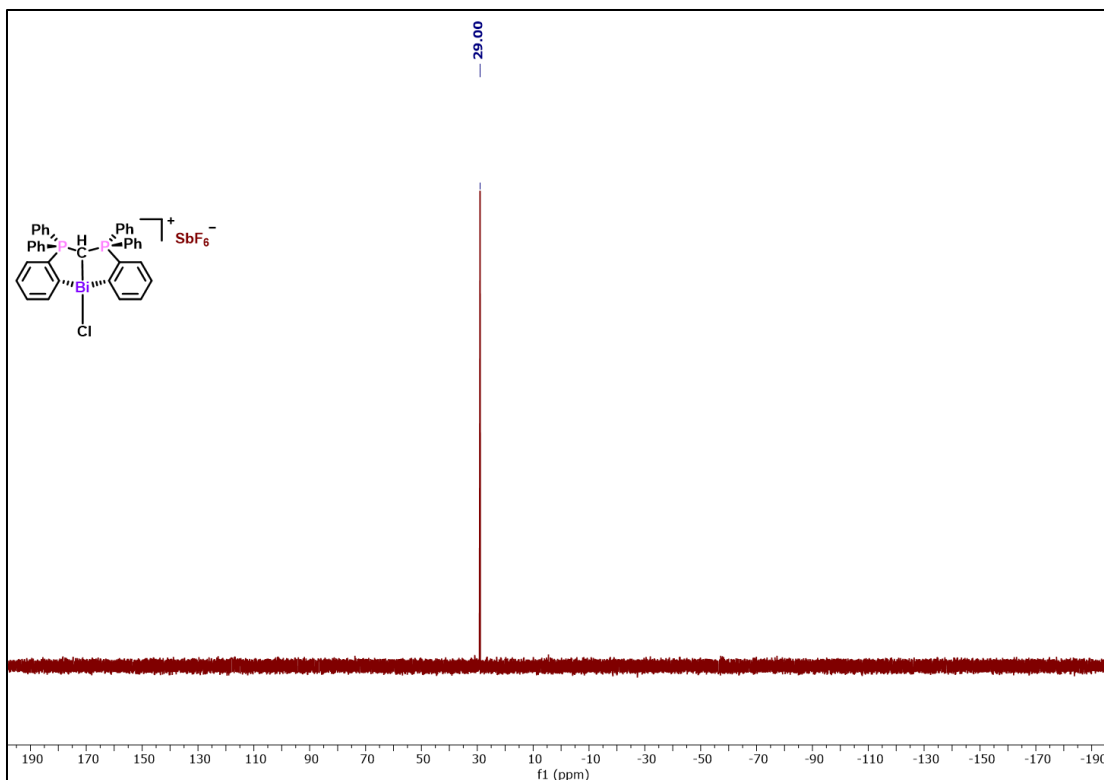


Figure A2.178. ^{31}P NMR spectrum of $7.7[\text{SbF}_6]$ (243 MHz, CD_2Cl_2 , 298 K).

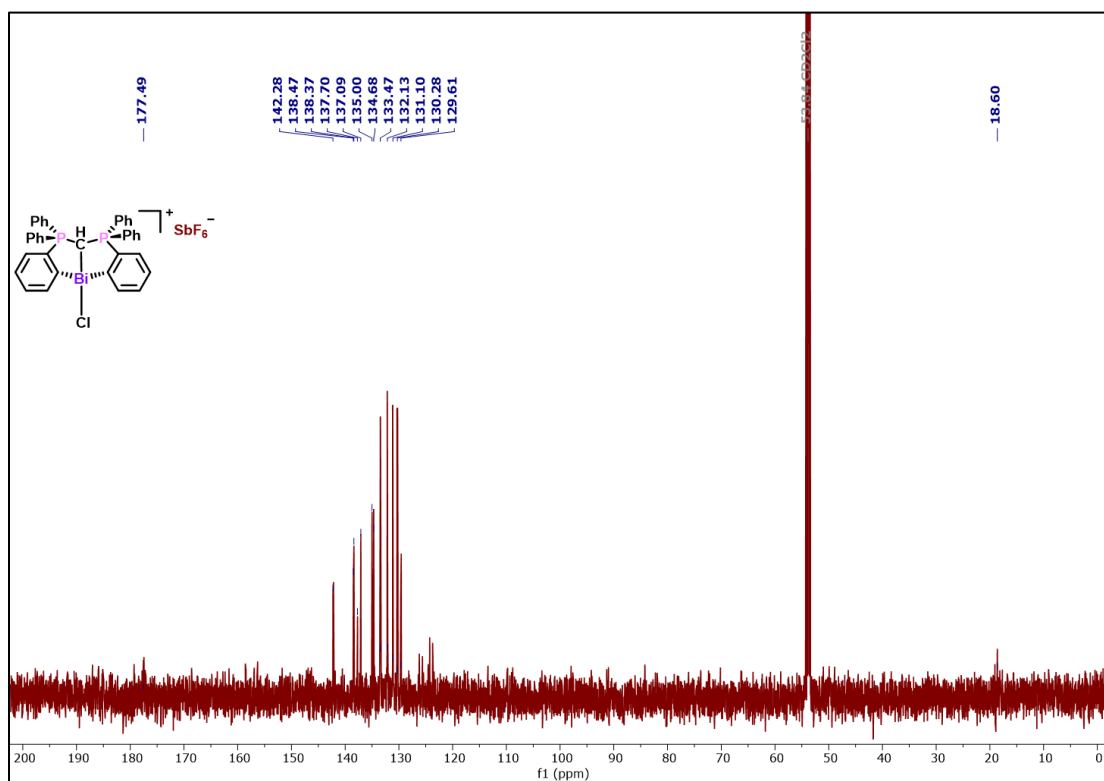


Figure A2.179. $^{13}\text{C}\{^1\text{H}\}$ NMR spectrum of $7.7[\text{SbF}_6]$ (150 MHz, CD_2Cl_2 , 298 K).

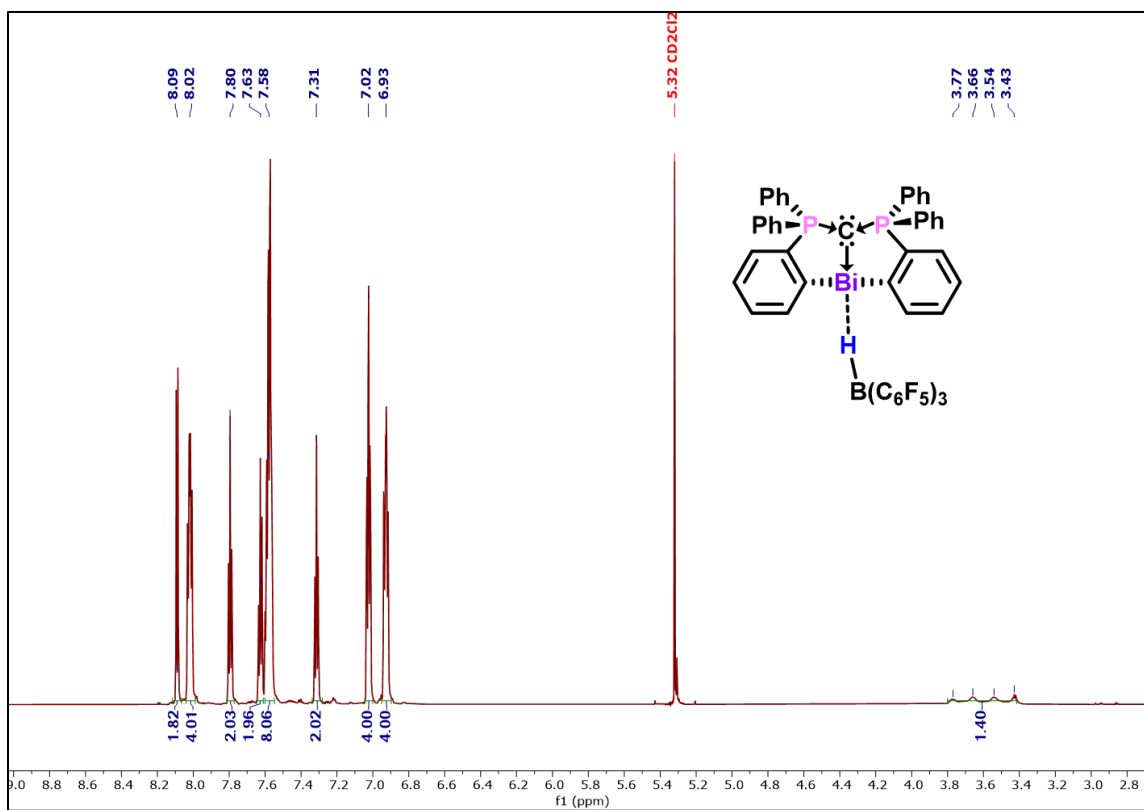


Figure A2.180. ¹H NMR spectrum of **7.9** (800 MHz, CD₂Cl₂, 298 K).

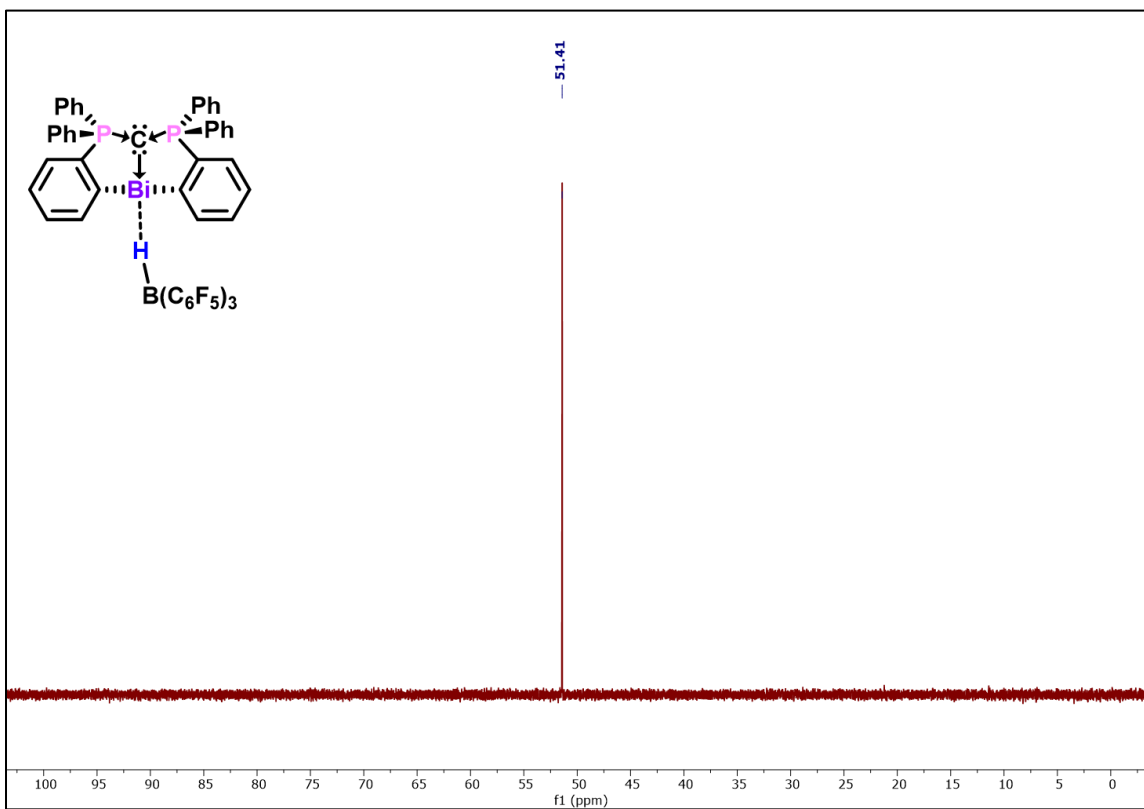


Figure A2.181. ³¹P NMR spectrum of **7.9** (243 MHz, CD₂Cl₂, 298 K).

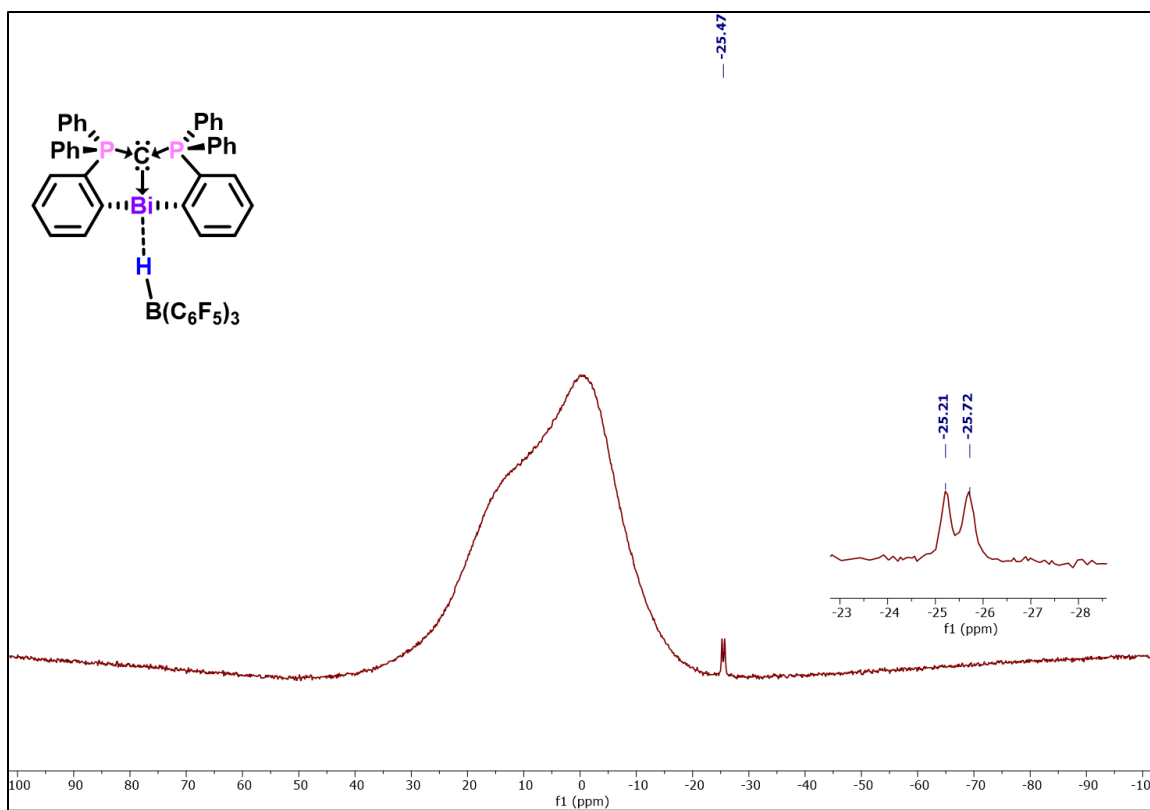


Figure A2.182. ^{11}B NMR spectrum of **7.9** (192 MHz, CD_2Cl_2 , 298 K).

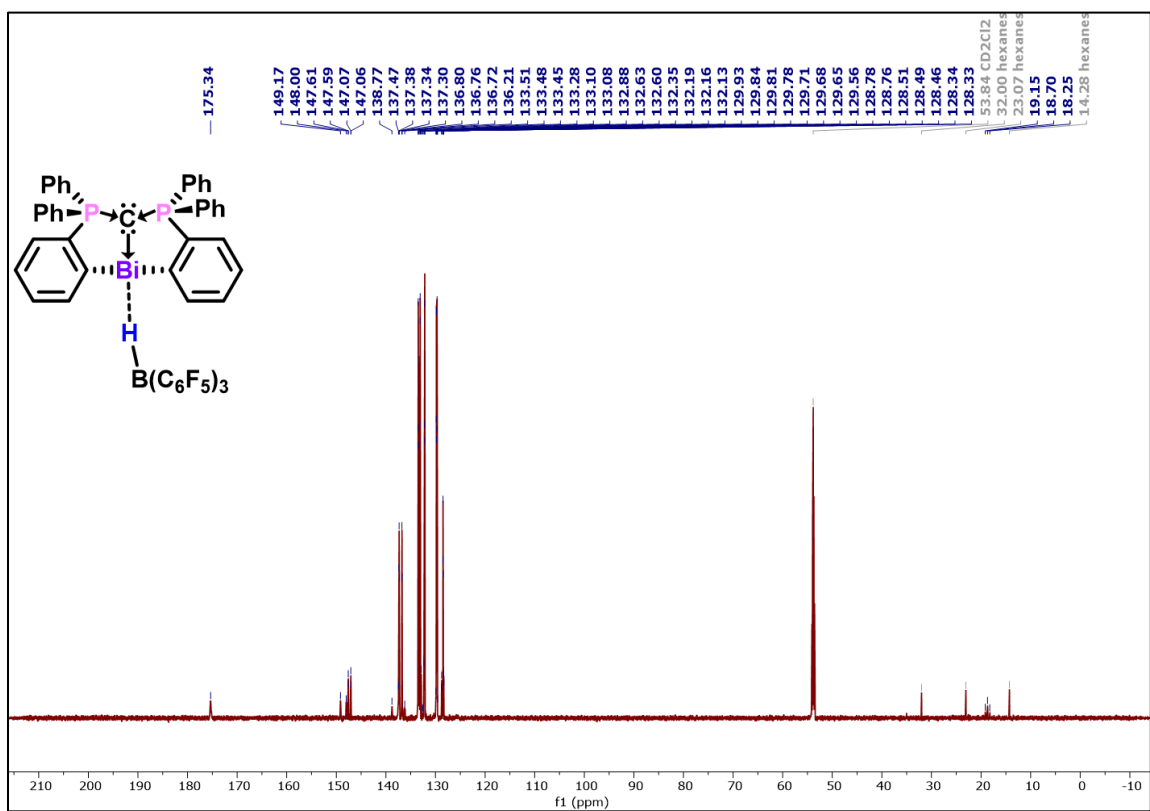


Figure A2.183. $^{13}\text{C}\{^1\text{H}\}$ NMR spectrum of **7.9** (201 MHz, CD_2Cl_2 , 298 K).

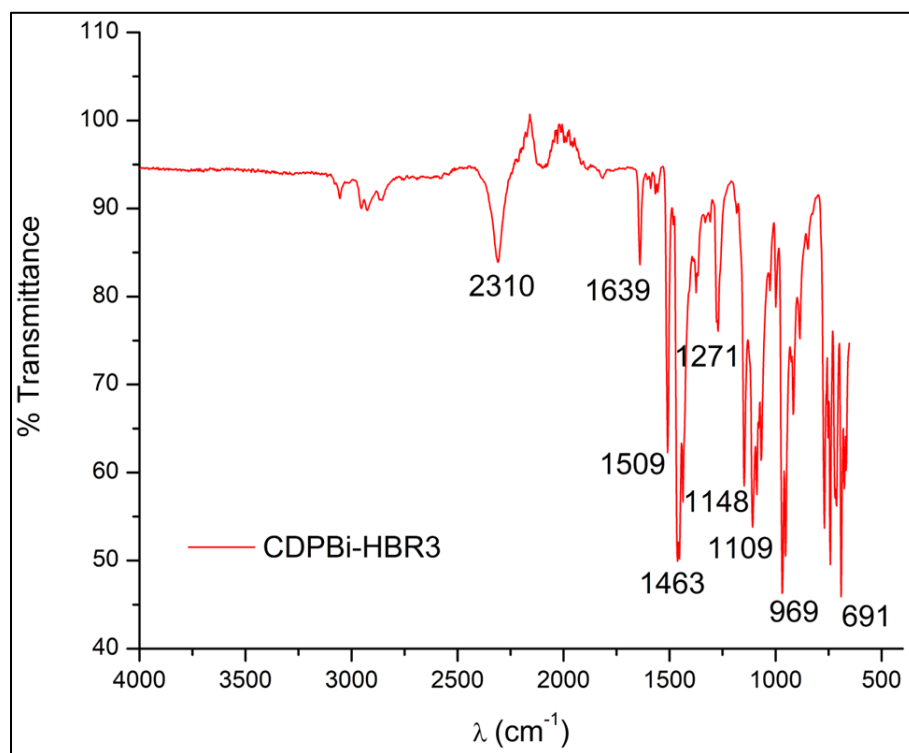


Figure A2.184. Solid-state FT-IR spectrum of **7.9**.

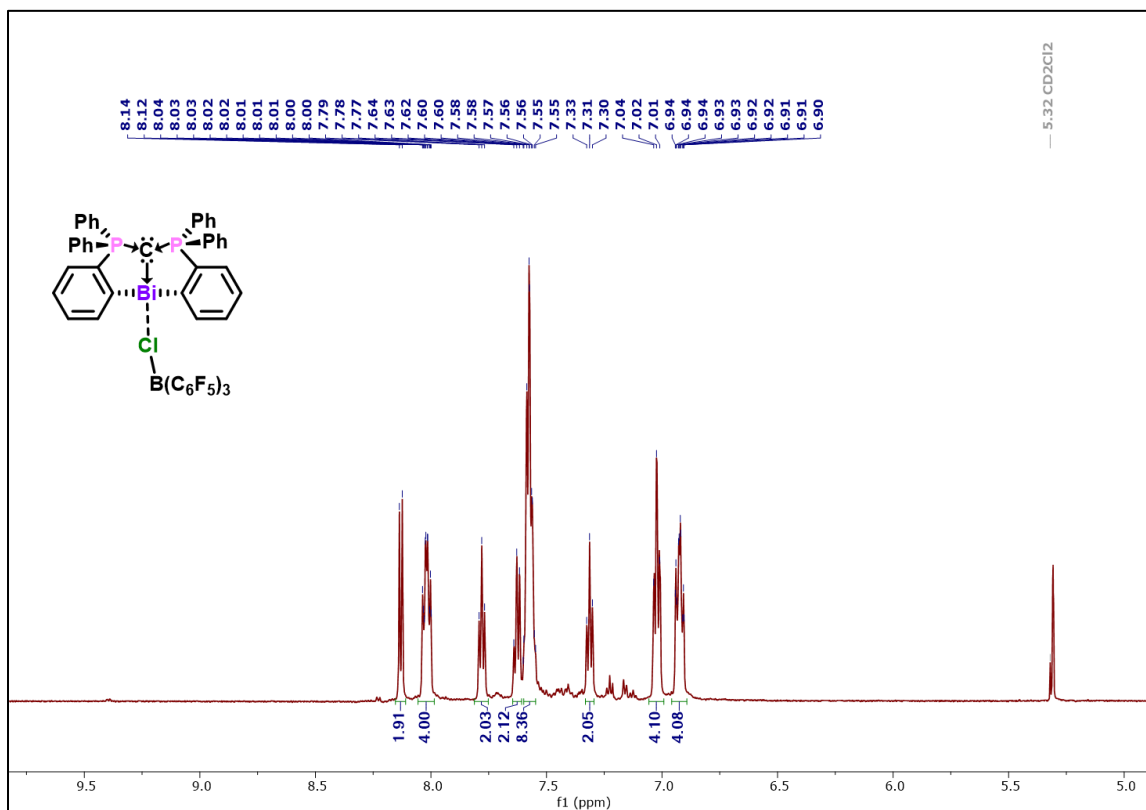


Figure A2.185. ^1H NMR spectrum of **7.10** (600 MHz, CD_2Cl_2 , 298 K).

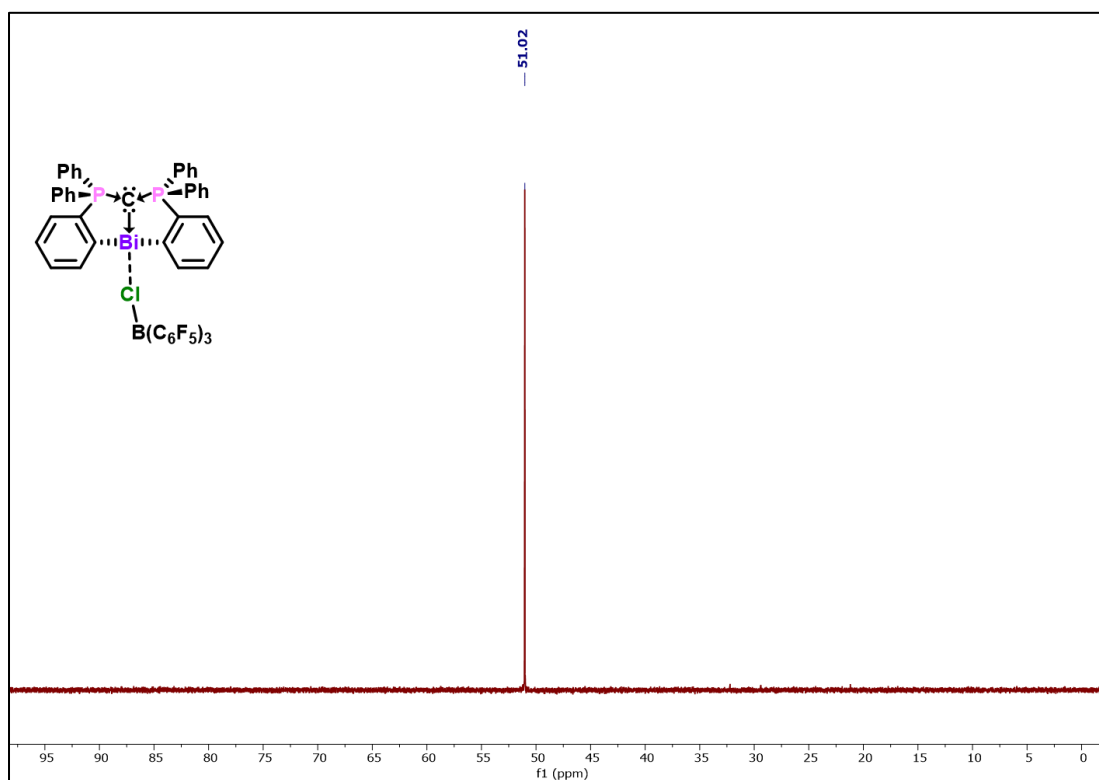


Figure A2.186. ^{31}P NMR spectrum of **7.10** (243 MHz, CD_2Cl_2 , 298 K).

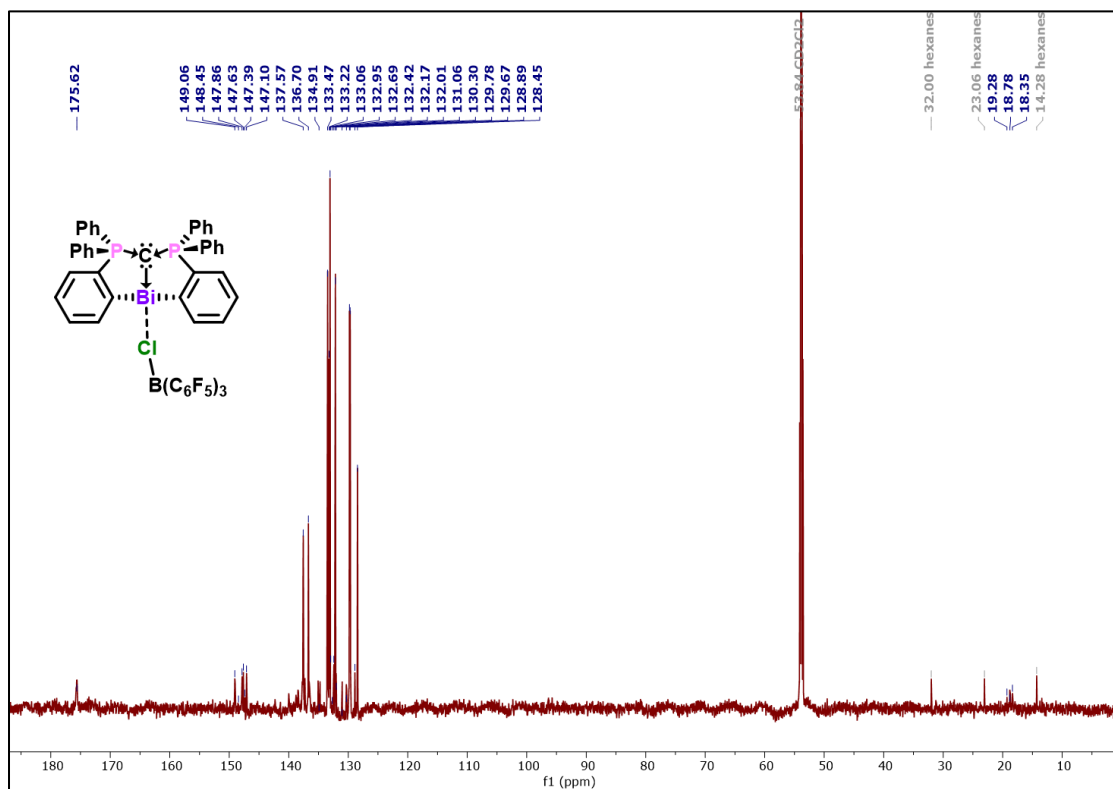


Figure A2.187. $^{13}\text{C}\{^1\text{H}\}$ NMR spectrum of **7.10** (201 MHz, CD_2Cl_2 , 298 K).

General considerations for catalysis experiments – The appropriate molar equivalents of catalyst and TEMPO (typically 13 mg, 0.0832 mmol) were combined in a J-Young NMR tube. A solution of PhSiH₃ in CD₂Cl₂ was added to the solids and their reaction monitored at regular intervals by ¹H NMR. Conversion was monitored by relative Si-H integrals for PhSiH₃ and PhH₂Si(OTEMP), and/or an internal hexamethylbenzene standard. Due to the presence of the TEMPO radical in solution, NMR was often obtained at warm temperatures (50 – 60 °C) for better signal resolution and more reliable integral ratios. TEMPO consumption was also indicated by the decolorization of the solution.

Table A2.3. Reactions conditions and conversion data for catalytic reactions

Entry	cat.	mol %	TEMPO/PhSiH ₃ (equiv)	condition	conversion ^a (%)
control	-	-	1/1	80 °C, 48 h	< 1
1	1	10	1/4	RT, 3 d	> 99 ^b
2	1	8	1/1	50 °C, 24 h	> 99 ^b
3	2	8	1/1	50 °C, 16 h	> 99 ^b
4	1	5	2/1	50 °C, 96 h	> 99 ^{b,c}

^aIn all cases, conversion was > 95% selective for PhH₂Si(OTEMP), and entries herein are based on ^bTEMPO consumption or ^csilane consumption.

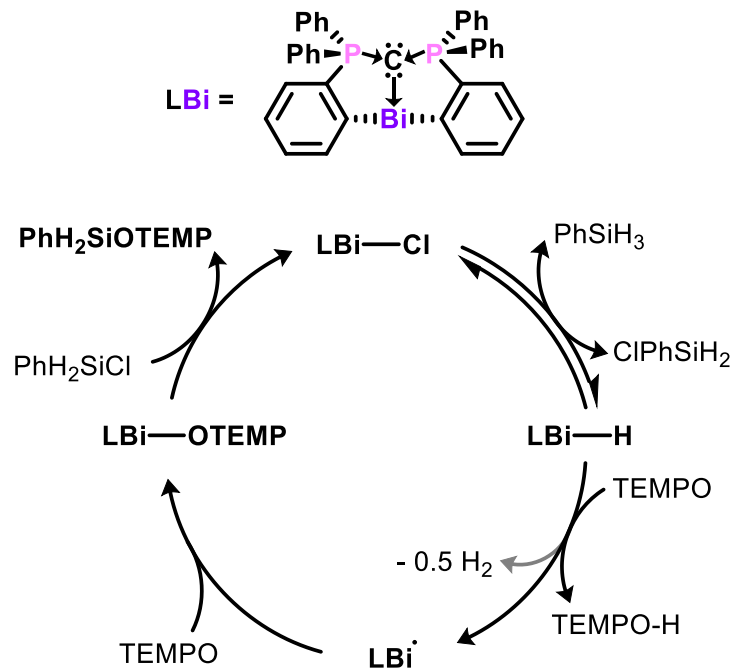


Figure A2.188. Proposed catalytic cycle inspired by literature.^{370, 371}

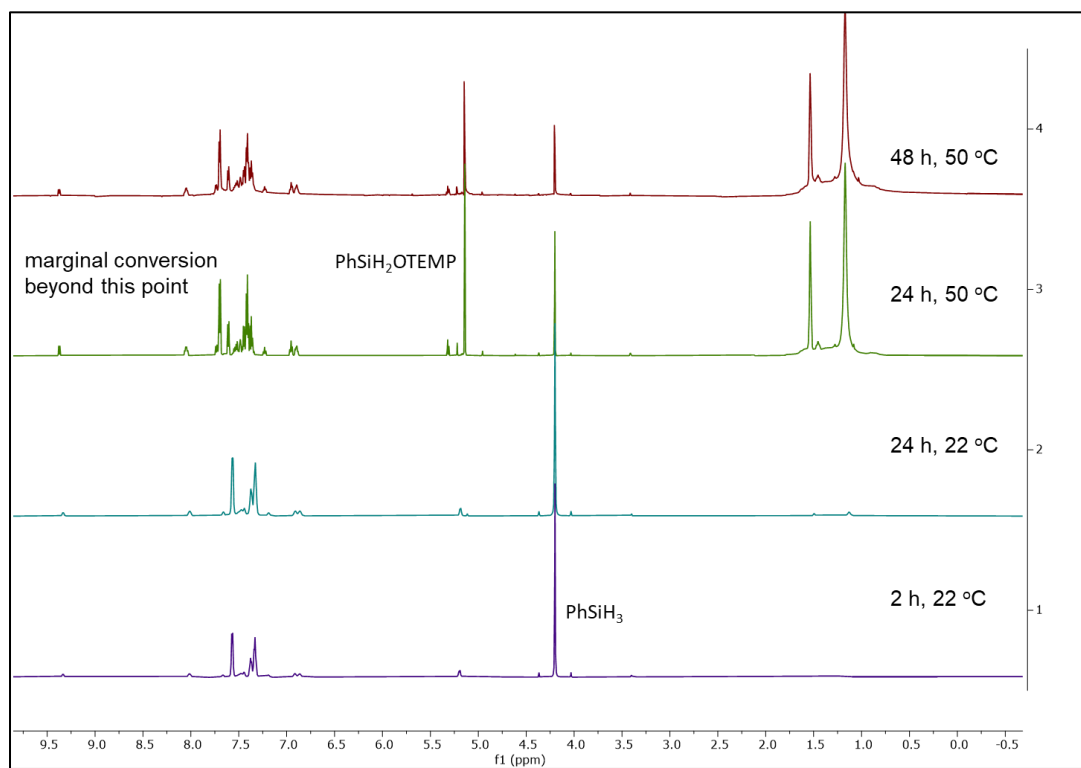


Figure A2.189. Stack plot of time-monitored ^1H NMR for entry 2 in Table A2.3.

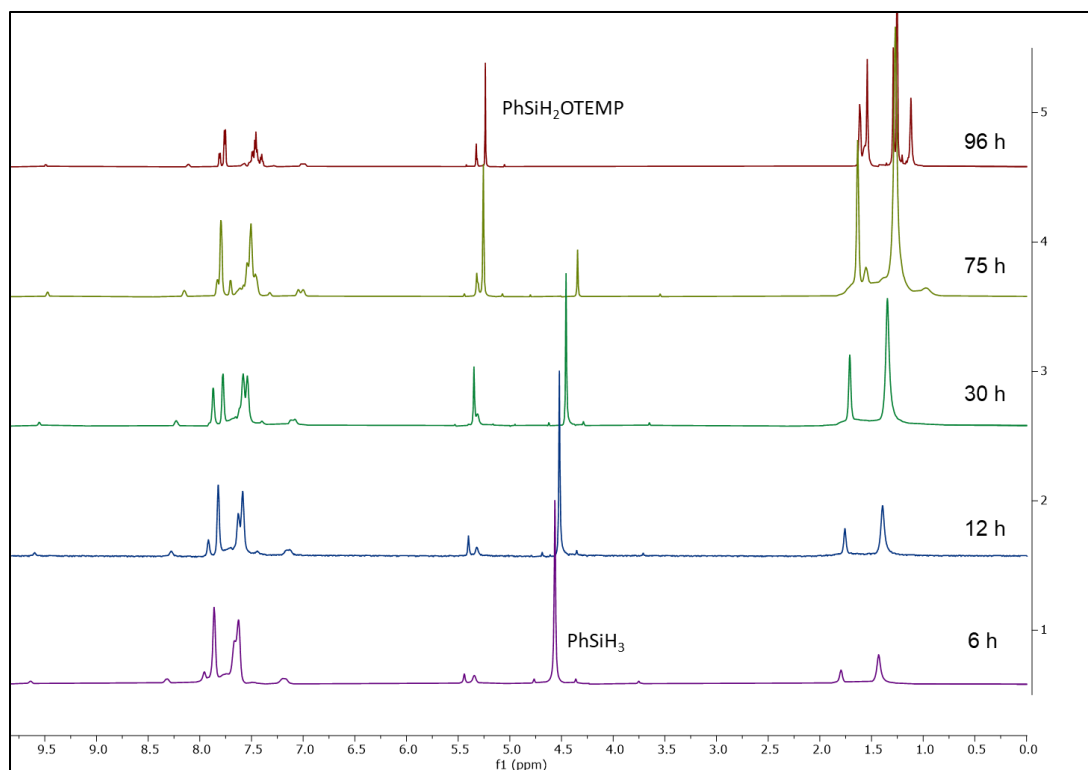


Figure A2.189. Stack plot of time-monitored ^1H NMR for entry 4 in Table Table A2.3. Reaction was conducted at 50 °C at all time intervals

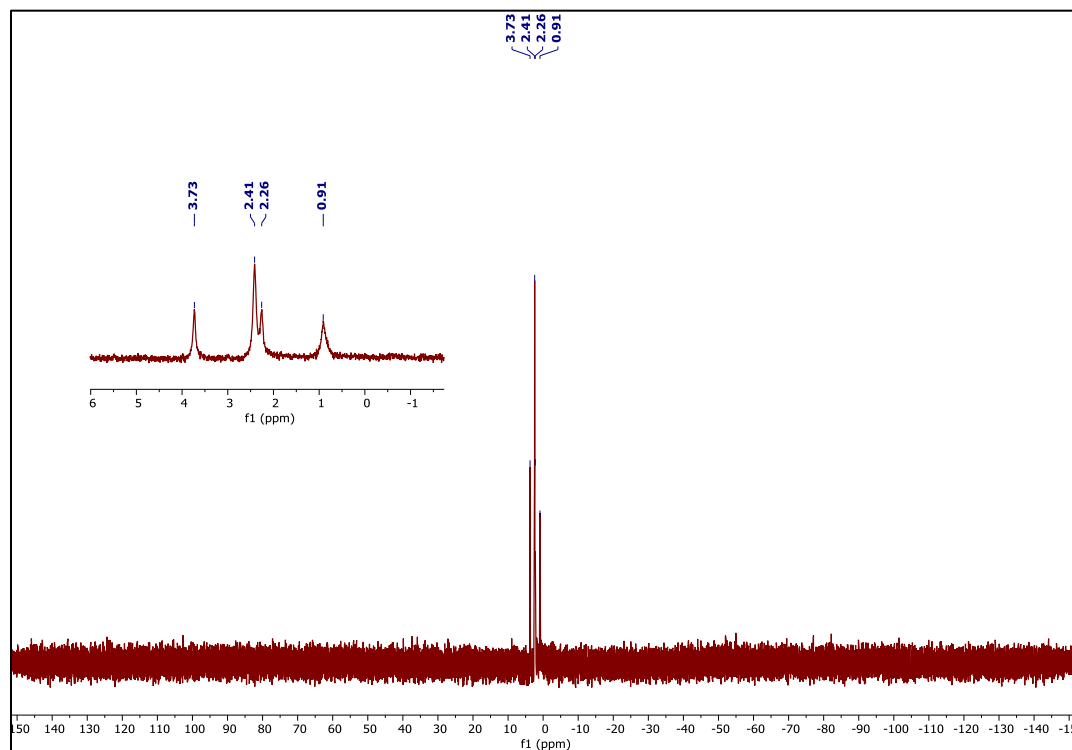


Figure A2.190. ^{31}P NMR spectrum of the reaction of **1** and XeF_2 prior to the crystallization of **11**.

Appendix III: Crystallographic Details and Crystal Structures

General Considerations.

Single crystal X-ray diffraction data were collected on a Bruker Kappa APEXII Duo diffractometer using a fine-focus sealed tube (Mo K_{α} , $\lambda = 0.71073 \text{ \AA}$) and a graphite monochromator or an Incoatec Microfocus I μ S (Cu K_{α} , $\lambda = 1.54178 \text{ \AA}$) and a multi-layer mirror monochromator. The frames were integrated with the Bruker SAINT software package⁴²⁷ using a narrow-frame algorithm. Data were corrected for absorption effects using the Multi-Scan method (SADABS).⁴²⁷ Each structure was solved and refined using the Bruker SHELXTL Software Package⁴²⁸ within APEX3⁴²⁷ and OLEX2.⁴²⁹ Non-hydrogen atoms were refined anisotropically. Hydrogen atoms were placed in geometrically calculated positions with $U_{iso} = 1.2U_{equiv}$ of the parent atom ($U_{iso} = 1.5U_{equiv}$ for methyl). Refinement details were compiled by Dr. Diane Dickie at the University of Virginia.

Chapter Two:

A single crystal of **2.1**, **2.1'**, **2.2**, **2.3**, **2.4**, **2.6**, **2.7** or **2.8** was coated with Paratone oil and mounted on a MiTeGen MicroLoop. The X-ray intensity data were measured on a Bruker Kappa APEXII Duo system. A fine-focus sealed tube (Mo K_{α} , $\lambda = 0.71073 \text{ \AA}$) and a graphite monochromator were used for **2.1**, **2.1'**, **2.3**, and **2.4** and an Incoatec Microfocus I μ S (Cu K_{α} , $\lambda = 1.54178 \text{ \AA}$) and a multi-layer mirror monochromator were used for **2.2**, **2.6**, **2.7** and **2.8**. The frames were integrated with the Bruker SAINT software package⁴²⁷ using a narrow-frame algorithm. Data were corrected for absorption effects using the Multi-Scan method (SADABS)⁴²⁷ (TWINABS for **2.8**). Each structure was solved and refined using the Bruker SHELXTL Software Package⁴²⁸ within APEX3⁴²⁷ and OLEX2.⁴²⁹ Non-hydrogen atoms were refined anisotropically. Hydrogen

atoms were placed in geometrically calculated positions with $U_{iso} = 1.2U_{equiv}$ of the parent atom ($U_{iso} = 1.5U_{equiv}$ for methyl).

For **2.2**, the co-crystallized toluene solvent was disordered over two positions. The relative occupancy was freely refined, with constraints on the anisotropic displacement parameters of the atoms in the minor component, and restraints on the minor component bonds. In **2.3**, the symmetry-disordered toluene solvent molecule was modeled at half-occupancy with constraints on the ring atoms. For **2.4**, two isopropyl groups were each found to be disordered over two positions. The relative occupancies of the two positions was freely refined, and constraints were used on the anisotropic displacement parameters of four of the six pairs of disordered atoms. A severely disordered mixture of hexane and toluene was located in the crystal lattice that could not be adequately modeled with or without restraints. Thus, the structure factors were modified using the PLATON SQUEEZE⁴³⁰ technique, in order to produce a “solvate-free” structure factor set. PLATON reported a total electron density of 488 e⁻ and total solvent accessible volume of 2244 Å³. In **2.6**, one isopropyl group and all of the co-crystallized toluene solvent molecules were disordered over two positions. The relative occupancies of each set of disordered atoms was freely refined, except for the C96-C102 toluene. It was set at 50% occupancy because the disorder was across an inversion center. Constraints and restraints were used on the anisotropic displacement parameters and bonds of most of the disordered atoms. In **2.7**, the relative occupancies of the disordered substituents were freely refined, and no constraints or restraints were needed. The twin domains of **2.8** were identified using CELL_NOW.⁴³¹ Starting with 1452 reflections, 835 reflections were fit to the first domain, 784 to the second domain (329 exclusively), with 288 unindexed reflection remaining. The twin domain was oriented at a 179.9° rotation about the real axis 1.000 0.000 0.003. The twin law was 1.000 -0.001 0.006 / 0.000 -1.000 -0.001 / -0.108

0.001 -1.000. It was refined on HKLF5 data, with the BASF for the twin domains refining to 0.46781.

Table A3.1. Crystallographic data table for **2.1, 2.1', 2.2, 2.3, 2.4, 2.6, 2.7** and **2.8**

	2.1	2.1'	2.2	2.3	2.4	2.6	2.7	2.8
CCDC number	1999999	2000000	2000001	2000002	2000003	2000004	2000528	2024372
Formula	C ₃₆ H ₅₆ Br ₂ MgN ₄	C ₃₄ H ₅₀ Br ₂ Cl ₂ MgN ₄	C ₅₁ H ₇₆ MgN ₆	C ₉₁ H ₁₃₆ Mg ₂ N ₁₂	C ₅₀ H ₈₀ MgN ₆	C ₁₉₇ H ₂₈₀ Mg ₄ N ₁₆	C ₅₂ H ₇₂ MgN ₄	C ₃₉ H ₆₀ BrK MgN ₄
FW (g/mol)	728.97	769.81	797.48	1446.73	789.51	2969.59	777.44	728.23
Temp (K)	100(2)	100(2)	250(2)	100(2)	100(2)	100(2)	100(2)	100(2)
λ (Å)	0.71073	0.71073	1.54178	0.71073	0.71073	1.54178	1.54178	1.54178
Size (mm)	0.041 x 0.094 x 0.167	0.108 x 0.175 x 0.320	0.061 x 0.102 x 0.120	0.120 x 0.160 x 0.193	0.134 x 0.310 x 0.310	0.154 x 0.179 x 0.194	0.102 x 0.138 x 0.207	0.219 x 0.230 x 0.320
Crystal habit	colorless plate	colorless block	yellow plate	yellow block	orange plate	yellow plate	orange block	yellow block
Crystal system	orthorhombic	orthorhombic	monoclinic	monoclinic	monoclinic	monoclinic	monoclinic	monoclinic
Space group	P b c n	P b c n	P 2 ₁ /n	P 2 ₁ /n	P 2 ₁ /c	P 2 ₁ /c	C 2/c	P 2 ₁ /m
a (Å)	12.697(3)	12.5665(6)	10.8688(11)	11.5799(11)	20.2478(16)	24.3383(13)	24.5919(10)	11.9392(5)
b (Å)	13.077(3)	13.2126(7)	33.513(4)	19.583(2)	12.1552(9)	19.8804(10)	9.2100(3)	20.5574(7)
c (Å)	22.755(6)	22.6670(10)	13.4596(13)	19.7914(19)	64.911(5)	19.3406(10)	22.8820(9)	16.2621(7)
α (°)	90	90	90	90	90	90	90	90
β (°)	90	90	91.808(7)	102.621(3)	90.376(3)	101.960(4)	113.755(3)	92.177(4)
γ (°)	90	90	90	90	90	90	90	90
Volume (Å ³)	3778.2(16)	3763.5(3)	4900.2(9)	4379.6(8)	15975.(2)	9154.9(8)	4743.5(3)	3988.5(3)
Z	4	4	4	2	12	2	4	4
Density (g/cm ³)	1.282	1.359	1.081	1.097	0.985	1.077	1.089	1.213
μ (mm ⁻¹)	2.191	2.341	0.594	0.077	0.068	0.592	0.592	2.713
F(000)	1528	1592	1744	1580	5208	3244	1696	1552
θ range (°)	1.79 to 23.32	1.80 to 28.31	2.64 to 68.40	1.48 to 25.80	1.25 to 26.39	1.85 to 59.10	3.93 to 68.36	2.72 to 68.34
Index ranges	-14 ≤ h ≤ 14 -14 ≤ k ≤ 10 -25 ≤ l ≤ 25	-16 ≤ h ≤ 16 -17 ≤ k ≤ 17 -30 ≤ l ≤ 30	-13 ≤ h ≤ 11 -40 ≤ k ≤ 37 -15 ≤ l ≤ 16	-14 ≤ h ≤ 14 -23 ≤ k ≤ 23 -21 ≤ l ≤ 24	-25 ≤ h ≤ 21 -14 ≤ k ≤ 15 -81 ≤ l ≤ 78	-27 ≤ h ≤ 27 -22 ≤ k ≤ 22 -21 ≤ l ≤ 18	-29 ≤ h ≤ 23 -11 ≤ k ≤ 11 -27 ≤ l ≤ 27	-14 ≤ h ≤ 14 0 ≤ k ≤ 24 0 ≤ l ≤ 19
Data / restraints / parameters	2732 / 0 / 201	4677 / 0 / 201	8961 / 0 / 567	8365 / 0 / 482	32361 / 0 / 1635	13162 / 546 / 1182	4328 / 0 / 315	7488 / 0 / 444
GOF on F ²	1.001	1.033	1.031	1.024	1.017	1.011	1.116	1.053
R ₁ (I > 2 σ (I))	0.0415	0.0346	0.0570	0.0559	0.0652	0.0954	0.0596	0.0674
wR ₂ (all data)	0.0878	0.0815	0.1647	0.1527	0.1497	0.3126	0.1687	0.1722

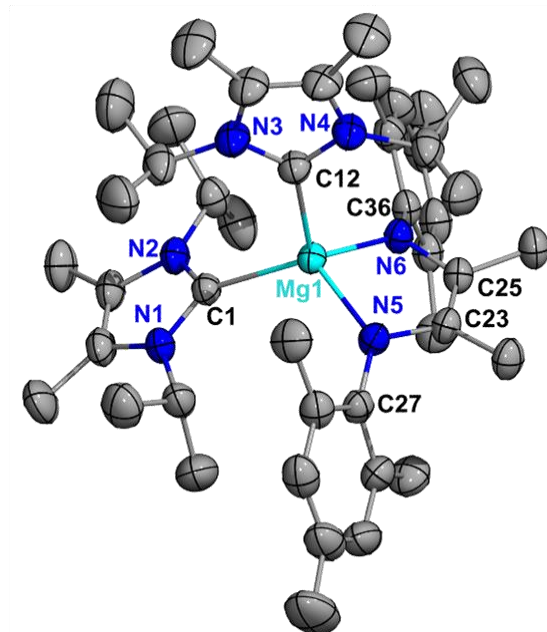


Figure A3.1. Molecular structure of **2.2** (thermal ellipsoids are shown at 50% probability, and H-atoms omitted for clarity).

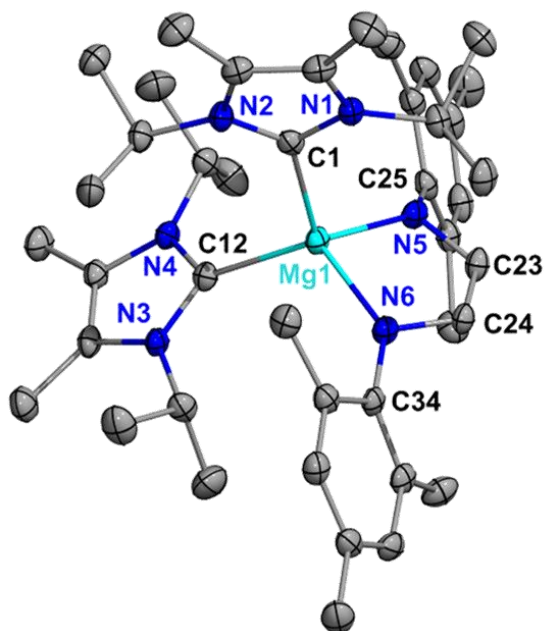


Figure A3.2. Molecular structure of **2.3**. Thermal ellipsoids are shown at 50% probability. H-atoms, and one co-crystallized toluene molecule omitted for clarity.

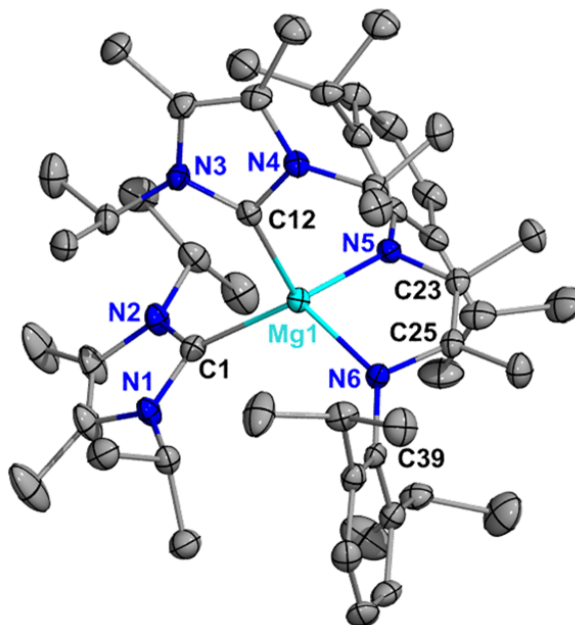


Figure A3.3. Molecular structure of **2.4** (thermal ellipsoids are shown at 50% probability, and H-atoms omitted for clarity). Only one of three chemically equivalent but crystallographically unique molecules in the asymmetric unit is shown.

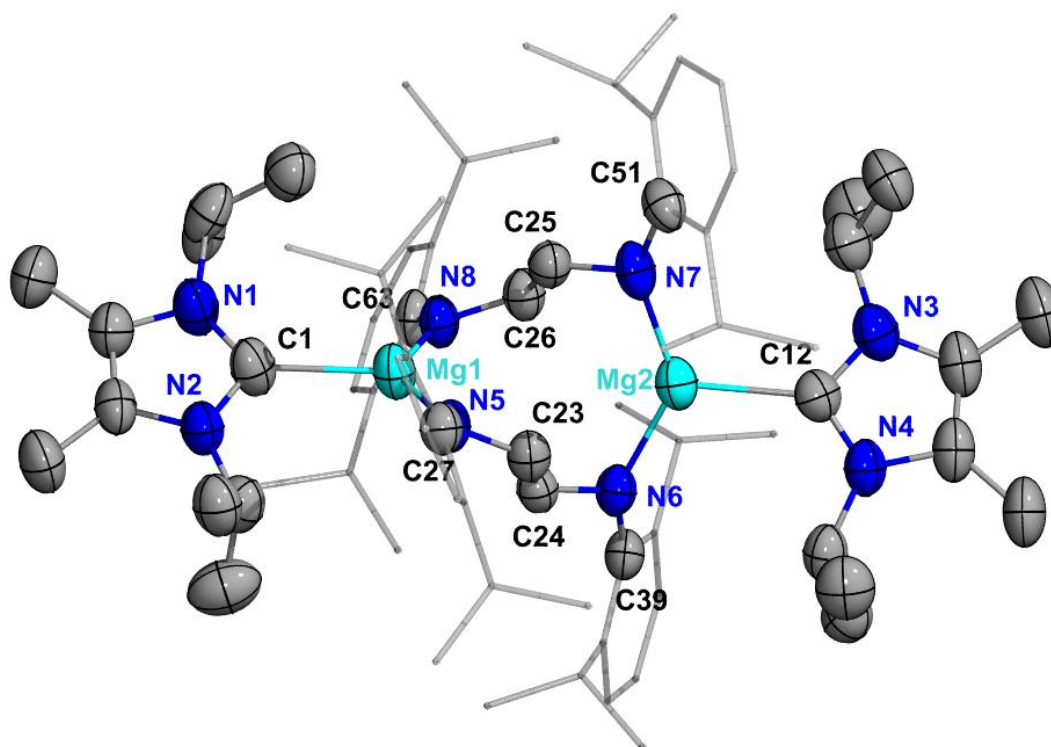


Figure A3.4. Molecular structure of **2.6**. For clarity, H atoms and co-crystallized toluene molecules have been omitted, and the Dipp groups are styled as wireframe. Only the major occupied positions are shown for the disordered isopropyl substituents on N2.

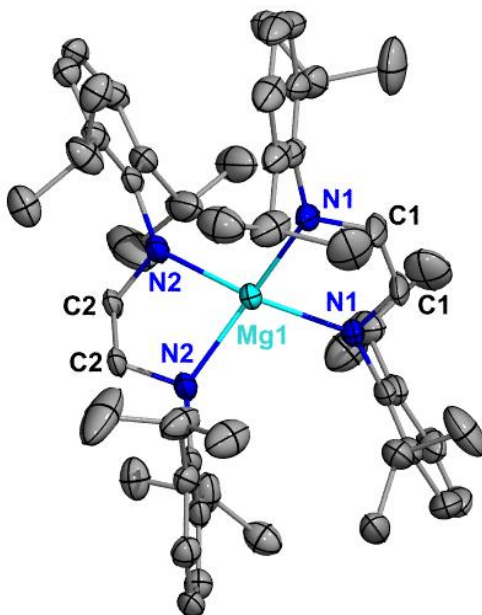


Figure A3.5. X-ray structure of compound **2.7**. Thermal ellipsoids are shown at 50% probability. For clarity, H atoms are omitted and only major occupied positions for the disordered C2 and isopropyl substituents are shown. Selected bond distances (Å) and angles (°): Mg1–N1: 2.0836(18); Mg1–N2: 2.0870(19); N1–C1: 1.323(3); N2–C2: 1.364(6); C1–C1': 1.388(5).

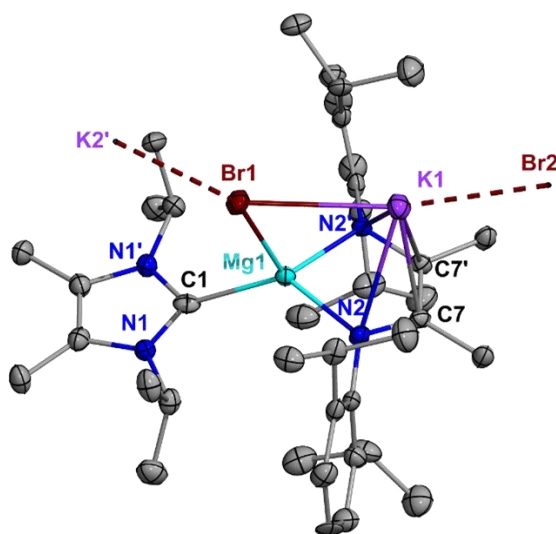


Figure A3.6. X-ray structure of compound **2.8** (thermal ellipsoids are shown at 50% probability, and H-atoms omitted for clarity). Selected bond distances (Å) and angles (°): Mg1–C1: 2.196(10); Mg2–C21: 2.210(11); Mg1–Br1: 2.606(3); Mg2–Br2: 2.591(3); Mg1–N2: 2.043(6); Mg2–N4: 2.029(6); C7–C7': 1.387(15); C27–C27': 1.370(15); Br1–K1: 3.233(2); Br1–K2: 3.136(2); Br2–K1: 3.103(2); Br2–K2: 3.246(2); K1–C7: 2.907(7); K1–N2: 2.936(6); K2–C27: 2.915(7); K2–N4: 2.927(6); N2–Mg1–N2': 83.9(3); N2–Mg1–C1: 129.7(2); C1–Mg1–Br1: 94.3(3); N2–Mg1–Br1: 109.45(19).

Chapter Three:

A suitable single crystal of each complex was coated with Paratone oil and mounted on a MiTeGen MicroLoop. The X-ray intensity data were measured on a Bruker Kappa APEXII Duo system. The Incoatec Microfocus I μ S (Cu K α , $\lambda = 1.54178$ Å) and a multi-layer mirror monochromator were used for **3.2**, **3.3**[BAr^F₄], **3.4**[BAr^F₄], **3.5**[BPh₄], and **3.8**, and the fine-focus sealed tube (Mo K α , $\lambda = 0.71073$ Å) and a graphite monochromator were used for **3.3**[BPh₄], **3.4**[BPh₄], and **3.7**. The frames were integrated with the Bruker SAINT software package⁴²⁷ using a narrow-frame algorithm. Data were corrected for absorption effects using the Multi-Scan method (SADABS).⁴²⁷ Each structure was solved and refined using the Bruker SHELXTL Software Package⁴²⁸ within APEX3⁴²⁷ and OLEX2.⁴²⁹ Non-hydrogen atoms were refined anisotropically. Hydrogen atoms were placed in geometrically calculated positions with $U_{iso} = 1.2U_{equiv}$ of the parent atom ($U_{iso} = 1.5U_{equiv}$ for methyl) unless otherwise specified below.⁴²⁷

In **3.2**, the best available crystal diffracted extremely weakly and it was not possible to collect data to the typical resolution. Nevertheless, enough data was obtained to unambiguously determine the connectivity of the structure. The C-H hydrogen atoms of the bridging methyl groups were located in the diffraction map and refined isotropically with $U_{iso} = 1.5U_{equiv}$ of the parent carbon and restraints on the bond distances. Several sites of disorder were identified in the structure. The relative occupancies of each disordered site was freely refined, and constraints and restraints were used as needed on the anisotropic displacement parameters and/or the bond lengths of the disordered atoms.

In **3.3**[BPh₄], both the cation and anion were extensively disordered. The relative occupancies of the disordered sites was freely refined. Constraints were used on the anisotropic displacement parameters of one disordered phenyl and one disordered imidazole. Constraints were also used on the bond lengths of the minor position of one disordered phenyl.

In **3.4**[**BAr^F₄**], one CF₃ group was extremely disordered by rotation. It was modeled over three positions with the sum set to 1 and with constraints on the anisotropic displacement parameters of the disordered atoms.

In **3.5**[**BPh₄**], the relative occupancies of the methyl and Br substituents was freely refined, and constraints were used on the anisotropic displacement parameters of the disorder atoms.

In **3.7**, a two-component twin was identified using CELL_NOW.⁴³¹ Starting with 1267 reflections, 1180 reflections were fit to the first domain, 1054 to the second domain (56 exclusively), with 31 unindexed reflection remaining. The twin domain was oriented at a 179.8° rotation about the reciprocal axis 0.004 0.000 1.000. The twin law was -0.996 0.003 0.008 / -0.006 -1.000 0.000 / 1.042 0.000 0.996. The structure was refined on HKLF5 data, with the BASF for the twin domains refining to 0.40527.

Table A3.2 Crystallographic details for compounds **3.2-3.5, 3.7** and **3.8**.

	3.2	3.3[BPh₄]	3.3[BAr^F₄]	3.4[BPh₄]	3.4[BAr^F₄]	3.5[BPh₄]	3.7	3.8
CCDC number	1998358	1998359	1998360	1998361	2018107	1998362	1998363	1998364
Formula	C ₁₁₆ H ₁₁₅ B ₂ Cl F ₄₈ Mg ₂ N ₈	C ₅₈ H ₈₃ BMg N ₆	C ₆₆ H ₇₅ BF ₂₄ M gN ₆	C ₅₇ H ₈₀ BBRm gN ₆	C ₆₅ H ₇₂ BBrF ₂ ₄ MgN ₆	C _{50.95} H _{70.84} B Br _{0.06} MgN ₄ O	C ₁₄ H ₂₄ Br ₂ MgN ₄	C ₄₂ H ₇₂ Br ₄ Mg ₂ N ₁₂
FW (g/mol)	2638.84	899.42	1443.44	964.30	1508.45	794.81	432.50 g/mol	1113.37
Temp (K)	100(2)	100(2)	100(2)	100(2)	100(2)	100(2)	100(2) K	100(2)
λ (Å)	1.54178	0.71073	1.54178	0.71073	0.71073	1.54178	0.71073 Å	1.54178
Size (mm)	0.045 x 0.119 x 0.126	0.354 x 0.357 x 0.420	0.041 x 0.136 x 0.211	0.092 x 0.101 x 0.189	0.182 x 0.412 x 0.697	0.009 x 0.092 x 0.17	0.160 x 0.172 x 0.332 mm	0.103 x 0.106 x 0.121
Crystal habit	colorless plate	colorless block	colorless plate	colorless rod	colorless block	colorless plate	colorless plate	colorless block
Crystal system	triclinic	monoclinic	monoclinic	monoclinic	monoclinic	triclinic	monoclinic	cubic
Space group	P -1	P 2 ₁ /c	P 2 ₁ /n	P 2 ₁ /n	P 2 ₁ /n	P -1	P 2 ₁ /n	P 2 ₁ 3
a (Å)	18.4203(19)	17.4055(8)	13.2568(8)	13.6535(9)	13.3434(13)	10.2417(10)	9.330(3)	17.1849(3)
b(Å)	18.6215(13)	16.3293(7)	29.5926(19)	18.0955(11)	29.497(3)	15.0602(14)	13.996(4)	17.1849(3)
c (Å)	20.3747(15)	20.5763(10)	18.5731(11)	22.0243(14)	18.5791(16)	15.7584(15)	14.737(6)	17.1849(3)
α (°)	81.055(4)	90	90	90	90	85.263(7)	90	90
β (°)	71.991(6)	111.0440(10)	104.157(4)	91.008(2)	104.397(3)	77.588(7)	107.376(10)	90
γ (°)	68.409(4)	90	90	90	90	81.071(7)	90	90
Volume (Å ³)	6173.2(9)	5458.1(4)	7065.0(8)	5440.6(6)	7082.9(11)		1836.6(11)	5075.1(3)
Z	2	4	4	4	4	2	4	4
Density (g/cm ³)	1.420	1.095	1.357	1.177	1.415	1.127	1.564 g/cm ³	1.457
μ (mm ⁻¹)	1.469	0.074	1.168	0.808	0.696	0.677	4.447 mm ⁻¹	4.439
F(000)	2700	1960	2984	2064	3088	863	872	2288
θ range (°)	2.28 to 58.31	1.25 to 25.39	2.87 to 68.76	1.74 to 25.71	1.32 to 27.57	2.88 to 68.63	2.05 to 26.44°	3.64 to 68.13
Index ranges	-20 ≤ h ≤ 19 -20 ≤ k ≤ 20 -22 ≤ l ≤ 22	-21 ≤ h ≤ 20 -19 ≤ k ≤ 19 -24 ≤ l ≤ 16	-14 ≤ h ≤ 15 -35 ≤ k ≤ 35 -22 ≤ l ≤ 22	-16 ≤ h ≤ 16 -19 ≤ k ≤ 22 -26 ≤ l ≤ 26	-17 ≤ h ≤ 17 -38 ≤ k ≤ 36 -23 ≤ l ≤ 24	-10 ≤ h ≤ 12 -18 ≤ k ≤ 18 -18 ≤ l ≤ 18	-11 ≤ h ≤ 11 0 ≤ k ≤ 17 0 ≤ l ≤ 18	-20 ≤ h ≤ 12 -14 ≤ k ≤ 20 -19 ≤ l ≤ 19
Independent reflns	17206 [R _{int} = 0.1425]	10035 [R _{int} = 0.0431]	12940 [R _{int} = 0.1640]	10347 [R _{int} = 0.1079]	16305 [R _{int} = 0.0293]	8529 [R _{int} = 0.0993]	3834 [R _{int} = 0.1411]	3133 [R _{int} = 0.0605]
Data / restraints /parameters	17206 / 312 / 1655	10035 / 0 / 898	12940 / 0 / 931	10347 / 0 / 613	16305 / 109 / 958	8529/0/540	3834 / 0 / 199	3113 / 0 / 189
GOF on F ²	1.025	1.071	0.977	0.984	1.018	1.016	1.054	1.058
R ₁ (I > 2σ(I))	0.1399	0.0488	0.0887	0.0535	0.0362	0.0542	0.0699	0.0348
wR ₂ (all data)	0.4036	0.1530	0.2802	0.0938	0.0913	0.1425	0.1917	0.0837

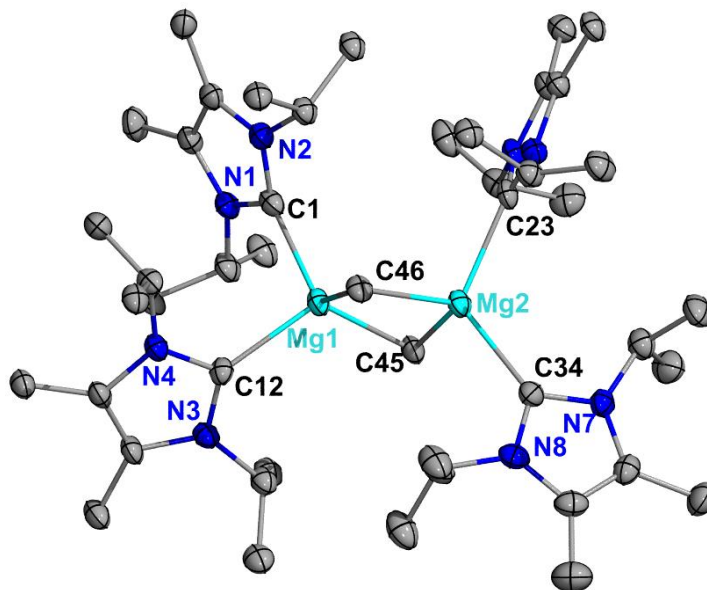


Figure A3.7. X-ray structure of compound **3.2** (thermal ellipsoids shown at 50% probability; H atoms, two BAR^{F}_4 anions and one co-crystallized $\text{C}_6\text{H}_5\text{Cl}$ molecule are omitted for clarity). Selected bond distances (Å) and angles ($^\circ$): Mg1–C1: 2.233(12); Mg1–C12: 2.209(10); Mg2–C23: 2.228(10); Mg2–C34: 2.212(11); Mg1–C45: 2.223(11); Mg1–C46: 2.246(10); Mg2–C45: 2.215(10); Mg2–C46: 2.285(11); C1–N1: 1.363(13); C1–N2: 1.356(13); C12–N3: 1.371(12); C12–N4: 1.353(12); C45–Mg1–C46: 102.7(4); Mg1–C46–Mg2: 74.3(3); C45–Mg2–C46: 101.7(4); Mg1–C45–Mg2: 76.1(4); C46–Mg2–C45–Mg1: 17.1(4).

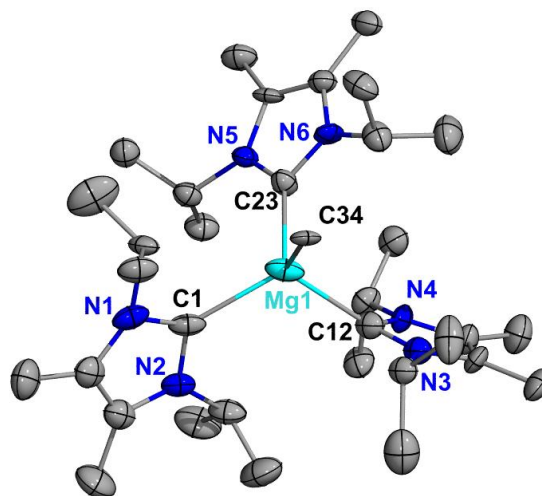


Figure A3.8. X-ray structure of compound **3.3**[BPh_4]. Thermal ellipsoids are shown at 50% probability. H-atoms and one non-coordinating BPh_4 anion are omitted for clarity. Selected bond distances (Å) and angles ($^\circ$): Mg1–C1: 2.277(2); Mg1–C12: 2.163(7); Mg1–C23: 2.271(2); Mg1–C34: 2.257(19); C1–Mg1–C12: 114.5(3); C1–Mg1–C23: 108.76(7); C1–Mg1–C34: 112.87(7); C12–Mg1–C23: 102.5(3); C12–Mg1–C34: 106.4(2); C23–Mg1–C34: 111.30(7).

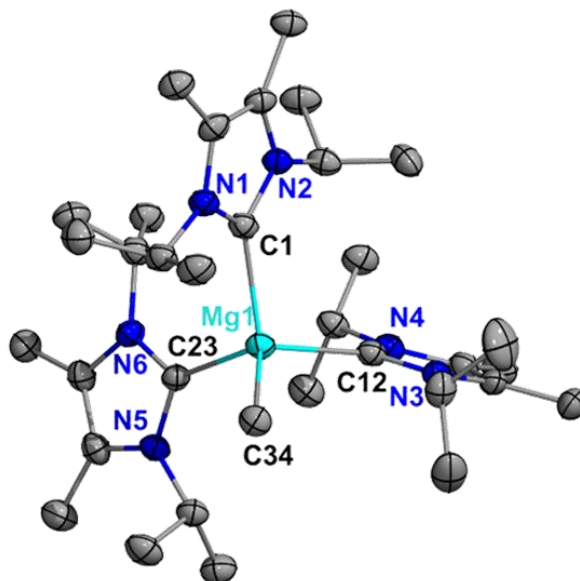


Figure A3.9. X-ray structure of compound **3.3**[BAr^F₄]. Thermal ellipsoids are shown at 30% probability. H-atoms and one non-coordinating BAr^F₄ anion are omitted for clarity. Selected bond distances (Å) and angles (°): Mg1–C1: 2.281(6); Mg1–C12: 2.276(6); Mg1–C23: 2.262(5); Mg1–C34: 2.154(5); C1–Mg1–C12: 108.85(19); C1–Mg1–C23: 111.4(2); C1–Mg1–C34: 109.8 (2); C12–Mg1–C23: 103.6(2); C12–Mg1–C34: 112.1(2); C23–Mg1–C34: 111.0(2).

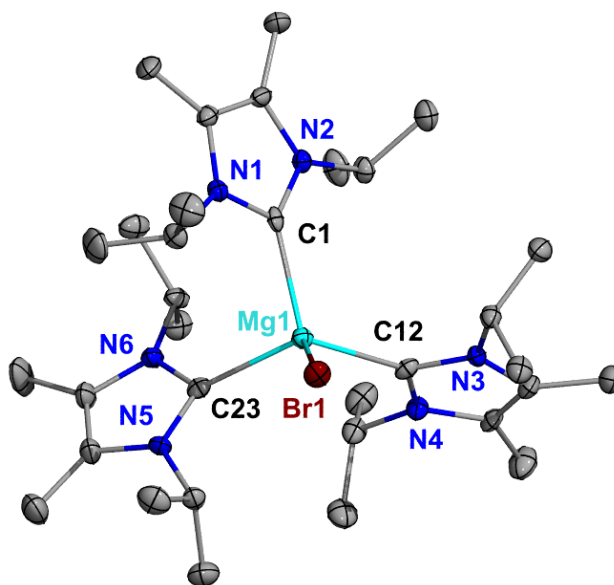


Figure A3.10. X-ray structure of compound **3.4**[BPh₄]. Thermal ellipsoids are shown at 50% probability. H-atoms and one non-coordinating BPh₄ anion are omitted for clarity. Selected bond distances (Å) and angles (°): Mg1–C1: 2.209(3); Mg1–C12: 2.210(3); Mg1–C23: 2.251(3); Mg1–Br1: 2.5195(9); C1–Mg1–C12: 115.31(11); C1–Mg1–C23: 101.59(10); C1–Mg1–Br1: 107.33(8); C12–Mg1–C23: 116.76(11); C12–Mg1–Br1: 105.54(8); C23–Mg1–Br1: 110.04(8).

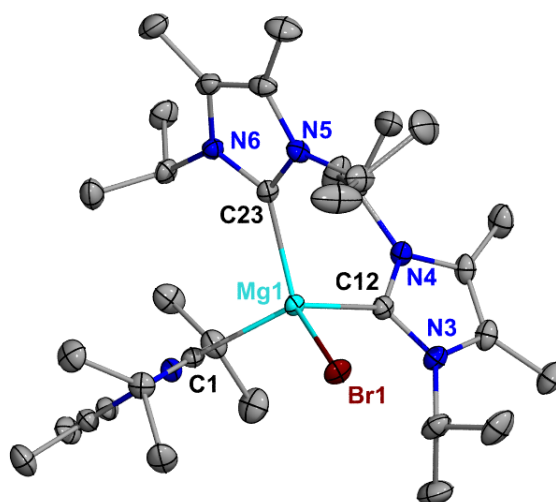


Figure A3.11. X-ray structure of compound **3.4**[BAr^F₄]. Thermal ellipsoids are shown at 50% probability. H-atoms and one non-coordinating BA^rF₄ anion are omitted for clarity. Selected bond distances (Å) and angles (°): Mg1–C1: 2.2360(18); Mg1–C12: 2.2554(18); Mg1–C23: 2.2434(18); Mg1–Br1: 2.4934(6); C1–Mg1–C12: 113.16(6); C1–Mg1–C23: 107.38(6); C1–Mg1–Br1: 107.99(5); C12–Mg1–C23: 111.00(7); C12–Mg1–Br1: 107.93(5); C23–Mg1–Br1: 109.29(5).

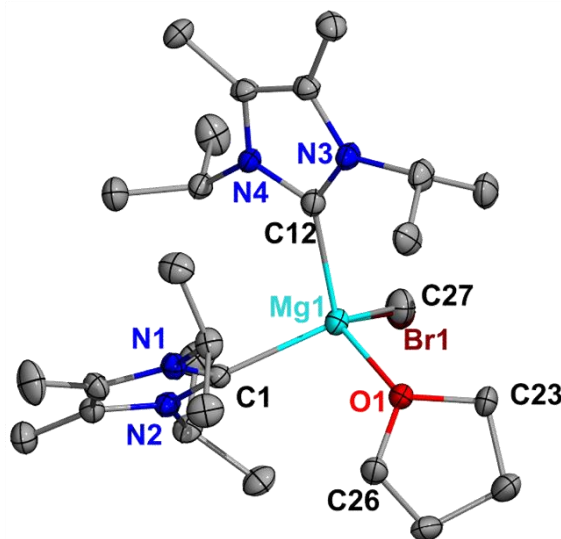


Figure A3.12. X-ray structure of compound **3.5**[BPh₄] including 4% co-crystallized [(ⁱPrNHC)₂(THF)Mg(Br)][BPh₄] (thermal ellipsoids shown at 50% probability; H atoms and non-coordinating BPh₄ anion are omitted for clarity). Selected bond distances (Å) and angles (°): Mg1–C1: 2.260(2); Mg1–C12: 2.246(3); Mg1–C27: 2.178(14); Mg1–O1: 2.0593(18); C1–N1: 1.365(5); C1–N2: 1.360(3); C1–Mg1–C12: 99.32(9); C1–Mg1–C27: 128.1(4); C12–Mg1–C27: 107.6(4); C12–Mg1–O1: 116.66(9).

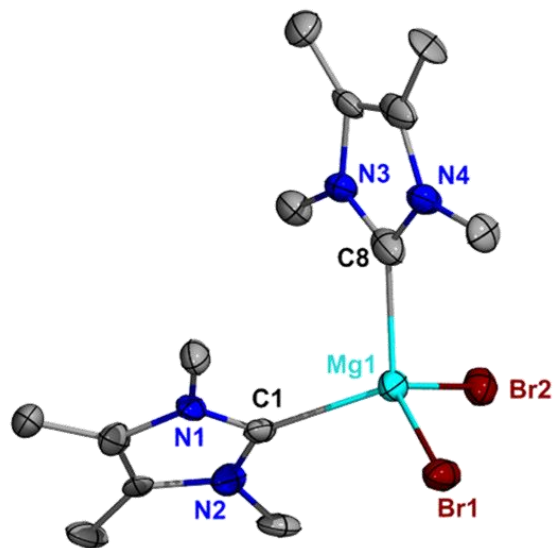


Figure A3.13. X-ray structure of compound **7** (thermal ellipsoids are shown at 50% probability; H-atoms omitted for clarity). Selected bond distances (Å) and angles (°): Mg1–C1: 2.234(13); Mg1–C12: 2.217(13); Mg1–Br1: 2.510(3); Mg1–Br2: 2.487(3); C1–N1: 1.333(13); C1–N2: 1.339(13); C8–N3: 1.352(15); C8–N4: 1.397(14); C1–Mg1–C8: 108.9(4); C1–Mg1–Br1: 106.3(3); C1–Mg1–Br2: 108.0(3); C8–Mg1–Br1: 110.9(4); C8–Mg1–Br2: 103.1(4); Br1–Mg1–Br2: 119.41(11); N1–C1–N2: 104.9(10); N4–C8–N3: 103.7(10)

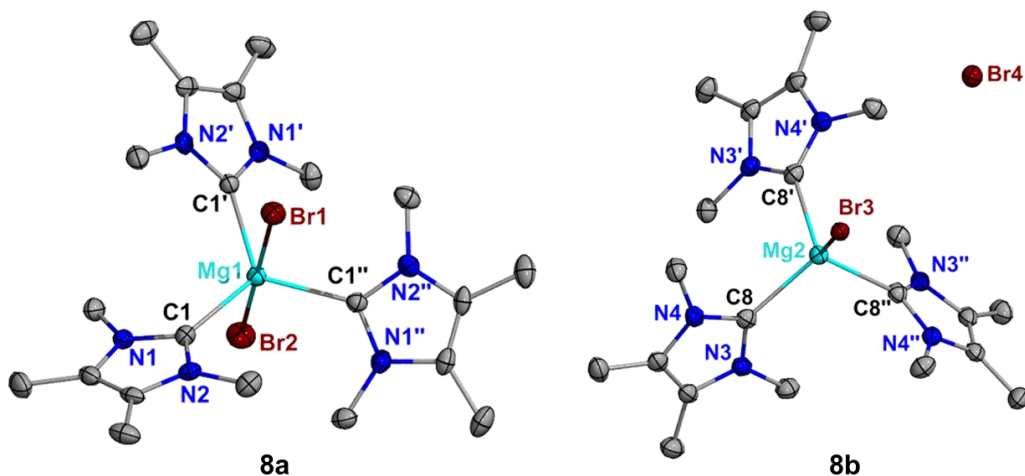


Figure A3.14. X-ray structure of compound **8a** and **8b** (thermal ellipsoids are shown at 50% probability; H-atoms omitted for clarity). Selected bond distances (Å) and angles (°): Mg1–C1: 2.214(5); Mg2–C8: 2.215(5); Mg1–Br1: 2.883(3); Mg1–Br2: 2.694(3); Mg2–Br3: 2.513(3); C1–N1: 1.361(7); C8–N4: 1.348(7); C1–Mg1–C1': 119.77(3); Br1–Mg1–Br2: 180.00(6); C1–Mg1–Br1: 87.25(16); C1–Mg1–Br2: 92.74(16); C8–Mg2–C8': 109.70(15); C8–Mg2–Br3: 109.24(15).

Chapter Four:

Single crystals of **4.1^{Me}**, **4.2^{iPr}**, **4.2^{iPr}·toluene**, **4.3^{Me}**, **4.4^{Me}·C₆H₅F**, **4.6**, **4.7^{iPr}·C₆H₅Br**, **4.9**, **4.10**, and **4.11** were coated with Paratone oil and mounted on a MiTeGen MicroLoop. The X-ray intensity data for **4.4^{Me}** were measured on a Bruker D8 Venture Photon III Kappa four-circle diffractometer system using an Incoatec I μ S 3.0 micro-focus sealed X-ray tube (Cu K α , $\lambda = 1.54178 \text{ \AA}$) and a HELIOS EF double bounce multilayer mirror monochromator. All others were measured on a Bruker Kappa APEXII Duo system. An Incoatec Microfocus I μ S (Cu K α , $\lambda = 1.54178 \text{ \AA}$) source and a multi-layer mirror monochromator were used for **4.1^{Me}** and **4.10** and a fine-focus sealed tube (Mo K α , $\lambda = 0.71073 \text{ \AA}$) and a graphite monochromator were used for all others. The frames were integrated with the Bruker SAINT software package⁴²⁷ using a narrow frame algorithm. Data were corrected for absorption effects using the multiscan method (TWINABS for **4.4^{Me}·C₆H₅F** and **4.6**, SADABS for all others).⁴²⁷ Each structure was solved and refined using the Bruker SHELXTL Software Package⁴²⁸ within APEX3⁴²⁷ and OLEX2.⁴²⁹ Non-hydrogen atoms were refined anisotropically. Hydrogen atoms were placed in geometrically calculated positions with $U_{\text{iso}} = 1.2U_{\text{equiv}}$ of the parent atom ($U_{\text{iso}} = 1.5U_{\text{equiv}}$ for methyl).

In **4.1^{Me}**, the relative occupancy of the substitutional disorder at the Mg was freely refined, with restraints on the disordered bond lengths and a constraint on the anisotropic displacement parameter of one pair of disordered atoms. In **4.2^{iPr}**, two isopropyl groups were disordered. The relative occupancy of each position was freely refined. Constraints were used on the anisotropic displacement parameters of some of the disordered atoms, and restraints were used on some of the disordered bonds. In **4.2^{iPr}·toluene**, the relative occupancy of the disordered positions was freely refined, with the toluene set at 50% to reflect its position on an inversion center. Constraints and restraints were used on the anisotropic displacement parameters and bond lengths of the most of the disordered atoms. In **4.3^{Me}**, the ethyl group was disordered over two positions. The relative

occupancy of the positions was freely refined, and no constraints or restraints were needed. In **4.10**, toluene solvent molecules were located in the crystal lattice. One was well-behaved but the remainder were severely disordered and could not be adequately modeled with or without restraints. Thus, the structure factors were modified using the PLATON SQUEEZE⁴³⁰ technique, in order to produce a “solvate-free” structure factor set. PLATON reported a total electron density of 79 e⁻ and total solvent accessible volume of 317 Å³. This corresponds to an additional 1.5 toluene molecules in the unit cell. In **4.4^{Me}**, OCP anion was disordered over three positions. The relative occupancy of the disordered atoms was freely refined with the sum of the parts set to equal 1. Restraints were used on the anisotropic displacement parameters and/or bond lengths of some of the disordered atoms.

Compounds **4.4^{Me}·C₆H₅F**, **4.6** and **4.9** each crystallized as a two-domain twin, identified by CELL_NOW.⁴³¹ The twin domain for **4.4^{Me}·C₆H₅F** was oriented at a 179.9° rotation about the reciprocal axis -0.014 1.000 -0.032. The twin law was -1.001 -0.028 -0.002 / -0.004 1.000 -0.009 / 0.004 -0.065 -0.999. The twin domain for **6** was oriented at a 180.0° rotation about the real axis 1.000 -0.002 -0.004. The twin law was 0.999 -0.004 -0.008 / -0.001 -1.000 0.000 / -0.237 0.001 -0.999. The twin domain for **9** was oriented at a 178.8° rotation about the reciprocal axis 0.988 1.000 0.001. The twin law was -0.004 0.993 -0.308 / 1.008 0.004 -0.287 / 0.018 -0.017 -0.999. These three structures were refined on HKLF5 data, with the BASF for the twin domains refining to 0.494 (**4.4^{Me}**), 0.48966 (**4.6**) and 0.19203 (**4.9**).

Table A3.3. Crystallographic data for **4.1^{Me}**, **4.2^{iPr}**, **4.2^{iPr}·toluene**, **4.3^{Me}** and **4.4^{Me}**

	4.1^{Me}	4.2^{iPr}	4.2^{iPr}·toluene	4.3^{Me}	4.4^{Me}	4.4^{Me}·C₆H₅F
CCDC number	2086364	2086365	2086366	2086367	2097942	2086368
Formula	C ₁₅ H ₂₇ BrMgN ₄	C ₂₄ H ₄₃ MgN ₄ OP	C ₅₅ H ₉₄ Mg ₂ N ₈ O ₂ P ₂	C ₂₀ H ₄₀ Mg ₂ N ₄ O ₂	C ₂₃ H ₃₉ MgN ₆ OP	C ₂₉ H ₄₄ FMgN ₆ OP
FW (g/mol)	367.62	458.90	1009.94	417.18	471.17	566.98
Temp (K)	100(2)	100(2)	100(2)	200(2)	100(2)	100(2)
λ (Å)	1.54178	0.71073	0.71073	0.71073	1.54178	0.71073
Size (mm)	0.086 x 0.154 x 0.243	0.220 x 0.294 x 0.335	0.282 x 0.453 x 0.547	0.151 x 0.187 x 0.305	0.098 x 0.172 x 0.381	0.106 x 0.261 x 0.262
Crystal habit	colorless plate	colorless block	colorless block	colorless plate	colourless needle	colorless plate
Crystal system	orthorhombic	orthorhombic	monoclinic	triclinic	monoclinic	triclinic
Space group	P na ₂₁	P na ₂₁	P 2 ₁ /n	P -1	P 2 ₁	P 1
a (Å)	13.5631(3)	13.7153(15)	12.155(2)	8.6750(8)	13.0406(4)	7.4357(10)
b (Å)	9.7053(2)	23.497(2)	18.446(3)	9.1705(8)	7.4809(2)	13.1361(16)
c (Å)	13.8094(2)	8.5710(9)	14.196(3)	9.4217(8)	14.2517(5)	17.650(3)
α (°)	90	90	90	105.182(2)	90	69.933(3)
β (°)	90	90	91.427(6)	104.780(2)	91.443(2)	88.373(4)
γ (°)	90	90	90	109.615(2)	90	89.214(3)
Volume (Å ³)	1817.79(6)	2762.2(5)	3181.9(10)	631.03(10)	1389.89(7)	1618.7(4)
Z	4	4	2	1	2	2
Density (g/cm ³)	1.343	1.104	1.054	1.098	1.126	1.163
μ (mm ⁻¹)	3.404	0.143	0.130	0.115	1.287	0.141
F(000)	768	1000	1100	228	508	608
θ range (°)	5.57 to 68.27	1.72 to 26.46	1.81 to 28.38	2.42 to 27.13	3.10 to 68.48	1.23 to 25.48
Index ranges	-16 ≤ h ≤ 16 -9 ≤ k ≤ 11 -16 ≤ l ≤ 16	-17 ≤ h ≤ 17 -29 ≤ k ≤ 29 -10 ≤ l ≤ 10	-16 ≤ h ≤ 16 -24 ≤ k ≤ 24 -18 ≤ l ≤ 18	-11 ≤ h ≤ 11 -8 ≤ k ≤ 11 -12 ≤ l ≤ 11	-15 ≤ h ≤ 15 -9 ≤ k ≤ 8 -17 ≤ l ≤ 17	-8 ≤ h ≤ 8 -14 ≤ k ≤ 15 0 ≤ l ≤ 21
Data / restraints / parameters	3330 / 3 / 212	5679 / 2 / 325	7944 / 6 / 401	2789 / 0 / 153	4958 / 11 / 347	6002 / 3 / 688
GOF on F ²	1.059	1.077	1.030	1.044	1.071	1.012
R ₁ (I > 2σ(I))	0.0376	0.0502	0.0575	0.0417	0.0496	0.0663
wR ₂ (all data)	0.0926	0.1273	0.1601	0.1185	0.1294	0.1618

Table A3.4. Crystallographic data for **4.6, 4.9 – 4.11**

	4.6	4.7^{iPr}·C₆H₅Br	4.9	4.10	4.11
CCDC number	2086369	2097943	2086370	2086371	2086372
Formula	C ₅₁ H ₈₀ N ₁₂ Na ₂ O ₂ P ₂	C ₃₄ H ₅₀ Br ₄ MgN ₄	C ₂₈ H ₅₀ Mg ₂ N ₄ O ₄ P ₂	C ₃₀ H ₄₄ MgN ₆ O ₂ P ₂	C ₁₅ H ₂₄ N ₄ OP ₂
FW (g/mol)	1001.19	858.73	617.28	606.96	338.32
Temp (K)	100(2)	100(2)	100(2)	100(2)	100(2)
λ (Å)	0.71073	0.71073	0.71073	1.54178	0.71073
Size (mm)	0.200 x 0.400 x 0.450	0.110 x 0.152 x 0.219	0.078 x 0.157 x 0.292	0.064 x 0.133 x 0.160	0.044 x 0.154 x 0.355
Crystal habit	colorless block	yellow block	colorless plate	colorless plate	colorless rod
Crystal system	monoclinic	orthorhombic	triclinic	triclinic	triclinic
Space group	P 2 ₁ /c	P b c n	P -1	P -1	P -1
a (Å)	23.643(3)	12.5952(8)	9.311(4)	11.3758(2)	9.7758(11)
b (Å)	11.9829(16)	13.2526(9)	9.422(4)	12.8027(4)	10.3750(11)
c (Å)	20.770(2)	22.7038(14)	10.345(4)	14.9412(3)	10.6004(12)
α (°)	90	90	78.802(11)	68.969(2)	111.862(3)
β (°)	96.347(3)	90	81.883(12)	72.489(2)	111.081(3)
γ (°)	90	90	82.314(11)	82.184(2)	97.916(3)
Volume (Å ³)	5848.3(13)	3789.7(4)	876.1(6)	1936.01(9)	884.04(17)
Z	4	4	1	2	2
Density (g/cm ³)	1.137	1.505	1.170	1.041	1.271
μ (mm ⁻¹)	0.136	4.292	0.195	1.420	0.253
F(000)	2152	1736	332	648	360
θ range (°)	1.73 to 25.45	1.79 to 29.61	2.02 to 25.75	3.29 to 68.39	2.23 to 28.34
Index ranges	-28 ≤ h ≤ 28 0 ≤ k ≤ 14 0 ≤ l ≤ 25	-17 ≤ h ≤ 17 -18 ≤ k ≤ 18 -31 ≤ l ≤ 31	-13 ≤ h ≤ 13 -15 ≤ k ≤ 15 -17 ≤ l ≤ 17	-13 ≤ h ≤ 13 -15 ≤ k ≤ 15 -17 ≤ l ≤ 17	-13 ≤ h ≤ 12 -13 ≤ k ≤ 13 -14 ≤ l ≤ 14
Data restraints / parameters	10560 / 0 / 648	5332 / 0 / 201	3337 / 0 / 189	7041 / 0 / 383	4406 / 0 / 207
GOF on F ²	1.055	1.021	1.075	1.040	1.042
R ₁ (I > 2σ(I))	0.0848	0.0270	0.1080	0.0661	0.0411
wR ₂ (all data)	0.2040	0.0522	0.3548	0.2002	0.0851

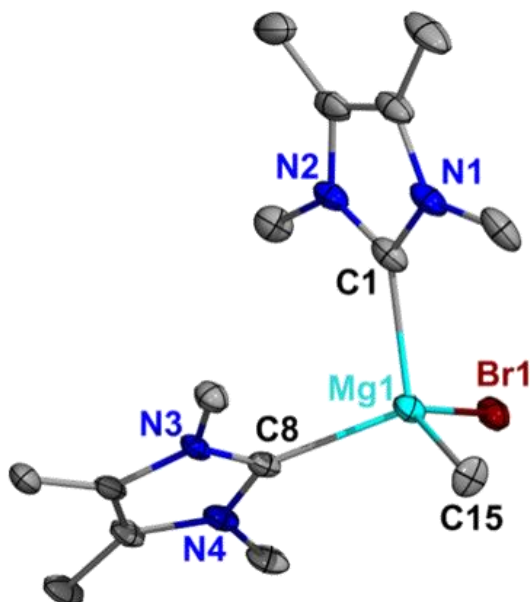


Figure A3.15. Molecular structure of 4.1^{Me} . Thermal ellipsoids are shown at 50% probability. Only the major occupied positions are shown for the disordered C15 and Br1 positions, and H atoms are omitted for clarity. Selected bond distances (Å) and angles (deg): Mg1–C15, 2.161(17); Mg1–C1, 2.253(7); Mg1–C8, 2.248(6); C1–N1, 1.363(7); C1–N2, 1.354(8), C15–Mg1–C1, 110.4(8); C15–Mg1–C8, 108.2(7); C8–Mg1–Br1, 108.06(17); C1–Mg1–Br1, 104.50(16).

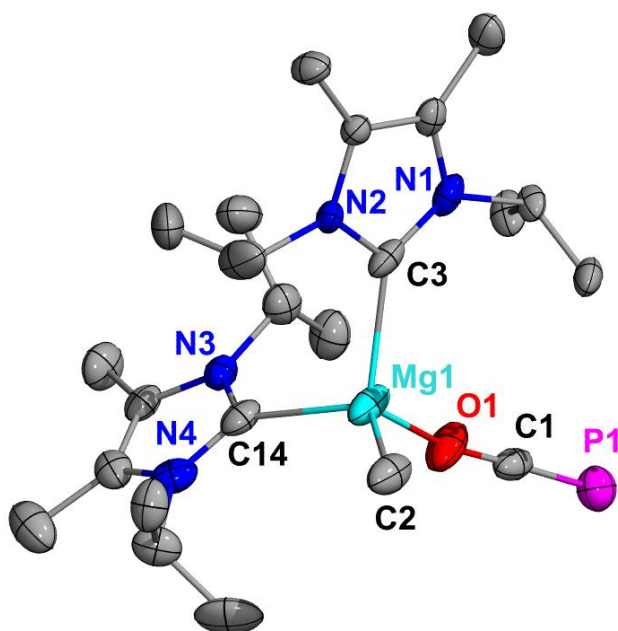


Figure A3.16. Molecular structure of 4.2^{iPr} with H atoms omitted for clarity. Selected bond distances (Å) and angles (deg): Mg1–O1, 1.982(3); O1–C1, 1.232(5); C1–P1, 1.559(5); Mg1–C2, 2.143(5); Mg1–C3, 2.266(4); Mg1–C14, 2.261(4); Mg1–O1–C1, 162.4(3); O1–C1–P1, 178.7(4); O1–Mg1–C2, 113.28(17); O1–Mg1–C14, 96.16(15).

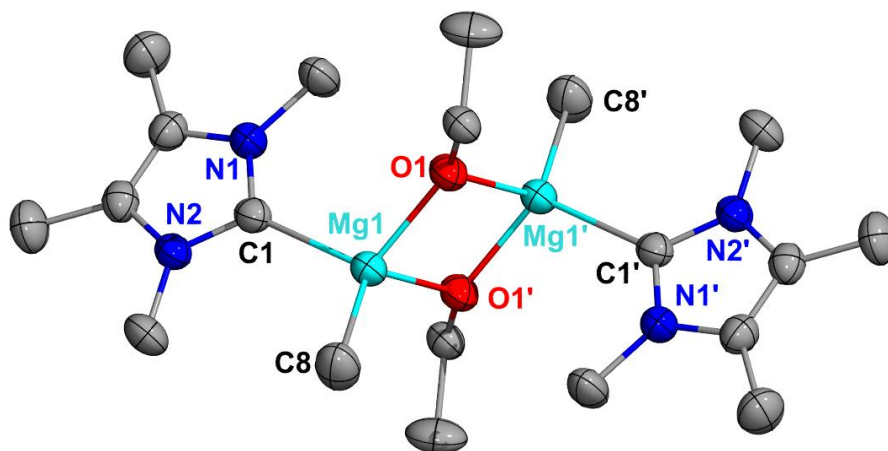


Figure A3.17. Molecular structure of 4.3^{Me} with H atoms omitted for clarity. Selected bond distances (Å) and angles (deg): Mg1–O1, 1.9659(13); Mg1–O1', 1.9868(13); Mg1–C1, 2.2649(18); Mg1–C8, 2.145(2), Mg1---Mg1', 2.9722(11); O1–Mg1–C1, 109.72(6); O1–Mg1–C8, 119.67(8); Mg1–O1–Mg1', 97.52(5).

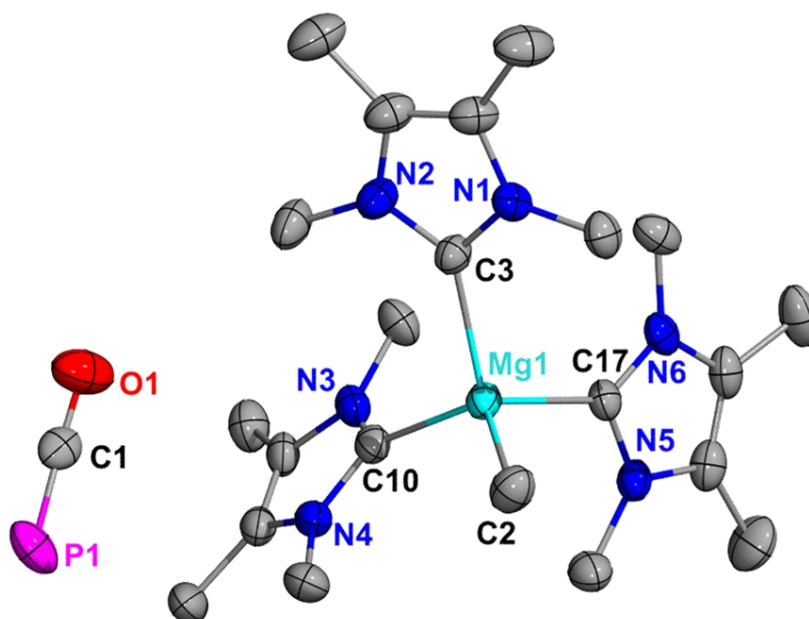


Figure A3.18. Molecular structure of 4.4^{Me} with H atoms omitted for clarity. Selected bond distances (Å) and angles (deg): C1–P1, 1.558(18); O1–C1, 1.111(16); Mg1–C2, 2.143(12); Mg1–C3, 2.241(13); Mg1–C10, 2.214(12); Mg1–C17, 2.216(11); O1–C1–P1, 176.6(13); C2–Mg1–C17, 118.5(5); C2–Mg1–C10, 108.7(5).

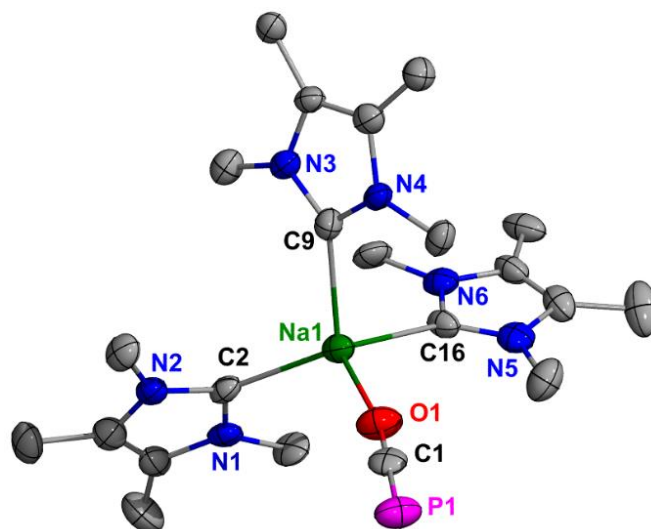


Figure A3.19. Molecular structure of **4.6** (thermal ellipsoids set at 50% probability; H atoms and co-crystallized toluene solvent are omitted for clarity). Only one of two crystallographically independent but chemically equivalent molecules in the asymmetric unit is represented. Selected bond distances (Å) and angles (deg): Na1–O1, 2.247(5); O1–C1, 1.215(5); C1–P1, 1.578(7); Na1–C2, 2.505(7); Na1–C9, 2.476(7); Na1–C16, 2.513(6); Na1–O1–C1, 167.2(5); O1–C1–P1, 179.2(6).

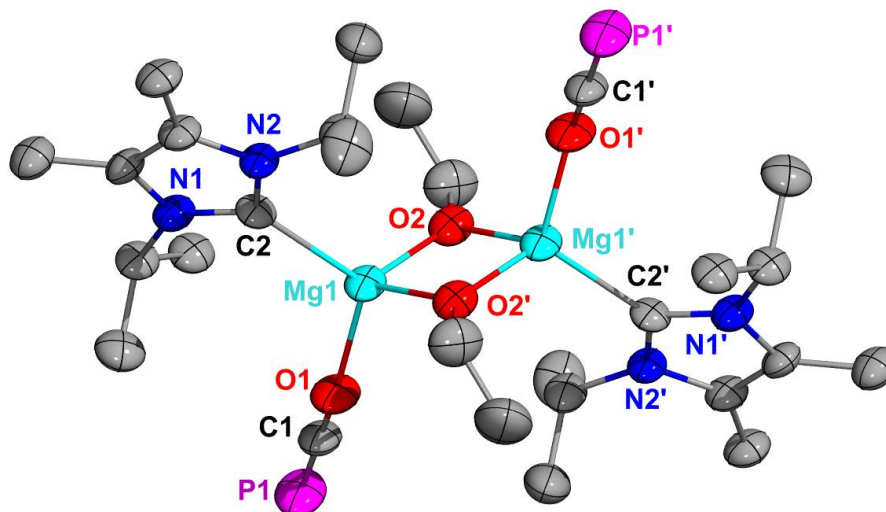


Figure A3.20. Molecular structure of **4.9** (thermal ellipsoids set at 50% probability; H atoms omitted for clarity). Selected bond distances (Å) and angles (deg): Mg1–O1, 1.938(4); Mg1–O2, 1.930(5); Mg1–O2', 1.953(4); O1–C1, 1.254(7); C1–P1, 1.545(6); Mg1–C2, 2.192(6); Mg1---Mg1, 2.885(4); Mg1–O1–C1, 145.9(5); O1–C1–P1, 179.3(6); O1–Mg1–C2, 112.6(2).

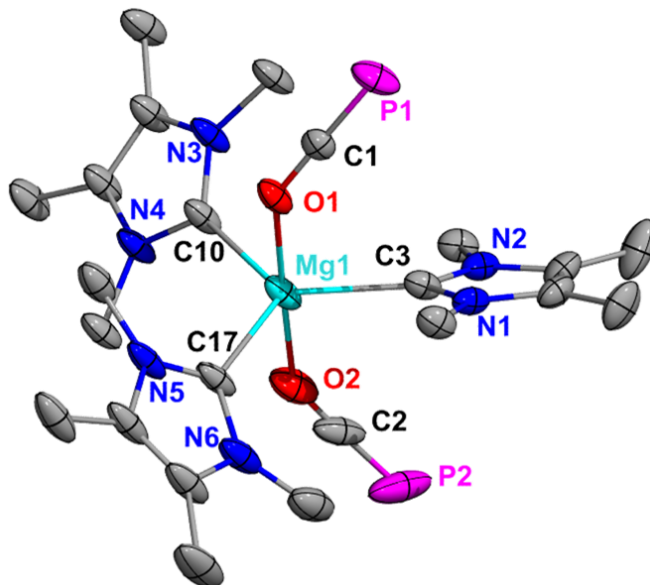


Figure A3.21. Molecular structure of **4.10** (thermal ellipsoids set at 30% probability; H atoms and co-crystallized solvent molecules omitted for clarity). Selected bond distances (Å) and angles (deg): Mg1–O1, 2.111(3); Mg1–O2, 2.143(2); Mg1–C3, 2.213(3); Mg1–C10, 2.216(3); Mg1–C17, 2.215(3); O1–C1, 1.208(3); O2–C2, 1.199(5); C1–P1, 1.575(3); C2–P2, 1.584(6); C1–O1–Mg1, 140.6(2); C2–O2–Mg1, 147.5(3); O1–Mg1–O2, 178.62(10); O2–Mg1–C3, 90.20(12); O1–Mg1–C3, 88.75(10); C17–Mg1–C3, 118.06(11); C10–Mg1–C3, 125.53(11).

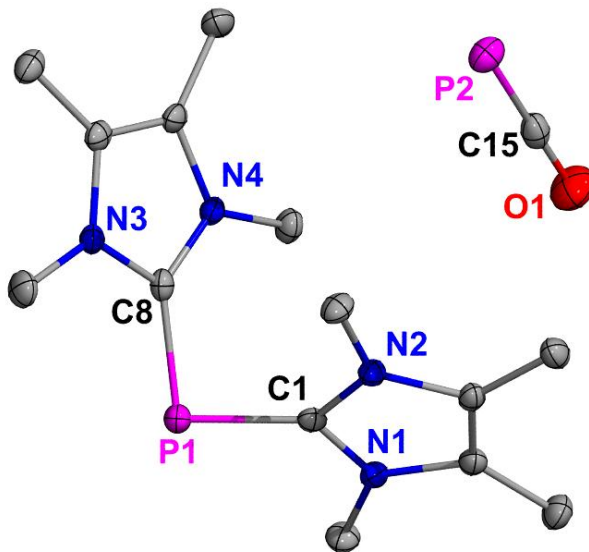


Figure A3.22. Molecular structure of **4.11** with H atoms omitted for clarity. Selected bond distances (Å) and angles (deg): P1–C1, 1.8045(18); P1–C8, 1.8055(18); C15–P2, 1.605(2); O1–C15, 1.196(2); C1–P1–C8, 96.63(8); O1–C15–P2, 179.00(17).

Chapter Five:

A single crystal of **5.2-5.9**, **5.11-5.13**, or **^{iPr}NHC-BN** was coated with Paratone oil and mounted on a MiTeGen MicroLoop. The X-ray intensity data were measured on a Bruker Kappa APEXII Duo system. A fine-focus sealed tube (Mo K α , $\lambda = 0.71073 \text{ \AA}$) and a graphite monochromator were used for **5.2**, **5.3**, **5.5** and **5.6**. An Incoatec Microfocus I μ S (Cu K α , $\lambda = 1.54178 \text{ \AA}$) and a multi-layer mirror monochromator were used for **5.4**, **5.11** and **5.13**. For **5.7**, **5.8**, **5.9**, **^{iPr}NHC-BN**, **5.12** the X-ray intensity data were measured on a Bruker D8 Venture Kappa four-circle diffractometer system equipped with an Incoatec I μ S 3.0 micro-focus sealed X-ray tube (Mo K α , $\lambda = 0.71073 \text{ \AA}$) and a HELIOS double bounce multilayer mirror monochromator.

The frames were integrated with the Bruker SAINT software package⁴²⁷ using a narrow-frame algorithm. Data were corrected for absorption effects using the Multi-Scan method (SADABS or TWINABS).⁴²⁷ Each structure was solved and refined using the Bruker SHELXTL Software Package⁴²⁸ within APEX3⁴²⁷ and OLEX2.⁴²⁹ Non-hydrogen atoms were refined anisotropically. The B-H hydrogen atoms were located in the electron density map and refined isotropically. All other hydrogen atoms were placed in geometrically calculated positions with $U_{iso} = 1.2U_{equiv}$ of the parent atom ($U_{iso} = 1.5U_{equiv}$ for methyl).

For **5.4**, a two-domain twin was identified using CELL_NOW.⁴³¹ Starting with 1270 reflections, 700 reflections were fit to the first domain, 701 to the second domain (258 exclusively), with 312 unindexed reflection remaining. The twin domain was oriented at a 179.9° rotation about the real axis 1.000 0.002 0.000. The twin law was 1.000 0.004 0.000 / 0.001 -1.000 0.001 / -0.162 -0.010 -1.000. The structure was refined on HKLF5 data, with the BASF for the twin domains refining to 0.48587. One toluene was symmetry-disordered and was modeled at 50% occupancy to reflect its special position. Another toluene molecule was disordered across three positions. The total occupancy was restricted to one and the relative occupancy of each of the three

positions was freely refined. Constraints and restraints were used on the anisotropic displacement parameters and bond lengths of most of the disordered atoms.

For **5.7**, the toluene solvent was modeled at half-occupancy because of its location on an inversion center.

For **5.13**, a two-domain twin was identified using CELL_NOW.⁴³¹ Starting with with 712 reflections, 511 reflections were fit to the first domain, 304 to the second domain (172 exclusively), with 29 unindexed reflection remaining. The twin domain was oriented at a 180.0° rotation about the real axis 0.046 1.000 0.042. The twin law was -0.998 0.039 0.002 / 0.091 0.990 0.083 / 0.008 0.196 -0.992. The structure was refined on HKLF5 data, with the BASF for the twin domains refining to 0.24281. For **5.12**, the relative occupancy of the disordered atoms was freely refined with restraints on the bond lengths of some of the disordered atoms.

Table A3.5. Crystallographic data for **5.2**, **ⁱPrNHC-BN**, **5.3**, **5.4**, **5.5**, and **5.6**

	5.2	ⁱPrNHC-BN	5.3	5.4	5.5	5.6
CCDC number	2171705	2171711	2171706	2171707	2171708	2193394
Formula	C ₂₁ H ₅₅ B ₂ MgN ₅ Si ₂	C ₁₃ H ₂₈ BN ₃	C ₂₆ H ₆₀ MgN ₆ Si ₄	C _{27.41} H _{58.90} B ₂ MgN ₅ Si ₂	C ₁₂ H ₅₄ B ₆ Mg ₄ N ₆ O	C ₁₂ H ₃₄ B ₂ MgN ₂ O ₂
FW (g/mol)	479.81	237.19	593.47	560.74	460.71	284.34
Temp (K)	100(2)	100(2)	100(2)	100(2)	100(2)	100(2)
λ (Å)	0.71073	0.71073	0.71073	1.54178	0.71073	0.71073
Size (mm)	0.124 x 0.436 x 0.556	0.154 x 0.213 x 0.242	0.337 x 0.383 x 0.460	0.050 x 0.093 x 0.394	0.238 x 0.368 x 0.592	0.187 x 0.258 x 0.443
Crystal habit	colorless plate	colorless block	colorless block	colorless plate	colorless block	colorless block
Crystal system	triclinic	orthorhombic	monoclinic	monoclinic	monoclinic	monoclinic
Space group	P -1	P 2 ₁ 2 ₁ 2 ₁	P 2 ₁ /n	C 2/c	P 2 ₁ /c	P 2 ₁ /c
a (Å)	9.0622(8)	9.6525(5)	11.6206(8)	40.4549(11)	10.8706(12)	13.4148(8)
b (Å)	12.2039(11)	10.7259(4)	18.9669(15)	8.6263(3)	17.3821(18)	11.8729(6)
c (Å)	15.8009(14)	14.4813(7)	16.7456(14)	25.2455(7)	16.1710(17)	12.2359(6)
α (°)	76.419(2)	90	90	90	90	90
β (°)	76.976(2)	90	98.879(2)	124.8810(10)	101.766(3)	110.843(2)
γ (°)	70.781(2)	90	90	90	90	90
Volume (Å ³)	1583.0(2)	1499.27(12)	3646.6(5)	7227.3(4)	2991.4(6)	1821.31(17)
Z	2	4	4	8	4	4
Density (g/cm ³)	1.007	1.051	1.081	1.031	1.023	1.037
μ (mm ⁻¹)	0.148	0.062	0.204	1.218	0.137	0.097
F(000)	532	528	1304	2467	1016	632
θ range (°)	1.34 to 31.55	2.36 to 27.50	1.63 to 33.17	2.66 to 68.36	1.74 to 29.63	1.62 to 27.15
Index ranges	-13 ≤ h ≤ 13 -17 ≤ k ≤ 17 -23 ≤ l ≤ 23	-12 ≤ h ≤ 12 -12 ≤ k ≤ 13 -18 ≤ l ≤ 18	-16 ≤ h ≤ 17 -29 ≤ k ≤ 29 -25 ≤ l ≤ 25	-48 ≤ h ≤ 39 0 ≤ k ≤ 10 0 ≤ l ≤ 30	-15 ≤ h ≤ 14 -24 ≤ k ≤ 24 -14 ≤ l ≤ 22	-16 ≤ h ≤ 17 -15 ≤ k ≤ 15 -15 ≤ l ≤ 15
Data / restraints / parameters	10557 / 0 / 316	3451 / 0 / 170	13910 / 0 / 354	6620 / 2 / 385	8434 / 0 / 346	4028 / 0 / 238
GOF on F ²	1.035	1.077	1.029	1.048	1.017	1.017
R ₁ (I > 2σ(I))	0.0327	0.0592	0.0343	0.0743	0.0381	0.0452
wR ₂ (all data)	0.0925	0.1487	0.0538	0.2142	0.0980	0.0715

Table A3.6. Crystallographic data for **5.7, 5.8, 5.9, 5.11, 5.12** and **5.13**

	5.7	5.8	5.9	5.11	5.12	5.13
CCDC number	2193395	2171709	2171710	2193396	2171713	2171712
Formula	C ₄₃ H ₈₄ B ₄ Mg ₂ N ₁₂	C ₁₅ H ₃₈ B ₂ MgN ₄	C ₁₉ H ₅₄ B ₄ MgN ₆	C ₁₅ H ₄₄ B ₄ MgN ₆	C ₁₇ H ₄₆ B ₃ MgN ₅	C ₂₃ H ₆₃ B ₃ MgN ₆ Si ₂
FW (g/mol)	861.08	320.42	434.23	376.11	377.33	536.71
Temp (K)	100(2)	100(2)	100(2)	100(2)	100(2)	100(2)
λ (Å)	0.71073	0.71073	0.71073	1.54178	0.71073	1.54178
Size (mm)	0.151 x 0.153 x 0.184	0.151 x 0.198 x 0.436	0.174 x 0.184 x 0.255	0.074 x 0.129 x 0.246	0.085 x 0.154 x 0.168	0.038 x 0.098 x 0.098mm
Crystal habit	colorless block	colorless rod	colorless plate	colorless rod	colourless block	colorless plates
Crystal system	monoclinic	monoclinic	monoclinic	orthorhombic	monoclinic	orthorhombic
Space group	C 2/c	C 2/c	I 2/a	P b c n	P 2 ₁ /c	P b c a
a (Å)	22.8029(10)	15.2889(15)	14.1303(12)	13.4094(4)	13.7539(7)	12.7469(7)
b (Å)	8.4951(4)	10.8916(9)	11.0611(4)	11.9712(3)	11.2856(6)	18.7862(9)
c (Å)	28.8056(14)	13.0380(11)	17.5569(7)	15.0129(5)	16.6542(7)	28.9521(16)
α (°)	90	90	90	90	90	90
β (°)	107.102(2)	104.238(3)	94.4890(10)	90	106.242(2)	90
γ (°)	90	90	90	90	90	90
Volume (Å ³)	5333.3(4)	2104.4(3)	2735.7(3)	2409.97(12)	2481.9(2)	6933.0(6)
Z	4	4	4	4	4	8
Density (g/cm ³)	1.072	1.011	1.054	1.037	1.010	1.028
μ (mm ⁻¹)	0.085	0.086	0.082	0.696	0.082	1.249
F(000)	1880	712	968	832	840	2384
θ range (°)	2.01 to 28.32	2.32 to 30.50	2.18 to 30.52	4.95 to 68.37°	2.21 to 28.32	3.05 to 67.77
Index ranges	-30 ≤ h ≤ 30 - 11 ≤ k ≤ 11 -38 ≤ l ≤ 38	-21 ≤ h ≤ 21 - 15 ≤ k ≤ 15 - 16 ≤ l ≤ 18	-19 ≤ h ≤ 20 -15 ≤ k ≤ 15 -25 ≤ l ≤ 24	-16 ≤ h ≤ 15 -14 ≤ k ≤ 14 -14 ≤ l ≤ 17	-15 ≤ h ≤ 18 -15 ≤ k ≤ 15 -20 ≤ l ≤ 22	0 ≤ h ≤ 15 0 ≤ k ≤ 22 0 ≤ l ≤ 34
Data / restraints / parameters	6636 / 0 / 328	3195 / 0 / 118	4186 / 0 / 164	2211 / 0 / 145	6170 / 7 / 313	6566 / 0 / 356
GOF on F ²	1.044	1.069	1.067	1.047	1.024	0.989
R ₁ (I > 2σ(I))	0.0499	0.0331	0.0425	0.0642	0.0505	0.1024
wR ₂ (all data)	0.1204	0.0962	0.1149	0.1967	0.1435	0.3361

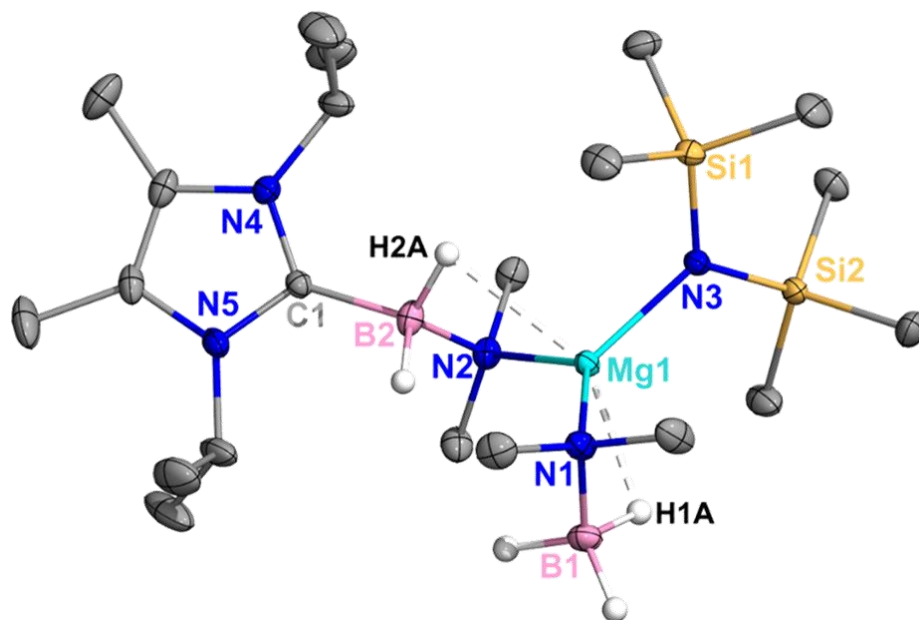


Figure A3.23. Molecular structure of **5.2**. H atoms omitted for clarity, with the exception of B–H hydrides which were isotropically refined. Selected bond distances (Å) and angles (°): Mg1–N1, 2.0944(8); Mg1–N2, 2.1301(8); Mg1–N3, 1.9964(8); Mg1–H1A, 2.095(14); Mg1–H2A, 2.373(13); C1–B2, 1.6250(13); B2–N2, 1.5653(13); B1–N1, 1.5721(13); N1–Mg1–N2, 131.96(3); N1–Mg1–N3, 115.79(3); N3–Mg1–N2, 111.73(3); B2–N2–Mg1, 83.67(5); B1–N1–Mg1, 82.76(5); H1A–Mg1–H2A, 147.3(5).

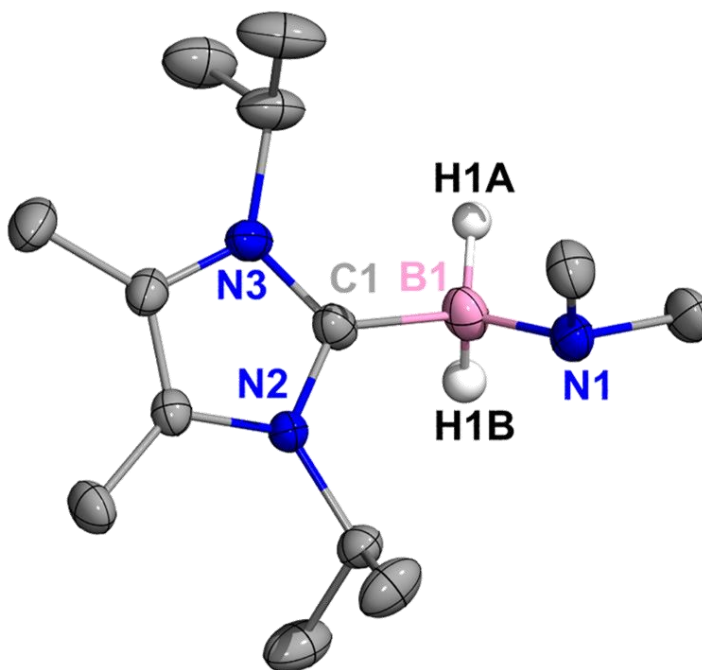


Figure A3.24. Molecular structure of ***i*PrNHC-BN**. H atoms omitted for clarity, with the exception of B–H hydrides which were isotropically refined. Selected bond distances (Å) and angles (°): B1–C1, 1.636(4); B1–N1, 1.516(4); B1–H1A, 1.13(4); B1–H1B, 1.10(4).

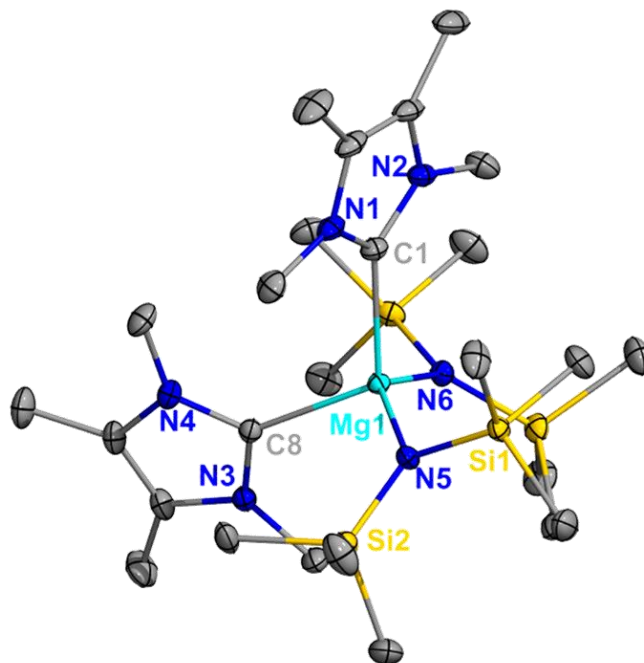


Figure A3.25. Molecular structure of **5.3**. Thermal ellipsoids at 30% probability and H atoms omitted for clarity. Selected bond distances (Å) and angles (°): Mg1–C1, 2.2878(10); Mg1–C8, 2.2743(10); Mg1–N5, 2.0696(9); Mg1–N6, 2.0780(9); C1–Mg1–C8, 115.53(4); C1–Mg1–N5, 98.28(4); C1–Mg1–N6, 109.45(4).

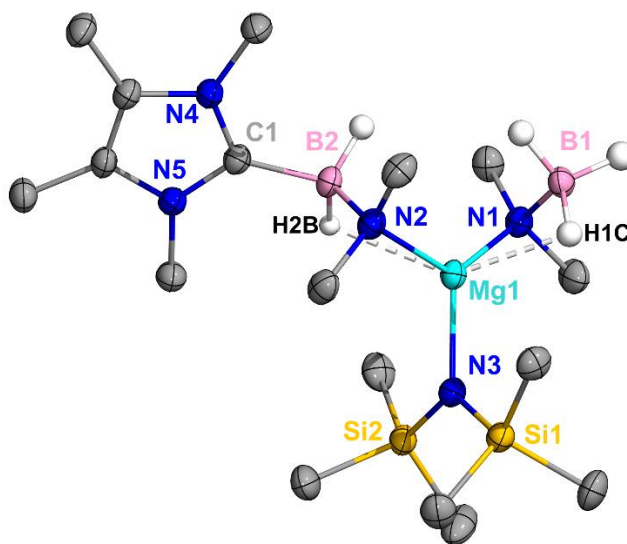


Figure A3.26. Molecular structure of **5.4**. H atoms omitted for clarity, with the exception of B–H hydrides which were isotropically refined. Selected bond distances (Å) and angles (°): Mg1–N1, 2.088(3); Mg1–N2, 2.116(3); Mg1–N3, 1.990(3); Mg1–H1C, 2.14(4); Mg1–H2B, 2.39(3); C1–B2, 1.625(5); B2–N2, 1.565(5); B1–N1, 1.560(5); N1–Mg1–N2, 129.83(13); N1–Mg1–N3, 117.26(13); N3–Mg1–N2, 112.18(13); B2–N2–Mg1, 90.1(2); B1–N1–Mg1, 82.1(2); H1C–Mg1–H2B, 140.1(13).

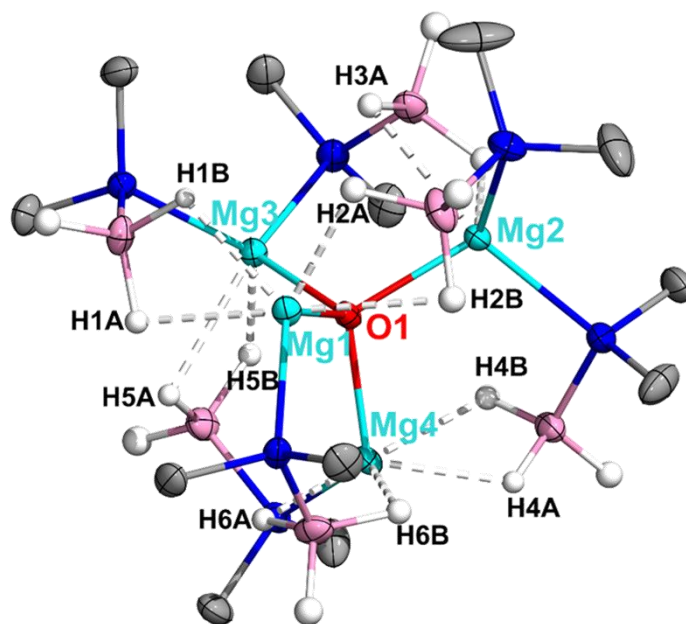


Figure A3.27. Molecular structure of **5.5**. H atoms omitted for clarity, with the exception of B–H hydrides which were isotropically refined. Selected bond distances (Å) and angles (°): Mg1–H1B, 1.975(15); Mg1–H2A, 1.949(17); Mg1–H1A, 2.132(16); Mg1–H2B, 2.254(17); Mg2–H3A, 2.313(16); Mg2–H3B, 1.960(17); Mg1–O1, 1.9718(9); Mg2–O1, 2.132(16); Mg1–N6, 2.0873(11); Mg2–N2, 2.1084(12); Mg2–N4, 2.1258(11); Mg1–O1–Mg2, 107.45(4); Mg1–O1–Mg3, 110.50(4); Mg3–O1–Mg4, 107.43(4); H3A–Mg2–H3B, 52.1(6); H1A–Mg1–H2B, 173.9(6).

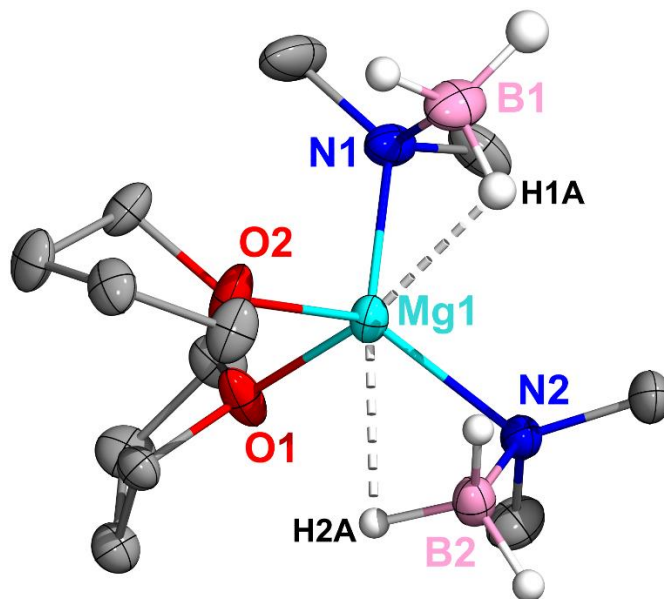


Figure A3.28. Molecular structure of **5.6**. H atoms omitted for clarity, with the exception of B–H hydrides which were isotropically refined. Selected bond distances (Å) and angles (°): Mg1–N1, 2.1034(15); Mg1–N2, 2.1176(14); Mg1–H1A, 2.16(2); Mg1–H2A, 2.353(19); B1–N1, 1.578(2); B2–N2, 1.571(2); N1–Mg1–N1', 113.79(6).

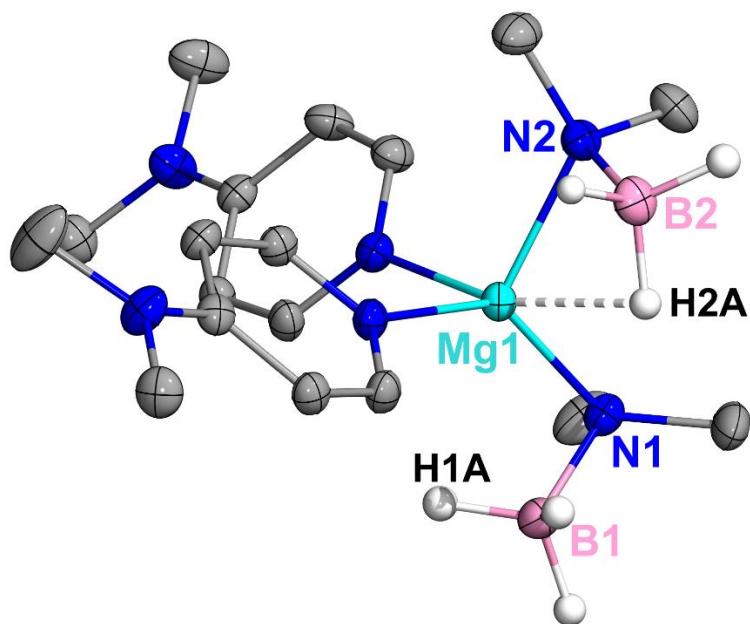


Figure A3.29. Molecular structure of **5.7**. H atoms omitted for clarity, with the exception of B–H hydrides which were isotropically refined. Selected bond distances (Å) and angles (°): Mg1–N1, 2.1099(14); Mg1–N2, 2.1147(14); Mg1–H2A, 2.210(18); B1–N1, 1.563(2); B2–N2, 1.581(2); N1–Mg1–N1', 113.18(6).

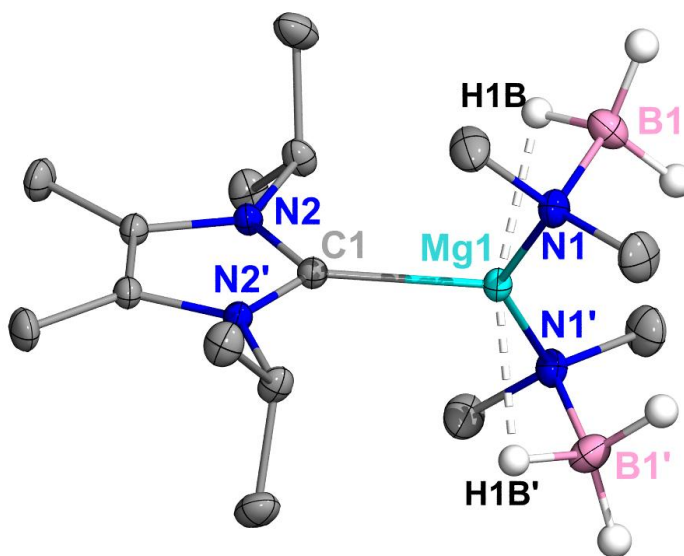


Figure A3.30. Molecular structure of **5.8**. H atoms omitted for clarity, with the exception of B–H hydrides which were isotropically refined. Selected bond distances (Å) and angles (°): Mg1–C1, 2.2062(10); Mg1–N1, 2.0848(7); Mg1–H1B, 2.104(13); B1–N1, 1.5707(11); N1–Mg1–C1, 108.385(19); N1–Mg1–N1', 143.23(4); H1B–Mg1–H1B', 161.82(3). Symmetry transformations used to generate equivalent atoms: $-x+1, y, -z+1/2$.

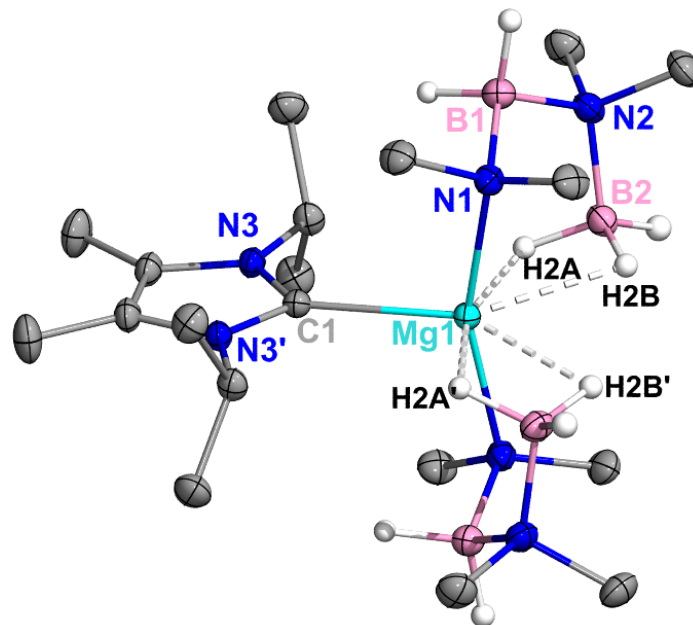


Figure A3.31. Molecular structure of **5.9**. H atoms omitted for clarity, with the exception of B–H hydrides which were isotropically refined. Selected bond distances (Å) and angles (°): Mg1–C1, 2.3450(16); Mg1–N1, 2.1663(9); Mg1–H2A, 2.107(14); Mg1–H2B, 2.295(15); B1–N1, 1.5607(16); B1–N2, 1.6115(16); B2–N2, 1.5846(16); N1–Mg1–C1, 100.24(3); N1–Mg1–N1', 159.51(6); H2A–Mg1–H2B, 50.0(5); H2B–Mg1–H2B', 64.0(5); H2A–Mg1–H2A', 161.3(5).

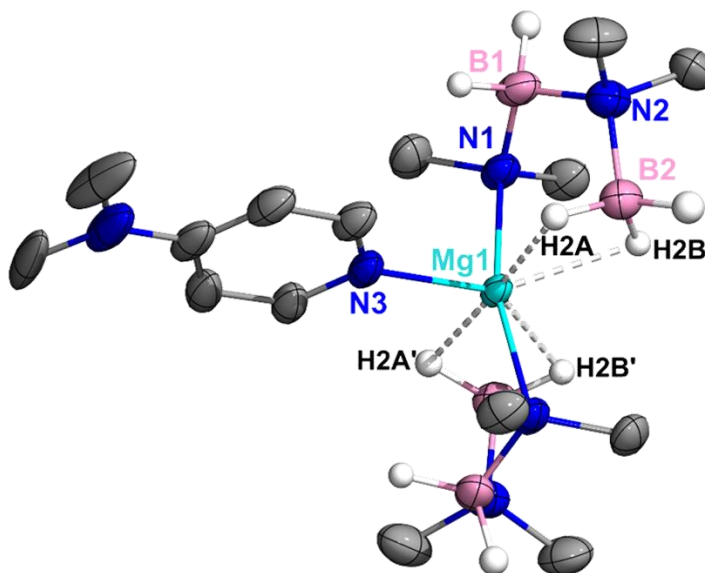


Figure A3.32. Molecular structure of **5.11**. H atoms omitted for clarity, with the exception of B–H hydrides which were isotropically refined. Selected bond distances (Å) and angles (°): Mg1–N3, 2.144(3); Mg1–N1, 2.1679(18); Mg1–H2A, 2.18(3); Mg1–H2B, 2.21(3); B1–N1, 1.547(4); B1–N2, 1.618(4); B2–N2, 1.580(3); N1–Mg1–C1, 100.24(3); N1–Mg1–N1', 163.16(12); H2A–Mg1–H2B, 53.4(10) Symmetry transformations used to generate equivalent atoms (A'): $-x+1, y, -z+3/2$

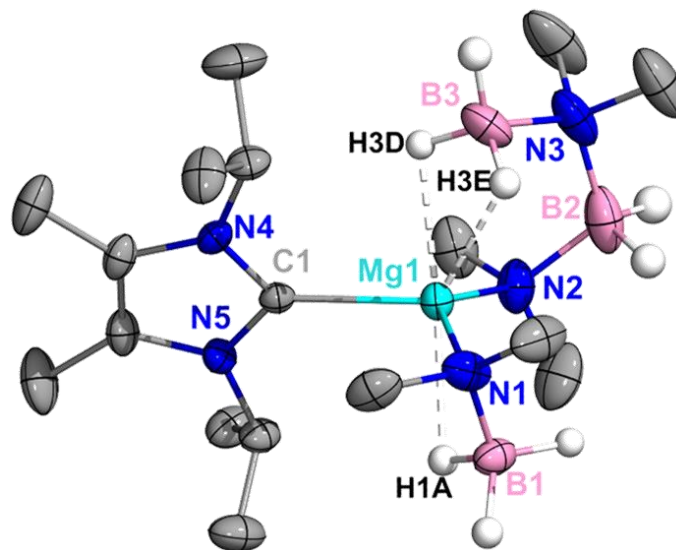


Figure A3.33. Molecular structure of **5.12**. H atoms omitted for clarity, with the exception of B–H hydrides which were isotropically refined. Selected bond distances (Å) and angles (°): Mg1–C1, 2.2287(15); Mg1–N1, 2.0843(14); Mg1–N2, 2.1328(14); Mg1–H1A, 2.20(2); Mg1–H3D, 2.222(19); Mg1–H3E, 2.09(2); B1–N1, 1.512(3); B2–N2, 1.581(3); B3–N3, 1.574(3); N1–Mg1–C1, 107.28(6); N1–Mg1–N2, 132.89(7); C1–Mg1–N2, 114.76(6); H1A–Mg1–H3D, 168.4(7); H1A–Mg1–H3E, 139.6(8); H3D–Mg1–H3E, 50.8(8).

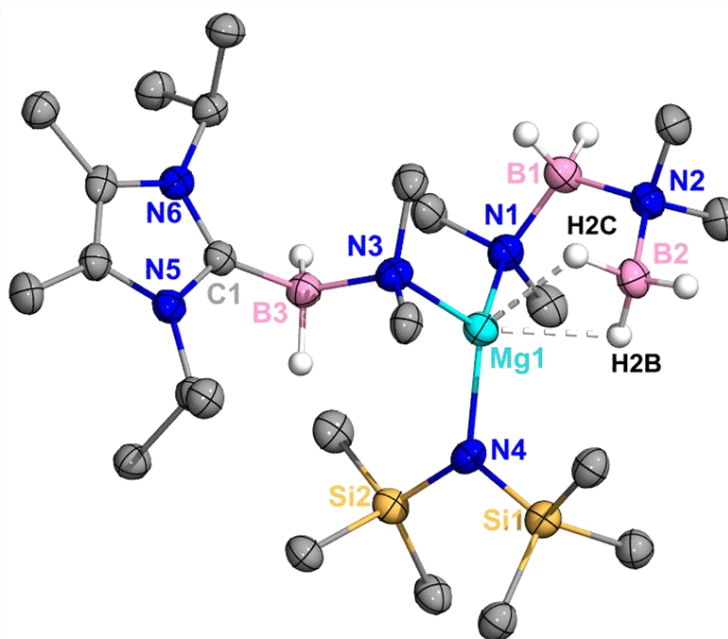


Figure A3.34. Molecular structure of **5.13**. H atoms omitted for clarity, with the exception of B–H hydrides which were isotropically refined. Selected bond distances (Å) and angles (°): Mg1–N3, 2.166(7); Mg1–N1, 2.137(7); Mg1–N4, 2.004(6); Mg1–H2B, 2.17(9); Mg1–H2C, 2.19(8); C1–B3, 1.633(11); B3–N3, 1.575(11); B1–N1, 1.579(11); B2–N2, 1.578(12); N4–Mg1–N3, 111.3(3); N4–Mg1–N1, 122.1(3); N3–Mg1–N1, 116.1(3).

Chapter Six:

A single crystal of **6.1**, **6.2**, **6.4**, **6.5**, **6.7**, **6.8**, **6.8'** or **6.9** was coated with Paratone oil and mounted on a MiTeGen MicroLoop. The X-ray diffraction data for **6.1**, **6.2**, **6.4**, **6.5**, **6.8**, and **6.8'** were measured on a Bruker Kappa APEXII Duo system using either a fine-focus sealed tube (Mo $K\alpha$, $\lambda = 0.71073 \text{ \AA}$) and a graphite monochromator (**6.1**, **6.2**, **6.5**, **6.8**, **6.8'**) or an Incoatec Microfocus I μ S (Cu $K\alpha$, $\lambda = 1.54178 \text{ \AA}$) and a multi-layer mirror monochromator (**6.4**). The X-ray diffraction data for **6.7** and **6.9** were measured on a Bruker D8 Venture PhotonIII Kappa four-circle diffractometer system equipped with an Incoatec I μ S 3.0 micro-focus sealed X-ray tube (Mo $K\alpha$, $\lambda = 0.71073 \text{ \AA}$) and a HELIOS double bounce multilayer mirror monochromator. The frames were integrated with the Bruker SAINT software package⁴²⁷ using a narrow-frame algorithm. Data were corrected for absorption effects using the multiscan method (SADABS).⁴²⁷ Each structure was solved and refined using the Bruker SHELXTL Software Package⁴²⁸ within APEX3⁴²⁷ and OLEX2.⁴²⁹ Non-hydrogen atoms were refined anisotropically. In **6.5**, the hydrogen atoms on methyls with close contacts to Ca (C28, C29, C61, C63) were located in the electron density map and refined isotropically. In **6.7**, **6.8**, **6.8'** and **6.9** the B-H hydrogen atoms were located in the electron density map and refined isotropically. All other hydrogen atoms in all structures were placed in geometrically calculated positions with $U_{iso} = 1.2U_{equiv}$ of the parent atom ($U_{iso} = 1.5U_{equiv}$ for methyl).

In **6.1**, the TWINROTMAT feature of Platon⁴³² was used to identify the twin law as -0.005 0.51 0.496 / 0.995 -0.49 0.496 / 0.995 0.51 -0.504, and the BASF values for the twin domains refined to 0.11567, 0.10904, and 0.09301. The relative occupancy of the disordered atoms was freely refined and no constraints or restraints were needed. In **6.2**, the relative occupancies of the disordered atoms were freely refined. Constraints were used on the anisotropic displacement parameters of the disordered nitrogen atoms only. Restraints were needed on the disordered C-N

bonds. In **6.7**, the relative occupancy of each disordered site was freely refined, with constraints and restraints used on the anisotropic displacement parameters or bond lengths of most of the disordered atoms. In **6.8'**, the symmetry-disordered toluene molecule was refined at half-occupancy with an AFIX 66 constraint on the ring atoms. In **6.9**, the relative occupancies of the disordered sites were freely refined. Constraints and restraints were used on the anisotropic displacement parameters and bond lengths of most of the disordered atoms.

Table A3.7. Crystallographic data for **6.1**, **6.2**, **6.4**, and **6.5**

	6.1	6.2	6.4	6.5
CCDC number	2088763	2088764	2088765	2088766
Formula	C ₂₀ H ₅₆ CaN ₂ O ₂ Si ₄	C ₂₃ H ₅₆ CaN ₄ Si ₄	C ₂₇ H ₆₄ CaN ₄ OSi ₄	C ₃₄ H ₇₁ CaN ₃ Si ₄
FW (g/mol)	509.10	541.15	613.26	674.37
Temp (K)	100(2)	100(2)	100(2)	100(2)
λ (Å)	0.71073	0.71073	1.54178	0.71073
Size (mm)	0.512 x 0.519 x 0.705	0.158 x 0.193 x 0.407	0.051 x 0.128 x 0.137	0.178 x 0.274 x 0.293
Crystal habit	colorless block	colorless block	colorless plate	colorless block
Crystal system	orthorhombic	monoclinic	triclinic	orthorhombic
Space group	A ba2	C 2/c	P -1	P cca
a (Å)	11.8580(18)	16.2020(19)	9.0128(3)	33.914(4)
b(Å)	16.5693(19)	13.4414(17)	10.6143(3)	23.973(2)
c (Å)	16.801(2)	16.653(2)	19.8066(6)	20.9363(19)
α (°)	90	90	88.649(2)	90
β (°)	90	109.593(3)	88.007(2)	90
γ (°)	90	90	80.083(2)	90
Volume (Å ³)	3301.0(7)	3416.7(7)	1865.05(10)	17022.(3)
Z	4	4	2	16
Density (g/cm ³)	1.024	1.052	1.092	1.053
μ (mm ⁻¹)	0.351	0.340	2.857	0.284
F(000)	1128	1192	676	5952
θ range (°)	1.72 to 30.76	2.02 to 29.62	2.23 to 68.39	1.20 to 25.34
Index ranges	-16 ≤ h ≤ 16 -23 ≤ k ≤ 23 -24 ≤ l ≤ 23	-22 ≤ h ≤ 22 -17 ≤ k ≤ 18 -23 ≤ l ≤ 23	-10 ≤ h ≤ 10 -12 ≤ k ≤ 12 -23 ≤ l ≤ 23	-40 ≤ h ≤ 33 -28 ≤ k ≤ 28 -25 ≤ l ≤ 24
Reflns collected	26468	35030	33219	122869
Independent reflns	5396 [R _{int} = 0.0927]	4807 [R _{int} = 0.0434]	6814 [R _{int} = 0.0696]	15482 [R _{int} = 0.1160]
Data / restraints /parameters	5396 / 1 / 164	4807 / 2 / 216	6814 / 0 / 352	15482 / 6 / 837
GOF on F ²	1.076	1.058	0.997	1.067
R ₁ (I > 2σ(I))	0.0985	0.0347	0.0462	0.0816
wR ₂ (all data)	0.2629	0.0906	0.1264	0.1919

Table A3.8. Crystallographic data for **6.7-6.9**

	6.7	6.8	6.8'	6.9
CCDC number	2176641	2176642	2176643	2176644
Formula	C ₂₆ H ₅₈ B ₂ CaN ₆	C ₃₄ H ₉₂ B ₆ Ca ₂ N ₁₀	C ₅₅ H ₁₁₆ B ₆ Ca ₂ N ₁₀	C ₁₄ H ₄₂ B ₃ CaN ₃ O ₂
FW (g/mol)	516.48	786.19	1062.59	357.01
Temp (K)	100(2)	100(2)	100(2)	100(2)
λ (Å)	0.71073	0.71073	0.71073	0.71073
Size (mm)	0.146 x 0.209 x 0.396	0.060 x 0.164 x 0.177	0.177 x 0.295 x 0.348	0.180 x 0.213 x 0.283
Crystal habit	colorless plate	colorless plate	colorless block	colorless plate
Crystal system	triclinic	triclinic	triclinic	triclinic
Space group	P -1	P -1	P -1	P -1
a (Å)	19.4399(9)	10.0998(10)	12.5844(17)	11.3042(9)
b (Å)	19.4639(8)	12.0913(11)	12.8733(17)	14.8213(13)
c (Å)	21.5397(8)	12.5437(13)	13.1308(17)	15.5337(14)
α (°)	101.6890(10)	113.654(3)	110.456(4)	65.992(3)
β (°)	99.2720(10)	112.234(3)	93.126(5)	88.400(3)
γ (°)	119.1900(10)	93.861(3)	118.850(4)	71.830(2)
Volume (Å ³)	6637.7(5)	1254.7(2)	1679.9(4)	2244.1(3)
Z	8	1	1	4
Density (g/cm ³)	1.034	1.041	1.050	1.057
μ (mm ⁻¹)	0.212	0.260	0.210	0.289
F(000)	2288	436	586	792
θ range (°)	1.84 to 28.27	1.90 to 29.64	1.72 to 27.57	2.04 to 26.05
Index ranges	-25 ≤ h ≤ 25 -25 ≤ k ≤ 25 -26 ≤ l ≤ 28	-14 ≤ h ≤ 13 -16 ≤ k ≤ 16 -17 ≤ l ≤ 17	-15 ≤ h ≤ 16 -16 ≤ k ≤ 16 -16 ≤ l ≤ 17	-12 ≤ h ≤ 13 -18 ≤ k ≤ 18 -19 ≤ l ≤ 19
Data / restraints / parameters	32860 / 16 / 1495	7069 / 0 / 279	7718 / 0 / 395	8837 / 103 / 541
GOF on F ²	1.038	1.011	1.028	1.075
R ₁ (I > 2 σ (I))	0.0572	0.0389	0.0437	0.0509
wR ₂ (all data)	0.1600	0.0856	0.1198	0.1392

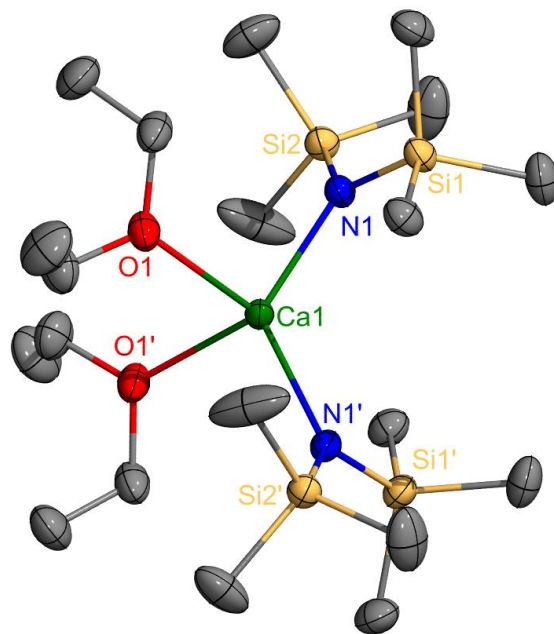


Figure A3.35. Molecular Structure of **6.1**.

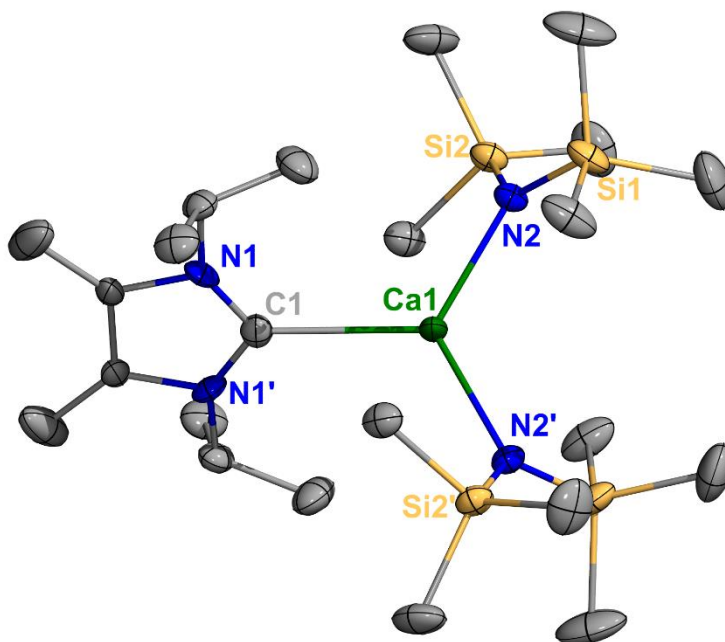


Figure A3.36. Molecular Structure of **6.2**. Thermal ellipsoids shown at 50% probability and H atoms omitted for clarity. Selected bond distances (Å) and angles (°): Ca1–N2: 2.280(3); Ca1–C1: 2.547(6); N1–C1: 1.350(7); N2–Ca1–N2: 122.3(2); N2–Ca1–C1: 118.83(12); N1–C1–N1: 113.9(6).

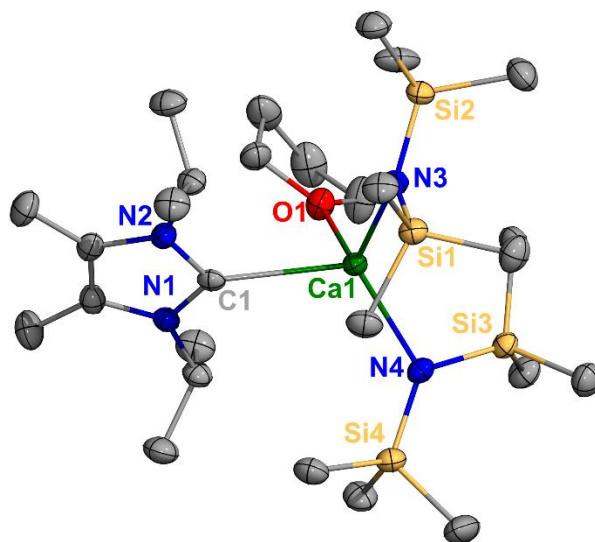


Figure A3.37. Molecular Structure of **6.4**. Thermal ellipsoids shown at 50% probability and H atoms omitted for clarity. Selected bond distances (Å) and angles (°): Ca1-N4: 2.3239(19); Ca1-N3: 2.3482(18); Ca1-O1: 2.4294(17); Ca1-C1: 2.617(2) N4-Ca1-N3: 122.22(7); N4-Ca1-O1.

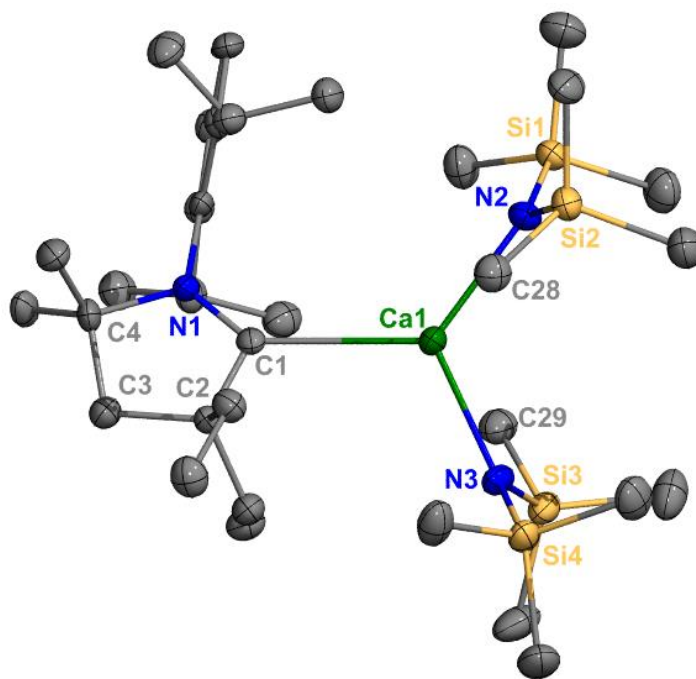


Figure A3.38. Molecular Structure of **6.5**. Thermal ellipsoids shown at 50% and H atoms omitted for clarity. Only one of two crystallographically unique but chemically equivalent molecules in the unit cell is shown. Selected bond distances (Å) and angles (°): Ca1-C1: 2.700(5); Ca1-N2: 2.296(4); Ca1-N3: 2.321(4); C1-N1: 1.308(6); C1-C2: 1.512(7); N2-Ca1-C1: 126.31(15); N3-Ca1-C1: 115.35(15); N3-Ca1-N2: 118.10(16).

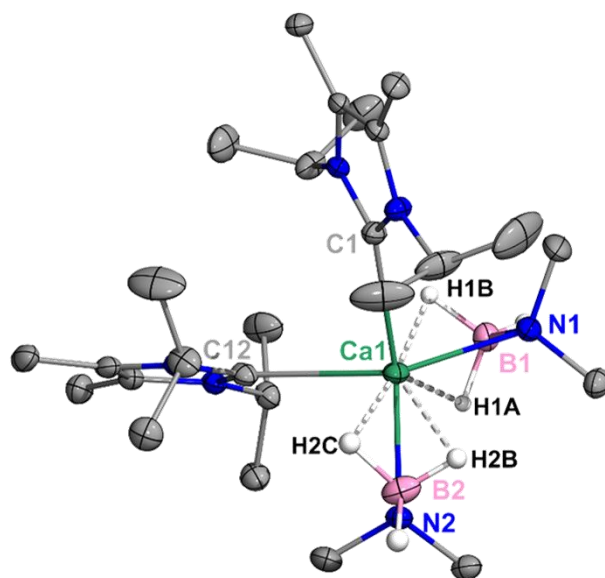


Figure A3.39. Molecular Structure of **6.7**. H atoms omitted for clarity, except for B–H hydrides, which were isotropically refined. Only one of two crystallographically unique but chemically equivalent molecules is shown. Selected bond distances (Å) and angles (°): Ca1–C1: 2.631(2); Ca1–C12: 2.672(3); Ca1–N1: 2.4445(19); Ca1–N2: 2.4492(17); B1–N1: 1.551(3); B2–N2: 1.539(3); N1–Ca1–N2: 108.29(6); H1B–Ca1–H2C: 174.2(9).

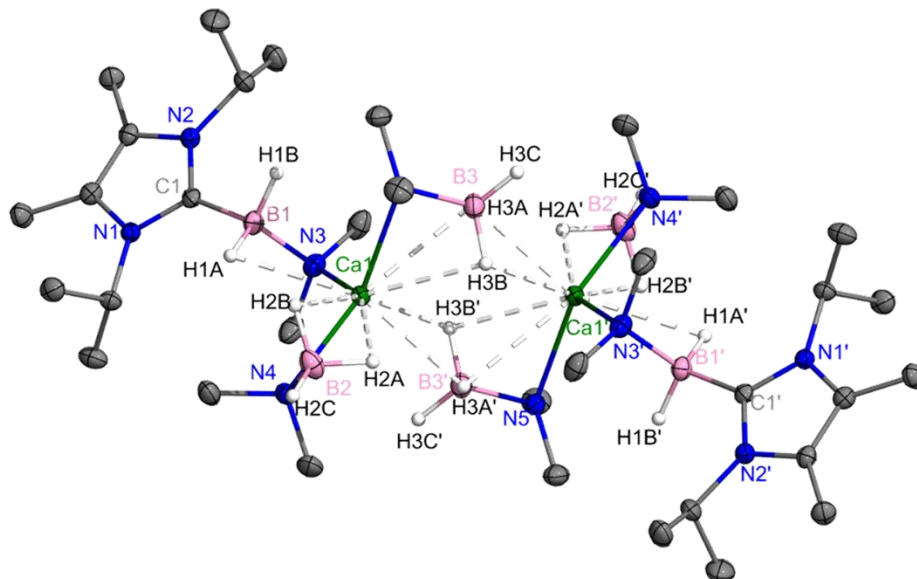


Figure A3.40. Molecular Structure of **6.8**. H atoms omitted for clarity, except for B–H hydrides, which were isotropically refined. Selected bond distances (Å) and angles (°): **8**: Ca1–N3: 2.4788(12); Ca1–N4: 2.4654(12); Ca1–N5: 2.5105(11); Ca1–H1A: 2.672(14); Ca1–H1B: 2.681(15); Ca1–H2A: 2.464(15); Ca1–H2B: 2.476(16); B1–N3: 1.5532(18); B1–C1: 1.6289(19); B2–N4: 1.550(2); B3–N5: 1.5388(19); N4–Ca1–N3: 104.95(4).

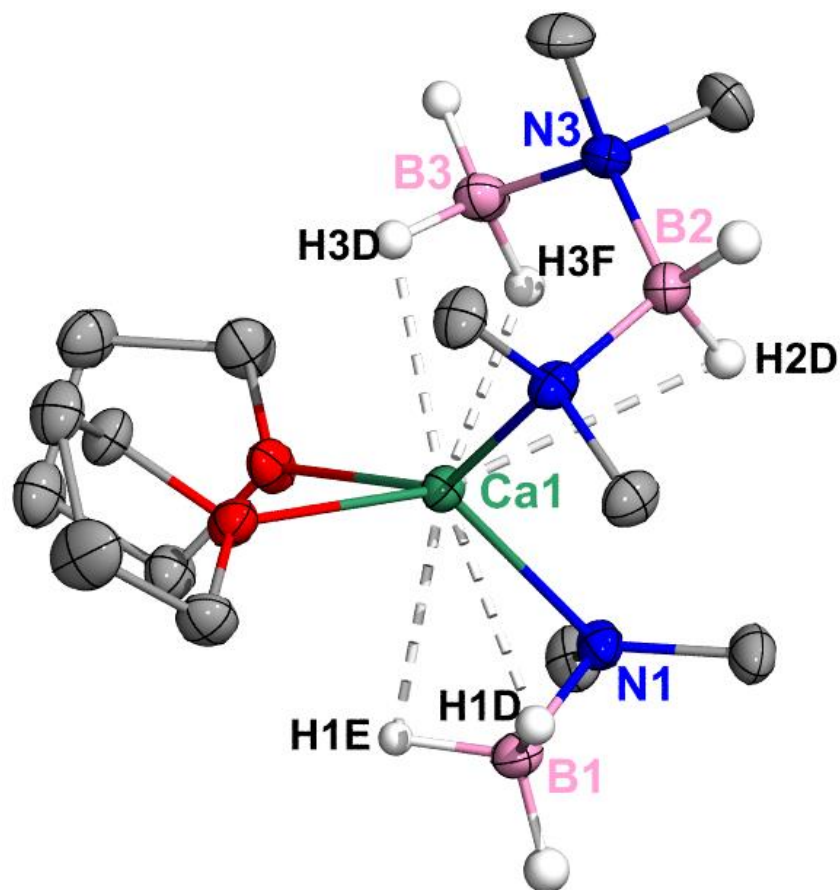


Figure A3.41. Molecular Structure of **6.9**. H atoms omitted for clarity, except for B–H hydrides which were isotropically refined. Only one of two crystallographically independent but chemically equivalent molecules in the asymmetric unit is represented. Only major positions for disordered atoms are shown. Selected bond distances (Å) and angles (°): Ca1–N1: 2.4166(19); Ca1–N3: 2.4733(18); Ca1–H1D: 2.53(3); Ca1–H1E: 2.46(2); Ca1–H2D: 2.42(3); Ca1–H2E: 2.35(2); B1–N1: 1.540(3); B2–N2: 1.574(3); B2–N3: 1.602(3); B3–N3: 1.566(3); N1–Ca1–N3: 113.35(6); H2D–Ca1–H1D: 155.5(9); H1E–Ca1–H2E: 135.5(8).

Chapter Seven:

Each single crystal was coated with Paratone oil and mounted on a MiTeGen MicroLoop. X-ray intensity data for **1**·CH₂Cl₂, **1**·THF, **2**·3CH₂Cl₂, **3**[BPh₄], **4**[BPh₄], **5**[BF₄]·2CH₂Cl₂, **5**[BAr^F₄]·Et₂O, **7**[AlOR^F₄]·CH₂Cl₂, **7**[SbF₆]·CH₂Cl₂, **8**[BF₄]₂·CH₂Cl₂, and **10** were measured on a Bruker Kappa APEXII Duo system using either a fine-focus sealed tube (Mo K_α, λ = 0.71073 Å) and a graphite monochromator or an Incoatec Microfocus I μ S (Cu K_α, λ = 1.54178 Å) and a multilayer mirror monochromator. Data for **2**·THF, **3**[NTf₂], **3**[NTf₂]·CH₂Cl₂, **5**[SbF₆]·CH₂Cl₂, **5**[SbF₆]·2THF, **5**[BPh₄]·2CH₂Cl₂, **5**[BPh₄]_a, **5**[BPh₄]_b, **6**[BPh₄]·CH₂Cl₂, **6**·THF, **9**·1.5CH₂Cl₂, **9**, and **9**·THF·benzene were measured on a Bruker D8 Venture Photon III Kappa four-circle diffractometer system using either an Incoatec I μ S 3.0 micro-focus sealed X-ray tube (Mo K_α, λ = 0.71073 Å) and a HELIOS double bounce multilayer mirror monochromator or an Incoatec I μ S 3.0 micro-focus sealed X-ray tube (Cu K_α, λ = 1.54178 Å) and a HELIOS EF double bounce multilayer mirror monochromator. All frames were integrated with the Bruker SAINT software package⁴²⁷ using a narrow-frame algorithm. Data were corrected for absorption effects using the Multi-Scan method (SADABS).⁴²⁷ Each structure was solved and refined using the Bruker SHELXTL Software Package⁴²⁸ within APEX3/4⁴²⁷ and OLEX2.⁴²⁹ Non-hydrogen atoms were refined anisotropically. The B-H hydrogen atoms in **9**·1.5CH₂Cl₂, **9** and **9**·THF·benzene were located in the electron density map and refined isotropically. All other hydrogen atoms were placed in geometrically calculated positions with $U_{iso} = 1.2U_{equiv}$ of the parent atom ($U_{iso} = 1.5U_{equiv}$ for methyl).

For **2**·3CH₂Cl₂, part of one dichloromethane solvent molecule was disordered over two positions. The relative occupancy was freely refined. No constraints or restraints were needed on the disordered atoms. For **2**·THF, the relative occupancy of the disordered atoms was freely refined. Restraints were used on the anisotropic displacement parameters and/or bond lengths of

some of the disordered atoms. For **3[NTf₂]**, the disordered triflimide anion was refined at 50% occupancy to reflect its location on a special position. For **3[NTf₂]**·**CH₂Cl₂**, the dichloromethane solvent was refined at 50% occupancy. The relative occupancies of the disordered anion and phenyl group were freely refined with constraints and restraints on the anisotropic displacement parameters and bond lengths of some of the disordered atoms.

For **4[BPh₄]**, several phenyl rings were disordered over two positions. The relative occupancy of the positions was freely refined. Constraints were used on the anisotropic displacement parameters of the disordered atoms and restraints were used on the disordered bonds. A mixture of hexane and CH₂Cl₂ solvents located in the crystal lattice was severely disordered and could not be adequately modeled with or without restraints. Thus, the structure factors were modified using the PLATON SQUEEZE⁴³⁰ technique, in order to produce a “solvate-free” structure factor set. PLATON reported a total electron density of 168 e⁻ and total solvent accessible volume of 529 Å³. For **5[BF₄]**·**2CH₂Cl₂**, the relative occupancy of the two sites of the disordered solvent was freely refined and restraints were used on the anisotropic displacement parameters of the disordered carbon atoms. For **5[SbF₆]**·**2THF**, the relative occupancy of the two positions of each disordered THF solvent molecule was freely refined, with a constraint on the anisotropic displacement parameters of most of the disordered atoms. For **5[BPh₄]**·**2CH₂Cl₂**, one molecule of dichloromethane solvent was partially disordered over two positions. The relative occupancy was free refined, and restraints were used on the disordered bonds. For **5[BPh₄]**_a****, the relative occupancy of the two sites of the disordered Bi and Ph was freely refined, with constraints and restraints on the anisotropic displacement parameters of the disordered carbon atoms. For **5[BAr^F₄]**·**Et₂O**, a two domain twin was identified using the “DOMAINS” feature of APEX4. The structure was refined on HKLF 5 data. The relative occupancy of each set of disordered atoms was

freely refined. Constraints and restraints were used on the anisotropic displacement parameters or bond lengths of most of the disordered atoms. Severely disordered Et₂O solvent located in the crystal lattice was severely disordered and could not be adequately modeled with or without restraints. Thus, the structure factors were modified using the PLATON SQUEEZE⁴³⁰ technique, in order to produce a “solvate-free” structure factor set. PLATON reported a total electron density of 164 e⁻ and total solvent accessible volume of 817 Å³.

For **7[AlOR^F₄]·CH₂Cl₂**, one CH₂Cl₂ solvent molecule was found to be disordered over two positions. The relative occupancy was freely refined, with constraints and restraints on the anisotropic displacement parameters and bond lengths of the disordered atoms. For **7[SbF₆]·CH₂Cl₂**, the relative occupancy of the two positions of the disordered SbF₆ anion was freely refined and no constraints or restraints were needed. For **8[NTf₂]₂**, the relative occupancies of the disordered fragments were freely refined, with constraints and restraints used on the anisotropic displacement parameters and bond lengths of the disordered CF₃ groups.

For **9·1.5CH₂Cl₂**, free refinement of the relative occupancy of the positions of the disordered CH₂Cl₂ solvent molecules gave a total of 1.5 molecules in the ASU, so the sum of the parts was then constrained to that value. Constraints and restraints were used on the anisotropic displacement parameters and bond lengths of most of the disordered atoms. For **9·THF·benzene**, the relative occupancy of the disordered THF sites was freely refined. Constraints and restraints were used on the anisotropic displacement parameters and bond lengths of most of the disordered atoms.

Table A3.9. Crystallographic data for compounds **7.1-7.3**

	1·CH₂Cl₂	1·THF	2·3CH₂Cl₂	2·THF	3[NTf₂]	3[NTf₂]·CH₂Cl₂	3[BPh₄]
CCDC number	2190040	2190041	2190042	2190043	2190044	2190045	2190046
Formula	C ₃₈ H ₃₀ BiCl ₃ P ₂	C ₄₁ H ₃₆ BiCl ₃ OP ₂	C ₇₇ H ₆₂ Bi ₂ Br ₂ Cl ₆ P ₄	C ₄₁ H ₃₆ BiBr ₂ OP ₂	C ₇₆ H ₅₆ Bi ₂ ClF ₆ NO ₄ P ₄ S ₂	C ₇₇ H ₅₈ Bi ₂ Cl ₃ F ₆ N ₃ O ₄ P ₄ S ₂	C ₉₉ H ₇₈ BBi ₂ Cl ₃ P ₄
FW (g/mol)	863.89	851.07	1901.62	895.53	1802.62	1887.55	1926.61
Temp (K)	100(2)	100(2)	100(2)	100(2)	100(2)	100(2)	100(2)
λ (Å)	0.71073	0.71073	0.71073	0.71073	0.71073	0.71073	0.71073
Size (mm)	0.051 x 0.121 x 0.182	0.135 x 0.243 x 0.338	0.186 x 0.187 x 0.221	0.047 x 0.089 x 0.121	0.106 x 0.108 x 0.159	0.095 x 0.095 x 0.192	0.103 x 0.190 x 0.234
Crystal habit	colorless rod	colourless block	colorless block	colourless block	colorless plate	colorless block	colourless block
Crystal system	monoclinic	monoclinic	orthorhombic	monoclinic	monoclinic	monoclinic	monoclinic
Space group	P 2 ₁ /c	P 2 ₁ /c	F dd2	P 2 ₁ /n	C 2/c	C 2/c	I 2
a (Å)	13.9385(10)	12.8399(9)	27.836(2)	13.7960(10)	12.3204(11)	20.8130(8)	22.9074(19)
b (Å)	24.8223(15)	15.6959(10)	31.238(2)	14.7901(9)	14.0505(12)	15.7948(6)	15.2482(7)
c (Å)	9.8769(7)	17.7597(12)	16.2200(13)	18.0901(11)	40.087(4)	24.9022(11)	24.1289(11)
α (°)	90	90	90	90	90	90	90
β (°)	106.176(2)	107.174(2)	90	107.574(2)	92.473(2)	112.515(2)	102.2100(10)
γ (°)	90	90	90	90	90	90	90
Volume (Å ³)	3282.0(4)	3419.6(4)	14104.0(19)	3518.9(4)	6932.9(11)	7562.3(5)	8237.5(9)
Z	4	4	8	4	4	4	4
Density (g/cm ³)	1.748	1.653	1.791	1.690	1.727	1.658	1.553
μ (mm ⁻¹)	5.742	5.360	6.480	6.269	5.328	4.957	4.490
F(000)	1688	1680	7376	1752	3520	3688	3816
θ range (°)	1.52 to 28.32	1.66 to 30.54°	1.59 to 31.58	2.07 to 28.32°	2.03 to 28.30	2.07 to 29.58°	1.11 to 28.31
Index ranges	-18 ≤ h ≤ 18 -22 ≤ k ≤ 33 -13 ≤ l ≤ 13	-18 ≤ h ≤ 17 -22 ≤ k ≤ 17 -21 ≤ l ≤ 25	-40 ≤ h ≤ 40 -45 ≤ k ≤ 45 -23 ≤ l ≤ 23	-18 ≤ h ≤ 18 -19 ≤ k ≤ 19 -24 ≤ l ≤ 24	-16 ≤ h ≤ 16 -17 ≤ k ≤ 18 -53 ≤ l ≤ 53	-27 ≤ h ≤ 28 -21 ≤ k ≤ 21 -34 ≤ l ≤ 34	-26 ≤ h ≤ 30 -20 ≤ k ≤ 20 -32 ≤ l ≤ 31
Reflns collected	45481	53749	66749	65004	45301	99286	91351
Independent reflns	8160 [R _{int} = 0.0772]	10463 [R _{int} = 0.0404]	11756 [R _{int} = 0.0395]	8724 [R _{int} = 0.0425]	8622 [R _{int} = 0.0334]	10593 [R _{int} = 0.0424]	20460 [R _{int} = 0.0743]
Data / restraints / parameters	8160 / 0 / 397	10463 / 0 / 415	11756 / 1 / 430	8724 / 154 / 522	8622 / 0 / 483	10593 / 103 / 554	20460 / 1 / 983
GOF on F ²	1.032	1.029	1.045	1.037	1.114	1.048	0.897
R ₁ (I > 2σ(I))	0.0381	0.0236	0.0199	0.0267	0.0217	0.0234	0.0339
wR ₂ (all data)	0.0626	0.0493	0.0416	0.0614	0.0418	0.0545	0.0642

Table A3.10. Crystallographic data for compounds 7.4-7.5

	4[BPh ₄]	5[BF ₄]·2C H ₂ Cl ₂	5[SbF ₆]·C H ₂ Cl ₂	5[SbF ₆]·2TH F	5[BPh ₄]·2C H ₂ Cl ₂	5[BPh ₄] _a	5[BPh ₄] _b	5[BAr ^F ₄]·Et ₂ O
CCDC number	2190032	2190033	2190034	2190035	2190036	2190037	2190038	2190039
Formula	C ₉₈ H ₇₆ BBi ₂ BrP ₄	C ₃₉ H ₃₂ BBiCl ₄ F ₄ P ₂	C ₃₈ H ₃₀ BiCl ₂ F ₆ P ₂ Sb	C ₈₆ H ₈₀ Bi ₂ F ₁₂ O ₃ P ₄ Sb ₂	C ₆₃ H ₅₂ BBiCl ₄ P _2	C ₆₁ H ₄₈ BB iP ₂	C ₆₁ H ₄₈ B BiP ₂	C ₁₄₂ H ₉₀ B ₂ Bi ₂ F ₄₈ OP ₄
FW (g/mol)	1886.14	1000.17	1064.19	2174.84	1232.57	1062.72	1062.72	3287.59
Temp (K)	100(2)	100(2)	100(2)	100(2)	100(2)	100(2)	100(2)	100(2)
λ (Å)	0.71073	0.71073	0.71073 Å	0.71073	0.71073	0.71073	0.71073	1.54178
Size (mm)	0.060 x 0.104 x 0.150	0.127 x 0.139 x 0.154	0.026 x 0.045 x 0.065	0.086 x 0.118 x 0.156	0.046 x 0.092 x 0.381	0.050 x 0.073 x 0.130	0.067 x 0.090 x 0.180	0.084 x 0.161 x 0.335
Crystal habit	colorless block	colorless block	colorless block	colorless block	colourless needle	colourless block	colorless plates	colorless plate
Crystal system	monoclinic	monoclinic	monoclinic	monoclinic	monoclinic	monoclinic	monoclinic	triclinic
Space group	I 2	P 2 ₁ /n	P 2 ₁ /n	P 2 ₁ /n	P 2 ₁ /c	P 2 ₁ /n	P 2 ₁ /c	P -1
a (Å)	23.2484(16)	14.4750(11)	14.514(2)	14.6201(8)	9.7614(3)	14.8800(4)	9.6590(11)	19.6981(11)
b (Å)	15.2556(9)	14.9982(11)	15.332(2)	15.6149(9)	24.3769(11)	17.9043(7)	21.913(2)	19.9898(10)
c (Å)	23.948(3)	17.2489(15)	17.5010(19)	17.6242(9)	22.5969(8)	17.9041(6)	22.478(3)	20.0319(11)
α (°)	90	90	90	90	90	90	90	64.780(3)
β (°)	102.288(2)	92.982(3)	95.396(4)	94.488(2)	95.8940(10)	102.0400(10)	99.596(5)	87.710(4)
γ (°)	90	90	90	90	90	90	90	89.555(4)
Volume (Å ³)	8299.0(11)	3739.6(5)	3877.2(9)	4011.1(4)	5348.6(3)	4665.0(3)	4691.1(9)	7129.8(7)
Z	4	4	4	2	4	4	4	2
Density (g/cm ³)	1.510	1.776	1.823	1.801	1.531	1.513	1.505	1.531
μ (mm ⁻¹)	4.840	5.136	5.505	5.197	3.597	3.889	3.868	6.206
F(000)	3720	1952	2040	2112	2464	2128	2128	3236
θ range (°)	1.38 to 26.09	1.79 to 27.48	1.94 to 26.41	1.88 to 29.59	2.00 to 29.60	1.98 to 28.32	2.06 to 29.74	2.25 to 68.34
Index ranges	-26 ≤ h ≤ 28 -18 ≤ k ≤ 18 -29 ≤ l ≤ 29	-18 ≤ h ≤ 18 -18 ≤ k ≤ 19 -22 ≤ l ≤ 22	-18 ≤ h ≤ 18 -19 ≤ k ≤ 15 -21 ≤ l ≤ 21	-20 ≤ h ≤ 20 -21 ≤ k ≤ 21 -24 ≤ l ≤ 24	-13 ≤ h ≤ 13 -33 ≤ k ≤ 33 -31 ≤ l ≤ 31	-19 ≤ h ≤ 19 -22 ≤ k ≤ 23 -23 ≤ l ≤ 23	-13 ≤ h ≤ 13 -30 ≤ k ≤ 30 -31 ≤ l ≤ 31	-23 ≤ h ≤ 23 -21 ≤ k ≤ 24 0 ≤ l ≤ 24
Reflns collected	50649	45504	44212	63537	94904	63018	82285	141325
Independent reflns	16423 [R _{int} = 0.0699]	8576 [R _{int} = 0.0606]	7949 [R _{int} = 0.1284]	11267 [R _{int} = 0.0512]	15026 [R _{int} = 0.0694]	11607 [R _{int} = 0.0802]	13247 [R _{int} = 0.0569]	25728 [R _{int} = 0.2193]
Data / restraints / parameters	16423 / 1 / 815	8576 / 6 / 488	7949 / 0 / 451	11267 / 0 / 528	15026 / 6 / 659	11607 / 174 / 626	13247 / 0 / 586	25728 / 284 / 1870
GOF on F ²	1.017	1.040	1.026	1.188	1.031	1.109	1.057	1.033
R ₁ (I > 2σ(I))	0.0480	0.0353	0.0491	0.0389	0.0363	0.0495	0.0340	0.1169
wR ₂ (all data)	0.0988	0.0830	0.1120	0.0754	0.0727	0.0896	0.0610	0.3313

Table A3.11. Crystallographic data for compounds **7.6-7.8**

	6[BPh₄]⁺·CH₂Cl₂	6·THF	7[AlOR^F₄]⁺·CH₂Cl₂	7[SbF₆]⁻·CH₂Cl₂	8[BF₄]₂⁻·CH₂Cl₂	8[NTf₂]₂
CCDC number	2190050	2190051	2190048	2190049	2190052	2190053
Formula	C ₆₂ H ₅₁ BBiCl ₃ P ₂	C ₆₅ H ₅₇ BBiCl ₃ OP ₂	C ₅₄ H ₃₁ AlBiBrCl ₂ F ₃ ₆ O ₄ P ₂	C ₃₈ H ₃₁ BiBrCl ₂ F ₆ P ₂ Sb	C ₃₈ H ₃₁ B ₂ BiCl ₂ F ₈ P ₂	C ₄₁ H ₂₉ BiF ₁₂ N ₂ O ₈ P ₂ S ₄
FW (g/mol)	1184.10	1171.28	1876.50	1145.11	1003.07	1304.82
Temp (K)	100(2)	100(2)	100(2)	100(2)	100(2)	100(2)
λ (Å)	0.71073	0.71073	0.71073	0.71073	0.71073	0.71073
Size (mm)	0.035 x 0.054 x 0.345	0.045 x 0.082 x 0.082	0.202 x 0.221 x 0.338	0.060 x 0.148 x 0.233	0.060 x 0.098 x 0.195	0.070 x 0.096 x 0.145
Crystal habit	colorless rod	colourless block	colourless block	colorless plate	colourless block	colourless block
Crystal system	monoclinic	monoclinic	triclinic	monoclinic	monoclinic	monoclinic
Space group	P 2 ₁ /c	P 2 ₁ /n	P -1	P 2 ₁ /c	P 2 ₁	P 2 ₁ /c
a (Å)	10.0344(6)	12.2039(14)	19.060(3)	10.2740(12)	10.0478(15)	20.4021(16)
b (Å)	16.1239(12)	32.890(3)	20.051(3)	20.703(3)	14.891(2)	13.3595(10)
c (Å)	32.236(2)	13.1093(11)	37.003(5)	17.863(2)	c13.273(2)	18.1407(17)
α (°)	90	90	93.491(4)	90	90	90
β (°)	97.311(2)	95.434(3)	93.277(4)	92.936(2)	107.421(3)	110.895(2)
γ (°)	90	90	112.195(4)	90	90	90
Volume (Å ³)	5173.2(6)	5238.2(9)	13020.(3)	3794.5(8)	1894.8(5)	4619.3(7)
Z	4	4	8	4	2	4
Density (g/cm ³)	1.520	1.485	1.915	2.004	1.758	1.876
μ (mm ⁻¹)	3.666	3.522	3.615	6.679	4.946	4.170
F(000)	2368	2360	7248	2184	976	2552
θ range (°)	2.05 to 26.07	1.99 to 27.52	1.10 to 26.12	1.51 to 31.57	1.61 to 28.29	1.86 to 27.52
Index ranges	-12 ≤ h ≤ 12 -17 ≤ k ≤ 19 -39 ≤ l ≤ 39	-15 ≤ h ≤ 15 -42 ≤ k ≤ 42 -13 ≤ l ≤ 17	-23 ≤ h ≤ 23 -24 ≤ k ≤ 24 -44 ≤ l ≤ 45	-15 ≤ h ≤ 15 -30 ≤ k ≤ 30 -26 ≤ l ≤ 26	-13 ≤ h ≤ 13 -19 ≤ k ≤ 19 -17 ≤ l ≤ 17	-26 ≤ h ≤ 26 -16 ≤ k ≤ 17 -23 ≤ l ≤ 22
Reflns collected	67445	66507	289932	55458	52131	61142
Independent reflns	10225 [R _{int} = 0.0962]	12018 [R _{int} = 0.1006]	51641 [R _{int} = 0.0909]	12682 [R _{int} = 0.0458]	9400 [R _{int} = 0.0474]	10623 [R _{int} = 0.1099]
Data / restraints / parameters	10225 / 0 / 622	12018 / 0 / 640	51641 / 7 / 3605	12682 / 0 / 506	9400 / 1 / 478	10623 / 15 / 636
GOF on F ²	1.116	1.012	1.094	1.030	1.018	1.125
R ₁ (I > 2σ(I))	0.0491	0.0425	0.0534	0.0312	0.0210	0.0573
wR ₂ (all data)	0.0819	0.0920	0.1273	0.0613	0.0440	0.1050

Table A3.12. Crystallographic data for compounds **7.9-7.12**

	9·1.5CH₂Cl₂	9	9·THF·benzene	10	11·CH₂Cl₂	12
CCDC number	2190026	2190027	2190028	2190029	2190030	2190031
Formula	C _{56.5} H ₃₂ BBiCl ₃ F ₁₅ P ₂	C ₅₅ H ₂₉ BBiF ₁₅ P ₂	C ₆₅ H ₄₃ BBiF ₁₅ O P ₂	C ₅₅ H ₂₈ BBiClF ₁₅ P ₂	C ₇₅ H ₅₈ Bi ₂ Cl ₈ P ₄	C ₇₄ H ₅₆ Bi ₂ F ₂₅ P ₄ S b ₃
FW (g/mol)	1386.45	1256.51	1406.72	1290.95	1784.65	2327.27
Temp (K)	100(2)	100(2)	100(2)	100(2)	100(2)	100(2)
λ (Å)	0.71073	0.71073	0.71073	0.71073	0.71073	0.71073
Size (mm)	0.227 x 0.251 x 0.397	0.091 x 0.177 x 0.192	0.100 x 0.182 x 0.338	0.074 x 0.130 x 0.225	0.155 x 0.182 x 0.292	0.140 x 0.140 x 0.249
Crystal habit	colourless block	colourless block	colourless plate	colourless block	red block	colourless block
Crystal system	monoclinic	triclinic	monoclinic	triclinic	monoclinic	monoclinic
Space group	P 2 ₁ /n	P -1	P 2 ₁ /n	P -1	P 2 ₁ /n	I 2/a
a (Å)	10.0148(4)	10.4207(4)	10.0376(7)	11.507(3)	9.3054(7)	14.4344(13)
b (Å)	23.6619(9)	13.5142(6)	23.5615(13)	14.131(3)	22.5570(19)	20.5806(16)
c (Å)	22.5969(10)	17.1038(7)	23.1027(13)	15.261(4)	15.8489(13)	26.191(3)
α (°)	90	100.8060(10)	90	88.629(7)	90	90
β (°)	95.837(2)	90.1570(10)	94.489(2)	75.966(7)	92.250(2)	95.860(3)
γ (°)	90	105.0230(10)	90	85.250(7)	90	90
Volume (Å ³)	5327.0(4)	2281.76(16)	5447.0(6)	2399.2(10)	3324.1(5)	7739.9(12)
Z	4	2	4	2	2	4
Density (g/cm ³)	1.729	1.829	1.715	1.787	1.783	1.997
μ (mm ⁻¹)	3.615 mm ⁻¹	4.036	3.393	3.895	5.750	5.751
F(000)	2705	1224	2776	1256	1740	4416
θ range (°)	1.95 to 32.03	2.03 to 33.16	1.94 to 29.59	1.38 to 26.44	1.57 to 29.62	1.26 to 26.50
Index ranges	-14 ≤ h ≤ 14 -35 ≤ k ≤ 30 -33 ≤ l ≤ 33	-16 ≤ h ≤ 13 -20 ≤ k ≤ 20 -26 ≤ l ≤ 26	-13 ≤ h ≤ 13 -32 ≤ k ≤ 32 -29 ≤ l ≤ 32	-14 ≤ h ≤ 14 -17 ≤ k ≤ 17 -19 ≤ l ≤ 19	-9 ≤ h ≤ 12 -28 ≤ k ≤ 31 -22 ≤ l ≤ 22	-18 ≤ h ≤ 18 -25 ≤ k ≤ 24 -32 ≤ l ≤ 32
Reflns collected	95436	61144	79141	48522	56876	41917
Independent reflns	18385 [R _{int} = 0.0450]	17271 [R _{int} = 0.0308]	15252 [R _{int} = 0.0569]	9846 [R _{int} = 0.1193]	9333 [R _{int} = 0.0459]	7981 [R _{int} = 0.0719]
Data / restraints / parameters	18385 / 46 / 769	17271 / 0 / 671	15252 / 28 / 779	9846 / 0 / 676	9333 / 0 / 415	7981 / 186 / 520
GOF on F ²	1.042	1.043	1.021	1.001	1.107	1.028
R ₁ (I > 2σ(I))	0.0262	0.0202	0.0327	0.0492	0.0344	0.0605
wR ₂ (all data)	0.0637	0.0482	0.0811	0.0901	0.0682	0.1698

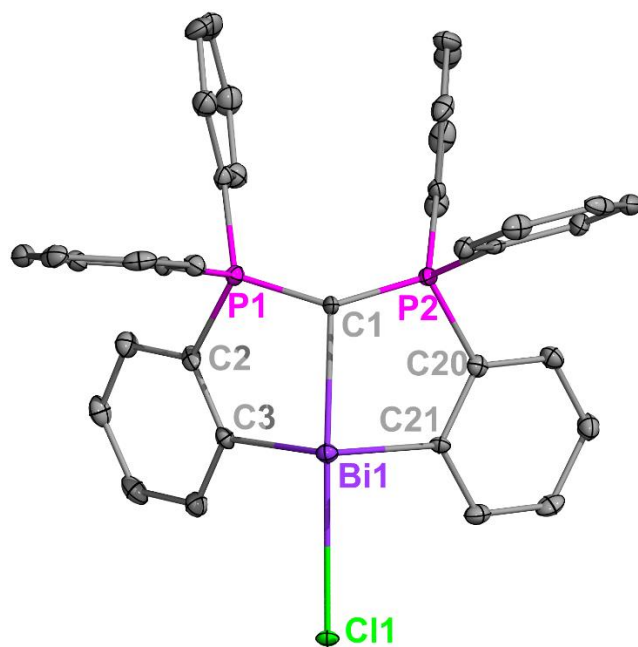


Figure A3.42. Molecular structure of **7.1**. Thermal ellipsoids set at 50% probability. Co-crystallized dichloromethane molecules and all H atoms are omitted for clarity. Selected bond distances (Å) and angles (°): Bi1–C1, 2.368(4); Bi1–Cl1, 3.0110(11); Bi1–C3, 2.279(4); Bi1–C21, 2.268(4); C1–P1, 1.677(4); C1–P2, 1.692(4); C3–Bi1–C21, 98.32(16); P1–C1–P2, 132.2(3).

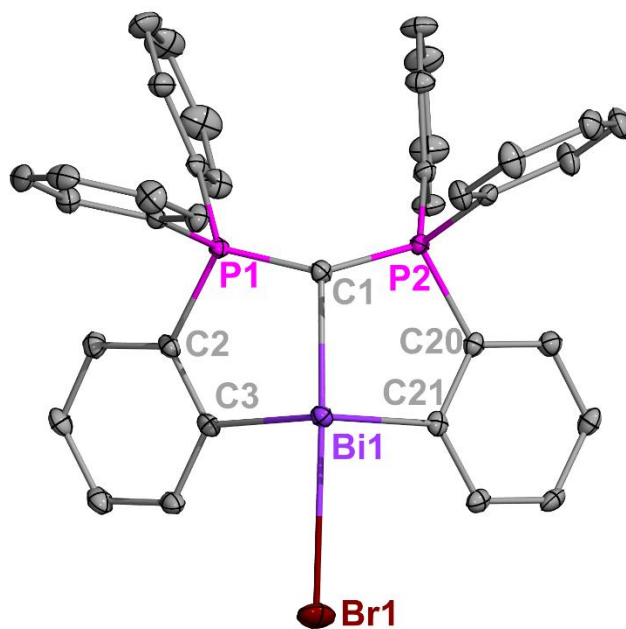


Figure A3.43. Molecular structure of **7.2**. Thermal ellipsoids set at 50% probability. Co-crystallized dichloromethane molecules and all H atoms are omitted for clarity. Selected bond distances (Å) and angles (°): Bi1–C1, 2.346(3); Bi1–Br1, 3.0826(4); Bi1–C3, 2.273(3); Bi1–C21, 2.275(3); C1–P1, 1.680(3); C1–P2, 1.686(3); C3–Bi1–C21, 102.12(11); P1–C1–P2, 134.9(2).

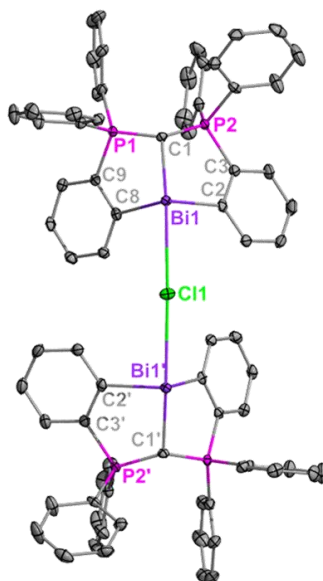


Figure A3.44. Molecular structure of **7.3[NTf₂]**. Thermal ellipsoids set at 50% probability. Co-crystallized solvent molecules, H atoms and one non-coordinating triflimide anion are omitted for clarity. Selected bond distances (Å) and angles (°): Bi1–C1, 2.295(2); Bi1–Cl1, 3.0939(3); Bi1–C2, 2.258(2); Bi1–C8, 2.290(2); C1–P1, 1.684(2); C1–P2, 1.691(2); C2–Bi1–C8, 100.46(8); P1–C1–P2, 128.7(14).

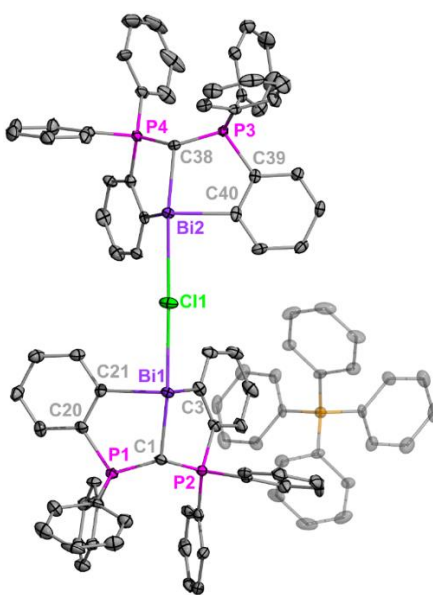


Figure A3.45. Molecular structure of **7.3[BPh₄]**. Thermal ellipsoids set at 50% probability, and H atoms are omitted for clarity. Selected bond distances (Å) and angles (°): Bi1–C1, 2.303(6); Bi2–C38, 2.307(6); Bi1–Cl1, 2.9494(16); Bi2–Cl1, 2.9778(16); Bi1–C3, 2.281(6); Bi1–C21, 2.268(7); C1–P1, 1.685(7); C1–P2, 1.690(7); Bi1–Cl1–Bi2, 172.75(8); C3–Bi1–C21, 103.3(2); P1–C1–P2, 130.8(4).

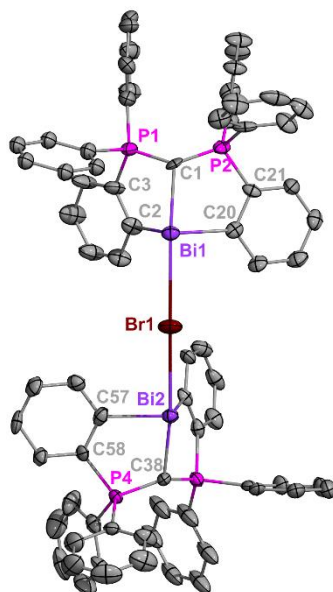


Figure A3.46. Molecular structure of **7.4[BPh₄]**. Thermal ellipsoids set at 50% probability, H atoms and one BPh₄ anion are omitted for clarity. Selected bond distances (Å) and angles (°): Bi1–C1, 2.291(11); Bi1–Br1, 3.0947(15); Bi2–Br1, 3.1184(15); Bi1–C2, 2.286(11); Bi1–C20, 2.258(11); C1–P1, 1.691(12); C1–P2, 1.674(11); C2–Bi1–C8, 101.7(4); P1–C1–P2, 131.5(8).

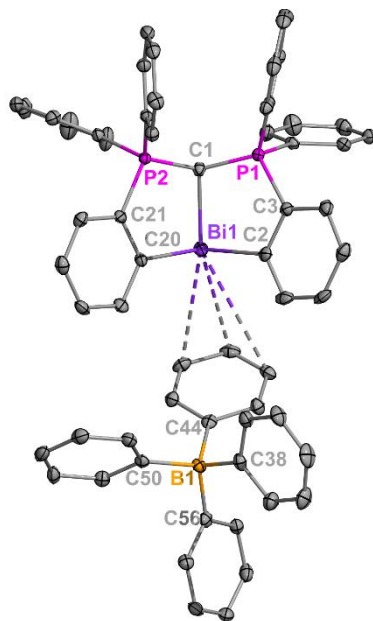


Figure A3.47. Molecular structure of **7.5[BPh₄]**. Thermal ellipsoids set at 50% probability, and H atoms are omitted for clarity. Selected bond distances (Å) and angles (°): Bi1–C1, 2.275(3); Bi1–C2, 2.261(3); Bi1–C20, 2.252(3); C1–P1, 1.692(3); C1–P2, 1.698(3); C2–Bi1–C20, 96.95(10); P1–C1–P2, 132.33(18).

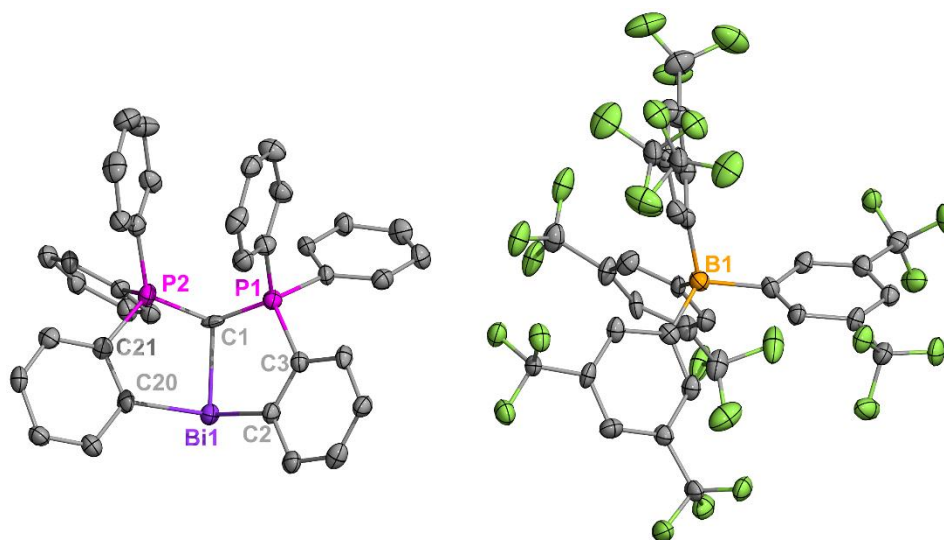


Figure A3.48. Molecular structure of $7.5[\text{BArF}_4]$. Thermal ellipsoids set at 50% probability, and H atoms are omitted for clarity. Selected bond distances (Å) and angles (°): Bi1–C1, 2.219(10); Bi1–C2, 2.227(14); Bi1–C20, 2.290(13); C1–P1, 1.705(16); C1–P2, 1.684(15); C2–Bi1–C20, 102.3(6); P1–C1–P2, 132.6(7).

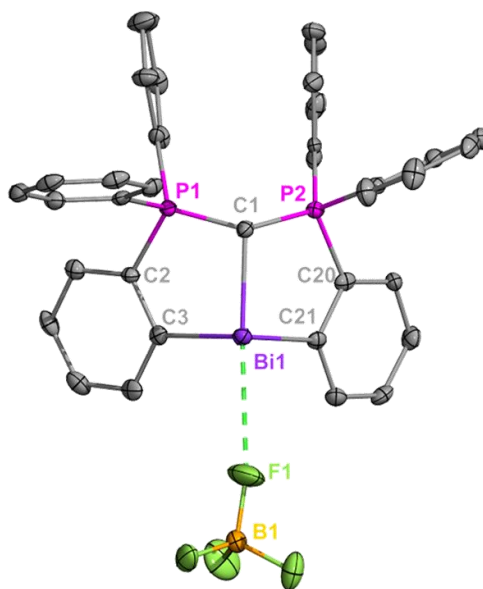


Figure A3.49. Molecular structure of $7.5[\text{BF}_4]$. Thermal ellipsoids set at 50% probability, and H atoms are omitted for clarity. Selected bond distances (Å) and angles (°): Bi1–C1, 2.275(4); Bi1–F1, 2.890; Bi1–C3, 2.260(5); Bi1–C21, 2.253(5); C1–P1, 1.704(5); C1–P2, 1.699(5); C3–Bi1–C21, 93.96(17); P1–C1–P2, 130.1(3).

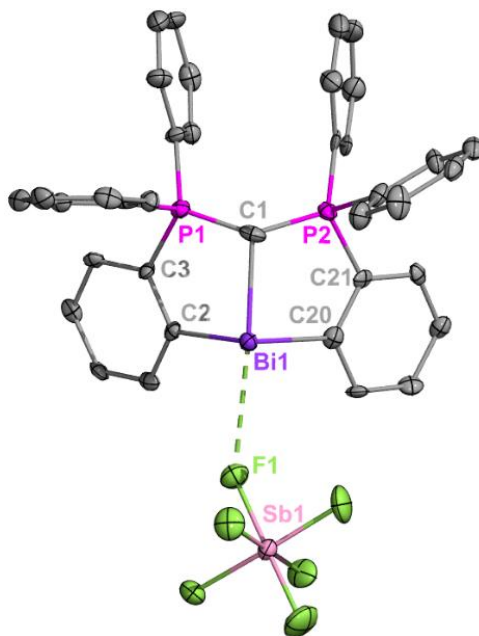


Figure A3.50. Molecular structure of **7.5[SbF₆]**. Thermal ellipsoids set at 50% probability, and H atoms are omitted for clarity. Selected bond distances (Å) and angles (°): Bi1–C1, 2.269(8); Bi1–F1, 2.926; Bi1–C2, 2.272(8); Bi1–C20, 2.257(8); C1–P1, 1.673(10); C1–P2, 1.712(9); C2–Bi1–C20, 96.4(3); P1–C1–P2, 131.3(5).

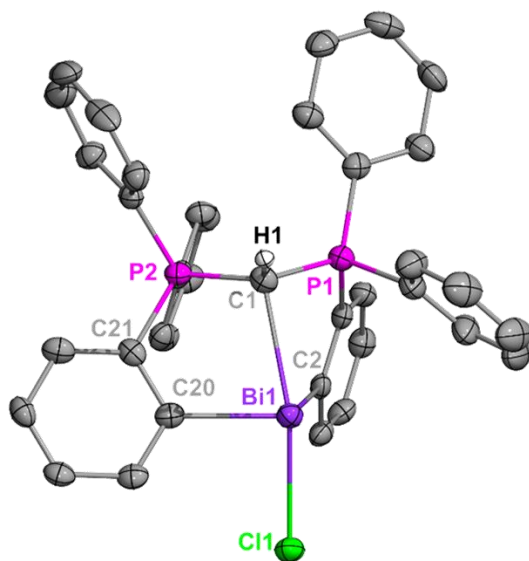


Figure A3.51. Molecular structure of **7.6[BPh₄]**. Thermal ellipsoids set at 50% probability, H atoms and one BPh₄ anion are omitted for clarity. Selected bond distances (Å) and angles (°): Bi1–C1, 2.609(5); Bi1–Cl1, 2.6324(14); Bi1–C2, 2.281(5); Bi1–C20, 2.263(5); C1–P1, 1.739(5); C1–P2, 1.763(6); C2–Bi1–C20, 102.97(18); P1–C1–P2, 124.2(3).

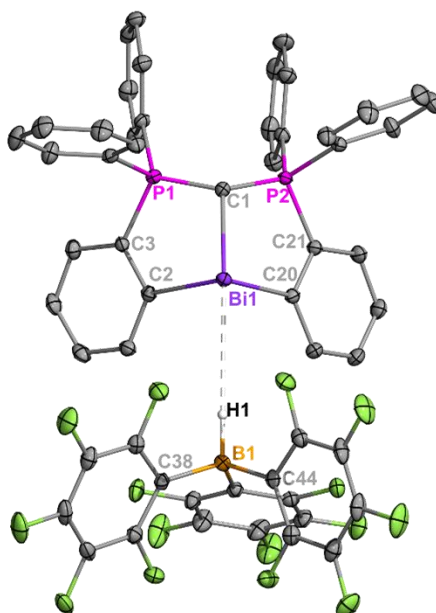


Figure A3.52. Molecular structure of **7.9**. Thermal ellipsoids are shown at 50 % probability, and aromatic protons omitted for clarity. B-H hydrides were isotropically refined. Selected bond distances (Å) and angles (°): Bi1–C1, 2.2773(18); Bi1–C2, 2.2676(19); Bi1–C20, 2.2488(18); Bi1–H1, 3.14(3); C1–P1, 1.6959(19); C1–P2, 1.6994(19); C2–Bi1–C20, 95.42(6); P1–C1–P2, 130.10(12).

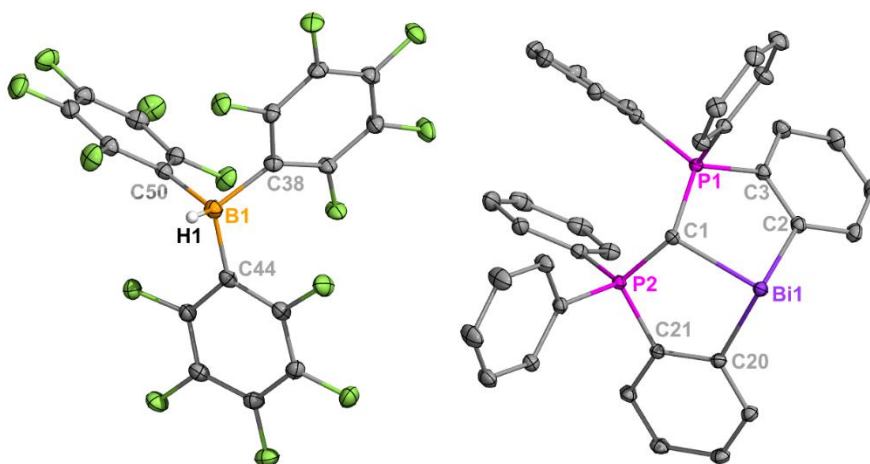


Figure A3.53. Molecular structure of **7.9'**. Thermal ellipsoids are shown at 50 % probability, and aromatic protons omitted for clarity. B-H hydrides were isotropically refined. Selected bond distances (Å) and angles (°): Bi1–C1, 2.2499(13); Bi1–C2, 2.2848(14); Bi1–C20, 2.2498(14); C1–P1, 1.6993(14); C1–P2, 1.6998(14); C2–Bi1–C20, 98.11(5); P1–C1–P2, 128.26(8).

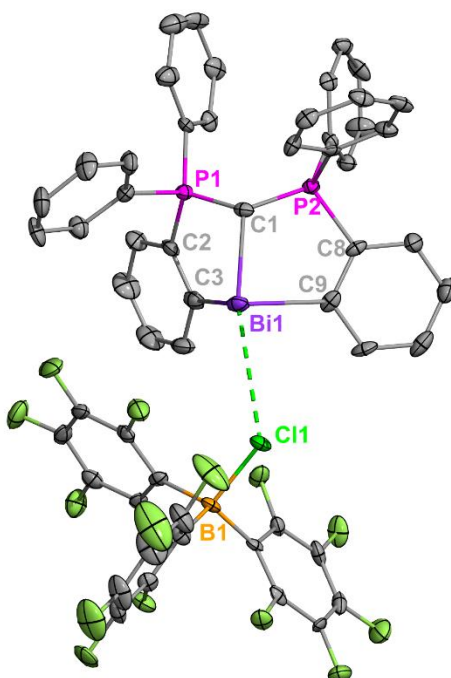


Figure A3.54. Molecular structure of **7.10**. Thermal ellipsoids set at 50% probability, and H atoms are omitted for clarity. Selected bond distances (Å) and angles (°): Bi1–C1, 2.259(5); B1–Cl1, 1.942(6); Bi1–C3, 2.293(6); Bi1–C9, 2.264(6); C1–P1, 1.695(6); C1–P2, 1.686(6); C3–Bi1–C9, 102.7(2); P1–C1–P2, 132.7(4).

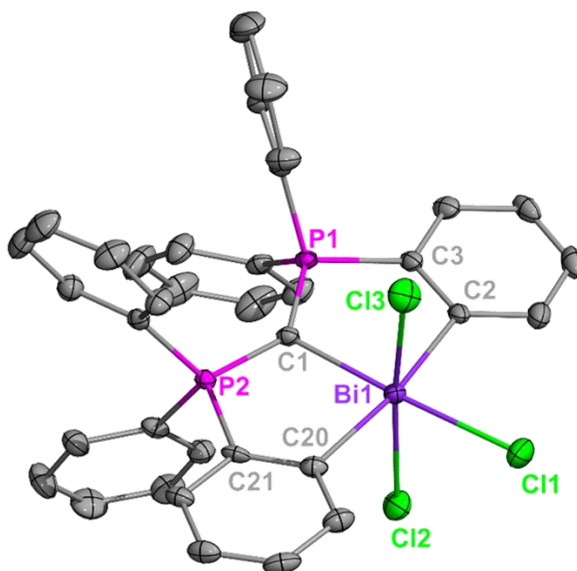


Figure A3.55. Molecular structure of **11**. Thermal ellipsoids shown at 50 % probability. Co-crystallized DCM molecules, and all aromatic protons are omitted for clarity. Selected bond distances (Å) and angles (°): Bi1–C1, 2.227(3); Bi1–Cl1, 2.5867(10); Bi1–Cl2, 2.5912(10); Bi1–Cl3, 2.5538(11); Bi1–C2, 2.231(4); Bi1–C20, 2.224(4); C1–P1, 1.681(3); C1–P2, 1.675(3); C2–Bi1–C20, 170.63(13); P1–C1–P2, 133.1(2).

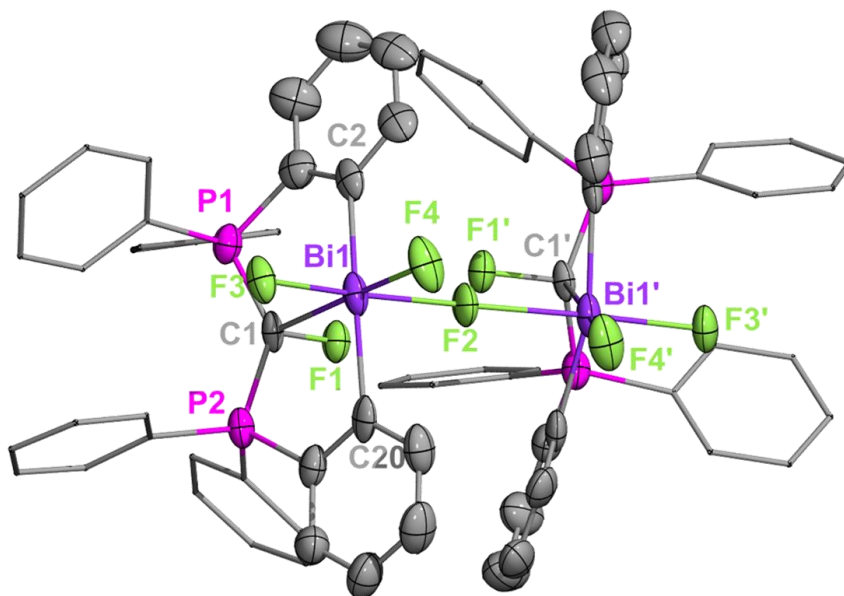


Figure A3.56. Molecular structure of **12**. Thermal ellipsoids shown at 50 % probability. Three non-coordinating SbF_6 anions, and all aromatic protons are omitted for clarity. A crystallographic two-fold rotational axis was found at F2. Selected bond distances (\AA) and angles ($^\circ$): Bi1–C1, 2.492(10); Bi1–F2, 2.2277(13); Bi1–F3, 2.057(6); Bi1–F4, 2.044(6); C1–F1, 1.440(11); Bi1–C2, 2.171(12); Bi1–C20, 2.182(13); C1–P1, 1.771(11); C1–P2, 1.791(11); C2–Bi1–C20, 162.4(4); P1–C1–P2, 135.8(6).

Appendix IV: Computational Details

Chapter Three:

Computations were performed by Nathan C. Frey under the supervision of Prof. Dr. Charles Edwin Webster (Mississippi State University).

The starting geometries of compounds **3.2²⁺**, **3.3⁺**, **3.4⁺**, **3.5⁺**, **3.7**, **3.8a**, and **3.8b** were each extracted from the X-ray crystal structures. All density functional theory geometry optimizations and corresponding harmonic vibrational frequency computations were carried out using Gaussian 16 Revision B.01⁴³³ at the ω B97X-D/BS1 level of theory.³¹² The default pruned UltraFine integration grids were used for all energy computations (99 radial shells with 590 points per shell (99,590) and pruned SG1 grids using 50 radial shells with 194 points per shell (50,194) for Hessians. The default SCF convergence criteria (10^{-8}) was used. The basis set (designated as BS1) utilized cc-pVDZ for Mg, C, O, N, and H and cc-pVDZ-PP for Br).^{315-317, 434, 435} For each compound, the Wiberg bond indices (WBI) formulated within the natural atomic orbital (NAO) basis and natural charges were calculated using NBO 3.1, as implemented in Gaussian 09 Revision D.01.⁴³⁶ Localized molecular orbitals were computed using Multiwfn⁴³⁷ 3.7 utilizing the Pipek-Mezey⁴³⁸ localization method with Mulliken population. Molecular orbitals were generated using Chemcraft (<http://www.chemcraftprog.com>) with a contour value of 0.05.⁴³⁹

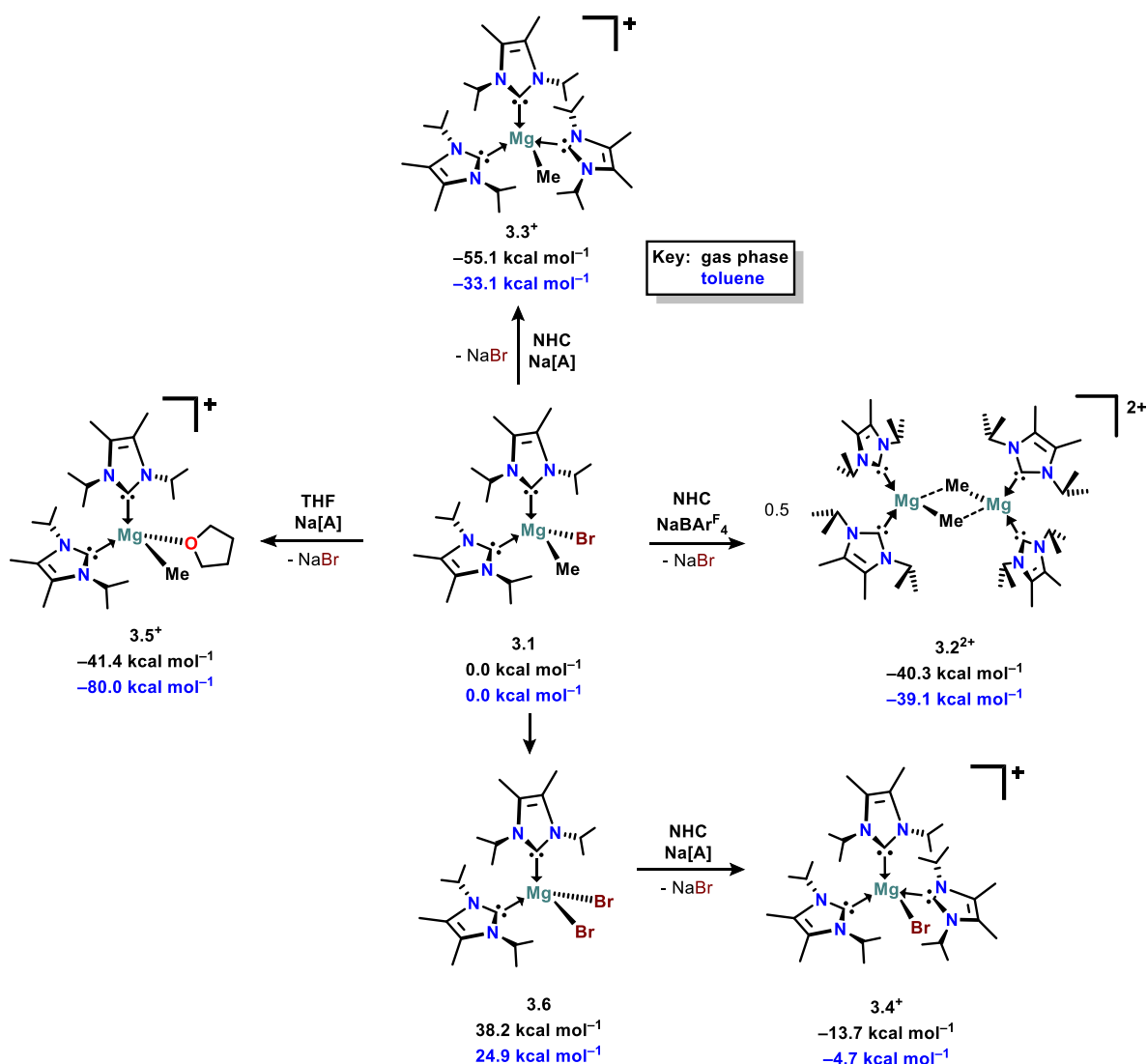
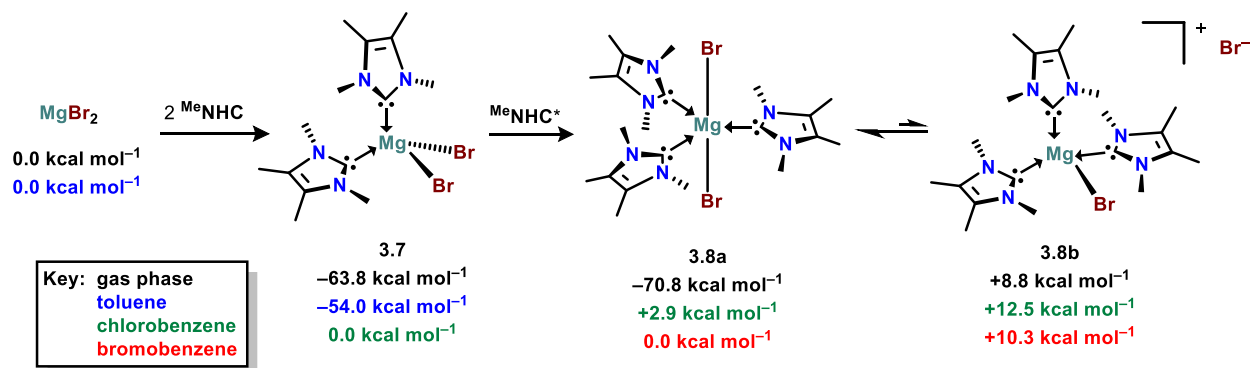


Figure A4.1. Energetics (ΔG) for halide abstraction reactions in gas phase (black, top) and toluene (blue, bottom).



*addition of only one MeNHC considered for reaction energetics

Figure A4.2. Energetics for MgBr₂ heterolysis reaction in gas phase (black), toluene (blue), chlorobenzene (green) and bromobenzene (red).

Table A4.1. WBI and Natural Charge values for reported compounds

3.2²⁺ [(ⁱPrNHC)₂Mg(μ-Me)]₂²⁺				3.3⁺ [(ⁱPrNHC)₃Mg(Me)]⁺			
Mg-R	R	WBI	Natural Charge	Mg-R	R	WBI	Natural Charge
	C ¹	0.3251	0.01667		C ¹	0.2872	0.06355
	C ¹²	0.2883	0.02710		C ¹²	0.3018	0.03134
	C ⁴⁵	0.2016	-1.45024		C ²³	0.2818	0.05076
	C ⁴⁶	0.2060	-1.45024		C ³⁴	0.4620	-1.19648
	Mg	-	1.26870		Mg	-	1.12977
3.4⁺ [(ⁱPrNHC)₃Mg(Br)]⁺				3.5⁺ [(ⁱPrNHC)₂(THF)Mg(Me)]⁺			
Mg-R	R	WBI	Natural Charge	Mg-R	R	WBI	Natural Charge
	C ¹	0.3053	0.02274		C ¹	0.2683	0.00976
	C ¹²	0.2953	0.03280		C ¹²	0.2670	0.02689
	C ²³	0.2832	0.03193		C ²⁷	0.3936	-1.30001
	Br ¹	0.4846	-0.66520		O ¹	0.1259	-0.69346
	Mg	-	1.12487		Mg	-	1.29442
3.7 (^{Me}NHC)₂MgBr₂				3.8a (^{Me}NHC)₃MgBr₂			
Mg-R	R	WBI	Natural Charge	Mg-R	R	WBI	Natural Charge
	C ¹	0.2874	0.07899		C ¹	0.2872	0.08595
	C ⁸	0.2874	0.07899		C ^{1'}	0.2872	0.08595
	Br ¹	0.4945	-0.68177		C ^{1''}	0.2872	0.08595
	Br ²	0.4945	-0.68177		Br ¹	0.3573	-0.73825
	Mg	-	1.07675		Br ²	0.3573	-0.73825
					Mg	-	1.02670
3.8b⁺ [(^{Me}NHC)₃MgBr]⁺							
Mg-R	R	WBI	Natural Charge				
	C ⁸	0.3231	0.04107				
	C ^{8'}	0.3176	0.04751				
	C ^{8''}	0.3209	0.03652				
	Br ³	0.5371	-0.65253				
	Mg	-	1.07605				

Table A4.2. WBI and natural charges for simplistic model Mg–R (R = ^{Me}NHC, ^{iPr}NHC, Br, (Br)₂, Me, O, THF) compounds

	WBI (Mg–R)	Natural charge (Mg)	Natural charge (R)
Mg(^{Me} NHC) ²⁺	0.3870	1.75189	–0.26126
Mg(^{iPr} NHC) ²⁺	0.3706	1.72138	–0.21918
MgBr ⁺	0.7178	1.59622	–0.59622
MgBr ₂	0.6246	1.29674	–0.64836
Mg(Me) ⁺	0.7994	1.44614	–1.26468
MgO ⁺	0.5641	1.67888	–0.67888
MgO	1.5202	1.00594	–1.00594
Mg(THF) ²⁺	0.1624	1.90383	–0.90464

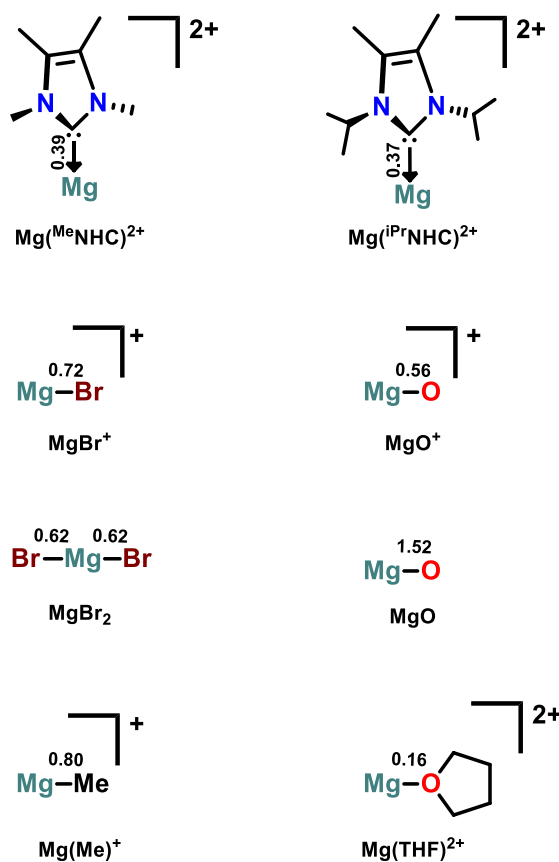
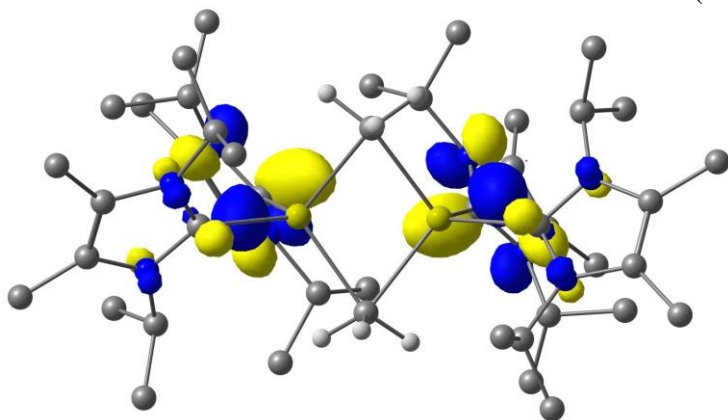


Figure A4.3: 2D representation of simplistic model Mg–R (R = ^{Me}NHC, ^{iPr}NHC, Br, (Br)₂, Me, O, THF) compounds with corresponding WBIs.

Molecular Orbitals for 3.2

MO 221 LUMO -2.92 eV (-0.10713 a.u.)



MO 220 HOMO -12.58 eV (-0.46225 a.u.)

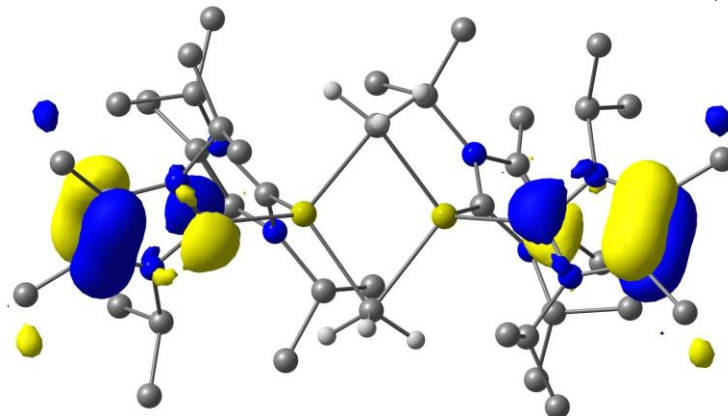


Figure A4.4. Frontier molecular orbitals (HOMO and LUMO) for **3.2**. Select hydrogen atoms not pictured for clarity.

MO 215 HOMO - 5 -14.13 eV (-0.51924 a.u.)

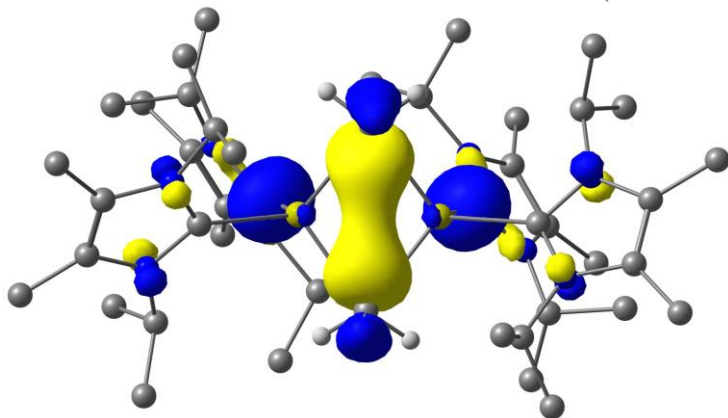


Figure A4.5. HOMO - 5 highlighting Mg(μ -Me) interaction in **3.2**. Select hydrogen atoms not pictured for clarity.

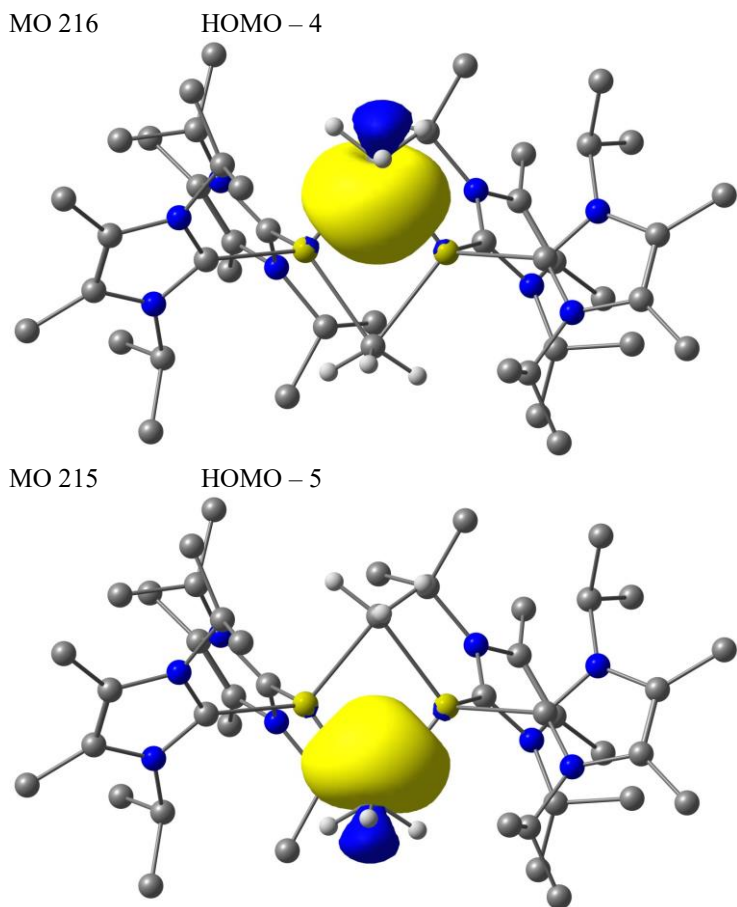


Figure A4.6. Pipek-Mezey Localized Molecular Orbitals for HOMO - 4 and HOMO - 5. Select hydrogen atoms not pictured for clarity.

Chapter Five:

Computations were performed by Nathan C. Frey under the supervision of Prof. Dr. Charles Edwin Webster (Mississippi State University).

All density functional theory computations were carried out using Gaussian 16 Revision C.01,⁴⁴⁰ using the default pruned UltraFine grids using 99 radial shells with 590 points per shell (99,590) and pruned SG1 grids using 50 radial shells with 194 points per shell (50,194) for Hessians. Default convergence for the SCF (10^{-8}) were used. All structures were optimized at the ω B97X-D/cc-pVDZ level of theory.³¹²⁻³¹⁷ To confirm that each stationary point was a minimum or transition state, analytical frequency computations were performed at the same level of theory. For each compound, the Wiberg bond indices (WBI) formulated within the natural atomic orbital (NAO) basis and natural charges were calculated using NBO 3.1,⁴⁴¹ as implemented in Gaussian 09 Revision D.01.⁴⁴² In versions of Gaussian prior to G16, the valence orbitals of Mg did not include the *p* orbitals. This omission will give different results than the default behavior of G16, in which the code was written to count *p* orbitals as valence orbitals for elements in groups 1A and 2A. The authors of Gaussian had intended to omit the *p* orbitals in transition metals and actinides/lanthanides but for Mg the code also omitted these *p* orbitals. Therefore, in order to directly compare to our earlier published results, we have used G09. For these complexes, the addition of IOp(6/90=2) to the route line for a G09 computation will provide the same results as those from G16. Mayer Bond Orders (MBO) were computed using Multiwfn.⁴³⁷ 3D representations of molecules were generated using JIMP2.⁴⁴³

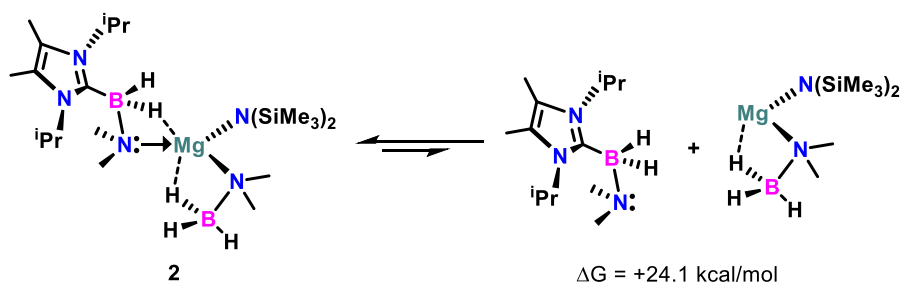


Figure A4.7. Free energy of ⁱPrNHC-BN dissociation from **5.2**

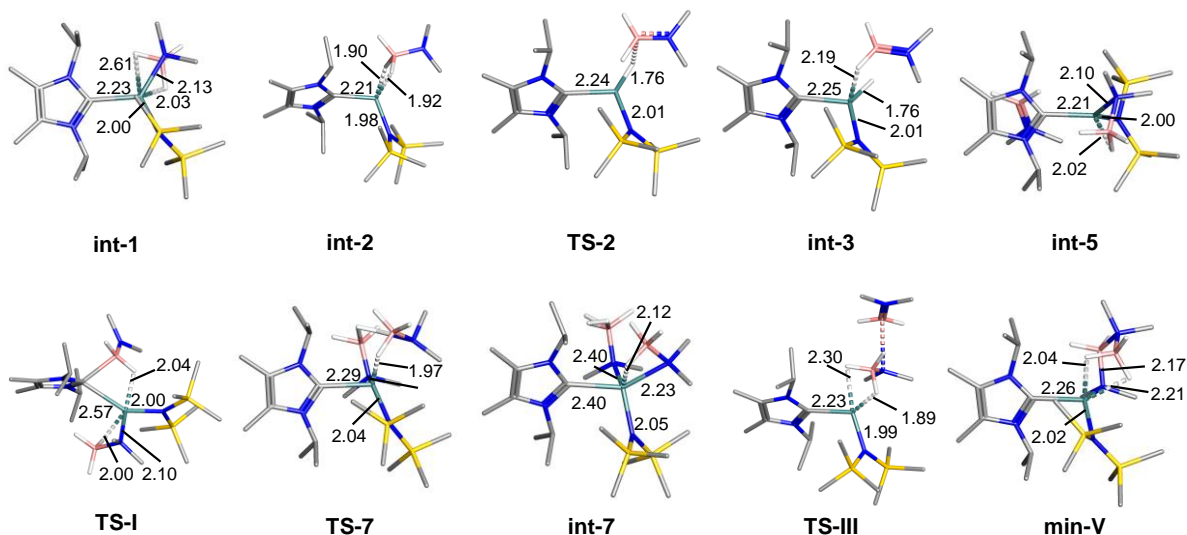


Figure A4.9. 3D representations of selected stationary points with relevant Mg–R (R = NHC, N, or H) bond lengths (in Å).

Table A4.3. Wiberg Bond Indices (WBI) and Mayer Bond Order (MBO) of N–B bonds for selected compounds

5.2			5.8		
N–B	WBI	MBO	N–B	WBI	MBO
N1–B1	0.7134	0.85	N1–B1	0.6903	0.83
N2–B2	0.6913	0.85	–	–	–
5.9			5.12		
N–B	WBI	MBO	N–B	WBI	MBO
N1–B1	0.6682	0.89	N1–B1	0.6941	0.85
N2–B1	0.5712	0.80	N2–B2	0.6576	0.85
N2–B2	0.6252	0.85	N3–B2	0.5715	0.80
–	–	–	N3–B3	0.6336	0.86

Table A4.4. Wiberg Bond Indices (WBI) and Mayer Bond Orders (MBO) of Mg–R for selected compounds

5.2				5.8			
Mg–R	R=	WBI	MBO	Mg–R	R=	WBI	MBO
	B1	0.0435	0.11		B1	0.0950	0.28
	B2	0.0655	0.26		C1	0.3008	0.58
	C1	–	–		N1	0.1248	0.43
	N1	0.0580	0.37		H1a	0.0426	0.15
	N2	0.0704	0.44		H1b	0.0519	0.18
	N3	0.1680	0.74		–	–	–
	H1a	0.0463	0.23		–	–	–
	H2a	0.0226	0.10		–	–	–
	H2b	0.0130	0.03		–	–	–
5.9				5.12			
Mg–R	R=	WBI	MBO	Mg–R	R=	WBI	MBO
	B1	0.0268	0.04		B1	0.0895	0.30
	B2	0.0652	0.29		B2	0.0271	0.05
	C1	0.2644	0.50		B3	0.0741	0.26
	N1	0.0775	0.39		C1	0.2768	0.57
	N2	0.0071	–0.00		N1	0.0944	0.41
	H2a	0.0427	0.18		N2	0.0998	0.41
	H2b	0.0310	0.16		N3	0.0059	–0.00
	–	–	–		H1a	0.0501	0.18
	–	–	–		H1c	0.0381	0.15
	–	–	–		H3d	0.0443	0.20
	–	–	–		H3e	0.0414	0.15

Chapter Six:

Computations were performed by Nathan C. Frey under the supervision of Prof. Dr. Charles Edwin Webster (Mississippi State University).

All density functional theory computations were carried out using Gaussian 16 Revision C.01,⁴⁴⁰ using the default pruned UltraFine grids using 99 radial shells with 590 points per shell (99,590) and pruned SG1 grids using 50 radial shells with 194 points per shell (50,194) for Hessians. Default convergence for the SCF (10^{-8}) were used. All structures were optimized at the ω B97X-D/cc-pVDZ level of theory.³¹²⁻³¹⁷ To confirm that each stationary point was a minimum or transition state, analytical frequency computations were performed at the same level of theory.

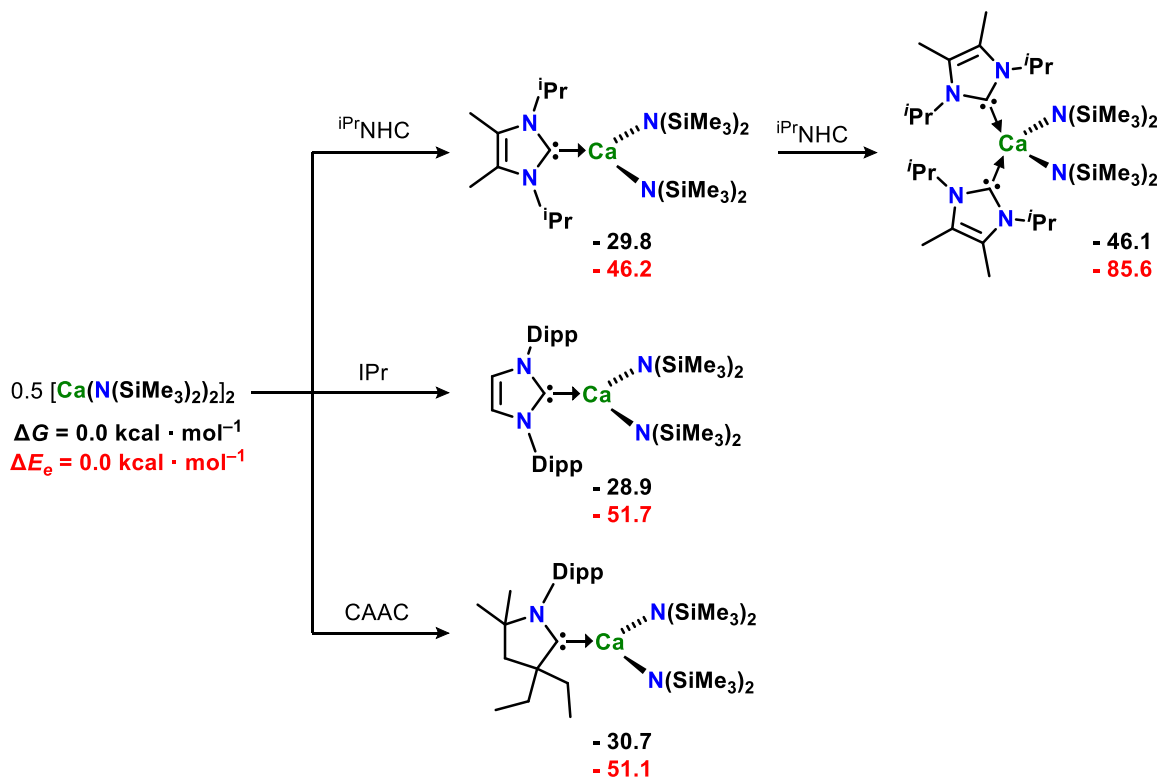


Figure A4.10. Computed (ω B97X-D/cc-pVDZ) complexation energies of carbenes and Ca(N(SiMe₃)₂)₂.

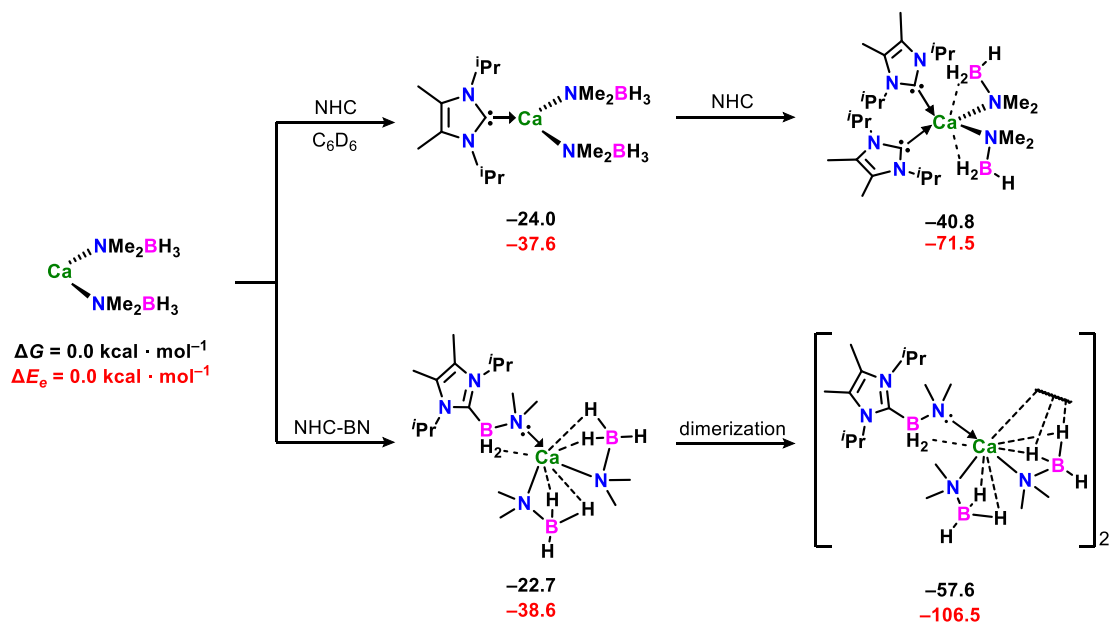


Figure A4.11. Computed (ω B97X-D/cc-pVDZ) complexation energies of NHC or NHC-BN and $\text{Ca}(\text{NMe}_2\text{BH}_3)_2$.

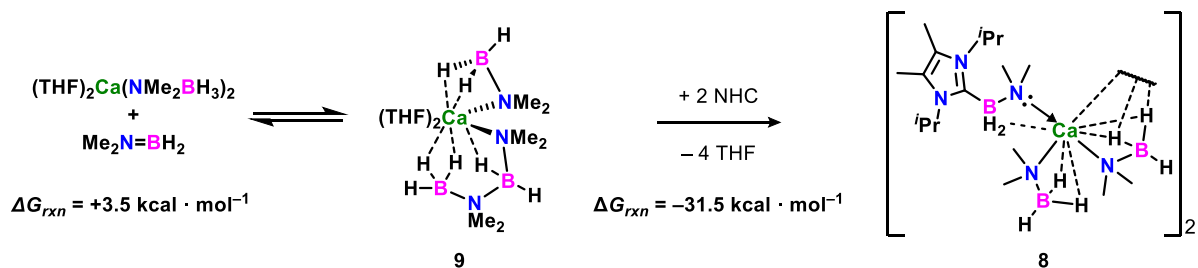
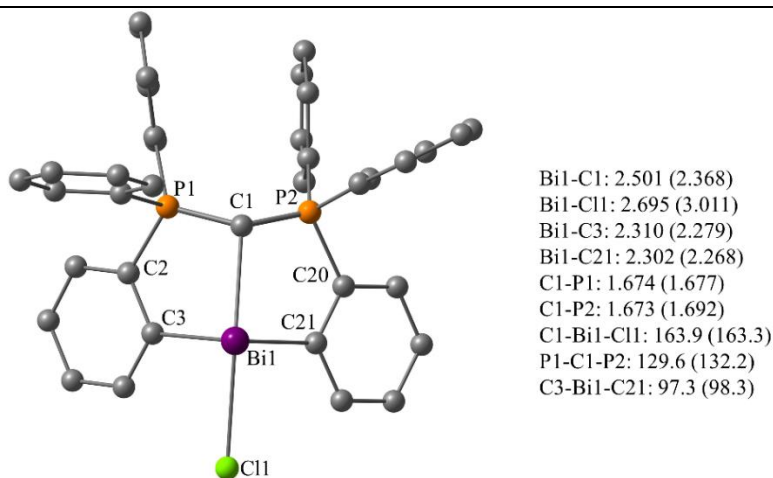


Figure A4.12. Computed (ω B97X-D/cc-pVDZ) energies of $\text{Me}_2\text{N}=\text{BH}_2$ elimination/migration in 6.9.

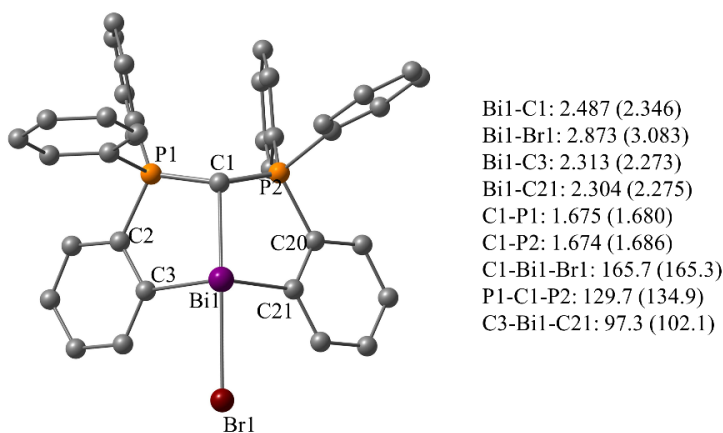
Chapter Seven:

Computations were performed by Dr. William Tiznado (Facultad de Ciencias Exactas, Universidad Andres Bello) and Dr. Sudip Pan (Philipps-Universität Marburg).

Geometry optimizations followed by harmonic vibrational frequency calculations of complexes **7.1**, **7.2**, **7.5⁺** and **7.12** were carried out at the BP86-D3(BJ)/def2-TZVPP level⁴⁴⁴⁻⁴⁴⁷ with and without solvation using Gaussian 16 program.⁴³³ The solvation effect was included by polarizable continuum model (PCM) using CH₂Cl₂ as solvent. The minimum energy nature of the complexes was ensured by the absence of any imaginary frequencies. The nature bond orbital (NBO) analysis was performed using NBO6 program.⁴⁴⁸ Quantum theory of atoms-in-molecules (QTAIM) analysis⁴¹⁵ was done using Multiwfn program⁴³⁷ at the BP86-D3(BJ)/def2-TZVPP level.



7.1 (C₁, ¹A)



7.2 (C₁, ¹A)

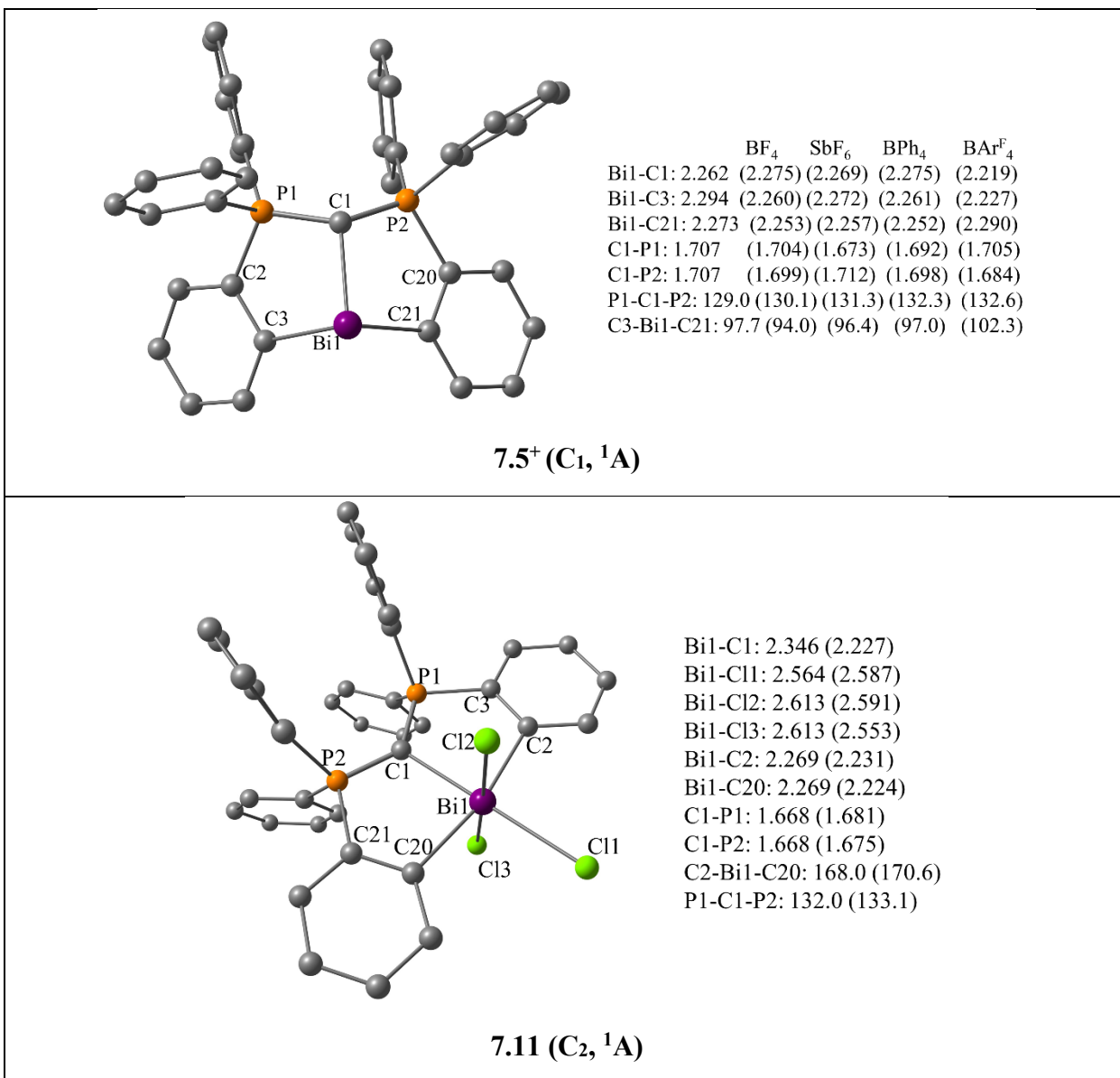
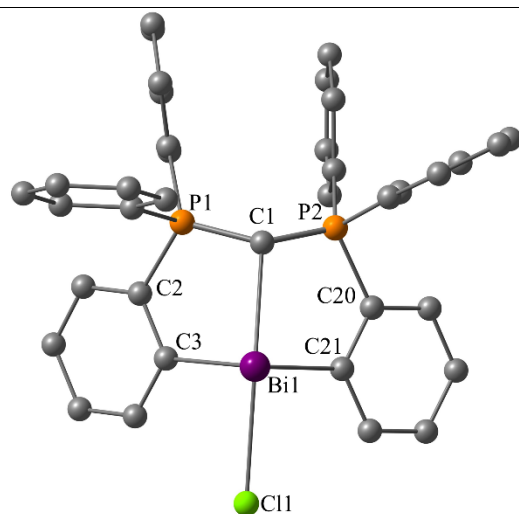
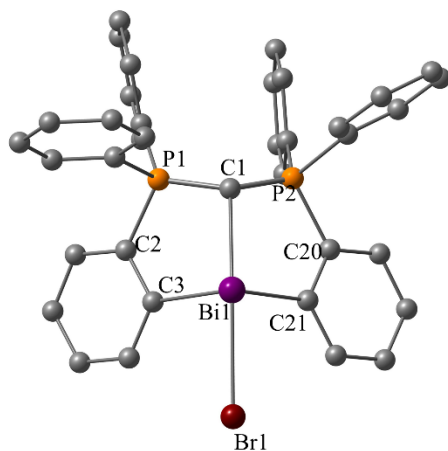


Figure A4.13. The minimum energy geometries of the studied complexes at the BP86-D3(BJ)/def2-TZVPP level. The computed (experimental) bond distances and angles are in Å and in degree, respectively.



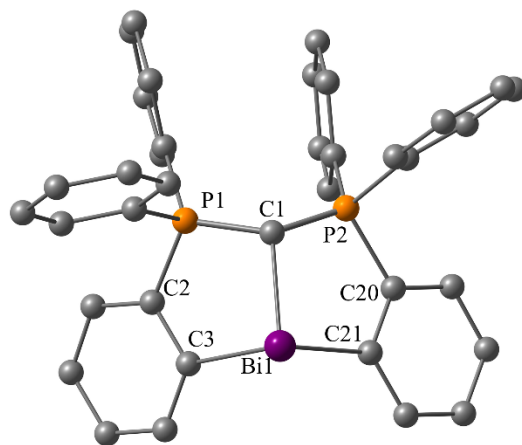
Bi1-C1: 2.396 (2.368)
 Bi1-Cl1: 2.876 (3.011)
 Bi1-C3: 2.309 (2.279)
 Bi1-C21: 2.296 (2.268)
 C1-P1: 1.684 (1.677)
 C1-P2: 1.684 (1.692)
 C1-Bi1-Cl1: 164.4 (163.3)
 P1-C1-P2: 129.0 (132.2)
 C3-Bi1-C21: 97.6 (98.3)

7.1 (C₁, ¹A)



Bi1-C1: 2.377 (2.346)
 Bi1-Br1: 3.089 (3.083)
 Bi1-C3: 2.310 (2.273)
 Bi1-C21: 2.296 (2.275)
 C1-P1: 1.686 (1.680)
 C1-P2: 1.686 (1.686)
 C1-Bi1-Br1: 166.3 (165.3)
 P1-C1-P2: 129.0 (134.9)
 C3-Bi1-C21: 97.5 (102.1)

7.2 (C₁, ¹A)



	BF ₄	SbF ₆	BPh ₄	BAr ^F ₄
Bi1-C1:	2.269 (2.275)	(2.269)	(2.275)	(2.219)
Bi1-C3:	2.297 (2.260)	(2.272)	(2.261)	(2.227)
Bi1-C21:	2.276 (2.253)	(2.257)	(2.252)	(2.290)
C1-P1:	1.705 (1.704)	(1.673)	(1.692)	(1.705)
C1-P2:	1.706 (1.699)	(1.712)	(1.698)	(1.684)
P1-C1-P2:	128.2 (130.1)	(131.3)	(132.3)	(132.6)
C3-Bi1-C21:	96.7 (94.0)	(96.4)	(97.0)	(102.3)

7.5⁺ (C₁, ¹A)

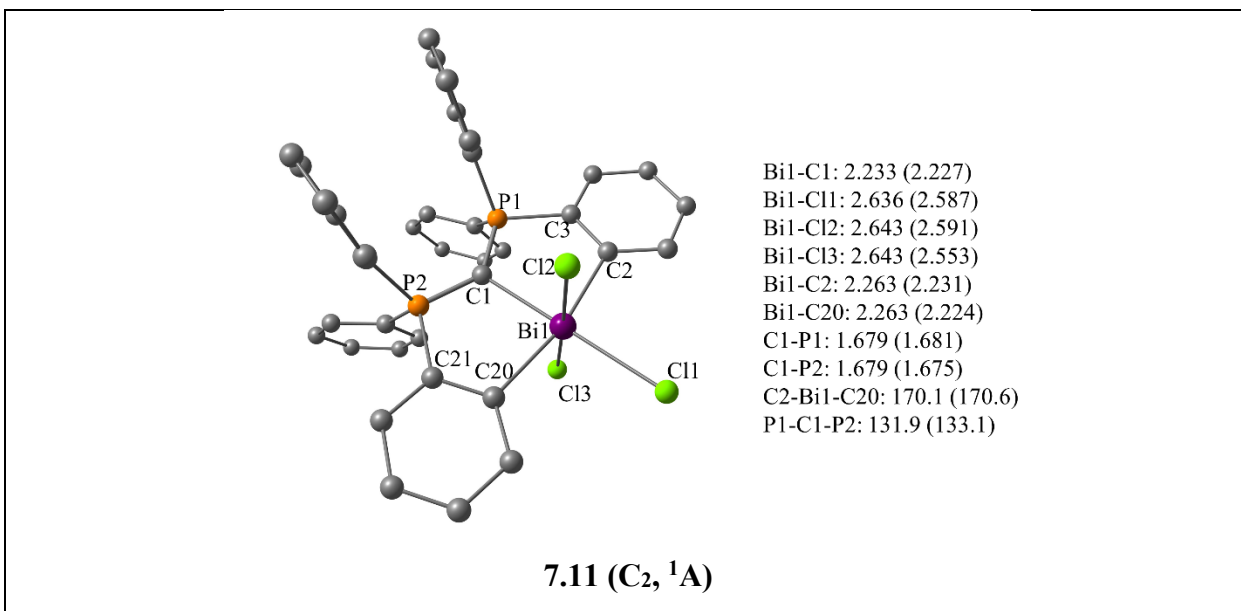
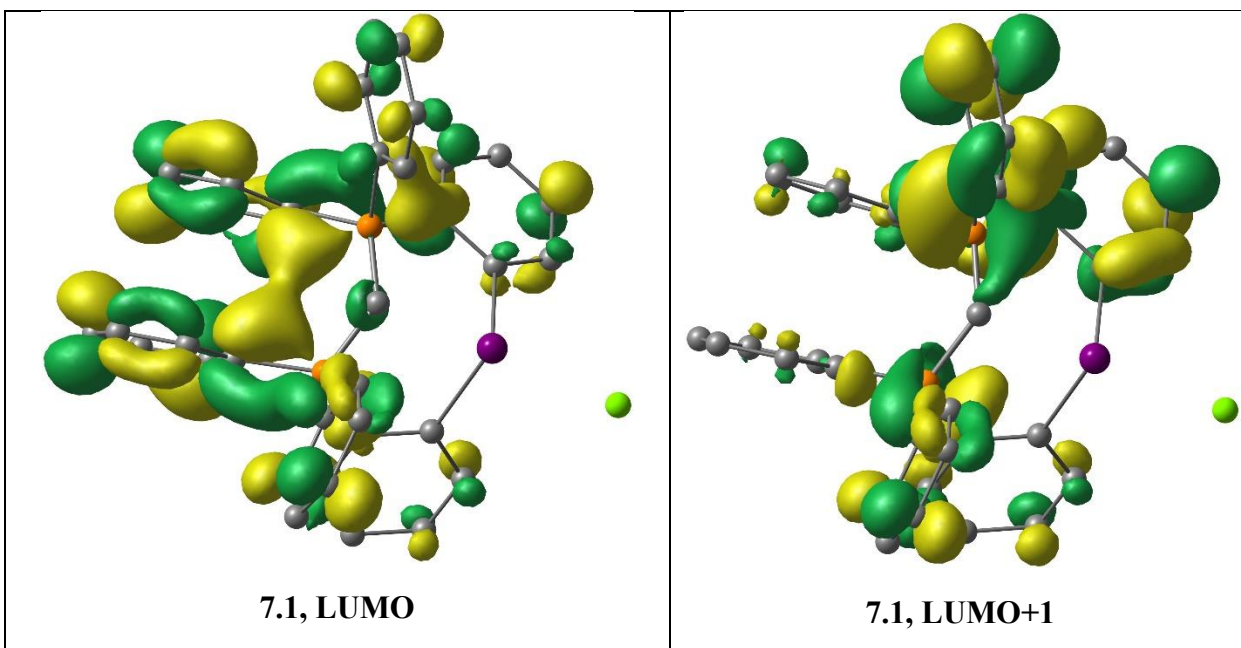
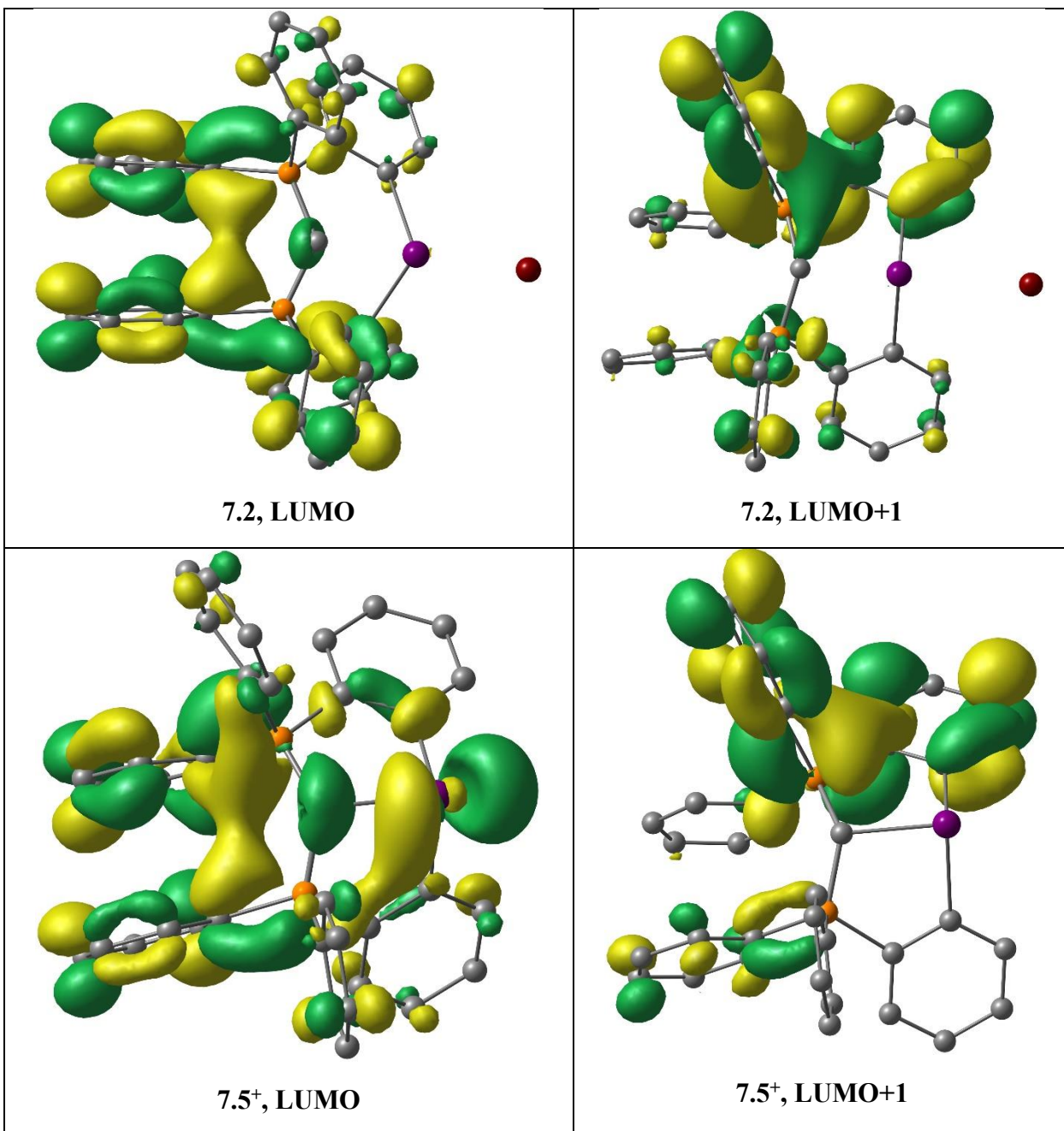


Figure A4.14. The minimum energy geometries of the studied complexes at the BP86-D3(BJ)/def2-TZVPP level with CPCM solvation model using CH₂Cl₂ as a solvent. The computed (experimental) bond distances and angles are in Å and in °, respectively.





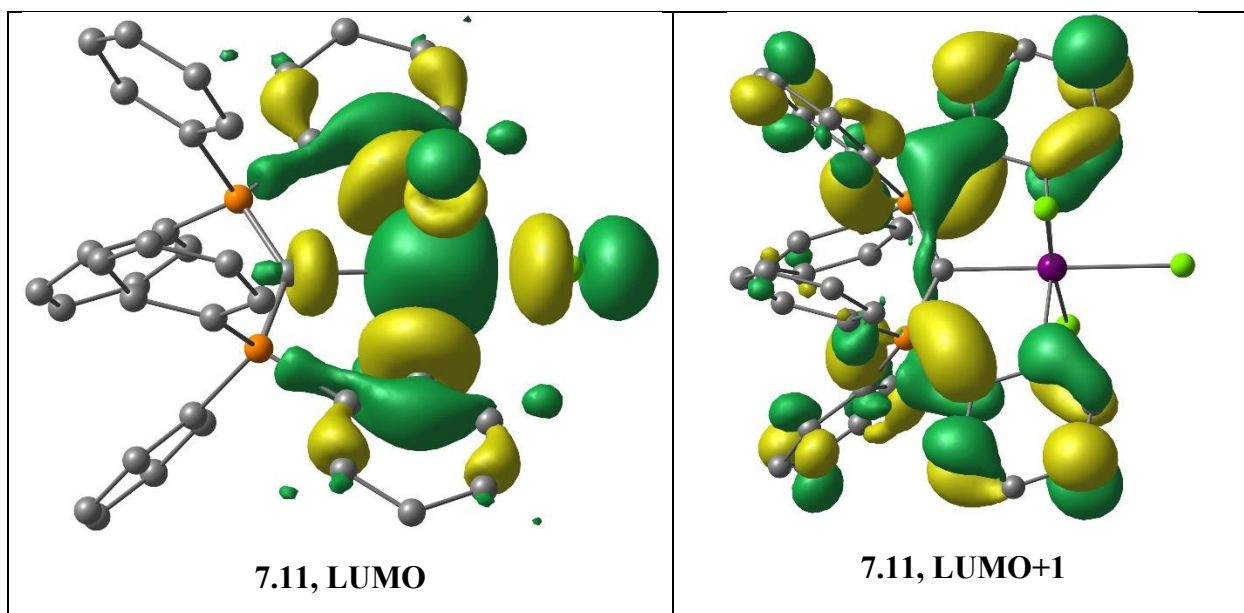


Figure A4.15. The shape of the LUMO and LUMO+1 of studied complexes at the BP86-D3(BJ)/def2-TZVPP level with CPCM solvation model using CH₂Cl₂ as a solvent.

Table 4.5. The NBO results of the studied complexes at the BP86-D3(BJ)/def2-TZVP level with CPCM solvation model using CH₂Cl₂ as a solvent.

Comple x	CDP _C -Bi σ-bond				Ph _C -Bi σ-bond				LP on CDP _C ^[a]	MBO	
	%C	%Bi	C	Bi	%C	%Bi	C	Bi		CDP _C -Bi	Bi-Ph _C
			2s:2p	6s:6p			2s:2p	6s:6p	2s:2p		
7.1	78	22	17:83	2:98	68	32	24:76	6:94	9:91	0.58	0.84
7.2	77	23	17:83	3:97	68	32	24:76	6:94	9:91	0.62	0.84
5	71	29	19:81	6:94	68	32	23:77	5:95	8:92	0.81	0.85
7.11					56	44	18:82	50:50	0:100(π)/ 23:77(σ)	0.68	0.64

^[a]Occupation number for π lone-pair ranges within 1.61 and 1.66 *e*, and the same for σ lone-pair in **11** is 1.44 *e*.

References

1. Harder, S., *Alkaline-earth metal compounds: oddities and applications*. Springer Berlin Heidelberg: Berlin, 2013; Vol. 45.
2. Harder, S., *Early Main Group Metal Catalysis: Concepts and Reactions*. Wiley-VCH: Weinheim, Germany, 2020.
3. Hill, M. S.; Liptrot, D. J.; Weetman, C., Alkaline earths as main group reagents in molecular catalysis. *Chem. Soc. Rev.* **2016**, *45*, 972-988.
4. Robertson, S. D.; Uzelac, M.; Mulvey, R. E., Alkali-Metal-Mediated Synergistic Effects in Polar Main Group Organometallic Chemistry. *Chem. Rev.* **2019**, *119*, 8332-8405.
5. Gil-Negrete, J. M.; Hevia, E., Main group bimetallic partnerships for cooperative catalysis. *Chem. Sci.* **2021**, *12*, 1982-1992.
6. Gentner, T. X.; Mulvey, R. E., Alkali-Metal Mediation: Diversity of Applications in Main-Group Organometallic Chemistry. *Angew. Chem. Int. Ed.* **2021**, *60*, 9247-9262.
7. Jones, C., Open questions in low oxidation state group 2 chemistry. *Commun. Chem.* **2020**, *3*, 159.
8. Stasch, A.; Jones, C., Stable dimeric magnesium(I) compounds: from chemical landmarks to versatile reagents. *Dalton Trans.* **2011**, *40*, 5659-5672.
9. Jones, C., Dimeric magnesium(I) β -diketimines: a new class of quasi-universal reducing agent. *Nat. Rev. Chem.* **2017**, *1*, 0059.
10. Jones, C.; Mountford, P.; Stasch, A.; Blake, M. P., s-Block Metal-Metal Bonds. In *Molecular Metal-Metal Bonds: Compounds, Synthesis, Properties*, Liddle, S. T., Ed. Wiley-VCH: Weinheim, 2015, pp 23-45.

11. 5 - Beryllium, Magnesium, Calcium, Strontium, Barium and Radium. In *Chemistry of the Elements (Second Edition)*, Greenwood, N. N.; Earnshaw, A., Eds. Butterworth-Heinemann: Oxford, 1997, <https://doi.org/10.1016/B978-0-7506-3365-9.50011-0pp> 107-138.
12. Buchner, M. R., Recent Contributions to the Coordination Chemistry of Beryllium. *Chem. Eur. J.* **2019**, *25*, 12018-12036.
13. Naglav, D.; Buchner, M. R.; Bendt, G.; Kraus, F.; Schulz, S., Off the Beaten Track—A Hitchhiker's Guide to Beryllium Chemistry. *Angew. Chem. Int. Ed.* **2016**, *55*, 10562-10576.
14. Perera, L. C.; Raymond, O.; Henderson, W.; Brothers, P. J.; Plieger, P. G., Advances in beryllium coordination chemistry. *Coord. Chem. Rev.* **2017**, *352*, 264-290.
15. Westerhausen, M., Recent Developments in the Organic Chemistry of Calcium – An Element with Unlimited Possibilities in Organometallic Chemistry? *Z. Anorg. Allg. Chem.* **2009**, *635*, 13-32.
16. Harder, S., From Limestone to Catalysis: Application of Calcium Compounds as Homogeneous Catalysts. *Chem. Rev.* **2010**, *110*, 3852-3876.
17. Sarazin, Y.; Carpentier, J.-F., Calcium, Strontium and Barium Homogeneous Catalysts for Fine Chemicals Synthesis. *Chem. Rec.* **2016**, *16*, 2482-2505.
18. Chapple, P. M.; Sarazin, Y., Contemporary Molecular Barium Chemistry. *Eur. J. Inorg. Chem.* **2020**, *2020*, 3321-3346.
19. Power, P. P., Main-group elements as transition metals. *Nature* **2010**, *463*, 171-177.
20. Weetman, C.; Inoue, S., The Road Travelled: After Main-Group Elements as Transition Metals. *ChemCatChem* **2018**, *10*, 4213-4228.
21. Chu, T.; Nikonov, G. I., Oxidative Addition and Reductive Elimination at Main-Group Element Centers. *Chem. Rev.* **2018**, *118*, 3608-3680.

22. Stephan, D. W., Catalysis, FLPs, and Beyond. *Chem* **2020**, *6*, 1520-1526.
23. Melen, R. L., Frontiers in molecular p-block chemistry: From structure to reactivity. *Science* **2019**, *363*, 479.
24. Lide, R. D., Ed., *CRC Handbook of Chemistry and Physics*. 77 ed.; CRC Press: Boca Raton, FL: 1993.
25. Green, S. P.; Jones, C.; Stasch, A., Stable magnesium(I) compounds with Mg-Mg bonds. *Science* **2007**, *318*, 1754-1757.
26. Arrowsmith, M.; Braunschweig, H.; Celik, M. A.; Dellermann, T.; Dewhurst, R. D.; Ewing, W. C.; Hammond, K.; Kramer, T.; Krummenacher, I.; Mies, J.; Radacki, K.; Schuster, J. K., Neutral zero-valent s-block complexes with strong multiple bonding. *Nat. Chem.* **2016**, *8*, 890-894.
27. Rösch, B.; Gentner, T. X.; Eysel, J.; Langer, J.; Elsen, H.; Harder, S., Strongly reducing magnesium(0) complexes. *Nature* **2021**, *592*, 717-721.
28. Wang, G.; Walley, J. E.; Dickie, D. A.; Pan, S.; Frenking, G.; Gilliard, R. J., A Stable, Crystalline Beryllium Radical Cation. *J. Am. Chem. Soc.* **2020**, *142*, 4560-4564.
29. Krieck, S.; Görls, H.; Yu, L.; Reiher, M.; Westerhausen, M., Stable "Inverse" Sandwich Complex with Unprecedented Organocalcium(I): Crystal Structures of [(thf)₂Mg(Br)-C₆H₂-2,4,6-Ph₃] and [(thf)₃Ca{μ-C₆H₃-1,3,5-Ph₃}Ca(thf)₃]. *J. Am. Chem. Soc.* **2009**, *131*, 2977-2985.
30. Rösch, B.; Gentner, T. X.; Langer, J.; Färber, C.; Eysel, J.; Zhao, L.; Ding, C.; Frenking, G.; Harder, S., Dinitrogen complexation and reduction at low-valent calcium. *Science* **2021**, *371*, 1125.

31. Brand, S.; Elsen, H.; Langer, J.; Donaubauer, W. A.; Hampel, F.; Harder, S., Facile Benzene Reduction by a Ca²⁺/AlI Lewis Acid/Base Combination. *Angew. Chem. Int. Ed.* **2018**, *57*, 14169-14173.
32. Schwamm, R. J.; Coles, M. P.; Hill, M. S.; Mahon, M. F.; McMullin, C. L.; Rajabi, N. A.; Wilson, A. S. S., A Stable Calcium Alumanyl. *Angew. Chem. Int. Ed.* **2020**, *59*, 3928-3932.
33. Yuvaraj, K.; Douair, I.; Paparo, A.; Maron, L.; Jones, C., Reductive Trimerization of CO to the Deltate Dianion Using Activated Magnesium(I) Compounds. *J. Am. Chem. Soc.* **2019**, *141*, 8764-8768.
34. Yuvaraj, K.; Douair, I.; Jones, D. D. L.; Maron, L.; Jones, C., Sterically controlled reductive oligomerisations of CO by activated magnesium(i) compounds: deltate vs. ethenediolate formation. *Chem. Sci.* **2020**, *11*, 3516-3522.
35. Paparo, A.; Yuvaraj, K.; Matthews, A. J. R.; Douair, I.; Maron, L.; Jones, C., Reductive Hexamerization of CO Involving Cooperativity Between Magnesium(I) Reductants and [Mo(CO)₆]: Synthesis of Well-Defined Magnesium Benzenehexolate Complexes**. *Angew. Chem. Int. Ed.* **2021**, *60*, 630-634.
36. Stegner, P.; Färber, C.; Oetzel, J.; Siemeling, U.; Wiesinger, M.; Langer, J.; Pan, S.; Holzmann, N.; Frenking, G.; Albold, U.; Sarkar, B.; Harder, S., d–d Dative Bonding Between Iron and the Alkaline-Earth Metals Calcium, Strontium, and Barium. *Angew. Chem. Int. Ed.* **2020**, *59*, 14615-14620.
37. Mukherjee, D.; Okuda, J., Molecular Magnesium Hydrides. *Angew. Chem. Int. Ed.* **2018**, *57*, 1458-1473.

38. Mukherjee, D.; Schuhknecht, D.; Okuda, J., Hydrido Complexes of Calcium: A New Family of Molecular Alkaline-Earth-Metal Compounds. *Angew. Chem. Int. Ed.* **2018**, *57*, 9590-9602.
39. Buchner, M. R.; Pan, S.; Poggel, C.; Spang, N.; Müller, M.; Frenking, G.; Sundermeyer, J., Di-ortho-beryllated Carbodiphosphorane: A Compound with a Metal–Carbon Double Bond to an Element of the s-Block. *Organometallics* **2020**, *39*, 3224-3231.
40. Wang, G.; Walley, J.; Dickie, D.; Molino, A.; Wilson, D.; Gilliard, R. J., s-Block Multiple Bonds: Isolation of a Beryllium Imido Complex. *Angew. Chem. Int. Ed.* **2021**, *60*, 9407-9411.
41. Roy, D. K.; Tröster, T.; Fantuzzi, F.; Dewhurst, R. D.; Lenczyk, C.; Radacki, K.; Pranckevicius, C.; Engels, B.; Braunschweig, H., Isolation and Reactivity of an Antiaromatic s-Block Metal Compound. *Angew. Chem. Int. Ed.* **2021**, *60*, 3812-3819.
42. Allred, A. L., Electronegativity values from thermochemical data. *J. Inorg. Nucl. Chem.* **1961**, *17*, 215-221.
43. Schlenk, W.; Schlenk, W., Über die Konstitution der Grignardschen Magnesiumverbindungen. *Ber. Dtsch. Chem. Ges.* **1929**, *62*, 920-924.
44. Seyferth, D., The Grignard Reagents. *Organometallics* **2009**, *28*, 1598-1605.
45. Westerhausen, M., Heavy Grignard reagents—Synthesis and reactivity of organocalcium compounds. *Coord. Chem. Rev.* **2008**, *252*, 1516-1531.
46. Westerhausen, M.; Gärtner, M.; Fischer, R.; Langer, J.; Yu, L.; Reiher, M., Heavy Grignard Reagents: Challenges and Possibilities of Aryl Alkaline Earth Metal Compounds. *Chem. Eur. J.* **2007**, *13*, 6292-6306.

47. Buchanan, W. D.; Allis, D. G.; Ruhlandt-Senge, K., Synthesis and stabilization—advances in organoalkaline earth metal chemistry. *Chem. Commun.* **2010**, *46*, 4449-4465.
48. Hanusa, T. P., New developments in the organometallic chemistry of calcium, strontium and barium. *Polyhedron* **1990**, *9*, 1345-1362.
49. Hanusa, T. P., Ligand influences on structure and reactivity in organoalkaline earth chemistry. *Chem. Rev.* **1993**, *93*, 1023-1036.
50. Westerhausen, M.; Koch, A.; Görls, H.; Krieck, S., Heavy Grignard Reagents: Synthesis, Physical and Structural Properties, Chemical Behavior, and Reactivity. *Chem. Eur. J.* **2017**, *23*, 1456-1483.
51. Langer, J.; Gärtner, M.; Fischer, R.; Görls, H.; Westerhausen, M., Reinvestigation of the reaction of strontium and barium with iodobenzene and molecular structure of the heavy Grignard reagent $[(\text{thf})_2\text{BaPh}_2]_4 \cdot (\text{thf})\text{BaO}$ with an oxygen-centered square Ba_5 pyramid. *Inorg. Chem. Commun.* **2007**, *10*, 1001-1004.
52. Wolf, B. M.; Stuhl, C.; Maichle-Mossmer, C.; Anwander, R., Dimethylcalcium. *J. Am. Chem. Soc.* **2018**, *140*, 2373-2383.
53. Ruspic, C.; Harder, S., Big Ligands for Stabilization of Small Functionalities in Calcium Chemistry. *Inorg. Chem.* **2007**, *46*, 10426-10433.
54. Barrett, A. G.; Casely, I. J.; Crimmin, M. R.; Hill, M. S.; Lachs, J. R.; Mahon, M. F.; Procopiou, P. A., Beta-diketiminato calcium and magnesium amides; model complexes for hydroamination catalysis. *Inorg. Chem.* **2009**, *48*, 4445-53.
55. Liptrot, D. J.; Hill, M. S.; Mahon, M. F.; MacDougall, D. J., Group 2 Promoted Hydrogen Release from $\text{NMe}_2\text{H} \cdot \text{BH}_3$: Intermediates and Catalysis. *Chem. Eur. J.* **2010**, *16*, 8508-8515.

56. Avent, A. G.; Crimmin, M. R.; Hill, M. S.; Hitchcock, P. B., Kinetic stability of heteroleptic (β -diketiminato) heavier alkaline-earth (Ca, Sr, Ba) amides. *Dalton Trans.* **2005**, 10.1039/B415468A, 278-284.
57. Stender, M.; Wright, R. J.; Eichler, B. E.; Prust, J.; Olmstead, M. M.; Roesky, H. W.; Power, P. P., The synthesis and structure of lithium derivatives of the sterically encumbered β -diketiminato ligand [$\{(2,6\text{-Pri}_2\text{H}_3\text{C}_6)\text{N}(\text{CH}_3)\text{C}\}_2\text{CH}\text{--}$], and a modified synthesis of the aminoimine precursor. *J. Chem. Soc., Dalton Trans.* **2001**, 10.1039/B103149J, 3465-3469.
58. Dove, A. P.; Gibson, V. C.; Hormnirun, P.; Marshall, E. L.; Segal, J. A.; White, A. J. P.; Williams, D. J., Low coordinate magnesium chemistry supported by a bulky β -diketiminato ligand. *Dalton Trans.* **2003**, 10.1039/B303550F, 3088-3097.
59. Arrowsmith, M.; Hill, M. S.; Kociok-Kohn, G.; MacDougall, D. J.; Mahon, M. F.; Mallov, I., Three-coordinate beryllium beta-diketiminates: synthesis and reduction chemistry. *Inorg. Chem.* **2012**, *51*, 13408-13418.
60. Hansch, C.; Leo, A.; Taft, R. W., A survey of Hammett substituent constants and resonance and field parameters. *Chem. Rev.* **1991**, *91*, 165-195.
61. Gentner, T. X.; Rösch, B.; Thum, K.; Langer, J.; Ballmann, G.; Pahl, J.; Donaubaue, W. A.; Hampel, F.; Harder, S., Heteroleptic Heavier Alkaline Earth Metal Amide Complexes Stabilized by a Superbulky β -Diketiminato Ligand. *Organometallics* **2019**, *38*, 2485-2493.
62. Causero, A.; Ballmann, G.; Pahl, J.; Färber, C.; Intemann, J.; Harder, S., β -Diketiminato calcium hydride complexes: the importance of solvent effects. *Dalton Trans.* **2017**, *46*, 1822-1831.
63. Sarish, S. P.; Roesky, H. W.; John, M.; Ringe, A.; Magull, J., Well-defined hydrocarbon soluble strontium fluoride and chloride complexes of composition $[\text{LSr}(\text{thf})(\mu\text{-}$

F)2Sr(thf)2L] and [LSr(thf)(μ -Cl)2Sr(thf)2L]. *Chem. Commun.* **2009**, 10.1039/B822148K, 2390-2392.

64. Liu, B.; Roisnel, T.; Carpentier, J.-F.; Sarazin, Y., When Bigger Is Better: Intermolecular Hydrofunctionalizations of Activated Alkenes Catalyzed by Heteroleptic Alkaline Earth Complexes. *Angew. Chem. Int. Ed.* **2012**, *51*, 4943-4946.

65. Roueindeji, H.; Ratsifitahina, A.; Roisnel, T.; Dorcet, V.; Kahlal, S.; Saillard, J.-Y.; Carpentier, J.-F.; Sarazin, Y., Metal...F-C Bonding in Low-Coordinate Alkaline Earth Fluoroarylamides. *Chem. Eur. J.* **2019**, *25*, 8854-8864.

66. Fischer, C. A.; Rösch, A.; Elsen, H.; Ballmann, G.; Wiesinger, M.; Langer, J.; Färber, C.; Harder, S., Lewis acidic alkaline earth metal complexes with a perfluorinated diphenylamide ligand. *Dalton Trans.* **2019**, *48*, 6757-6766.

67. Rösch, B.; Gentner, T. X.; Elsen, H.; Fischer, C. A.; Langer, J.; Wiesinger, M.; Harder, S., Nucleophilic Aromatic Substitution at Benzene with Powerful Strontium Hydride and Alkyl Complexes. *Angew. Chem. Int. Ed.* **2019**, *58*, 5396-5401.

68. Wilson, A. S. S.; Hill, M. S.; Mahon, M. F.; Dinoi, C.; Maron, L., Organocalcium-mediated nucleophilic alkylation of benzene. *Science* **2017**, *358*, 1168-1171.

69. Crimmin, M. R.; Hill, M. S., Homogeneous Catalysis with Organometallic Complexes of Group 2. In *Alkaline-Earth Metal Compounds: Oddities and Applications*, Harder, S., Ed. Springer Berlin Heidelberg: Berlin, Heidelberg, 2013, 10.1007/978-3-642-36270-5_6pp 191-241.

70. Harder, S.; Brettar, J., Rational Design of a Well-Defined Soluble Calcium Hydride Complex. *Angew. Chem. Int. Ed.* **2006**, *45*, 3474-3478.

71. Causero, A.; Ballmann, G.; Pahl, J.; Zijlstra, H.; Färber, C.; Harder, S., Stabilization of Calcium Hydride Complexes by Fine Tuning of Amidinate Ligands. *Organometallics* **2016**, *35*, 3350-3360.
72. Shi, X.; Hou, C.; Zhou, C.; Song, Y.; Cheng, J., A Molecular Barium Hydrido Complex Stabilized by a Super-Bulky Hydrotris(pyrazolyl)borate Ligand. *Angew. Chem. Int. Ed.* **2017**, *56*, 16650-16653.
73. Höllerhage, T.; Carpentier, A.; Spaniol, T. P.; Maron, L.; Englert, U.; Okuda, J., Cationic strontium hydride complexes supported by an NNNN-type macrocycle. *Chem. Commun.* **2021**, 10.1039/D1CC02040D.
74. Shi, X.; Qin, G.; Wang, Y.; Zhao, L.; Liu, Z.; Cheng, J., Super-Bulky Penta-arylcyclopentadienyl Ligands: Isolation of the Full Range of Half-Sandwich Heavy Alkaline-Earth Metal Hydrides. *Angew. Chem. Int. Ed.* **2019**, *58*, 4356-4360.
75. Chapple, P. M.; Kahlal, S.; Cartron, J.; Roisnel, T.; Dorcet, V.; Cordier, M.; Saillard, J.-Y.; Carpentier, J.-F.; Sarazin, Y., Bis(imino)carbazolate: A Master Key for Barium Chemistry. *Angew. Chem. Int. Ed.* **2020**, *59*, 9120-9126.
76. Williams, R. A.; Hanusa, T. P.; Huffman, J. C., Synthesis and crystallographic characterization of $(\text{Me}_5\text{C}_5)_2\text{Ca}(\text{Me}_3\text{SiC}\equiv\text{C}\equiv\text{CSiMe}_3)$: the first monomeric diyne complex of a main-group element. *J. Am. Chem. Soc.* **1990**, *112*, 2454-2455.
77. Sockwell, S. C.; Hanusa, T. P.; Huffman, J. C., Formation and reactions of mono- and bis(peralkylcyclopentadienyl) complexes of calcium and barium. The x-ray crystal structure of $[\text{cyclic}][(\text{Me}_4\text{EtC}_5)\text{Ca}(\mu\text{-NSiMe}_2\text{CH}_2\text{CH}_2\text{SiMe}_2)]_2$. *J. Am. Chem. Soc.* **1992**, *114*, 3393-3399.

78. Hays, M. L.; Hanusa, T. P.; Nile, T. A., Synthesis and X-ray crystal structures of alkaline-earth metallocenes with pendant substituents. *J. Organomet. Chem.* **1996**, *514*, 73-79.
79. Arduengo, A. J.; Davidson, F.; Krafczyk, R.; Marshall, W. J.; Tamm, M., Adducts of Carbenes with Group II and XII Metallocenes†. *Organometallics* **1998**, *17*, 3375-3382.
80. Margl, P.; Schwarz, K.; Bloechl, P. E., Fluxional Dynamics of Beryllocene. *J. Am. Chem. Soc.* **1994**, *116*, 11177-11178.
81. Pal, R.; Mebs, S.; Shi, M. W.; Jayatilaka, D.; Krzeszczakowska, J. M.; Malaspina, L. A.; Wiecko, M.; Luger, P.; Hesse, M.; Chen, Y.-S.; Beckmann, J.; Grabowsky, S., Linear MgCp*₂ vs Bent CaCp*₂: London Dispersion, Ligand-Induced Charge Localizations, and Pseudo-Pregostic C–H···Ca Interactions. *Inorg. Chem.* **2018**, *57*, 4906-4920.
82. Bauer, H.; Thum, K.; Alonso, M.; Fischer, C.; Harder, S., Alkene Transfer Hydrogenation with Alkaline-Earth Metal Catalysts. *Angew. Chem. Int. Ed. Engl.* **2019**, *58*, 4248-4253.
83. Wiesinger, M.; Maitland, B.; Färber, C.; Ballmann, G.; Fischer, C.; Elsen, H.; Harder, S., Simple Access to the Heaviest Alkaline Earth Metal Hydride: A Strongly Reducing Hydrocarbon-Soluble Barium Hydride Cluster. *Angew. Chem. Int. Ed.* **2017**, *56*, 16654-16659.
84. Bauer, H.; Alonso, M.; Färber, C.; Elsen, H.; Pahl, J.; Causero, A.; Ballmann, G.; De Proft, F.; Harder, S., Imine hydrogenation with simple alkaline earth metal catalysts. *Nat. Catal.* **2018**, *1*, 40-47.
85. Martin, J.; Knüpfer, C.; Eyselien, J.; Färber, C.; Grams, S.; Langer, J.; Thum, K.; Wiesinger, M.; Harder, S., Highly Active Superbulky Alkaline Earth Metal Amide Catalysts for Hydrogenation of Challenging Alkenes and Aromatic Rings. *Angew. Chem. Int. Ed.* **2020**, *59*, 9102-9112.

86. Naglav, D.; Neumann, A.; Bläser, D.; Wölper, C.; Haack, R.; Jansen, G.; Schulz, S., Bonding situation in Be[N(SiMe₃)₂]₂ – an experimental and computational study. *Chem. Commun.* **2015**, *51*, 3889-3891.
87. Walley, J. E.; Breiner, G.; Wang, G.; Dickie, D. A.; Molino, A.; Dutton, J. L.; Wilson, D. J. D.; Gilliard, J. R. J., s-Block carbodicarbene chemistry: C(sp³)–H activation and cyclization mediated by a beryllium center. *Chem. Commun.* **2019**, *55*, 1967-1970.
88. Schuhknecht, D.; Spaniol, T. P.; Maron, L.; Okuda, J., Regioselective Hydrosilylation of Olefins Catalyzed by a Molecular Calcium Hydride Cation. *Angew. Chem. Int. Ed.* **2020**, *59*, 310-314.
89. Lemmerz, L. E.; Mukherjee, D.; Spaniol, T. P.; Wong, A.; Ménard, G.; Maron, L.; Okuda, J., Cationic magnesium hydride [MgH]⁺ stabilized by an NNNN-type macrocycle. *Chem. Commun.* **2019**, *55*, 3199-3202.
90. Schnitzler, S.; Spaniol, T. P.; Maron, L.; Okuda, J., Formation and Reactivity of a Molecular Magnesium Hydride with a Terminal Mg-H Bond. *Chem. Eur. J.* **2015**, *21*, 11330-4.
91. Wiesinger, M.; Maitland, B.; Elsen, H.; Pahl, J.; Harder, S., Stabilizing Magnesium Hydride Complexes with Neutral Ligands. *Eur. J. Inorg. Chem.* **2019**, *2019*, 4433-4439.
92. Schuhknecht, D.; Spaniol, T. P.; Yang, Y.; Maron, L.; Okuda, J., Reactivity of a Molecular Calcium Hydride Cation ([CaH]⁺) Supported by an NNNN Macrocycle. *Inorg. Chem.* **2020**, *59*, 9406-9415.
93. Leich, V.; Spaniol, T. P.; Maron, L.; Okuda, J., Molecular Calcium Hydride: Dicalcium Trihydride Cation Stabilized by a Neutral NNNN-Type Macrocyclic Ligand. *Angew. Chem. Int. Ed.* **2016**, *55*, 4794-4797.

94. Martin, D.; Beckerle, K.; Schnitzler, S.; Spaniol, T. P.; Maron, L.; Okuda, J., Discrete Magnesium Hydride Aggregates: A Cationic Mg₁₃H₁₈ Cluster Stabilized by NNNN-Type Macrocycles. *Angew. Chem. Int. Ed.* **2015**, *54*, 4115-4118.
95. Jochmann, P.; Davin, J. P.; Spaniol, T. P.; Maron, L.; Okuda, J., A Cationic Calcium Hydride Cluster Stabilized by Cyclen-Derived Macrocyclic N,N,N,N Ligands. *Angew. Chem. Int. Ed.* **2012**, *51*, 4452-4455.
96. Schuhknecht, D.; Spaniol, T. P.; Douair, I.; Maron, L.; Okuda, J., A tetranuclear calcium hydride cluster with a highly symmetric [Ca₄H₆]²⁺ core. *Chem. Commun.* **2019**, *55*, 14837-14839.
97. Munz, D., Pushing Electrons—Which Carbene Ligand for Which Application? *Organometallics* **2018**, *37*, 275-289.
98. Nesterov, V.; Reiter, D.; Bag, P.; Frisch, P.; Holzner, R.; Porzelt, A.; Inoue, S., NHCs in Main Group Chemistry. *Chem. Rev.* **2018**, *118*, 9678-9842.
99. Rösch, B.; Harder, S., New horizons in low oxidation state group 2 metal chemistry. *Chem. Commun.* **2021**, *57*, 9354-9365.
100. Freeman, L. A.; Walley, J. E.; Gilliard, R. J., Synthesis and reactivity of low-oxidation-state alkaline earth metal complexes. *Nature Synthesis* **2022**, *1*, 439-448.
101. Arrowsmith, M.; Hill, M. S.; Kociok-Kohn, G.; MacDougall, D. J.; Mahon, M. F., Beryllium-induced C-N bond activation and ring opening of an N-heterocyclic carbene. *Angew. Chem. Int. Ed. Engl.* **2012**, *51*, 2098-2100.
102. Lapshin, I. V.; Basalov, I. V.; Lyssenko, K. A.; Cherkasov, A. V.; Trifonov, A. A., CaII, YbII and SmII Bis(Amido) Complexes Coordinated by NHC Ligands: Efficient Catalysts

for Highly Regio- and Chemoselective Consecutive Hydrophosphinations with PH₃. *Chem. Eur. J.* **2019**, *25*, 459-463.

103. Li, N.; Guan, B.-T., A Dialkyl Calcium Carbene Adduct: Synthesis, Structure, and Catalytic Cross-Dehydrocoupling of Silanes with Amines. *Eur. J. Inorg. Chem.* **2019**, *2019*, 2231-2235.

104. Arrowsmith, M.; Hill, M. S.; MacDougall, D. J.; Mahon, M. F., A hydride-rich magnesium cluster. *Angew. Chem. Int. Ed.* **2009**, *48*, 4013-4016.

105. Obi, A.; Frey, N.; Dickie, D.; Webster, C. E.; Gilliard, R. J., N-Heterocyclic Carbene-Assisted Reversible Migratory Coupling of Aminoborane at Magnesium. *Angew. Chem. Int. Ed.* **2022**, *n/a*, e202211496.

106. Freeman, L. A.; Walley, J. E.; Obi, A. D.; Wang, G.; Dickie, D. A.; Molino, A.; Wilson, D. J. D.; Gilliard, R. J., Stepwise Reduction at Magnesium and Beryllium: Cooperative Effects of Carbenes with Redox Non-Innocent α -Diimines. *Inorg. Chem.* **2019**, *58*, 10554-10568.

107. Obi, A. D.; Freeman, L. A.; Dickie, D. A.; Gilliard, R. J., N-Heterocyclic Carbene-Mediated Ring Opening of Reduced Diazamagnesacycles. *Organometallics* **2020**, *39*, 4575-4583.

108. Wong, Y. O.; Freeman, L. A.; Agakidou, A. D.; Dickie, D. A.; Webster, C. E.; Gilliard, R. J., Two Carbenes versus One in Magnesium Chemistry: Synthesis of Terminal Dihalide, Dialkyl, and Grignard Reagents. *Organometallics* **2019**, *38*, 688-696.

109. Obi, A. D.; Walley, J. E.; Frey, N. C.; Wong, Y. O.; Dickie, D. A.; Webster, C. E.; Gilliard, R. J., Tris(carbene) Stabilization of Monomeric Magnesium Cations: A Neutral, Nontethered Ligand Approach. *Organometallics* **2020**, *39*, 4329-4339.

110. Schuster, J. K.; Roy, D. K.; Lenczyk, C.; Mies, J.; Braunschweig, H., New Outcomes of Beryllium Chemistry: Lewis Base Adducts for Salt Elimination Reactions. *Inorg. Chem.* **2019**, *58*, 2652-2658.
111. Herrmann, W. A.; Runte, O.; Artus, G., Synthesis and structure of an ionic beryllium-“carbene” complex. *J. Organomet. Chem.* **1995**, *501*, C1-C4.
112. Arduengo, A. J.; Harlow, R. L.; Kline, M., A stable crystalline carbene. *J. Am. Chem. Soc.* **1991**, *113*, 361-363.
113. Arduengo, A. J.; Dias, H. V. R.; Harlow, R. L.; Kline, M., Electronic stabilization of nucleophilic carbenes. *J. Am. Chem. Soc.* **1992**, *114*, 5530-5534.
114. Hopkinson, M. N.; Richter, C.; Schedler, M.; Glorius, F., An overview of N-heterocyclic carbenes. *Nature* **2014**, *510*, 485-496.
115. Lavallo, V.; Canac, Y.; Prasang, C.; Donnadiou, B.; Bertrand, G., Stable cyclic (alkyl)(amino)carbenes as rigid or flexible, bulky, electron-rich ligands for transition-metal catalysts: a quaternary carbon atom makes the difference. *Angew. Chem. Int. Ed.* **2005**, *44*, 5705-5709.
116. Melaimi, M.; Jazzar, R.; Soleilhavoup, M.; Bertrand, G., Cyclic (Alkyl)(amino)carbenes (CAACs): Recent Developments. *Angew. Chem. Int. Ed.* **2017**, *56*, 10046-10068.
117. Soleilhavoup, M.; Bertrand, G., Cyclic (alkyl)(amino)carbenes (CAACs): stable carbenes on the rise. *Acc. Chem. Res.* **2015**, *48*, 256-266.
118. Martin, C. D.; Soleilhavoup, M.; Bertrand, G., Carbene-Stabilized Main Group Radicals and Radical Ions. *Chem Sci* **2013**, *4*, 3020-3030.

119. Paparo, A.; Best, S. P.; Yuvaraj, K.; Jones, C., Neutral, Anionic, and Paramagnetic 1,3,2-Diazaberyllacycles Derived from Reduced 1,4-Diazabutadienes. *Organometallics* **2020**, *39*, 4208-4213.
120. Turner, Z. R., Chemically Non-Innocent Cyclic (Alkyl)(Amino)Carbenes: Ligand Rearrangement, C-H and C-F Bond Activation. *Chem. Eur. J.* **2016**, *22*, 11461-11468.
121. Turner, Z. R.; Buffet, J.-C., Group 1 and 2 cyclic (alkyl)(amino)carbene complexes. *Dalton Trans.* **2015**, *44*, 12985-12989.
122. Ramirez, F.; Desai, N. B.; Hansen, B.; McKelvie, N., HEXAPHENYLCARBODIPHOSPHORANE, (C₆H₅)₃PCP(C₆H₅)₃. *J. Am. Chem. Soc.* **1961**, *83*, 3539-3540.
123. Tonner, R.; Öxler, F.; Neumüller, B.; Petz, W.; Frenking, G., Carbodiphosphoranes: The Chemistry of Divalent Carbon(0). *Angew. Chem. Int. Ed.* **2006**, *45*, 8038-8042.
124. Petz, W.; Kutschera, C.; Neumüller, B., Reaction of the Carbodiphosphorane Ph₃PCPPh₃ with Platinum(II) and -(0) Compounds: Platinum Induced Activation of C–H Bonds. *Organometallics* **2005**, *24*, 5038-5043.
125. Marrot, S.; Kato, T.; Gornitzka, H.; Baceiredo, A., Cyclic Carbodiphosphoranes: Strongly Nucleophilic σ -Donor Ligands. *Angew. Chem. Int. Ed.* **2006**, *45*, 2598-2601.
126. Tonner, R.; Frenking, G., C(NHC)₂: Divalent Carbon(0) Compounds with N-Heterocyclic Carbene Ligands—Theoretical Evidence for a Class of Molecules with Promising Chemical Properties. *Angew. Chem. Int. Ed.* **2007**, *46*, 8695-8698.
127. Dyker, C. A.; Lavallo, V.; Donnadiou, B.; Bertrand, G., Synthesis of an extremely bent acyclic allene (a "carbodicarbene"): a strong donor ligand. *Angew. Chem. Int. Ed.* **2008**, *47*, 3206-9.

128. Petz, W., Addition compounds between carbones, CL_2 , and main group Lewis acids: A new glance at old and new compounds. *Coord. Chem. Rev.* **2015**, *291*, 1-27.
129. Liu, S.; Chen, W.-C.; Ong, T.-G., Synthesis and Structure of Carbodicarbenes and Their Application in Catalysis. In *Modern Ylide Chemistry: Applications in Ligand Design, Organic and Catalytic Transformations*, Gessner, V. H., Ed. Springer International Publishing: Cham, 2018, 10.1007/430_2017_20pp 51-71.
130. Chen, W.-C.; Hsu, Y.-C.; Lee, C.-Y.; Yap, G. P. A.; Ong, T.-G., Synthetic Modification of Acyclic Bent Allenes (Carbodicarbenes) and Further Studies on Their Structural Implications and Reactivities. *Organometallics* **2013**, *32*, 2435-2442.
131. Chen, W.-C.; Shen, J.-S.; Jurca, T.; Peng, C.-J.; Lin, Y.-H.; Wang, Y.-P.; Shih, W.-C.; Yap, G. P. A.; Ong, T.-G., Expanding the Ligand Framework Diversity of Carbodicarbenes and Direct Detection of Boron Activation in the Methylation of Amines with CO_2 . *Angew. Chem. Int. Ed.* **2015**, *54*, 15207-15212.
132. Aweke, B. S.; Yu, C.-H.; Zhi, M.; Chen, W.-C.; Yap, G. P. A.; Zhao, L.; Ong, T.-G., A Bis-(carbone) Pincer Ligand and Its Coordinative Behavior toward Multi-Metallic Configurations. *Angew. Chem. Int. Ed.* **2022**, *61*, e202201884.
133. Liu, S.-k.; Chen, W.-C.; Yap, G. P. A.; Ong, T.-G., Synthesis of Carbophosphinocarbene and Their Donating Ability: Expansion of the Carbone Class. *Organometallics* **2020**, *39*, 4395-4401.
134. Petz, W.; Dehnicke, K.; Holzmann, N.; Frenking, G.; Neumüller, B., The Reaction of $BeCl_2$ with Carbodiphosphorane $C(PPh_3)_2$; Experimental and Theoretical Studies. *Z. Anorg. Allg. Chem.* **2011**, *637*, 1702-1710.

135. Hollister, K. K.; Molino, A.; Breiner, G.; Walley, J. E.; Wentz, K. E.; Conley, A. M.; Dickie, D. A.; Wilson, D. J. D.; Gilliard, R. J., Air-Stable Thermoluminescent Carbodicarbene-Borafluorenium Ions. *J. Am. Chem. Soc.* **2022**, *144*, 590-598.
136. Quinlivan, P. J.; Shlian, D. G.; Amemiya, E.; Parkin, G., Reactivity of the carbodiphosphorane, (Ph₃P)₂C, towards main group metal alkyl compounds: coordination and cyclometalation. *Dalton Trans.* **2019**, *48*, 9139-9151.
137. Braunschweig, H.; Dewhurst, R. D.; Hammond, K.; Mies, J.; Radacki, K.; Vargas, A., Ambient-Temperature Isolation of a Compound with a Boron-Boron Triple Bond. *Science* **2012**, *336*, 1420-1422.
138. Wang, Y.; Chen, M.; Xie, Y.; Wei, P.; Schaefer, H. F.; Schleyer, P. v. R.; Robinson, G. H., Stabilization of elusive silicon oxides. *Nat. Chem.* **2015**, *7*, 509-513.
139. Wilson, D. J. D.; Dutton, J. L., Recent Advances in the Field of Main-Group Mono- and Diatomic “Allotropes” Stabilised by Neutral Ligands. *Chem. Eur. J.* **2013**, *19*, 13626-13637.
140. Chen, W.-C.; Lee, C.-Y.; Lin, B.-C.; Hsu, Y.-C.; Shen, J.-S.; Hsu, C.-P.; Yap, G. P. A.; Ong, T.-G., The Elusive Three-Coordinate Dicationic Hydrido Boron Complex. *J. Am. Chem. Soc.* **2014**, *136*, 914-917.
141. Đorđević, N.; Ganguly, R.; Petković, M.; Vidović, D., Bis(carbodicarbene)phosphenium trication: the case against hypervalency. *Chem. Commun.* **2016**, *52*, 9789-9792.
142. Walley, J.; Warring, L.; Wang, G.; Dickie, D. A.; Pan, S.; Frenking, G.; Gilliard, R. J., Carbodicarbene Bismaalkene Cations: Unravelling the Complexities of Carbene versus Carbene in Heavy Pnictogen Chemistry. *Angew. Chem. Int. Ed.* **2021**, *60*, 6682-6690.

143. Wang, G.; Freeman, L. A.; Dickie, D. A.; Mokrai, R.; Benkő, Z.; Gilliard, R. J., Highly Reactive Cyclic(alkyl)(amino) Carbene- and N-Heterocyclic Carbene-Bismuth(III) Complexes: Synthesis, Structure, and Computations. *Inorg. Chem.* **2018**, *57*, 11687-11695.
144. Waters, J. B.; Chen, Q.; Everitt, T. A.; Goicoechea, J. M., N-Heterocyclic carbene adducts of the heavier group 15 tribromides. Normal to abnormal isomerism and bromide ion abstraction. *Dalton Trans.* **2017**, *46*, 12053-12066.
145. Münzer, J. E.; Kneusels, N.-J. H.; Weinert, B.; Neumüller, B.; Kuzu, I., Hexaphenyl carbodiphosphorane adducts of heavier group 15 element trichlorides: syntheses, properties and reactivities. *Dalton Trans.* **2019**, *48*, 11076-11085.
146. Czernetzki, C.; Arrowsmith, M.; Fantuzzi, F.; Gärtner, A.; Tröster, T.; Krummenacher, I.; Schorr, F.; Braunschweig, H., A Neutral Beryllium(I) Radical. *Angew. Chem. Int. Ed.* **2021**, *60*, 20776-20780.
147. Jones, C.; Stasch, A., Stable Molecular Magnesium(I) Dimers: A Fundamentally Appealing Yet Synthetically Versatile Compound Class. In *Alkaline-Earth Metal Compounds: Oddities and Applications*, Harder, S., Ed. Springer Berlin Heidelberg: Berlin, Heidelberg, 2013, 10.1007/978-3-642-36270-5_3pp 73-101.
148. Liu, H.-Y.; Schwamm, R. J.; Neale, S. E.; Hill, M. S.; McMullin, C. L.; Mahon, M. F., Reductive Dimerization of CO by a Na/Mg(I) Diamide. *J. Am. Chem. Soc.* **2021**, *143*, 17851-17856.
149. Boutland, A. J.; Carroll, A.; Alvarez Lamsfus, C.; Stasch, A.; Maron, L.; Jones, C., Reversible Insertion of a C=C Bond into Magnesium(I) Dimers: Generation of Highly Active 1,2-Dimagnesioethane Compounds. *J. Am. Chem. Soc.* **2017**, *139*, 18190-18193.

150. Wang, G.; Freeman, L. A.; Dickie, D. A.; Mokrai, R.; Benkő, Z.; Gilliard, R. J., Isolation of Cyclic(Alkyl)(Amino) Carbene–Bismuthinidene Mediated by a Beryllium(0) Complex. *Chem. Eur. J.* **2019**, *25*, 4335-4339.
151. Labinger, J. A., Tutorial on Oxidative Addition. *Organometallics* **2015**, *34*, 4784-4795.
152. Lyaskovskyy, V.; de Bruin, B., Redox Non-Innocent Ligands: Versatile New Tools to Control Catalytic Reactions. *ACS Catal.* **2012**, *2*, 270-279.
153. Fedushkin, I. L.; Khvoynova, N. M.; Skatova, A. A.; Fukin, G. K., Oxidative Addition of Phenylacetylene through C–H Bond Cleavage To Form the MgII–dpp-bian Complex: Molecular Structure of [Mg{dpp-bian(H)}(CCPh)(thf)₂] and Its Diphenylketone Insertion Product [Mg(dpp-bian)–{OC(Ph)₂CCPh}(thf)]. *Angew. Chem. Int. Ed.* **2003**, *42*, 5223-5226.
154. Arrowsmith, M.; Hill, M. S.; Kociok-Köhn, G., Activation of N-Heterocyclic Carbenes by {BeH₂} and {Be(H)(Me)} Fragments. *Organometallics* **2015**, *34*, 653-662.
155. Fedushkin, I. L.; Chudakova, V. A.; Skatova, A. A.; Khvoynova, N. M.; Kurskii, Y. A.; Glukhova, T. A.; Fukin, G. K.; Dechert, S.; Hummert, M.; Schumann, H., Monomeric Magnesium and Calcium Complexes containing the Rigid, Dianionic 1, 2-Bis[(2, 5-di-tert-butylphenyl)imino]acenaphthene (dtb-BIAN) and 1, 2-Bis[(2-biphenyl)imino]acenaphthene (bph-BIAN) Ligands. *Z. Anorg. Allg. Chem.* **2004**, *630*, 501-507.
156. Fedushkin, I. L.; Skatova, A. A.; Chudakova, V. A.; Cherkasov, V. K.; Dechert, S.; Schumann, H., Magnesium and calcium complexes with two diimine radical-anion ligands. Molecular structure of the Ca complex with 1,2-bis[(2,6-diisopropylphenyl)imino]acenaphthene. *Russ. Chem. Bull.* **2004**, *53*, 2142-2147.
157. Fedushkin, I. L.; Chudakova, V. A.; Skatova, A. A.; Fukin, G. K., Solvent-free alkali and alkaline earth metal complexes of di-imine ligands. *Heteroat. Chem* **2005**, *16*, 663-670.

158. Fedushkin, I. L.; Morozov, A. G.; Rassadin, O. V.; Fukin, G. K., Addition of nitriles to alkaline earth metal complexes of 1,2-bis[(phenyl)imino]acenaphthenes. *Chem. Eur. J.* **2005**, *11*, 5749-5757.
159. Bailey, P. J.; Dick, C. M.; Fabre, S.; Parsons, S.; Yellowlees, L. J., Complexation of dimethylmagnesium with alpha-diimines; structural and EPR characterisation of single electron and alkyl transfer products. *Dalton Trans.* **2006**, 10.1039/b514591k, 1602-1610.
160. Kruczyński, T.; Henke, P.; Augenstein, T.; Arleth, N.; Breher, F.; Schnöckel, H., From MgBr via single-electron transfer (SET) to a paramagnetic Mg(II) compound and back to Mg(I): [MgBr(L(1))]2 and [K(thf)3]2[Mg2(L(1))2], L(1) = RN=C(Me)C(Me)=NR, R = 2,6-diisopropylphenyl. *Chem. Commun.* **2014**, *50*, 15677-15680.
161. Panda, T. K.; Kaneko, H.; Michel, O.; Pal, K.; Tsurugi, H.; Törnroos, K. W.; Anwander, R.; Mashima, K., Dianion and Monoanion Ligation of 1,4-Diaza-1,3-butadiene to Barium, Strontium, and Calcium. *Organometallics* **2012**, *31*, 3178-3184.
162. Liu, Y.; Zhao, Y.; Yang, X.-J.; Li, S.; Gao, J.; Yang, P.; Xia, Y.; Wu, B., Calcium Complexes of Noninnocent α -Diimine Ligands. *Organometallics* **2011**, *30*, 1599-1606.
163. Anga, S.; Bhattacharjee, J.; Harinath, A.; Panda, T. K., Synthesis, structure and reactivity study of magnesium amidinato complexes derived from carbodiimides and N,N'-bis(2,6-diisopropylphenyl)-1,4-diaza-butadiene ligands. *Dalton Trans.* **2015**, *44*, 955-65.
164. Gao, J.; Liu, Y.; Zhao, Y.; Yang, X.-J.; Sui, Y., Syntheses and Structures of Magnesium Complexes with Reduced α -Diimine Ligands. *Organometallics* **2011**, *30*, 6071-6077.

165. Liu, Y.; Li, S.; Yang, X. J.; Yang, P.; Wu, B., Magnesium-magnesium bond stabilized by a doubly reduced alpha-diimine: synthesis and structure of $[K(THF)_3]_2[LMg-MgL]$ ($L = [(2,6\text{-}(i)Pr_2C_6H_3)NC(Me)]_2(2-)$). *J. Am. Chem. Soc.* **2009**, *131*, 4210-4211.
166. Ma, M.; Wang, H.; Wang, J.; Shen, L.; Zhao, Y.; Xu, W. H.; Wu, B.; Yang, X. J., Mg-Mg-bonded compounds with N,N'-dipp-substituted phenanthrene-diamido and o-phenylene-diamino ligands. *Dalton Trans.* **2019**, *48*, 2295-2299.
167. Wang, J.; Wang, J.; Shen, L.; Zhao, Y.; Wu, B.; Yang, X.-J., Reactions of Dianionic α -Diimine-Supported Dimagnesium(I) Compound $[K(THF)_3]_2[LMg-MgL]$ with Nitriles. *Organometallics* **2019**, *38*, 2674-2682.
168. Arduengo, A. J.; Krafczyk, R.; Schmutzler, R.; Craig, H. A.; Goerlich, J. R.; Marshall, W. J.; Unverzagt, M., Imidazolylienes, imidazolinylienes and imidazolidines. *Tetrahedron* **1999**, *55*, 14523-14534.
169. Diez-Gonzalez, S.; Marion, N.; Nolan, S. P., N-heterocyclic carbenes in late transition metal catalysis. *Chem. Rev.* **2009**, *109*, 3612-3676.
170. Jędrzkiewicz, D.; Mai, J.; Langer, J.; Mathe, Z.; Patel, N.; DeBeer, S.; Harder, S., Access to a Labile Monomeric Magnesium Radical by Ball-Milling. *Angew. Chem. Int. Ed.* **2022**, *61*, e202200511.
171. Andrada, D. M.; Salvador Sedano, P.; Corral, I.; Jana, A.; Danés, S.; Gimferrer, M.; Vos, E.; Yildiz, C. B., The Oxidation State in Low-Valent Beryllium and Magnesium Compounds. *Chem. Sci.* **2022**, *13*, 6583-6591.
172. Breitwieser, K.; Bahmann, H.; Weiss, R.; Munz, D., Gauging Radical Stabilization with Carbenes. *Angew. Chem. Int. Ed.* **2022**, *61*, e202206390.

173. Walley, J. E.; Wong, Y.-O.; Freeman, L. A.; Dickie, D. A.; Gilliard, R. J., N-Heterocyclic Carbene-Supported Aryl- and Alk- oxides of Beryllium and Magnesium. *Catalysts* **2019**, *9*, 934-945.
174. Freeman, L. A.; Walley, J. E.; Dickie, D. A.; Gilliard, R. J., Low-nuclearity magnesium hydride complexes stabilized by N-heterocyclic carbenes. *Dalton Trans.* **2019**, *48*, 17174-17178.
175. Pahl, J.; Brand, S.; Elsen, H.; Harder, S., Highly Lewis acidic cationic alkaline earth metal complexes. *Chem. Commun.* **2018**, *54*, 8685-8688.
176. Panda, T. K.; Kaneko, H.; Pal, K.; Tsurugi, H.; Mashima, K., Salt Metathesis and Direct Reduction Reactions Leading to Group 3 Metal Complexes with a N,N' -Bis(2,6-diisopropylphenyl)-1,4-diaza-1,3-butadiene Ligand and Their Solid-State Structures. *Organometallics* **2010**, *29*, 2610-2615.
177. Thiele, K.-H.; Lorenz, V.; Thiele, G.; Zönnchen, P.; Scholz, J., [Be(dad)₂]: Synthesis and Structure of a Diazabutadieneberyllium Complex. *Angew. Chem. Int. Ed. Engl.* **1994**, *33*, 1372-1373.
178. Gardiner, M. G.; Hanson, G. R.; Henderson, M. J.; Lee, F. C.; Raston, C. L., Paramagnetic Bis(1,4-di-tert-butyl-1,4-diazabutadiene) Adducts of Lithium, Magnesium, and Zinc. *Inorg. Chem.* **1994**, *33*, 2456-2461.
179. Corvaja, C.; Pasimeni, L., Hyperfine splitting in the ESR spectra of random oriented alkali earth biradical chelates. *Chem. Phys. Lett.* **1976**, *39*, 261-264.
180. Gardinier, J. R.; Gabbai, F. P., Reaction of N,N' -bis(mesityl)ethylenediamine with triethylaluminium. Formation of ten-membered aluminium amide heterocycles. *New Journal of Chemistry* **2001**, *25*, 1567-1571.

181. Notably, we observed the presence of free iPrNHC in saturated NMR solutions of 2-5, corroborating the plausibility of initial NHC dissociation.
182. Tapu, D.; Dixon, D. A.; Roe, C., ¹³C NMR Spectroscopy of “Arduengo-type” Carbenes and Their Derivatives. *Chem. Rev.* **2009**, *109*, 3385-3407.
183. Scholz, J.; Görls, H.; Schumann, H.; Weimann, R., Reaction of Samarium 1,4-Diaza-1,3-diene Complexes with Ketones: Generation of a New Versatile Tridentate Ligand via 1,3-Dipolar Cycloaddition. *Organometallics* **2001**, *20*, 4394-4402.
184. Pyykkö, P.; Atsumi, M., Molecular Single-Bond Covalent Radii for Elements 1–118. *Chem. Eur. J.* **2009**, *15*, 186-197.
185. Penafiel, J.; Maron, L.; Harder, S., Early main group metal catalysis: how important is the metal? *Angew. Chem. Int. Ed.* **2015**, *54*, 201-206.
186. Harder, S., Introduction to Early Main Group Organometallic Chemistry and Catalysis. In *Early Main Group Metal Catalysis*, Harder, S., Ed. 2020, 10.1002/9783527818020.ch1pp 1-29.
187. Rauch, M.; Parkin, G., Zinc and Magnesium Catalysts for the Hydrosilylation of Carbon Dioxide. *J. Am. Chem. Soc.* **2017**, *139*, 18162-18165.
188. Wilson, A. S. S.; Dinoi, C.; Hill, M. S.; Mahon, M. F.; Maron, L., Heterolysis of Dihydrogen by Nucleophilic Calcium Alkyls. *Angew. Chem. Int. Ed.* **2018**, *57*, 15500-15504.
189. Anker, M. D.; Arrowsmith, M.; Bellham, P.; Hill, M. S.; Kociok-Köhn, G.; Liptrot, D. J.; Mahon, M. F.; Weetman, C., Selective reduction of CO₂ to a methanol equivalent by B(C₆F₅)₃-activated alkaline earth catalysis. *Chem. Sci.* **2014**, *5*, 2826-2830.
190. Brand, S.; Elsen, H.; Langer, J.; Grams, S.; Harder, S., Calcium-Catalyzed Arene C–H Bond Activation by Low-Valent AlI. *Angew. Chem. Int. Ed.* **2019**, *58*, 15496-15503.

191. Garcia, L.; Dinoi, C.; Mahon, M. F.; Maron, L.; Hill, M. S., Magnesium hydride alkene insertion and catalytic hydrosilylation. *Chem. Sci.* **2019**, *10*, 8108-8118.
192. Garcia, L.; Anker, M. D.; Mahon, M. F.; Maron, L.; Hill, M. S., Coordination of arenes and phosphines by charge separated alkaline earth cations. *Dalton Trans.* **2018**, *47*, 12684-12693.
193. Pahl, J.; Elsen, H.; Friedrich, A.; Harder, S., Unsupported metal silyl ether coordination. *Chem. Commun.* **2018**, *54*, 7846-7849.
194. Pahl, J.; Friedrich, A.; Elsen, H.; Harder, S., Cationic Magnesium π -Arene Complexes. *Organometallics* **2018**, *37*, 2901-2909.
195. Pahl, J.; Stennett, T. E.; Volland, M.; Guldi, D. M.; Harder, S., Complexation and Versatile Reactivity of a Highly Lewis Acidic Cationic Mg Complex with Alkynes and Phosphines. *Chem. Eur. J.* **2019**, *25*, 2025-2034.
196. Friedrich, A.; Pahl, J.; Elsen, H.; Harder, S., Bulky cationic beta-diketimate magnesium complexes. *Dalton Trans.* **2019**, *48*, 5560-5568.
197. Garcia, L.; Mahon, M. F.; Hill, M. S., Multimetallic Alkaline-Earth Hydride Cations. *Organometallics* **2019**, *38*, 3778-3785.
198. Bruyere, J.-C.; Gourlaouen, C.; Karmazin, L.; Bailly, C.; Boudon, C.; Ruhlmann, L.; de Frémont, P.; Dagorne, S., Synthesis and Characterization of Neutral and Cationic Magnesium Complexes Supported by NHC Ligands. *Organometallics* **2019**, *38*, 2748-2757.
199. Bourissou, D.; Guerret, O.; Gabbai, F. P.; Bertrand, G., Stable Carbenes. *Chem. Rev.* **2000**, *100*, 39-92.

200. Bellemin-Laponnaz, S.; Dagorne, S., Group 1 and 2 and Early Transition Metal Complexes Bearing N-Heterocyclic Carbene Ligands: Coordination Chemistry, Reactivity, and Applications. *Chem. Rev.* **2014**, *114*, 8747-8774.
201. Zhao, Q.; Meng, G.; Nolan, S. P.; Szostak, M., N-Heterocyclic Carbene Complexes in C–H Activation Reactions. *Chem. Rev.* **2020**, *120*, 1981-2048.
202. Groom, C. R.; Bruno, I. J.; Lightfoot, M. P.; Ward, S. C., The Cambridge Structural Database. *Acta Crystallogr. Sect. B.* **2016**, *72*, 171-179.
203. Martínez-Martínez, A. J.; Fuentes, M. Á.; Hernán-Gómez, A.; Hevia, E.; Kennedy, A. R.; Mulvey, R. E.; O'Hara, C. T., Alkali-Metal-Mediated Magnesiations of an N-Heterocyclic Carbene: Normal, Abnormal, and “Paranormal” Reactivity in a Single Tritopic Molecule. *Angew. Chem. Int. Ed.* **2015**, *54*, 14075-14079.
204. Jones, C.; Yuvaraj, K.; Douair, I.; Maron, L., Activation of Ethylene by N-Heterocyclic Carbene Coordinated Magnesium(I) Compounds. *Chem. Eur. J.* **2020**, 10.1002/chem.202002380.
205. Walley, J. E.; Obi, A. D.; Breiner, G.; Wang, G.; Dickie, D. A.; Molino, A.; Dutton, J. L.; Wilson, D. J. D.; Gilliard, R. J., Cyclic(alkyl)(amino) Carbene-Promoted Ring Expansion of a Carbodicarbene Beryllacycle. *Inorg. Chem.* **2019**, *58*, 11118-11126.
206. Kennedy, A. R.; Mulvey, R. E.; Robertson, S. D., N-Heterocyclic carbene stabilized adducts of alkyl magnesium amide, bisalkyl magnesium and Grignard reagents: trapping oligomeric organo s-block fragments with NHCs. *Dalton Trans.* **2010**, *39*, 9091-9099.
207. In this article, bis- and tris-carbene stabilization refer to the coordination of two or three untethered carbene units to a single magnesium atom. This notation is also used in literature for neutral or anionic chelates housing tethered NHC units. Indeed, there exists only one example of

- tethered tris-NHC coordination to magnesium. See Nieto, I.; Cervantes-Lee, F.; Smith, J. M., A new synthetic route to bulky “second generation” tris(imidazol-2-ylidene)borate ligands: synthesis of a four coordinate iron(ii) complex. *Chem. Commun.* 2005, 3811-3813.
208. Bailey, P. J.; Coxall, R. A.; Dick, C. M.; Fabre, S.; Parsons, S.; Yellowlees, L. J., Structural and EPR characterisation of single electron and alkyl transfer products from reaction of dimethyl magnesium with bulky α -diimine ligands. *Chem. Commun.* **2005**, 10.1039/B505697G, 4563-4565.
209. Gibson, V. C.; Segal, J. A.; White, A. J. P.; Williams, D. J., Novel Mono-alkyl Magnesium Complexes Stabilized by a Bulky β -Diketimate Ligand: Structural Characterization of a Coordinatively Unsaturated Trigonal System. *J. Am. Chem. Soc.* **2000**, *122*, 7120-7121.
210. Bailey, P. J.; Dick, C. M. E.; Fabre, S.; Parsons, S., Synthesis and characterisation of magnesium methyl complexes with monoanionic chelating nitrogen donor ligands and their reaction with dioxygen. *J. Chem. Soc., Dalton Trans.* **2000**, 10.1039/B001316L, 1655-1661.
211. Stuhl, C.; Anwender, R., Dimethylmagnesium revisited. *Dalton Trans.* **2018**, *47*, 12546-12552.
212. Michel, O.; Meermann, C.; Törnroos, K. W.; Anwender, R., Alkaline-Earth Metal Alkylaluminate Chemistry Revisited. *Organometallics* **2009**, *28*, 4783-4790.
213. Viebrock, H.; Behrens, U.; Weiss, E., A Novel Organomagnesium Compound Consisting of Two Triple-Decker Cations [LMg(μ -Me(3)MgL)]⁺ and an Octamethyltrimagnesate Anion: [{Me₂Mg(μ -Me)₂ }₂Mg]₂⁻. *Angew. Chem. Int. Ed. Engl.* **1994**, *33*, 1257-1259.

214. Peltzer, R. M.; Eisenstein, O.; Nova, A.; Cascella, M., How Solvent Dynamics Controls the Schlenk Equilibrium of Grignard Reagents: A Computational Study of CH₃MgCl in Tetrahydrofuran. *J. Phys. Chem. B* **2017**, *121*, 4226-4237.
215. Peltzer, R. M.; Gauss, J.; Eisenstein, O.; Cascella, M., The Grignard Reaction – Unraveling a Chemical Puzzle. *J. Am. Chem. Soc.* **2020**, *142*, 2984-2994.
216. Obi, A. D.; Dickie, D. A.; Gilliard, R. J., CCDC 2009525: Experimental Crystal Structure Determination. *CSD Communication* **2020**, 10.5517/ccdc.csd.cc25g2d4.
217. Kuhn, N.; Kratz, T., Synthesis of Imidazol-2-ylidenes by Reduction of Imidazole-2(3H)-thiones. *Synthesis* **1993**, *1993*, 561-562.
218. Mantina, M.; Chamberlin, A. C.; Valero, R.; Cramer, C. J.; Truhlar, D. G., Consistent van der Waals Radii for the Whole Main Group. *J. Phys. Chem. A* **2009**, *113*, 5806-5812.
219. Couchman, S. A.; Holzmann, N.; Frenking, G.; Wilson, D. J.; Dutton, J. L., Beryllium chemistry the safe way: a theoretical evaluation of low oxidation state beryllium compounds. *Dalton Trans.* **2013**, *42*, 11375-11384.
220. De, S.; Parameswaran, P., Neutral tricoordinated beryllium(0) compounds – isostructural to BH₃ but isoelectronic to NH₃. *Dalton Trans.* **2013**, *42*, 4650-4656.
221. Rit, A.; Zanardi, A.; Spaniol, T. P.; Maron, L.; Okuda, J., A Cationic Zinc Hydride Cluster Stabilized by an N-Heterocyclic Carbene: Synthesis, Reactivity, and Hydrosilylation Catalysis. *Angew. Chem. Int. Ed.* **2014**, *53*, 13273-13277.
222. Goicoechea, J. M.; Grützmacher, H., The Chemistry of the 2-Phosphaethynolate Anion. *Angew. Chem. Int. Ed.* **2018**, *57*, 16968-16994.
223. Weber, L., 2-Phospha- and 2-Arsaethynolates – Versatile Building Blocks in Modern Synthetic Chemistry. *Eur. J. Inorg. Chem.* **2018**, *2018*, 2175-2227.

224. Heift, D.; Benko, Z.; Grutzmacher, H., Is the phosphaehtynolate anion, (OCP)(-), an ambident nucleophile? A spectroscopic and computational study. *Dalton Trans.* **2014**, *43*, 5920-5928.
225. Becker, G.; Schwarz, W.; Seidler, N.; Westerhausen, M., Acyl- und Alkylidenphosphane. XXXIII. Lithoxy-methylidenphosphan · DME und -methylidinphosphan · 2 DME — Synthese und Struktur. *Z. Anorg. Allg. Chem.* **1992**, *612*, 72-82.
226. Puschmann, F. F.; Stein, D.; Heift, D.; Hendriksen, C.; Gal, Z. A.; Grützmacher, H.-F.; Grützmacher, H., Phosphination of Carbon Monoxide: A Simple Synthesis of Sodium Phosphaehtynolate (NaOCP). *Angew. Chem. Int. Ed.* **2011**, *50*, 8420-8423.
227. Krummenacher, I.; Cummins, C. C., Carbon–phosphorus triple bond formation through multiple bond metathesis of an anionic niobium phosphide with carbon dioxide. *Polyhedron* **2012**, *32*, 10-13.
228. Jupp, A. R.; Goicoechea, J. M., The 2-Phosphaehtynolate Anion: A Convenient Synthesis and [2+2] Cycloaddition Chemistry. *Angew. Chem. Int. Ed.* **2013**, *52*, 10064-10067.
229. Heift, D.; Benkő, Z.; Grützmacher, H., Coulomb repulsion versus cycloaddition: formation of anionic four-membered rings from sodium phosphaehtynolate, Na(OCP). *Dalton Trans.* **2014**, *43*, 831-840.
230. Gilliard, R. J.; Heift, D.; Benkő, Z.; Keiser, J. M.; Rheingold, A. L.; Grützmacher, H.; Protasiewicz, J. D., An isolable magnesium diphosphaehtynolate complex. *Dalton Trans.* **2018**, *47*, 666-669.
231. Westerhausen, M.; Schneiderbauer, S.; Piotrowski, H.; Suter, M.; Nöth, H., Synthesis of alkaline earth metal bis(2-phosphaehtynolates). *J. Organomet. Chem.* **2002**, *643-644*, 189-193.

232. Wilson, D. W. N.; Urwin, S. J.; Yang, E. S.; Goicoechea, J. M., A Cyaphide Transfer Reagent. *J. Am. Chem. Soc.* **2021**, *143*, 10367-10373.
233. Doddi, A.; Peters, M.; Tamm, M., N-Heterocyclic Carbene Adducts of Main Group Elements and Their Use as Ligands in Transition Metal Chemistry. *Chem. Rev.* **2019**, *119*, 6994-7112.
234. Langer, J.; Kriek, S.; Fischer, R.; Görls, H.; Walther, D.; Westerhausen, M., 1,4-Dioxane Adducts of Grignard Reagents: Synthesis, Ether Fragmentation Reactions, and Structural Diversity of Grignard Reagent/1,4-Dioxane Complexes. *Organometallics* **2009**, *28*, 5814-5820.
235. Maercker, A., Ether Cleavage with Organo-Alkali-Metal Compounds and Alkali Metals. *Angew. Chem. Int. Ed. Engl.* **1987**, *26*, 972-989.
236. Friedrich, A.; Pahl, J.; Eysel, J.; Langer, J.; van Eikema Hommes, N.; Görling, A.; Harder, S., Magnesium–halobenzene bonding: mapping the halogen sigma-hole with a Lewis-acidic complex. *Chem. Sci.* **2021**, *12*, 2410-2418.
237. Jost, M.; Finger, L. H.; Sundermeyer, J.; von Hänisch, C., Simple access to ionic liquids and organic salts containing the phosphoethynolate (PCO⁻) and Zintl (Sb₁₁₃⁻) anions. *Chem. Commun.* **2016**, *52*, 11646-11648.
238. Walley, J. E.; Warring, L. S.; Kertész, E.; Wang, G.; Dickie, D. A.; Benkő, Z.; Gilliard, R. J., Indirect Access to Carbene Adducts of Bismuth- and Antimony-Substituted Phosphaketene and Their Unusual Thermal Transformation to Dipnictines and [(NHC)₂OCP][OCP]. *Inorg. Chem.* **2021**, *60*, 4733-4743.
239. Liu, L. L.; Ruiz, D. A.; Dahcheh, F.; Bertrand, G.; Suter, R.; Tondreau, A. M.; Grützmacher, H., Isolation of Au-, Co-η¹PCO and Cu-η²PCO complexes, conversion of an Ir-

- η^1 PCO complex into a dimetalladiphosphene, and an interaction-free PCO anion. *Chem. Sci.* **2016**, *7*, 2335-2341.
240. Mei, Y.; Borger, J. E.; Wu, D.-J.; Grützmacher, H., Salen supported Al-O-C \equiv P and Ga-P=C=O complexes. *Dalton Trans.* **2019**, *48*, 4370-4374.
241. Bestgen, S.; Chen, Q.; Rees, N. H.; Goicoechea, J. M., Synthesis and reactivity of rare-earth metal phosphoethynolates. *Dalton Trans.* **2018**, *47*, 13016-13024.
242. Camp, C.; Settineri, N.; Lefèvre, J.; Jupp, A. R.; Goicoechea, J. M.; Maron, L.; Arnold, J., Uranium and thorium complexes of the phosphoethynolate ion. *Chem. Sci.* **2015**, *6*, 6379-6384.
243. Wilson, D. W. N.; Hinz, A.; Goicoechea, J. M., An Isolable Phosphoethynolatorborane and Its Reactivity. *Angew. Chem. Int. Ed.* **2018**, *57*, 2188-2193.
244. Alidori, S.; Heift, D.; Santiso-Quinones, G.; Benkő, Z.; Grützmacher, H.; Caporali, M.; Gonsalvi, L.; Rossin, A.; Peruzzini, M., Synthesis and Characterization of Terminal [Re(XCO)(CO)₂(triphos)] (X=N, P): Isocyanate versus Phosphoethynolate Complexes. *Chem. Eur. J.* **2012**, *18*, 14805-14811.
245. Hou, G.-L.; Chen, B.; Transue, W. J.; Yang, Z.; Grützmacher, H.; Driess, M.; Cummins, C. C.; Borden, W. T.; Wang, X.-B., Spectroscopic Characterization, Computational Investigation, and Comparisons of ECX⁻ (E = As, P, and N; X = S and O) Anions. *J. Am. Chem. Soc.* **2017**, *139*, 8922-8930.
246. Mielke, Z.; Andrews, L., Infrared detection of the PCO radical and HPCO molecule. *Chem. Phys. Lett.* **1991**, *181*, 355-360.
247. Hinz, A.; Schulz, A.; Villinger, A., On the behaviour of biradicaloid [P(μ -NTer)]₂ towards Lewis acids and bases. *Chem. Commun.* **2016**, *52*, 6328-6331.

248. Henne, F. D.; Dickschat, A. T.; Hennersdorf, F.; Feldmann, K. O.; Weigand, J. J., Synthesis of Selected Cationic Pnictanes $[\text{LnPnX}_{3-n}]_{n+}$ (L = Imidazolium-2-yl; Pn = P, As; n = 1–3) and Replacement Reactions with Pseudohalogenes. *Inorg. Chem.* **2015**, *54*, 6849-6861.
249. Ellis, B. D.; Dyker, C. A.; Decken, A.; Macdonald, C. L. B., The synthesis, characterisation and electronic structure of N-heterocyclic carbene adducts of PI cations. *Chem. Commun.* **2005**, 10.1039/B500692A, 1965-1967.
250. Ellis, B. D.; Macdonald, C. L. B., Stable compounds containing heavier group 15 elements in the +1 oxidation state. *Coord. Chem. Rev.* **2007**, *251*, 936-973.
251. Back, O.; Kuchenbeiser, G.; Donnadiou, B.; Bertrand, G., Nonmetal-Mediated Fragmentation of P₄: Isolation of P₁ and P₂ Bis(carbene) Adducts. *Angew. Chem. Int. Ed.* **2009**, *48*, 5530-5533.
252. Binder, J. F.; Swidan, A. a.; Macdonald, C. L. B., Synthesis of Heteroleptic Phosphorus(I) Cations by P⁺ Transfer. *Inorg. Chem.* **2018**, *57*, 11717-11725.
253. Yang, W.; Krantz, K. E.; Dickie, D. A.; Molino, A.; Wilson, D. J. D.; Gilliard Jr, R. J., Crystalline BP-Doped Phenanthryne via Photolysis of The Elusive Boraphosphaketene. *Angew. Chem. Int. Ed.* **2020**, *59*, 3971-3975.
254. Sharma, M. K.; Wölper, C.; Haberhauer, G.; Schulz, S., Multi-Talented Gallaphosphene for Ga–P–Ga Heteroallyl Cation Generation, CO₂ Storage, and C(sp³)–H Bond Activation. *Angew. Chem. Int. Ed.* **2021**, *60*, 6784-6790.
255. Wilson, D. W. N.; Feld, J.; Goicoechea, J. M., A Phosphanyl-Phosphagallene that Functions as a Frustrated Lewis Pair. *Angew. Chem. Int. Ed.* **2020**, *59*, 20914-20918.
256. Liu, L.; Ruiz, David A.; Munz, D.; Bertrand, G., A Singlet Phosphinidene Stable at Room Temperature. *Chem* **2016**, *1*, 147-153.

257. Hagspiel, S.; Fantuzzi, F.; Dewhurst, R. D.; Gärtner, A.; Lindl, F.; Lamprecht, A.; Braunschweig, H., Adducts of the Parent Boraphosphaketene H₂BPCO and their Decarbonylative Insertion Chemistry. *Angew. Chem. Int. Ed.* **2021**, *60*, 13666-13670.
258. Wilson, D. W. N.; Myers, W. K.; Goicoechea, J. M., Synthesis and decarbonylation chemistry of gallium phosphaketenes. *Dalton Trans.* **2020**, *49*, 15249-15255.
259. Heift, D.; Benkő, Z.; Grützmacher, H., Phosphaketenes as Building Blocks for the Synthesis of Triphospha Heterocycles. *Chem. Eur. J.* **2014**, *20*, 11326-11330.
260. Heift, D.; Benkő, Z.; Grützmacher, H.; Jupp, A. R.; Goicoechea, J. M., Cyclo-oligomerization of isocyanates with Na(PH₂) or Na(OCP) as “P⁻” anion sources. *Chem. Sci.* **2015**, *6*, 4017-4024.
261. Wilson, D. W. N.; Franco, M. P.; Myers, W. K.; McGrady, J. E.; Goicoechea, J. M., Base induced isomerisation of a phosphaehtynolato-borane: mechanistic insights into boryl migration and decarbonylation to afford a triplet phosphinidene. *Chem. Sci.* **2020**, *11*, 862-869.
262. Li, Z.; Chen, X.; Li, Y.; Su, C.-Y.; Grützmacher, H., N-Heterocyclic carbene phosphaketene adducts as precursors to carbene–phosphinidene adducts and a rearranged π -system. *Chem. Commun.* **2016**, *52*, 11343-11346.
263. Robinson, T. P.; Cowley, M. J.; Scheschkewitz, D.; Goicoechea, J. M., Phosphide Delivery to a Cyclotrisilene. *Angew. Chem. Int. Ed.* **2015**, *54*, 683-686.
264. Hansmann, M. M.; Bertrand, G., Transition-Metal-like Behavior of Main Group Elements: Ligand Exchange at a Phosphinidene. *J. Am. Chem. Soc.* **2016**, *138*, 15885-15888.
265. Tondreau, A. M.; Benkő, Z.; Harmer, J. R.; Grützmacher, H., Sodium phosphaehtynolate, Na(OCP), as a “P” transfer reagent for the synthesis of N-heterocyclic carbene supported P₃ and PAsP radicals. *Chem. Sci.* **2014**, *5*, 1545-1554.

266. Rossin, A.; Peruzzini, M., Ammonia–Borane and Amine–Borane Dehydrogenation Mediated by Complex Metal Hydrides. *Chem. Rev.* **2016**, *116*, 8848-8872.
267. Kumar, R.; Karkamkar, A.; Bowden, M.; Autrey, T., Solid-state hydrogen rich boron–nitrogen compounds for energy storage. *Chem. Soc. Rev.* **2019**, *48*, 5350-5380.
268. Graetz, J., New approaches to hydrogen storage. *Chem. Soc. Rev.* **2009**, *38*, 73-82.
269. Marder, T. B., Will We Soon Be Fueling our Automobiles with Ammonia–Borane? *Angew. Chem. Int. Ed.* **2007**, *46*, 8116-8118.
270. Stennett, T. E.; Harder, S., s-Block amidoboranes: syntheses, structures, reactivity and applications. *Chem. Soc. Rev.* **2016**, *45*, 1112-1128.
271. Hamilton, C. W.; Baker, R. T.; Staubitz, A.; Manners, I., B–N compounds for chemical hydrogen storage. *Chem. Soc. Rev.* **2009**, *38*, 279-293.
272. Chua, Y. S.; Chen, P.; Wu, G.; Xiong, Z., Development of amidoboranes for hydrogen storage. *Chem. Commun.* **2011**, *47*, 5116-5129.
273. Karkamkar, A.; Aardahl, C.; Autrey, T., Recent developments on hydrogen release from ammonia borane. *Mater. Matters* **2007**, *2*, 6-9.
274. Smythe, N. C.; Gordon, J. C., Ammonia Borane as a Hydrogen Carrier: Dehydrogenation and Regeneration. *Eur. J. Inorg. Chem.* **2010**, *2010*, 509-521.
275. Diyabalanage, H. V. K.; Shrestha, R. P.; Semelsberger, T. A.; Scott, B. L.; Bowden, M. E.; Davis, B. L.; Burrell, A. K., Calcium Amidotrihydroborate: A Hydrogen Storage Material. *Angew. Chem. Int. Ed.* **2007**, *46*, 8995-8997.
276. Diyabalanage, H. V. K.; Nakagawa, T.; Shrestha, R. P.; Semelsberger, T. A.; Davis, B. L.; Scott, B. L.; Burrell, A. K.; David, W. I. F.; Ryan, K. R.; Jones, M. O.; Edwards, P. P.,

- Potassium(I) Amidotrihydroborate: Structure and Hydrogen Release. *J. Am. Chem. Soc.* **2010**, *132*, 11836-11837.
277. Xiong, Z.; Yong, C. K.; Wu, G.; Chen, P.; Shaw, W.; Karkamkar, A.; Autrey, T.; Jones, M. O.; Johnson, S. R.; Edwards, P. P.; David, W. I. F., High-capacity hydrogen storage in lithium and sodium amidoboranes. *Nat. Mater.* **2008**, *7*, 138-141.
278. Zhang, Q.; Tang, C.; Fang, C.; Fang, F.; Sun, D.; Ouyang, L.; Zhu, M., Synthesis, Crystal Structure, and Thermal Decomposition of Strontium Amidoborane. *J. Phys, Chem. C* **2010**, *114*, 1709-1714.
279. Luo, J.; Kang, X.; Wang, P., Synthesis, formation mechanism, and dehydrogenation properties of the long-sought $Mg(NH_2BH_3)_2$ compound. *Energy Environ. Sci.* **2013**, *6*, 1018-1025.
280. Wu, H.; Zhou, W.; Yildirim, T., Alkali and Alkaline-Earth Metal Amidoboranes: Structure, Crystal Chemistry, and Hydrogen Storage Properties. *J. Am. Chem. Soc.* **2008**, *130*, 14834-14839.
281. Chua, Y. S.; Wu, G.; Xiong, Z.; Karkamkar, A.; Guo, J.; Jian, M.; Wong, M. W.; Autrey, T.; Chen, P., Synthesis, structure and dehydrogenation of magnesium amidoborane monoammoniate. *Chem. Commun.* **2010**, *46*, 5752-5754.
282. Kang, X.; Wu, H.; Luo, J.; Zhou, W.; Wang, P., A simple and efficient approach to synthesize amidoborane ammoniates: case study for $Mg(NH_2BH_3)_2(NH_3)_3$ with unusual coordination structure. *J. Mater. Chem.* **2012**, *22*, 13174-13179.
283. Wu, H.; Zhou, W.; Pinkerton, F. E.; Meyer, M. S.; Yao, Q.; Gadipelli, S.; Udovic, T. J.; Yildirim, T.; Rush, J. J., Sodium magnesium amidoborane: the first mixed-metal amidoborane. *Chem. Commun.* **2011**, *47*, 4102-4104.

284. Chua, Y. S.; Li, W.; Wu, G.; Xiong, Z.; Chen, P., From Exothermic to Endothermic Dehydrogenation – Interaction of Monoammoniate of Magnesium Amidoborane and Metal Hydrides. *Chem. Mater.* **2012**, *24*, 3574-3581.
285. Chua, Y. S.; Wu, H.; Zhou, W.; Udovic, T. J.; Wu, G.; Xiong, Z.; Wong, M. W.; Chen, P., Monoammoniate of Calcium Amidoborane: Synthesis, Structure, and Hydrogen-Storage Properties. *Inorg. Chem.* **2012**, *51*, 1599-1603.
286. Nolla-Saltiel, R.; Geer, A. M.; Lewis, W.; Blake, A. J.; Kays, D. L., Dehydrogenation of dimethylamine-borane mediated by Group 1 pincer complexes. *Chem. Commun.* **2018**, *54*, 1825-1828.
287. Ried, A. C. A.; Taylor, L. J.; Geer, A. M.; Williams, H. E. L.; Lewis, W.; Blake, A. J.; Kays, D. L., A Highly Active Bidentate Magnesium Catalyst for Amine-Borane Dehydrocoupling: Kinetic and Mechanistic Studies. *Chem. Eur. J.* **2019**, *25*, 6840-6846.
288. Wirtz, L.; Haider, W.; Huch, V.; Zimmer, M.; Schäfer, A., Magnesocenophane-Catalyzed Amine Borane Dehydrocoupling. *Chem. Eur. J.* **2020**, *26*, 6176-6184.
289. Bellham, P.; Hill, M. S.; Kociok-Köhn, G., Alkali metal-mediated dehydrocoupling of Me₂NH·BH₃. *Dalton Trans.* **2015**, *44*, 12078-12081.
290. Bellham, P.; Anker, M. D.; Hill, M. S.; Kociok-Köhn, G.; Mahon, M. F., The significance of secondary interactions during alkaline earth-promoted dehydrogenation of dialkylamine-boranes. *Dalton Trans.* **2016**, *45*, 13969-13978.
291. Jones, C.; Bonyhady, S. J.; Nembenna, S.; Stasch, A., New Routes to Soluble Magnesium Amidoborane Complexes. *Eur. J. Inorg. Chem.* **2012**, *2012*, 2596-2601.

292. Spielmann, J.; Harder, S., Hydrogen Elimination in Bulky Calcium Amidoborane Complexes: Isolation of a Calcium Borylamide Complex. *J. Am. Chem. Soc.* **2009**, *131*, 5064-5065.
293. Spielmann, J.; Jansen, G.; Bandmann, H.; Harder, S., Calcium Amidoborane Hydrogen Storage Materials: Crystal Structures of Decomposition Products. *Angew. Chem. Int. Ed.* **2008**, *47*, 6290-6295.
294. Spielmann, J.; Piesik, D. F. J.; Harder, S., Thermal Decomposition of Mono- and Bimetallic Magnesium Amidoborane Complexes. *Chem. Eur. J.* **2010**, *16*, 8307-8318.
295. Spielmann, J.; Bolte, M.; Harder, S., Synthesis and structure of a magnesium–amidoborane complex and its role in catalytic formation of a new bis-aminoborane ligand. *Chem. Commun.* **2009**, 10.1039/B914979A, 6934-6936.
296. Hill, M. S.; Hodgson, M.; Liptrot, D. J.; Mahon, M. F., Stoichiometric reactivity of dialkylamine boranes with alkaline earth silylamides. *Dalton Trans.* **2011**, *40*, 7783-7790.
297. Bellham, P.; Hill, M. S.; Kociok-Köhn, G.; Liptrot, D. J., Alkaline earth alkyl insertion chemistry of in situ generated aminoboranes. *Dalton Trans.* **2013**, *42*, 737-745.
298. Hill, M. S.; Kociok-Köhn, G.; Robinson, T. P., Group 3-centred dehydrocoupling of Me₂NH·BH₃. *Chem. Commun.* **2010**, *46*, 7587-7589.
299. Daly, S. R.; Bellott, B. J.; Nesbit, M. A.; Girolami, G. S., Synthesis and Structural Diversity of Barium (N,N-Dimethylamino)diboranates. *Inorg. Chem.* **2012**, *51*, 6449-6459.
300. Dunbar, A. C.; Girolami, G. S., Synthesis and Characterization of Calcium N,N-Dimethylaminodiboranates as Possible Chemical Vapor Deposition Precursors. *Inorg. Chem.* **2014**, *53*, 888-896.

301. Dunbar, A. C.; Joseph Lastowski, R.; Girolami, G. S., Synthesis and Characterization of Strontium N,N-Dimethylaminodiboranates as Possible Chemical Vapor Deposition Precursors. *Inorg. Chem.* **2020**, *59*, 16893-16904.
302. Kim, D. Y.; Girolami, G. S., Highly Volatile Magnesium Complexes with the Aminodiboranate Anion, a New Chelating Borohydride. Synthesis and Characterization of Mg(H₃BNMe₂BH₃)₂ and Related Compounds. *Inorg. Chem.* **2010**, *49*, 4942-4948.
303. Obi, A. D.; Machost, H. R.; Dickie, D. A.; Gilliard, R. J., A Thermally Stable Magnesium Phosphaethynolate Grignard Complex. *Inorg. Chem.* **2021**, *60*, 12481-12488.
304. Sabourin, K. J.; Malcolm, A. C.; McDonald, R.; Ferguson, M. J.; Rivard, E., Metal-free dehydrogenation of amine-boranes by an N-heterocyclic carbene. *Dalton Trans.* **2013**, *42*, 4625-4632.
305. Oldroyd, N. L.; Chitnis, S. S.; Annibale, V. T.; Arz, M. I.; Sparkes, H. A.; Manners, I., Metal-free dehydropolymerisation of phosphine-boranes using cyclic (alkyl)(amino)carbenes as hydrogen acceptors. *Nat. Commun.* **2019**, *10*, 1370.
306. Stubbs, N. E.; Jurca, T.; Leitao, E. M.; Woodall, C. H.; Manners, I., Polyaminoborane main chain scission using N-heterocyclic carbenes; formation of donor-stabilised monomeric aminoboranes. *Chem. Commun.* **2013**, *49*, 9098-9100.
307. Malcolm, A. C.; Sabourin, K. J.; McDonald, R.; Ferguson, M. J.; Rivard, E., Donor-Acceptor Complexation and Dehydrogenation Chemistry of Aminoboranes. *Inorg. Chem.* **2012**, *51*, 12905-12916.
308. Deposition Numbers 2171705, 2171706, 2171707, 2171708, 2171709, 2171710, 2171711, 2171712, 2171713, 2193394, 2193395, and 2193396 contain the supplementary crystallographic data for this paper. These data are provided free of charge by the joint

Cambridge Crystallographic Data Centre and Fachinformationszentrum Karlsruhe Access
Structures service www.ccdc.cam.ac.uk/structures

309. iPrNHC-BN was independently prepared from the reaction of [Me₂NBH₂]₂ and iPrNHC (80 C, 2 h), and fully characterized by heteronuclear NMR and X-ray crystallography. See SI for details
310. Jana, A.; Schulzke, C.; Roesky, H. W., Oxidative Addition of Ammonia at a Silicon(II) Center and an Unprecedented Hydrogenation Reaction of Compounds with Low-Valent Group 14 Elements Using Ammonia Borane. *J. Am. Chem. Soc.* **2009**, *131*, 4600-4601.
311. Johnson, H. C.; Robertson, A. P. M.; Chaplin, A. B.; Sewell, L. J.; Thompson, A. L.; Haddow, M. F.; Manners, I.; Weller, A. S., Catching the First Oligomerization Event in the Catalytic Formation of Polyaminoboranes: H₃B·NMeHBH₂·NMeH₂ Bound to Iridium. *J. Am. Chem. Soc.* **2011**, *133*, 11076-11079.
312. Chai, J.-D.; Head-Gordon, M., Long-range corrected hybrid density functionals with damped atom–atom dispersion corrections. *Phys. Chem. Chem. Phys.* **2008**, *10*, 6615-6620.
313. Jr., T. H. D., Gaussian basis sets for use in correlated molecular calculations. I. The atoms boron through neon and hydrogen. *J. Chem. Phys.* **1989**, *90*, 1007-1023.
314. Kendall, R. A.; Jr., T. H. D.; Harrison, R. J., Electron affinities of the first - row atoms revisited. Systematic basis sets and wave functions. *J. Chem. Phys.* **1992**, *96*, 6796-6806.
315. Peterson, K. A., Systematically convergent basis sets with relativistic pseudopotentials. I. Correlation consistent basis sets for the post-d group 13–15 elements. *J. Chem. Phys.* **2003**, *119*, 11099-11112.
316. Peterson, K. A.; Figgen, D.; Goll, E.; Stoll, H.; Dolg, M., Systematically convergent basis sets with relativistic pseudopotentials. II. Small-core pseudopotentials and correlation

- consistent basis sets for the post-d group 16–18 elements. *J. Chem. Phys.* **2003**, *119*, 11113-11123.
317. Peterson, K. A.; Shepler, B. C.; Figgen, D.; Stoll, H., On the Spectroscopic and Thermochemical Properties of ClO, BrO, IO, and Their Anions. *J. Phys. Chem. A* **2006**, *110*, 13877-13883.
318. Butera, V.; Russo, N.; Sicilia, E., Hydrogen Release from Dialkylamine–Boranes Promoted by Mg and Ca Complexes: A DFT Analysis of the Reaction Mechanism. *Chem. Eur. J.* **2014**, *20*, 5967-5976.
319. Barrett, A. G. M.; Crimmin, M. R.; Hill, M. S.; Procopiou, P. A., Heterofunctionalization catalysis with organometallic complexes of calcium, strontium and barium. *Proc. R. Soc. A.* **2010**, *466*, 927-963.
320. Westerhausen, M.; Koch, A.; Görls, H.; Krieck, S., Heavy Grignard Reagents: Synthesis, Physical and Structural Properties, Chemical Behavior, and Reactivity. *Chem. Eur. J.* **2016**, *23*, 1456-1483.
321. Westerhausen, M., 100 Years after Grignard: Where Does the Organometallic Chemistry of the Heavy Alkaline Earth Metals Stand Today? *Angew. Chem. Int. Ed.* **2001**, *40*, 2975-2977.
322. Speight, I. R.; Chmely, S. C.; Hanusa, T. P.; Rheingold, A. L., Mechanochemically directed metathesis in Group 2 chemistry: Calcium amide formation without solvent. *Chem. Commun.* **2019**, *55*, 2202-2205.
323. Gao, P.; Jiang, J.; Maeda, S.; Kubota, K.; Ito, H., Mechanochemically Generated Calcium-Based Heavy Grignard Reagents and Their Application to Carbon–Carbon Bond-Forming Reactions. *Angew. Chem. Int. Ed.* **2022**, *n/a*, e202207118.

324. Westerhausen, M., Synthesis and spectroscopic properties of bis(trimethylsilyl)amides of the alkaline-earth metals magnesium, calcium, strontium, and barium. *Inorg. Chem.* **1991**, *30*, 96-101.
325. Cloke, F. G. N.; Hitchcock, P. B.; Lappert, M. F.; Lawless, G. A.; Royo, B., Lipophilic strontium and calcium alkyls, amides and phenoxides; X-ray structures of the crystalline square-planar [$\{\text{trans-Sr}(\text{NR}')_2(\mu\text{-}1,4\text{-dioxane})\}^\infty$] and tetrahedral [$\text{CaR}_2(1,4\text{-dioxane})_2$]; $\text{R}' = \text{SiMe}_3$, $\text{R} = \text{CH}(\text{SiMe}_3)_2$. *J. Chem. Soc., Chem. Commun.* **1991**, 10.1039/C39910000724, 724-726.
326. Koch, A.; Wirgenings, M.; Kriek, S.; Görls, H.; Pohnert, G.; Westerhausen, M., Hydrocarbon-Soluble Bis(trimethylsilylmethyl)calcium and Calcium–Iodine Exchange Reactions at sp^2 -Hybridized Carbon Atoms. *Organometallics* **2017**, *36*, 3981-3986.
327. Harder, S.; Feil, F.; Weeber, A., Structure of a Benzylcalcium Diastereomer: An Initiator for the Anionic Polymerization of Styrene. *Organometallics* **2001**, *20*, 1044-1046.
328. Crimmin, M. R.; Barrett, A. G. M.; Hill, M. S.; MacDougall, D. J.; Mahon, M. F.; Procopiou, P. A., Bis(trimethylsilyl)methyl Derivatives of Calcium, Strontium and Barium: Potentially Useful Dialkyls of the Heavy Alkaline Earth Elements. *Chem. Eur. J.* **2008**, *14*, 11292-11295.
329. Yan, K.; Upton, B. M.; Ellern, A.; Sadow, A. D., Lewis Acid-Mediated β -Hydride Abstraction Reactions of Divalent $\text{M}(\text{C}(\text{SiHMe}_2)_3)_2\text{THF}_2$ ($\text{M} = \text{Ca}, \text{Yb}$). *J. Am. Chem. Soc.* **2009**, *131*, 15110-15111.
330. Feil, F.; Harder, S., α,α -Bis(trimethylsilyl)-Substituted Benzyl Complexes of Potassium and Calcium. *Organometallics* **2000**, *19*, 5010-5015.

331. Eaborn, C.; B. Hitchcock, P., The first structurally characterised solvent-free ζ -bonded diorganocalcium, $\text{Ca}[\text{C}(\text{SiMe}_3)_3]_2$. *Chem. Commun.* **1997**, 10.1039/A703972G, 1961-1962.
332. Hitchcock, P. B.; Khvostov, A. V.; Lappert, M. F., Synthesis and structures of crystalline bis(trimethylsilyl)methanido complexes of potassium, calcium and ytterbium. *J. Organomet. Chem.* **2002**, 663, 263-268.
333. Coles, M. P., The role of the bis-trimethylsilylamido ligand, $[\text{N}\{\text{SiMe}_3\}_2]^-$, in main group chemistry. Part 1: Structural chemistry of the s-block elements. *Coord. Chem. Rev.* **2015**, 297-298, 2-23.
334. Hanusa, T. P., New Developments in the Cyclopentadienyl Chemistry of the Alkaline-Earth Metals. *Organometallics* **2002**, 21, 2559-2571.
335. Maitland, B.; Wiesinger, M.; Langer, J.; Ballmann, G.; Pahl, J.; Elsen, H.; Farber, C.; Harder, S., A Simple Route to Calcium and Strontium Hydride Clusters. *Angew. Chem. Int. Ed.* **2017**, 56, 11880-11884.
336. Brinkmann, C.; Barrett, A. G. M.; Hill, M. S.; Procopiou, P. A., Heavier Alkaline Earth Catalysts for the Intermolecular Hydroamination of Vinylarenes, Dienes, and Alkynes. *J. Am. Chem. Soc.* **2012**, 134, 2193-2207.
337. Arrowsmith, M.; Crimmin, M. R.; Hill, M. S.; Lomas, S. L.; Heng, M. S.; Hitchcock, P. B.; Kociok-Köhn, G., Catalytic hydroacetylenation of carbodiimides with homoleptic alkaline earth hexamethyldisilazides. *Dalton Trans.* **2014**, 43, 14249-14256.
338. Liptrot, D. J., *Group 2 Mediated Dehydrocoupling*. Springer International Publishing: 2015.

339. Chisholm, M. H.; Gallucci, J.; Phomphrai, K., Lactide polymerization by well-defined calcium coordination complexes: comparisons with related magnesium and zinc chemistry. *Chem. Commun.* **2003**, 10.1039/B208679D, 48-49.
340. Chapple, P. M.; Cordier, M.; Dorcet, V.; Roisnel, T.; Carpentier, J.-F.; Sarazin, Y., A versatile nitrogen ligand for alkaline-earth chemistry. *Dalton Trans.* **2020**, *49*, 11878-11889.
341. Crimmin, M. R.; Casely, I. J.; Hill, M. S., Calcium-Mediated Intramolecular Hydroamination Catalysis. *J. Am. Chem. Soc.* **2005**, *127*, 2042-2043.
342. Hu, H.; Cui, C., Synthesis of Calcium and Ytterbium Complexes Supported by a Tridentate Imino-Amidinate Ligand and Their Application in the Intermolecular Hydrophosphination of Alkenes and Alkynes. *Organometallics* **2012**, *31*, 1208-1211.
343. Ballmann, G.; Rösch, B.; Harder, S., Stabilization of Heteroleptic Heavier Alkaline Earth Metal Complexes with an Encapsulating Dipyrromethene Ligand. *Eur. J. Inorg. Chem.* **2019**, *2019*, 3683-3689.
344. Pearce, K. G.; Dinoi, C.; Hill, M. S.; Mahon, M. F.; Maron, L.; Schwamm, R. S.; Wilson, A. S. S., Synthesis of Molecular Phenylcalcium Derivatives: Application to the Formation of Biaryls. *Angew. Chem. Int. Ed.* **2022**, *61*, e202200305.
345. Koch, A.; Kriek, S.; Görls, H.; Westerhausen, M., Alkaline Earth Metal–Carbene Complexes with the Versatile Tridentate 2,6-Bis(3-mesitylimidazol-2-ylidene)pyridine Ligand. *Organometallics* **2017**, *36*, 994-1000.
346. He, X.; Allan, J. F.; Noll, B. C.; Kennedy, A. R.; Henderson, K. W., Stereoselective Enolizations Mediated by Magnesium and Calcium Bisamides: Contrasting Aggregation Behavior in Solution and in the Solid State. *J. Am. Chem. Soc.* **2005**, *127*, 6920-6921.

347. Barrett, A. G. M.; Crimmin, M. R.; Hill, M. S.; Kociok-Köhn, G.; MacDougall, D. J.; Mahon, M. F.; Procopiou, P. A., Synthesis, Characterization, and Solution Lability of N-Heterocyclic Carbene Adducts of the Heavier Group 2 Bis(trimethylsilyl)amides. *Organometallics* **2008**, *27*, 3939-3946.
348. Thomas-Hargreaves, L. R.; Pan, S.; Ivlev, S. I.; Frenking, G.; Buchner, M. R., π Back-Donation from a Beryllium Dibromide Fragment at the Expense of Its σ Strength. *Inorg. Chem.* **2022**, *61*, 700-705.
349. Schwarz, N.; Sun, X.; Yadav, R.; Köpfe, R.; Simler, T.; Roesky, P. W., Application of the Redox-Transmetalation Procedure to Access Divalent Lanthanide and Alkaline-Earth NHC Complexes**. *Chem. Eur. J.* **2021**, *27*, 12857-12865.
350. Owing to the propensity of the diethylether to evaporate under even short periods of vacuum, the yield given for 1 is calculated from the amount of solvent-free complex that is obtained after drying the product under reduced pressure. Please see SI for further experimental details.
351. He, X.; Noll, B. C.; Beatty, A.; Mulvey, R. E.; Henderson, K. W., Ketone Deprotonation Mediated by Mono- and Heterobimetallic Alkali and Alkaline Earth Metal Amide Bases: Structural Characterization of Potassium, Calcium, and Mixed Potassium–Calcium Enolates. *J. Am. Chem. Soc.* **2004**, *126*, 7444-7445.
352. Johns, A. M.; Chmely, S. C.; Hanusa, T. P., Solution Interaction of Potassium and Calcium Bis(trimethylsilyl)amides; Preparation of $\text{Ca}[\text{N}(\text{SiMe}_3)_2]_2$ from Dibenzylcalcium. *Inorg. Chem.* **2009**, *48*, 1380-1384.
353. Freeman, L. A.; Obi, A. D.; Machost, H. R.; Molino, A.; Nichols, A. W.; Dickie, D. A.; Wilson, D. J. D.; Machan, C. W.; Gilliard, R. J., Soluble, crystalline, and thermally stable

alkali CO₂⁻ and carbonite (CO₂²⁻) clusters supported by cyclic(alkyl)(amino) carbenes. *Chem. Sci.* **2021**, *12*, 3544-3550.

354. For examples of main group M(HMDS)₂ (M = Mg, Zn, Ge, Sn) reactivity with CO₂, see Felix, A. M.; Boro, B. J.; Dickie, D. A.; Tang, Y.; Saria, J. A.; Moasser, B.; Stewart, C. A.; Frost, B. J.; Kemp, R. A., Insertion of CO₂ into divalent group 2 and 12 bis(silylamides). *Main Group Chem.* 2012, *11*, 13-29 and references therein. To the best of our knowledge, examples involving Ca(HMDS)₂ are unreported, and our preliminary investigations are thus far inconclusive, and outside the scope of this study.

355. Greenwood, N. N.; Earnshaw, A., *Chemistry of the Elements*. Elsevier: 2012.

356. Baker, R. J.; Davies, A. J.; Jones, C.; Kloth, M., Structural and spectroscopic studies of carbene and N-donor ligand complexes of Group 13 hydrides and halides. *J. Organomet. Chem.* **2002**, *656*, 203-210.

357. D. Francis, M.; E. Hibbs, D.; B. Hursthouse, M.; Jones, C.; A. Smithies, N., Carbene complexes of Group 13 trihydrides: synthesis and characterisation of [MH₃{ \wedge CN(Pri)C₂Me₂N \vee (Pri)}], M = Al, Ga or In. *J. Chem. Soc., Dalton Trans.* **1998**, 10.1039/A805766D, 3249-3254.

358. Moon, H. W.; Cornella, J., Bismuth Redox Catalysis: An Emerging Main-Group Platform for Organic Synthesis. *ACS Catal.* **2022**, *12*, 1382-1393.

359. Lipshultz, J. M.; Li, G.; Radosevich, A. T., Main Group Redox Catalysis of Organopnictogens: Vertical Periodic Trends and Emerging Opportunities in Group 15. *J. Am. Chem. Soc.* **2021**, *143*, 1699-1721.

360. Coughlin, O.; Benjamin, S. L., 3.11 - Arsenic, Antimony and Bismuth. In *Comprehensive Coordination Chemistry III*, Constable, E. C.; Parkin, G.; Que Jr, L., Eds. Elsevier: Oxford, 2021, <https://doi.org/10.1016/B978-0-08-102688-5.00051-9> 321-417.

361. Cornella, J.; Pang, Y., Organometallic Compounds of Arsenic, Antimony and Bismuth. In *Reference Module in Chemistry, Molecular Sciences and Chemical Engineering*, Elsevier: 2021, <https://doi.org/10.1016/B978-0-12-820206-7.00128-1>.
362. Chitnis, S. S.; Hynes, T., Antimony and Bismuth Complexes in Organic Synthesis. In *Reference Module in Chemistry, Molecular Sciences and Chemical Engineering*, Elsevier: 2021, <https://doi.org/10.1016/B978-0-12-820206-7.00025-1>.
363. Mohan, R., Green bismuth. *Nat. Chem.* **2010**, *2*, 336-336.
364. Wedler, H. B.; Wendelboe, P.; Power, P. P., Second-Order Jahn–Teller (SOJT) Structural Distortions in Multiply Bonded Higher Main Group Compounds. *Organometallics* **2018**, *37*, 2929-2936.
365. Power, P. P., An Update on Multiple Bonding between Heavier Main Group Elements: The Importance of Pauli Repulsion, Charge-Shift Character, and London Dispersion Force Effects. *Organometallics* **2020**, *39*, 4127-4138.
366. Abbenseth, J.; Goicoechea, J. M., Recent developments in the chemistry of non-trigonal pnictogen pincer compounds: from bonding to catalysis. *Chem. Sci.* **2020**, *11*, 9728-9740.
367. Lichtenberg, C., Molecular bismuth(III) monocations: structure, bonding, reactivity, and catalysis. *Chem. Commun.* **2021**, *57*, 4483-4495.
368. Andleeb, S.; Imtiaz ud, D., Recent progress in designing the synthetic strategies for bismuth based complexes. *J. Organomet. Chem.* **2019**, *898*, 120871.
369. Ishida, S.; Hirakawa, F.; Furukawa, K.; Yoza, K.; Iwamoto, T., Persistent Antimony- and Bismuth-Centered Radicals in Solution. *Angew. Chem. Int. Ed.* **2014**, *53*, 11172-11176.
370. Schwamm, R. J.; Lein, M.; Coles, M. P.; Fitchett, C. M., Catalytic oxidative coupling promoted by bismuth TEMPOxide complexes. *Chem. Commun.* **2018**, *54*, 916-919.

371. Ramler, J.; Krummenacher, I.; Lichtenberg, C., Well-Defined, Molecular Bismuth Compounds: Catalysts in Photochemically Induced Radical Dehydrocoupling Reactions. *Chem. Eur. J.* **2020**, *26*, 14551-14555.
372. Mukhopadhyay, D. P.; Schleier, D.; Wirsing, S.; Ramler, J.; Kaiser, D.; Reusch, E.; Hemberger, P.; Preitschopf, T.; Krummenacher, I.; Engels, B.; Fischer, I.; Lichtenberg, C., Methylbismuth: an organometallic bismuthinidene biradical. *Chem. Sci.* **2020**, *11*, 7562-7568.
373. Oberdorf, K.; Hanft, A.; Ramler, J.; Krummenacher, I.; Bickelhaupt, F. M.; Poater, J.; Lichtenberg, C., Bismuth Amides Mediate Facile and Highly Selective Pn–Pn Radical-Coupling Reactions (Pn=N, P, As). *Angew. Chem. Int. Ed.* **2021**, *60*, 6441-6445.
374. Schwamm, R. J.; Lein, M.; Coles, M. P.; Fitchett, C. M., Bi–P Bond Homolysis as a Route to Reduced Bismuth Compounds and Reversible Activation of P₄. *Angew. Chem. Int. Ed.* **2016**, *55*, 14798-14801.
375. Planas, O.; Wang, F.; Leutzsch, M.; Cornella, J., Fluorination of arylboronic esters enabled by bismuth redox catalysis. *Science* **2020**, *367*, 313-317.
376. Ramler, J.; Krummenacher, I.; Lichtenberg, C., Bismuth Compounds in Radical Catalysis: Transition Metal Bismuthanes Facilitate Thermally Induced Cycloisomerizations. *Angew. Chem. Int. Ed.* **2019**, *58*, 12924-12929.
377. Pang, Y.; Leutzsch, M.; Nöthling, N.; Cornella, J., Catalytic Activation of N₂O at a Low-Valent Bismuth Redox Platform. *J. Am. Chem. Soc.* **2020**, *142*, 19473-19479.
378. Gimferrer, M.; Danés, S.; Andrada, D. M.; Salvador, P., Unveiling the Electronic Structure of the Bi(+1)/Bi(+3) Redox Couple on NCN and NNN Pincer Complexes. *Inorg. Chem.* **2021**, *60*, 17657-17668.

379. Schwamm, R. J.; Harmer, J. R.; Lein, M.; Fitchett, C. M.; Granville, S.; Coles, M. P., Isolation and Characterization of a Bismuth(II) Radical. *Angew. Chem. Int. Ed.* **2015**, *54*, 10630-10633.
380. Turner, Z. R., Bismuth Pyridine Dipyrrolide Complexes: a Transient Bi(II) Species Which Ring Opens Cyclic Ethers. *Inorg. Chem.* **2019**, *58*, 14212-14227.
381. Ramler, J.; Schwarzmann, J.; Stoy, A.; Lichtenberg, C., Two Faces of the Bi–O Bond: Photochemically and Thermally Induced Dehydrocoupling for Si–O Bond Formation. *Eur. J. Inorg. Chem.* **2022**, *2022*, e202100934.
382. Kindervater, M. B.; Marczenko, K. M.; Werner-Zwanziger, U.; Chitnis, S. S., A Redox-Confused Bismuth(I/III) Triamide with a T-Shaped Planar Ground State. *Angew. Chem. Int. Ed.* **2019**, *58*, 7850-7855.
383. Deb, R.; Balakrishna, P.; Majumdar, M., Recent Developments in the Chemistry of Pn(I) (Pn=N, P, As, Sb, Bi) Cations. *Chem. Asian J.* **2022**, *17*, e202101133.
384. Wang, F.; Planas, O.; Cornella, J., Bi(I)-Catalyzed Transfer-Hydrogenation with Ammonia-Borane. *J. Am. Chem. Soc.* **2019**, *141*, 4235-4240.
385. Šimon, P.; de Proft, F.; Jambor, R.; Růžička, A.; Dostál, L., Monomeric Organoantimony(I) and Organobismuth(I) Compounds Stabilized by an NCN Chelating Ligand: Syntheses and Structures. *Angew. Chem. Int. Ed.* **2010**, *49*, 5468-5471.
386. Deka, R.; Orthaber, A., Carbene chemistry of arsenic, antimony, and bismuth: origin, evolution and future prospects. *Dalton Trans.* **2022**, *51*, 8540-8556.
387. Aprile, A.; Corbo, R.; Vin Tan, K.; Wilson, D. J. D.; Dutton, J. L., The first bismuth–NHC complexes. *Dalton Trans.* **2014**, *43*, 764-768.

388. Wilson, D. J. D.; Couchman, S. A.; Dutton, J. L., Are N-Heterocyclic Carbenes “Better” Ligands than Phosphines in Main Group Chemistry? A Theoretical Case Study of Ligand-Stabilized E₂ Molecules, L-E-E-L (L = NHC, phosphine; E = C, Si, Ge, Sn, Pb, N, P, As, Sb, Bi). *Inorg. Chem.* **2012**, *51*, 7657-7668.
389. Siddiqui, M. M.; Sarkar, S. K.; Nazish, M.; Morganti, M.; Köhler, C.; Cai, J.; Zhao, L.; Herbst-Irmer, R.; Stalke, D.; Frenking, G.; Roesky, H. W., Donor-Stabilized Antimony(I) and Bismuth(I) Ions: Heavier Valence Isoelectronic Analogues of Carbenes. *J. Am. Chem. Soc.* **2021**, *143*, 1301-1306.
390. Dobrovetsky, R.; Stephan, D. W., Catalytic Reduction of CO₂ to CO by Using Zinc(II) and In Situ Generated Carbodiphosphoranes. *Angew. Chem. Int. Ed.* **2013**, *52*, 2516-2519.
391. Liu, S.-k.; Shih, W.-C.; Chen, W.-C.; Ong, T.-G., Carbodicarbenes and their Captodative Behavior in Catalysis. *ChemCatChem* **2018**, *10*, 1483-1498.
392. Thirumoorthi, R.; Chivers, T.; Gendy, C.; Vargas-Baca, I., CH–NH Tautomerism in the Products of the Reactions of the Methanide [HC(PPh₂NSiMe₃)₂][–] with Pnictogen and Tellurium Iodides. *Organometallics* **2013**, *32*, 5360-5373.
393. Thirumoorthi, R.; Chivers, T.; Vargas-Baca, I., S,C,S-Pnictogen bonding in pincer complexes of the methanediide [C(Ph₂PS)₂]₂[–]. *Dalton Trans.* **2011**, *40*, 8086-8088.
394. Sindlinger, C. P.; Stasch, A.; Wesemann, L., Heavy Group 15 Element Compounds of a Sterically Demanding Bis(iminophosphorane)methanide and -methanediide. *Organometallics* **2014**, *33*, 322-328.
395. Böttger, S. C.; Poggel, C.; Sundermeyer, J., ortho-Directed Dilithiation of Hexaphenyl-carbodiphosphorane. *Organometallics* **2020**, *39*, 3789-3793.

396. Henceforth, the carbodiphosphoranyl dianion is denoted as "CDP" whereas the neutral carbodiphosphorane ligand will be specifically described as "neutral CDP" or "monodentate CDP"
397. Notably, several solvates of 1 and 2, as well as most of the compounds described in this manuscript, were crystallographically identified, and their cifs included in the supporting information
398. Balasubramaniam, S.; Kumar, S.; Andrews, A. P.; Varghese, B.; Jemmis, E. D.; Venugopal, A., A Dicationic Bismuth(III) Lewis Acid: Catalytic Hydrosilylation of Olefins. *Eur. J. Inorg. Chem.* **2019**, 2019, 3257-3257.
399. Bao, M.; Hayashi, T.; Shimada, S., Cationic Organobismuth Complex with 5,6,7,12-Tetrahydrodibenz[c,f][1,5]azabismocine Framework and Its Coordination Complexes with Neutral Molecules. *Organometallics* **2007**, 26, 1816-1822.
400. Toma, A.; Raț, C. I.; Silvestru, A.; Ruffer, T.; Lang, H.; Mehring, M., Heterocyclic bismuth(III) compounds with transannular S→Bi interactions. An experimental and theoretical approach. *J. Organomet. Chem.* **2016**, 806, 5-11.
401. Yin, S.-F.; Maruyama, J.; Yamashita, T.; Shimada, S., Efficient Fixation of Carbon Dioxide by Hypervalent Organobismuth Oxide, Hydroxide, and Alkoxide. *Angew. Chem. Int. Ed.* **2008**, 47, 6590-6593.
402. Shimada, S.; Yamazaki, O.; Tanaka, T.; Suzuki, Y.; Tanaka, M., Synthesis and structure of 5,6,7,12-tetrahydrodibenz[c,f][1,5]azabismocines. *J. Organomet. Chem.* **2004**, 689, 3012-3023.

403. Casely, I. J.; Ziller, J. W.; Mincher, B. J.; Evans, W. J., Bismuth Coordination Chemistry with Allyl, Alkoxide, Aryloxy, and Tetraphenylborate Ligands and the {[2,6-(Me₂NCH₂)₂C₆H₃]₂Bi}⁺ Cation. *Inorg. Chem.* **2011**, *50*, 1513-1520.
404. Carden, J. L.; Dasgupta, A.; Melen, R. L., Halogenated triarylboranes: synthesis, properties and applications in catalysis. *Chem. Soc. Rev.* **2020**, *49*, 1706-1725.
405. Roy, M. M. D.; Omaña, A. A.; Wilson, A. S. S.; Hill, M. S.; Aldridge, S.; Rivard, E., Molecular Main Group Metal Hydrides. *Chem. Rev.* **2021**, *121*, 12784-12965.
406. Hardman, N. J.; Twamley, B.; Power, P. P., (2,6-Mes₂H₃C₆)₂BiH, a Stable, Molecular Hydride of a Main Group Element of the Sixth Period, and Its Conversion to the Dibismuthene (2,6-Mes₂H₃C₆)BiBi(2,6-Mes₂C₆H₃). *Angew. Chem. Int. Ed.* **2000**, *39*, 2771-2773.
407. Lawson, J. R.; Melen, R. L., Tris(pentafluorophenyl)borane and Beyond: Modern Advances in Borylation Chemistry. *Inorg. Chem.* **2017**, *56*, 8627-8643.
408. Lampland, N. L.; Pindwal, A.; Neal, S. R.; Schlauderer, S.; Ellern, A.; Sadow, A. D., Magnesium-catalyzed hydrosilylation of α,β -unsaturated esters. *Chem. Sci.* **2015**, *6*, 6901-6907.
409. Sadow, A. D.; Tilley, T. D., Enhanced Reactivity of Cationic Hafnocene Complexes toward σ -Bond Metathesis Reactions. Si-H and Si-C Bond Activations in Stoichiometric and Catalytic Organosilane Conversions. *Organometallics* **2003**, *22*, 3577-3585.
410. Janssen-Müller, D.; Oestreich, M., Transition-Metal-Like Catalysis with a Main-Group Element: Bismuth-Catalyzed C-F Coupling of Aryl Boronic Esters. *Angew. Chem. Int. Ed.* **2020**, *59*, 8328-8330.
411. Gray, P. A.; Burford, N., Coordination complexes of pnictogen(V) cations. *Coord. Chem. Rev.* **2016**, *324*, 1-16.

412. Sakabe, M.; Sato, S., Isolation and Structural Determination of a Hexacoordinated Antimony(V) Dication. *Chem. Eur. J.* **2021**, *27*, 5658-5665.
413. Frazee, C.; Burford, N.; McDonald, R.; Ferguson, M. J.; Decken, A.; Patrick, B. O., Complexes of Stiboranium Mono-, Di-, and Trications. *Chem. Eur. J.* **2018**, *24*, 4011-4013.
414. Ugi, I.; Marquarding, D.; Klusacek, H.; Gillespie, P.; Ramirez, F., Berry pseudorotation and turnstile rotation. *Acc. Chem. Res.* **1971**, *4*, 288-296.
415. Bader, R. F. W., *Atoms in Molecules: A Quantum Theory*. Clarendon Press: Oxford, UK, 1990.
416. Cremer, D.; Kraka, E., Chemical Bonds without Bonding Electron Density? Does the Difference Electron-Density Analysis Suffice for a Description of the Chemical Bond? *Angew. Chem. Int. Ed.* **1984**, *23*, 627-628.
417. Frenking, G.; Tonner, R.; Klein, S.; Takagi, N.; Shimizu, T.; Krapp, A.; Pandey, K. K.; Parameswaran, P., New bonding modes of carbon and heavier group 14 atoms Si–Pb. *Chem. Soc. Rev.* **2014**, *43*, 5106-5139.
418. Zhao, L.; Chai, C.; Petz, W.; Frenking, G., Carbones and Carbon Atom as Ligands in Transition Metal Complexes. *Molecules* **2020**, *25*, 4943-4990.
419. Kroll, A.; Steinert, H.; Scharf, L. T.; Scherpf, T.; Mallick, B.; Gessner, V. H., A diamino-substituted carbodiphosphorane as strong C-donor and weak N-donor: isolation of monomeric trigonal-planar L·ZnCl₂. *Chem. Commun.* **2020**, *56*, 8051-8054.
420. Fulmer, G. R.; Miller, A. J. M.; Sherden, N. H.; Gottlieb, H. E.; Nudelman, A.; Stoltz, B. M.; Bercaw, J. E.; Goldberg, K. I., NMR Chemical Shifts of Trace Impurities: Common Laboratory Solvents, Organics, and Gases in Deuterated Solvents Relevant to the Organometallic Chemist. *Organometallics* **2010**, *29*, 2176-2179.

421. Macchioni, A., Ion Pairing in Transition-Metal Organometallic Chemistry. *Chem. Rev.* **2005**, *105*, 2039-2074.
422. Geer, A. M.; Tejel, C.; López, J. A.; Ciriano, M. A., Terminal Imido Rhodium Complexes. *Angew. Chem. Int. Ed.* **2014**, *53*, 5614-5618.
423. Yakelis, N. A.; Bergman, R. G., Safe Preparation and Purification of Sodium Tetrakis[(3,5-trifluoromethyl)phenyl]borate (NaBArF24): Reliable and Sensitive Analysis of Water in Solutions of Fluorinated Tetraarylborates. *Organometallics* **2005**, *24*, 3579-3581.
424. Ansell, M. B.; Roberts, D. E.; Cloke, F. G. N.; Navarro, O.; Spencer, J., Synthesis of an [(NHC)₂Pd(SiMe₃)₂] Complex and Catalytic cis-Bis(silyl)ations of Alkynes with Unactivated Disilanes. *Angew. Chem. Int. Ed.* **2015**, *54*, 5578-5582.
425. Vargas, W.; English, U.; Ruhlandt-Senge, K., A Novel Group of Alkaline Earth Metal Amides: Syntheses and Characterization of M[N(2,6-iPr₂C₆H₃)(SiMe₃)₂](THF)₂ (M = Mg, Ca, Sr, Ba) and the Linear, Two-Coordinate Mg[N(2,6-iPr₂C₆H₃)(SiMe₃)₂]₂. *Inorg. Chem.* **2002**, *41*, 5602-5608.
426. Hoerger, C. J.; Heinemann, F. W.; Louyriac, E.; Maron, L.; Grützmacher, H.; Meyer, K., Formation of a Uranium-Bound η¹-Cyaphide (CP⁻) Ligand via Activation and C–O Bond Cleavage of Phosphaethynolate (OCP⁻). *Organometallics* **2017**, *36*, 4351-4354.
427. Bruker *Saint; SADABS; APEX3*, Bruker AXS Inc.: Madison, Wisconsin, USA, 2012
428. Sheldrick, G. M., SHELXT– Integrated space-group and crystal-structure determination. *Acta Crystallogr., Sect. A: Found. Crystallogr.* **2015**, *71*, 3-8.
429. Dolomanov, O. V.; Bourhis, L. J.; Gildea, R. J.; Howard, J. A. K.; Puschmann, H., OLEX2: a complete structure solution, refinement and analysis program. *J. Appl. Crystallogr.* **2009**, *42*, 339-341.

430. Spek, A. L., PLATON SQUEEZE: a tool for the calculation of the disordered solvent contribution to the calculated structure factors. *Acta Crystallographica Section C: Structural Chemistry* **2015**, *71*, 9-18.
431. Sheldrick, G. *CELL_NOW, version 2008/4*, Georg-August-Universität Göttingen: Göttingen, Germany, 2008
432. Spek, A. L., Structure validation in chemical crystallography. *Acta Crystallogr. Sect. D. Biol. Crystallogr.* **2009**, *65*, 148-155.
433. Frisch, M. J.; Trucks, G. W.; Schlegel, H. B.; Scuseria, G. E.; Robb, M. A.; Cheeseman, J. R.; Scalmani, G.; Barone, V.; Petersson, G. A.; Nakatsuji, H.; Li, X.; Caricato, M.; Marenich, A. V.; Bloino, J.; Janesko, B. G.; Gomperts, R.; Mennucci, B.; Hratchian, H. P.; Ortiz, J. V.; Izmaylov, A. F.; Sonnenberg, J. L.; Williams; Ding, F.; Lipparini, F.; Egidi, F.; Goings, J.; Peng, B.; Petrone, A.; Henderson, T.; Ranasinghe, D.; Zakrzewski, V. G.; Gao, J.; Rega, N.; Zheng, G.; Liang, W.; Hada, M.; Ehara, M.; Toyota, K.; Fukuda, R.; Hasegawa, J.; Ishida, M.; Nakajima, T.; Honda, Y.; Kitao, O.; Nakai, H.; Vreven, T.; Throssell, K.; Montgomery Jr., J. A.; Peralta, J. E.; Ogliaro, F.; Bearpark, M. J.; Heyd, J. J.; Brothers, E. N.; Kudin, K. N.; Staroverov, V. N.; Keith, T. A.; Kobayashi, R.; Normand, J.; Raghavachari, K.; Rendell, A. P.; Burant, J. C.; Iyengar, S. S.; Tomasi, J.; Cossi, M.; Millam, J. M.; Klene, M.; Adamo, C.; Cammi, R.; Ochterski, J. W.; Martin, R. L.; Morokuma, K.; Farkas, O.; Foresman, J. B.; Fox, D. J. *Gaussian 16 Revision B.01*, Wallingford, CT, 2016
434. Kendall, R. A.; Dunning, T. H.; Harrison, R. J., Electron affinities of the first - row atoms revisited. Systematic basis sets and wave functions. *J. Chem. Phys.* **1992**, *96*, 6796-6806.
435. Dunning Jr, T. H., Gaussian basis sets for use in correlated molecular calculations. I. The atoms boron through neon and hydrogen. *J. Chem. Phys.* **1989**, *90*, 1007-1023.

436. Frisch, M. J.; Trucks, G. W.; Schlegel, H. B.; Scuseria, G. E.; Robb, M. A.; Cheeseman, J. R.; Scalmani, G.; Barone, V.; Petersson, G. A.; Nakatsuji, H.; Li, X.; Caricato, M.; Marenich, A. V.; Bloino, J.; Janesko, B. G.; Gomperts, R.; Mennucci, B.; Hratchian, H. P.; Ortiz, J. V.; Izmaylov, A. F.; Sonnenberg, J. L.; Williams; Ding, F.; Lipparini, F.; Egidi, F.; Goings, J.; Peng, B.; Petrone, A.; Henderson, T.; Ranasinghe, D.; Zakrzewski, V. G.; Gao, J.; Rega, N.; Zheng, G.; Liang, W.; Hada, M.; Ehara, M.; Toyota, K.; Fukuda, R.; Hasegawa, J.; Ishida, M.; Nakajima, T.; Honda, Y.; Kitao, O.; Nakai, H.; Vreven, T.; Throssell, K.; Montgomery Jr., J. A.; Peralta, J. E.; Ogliaro, F.; Bearpark, M. J.; Heyd, J. J.; Brothers, E. N.; Kudin, K. N.; Staroverov, V. N.; Keith, T. A.; Kobayashi, R.; Normand, J.; Raghavachari, K.; Rendell, A. P.; Burant, J. C.; Iyengar, S. S.; Tomasi, J.; Cossi, M.; Millam, J. M.; Klene, M.; Adamo, C.; Cammi, R.; Ochterski, J. W.; Martin, R. L.; Morokuma, K.; Farkas, O.; Foresman, J. B.; Fox, D. J. *Gaussian 09 Revision D. 01*, Wallingford, CT, 2016
437. Lu, T.; Chen, F., Multiwfn: A multifunctional wavefunction analyzer. *J. Comput. Chem.* **2012**, *33*, 580-592.
438. Pipek, J.; Mezey, P. G., A fast intrinsic localization procedure applicable for ab initio and semiempirical linear combination of atomic orbital wave functions. *J. Chem. Phys.* **1989**, *90*, 4916-4926.
439. Zhurko, G. A. Chemcraft. Ivanonvo, Russia 2005.
440. Frisch, M. J.; Trucks, G. W.; Schlegel, H. B.; Scuseria, G. E.; Robb, M. A.; Cheeseman, J. R.; Scalmani, G.; Barone, V.; Petersson, G. A.; Nakatsuji, H.; Li, X.; Caricato, M.; Marenich, A. V.; Bloino, J.; Janesko, B. G.; Gomperts, R.; Mennucci, B.; Hratchian, H. P.; Ortiz, J. V.; Izmaylov, A. F.; Sonnenberg, J. L.; Williams; Ding, F.; Lipparini, F.; Egidi, F.; Goings, J.; Peng, B.; Petrone, A.; Henderson, T.; Ranasinghe, D.; Zakrzewski, V. G.;

Gao, J.; Rega, N.; Zheng, G.; Liang, W.; Hada, M.; Ehara, M.; Toyota, K.; Fukuda, R.; Hasegawa, J.; Ishida, M.; Nakajima, T.; Honda, Y.; Kitao, O.; Nakai, H.; Vreven, T.; Throssell, K.; Montgomery Jr., J. A.; Peralta, J. E.; Ogliaro, F.; Bearpark, M. J.; Heyd, J. J.; Brothers, E. N.; Kudin, K. N.; Staroverov, V. N.; Keith, T. A.; Kobayashi, R.; Normand, J.; Raghavachari, K.; Rendell, A. P.; Burant, J. C.; Iyengar, S. S.; Tomasi, J.; Cossi, M.; Millam, J. M.; Klene, M.; Adamo, C.; Cammi, R.; Ochterski, J. W.; Martin, R. L.; Morokuma, K.; Farkas, O.; Foresman, J. B.; Fox, D. J. *Gaussian 16 Rev. C.01*, Wallingford, CT, 2016

441. Glendening, E.; Reed, A.; Carpenter, J.; Weinhold, F., NBO Version 3.1. **1998**.

442. M. J. Frisch, G. W. T., H. B. Schlegel, G. E. Scuseria, M. A. Robb, J. R. Cheeseman, G. Scalmani, V. Barone, B. Mennucci, G. A. Petersson, H. Nakatsuji, M. Caricato, X. Li, H. P. Hratchian, A. F. Izmaylov, J. Bloino, G. Zheng, J. L. Sonnenberg, M. Hada, M. Ehara, K. Toyota, R. Fukuda, J. Hasegawa, M. Ishida, T. Nakajima, Y. Honda, O. Kitao, H. Nakai, T. Vreven, J. A. Montgomery, Jr., J. E. Peralta, F. Ogliaro, M. Bearpark, J. J. Heyd, E. Brothers, K. N. Kudin, V. N. Staroverov, R. Kobayashi, J. Normand, K. Raghavachari, A. Rendell, J. C. Burant, S. S. Iyengar, J. Tomasi, M. Cossi, N. Rega, J. M. Millam, M. Klene, J. E. Knox, J. B. Cross, V. Bakken, C. Adamo, J. Jaramillo, R. Gomperts, R. E. Stratmann, O. Yazyev, A. J. Austin, R. Cammi, C. Pomelli, J. W. Ochterski, R. L. Martin, K. Morokuma, V. G. Zakrzewski, G. A. Voth, P. Salvador, J. J. Dannenberg, S. Dapprich, A. D. Daniels, O. Farkas, J. B. Foresman, J. V. Ortiz, J. Cioslowski, and D. J. Fox *Gaussian 09 Rev. D.01*, Wallingford, CT, 2009

443. Manson, J. W., C. E.; Pérez, L. M.; Hall, M. B. *Jimp 2*.

<http://www.chem.tamu.edu/jimp2/index.html>.

444. Becke, A. D., Density-functional exchange-energy approximation with correct asymptotic behavior. *Physical Review A* **1988**, *38*, 3098-3100.
445. Perdew, J. P., Density-functional approximation for the correlation energy of the inhomogeneous electron gas. *Phys. Rev. B* **1986**, *33*, 8822-8824.
446. Grimme, S.; Ehrlich, S.; Goerigk, L., Effect of the damping function in dispersion corrected density functional theory. *J. Comput. Chem.* **2011**, *32*, 1456-1465.
447. Grimme, S.; Antony, J.; Ehrlich, S.; Krieg, H., A consistent and accurate ab initio parametrization of density functional dispersion correction (DFT-D) for the 94 elements H-Pu. *J. Chem. Phys.* **2010**, *132*, 154104.
448. Glendening, E. D.; Landis, C. R.; Weinhold, F., NBO 6.0: Natural bond orbital analysis program. *J. Comput. Chem.* **2013**, *34*, 1429-1437.